


FRICION WEAR LUBRICATION



Tribology Handbook

**FRICTION
WEAR
LUBRICATION**

VOL. 1

ТРЕНИЕ, ИЗНАШИВАНИЕ И СМАЗКА

Под редакцией И. В. КРАГЕЛЬСКОГО и В. В. АЛИСИНА

Издательство «Машиностроение», Москва

FRICION WEAR LUBRICATION

Vol. 1

Tribology Handbook

Edited by Prof. I. V. KRAGELSKY

D. Sc. (Eng.)

V. V. ALISIN

Cand. Sc. (Eng.)

Institute for Machine Sciences, Moscow

Translated from

the Russian

by

Felix Palkin

and Valerian Palkin

Mir Publishers

Moscow

*First published 1981
Revised from the 1978 Russian edition*

The Russian Alphabet and Transliteration

Аа	a	Кк	k	Хх	kh
Бб	b	Лл	l	Цц	ts
Вв	v	Мм	m	Чч	ch
Гг	g	Нн	n	Шш	sh
Дд	d	Оо	o	Щщ	shch
Ее	e	Пп	p	Ъ	"
Ёё	ë	Рр	r	Ы	y
Жж	zh	Сс	s	Ь	'
Зз	z	Тт	t	Ээ	e
Ии	i	Уу	u	Юю	yu
Йй	y	Фф	f	Яя	ya

The Greek Alphabet

Αα	Alpha	Ιι	Iota	Ρρ	Rho
Ββ	Beta	Κκ	Kappa	Σσ	Sigma
Γγ	Gamma	Λλ	Lambda	Ττ	Tau
Δδ	Delta	Μμ	Mu	Υυ	Upsilon
Εε	Epsilon	Νν	Nu	Φφ	Phi
Ζζ	Zeta	Ξξ	Xi	Χχ	Chi
Ηη	Eta	Οο	Omicron	Ψψ	Psi
Θθ	Theta	Ππ	Pi	Ωω	Omega

На английском языке

© Издательство «Машиностроение», 1978

© English translation, Mir Publishers, 1981

CONTENTS

Preface	9
Notation	10
Chapter 1. The Contact of Solids [Professor N. B. Demkin, D. Sc. (Eng.)]	
1.1. Contact of Ideally Smooth Surfaces	13
1.2. Surface Quality of Machine Parts	17
1.2.1. Physico-Mechanical Properties of Surface Layers	17
1.2.2. Characteristics of Surface Geometry	18
1.2.3. Methods for Determining Characteristics of Surface Geometry	22
1.3. Contact of Rough Surfaces	32
1.3.1. Interaction of Surface Peaks	32
1.3.2. Real and Contour Areas of Contact	33
1.3.3. Calculation of the Real Area of Contact and Real Pressure	34
1.3.4. Calculation of the Contour Area of Contact and Contour Pressure	38
1.3.5. Calculation of Approach Between Surfaces	41
1.3.6. Calculation of Intercontact Space Volume	43
1.3.7. Calculation of the Number of Spots in Real Contact, Their Average Area and Spacing	44
1.4. Rheological Properties of Contact	45
1.5. Methods and Instruments for Research on Properties of Contacts	47
1.5.1. Measurement of Real Contact Area	47
1.5.2. Measurement of Contact Deformations	52
References	52
Chapter 2. Calculation of Coefficients of External Friction and Preliminary Displacement [Professor N. M. Mikhin, D. Sc. (Eng.)]	
2.1. Main Concepts and Definitions	54
2.2. Interaction of Solids	56
2.3. Factors Affecting the Coefficient of External Static Friction	69
2.3.1. Contour Pressure	69
2.3.2. Surface Roughness	73
2.3.3. Mechanical Properties of Contacting Materials	76
2.3.4. Temperature of Solids in Contact	79
2.4. Methods for Determining Quantities Required for Calculation of the Coefficient of External Static Friction	80
2.5. Method for Calculation of the Coefficient of Friction	88
2.6. Preliminary Displacement	94
References	99

Chapter 3. Calculation of Wear Rate [Professor I. V. Kragelsky, D. Sc. (Eng.), V. V. Alisin, Cand. Sc. (Eng.)]

3.1. General Characteristics of Wear of Materials	102
3.2. Physical Model of Wear	104
3.3. Main Design Relationships	112
3.4. Factors Affecting Wear Rate	114
References	118

Chapter 4. Calculation of Tribological Joints for Wear [Professor A. S. Pro-nikov, D. Sc. (Eng.)]

4.1. Wear in Tribological Joints	119
4.1.1. Basic Laws of Wear in Materials	119
4.1.2. Wear of the Surface and Joint	120
4.1.3. Classification of Joints by Wear Conditions	122
4.2. Wear Calculation Methods for Tribological Joints	125
4.2.1. The Use of the Contact Condition	125
4.2.2. Rectilinear Guideways	128
4.2.3. Joints with Variable Contact Conditions	130
4.2.4. Running-in of Inaccurate or Deformed Parts	135
4.2.5. Pairs with Small Relative Displacements	138
4.3. Wear Calculation with Allowance for Stiffness	140
4.3.1. Contact Problem for Wearing Joints	140
4.3.2. Transition of Static Pressure Diagram into Dynamic One	142
4.3.3. Rigidly Linked Joints	144
4.4. Calculation of Wear Limits	146
4.4.1. The Allowable Amounts of Wear	146
4.4.2. Wear Limits for Multi-Link Mechanisms	147
4.5. Calculation for Reliability of Joints	148
4.5.1. Reliability Parameters	148
4.5.2. Example of Calculation for Wear Life and Probability of Failure-Free Operation	150
4.5.3. Predicting the Wear of Joints	151
4.5.4. Effect of Wear on Functional Properties of a Machine	152
4.5.5. Diagram for Calculation of a Machine for Reliability	154
References	156

Chapter 5. Choice of Materials for Rubbing Parts [BSSR Academician V. A. Bely, A. U. Sviridenok, D. Sc. (Eng.)]

5.1. Analysis of Operating Conditions and Drawing up of Specifications	158
5.2. Preliminary Choice of Material	162
5.2.1. General Data	162
5.2.2. Polymer-Base Materials	162
5.2.3. Laminated Materials	182
5.2.4. Carbon-Graphite Materials	184
5.2.5. Metal-Ceramic Materials	186
5.3. Assessment of Performance of Tribological Joints at Design Stage	189
5.4. The Final Choice of Material	196
References	197

Chapter 6. Metals for Rubbing Components

6.1. Structural Changes of Metals in Friction [Professor I. M. Lyubars-ky, Dr. Sc. (Eng.)]	199
--	-----

6.1.1. General	199
6.1.2. Structure and Properties	199
6.1.3. Metal Strengthening	200
6.1.4. Secondary Processes in Friction	203
6.1.5. Main Methods of Metal Structure Analysis	207
6.1.6. Recommendations	207
6.2. Thermo-Chemical Treatment as a Means for Increasing the Wear Resistance of Metals [Yu. M. Vinogradov, D. Sc. (Eng.)]	208
6.2.1. Process Features	208
6.2.2. TCT Processes and Their Application	209
6.2.3. Assessing the Effectiveness of TCT	216
6.3. Friction and Wear of Metals at High Sliding Speeds [V. A. Ba- lakin, Cand. Sc. (Eng.)]	218
References	222
 Chapter 7. Metallic Antifriction Materials [Professor N. A. Bushe, D. Sc. (Eng.)]	
7.1. Brief Characteristics of Bearing Alloys	223
7.1.1. Babbitt Metals	223
7.1.2. Copper-Base Alloys	226
7.1.3. Aluminium-Base Alloys	229
7.1.4. Link-Base Alloys	231
7.1.5. Ferrous Alloys	232
7.1.6. Sintered Alloys	235
7.2. Comparative Evaluation of Bearing Materials Properties	235
7.2.1. Fatigue Strength	235
7.2.2. Running-in	242
7.2.3. Wear Resistance	244
7.2.4. Compatibility of Sliding-Pair Elements	246
7.2.5. Resistance to Scoring	249
7.3. Selection of Bearing Alloys	251
References	252
 Chapter 8. Manufacturing Methods for Improving the Wear Resistance of Materials and Tribological Joints [Professor E. V. Ryzrov, D. Sc. (Eng.)]	
8.1. General	255
8.2. Machining Methods	257
8.3. Surface Treatment by Plastic Deformation	269
8.4. Heat Treatment (Surface Hardening)	274
8.5. Surface Coating	275
8.6. Hard-Facing	277
8.7. Metal Spraying	283
References	289
 Chapter 9. Lubricants and Additives	
9.1. Engine Oils [V. D. Reznikov, Cand. Sc. (Eng.)]	290
9.1.1. Classification by Viscosity and the Main Principles of Oil Selection	291
9.1.2. Classification by Service Properties and the Main Principles of Selection	294
9.2. Transmission Oils for Automotive Applications [I.E. Vinogradov, D. Sc. (Eng.)]	295
9.2.1. Viscosity and Its Dependence on Temperature	295
9.2.2. Basics of Oil and Additive Selection	301
9.2.3. Types and Properties of Additives	306
9.2.4. Requirements for Transmission Oils	312

9.3. Industrial Oils [K. M. Badyshtova, Cand. Sc. (Eng)]	319
9.3.1. Main Properties	323
9.3.2. Modern Oil Assortment	329
9.4. Greases [Yu. L. Ishchuk, Cand. Sc. (Eng.)]	333
9.4.1. Properties	333
9.4.2. Assortment and Application of Greases	345
9.5. Solid Lubricants and Coatings for Operation in Vacuum [G. I. Tro- yanovskaya, Cand. Sc. (Eng.)]	352
9.5.1. Solid Lubricants	352
9.5.2. Self-Lubricating Materials	354
9.5.3. Frictional Characteristics of Solid Lubricants and Self-Lubr- icating Materials	357
9.5.4. Solid Lubricant Coatings with Polymer Binders	361
9.5.5. Soft Metal Coatings	363
References	365

Chapter 10. Thermal Stability of Boundary Lubrication Films and Solid Lubricant Films [R. M. Matveevsky, D. Sc. (Eng.)]

10.1. Influence of the Nature of Oil, Additive and Grease	370
10.2. Influence of the Rubbing Surface Material	375
10.3. Influence of Gas Medium	378
10.4. Thermal Stability of Solid Lubricant Coatings	379
References	381

The evolution of mechanical engineering gives rise to new fields of study, whose development is dictated by practical needs.

At its early stage, machine design was primarily concerned with kinematical analysis of machine parts in relative motion. The need for strength calculation emerged later on, when high-power engines came into existence.

Recent years have seen the advent and development of a third branch of machine design, which has been called tribology (after the Greek word *tribos* meaning to rub). The essence of this branch of study is research into the contact interaction of solids in relative motion that produces friction in the contact area. The frictional forces not only reduce the useful power of engines, but also cause changes in the dimensions of mating parts and, consequently, impair the accuracy of machines. Under unfavourable conditions, external friction is transformed into internal friction causing the galling of frictional surfaces, which may lead to their seizure, that is, to a failure in the machine.

In some cases, however, frictional forces are beneficial (for instance, in brakes, friction transmission, and similar mechanisms).

Soviet scientists have vastly contributed to the development of tribology, and the present handbook summarizes the results of their research on the friction and wear of machine parts and gives data on lubricants and lube additives for various sliding and rolling contact joints operating under a variety of conditions.

The handbook is compiled by a large body of leading scientists. It is conceived as an aid to design engineers in choosing materials and lubricants for the given rubbing conditions, and may also prove helpful to repair and maintenance engineers.

This is the first tribology handbook to be ever published in this country, so some imperfections in its content and setup seem to be inevitable. The authors, therefore, will accept with gratitude all suggestions aimed at the improvement of this work.

NOTATION

A_a	= apparent area of contact
A_c	= contour area of contact
A_r	= real area of contact
N	= normal load
T	= frictional force
W	= work of friction
p_a, p_c, p_r	= nominal, contour, and real pressure, respectively
M	= moment of external forces
M_T	= frictional moment
t	= time
ω	= angular velocity
v	= linear velocity
τ	= tangential stress
σ	= normal stress
μ	= Poisson's ratio
E	= modulus of elasticity
σ_y	= yield limit
HB, HRC, HV	= Brinell, Rockwell, and Vickers hardness, respectively
H	= microhardness
α_h	= coefficient of hysteresis loss
σ_0	= frictional fatigue parameter
t_y	= degree of frictional fatigue curve for elastic contact
n	= number of loading cycles causing destruction of the deformed volume of material; number of revolutions
ρ	= density
$\Theta = \frac{1-\mu^2}{E}$	= elastic constant of material (if both surfaces are deformed, $\Theta_\Sigma = \Theta_1 + \Theta_2$)
d	= diameter of contact spot
R_{\max}	= maximum height of profile irregularities
n_p	= reference length of profile

t_p	= relative reference length of profile
p	= level of profile section
H_b	= height of waveform
R_b	= curvature radius of wave crests
S_b	= spacing (wavelength) of waveforms
Ra	= arithmetic mean deviation of the profile
Rz	= ten-point height of irregularities
S_m	= mean spacing of profile irregularities
Δ_0	= maximum form error
r_{tr}	= transverse curvature radius of irregularity
r_{ln}	= longitudinal curvature radius of irregularity
$r = \frac{r_{tr}r_{ln}}{r_{tr}+r_{ln}}$	= effective curvature radius of irregularity
b, v	= parameters of bearing-area curve
ϵ	= relative approach
$\Delta = \frac{R_{\max}}{vb^{1/v}}$	= complex parameter of surface roughness
f	= coefficient of sliding friction (dimensionless); oscillation frequency
f_{ml}	= molecular component of coefficient of friction
f_{mc}	= mechanical component of coefficient of friction
I	= linear wear rate
I_M	= wear rate in terms of mass
i_n	= specific linear wear
τ_0	= resistance to shear with normal pressure extrapolated to zero
β	= coefficient of strengthening of molecular bond (dimensionless)
U	= linear wear
U_M	= wear in terms of mass
U_V	= wear in terms of volume
h	= depth of penetration
V_s	= volume of intercontact space
h_m	= mean clearance
a_τ	= tangential contact displacements
γ	= time wear rate
θ_s	= mean surface temperature
θ	= bulk temperature
η	= dynamic viscosity
ν	= kinematic viscosity
N_c	= number of loading cycles

THE CONTACT OF SOLIDS

The interaction of solids occurring in the frictional area can only be understood properly if the surface geometry of the mating parts is taken into account. The theory of contact of rough surfaces is based on the classical solutions of problems for the elastic and plastic types of contact and on the results of research into surface quality.

The solutions to the contact problems are obtained for solids having true geometric form and ideal physico-mechanical properties, whereas actual surface irregularities in machine parts are much varied in form and their properties are far from ideal. For this reason, the characteristics of a contact are calculated with the use of statistical methods that make it possible to describe the deformation of a certain averaged surface peak and account for the laws of distribution of surface peaks and waves. Such an approach gives formulas sufficiently accurate for engineering calculations.

1.1. CONTACT OF IDEALLY SMOOTH SURFACES

Depending on the type of stress conditions in the contact area, the contact of two solids can be either elastic or plastic.

The theory of contact deformations in elastic solids considers two problems—one where the initial contact is made at a point and the other where it is made along a line. The problems are solved on the following assumptions: (1) the contacting bodies are smooth and homogeneous; (2) only elastic deformations take place in the contact area; (3) the contact forces are normal to the joint surface; and (4) the contact area is small compared with the area of the contacting

surfaces. Friction arising in the contact area at the time the load is applied is neglected*. Hertz has shown that the contact area is generally an ellipse which in extreme cases can be transformed into a circle or a strip limited by parallel lines. The first extreme case corresponds to the contact of two spherical bodies or two identical cylinders with mutually perpendicular axes. The second case occurs where the contact is made by two cylinders with parallel axes.

Data on the distribution of pressure over the contact area for bodies of various shapes are listed in Table 1.1.

Table 1.1

Distribution of pressure over elastic-contact area of two curvilinear bodies

Initial contact and shape of touching bodies	Law of pressure distribution	Sketch
Point contact; surfaces of different curvatures	$p(x, y) = p_{\max} \sqrt{1 - \left(\frac{x}{a}\right)^2 - \left(\frac{y}{b}\right)^2}$ <p>contact area is an ellipse with half-axes a and b</p>	
Point contact; spheres, or cylinders of identical radii with crossed (perpendicular) axes	$p(x, y) = p_{\max} \sqrt{1 - \left(\frac{p_{xy}}{\rho}\right)^2}$ <p>contact area is a circle</p>	
Line contact; cylinders with parallel axes	$p(x, y) = p_{\max} \sqrt{\left(\frac{y}{c}\right)^2}$	

Designations: $p(x, y)$ = pressure at a point with coordinates x and y ; p_{\max} = maximum pressure; ρ = radius of contact-area circle.

The relationship between the mean and maximum stresses for elliptical and circular contact areas is

$$p_m = \frac{2}{3} p_{\max}$$

* Solutions in a more general form are known; in engineering calculations, however, contact friction commonly is not taken into account.

Table 1.2

Calculation formulas for contact area, maximum pressure, and approach in elastic contact of curvilinear bodies

Type of contact	Calculation formulas																												
1. Two spheres. Contact area is a circle	$\rho = 0.909 \sqrt[3]{\Theta_{\Sigma} r N}$ $p_{\max} = 0.578 \sqrt[3]{\frac{N}{\Theta_{\Sigma}^2 r^2}}$ $h = 0.825 \sqrt[3]{\frac{\Theta_{\Sigma} N^2}{r}}$																												
2. Sphere with plane. Contact area is a circle	In formulas relating to Type 1 contact, substitute r_{sp} for r (r_{sp} = radius of sphere)																												
3. Convex sphere with concave sphere ($r_1 \gg r_2$). Contact area is a circle	In formulas relating to Type 1 contact, insert $r = \frac{r_1 r_2}{r_1 - r_2}$																												
4. Two cylinders with mutually perpendicular axes. Contact area is an ellipse with half-axes a_e and b_e	$a_e = \beta_1 \sqrt{r \Theta_{\Sigma} N}, \quad b_e = \beta_2 a_e$ <p>contact area $A = \pi a_e b_e = \pi \beta_2 a_e^2$</p> $p_{\max} = \frac{1.5 N}{A}, \quad h = \beta_3 \sqrt[3]{\frac{N}{\Theta_{\Sigma}^2 r}}$ <table><tr><td>r_1/r_2</td><td>1</td><td>1.5</td><td>2</td><td>3</td><td>6</td><td>10</td></tr><tr><td>β_1</td><td>1.144</td><td>1.317</td><td>1.459</td><td>1.701</td><td>2.226</td><td>2.740</td></tr><tr><td>β_2</td><td>1.000</td><td>0.765</td><td>0.632</td><td>0.482</td><td>0.308</td><td>0.221</td></tr><tr><td>β_3</td><td>1.651</td><td>1.635</td><td>1.607</td><td>1.548</td><td>1.405</td><td>1.280</td></tr></table>	r_1/r_2	1	1.5	2	3	6	10	β_1	1.144	1.317	1.459	1.701	2.226	2.740	β_2	1.000	0.765	0.632	0.482	0.308	0.221	β_3	1.651	1.635	1.607	1.548	1.405	1.280
r_1/r_2	1	1.5	2	3	6	10																							
β_1	1.144	1.317	1.459	1.701	2.226	2.740																							
β_2	1.000	0.765	0.632	0.482	0.308	0.221																							
β_3	1.651	1.635	1.607	1.548	1.405	1.280																							
5. Two cylinders with mutually perpendicular axes and equal radii. Contact area is a circle	$\rho = 0.909 \sqrt[3]{\Theta_{\Sigma} r N}, \quad p_{\max} = 0.578 \sqrt[3]{\frac{N}{\Theta_{\Sigma} r}}$ $h = 0.825 \sqrt[3]{\frac{\Theta_{\Sigma}^2 N^2}{r}}$																												
6. Two cylinders with parallel axes (both surfaces are convex). Contact area is a rectangle with a width of 2ρ	$\rho = 1.128 \sqrt{\Theta_{\Sigma} r N l}, \quad p_{\max} = 0.564 \sqrt{\frac{N l}{\Theta_{\Sigma} r}}$ $h = \frac{2 N l}{\pi} \left[\Theta_1 \left(\ln \frac{2 r_1}{\rho} + 0.407 \right) + \Theta_2 \left(\ln \frac{2 r_2}{\rho} + 0.407 \right) \right]$																												
7. Cylinder with a plane. Contact area is a rectangle with a width of 2ρ	In formulas relating to Type 6 contact, substitute r_c for r (r_c = radius of cylinder)																												

Table 1.2 (cont.)

Type of contact	Calculation formulas																																								
8. Cylindrical surface with parallel concave cylindrical surface ($r_1 \gg \gg r_2$). Contact area is a rectangle with a width of 2ρ	In formulas relating to Type 6 contact, take $r = \frac{r_1 r_2}{r_1 - r_2}$																																								
9. Two curvilinear bodies touching at a single point before deformation. Contact area is generally an ellipse with half-axes a_e and b_e	$a_e = n_a \sqrt[3]{\frac{3}{2} \frac{\Theta_\Sigma N}{K_\Sigma}}, \quad b_e = n_b \sqrt[3]{\frac{3}{2} \frac{\Theta_\Sigma N}{K_\Sigma}}$ $p_{\max} = \frac{1}{\pi n_a n_b} \sqrt[3]{\frac{3}{2} \left(\frac{K_\Sigma}{\Theta_\Sigma} \right)^2 N}$ $h = \frac{n_\delta}{2} \sqrt[3]{\frac{9}{4} \Theta_\Sigma^2 K_\Sigma N^2}$ $K_\Sigma = \frac{1}{r_{11}} + \frac{1}{r_{12}} + \frac{1}{r_{21}} + \frac{1}{r_{22}}$																																								
	<table><tr><th>b_e/a_e</th><th>l^2</th><th>n_a</th><th>n_b</th><th>n_δ</th></tr><tr><td>1</td><td>0.00</td><td>1.00</td><td>1.00</td><td>1.00</td></tr><tr><td>0.8</td><td>0.36</td><td>1.12</td><td>0.91</td><td>0.99</td></tr><tr><td>0.6</td><td>0.64</td><td>1.27</td><td>0.81</td><td>0.97</td></tr><tr><td>0.4</td><td>0.84</td><td>1.66</td><td>0.66</td><td>0.90</td></tr><tr><td>0.2</td><td>0.96</td><td>2.27</td><td>0.50</td><td>0.73</td></tr><tr><td>0.1</td><td>0.99</td><td>4.01</td><td>0.40</td><td>0.59</td></tr><tr><td>0.05</td><td>0.997</td><td>5.98</td><td>0.33</td><td>0.46</td></tr></table>	b_e/a_e	l^2	n_a	n_b	n_δ	1	0.00	1.00	1.00	1.00	0.8	0.36	1.12	0.91	0.99	0.6	0.64	1.27	0.81	0.97	0.4	0.84	1.66	0.66	0.90	0.2	0.96	2.27	0.50	0.73	0.1	0.99	4.01	0.40	0.59	0.05	0.997	5.98	0.33	0.46
b_e/a_e	l^2	n_a	n_b	n_δ																																					
1	0.00	1.00	1.00	1.00																																					
0.8	0.36	1.12	0.91	0.99																																					
0.6	0.64	1.27	0.81	0.97																																					
0.4	0.84	1.66	0.66	0.90																																					
0.2	0.96	2.27	0.50	0.73																																					
0.1	0.99	4.01	0.40	0.59																																					
0.05	0.997	5.98	0.33	0.46																																					

Designations: N_l = normal load per unit length; p_{\max} = maximum pressure on the contact area; ρ = radius or half the width of the contact area; $\Theta_\Sigma = \Theta_1 + \Theta_2$ = elastic constant for two deformed bodies; $r = \frac{r_1 r_2}{r_1 + r_2}, \frac{1}{r_{11}}, \frac{1}{r_{22}}, \frac{1}{r_{12}}, \frac{1}{r_{21}}$ = main curvatures at the contact point; a_e and b_e = half-axes of the contact ellipse; l = eccentricity.

Table 1.2 lists formulas for calculating the contact area, approach, and maximum pressure in various instances of elastic interaction between smooth surfaces.

With plastic deformation, the mean contact pressure is given by

$$p_m = c\sigma_y$$

where c = factor allowing for shape of surface irregularities and strain hardening of part material, σ_y = yield limit.

For plastic contact of a sphere, $c \approx 3$ [7] (for strain-hardened material). For practical purposes, the mean contact pressure may be considered equal to hardness.

Strain hardness can be estimated by the Mayer formula

$$N = gd^n$$

where d = diameter of impression; g and n = factors allowing for properties of material, which are reduced in strain hardening.

1.2. SURFACE QUALITY OF MACHINE PARTS

1.2.1. Physico-Mechanical Properties of Surface Layers

The properties of the surface layers of a machine part substantially differ from the bulk properties of the material it is made from [4]. The force field created by the atoms of the outer layer has a high adsorption capacity; as a result, the surface is normally coated with adsorbed layers of air, water and various organic substances. The adsorbed surface-active substances have the effect of weakening the interaction between the atoms disposed at the surface. Penetrating into microcracks, surface-active substances build up a pressure making for further development of the cracks inside the solid and weaken the strength of the outer layer (the Rebinder effect).

A metal surface is usually coated with oxide films whose formation is particularly intensive at elevated temperatures. The properties of the surface layer of a material depend significantly on the method of its machining. Where the material is machined with a single-point cutting tool, a plastic deformation zone, in which the grains of the material are crushed, forms in front of the tool face. The layer of altered structure extends inside to a depth of tens of micrometers; after rough machining, its depth can reach hundreds of micrometers. Similar phenomena also take place in grinding. The application of fine-grained abrasives at low grinding speeds minimizes the roughness of the ground surface and the thickness of the deformed layer.

Processes attending friction also strongly affect the properties of surface layers. Because the peaks of asperities on the mating surfaces mutually penetrate as the surfaces move tangentially relative to each other, plastic-elastic re-deformation occurs in the surface layers. The depth of the deformed layer depends on the sliding speed; namely, it decreases with increasing speed. Repeated elastic deformations of the surface give rise to fatigue phenomena. Plastic and elastic deformations in the surface layer not only lead to changes in its properties, but also produce a new microprofile typical of the

given frictional conditions. High temperatures attending friction result in the annealing and softening of the surface layer, smoothing of microirregularities, structural changes of the material, and the development of diffusion processes. The temperature gradient through the depth of the material also has significant influence on the properties of the frictional surface: it produces a gradient of mechanical properties. The changed structure of the surface layer substantially alters its mechanical properties. These properties can be evaluated by measuring the microhardness of the surface layer. The surface layer of metals normally shows a high hardness which is due to strain hardening. This hardened layer can be detected by X-ray diffraction analysis.

1.2.2. Characteristics of Surface Geometry

Surface irregularities in machine parts are classified into form errors, waviness, and roughness. *Form errors* are separate, irregular deviations of the surface from its true form (convexity, concavity, taper, etc.). *Waviness* is a pattern of periodically recurring peaks and valleys of the same order of magnitude, which are spaced apart

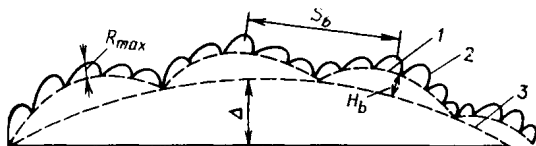


Fig. 1.1. Diagram of surface geometry of a solid
1—waviness; 2—roughness; 3—form errors

at a distance (wave spacing S_b) that substantially exceeds their height H_b ($S_b/H_b > 40$).

By surface *roughness* is meant a multitude of irregularities with a relatively short spacing (2 to 800 μm) and height (0.03 to 400 μm).

Form deviations, waviness and roughness are shown schematically in Fig. 1.1. Surface-roughness parameters are given in Table 1.3. They are determined by analyzing profile graphs that represent a surface profile on an enlarged scale (Fig. 1.2).

The *sampling length* l (Fig. 1.3) is the length of the reference line used for isolating surface irregularities that characterize surface roughness and for determining the numerical values of the latter. The *mean line* (M_1M_2) is a reference line having the form of the nominal profile and drawn so that within the sampling length the root-mean-square deviation of the profile from this line is a minimum. The *line of profile peaks* (A_1A_2) is a line equidistant from the mean line and passing through the highest peak of the profile within the sampling length; the *line of profile valleys* (B_1B_2) is a line equidistant

from the mean line passing through the lowest point of the profile within the sampling length.

The sampling length is selected in accordance with GOST* 2789-73, depending on the surface irregularity height and the roughness class.

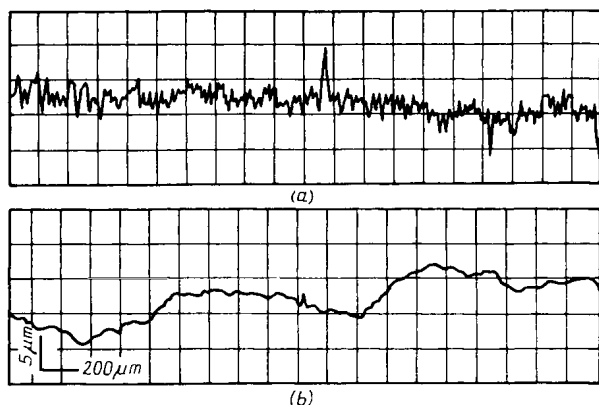


Fig. 1.2. Profile graphs of a steel surface (vertical magnification is 40 times the horizontal one)

(a) transverse trace; (b) longitudinal trace

It should be noted that with a larger sampling length the roughness parameters can be determined more accurately; the effect of waviness

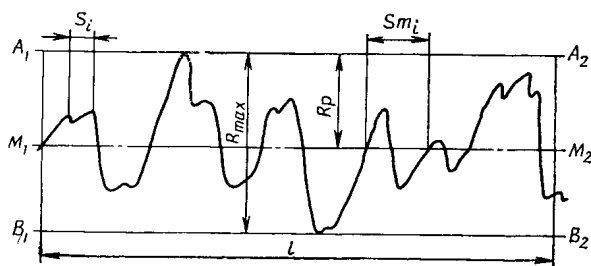


Fig. 1.3. Surface roughness parameters

on measurement results, however, becomes more pronounced.

In calculations for contact interaction, one has to use a number of additional surface characteristics along with the standard characteristics. The additional characteristics are listed in Table 1.4. The *bearing-area curve* of the profile characterizes the distribution of the

* GOST is a transliterated acronym meaning a Basic State Standard of the USSR.— *Translation editor.*

Table 1.3

Classes of surface roughness and values of sampling length
(according to GOST 2789-73)

Surface roughness classes	Division	Roughness parameters		Sampling length l , mm	Surface roughness classes	Division	Roughness parameters		Sampling length l , mm
		Ra , μm	Rz , μm				Ra , μm	Rz , μm	
1	—	—	320-160	8.0	10	a	0.160-0.125	—	0.25
2	—	—	160-80			b	0.125-0.100		
3	—	—	80-40			c	0.100-0.080		
4	—	—	40-20	2.5	11	a	0.080-0.063	—	
5	—	—	20-10			b	0.063-0.050		
						c	0.050-0.040		
6	a b c	2.5-2.0 2.0-1.6 1.6-1.25	—	0.8	12	a	0.040-0.032	—	
			b			0.032-0.025			
			c			0.025-0.020			
7	a b c	1.25-1.0 1.0-0.8 0.8-0.63	—		13	a	—	0.100-0.080	0.08
			b			0.080-0.063			
			c			0.063-0.050			
8	a b c	0.63-0.50 0.50-0.40 0.4-0.32	—		14	a	—	0.05-0.04	
			b			0.032-0.04			
			c			0.032-0.025			
9	a b c	0.32-0.25 0.25-0.20 0.20-0.16	—	0.25					

material over the height of the rough layer (Fig. 1.4). To plot the curve, the profile graph is broken into a number of horizontal levels

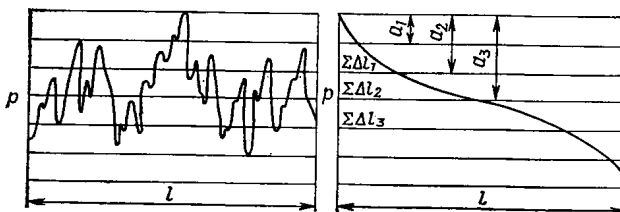


Fig. 1.4. Plotting the bearing-area curve

parallel to the mean line, and then the sections limiting the widths Δl_i of the peaks at a given level p are added together.

The bearing-area curve is plotted predominantly in terms of relative units. In this case, the ratio of the sum of the peak sections at a given level to the length of the profile graph is plotted on the abscissa, and the ratio of the approach a to R_{\max} (or to R_p) is plotted

Table 1.4

Additional characteristics of surface roughness and waviness used for friction and wear calculations

Parameter	Definition
<i>Roughness</i>	
Height of the maximum peak of the profile (height of crushing) R_p	Distance between the line of profile peaks and the mean line
Mean curvature radius r of profile peaks	Mean value of curvature of profile peaks, obtained for five maximum peaks within the sampling length
Mean angle of inclination of profile irregularities φ	Mean angle of inclination of profile irregularity flanks to the mean line within the sampling length
Parameters v and b of the bearing-area curve	Parameters of an exponential approximation of the initial portion of the bearing-area curve (from the origin to the mean line) plotted in terms of relative units
<i>Waviness</i>	
Maximum height of waves H_b	Distance between the line of wave crests and the line of wave valleys within the sampling length l_b of the waveform graph
Mean wavelength S_b	Mean distance between wave crests within the sampling length l_b ; $l_b \geq 5S_b$
Mean curvature radius r_b of wave crests	Mean value of the wave curvature radius within the sampling length

on the ordinate. Then the initial portion of the bearing-area curve can be represented in the form [4, 9]

$$tp = \frac{\Sigma \Delta l_p}{l} = \frac{A_p}{A_c} = b \left(\frac{a}{R_{\max}} \right)^v = t_m \left(\frac{a}{R_p} \right)^v \quad (1.1)$$

where $\Sigma \Delta l_p$ = reference length of the profile at the level p ; A_p = area of the peak sections at the level p ; t_m = relative reference length of the profile at the level of the mean line.

Waviness parameters are not yet standardized, although waviness has a marked effect on the properties of contact between surfaces. The most important characteristics of waviness, required for estimating the properties of a contact (see Table 1.4), can be obtained by analyzing waveform graphs. The graphs to be analyzed should contain not less than five waves.

The properties of a contact may be greatly influenced by surface form deviations resulting in that the surfaces touch at separate locations only. Form deviations are usually characterized by the maximum error Δ . These deviations alter the law of distribution of the

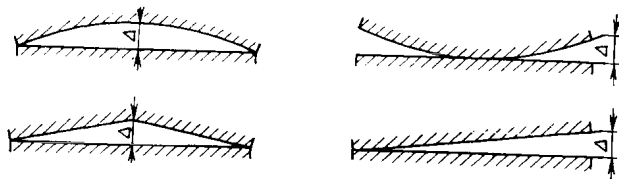


Fig. 1.5. Types of surface form deviations

wave peak height and the sequence in which the waves come into contact as the load is increased. Some types of form deviations are illustrated in Fig. 1.5 [11, 14].

1.2.3. Methods for Determining Characteristics of Surface Geometry

In order to find the parameters of surface geometry, several (not less than five) sections most characteristic of the surface being tested are chosen and their profile graphs are recorded. The length of the profile section to be investigated should not be smaller than the sampling length.

The arithmetic mean deviation of the profile, Ra , is read directly from the scale of a profilometer/surface-analyzer (for instance, Model 201 made by the Moscow "Kalibr Works").

For determining R_{max} and Rp , at least five sections of the profile graphs are selected and the mean line is drawn for each section. The position of the mean line is found most easily by the method of averages as follows. A horizontal line parallel to the given profile section is drawn some distance below the deepest valley, and the ordinates y_1, y_2, \dots, y_n of the profile are measured from this horizontal every 2 mm. The values thus obtained are divided into two equal groups (y_1 through $y_{n/2}$ and $y_{n/2}$ through y_n) for the left- and right-hand portions of the profile graph. The mean line is drawn through two points with coordinates x', y' , and x'', y'' :

$$x' = \frac{x_1 + x_{n/2}}{2}, \quad y' = \frac{\sum_{i=1}^{n/2} y_i}{n/2}$$

$$x'' = \frac{x_{n/2} + x_n}{2}, \quad y'' = \frac{\sum_{i=n/2}^n y_i}{n/2}$$

The lines of profile peaks and valleys are then drawn within the sampling length. The distance from the line of peaks to the line of valleys will be equal to $R_{\max i}$, and that from the line of peaks to the mean line, to Rp_i . For calculations, the mean value for the five different surface profile sections is taken:

$$R_{\max} = \frac{1}{5} \sum_1^5 R_{\max i}, \quad Rp = \frac{1}{5} \sum_1^5 Rp_i$$

To calculate the parameters of the bearing-area curve, the relative reference length t_{m_i} of the profile along the mean line is first determined for the five profile graph sections whose length is equal to the sampling length, and then the mean value of the five values thus obtained is found:

$$t_m = \frac{1}{5} \sum_1^5 t_{m_i}$$

where $t_{m_i} = \frac{1}{l} \sum_1^n \Delta l_{m_i}$, Δl_{m_i} = length of peak section at the level of the mean line, and l = sampling length.

The parameters v and b of the bearing-area curve are calculated by the formulas [5]

$$v = 2t_m \frac{Rp}{Ra} - 1, \quad b = t_m \left(\frac{R_{\max}}{Rp} \right)^v \quad (1.2)$$

Formula (1.1) with the parameters found from the relationships (1.2) describes the initial section of the bearing-area curve up to the mean line.

Example 1. For five profile graphs taken from different sections of a test surface the following values are obtained: $t_{m_i} = 0.5, 0.6, 0.51, 0.55$, and 0.5 ; $Rp_i = 3.2, 3.4, 3.5, 3.0$, and $3.3 \mu\text{m}$, $Ra_i = 1.4, 1.31, 1.30, 1.35$, and $1.35 \mu\text{m}$; $R_{\max i} = 6.5, 6.9, 7.1, 6.1$, and $6.3 \mu\text{m}$.

$$\text{Then } t_m = \frac{0.5 + 0.6 + 0.51 + 0.55 + 0.5}{5} = 0.53 \mu\text{m}$$

$$Rp = \frac{3.2 + 3.4 + 3.5 + 3.0 + 3.3}{5} = 3.28 \mu\text{m}$$

$$R_{\max} = \frac{6.5 + 6.9 + 7.1 + 6.1 + 6.3}{5} = 6.58 \mu\text{m}$$

$$Ra = \frac{1.4 + 1.31 + 1.30 + 1.35 + 1.35}{5} = 1.34 \mu\text{m}$$

whence

$$v = 2 \times 0.53 \frac{3.28}{1.34} - 1 = 1.58$$

$$b = 0.53 \left(\frac{6.58}{3.28} \right)^{1.58} = 1.6$$

For the contact of two rough surfaces, the parameters v and b are expressed by

$$v = v_1 + v_2, \quad b = \frac{K_2 b_1 b_2 (R_{\max_1} + R_{\max_2})^{v_1 + v_2}}{R_{\max_1}^{v_1} R_{\max_2}^{v_2}} \quad (1.3)$$

where $K_2 = \frac{\Gamma(v_1 + 1) \Gamma(v_2 + 1)}{\Gamma(v_1 + v_2 + 1)}$

The curvature radii of surface peaks are determined from profile graphs recorded by tracing the surface in transverse and longitudinal directions. For calculation, at least five highest peaks are taken and

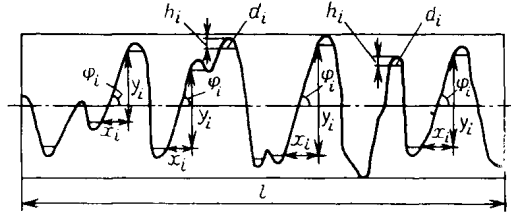


Fig. 1.6. Diagram for calculating crest curvature radii and angles of inclination of surface irregularities

the section width d_i is found at a distance h_i from the crest, equal to $0.3 Ra$ or $0.06 R_{\max}$ (Fig. 1.6). The radius of each peak will then be given by

$$r_{pi} = \frac{\gamma_v}{\gamma_h^2} \frac{d_i^2}{8h_i} \quad (1.4)$$

where γ_v and γ_h = vertical and horizontal magnifications.

Formula (1.4) is used for calculating both the transverse radius r_{tr} from the transverse (across-the-lay) profile graph and the longitudinal radius r_{ln} from the longitudinal (along-the-lay) profile graph.

The mean radius will be

$$r_p = \frac{l}{k} \sum_{i=1}^k r_{pi} \quad (1.5)$$

The length of the longitudinal profile graph should be taken greater than the sampling length so as to include at least five peaks. Where the surface roughness is not sufficiently uniform, a number of profile graphs taken from different areas of the surface are analyzed.

The effective radius r used for calculation is determined as the geometric mean of the longitudinal and transverse radii:

$$r = \sqrt{r_{tr} r_{ln}} \quad (1.6)$$

where r_{tr} and r_{ln} = mean values of the curvature radii for the transverse and longitudinal profile graphs, respectively.

Where the radius of a whole peak (modelled by a hemispherical segment) rather than the curvature radius needs to be determined, the width of the peak sections is taken along the mean line.

Typical values for the curvature radii of peaks on surfaces processed by various machining methods are given in Table 1.5.

Table 1.5

Profile peak curvature radii for surfaces machined by various methods

Machining method	Surface roughness class	Radius (μm)	
		transverse r_{tr}	longitudinal r_{ln}
Grinding	6-7	4-10	100-300
Turning	8-9	10-40	100-300
	5-6	20-40	400-500
	7-8	40-120	—
Milling	4-5	30-60	400-500
	6-7	60-80	—
Polishing	8-9	300-700	300-700
	10	500-1000	500-1000
Lapping	10-12	20-70	—

It has been proposed recently [8] to assess surface roughness by a complex characteristic $\Delta = R_{\max}/rb^{1/\nu}$, allowing for the acuteness of peaks and their height distribution. Surface roughness parameters for the main machining methods and run-in surfaces are given in Tables 1.6 through 1.9 (these tables are compiled by V. S. Komalov using the data obtained by E. V. Ryzhov).

Example 2. Calculate the curvature radius of peaks for an across-the-lay profile graph recorded with a horizontal magnification $\gamma_h = 400$ and a vertical magnification $\gamma_v = 1,000$. The maximum height of the profile, $R_{\max} = 42$ mm. The width of the profile section for seven highest peaks is found at a distance of $0.06 R_{\max} = 2.5$ mm from their crests: $d_{tri} = 6, 8, 5.5, 12, 7.5$, and 6.3 mm.

Then

$$\frac{1}{k} \sum d_{tri}^2 = \frac{6^2 + 8^2 + 5.5^2 + 6^2 + 12^2 + 7.5^2 + 6.3^2}{7} = 5.81 \text{ mm}^2$$

$$r_{tr} = \frac{\gamma_v \sum_1^h d_{tri}^2}{8\gamma_h^2 h k} = \frac{1,000 \times 5.8}{8 \times 400^2 \times 2.5} = 18 \text{ } \mu\text{m}$$

Table 1.6

Approximate values of roughness parameters for steel surfaces machined by different methods *

Machining method	Surface roughness class	R_{\max} , μm	r , μm	b	v	Δ
Cylindrical grinding	7	9.4	8	0.6	2.0	1.6×10^{-1}
	8	4.7	12	0.9	1.9	4.1×10^{-2}
	9	2.4	20	1.3	1.9	9.6×10^{-2}
	10	1.2	30	2.0	1.9	2.8×10^{-2}
Internal grinding	6	18	5	0.6	2.0	49.6×10^{-1}
	7	9.4	8	0.9	1.9	13.0×10^{-1}
	8	4.7	13	1.1	1.8	3.6×10^{-1}
	9	2.4	18	1.4	1.7	1.1×10^{-1}
Surface grinding	5	37	35	0.6	2.2	1.24×10^0
	6	18	100	0.9	1.9	2×10^{-1}
	7	9.4	180	1.0	1.8	6×10^{-2}
	8	4.7	370	1.6	1.8	1.3×10^{-2}
	9	2.4	550	2.3	1.6	2.64×10^{-3}
Polishing	8	4.7	230	2.0	1.7	1.4×10^{-2}
	9	2.4	450	2.5	1.6	3.0×10^{-3}
	10	1.2	670	3.5	1.5	7.8×10^{-4}
Turning	5	37	15	1.0	2.1	2.50×10^0
	6	18	20	1.4	1.9	7.9×10^{-1}
	7	9.4	35	1.8	1.8	1.9×10^{-1}
	8	4.7	55	2.0	1.6	6.3×10^{-2}
Face milling	5	37	420	0.4	2.2	1.4×10^{-1}
	6	18	900	0.5	1.6	3.0×10^{-2}
	7	8	1300	0.6	1.4	1×10^{-2}
Lapping of cylindrical surfaces	10	1.2	30	2.5	1.5	2.2×10^{-2}
	11	0.6	40	2.6	1.4	7.7×10^{-3}
	12	0.3	55	2.6	1.3	2.6×10^{-3}
	13	0.15	75	3.3	1.2	7.4×10^{-4}
Lapping of planes	10	1.2	300	2.4	1.6	2.34×10^{-3}
	11	0.6	500	3.0	1.4	3.5×10^{-4}
	12	0.3	1000	3.3	1.2	1.2×10^{-4}
	13	0.15	3000	4.5	1.1	1.35×10^{-5}
Honing	8	4.7	15	0.7	1.8	0.37×10^{-2}
	9	2.4	20	1.0	1.7	1.2×10^{-1}
	10	1.2	35	1.9	1.6	2.26×10^{-2}
	11	0.6	70	2.5	1.6	4.65×10^{-3}

* The table is taken by editor I. V. Kragelsky from [8, 14].

Table 1.7

Approximate values of roughness parameters for internal cylindrical surfaces finished by various methods (steel parts) *

Finishing method	Surface roughness class	R_{\max} , μm	r , μm	R_a , μm	b	v	Δ
Lapping	10	0.84	30	0.14	2.5	1.5	1.53×10^{-2}
		0.66	33	0.11	2.5	1.5	1.08×10^{-2}
		0.54	36	0.09	2.4	1.4	8.2×10^{-3}
	11	0.43	40	0.071	2.5	1.4	5.46×10^{-3}
		0.33	45	0.066	2.5	1.4	3.83×10^{-3}
		0.27	50	0.055	2.6	1.4	2.75×10^{-3}
	12	0.21	55	0.036	2.6	1.3	1.87×10^{-3}
		0.16	62	0.030	2.5	1.4	1.3×10^{-3}
		0.13	70	0.022	2.5	1.3	9.1×10^{-4}
	13	0.10	80	0.018	3.3	1.2	5.4×10^{-4}
		0.08	75	0.014	2.8	1.4	3.9×10^{-4}
		0.06	85	0.010	2.9	1.5	2.9×10^{-4}
Diamond burnishing	9	1.50	1300	0.25	0.9	1.0	1.15×10^{-3}
		1.32	1300	0.22	2.1	1.2	5.4×10^{-4}
		1.20	1230	0.20	0.9	1.2	1.0×10^{-4}
	10	0.84	2300	0.14	1.0	1.4	3.6×10^{-4}
		0.72	2200	0.12	1.0	1.3	3.3×10^{-4}
		0.60	2400	0.12	1.1	0.5	2.34×10^{-4}
	11	0.32	2400	0.066	1.6	1.5	1.15×10^{-4}
		0.24	2600	0.058	2.0	1.0	1.0×10^{-4}
		0.39	2800	0.040	2.0	1.2	6×10^{-5}
	12	0.22	3100	0.30	2.5	1.5	3.9×10^{-5}
		0.17	3150	0.029	2.0	1.2	2.9×10^{-5}
		0.21	3200	0.025	3.5	1.8	2.4×10^{-5}

* The table is taken by editor I. V. Kragelsky from [8, 14].

Table 1.8

Approximate values of roughness parameters for cast-iron surfaces machined by various methods *

Machining method	Surface roughness class	R_{\max} , μm	r , μm	b	v	Δ
Cylindrical grinding	6	11	50	0.70	1.9	2.72×10^{-1}
	7	7.2	85	1.20	1.9	6.5×10^{-2}
	8	3.5	150	1.25	1.8	2.0×10^{-2}
	9	1.8	190	1.55	1.7	7.5×10^{-3}

Table 1.8 (cont.)

Machining method	Surface roughness class	R_{\max} , μm	r , μm	b	v	Δ
Internal grinding	6	11	12	1.60	2.6	8.0×10^{-1}
	7	7.4	16	1.75	2.4	3.7×10^{-1}
	8	3.6	25	1.95	2.3	1.8×10^{-1}
	9	1.7	45	2.10	2.2	7.7×10^{-2}
Face milling	5	23	40	0.42	2.0	8.9×10^{-1}
	6	11	60	0.70	1.9	2.3×10^{-1}
	7	6.9	90	0.75	1.8	9.5×10^{-2}
Turning	4	48	25	1.10	1.9	1.85×10^{-1}
	5	21	37	1.20	1.8	5.4×10^{-1}
	6	12	60	1.45	1.7	1.54×10^{-1}
	7	7.4	130	1.50	1.6	4.4×10^{-2}
Plain milling	4	29	17	1.40	2.8	2.54×10^0
	5	23	20	1.60	2.6	9.6×10^{-1}
	6	11	25	1.70	2.4	3.7×10^{-1}
	7	7.2	50	2.10	2.1	1.07×10^{-1}
Boring	5	23	12	0.72	2.2	2.2×10^0
	6	11	13	1.00	2.2	8.85×10^{-1}
	7	6.9	15	1.15	2.1	4.3×10^{-1}
	8	3.8	20	1.75	2.0	1.41×10^{-1}
Lapping of planes	10	0.98	15	2.00	1.3	3.9×10^{-2}
	11	0.42	20	2.30	1.2	1.05×10^{-2}
	12	0.23	40	2.40	1.1	2.6×10^{-3}
	13	0.18	55	3.10	1.0	1.6×10^{-3}
Shaping	4	48	18	0.75	2.2	3.0×10^0
	5	22	25	0.90	2.0	9.3×10^{-1}
	6	11	100	1.20	1.9	1.05×10^{-1}
	7	6.9	150	1.6	1.9	3.5×10^{-2}

* The table is taken by editor I. V. Kragelsky from [8, 14].

Table 1.9

Approximate values of roughness parameters for various run-in surfaces [8]

Components examined	Surface roughness class	R_{\max} , μm	r , μm	b	v	Ra , μm	Δ
Steel surfaces at places of contact with rubber lip packings	9	0.72	180	3.1	3.0	0.13	2.7×10^{-10}
Plain bearings (journal from steel Grade 2X13)	9	0.84	58	1.8	2.0	0.15	1.1×10^{-2}
Cast-iron piston ring	11	0.15	85	1.8	2.3	0.03	1.4×10^{-3}
Adjustable jib in Model 1A63 lathe	11	0.15	100	3.0	1.8	0.03	1.1×10^{-3}
Plain bearing (bush from metal-ceramics containing MoS_2)	7	5.40	77	3.5	1.8	0.09	3.5×10^{-2}
Outer plate of friction clutch in Model 1A62 lathe	10	0.60	46	1.4	2.1	0.10	1.10×10^{-2}
Inner plate of friction clutch in Model 1A62 lathe	9	1.8	60	2.8	2.2	0.32	1.9×10^{-2}
Guideways (in steam hammer)	8	3.6	19	1.0	1.2	0.67	0.2×10^{-1}
Circular slot in cluster gear	7	7.3	35	1.6	1.4	1.27	1.5×10^{-1}
Dises and shoes in aircraft brake made from: retinax	7	4	30	4.0	2.4	0.70	74×10^{-2}
ΦМК-11	7	6.5	120	3.5	2.5	1.15	3.3×10^{-2}
МКБ-50	7	6	15	1.1	2.1	0.91	3.7×10^{-1}
ΨНМХ	8	4	76	1.0	2.1	0.65	5.3×10^{-2}
steel Grade 30XFCA	7	5	82	1.0	2.2	0.78	5.5×10^{-2}
Cylindrical liner	9	1.2	1000	—	1.0	0.04	1.2×10^{-3}
Piston ring	10-11	0.48	270	—	0.4	0.02	1.7×10^{-3}
Crankshaft (main and rod journals)	9	1.6	500	—	1.2	0.05	3.1×10^{-3}
Crankshaft bearing bushes	8-9	2.6	300	—	—	0.42	86×10^{-3}
Gudgeon pin	11	6.7	300	—	—	0.11	2.2×10^{-2}
Bearing bush in conrod small end	10	7.0	250	—	—	0.112	2.8×10^{-2}
Piston (pin-bore)	9	1.1	220	—	—	0.18	5.0×10^{-3}
Diesel injector	—	0.6	35	3.8	1.9	0.1	1.7×10^{-2}
Conrod bearing liner in Model Volga M-21 car	—	1.3	54	1.2	2.0	0.24	2.4×10^{-2}

Correspondingly, for a longitudinal profile graph of the surface, recorded at $\gamma_v = 4,000$ and $\gamma_h = 1,000$, $d_{lni} = 50, 58, 70, 93$, and 51.5 mm (at $0.06R_{\max} = 2.5$ mm), whence

$$\frac{1}{k} \sum_1^k d_{lni} = \frac{50^2 + 58^2 + 70^2 + 93^2 + 51.5^2}{5} = 4,413 \text{ mm}^2$$

$$r_{ln} = \frac{4,000}{(1,000)^2} \frac{4,413}{8 \times 2.5} = 0.883 \text{ mm} = 883 \text{ } \mu\text{m}$$

whence, the effective radius

$$r = \sqrt{18 \times 883} = 126 \text{ } \mu\text{m}$$

The angle φ at which the profile elements are inclined to the mean line is computed by the formula [15]

$$\tan \varphi_i = \frac{\gamma_h y_i}{\gamma_v x_i} \quad (1.7)$$

where x_i and y_i = legs of a triangle formed by (a) a perpendicular (y_i) to the mean line, drawn from the profile point spaced from the crest at a distance of $0.06 R_{\max}$ ($0.3 Ra$), (b) a line-segment (x_i) passing parallel to the mean line through the profile point spaced from the valley bottom at a distance of $0.06 R_{\max}$ ($0.3 Ra$) and up to the intersection with the perpendicular, and (c) the straight line connecting the above-mentioned points of the profile (see Fig. 1.6).

In calculations, use is made of the mean slope of the profile elements:

$$\tan \varphi = \frac{1}{n} \sum_1^n \tan \varphi_i \quad (1.8)$$

where n = number of angles measured.

Waviness parameters are found from waveform profile graphs. The method for obtaining the maximum height H_b of waves and the mean wavelength S_b is essentially the same as that for obtaining the roughness parameters R_{\max} and S_m and, therefore, needs no special explanation. It should only be noted that the length of a waveform graph must equal at least five S_b .

The transverse wave crest radius r_{b, tr_i} is found from a formula similar to formula (1.4), namely,

$$r_{b, tr_i} = \frac{\gamma_v d_{b_i}^2}{\gamma_h^2 8 h_{b_i}} \quad (1.9)$$

where d_{b_i} = length of a wave section by the mean line and h_{b_i} = distance between the crest of a wave and the mean line.

For calculations use is made of the mean value

$$r_{b, tr} = \frac{1}{k} \sum_1^k r_{b, tr_i}$$

determined for not less than five waves. The longitudinal wave crest radius is found in a similar way. The wave effective radius

value, used in calculations, is then obtained from the formula

$$r_b = \sqrt{r_{b, tr} r_{b, ln}} \quad (1.10)$$

The wave crest radius varies within the range from 10 to 1,000 mm; the waviness parameters for different machining methods are listed in Tables 1.10 and 1.11.

Table 1.10

Approximate values of transverse waviness parameters

Machining method and class of surface roughness	H_b , μm	S_b , μm	R_b , mm	$\frac{S_b}{H_b}$
<i>Steel parts</i>				
Internal grinding, 6th-9th	0.6-4.5	500-1400	10-80	100-1350
Cylindrical grinding, 7th-9th	0.75-3	250-500	10-25	165-400
Surface grinding, 5th-9th	1.2-13	750-1400	15-50	100-700
Boring, 5th-8th	2-3.5	1000-1500	15-55	300-750
Shaping, 4th-7th	2-6	400-1700	10-30	200-350
Honing, 8th-11th	0.1-0.8	150-700	2.5-40	200-7000
Reaming, 6th-9th	0.5-4	300-500	5-50	100-1000
Polishing, 8th-10th	0.3-1.5	150-350	10-25	200-500
Lapping of planes, 11th-12th	0.1-0.35	60-100	5-10	300-600
Lapping of cylindrical surfaces, 10th-13th	0.05-0.15	35-120	2.5-10	400-700
Scraping, 8th	3.5-6	5000-5500	600-1000	800-1600
<i>Cast-iron parts</i>				
Internal grinding, 6th-8th	1-3	450-1400	5-400	120-450
Cylindrical grinding, 6th-9th	0.5-7.5	550-1000	10-100	80-1850
Scraping, 8th	4.5-7	4000	450	600-900
Surface grinding, 6th-9th	0.8-4	500-900	20-80	200-800
Boring, 5th-9th	0.5-10	400-1000	5-50	40-850
Face milling, 7th	2.5	800	85	300
Turning, 7th	1	1000	50	1000

Table 1.11

Approximate values of longitudinal waviness parameters (from E. V. Ryzhov)

Machining method and class of surface roughness	H_b , μm	S_b , μm	R_b , mm	$\frac{S_b}{H_b}$
<i>Steel parts</i>				
Surface grinding, 5th-9th	1.2-12	2.4-3.5	30-350	280-2900
Shaping, 4th-7th	1-12	1-5	40-100	320-1000
Plain milling, 4th-6th	7.5-40	1.7-3.4	5-45	60-270
Broaching, 7th-9th	0.4-3	0.7-0.9	20-80	300-1750
Lapping of planes, 10th-11th	0.25-0.5	1-1.5	150-850	2000-6000
Scraping, 8th	3.5-6	6000-7500	1100-1700	1000-2000
<i>Cast-iron parts</i>				
Surface grinding, 6th-9th	1.3-9	1.8-2.3	40-200	200-1770
Plain milling, 4th-7th	7.5-30	1.6-2.5	10-60	83-267
Shaping, 4th	12	1.65	20	140
Scraping, 8th	4.5-7	7000	1200	1000-1600

1.3. CONTACT OF ROUGH SURFACES

1.3.1. Interaction of Surface Peaks

When two rough surfaces acted upon by a normal force come into contact, the opposite surface peaks to make the contact first are those for which the sum of the heights is the largest. As the load is increased, new pairs of opposite peaks having ever smaller sum of heights will be coming into contact. Once in contact, the surface peaks become deformed. This deformation at first is elastic. When the load exceeds a certain critical magnitude, however, the deformation will change into plastic or, rather, elastic-plastic, because the material under a permanently deformed peak will deflect elastically.

The increasing load gives rise to elastic deformation of surface waves on which surface asperities are located. This deformation leads to an increase in the contour area of contact and, as a result, to an increase in the number of peaks sustaining the load. Since the peaks differ in height, the deformation of various peaks on one and the same surface will be different at any instant of time. The pairs of the highest peaks in contact will be deformed most, whereas peaks whose height is smaller than average usually do not come into contact even at high loads.

When the touching surfaces differ in hardness, the peaks of the harder surface penetrate those of the softer surface. The peaks of the latter are crushed and their shape changes. In this case, the properties of the contact will be influenced by the surface form errors of the harder body and by the mechanical properties of the softer body.

The behaviour of contact at the first application and repeated applications of normal load is different. Plastic deformations predominate at the first loading of metal surfaces whose roughness is not very small ($Ra > 0.16$). The next loading cycle effected without altering the mutual position of the surfaces will give purely elastic contact deformation. If one surface is shifted with respect to the mating surface, however, other pairs of yet undeformed peaks will come into contact, and contact deformation will again be essentially plastic.

If the touching surfaces slide relative to each other, they first run in, changing their geometry; as a result, there develops roughness of a certain constant magnitude typical of given rubbing conditions. During the running-in process the physico-mechanical properties of surface layers also change because plastic deformations normally predominate in the contact. For this reason, the original surface geometry and original properties of the surfaces in contact will determine the characteristics of a contact during the initial

phase of running-in only. When the running-in process becomes stable, the surface geometry is reproduced over and over again, and the surface layer properties do not alter significantly, the plastic contact of the peaks of surface irregularities being predominant.

1.3.2. Real and Contour Areas of Contact

In interacting machine parts, the irregularities of the mating surfaces are out of contact over a considerable portion of the apparent contact area because of surface waviness and form errors. For

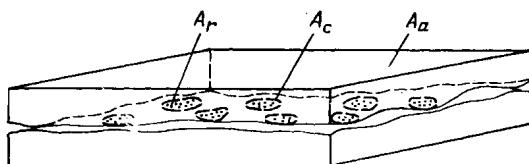


Fig. 1.7. Real area (A_r), contour area (A_c), and apparent area (A_a) of contact

this reason, the contact area hardly depends on the geometric area of the mating parts. It is exactly this fact that lies behind the conclusion by Coulomb that the frictional force is independent of the apparent contact area of the rubbing surfaces.

Waviness results in the contact spots grouping in separate areas at waveform crests (Fig. 1.7); a total of these areas forms the *contour area of contact*, A_c . This area may be defined as the area over which the surface waves make contact. This contact is obviously intermittent because of surface roughness. Since the distinction between roughness and waviness is conventional to a considerable degree, the boundaries of the contour area may be identified on the basis of the following definition. The contour area is to be taken to mean the area within which the contact of the irregularities occurs, the distance between the contact spots not exceeding the sampling length specified by the Standard for measuring a given magnitude of surface roughness.

Where one of the mating surfaces has waviness and the other is relatively flat, the contour area of contact will characterize the frictional area over which the surfaces wear as a result of interaction of their irregularities. In approximate measurements of the area of contact, for instance by the pigment transfer method, it is precisely the contour area that is measured.

The *real area of contact*, A_r , is to be taken to mean the area within which the irregularities forming surface roughness are in contact. The real area of contact approaches in magnitude the area where the atoms and molecules of substance interact, although these two areas are not identical in some cases (see specifically Ch. 2). Apart

from the irregularities, machined surfaces also have sub-irregularities whose study is now only beginning.

The real area of contact is usually small; it amounts to not over 0.01 to 0.1 percent of the apparent contact area. The actual contact spots, developed through the deformation of separate irregularities, are 3 to 50 μm in diameter.

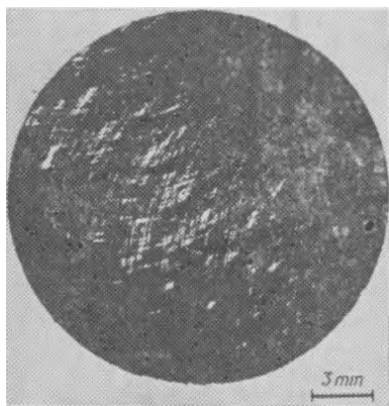


Fig. 1.8. Area of contact between ground steel parts

The normal load per unit area of real contact characterizes the *real pressure* p_r . This pressure is close to the material hardness for plastic contact and is substantially lower for elastic contact. The contour area of contact commonly comes to 5 to 15 percent of the apparent contact area. If the apparent contact area is not very large and waviness may be neglected, the contour area of contact may be considered to be equal to the apparent area. The normal load per unit contour area of contact characterizes the *contour pressure* p_c . The contour pressure is usually

several times the nominal one.

A photograph of the contact area of two ground steel specimens, on which the real and the contour areas of contact are clearly identifiable, is given in Fig. 1.8. The photograph was obtained by means of two thin graphite films.

With increasing nominal contact pressure, the contour pressure changes relatively little, and the real pressure remains practically invariable.

1.3.3. Calculation of the Real Area of Contact and Real Pressure

The real pressure can be calculated with the use of relationship derived on the basis of a rough surface model in the form of a set of spherical segments with a radius r [3, 10, 14]. Because r is determined as the geometric mean of the transverse and the longitudinal radii, such a model is also suitable for peaks of elongated ellipsoidal shape. The formula is derived under the assumption that for elastic contact the deformation of separate peaks is governed by the Hertz relationships, whereas for plastic contact the average contact stress is equal to the microhardness H (for a number of materials the microhardness may be considered to be approximately equal to the Brinell and Vickers hardness number, that is, $H \approx HB \approx HV$). Taking

into account these assumptions and also assuming that the material in a rough layer is distributed in accordance with formula (1.1), we shall obtain the following expression for the mean real contact pressure p_r :

$$p_r = (K_3 B)^{\frac{\nu}{\nu + \omega}} \left(\frac{Rp}{r}\right)^{\frac{\omega \nu}{\nu + \omega}} \left(\frac{N}{\alpha t_m A_c}\right)^{\frac{\omega}{\nu + \omega}} \tag{1.11}$$

where α = elastic deflection factor and ω and B = factors characterizing the deformation properties of the material; the values of these factors are given in Table 1.12.

Table 1.12

Values of ω , B , and α for various types of contact

Type of deformation	Surfaces	ω	B	α
Elastic	Metal surfaces with $Ra \leq 0.16 \text{ }\mu\text{m}$; polymers	0.5	$0.43/\Theta$	0.5
Plastic	Metal surfaces, $Ra > 0.16 \text{ }\mu\text{m}$	0	H	1

Tables 1.12 and 1.13 list the values of α not only for the elastic

Table 1.13

Coefficient α for elastic-plastic contact

HB	S_m/Rz					
	1	10	20	30	40	50
50	1.0	0.85	0.75	0.65	0.55	0.50
100	0.90	0.75	0.56	0.50	0.50	0.50
200	0.80	0.56	0.50	0.50	0.50	0.50
400	0.70	0.50	0.50	0.50	0.50	0.50

and plastic types of contact, but also for elastic-plastic contact, this enabling one to evaluate the deflection of peaks during plastic contact for different surfaces.

The coefficient K_3 is calculated by the formula

$$K_3 = \frac{\Gamma(\nu + 1) \Gamma(\omega + 2)}{\Gamma(\nu + \omega + 1)} \tag{1.12}$$

Some values of K_3 are given in Table 1.14.

Table 1.14

Values of coefficient K_3 for some values of ω and ν

ω	ν		
	2	3	4
0	1	1	1
0.2	0.94	0.85	0.81
0.4	0.83	0.73	0.69
0.5	0.80	0.69	0.61

Note: At $\nu = 1$, $K_3 = 1$ for all the values of ω .

Table 1.15

Approximate formulas for computing real pressure

Type of deformation	Surfaces and pressure	Calculation formula	Note
Elastic	Two rough surfaces	$p_r = 0.61 \left(\frac{Ra}{r\Theta^2} \right)^{0.43} p_c^{0.14}$	$r = \frac{r_1 r_2}{r_1 + r_2}$
	Rough surface with smooth surface	$p_r = 0.8 \left(\frac{Ra}{r\Theta^2} \right)^{0.4} p_c^{0.2}$	
Plastic	$p_c \leq \frac{1}{3} HB$	$p_r \approx H$	For the contact of surfaces from dissimilar materials, the smaller value of microhardness is taken for calculation
	$p_c > \frac{1}{3} HB$	$p_r \approx p_c - 0.4 \sqrt{\frac{H^3}{p_c}}$	
Repeated loading of plastically deformed surfaces	Two rough surfaces	$p_r \approx H \left(\frac{N}{N_0} \right)^{1/3}$	The formulas hold true if the surfaces were not displaced after the first loading
	Rough surface with smooth surface	$p_r \approx H \left(\frac{N}{N_0} \right)^{1/2}$	

Designation: N_0 = normal load at the first loading.

When plastic deformation occurs on the first application of load, the second and succeeding loading cycles effected without alteration of the mutual position of the surfaces will result in elastic deformation until the normal load N exceeds the initial load N_0 . In this

case

$$p_r = H \left(\frac{N}{N_0} \right)^{1/\nu} (N \leq N_0) \quad (1.13)$$

where H = microhardness.

Plastic contact at high pressures is a special case. If $p_c > \frac{1}{3} HB$, the contact pressure will exceed the hardness of the material because the interaction of the deformed peaks will result in hindered plastic deformation [2].

Using formulas (1.11) and (1.13) and substituting the appropriate values of parameters for surface geometry and material, the magni-

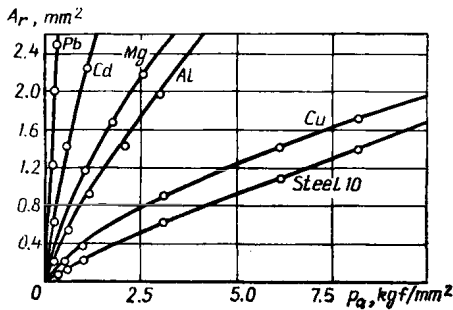


Fig. 1.9. Relationship between the real area of contact and contour pressure

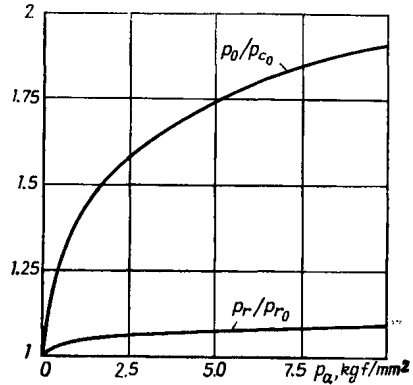


Fig. 1.10. Real and contour pressures as a function of nominal pressure

tude of the real pressure can be computed for various cases. To simplify calculations, approximate formulas for the real pressure (see Table 1.15) can be derived by substituting typical values of the parameters into formula (1.11).

The real contact area is computed by the formula

$$A_r = \frac{N}{p_r} = A_c \frac{p_c}{p_r}$$

The relationship between the real area of contact and the contour pressure for various metals at $40 \mu\text{m } R_z$ is shown on the graph in Fig. 1.9. Figure 1.10 is a graphical representation of the real and contour pressures as a function of the normal load.

Example 3. Calculate the real pressure for the contact of two identical steel surfaces.

$$\begin{aligned} Ra_1 &= Ra_2 = 0.08 \mu\text{m}; r_{tr} = 160 \mu\text{m}, r_{ln} = 800 \mu\text{m}, \\ E &= 2 \times 10^4 \text{ kgf/mm}^2, \mu = 0.3, p_c = 2 \text{ kgf/mm}^2 \end{aligned}$$

According to Table 1.12, the contact will be elastic, and the appropriate formula is chosen from Table 1.15. Then,

$$r = \sqrt{r_{tr} r_{ln}} = \sqrt{160 \times 800} = 358 \text{ } \mu\text{m}$$

$$Ra = Ra_1 + Ra_2 = 0.08 + 0.08 = 0.16 \text{ } \mu\text{m}$$

$$\Theta_{\Sigma} = \frac{1 - \mu_1^2}{E_1} + \frac{1 - \mu_2^2}{E_2} = \frac{2(1 - \mu^2)}{E} = 9 \times 10^{-5} \text{ mm}^2/\text{kgf}$$

Substituting the above values into the formula for p_r , we will find

$$p_r \approx \frac{0.61}{\Theta_{\Sigma}^{0.86}} \left(\frac{Ra}{r} \right)^{0.43} p_c^{0.14} \approx 73 \text{ kgf/mm}^2$$

1.3.4. Calculation of the Contour Area of Contact and Contour Pressure

For small-area surfaces on which waviness is not identified, the contour area of contact will be equal to the apparent area, that is, $A_c = A_a$. The contour area is calculated with the use of the model

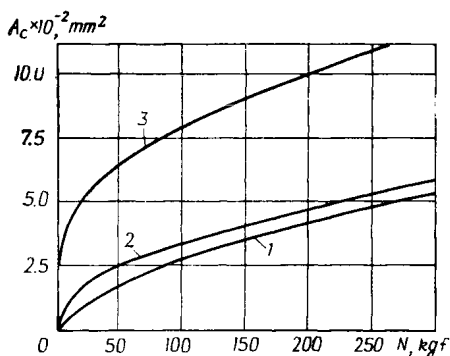


Fig. 1.11. Relationship between the contour area of contact and surface roughness 1—smooth surface; 2—4 = $\mu\text{m} R_{\text{max}}$; 3—40 $\text{mR}\mu_{\text{max}}$

of spherical- or elliptical-segment waveforms. If the waveform is close to a cylinder, it is, as a rule, not straight in the longitudinal direction; here the longitudinal curvature radius can be determined and, with its aid, the effective radius obtained, which characterizes the waveform for this case as well [formula (1.6)]. Where surface roughness is low ($R_{\text{max}} < 0.1 H_b$), the waveforms may be regarded as smooth and the relationships based on the Hertz formulas may be employed for calculations. With a coarse finish

($R_{\text{max}} \geq 0.1 H_b$), the asperities on the crests of the waves subject to deformation have the mutual effect of deflecting some contact area portions; this effect is due to the combined action of the contacting peaks located on these portions. The interaction of the asperities leads to a more uniform distribution of pressure and to substantial increase in the contact area as compared with that computed by the Hertz formulas [5].

Curves illustrating the difference in the contour contact areas between rough and smooth steel spheres are given in Fig. 1.11. As is clearly seen from the graph, the difference is particularly large at small loads and coarse finish. With wavy surfaces, the effect of roughness on the contour area is still greater, because in loading

Table 1.16

Formulas for computing the contour area of contact and contour pressure

A. $R_{\max} < 0.1 H_b$

Number of waves in contact, n_b	Conditions	Calculation formulas	Designations
≤ 3	Small apparent area of contact, A_a , commensurable with S_b^2 ; small loads	$A_c = 2.8 n_b^{1/3} (\Theta_\Sigma R_b N)^{2/3}$ $p_c = \frac{0.36}{(\Theta_\Sigma R_b)^{2/3}} \left(\frac{N}{n_b} \right)^{1/3}$	$R_b = \frac{R_{b1} R_{b2}}{R_{b1} + R_{b2}}$
> 3	Apparent area of contact A_a , substantially larger than S_b^2	$A_c = 2.2 A_a^{0.14} \left(\frac{R_b}{H_b} \right)^{0.43} (\Theta_\Sigma N)^{0.86}$ $p_c = 0.45 \left(\frac{H_b}{R_b \Theta^2} \right)^{0.43} p_a^{0.14}$	—

B. $R_{\max} \geq 0.1 H_b$

Number of waves in contact, n_b	Deformation of asperities or condition of surface	Calculation formulas
≤ 3	Plastic	$A_c \simeq \pi n_b \left[\left(\frac{3 \Theta_\Sigma R_b N}{4 n_b} \right)^{0.89} + 1.8 R_p R_b \left(\frac{N}{n_b H} \right)^{0.33} \right]^{0.75}$
	Elastic	$A_c \simeq \pi n_b \left[\left(\frac{3 \Theta_\Sigma R_b N}{4 n_b} \right)^{0.86} + 2.6 R_p R_b \left(\frac{r}{R_p} \right)^{0.14} \left(\frac{\Theta_\Sigma N}{n_b} \right)^{0.28} \right]^{0.78}$
> 3	Wavy surface with a plane	$v_b = 2$ $K_w = 1.8$ $A_c = A_a K_b K_w \left[\left(\frac{2 R_b}{H_b} \right)^{1/2} \Theta_\Sigma p_a \right]^{\frac{v_b}{v_b + \delta}}$
	Both surfaces are wavy	$v_b = 3$ $K_w = 2.4$ $p_c = \frac{1}{K_w K_b} \left(\frac{H_b}{2 R_b \Theta^2} \right)^{\frac{v_b}{2(v_b + \delta)}} p_a^{\frac{\delta}{v_b + \delta}}$

Note: To a first approximation, $R_p \approx \frac{1}{2} R_{\max}$.

such a surface, there is always a number of waves that have just come into contact and, hence, taking a small load. Formulas for calculating the contour area of contact and the contour pressure are given in Tables 1.16 and 1.17.

Table 1.17

Values of coefficients in the formulas of Table 1.16

Type of deformation of asperities	$\frac{1}{\Theta_{\Sigma} H}$	Coefficient	R_{\max}/H_b					
			0.1	0.2	0.4	0.8	1.6	3.2
Plastic	50	K_{b1}	1.05	1.15	1.20	1.35	1.55	2.1
		δ_1	0.60	0.70	0.85	1.15	1.50	2.3
		K_{b2}	0.95	0.9	0.85	0.85	1.10	1.5
		δ_2	0.7	1.05	1.45	2.15	3.15	3.9
	100	K_{b1}	1.10	1.17	1.28	1.45	1.75	2.6
		δ_1	0.65	0.8	1.0	1.3	1.65	2.0
		K_{b2}	0.95	0.88	0.85	0.9	1.2	2.1
		δ_2	0.75	1.10	1.60	2.4	3.4	4.0
	200	K_{b1}	1.13	1.20	1.35	1.55	2.1	3.3
		δ_1	0.70	0.85	1.10	1.50	2.35	2.0
		K_{b2}	0.90	0.85	0.85	0.93	1.35	2.5
		δ_2	0.80	1.2	1.7	2.6	3.6	4.0
Elastic	—	K_{b1}	1.05	1.06	1.14	1.25	1.5	2.1
		δ_1	0.65	0.80	1.05	1.4	1.95	2.4
		K_{b2}	0.88	0.85	0.80	0.85	1.1	1.8
		δ_2	0.75	1.1	1.7	2.6	2.6	4.5

Note. Index 1 relates to two rough surfaces, and 2 to a rough surface in contact with a smooth surface.

In these calculations, distinction is made between the following cases: (a) small and large height of surface peaks with respect to the height of waves; (b) elastic and plastic deformation of irregularities (see Table 1.12); (c) small number of waves (1 to 3), which does not change with the increase in the load, and a large number of waves which progressively come into contact as the load rises. It should be noted that even with a large number of waves, but at a small load, from one to three waves only can be in contact; and (d) both mating surfaces have waviness, or one is wavy, whereas the other can be regarded as flat.

When calculating the contour area of contact, it should be borne in mind that since the real area of contact depends but little on the contour area, determining the contour area approximately is suffi-

cient for solving the problems of friction and wear. Indeed, a 100-per-cent error in finding the contour area will give only an error of about 12 percent in finding the real area of contact.

If the calculation by the formulas from Table 1.16 yields $A_c > A_a$, it means that for the surfaces under consideration the formula does not hold true at a given load, and here A_c should be taken equal to A_a .

Example 4. Calculate the contour area of contact of two steel surfaces: $R_{a1} = R_{a2} = 1.6 \mu\text{m}$, $H_{b1} = 10 \mu\text{m}$; $H_{b2} = 20 \mu\text{m}$, $R_{b1} = 100 \text{ mm}$, $R_{b2} = 150 \text{ mm}$, $E_1 = E_2 = 2 \times 10^4 \text{ kgf/mm}^2$, $A_a = 2500 \text{ mm}^2$, $\mu_1 = \mu_2 = 0.3$, $H_1 = H_2 = 100 \text{ kgf/mm}^2$; $P_a = 1 \text{ kgf/mm}^2$.

The calculation is made according to Table 1.16. In the present case

$$\nu_b = 3, \quad K_b = 2.38, \quad R_b = \frac{R_{b1}R_{b2}}{R_{b1} + R_{b2}} = 60,$$

$$\Theta_\Sigma = 9 \times 10^{-5} \text{ mm}^2/\text{kgf}$$

$\frac{1}{\Theta H} = 111$, $R_{\max}/H_{b1} \approx 5R_{a1}/H_b = 0.8$ (the larger value is taken). From Table 1.15 $K_{b1} = 1.8$, $\delta_1 = 1.7$. Substituting the obtained values in the formula for A_c , we shall have $A_c = 420 \text{ mm}^2$.

1.3.5. Calculation of Approach Between Surfaces

The penetration, crushing, and elastic deformation of surface asperities under load have the effect of bringing the two contacting surfaces closer together. In some cases, the magnitude of approach determines the character of friction and wear of the surfaces, because the mode of interaction, the real area of contact, and the size of contact spots depend on the depth of penetration. Three types of approach should be distinguished: approach due to the deformation of asperities, h , approach due to the deformation of waves, h_b , and the total approach due to both factors, $h_\Sigma = h + h_b$.

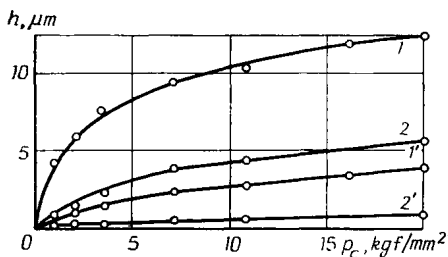


Fig. 1.12. Relationship between approach and contour pressure
1 and 2—initial loading of two rough surfaces (1), and a rough surface with a smooth surface (2); 1' and 2'—repeated loading of the same surfaces

Formulas for calculating the approach due to the deformation of asperities are given in Table 1.18.

Figure 1.12 presents the relationship between the approach and the contour pressure at the first loading (1, 2) and the second loading (1', 2') of the contact area.

Table 1.18

Formulas for calculating approach

Type of surface	Contact conditions and the scope of the formula	Formula	Note
Non-wavy	General formula	$h = Rp \left(\frac{p_c}{\alpha t_m p_r} \right)^{1/v}$	Rp , t_m , v —see p. 23; p_r is computed by formulas in Table 1.15, and p_c , by formulas in Table 1.16 with coefficients in Table 1.17
	Approximate formula for the contact of two rough surfaces	$h \approx 3.4 Ra \left(\frac{p_c}{p_r} \right)^{1/3}$	
	Approximate formula for the contact of a rough surface with a smooth surface	$h \approx 4.1 Ra \left(\frac{p_c}{p_r} \right)^{1/2}$	
	Repeated application of load to plastic contact	$h = \frac{1 - \alpha^{1/2}}{\alpha^{1/2}} Rp \left(\frac{2p_c}{H} \right)^{1/3}$	α —see Tables 1.12 and 1.13. The surfaces are loaded repeatedly without relative displacement
Wavy	Wavy surface in contact with a plane	$h_\Sigma = h + 3.83 H_b^{0.8} R_b^{0.2} (\Theta_\Sigma p_a)^{0.4}$	Values of h are computed by the above formulas in this table
	Both contacting surfaces are wavy	$h_\Sigma = h + 1.8 H_b^{0.85} R_b^{0.15} (\Theta_\Sigma p_a)^{0.3}$	

Example 5. Calculate the approach of two identical steel surfaces having $Rz_1 = Rz_2 = 0.3 \text{ } \mu\text{m}$, $r = 300 \text{ } \mu\text{m}$, $E = 2 \times 10^4 \text{ kgf/mm}^2$, $\mu = 0.3$ at a pressure $p_c = 1 \text{ kgf/mm}^2$.

$$Rz = Rz_1 + Rz_2 = 0.6 \text{ } \mu\text{m}, \quad r = \frac{r_1 r_2}{r_1 + r_2} = 150 \text{ } \mu\text{m}, \quad \Theta_\Sigma =$$

$$= \frac{2(1 - \mu^2)}{E} = 9 \times 10^{-5} \text{ mm}^2/\text{kgf}$$

The calculation formula is chosen from Table 1.18. First, p_r must be calculated, using the appropriate formula from Table 1.15. With $Ra \approx 0.2Rz = 0.12 \text{ } \mu\text{m}$, we shall have $p_r \approx 4.3 \text{ kgf/mm}^2$. Inserting the appropriate values into the formula from Table 1.18, we obtain $h \approx 0.25 \text{ } \mu\text{m}$.

1.3.6. Calculation of Intercontact Space Volume

The intercontact space volume and the associated average amount of clearance between the contacting surfaces to a great extent determine the thermal resistance of the joint and its tightness. This volume depends on the form of the bearing-area curve of the two mating surfaces and the amount of their approach under a normal load. For wavy surfaces, their profile and deformation are of decisive importance. Table 1.19 lists formulas for calculating the intercontact space volume and the average amount of clearance between the surfaces in contact. Curves showing the change of the intercontact space volume with load for steel parts are presented in Fig. 1.13.

Example 6. Determine the volume of the intercontact space between two flat copper surfaces having $Ra_1 = 5 \text{ } \mu\text{m}$, $Ra_2 = 0.3 \text{ } \mu\text{m}$, $HB_1 = HB_2 = 70 \text{ kgf/mm}^2$, $A_a = 100 \text{ mm}^2$, $N = 100 \text{ kgf}$.

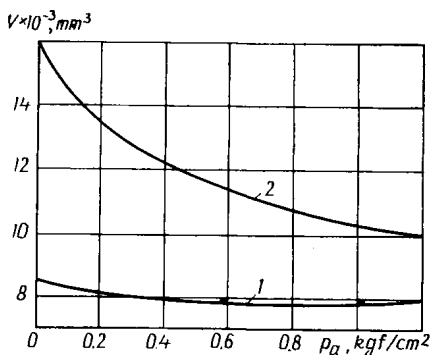


Fig. 1.13. Variation of intercontact space volume for steel surfaces
1—without waviness; 2—with waviness

Table 1.19

Formulas for calculating the intercontact space volume V_s and mean clearance width h_m

Contact conditions	Formulas	Note
General formulas for rough surfaces	$V_s = \left[1 - \left(\frac{p_c}{\alpha t_m p_r} \right)^{1/\nu} \right] (Rp_1 + Rp_2) A_c$ $h_m = \left[1 - \left(\frac{p_c}{\alpha t_m p_r} \right)^{1/\nu} \right] (Rp_1 + Rp_2)$	For calculation of p_r see Table 1.15, for p_c , Tables 1.16 and 1.17, for ν and t_m see p. 23
Contact of two rough surfaces	$V_s \simeq \left[1 - 3.3 \left(\frac{p_c}{p_r} \right)^{1/3} \right] (Rp_1 + Rp_2) A_c$ $h_m \simeq \left[1 - 3.3 \left(\frac{p_c}{p_r} \right)^{1/3} \right] (Rp_1 + Rp_2)$	
Contact of rough surface with smooth surface	$V_s \simeq \left[1 - 3.6 \left(\frac{p_c}{p_r} \right)^{1/2} \right] R_p A_c$ $h_m \simeq \left[1 - 3.6 \left(\frac{p_c}{p_r} \right)^{1/2} \right] R_p$	
Contact of two wavy and rough surfaces	$V_s = \left(\frac{H_{b1}}{2} + \frac{H_{b2}}{2} + Rp_1 + Rp_2 - h_\Sigma \right) A_c$ $h_m = \frac{H_{b1}}{2} + \frac{H_{b2}}{2} + Rp_1 + Rp_2 - h_\Sigma$	For calculation of h_Σ see Table 1.18

Since $Ra_1/Ra_2 = 16.7$, the second surface can be considered flat for calculation purposes: $p_r = H \approx HB = 70 \text{ kgf/mm}^2$; with waviness being absent, $A_c = A_a$ and $p_c = p_a$; $Rp \approx 2.5 \text{ Ra} = 12.5 \text{ }\mu\text{m}$.

Then, according to Table 1.19,

$$V_s = \left[1 - 3.6 \left(\frac{p_c}{p_r} \right)^{1/2} \right] A_c R p = \\ = \{ 1 - 3.6 [100/(70 \times 100)]^{1/2} \} 100 \times 2.5 \times 0.005 = 0.71 \text{ mm}^3$$

1.3.7. Calculation of the Number of Spots in Real Contact, Their Average Area and Spacing

The spots of the real contact are the places where elementary interactions between surfaces occur; these interactions give rise to friction and wear. The area of the contact spots determines the size of worn-off particles, the time of interaction at a single contact spot and the temperature developing from friction. The average spacing of contact spots defines the frequency of their interactions. The number of contact spots is calculated on the basis of a hemispherical model of rough surface, whose application enables one to determine the law of distribution of asperity crests throughout the height of the rough layer, proceeding from the law of distribution of the material (the bearing-area curve). Formulas for calculating the number of contact spots are presented in Table 1.20.

Table 1.20

Formulas for determining the number of real contact spots, n_r , their average area ΔA_r , and average distance between them, S_r

Surfaces in contact	Formulas	Note
Two rough surfaces	$n_r = \frac{3.1 A_c}{K_r r R a} \left(\frac{p_c}{p_r} \right)^{0.66}$ $S_r = 0.57 (K_r r R a)^{0.5} \left(\frac{p_r}{p_c} \right)^{0.33}$ $\Delta A_r = 0.33 K_r r R a \left(\frac{p_c}{p_r} \right)^{0.33}$	For elastic contact of asperities (see Table 1.12) $K_r = 11$, and for plastic contact $K_r = 21$
Rough surface with smooth surface	$n_r = \frac{2 A_c}{K_r r R a} \left(\frac{p_c}{p_r} \right)^{0.5}$ $S_r = 0.7 (K_r r R a)^{0.5} \left(\frac{p_r}{p_c} \right)^{0.5}$ $\Delta A_r = 0.5 K_r r R a \left(\frac{p_c}{p_r} \right)^{0.5}$	For determining r and Ra see p. 23-24, and for determining p_r and p_c see Tables 1.15, 1.16, and 1.17

Example 7. Calculate the average area and the number of contact spots for identical steel surfaces ($Rz = 40 \mu\text{m}$, $r = 100 \mu\text{m}$, $A_c = 200 \text{ mm}^2$, $N = 200 \text{ kgf}$, $HB = 300 \text{ kgf/mm}^2$). Then $Ra \approx 1/4 Rz = 10 \mu\text{m}$, $p_c = 1 \text{ kgf/mm}^2$, $p_r = 300 \text{ kgf/mm}^2$, and, since the contact is plastic, $K_r = 21$. Substituting the values of the parameters into the formula for the contact of two rough surfaces (Table 1.20), we shall have

$$n_r = \frac{200}{0.33 \times 21 \times 0.1 \times 0.01} (1/300)^{0.66} = 641 \text{ spots}$$

$$\Delta A_r = 0.33 \times 21 \times 0.1 \times 0.01 (1/330)^{0.33} = 0.001 \text{ mm}^2$$

The average diameter of the contact spot $d = \sqrt{\Delta A} = 31.6 \mu\text{m}$.

1.4. RHEOLOGICAL PROPERTIES OF CONTACT

The real pressure on the contact is very high; it gives rise to plastic deformation of surface peaks, and, in some instances, causes the material at the contact to creep. As a result, the characteristics of the contact change as the load application time grows longer. The relation between the deformation of the contact and time is determined by the properties of the material, its homological temperature, surface roughness, and the applied load. Metals creep intensively at a homological temperature of over 0.4; however, creep occurs at room temperature as well, even with such materials as steel [6].

It has been shown experimentally that the rate of pressure drop in indenting a viscous plastic medium with a rigid sphere is an exponential function of the stress effective at a given instant of time; here, the contact pressure will be expressed as

$$p_t = HB (t_{HB}/t)^m$$

where t_{HB} = time of keeping the indenter under load in a Brinell hardness test and m = rheological constant of the material under test.

Formulas for calculating the real contact area and the approach of surfaces as a function of time are given in Table 1.21, and the values of the rheological constant for some metals and alloys are given in Table 1.22. For other materials the constant m can be found experimentally, using the above formula. As can be seen from Table 1.22, the creep of hard metals is very low at normal temperatures. For assessing the behaviour of a contact at high temperatures, the value of m at a given temperature needs to be determined beforehand. To a first approximation, the value of m at the appropriate homological temperature, taken from Table 1.22, may be used for rough evaluation of the contact behaviour.

Example 8. Calculate the additional contact deformation of two parts made from steel Grade 35 ($\nu = 1.5$) at room temperature in 24 hours from the moment the parts were placed under load. The load application time $t_1 = 1 \text{ min}$. From Table 1.22, $m = 0.0067$; for two rough surfaces $v_2 = v_1 + v_2 = 1.5 + 1.5 = 3$, $t_2 = 24 \times 3,600 = 86,400 \text{ s}$.

Table 1.21

Formulas for determining the real area of contact and approach of metal surfaces as a function of time

Contact conditions	Formula	Note
One of the surfaces in contact is plastically deformed	$A_{rt} = \frac{N}{HBt_{HB}^m} (t_2^m - t_1^m)$ $h_t = Rp \left(\frac{p_c}{t_m HB} \right)^{1/\nu} \left[\left(\frac{t_2}{t_1} \right)^{m/\nu} - \left(\frac{t_1}{t_{HB}} \right)^{m/\nu} \right]$ $A_{rt}/A_{r1} = (t/t_1)^m - 1$ $h_t/h_1 = (t/t_1)^m - 1$	Hardness of the softer material and roughness of the harder material are to be used for calculation

Designations: A_{rt} = change in real contact area over the period of time $t_2 - t_1$; t_m = relative reference length along the mean line; a_t = change in approach over the period of time $t_2 - t_1$; A_{r1} and a_1 = real contact area and approach at the moment t_1 , respectively.

Table 1.22

Values of m for various materials (after P. D. Netyagov)

Material	T_H^*	HB	m	Material	T_H^*	HB	m
Tin	0.56	5.5	0.096	Silver	0.38	33.2	0.049
Cadmium	0.48	28.1	0.066		0.44	20.0	0.085
Lead	0.46	4.5	0.065		0.56	11.6	0.115
Zinc	0.42	34.5	0.056				
Magnesium	0.32	34.8	0.026				
Silver	0.24	66.0	0.014	BT1-1	0.14	101	0.021
	0.35	37.5	0.031	BAД-1Φ	—	118	0.0076
				Steel Grade 20X13	0.17	280	0.0074
				Steel Grade 35	—	257	0.0067

* Homological temperature, equal to the ratio of the temperature during the experiment to the melting temperature in kelvins.

Substituting the above values into the formula from Table 1.21, we shall have

$$\frac{\Delta h_t}{h_1} = \left(\frac{t_2}{t_1} \right)^{m/v} - 1 = \left(\frac{86,400}{60} \right)^{\frac{0.0067}{3}} - 1 = 0.0163$$

that is, deformation increases only by 1.6 percent.

1.5. METHODS AND INSTRUMENTS FOR RESEARCH ON PROPERTIES OF CONTACT

1.5.1. Measurement of Real Contact Area

Modern methods for determining the real area of contact [3] can be divided into five groups (Table 1.23).

Group 1. Electrical and thermal conductivity are found by the Holm formula. The total contact resistance equals the sum of the material spreading resistance, dependent on the contour area of contact, and the resistance determined by the number and area of the real-contact spots:

$$R = \frac{1}{2\lambda\rho_c} + \frac{1}{2\lambda\rho n_r}$$

where R = electrical resistance, λ = specific conductivity of the material, ρ_c and ρ = radii of contour and real contact areas and n_r = number of spots of real contact.

This formula also holds true for the calculation of thermal conductivity of the contact. For the assessment of the real contact area through electrical conductivity, data on the number and area of contact spots are required; in addition, the effect of surface films and foreign matter fouling the surface is difficult to estimate. For these reasons, the results obtained by the electrical conductivity method need to be verified by other methods. The accuracy of determining the contact area by thermal conductivity is greatly influenced by the thermal conductivity of the gas filling the between-contact space; here the area and the number of contact spots must also be known. This method has not found wide application because the measurement of heat flows with adequate accuracy presents some difficulty.

The use of ultrasound for assessing the contact area requires the consideration of the interference phenomena, which depend, in particular, on the shape and size of test specimens. Moreover, as the length of ultrasonic waves is substantially greater than the contact spot diameter, the relationship between the conductivity and the wavelength needs to be found, and the conductivity at a wavelength approaching zero is bound to be determined by interpolation. Without careful consideration of these factors, the method can only be used for comparative measurements.

Table 1.23

Methods for determining real area of contact

Group of methods	Method of obtaining information	Application	Note
1. Based on contact conductivity	By electrical conductivity	Metals in stationary and sliding contact	Necessary to verify by other methods
	By thermal conductivity	Metals in stationary contact	
	By ultrasonic conductivity	Any solids in stationary and sliding contact	
2. Geometric	By approach of surfaces	Any solids in stationary and sliding contact, $Ra \geq 0.6 \mu m$	—
	By data obtained in indenting the surface with a large-radius sphere	Any solids in stationary contact, $Ra \geq 0.6 \mu m$	
3. Based on use of thin films	By rupture of lumiphore-containing films	Any solids in stationary contact, $Ra \geq 1.2 \mu m$	Necessary to verify by other methods
	By rupture of films containing radioactive isotopes	Any solids in stationary contact, $Ra \geq 0.16 \mu m$	
	By rupture of carbon films		
4. Optical	By disturbance of total internal reflection	One of the surfaces is transparent, hard, and smooth; contact stationary or sliding, $Ra \geq 0.6 \mu m$	—
	By absence of diffusion at contact spots	Both surfaces are transparent; stationary and sliding contact, $Ra \geq 1.2 \mu m$	
	By change in interference pattern at contact spots	One of the surfaces is transparent, hard, smooth, and coated with a reflecting film; stationary contact $Ra \geq 1.2 \mu m$	
5. By change in physico-chemical properties in contact areas	Etching and selective depositing of metal at contact spots	Metal surfaces in stationary contact	Methods are developed insufficiently

Group 2. The method based on the measurement of the approach of surfaces requires the knowledge of the relationship between the real contact area and the approach. Here, profile graphs of the rough surface are recorded before the latter is brought into contact with the smooth surface. These graphs are the source for determining the parameters of the bearing-area curve. When the rough surface for which the bearing-area curve is plotted makes contact with a smooth, hard surface, the real contact area may be considered, to some approximation for plastic contact, to be equal to the corresponding abscissa of the bearing-area curve. Thus, by measuring the approach between the rough and smooth surfaces, some idea of the real contact area can be gained.

The method is rather difficult to carry out, because it requires a careful study of the geometry of the rough contacting surface on the basis of a large number of surface profile graphs.

Another geometric method for determining the real contact area, the approach, and the parameters of the bearing-area curve is based on measuring deformation from indenting a rough surface with a spherical indenter of a large radius ($r = 100$ to 200 mm).

Group 3. Measuring the real contact area with the aid of thin films is extensively applied in engineering practice. For instance, the real contact area can be roughly assessed by measuring the area or luminous properties of an impression obtained on a carbon-paper sheet placed between the contacting surfaces. Another technique involves applying a thin film to one of the mating surfaces and, after bringing them in and out of contact, locations are examined where the film has broken or where it has been transferred to the other surface because of the adhesion and deformation of the asperities.

In order to obtain an impression that corresponds to the real rather than the contour area of contact, the layer to be applied must be very thin; otherwise, it will fill the valleys of the profile and thus will substantially alter the geometry of the contacting surfaces. The thickness of the layer must be much smaller than the height of the profile peaks. Various methods are employed for identifying such a thin layer.

The real area of contact can also be determined with the aid of a luminescent pigment. A thin layer of the pigment-containing substance diluted in a volatile solvent is applied to the test surface. After the solvent has evaporated, the coloured surface is brought into contact with the uncoloured one. The film is transferred to the mating surface at the contact points. When this surface is exposed to ultraviolet rays, the luminescent pigment becomes activated and starts radiating light rays in the visible region of the spectrum. A photograph of the real contact area can be obtained in this way. The accuracy of the method depends largely on the properties of the film containing the luminescent pigment. Our investigations have shown that the commonly applied rosin films yield no good results.

One more method of this group for determining the real contact area is the radioactive-isotope method. One of the contacting surfaces is activated or coated with a layer of radioactive substance. While the surfaces are in contact, the active isotopes transfer to the inactive surface at the contact points. The distribution of isotopes

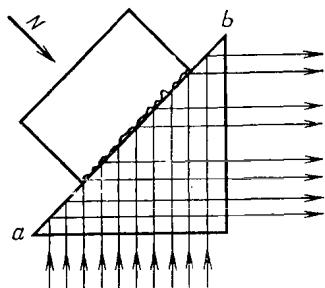


Fig. 1.14. Principle of optical measurement of the real area of contact

over the surface of the nonactivated specimen is determined by means of autoradiography. A fine-grain film is used as a material for autoradiographs. The advantage of this method is high sensitivity. The uniform radiation of isotopes in all directions, however, will affect the size of the impression for a given group of radioactive atoms, which will depend on the exposition, the sensitivity of the photographic film, the quantity of radioactive isotopes and the developing conditions.

The method of measuring the real area of contact with the aid of a carbon film deposited on one of the mating surfaces by spraying in vacuum is most simple and effective. When the test specimens are brought together the film breaks at the points of contact. After the specimens are taken apart, light contact spots are clearly identified

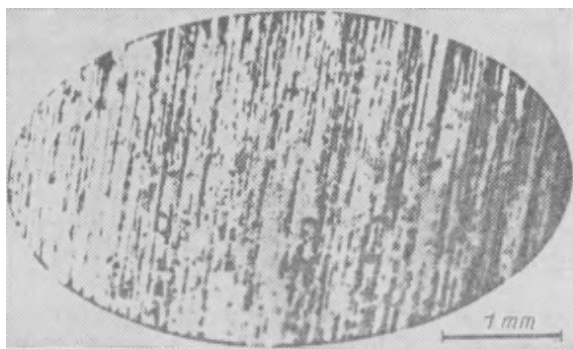


Fig. 1.15. Image of contact spots obtained by optical method

on the dark carbon-film background. A carbon-film layer 40 to 50 μm thick can be detected visually. The use of films of such a small thickness allows the real contact area for surfaces with $Ra \geq 0.08 \mu\text{m}$ to be measured.

Group 4. Optical methods for measuring the real contact area involve viewing this area through one (or both) of the test specimens made of transparent material. Related to these methods is one in

which the contact of a rough surface with an optical prism (Fig. 1.14) results in the upsetting of total internal reflection. A parallel beam of light is directed onto the contacting face of the prism at an angle exceeding the critical angle. The total internal reflection is upset at the contact points, and these points are identified in the reflected light as dark spots on a bright background (Fig. 1.15). The method is applicable to determining the real contact area between a rough and a smooth surface in motion as well as in stationary conditions. The drawbacks to the method are its unsuitability for the study of contact between two rough surfaces and the measuring error due to light's penetration into the second medium during total internal reflection.

There is an optical method of measuring the real contact area of two rough transparent specimens, based on the passage of a parallel beam of light through their interface. While the light rays pass through the points of contact without refraction, light is dissipated at the places where there is no contact (Fig. 1.16). As a result, the contacting points are seen in transmitted light as brightly luminous spots on a grey background.

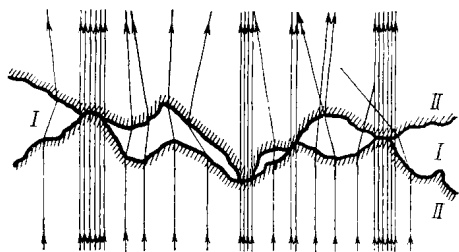


Fig. 1.16. Determining the real area of contact in transmitted light

This method allows the real contact area of two rough surfaces to be studied both in stationary conditions and in motion. The disadvantage of the method is a very limited range of the test materials, since both specimens must be transparent.

An optical method for determining the real area of contact is known, wherein the phase-contrast effect is used. The rough surface to be investigated is brought into contact with a polished glass plate coated with a silver film; at the points of contact, the glass and, accordingly, the silver film become somewhat deformed. Observing the film through the glass plate with the aid of a microscope and using the phase-contrast method, one can detect minute irregularities of the film and thus locate the contact spots. The method has a very high resolution and makes it possible to identify small contact spots. However, it is unsuitable for testing specimens in motion and also those with a fine surface finish, because here the deformation of glass will not correspond to the contact area.

Group 5. The deformation of surface asperities in contact and friction at contact spots cause a sharp increase in dislocation density, which intensifies diffusion processes and gives rise to exoelectron emission. These phenomena can be employed for determining the real contact area. For instance, etching in acid vapours and selective deposition of metal from a solution can be used to identify the

contact area. Such techniques, however, have not yet been sufficiently developed.

More detailed descriptions of the methods for determining the real area of contact and the list of references on the subject are given in [3].

1.5.2. Measurement of Contact Deformations

Experimental measurement of contact deformations presents difficulties associated with the requirement for high measuring accuracy, because the deformations of surfaces machined to a fine finish are as small as tenths and hundredths of a millimetre. Such high-accuracy measurements are greatly affected by extraneous factors. The adverse factors here are the bulk deformation of specimens, deformations in the measuring system, misalignments, thermal deformations and so on.

The simplest method of measuring contact deformations involves placing a number of strain gauges at points located as near as possible to the contact point. To eliminate the influence of misalignments, the average of the readings from the gauges is taken. Such tensometers, however, are not accurate enough and their indications are affected by the deformation where the tensometer locating fins contact the specimens, as well as the deformation of the specimens between the locating points.

A much higher accuracy can be achieved by using strain gauges, inductive transducers, mechanically controlled electron valves, opticators, air gauges, and optomechanical devices that allow deformations of $0.1\text{ }\mu\text{m}$ and smaller to be measured. The use of interferometry offers a particularly high accuracy.

Improved accuracy can be obtained by measuring the total contact deformation of a stack of specimens having identical surfaces [1]; in this case very small contact deformations can be measured. Methods for measuring contact deformations are treated in more detail in [3, 10, 11, 14].

REFERENCES

1. Ахматов А. С. Молекулярная физика граничного трения. М., Физматгиз, 1963.
2. Демкин Н. Б., Измайлов В. В., Саватеев В. М. О величине фактического давления при пластическом контакте.— В кн.: Надежность и долговечность деталей машин. Калинин, КПИ, 1974, с. 29—36.
3. Демкин Н. Б. Контактное взаимодействие шероховатых поверхностей. М., «Наука», 1970.
4. Демкин Н. Б., Короухов М. А. Формирование площади контакта при трении металлов.— В кн.: Физико-химическая механика фрикционного взаимодействия. М., «Наука», 1971.
5. Демкин Н. Б., Коротков М. А., Алексеев В. М. Методика расчета характеристик фрикционного контакта.— В кн.: Расчет и моделирование

режима работы тормозных и фрикционных устройств. М., «Наука», 1974, с. 5—15.

6. Демкин Н. Б., Нетягов П. Д. Исследование реологических свойств контакта шероховатых поверхностей. «Известия вузов. Машиностроение», 1973, № 3, с. 18—24.

7. Ишлинский А. Ю. Осесимметричная задача теории пластичности и проба Бринелля. — «Прикладная математика и механика», 1944, т. 8, вып. 3, с. 201—224.

8. Комбалов В. С. Влияние шероховатости твердых тел на трение и износ. М., «Наука», 1974.

9. Крагельский И. В., Демкин Н. Б. Определение фактической площади касания. — В кн.: Трение и износ в машинах, т. 14, М., изд-во АН СССР, 1960, с. 37—62.

10. Крагельский И. В. Трение и износ. М., «Машиностроение», 1968.

11. Левина З. М., Решетов Д. Н. Контактная жесткость машин. М., «Машиностроение», 1971.

12. Михин Н. М. О связи площади касания и сближения при неподвижном и скользящем контактах. — В кн.: Трение твердых тел. М., «Наука», 1964, с. 62—66.

13. Расчеты на прочность в машиностроении, т. 2. Под ред. С. Д. Пономарева. М., Машгиз, 1959.

14. Рыжов Э. В. Контактная жесткость деталей машин. М., «Машиностроение», 1966.

15. Характеристики микрогеометрии, определяющие контактное взаимодействие шероховатых поверхностей (методика определения). М., НИИМАШ; 1973.

CALCULATION OF COEFFICIENTS OF EXTERNAL FRICTION AND PRELIMINARY DISPLACEMENT

2.1. MAIN CONCEPTS AND DEFINITIONS

External friction of solids is a complex phenomenon depending on various processes that occur in the real areas of contact and in thin surface layers during relative tangential movement of the bodies. By the frictional force T is meant the force of resistance to relative displacement of solids, which is directed oppositely to this displacement. The external forces of friction are nonconservative, that is, the work of the frictional forces depends on the distance over which the solids are displaced. The magnitude of the external frictional force is determined generally by the displacement of solids in a tangential direction; depending on this displacement, distinction is made between the force of external static friction, the partial force of external static friction, and the force of external kinetic friction.

The *partial force of external static friction* is the force of resistance to motion in the case of small, partially reversible tangential displacements called preliminary displacements. This force occurs in tribological joints where no continuous sliding takes place under the effect of forces applied to the contacting bodies. The force of external static friction is the magnitude of the partial force of external static friction that corresponds to the maximum preliminary displacement.

The *force of external sliding friction* is the resistance to tangential displacement of contacting bodies, which does not depend on the magnitude of the displacement [20].

External friction involves an intensive deformation of the outer layer on the softer body by the penetrating harder-surface asperities [26, 59]. It should be noted that not all processes of deformation of the surface layer may be called external friction; in fact, external friction only involves such a deformation due to the relative tangen-

tial displacement of the contacting bodies as is not attended by breaks in the integrity of the material, the deformation of the material under the thin outer layer being negligibly small.

As to the kinematic character of relative displacement, distinction is made between sliding friction and rolling friction, which frequently accompany each other.

Because external friction is governed by processes occurring in very thin subsurface layers and at the boundary separating the solid bodies in the real contact areas, the frictional force depends on the physico-mechanical properties of these subsurface layers. The properties of these layers differ from the properties of the layers lying underneath [6]. The cause is that the interatomic (intermolecular, interionic) forces are not symmetrical in the subsurface layers and the atoms (molecules, ions) cannot take the positions that correspond to the minimum level of energy in the bulk of the material. The structure of the subsurface layers is also distorted by machining the surface and by the deformation of these layers and changes in temperature in the process of friction. For these reasons, the internal energy of the subsurface layers will be higher than the energy in the bulk of the metal (material).

Atoms (molecules) of the ambient medium are adsorbed on the surface of the solid body and, owing to chemisorption, form films of chemical compounds with the solid. In the simplest case these are oxide films. Thus, the subsurface layers generally have a distorted structure, and contain oxide films and one, at least in the ambience of air, monolayer of adsorbed vapours of water or gases. In order to decrease the interaction between solids in contact, use is very frequently made of lubrication. As a result, the interaction of bodies in the case of external friction occurs between the films coating the bodies rather than between the bodies themselves. Depending on the surface condition of the solids, distinction is drawn between friction without lubrication, boundary friction, and fluid friction.

Friction without lubrication is the friction of two solids whose interface is not provided positively with lubrication of any kind. Sometimes such an interaction of rubbing bodies is called *dry friction*.

Boundary friction is the friction of two solids having at their interface a fluid layer whose properties differ from those of the bulk lubricant [21]. Investigations conducted by B. V. Deryagin [12] and his co-workers have shown that the properties of a fluid layer 0.1 μm thick usually differ from those of the bulk fluid and, therefore, the conventional hydrodynamic equations do not apply to such thin layers.

The coefficient of sliding friction is the ratio of the sliding frictional force to the normal component of the external forces that act on the rubbing surfaces.

2.2. INTERACTION OF SOLIDS

The molecular-mechanical theory of friction (known in other countries as the adhesion-deformational theory), first put forward by I. V. Kragelsky in the USSR in 1939 [18], has recently found extensive use for the explanation of interaction between solids in contact. Let us consider the main points of the molecular-mechanical theory of friction on the basis of the modern concepts of frictional interaction of solids.

The penetration of the harder asperities into the softer mating surface in the real areas of contact between two bodies is accounted for by their differing mechanical properties, variations in these properties at separate portions of the bodies [14], and differences in the geometric outlines of the contact areas [36]. For this reason, the sliding of one body relative to the other will have the effect of deforming the softer surface layer by the harder asperities. The resistance of the surface layers to deformation in sliding is called the mechanical (or deformational) component of the friction force. It can be calculated on the basis of the mechanical properties of the surface layers, the geometric shape of the asperities, and the stress conditions in the contact area, using the main principles of the mechanics of solids.

Along with the deformation of the surface layers in external friction, perceptible molecular interactions are detected at the portions of the contacting bodies that are separated by as small distances as 10^{-7} cm. Resistance to relative sliding, which is the result of these interactions, has been called the molecular component of the frictional force. This component is frequently referred to as the adhesion component; the term, however, is not accurate, because adhesion means joining or sticking, whereas the molecular interactions are characterized by both attraction and repulsion forces.

Taking into account that the material will undergo deformation at the contact areas until the interatomic (intermolecular) repulsion forces equalize the attraction forces, the real contact area may be defined as a combination of elementary areas in which this equality is realized. It can be assumed that the area over which the molecular interactions manifest themselves appreciably coincides with the real contact area for surfaces finished to lower than the 12th class of surface roughness.

Owing to the presence on the surfaces of solids of films whose thickness and structure depend on the surroundings, it has not yet been possible to calculate theoretically the molecular component of the friction force for actual operating conditions. Therefore, this component is calculated by the molecular component of the external coefficient of friction, found experimentally, (see p. 81) and by the average normal stresses acting in the real areas of contact. For superfinished surfaces of the 13th and higher classes of surface rough-

ness, the molecular component must be determined with due regard for noncontact interactions.

The total force of external friction will be equal to the sum of two components—the molecular component T_{ml} and the mechanical component T_{mc} :

$$T = T_{ml} + T_{mc} \quad (2.1)$$

It should be noted that the molecular and mechanical components of the frictional force are interrelated, and the arithmetic sum can only be taken for a rough estimate of the total frictional force.

To find the frictional force, it is necessary to know the type of deformation in the contact areas and the geometric shapes of asperities. The deformations in the real contact areas depend on the mechanical properties of the rubbing solids, the magnitude of the applied force, and the microtopography of the surfaces.

The hemispherical model of a rough surface [22, 27] has gained the widest application for calculating the interaction between solids in friction. Calculations [46] show that in the penetration area, where external friction conditions are effective, the use of the hemispherical model of a separate asperity gives an error of not over 10 percent in determining the real contact area, not over 4 percent in determining the average normal stresses in the contact areas, and from 3 to 7 percent in determining the coefficient of friction.

These facts suggest the following important conclusions. First, the distributions of the peaks of the asperities by height for a real component and a hemispherical model of a rough surface are described by one and the same function, assuming that the relationship between the contact area and the approach for the hemispherical model is determined by the bearing-area curve of the real body and that the contact area is formed by separate contact spots whose average areas in the model and in the real body are the same. Second, the identical magnitudes of approach for a real surface and for a hemispherical model of the asperities of a rough surface correspond to identical contact areas, identical loads and identical friction forces in sliding.

Taking into account that in the contact of solids the harder portions penetrate into the softer ones and that the deformation of the former is insignificant, one of the bodies can be considered absolutely rigid as far as the interaction of the bodies is concerned. The contact of the rough surface with a plane will be discrete. The mutual influence of separate deformation zones can be neglected when calculating the contact interaction, since this influence is small during elastic deformations in the contact areas [34] and comes into play during plastic deformations [13] with a relative approach $\varepsilon \approx 0.5$, at which conventional tribological joints do not work.

Solution to the problem of a hemisphere sliding along a plane being deformed has shown that the upsetting of integrity arises dur-

ing the penetrations [22]

$$\frac{h}{r} \leq \frac{1}{2} \left(1 - \frac{2\tau_n}{\sigma_T} \right) \quad (2.2)$$

With regard to the relationship between the approach h and the contour pressure p_c

$$h = \frac{R_{\max}}{b^{1/\nu}} \left(\frac{2p_c}{HB} \right)^{1/\nu} \quad (2.3)$$

we shall obtain the following expression for the maximum values of p_c which, when exceeded, will give rise to a break in the external friction conditions:

$$p_c = \frac{HB}{2^{\nu+1}\Delta^{\nu}} \left(1 - \frac{6\tau_n}{HB} \right)^{\nu}$$

For the most widespread classes of surface finish, $b = 2$ and $\nu = 2$; hence

$$p_c = \frac{0.125HB}{\Delta^2} \left(1 - \frac{6\tau_n}{HB} \right)^2 \quad (2.4)$$

The graphs of the relationship between p_c and $\frac{\tau_n}{HB}$, according to formula (2.4), for different values of $\frac{rb^{1/\nu}}{R_{\max}}$ is given in Fig. 2.1. Calculations made by formula (2.4) show that the tangential stresses caused by molecular interactions in real contact areas substantially affect the level of p_c determining the threshold of external friction. At $\tau_n = 0.4 \sigma_T$ external friction takes place even with relatively coarse-finished surfaces and considerable contour pressures

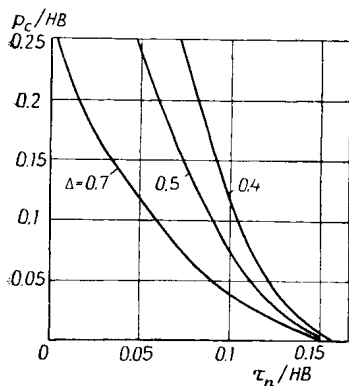


Fig. 2.1. Relationship between p_c/HB and τ_n/HB

$\left(\frac{p_c}{HB} > 0.04 \right)$. As τ_n is getting closer to $\frac{\sigma_T}{2}$, the threshold of external friction shifts toward the lower-value zone of pressures, and the external friction becomes possible only for fine-finished surfaces (the 9th-10th classes of surface roughness at small loads).

The tangential stresses τ_n arising at the interface owing to molecular interactions are a function of normal stresses [27, 28, 43, 44]:

$$\tau_n = \tau_0 + \beta p_r \quad (2.5)$$

The constants τ_0 and β , called frictional parameters later in the text, depend on the operating conditions of a tribological joint. Assuming that at the interface of two solids there is always the so-called third body incorporating the films of lubricants, oxides, adsorbed

vapours, and gases, and considering that, along with the bulk deformation of the surface layers, external friction involves a viscous flow in the third body, the following expressions for the frictional parameters τ_0 and β can be derived:

$$\tau_0 = A(T) c_1 e^{\frac{\beta_1}{kT}} \quad (2.6)$$

$$\beta = \frac{A(T) c_1 e^{\frac{\beta_1}{kT}} \gamma}{kT} \quad (2.7)$$

where $A(T)$ = a function of temperature [55]; $c_1 = \frac{dv}{dz}$ = speed gradient, β_1 and γ = constants at a constant temperature, and k = Boltzmann constant.

The contact interaction of sliding solids will be markedly influenced by the type of deformation in the contact area and the extent of density of the contact. Elastic, elastic-plastic, and plastic deformations can take place in the real contact areas. Elastic-plastic deformations are most frequent. In some cases, however, calculations may be made on the assumption that only elastic deformations (at contour pressures $p_c \leq 100$ kgf/cm² for surfaces finished to the 10th or higher classes of surface roughness) or plastic deformations (at contour pressure $p_c > 100$ kgf/cm² or for surfaces finished to the 8th class of surface roughness) occur in the contact areas. The interaction of solids in the case of elastic-plastic deformations is still not clearly understood. We shall present, therefore, formulas for calculating the coefficient of external friction for the elastic and plastic deformations only.

Elastic contact takes place where the maximum stresses at the asperity that has penetrated deepest are lower than the Brinell hardness of the softer component of the sliding pair [23, 31]; it corresponds to the approach

$$\frac{h}{r} = 2.4 (1 - \mu^2)^2 \left(\frac{HB}{E} \right)^2 \quad (2.8)$$

and the contour pressure

$$p_c \leq \frac{2.4^{\frac{2v+1}{2}} v(v-1) k_1 HB^{2v+1} (1 - \mu^2)^{2v}}{5E^{2v} \Delta^v}$$

where k_1 = integration constant dependent on v .

A graph showing k_1 and $v(v-1)$ as a function of v is given in Fig. 2.2. For the most often used values of surface roughness in engineering components ($v = 2$, $b = 2$)

$$p_c = \frac{1.4}{\Delta^2} \frac{HB^5 (1 - \mu^2)^4}{E^4} \quad (2.9)$$

The variation in the contour pressures p_c that cause the transition of elastic to elastic-plastic deformations as a function of surface

roughness at different $\frac{HB}{E}$ ratios is represented graphically in Fig. 2.3. Thus, with materials having a high modulus of elasticity (for instance, metals), elastic contact at the initial loading is only possible for fine-finished surfaces with $\Delta \leq 0.005$, that is, for the 10th to 11th classes of surface roughness. With polymers, elastic contact is possible at considerable values of $\frac{p_c}{HB}$ and with surfaces finished to lower classes of roughness than metals.

With elastic deformations in the contact areas, the mechanical component of external friction force arises from incomplete elasti-

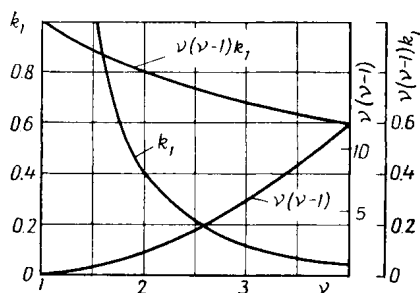


Fig. 2.2. Dependence of k_1 and $k_1 v(v-1)$ on v

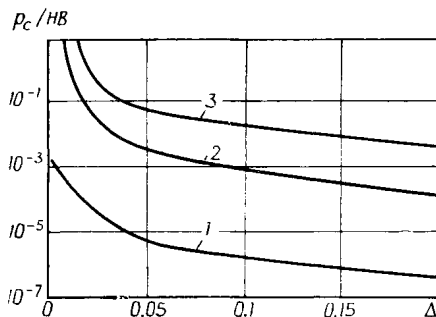


Fig. 2.3. Relation between p_c and Δ
1— $\frac{HB}{E} = 0.01$, $\mu = 0.3$; 2— $\frac{HB}{E} = 0.05$,
 $\mu = 0.5$; 3— $\frac{HB}{E} = 0.1$; $\mu = 0.5$

city of solids. For this reason, deforming the surface layer of the softer body by the penetrating asperities arouses the resistance to relative sliding, which is due to hysteresis losses. Given below are formulas for calculating the external friction coefficient for elastic deformation in the contact area.

Sparse contact takes place where the number of contacting asperities, n_r , is smaller than the number of asperities at the contour contact area, n_c , which corresponds to contour pressures [46]

$$p_c < p_{cs} = \frac{8 \times 10^{-2} \Delta^{1/2} E}{(b^{1/v} v)^{\frac{2v+1}{2v-1}} (1-\mu^2)} \quad (2.10)$$

or, for the normally employed engineering surface roughness classes ($v = 2$, $b = 2$)

$$p_{cs} \geq 6 \times 10^{-3} \Delta^{1/2} \frac{E}{(1-\mu^2)} \quad (2.11)$$

A graph showing the relationship between $\frac{p_{cs}(1-\mu^2)}{E}$, computed by formula (2.11), and the ratio $\Delta = \frac{R_{\max}}{rb^{1/v}}$ is presented in Fig. 2.4.

Apparently, elastic deformations at the contact areas can result in a dense contact only where the softer material in the sliding pair has a low elastic modulus. For materials with a high elastic modulus, the contour pressure that causes dense contact turns out to be higher than the contour pressures that correspond to the transition from elastic to elastic-plastic deformations in the contact area.

The coefficient of external static friction, equal to the ratio of the frictional force to the normal load, will be the sum of the molecular and the mechanical component [45]:

$$f = \frac{2.4\tau_0(1-\mu^2)r^{1/2}}{\nu(\nu-1)k_1Eh^{1/2}} + \beta + \frac{0.4\alpha_f h^{1/2}}{k_1\nu(\nu-1)r^{1/2}} \quad (2.12)$$

where α_f = coefficient of hysteresis losses in complex stress conditions. For a sliding spherical indenter [60] $\alpha_f = 2.5\alpha_h$, where α_h = coefficient of hysteresis losses in simple tension-compression. The values of α_h for different materials are listed in Table 2.1.

Table 2.1

Values of the coefficient of hysteresis losses, α_h

Material	α_h	Material	α_h
Hard copper	0.04	Rubber	0.09-0.13
Phosphor bronze	0.04	Wood	0.2
Duralumin	0.03	Hide	
Hardened steel	0.02	raw	0.06
Plastics	0.08-0.12	deaired	0.1

For the most common surface finishes ($\nu = 2$, $b = 2$)

$$f = \frac{3\tau_0(1-\mu^2)r^{1/2}}{Eh^{1/2}} + \beta + 0.17\alpha_f \left(\frac{h}{r}\right)^{1/2} \quad (2.13)$$

From formulas (2.12) and (2.13) it follows that the predominance of one of the components in the total coefficient of friction depends on the operating conditions of a given sliding pair (the values of τ_0 and β and the approach h), on the surface roughness characteristics r and ν , and on the mechanical properties of the softer component in the sliding pair (E and μ). With elastic deformations effective in the contact area, the mechanical component of the coefficient of external friction can be ignored, as compared with the molecular

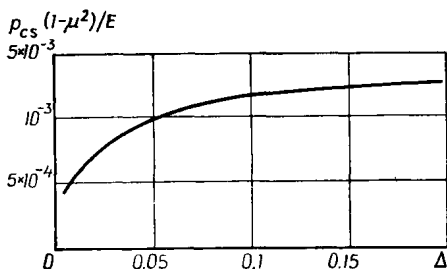


Fig.2.4. Relation between $\frac{p_{cs}(1-\mu^2)}{E}$ and Δ

component, for materials with high elastic moduli and low hysteresis loss factors, and also for materials with low elastic moduli (rubber, plastics) when the magnitude of the molecular component is high ($f_{ml} > 0.3$). If sliding materials with a low elastic modulus are efficiently lubricated, the mechanical component cannot be neglected; this condition, for example, occurs when rubber slides with a boundary lubrication by water or in processing semifinished leather articles [44]. For this reason, in sliding pairs that require a stable coefficient of friction, the conditions should be set up wherein the mechanical component is predominant, that is, effective boundary lubrication must be provided. This requirement is satisfied, in particular, in road building, where surface-coating layers at steep grades and curves have a coarse roughness, which secures a satisfactory adhesion of vehicle wheels to the road surface in rainy weather.

It should be noted that with a closer approach between the mating surfaces the molecular component of the coefficient of friction decreases, whereas the mechanical component increases. Such alteration of the components shows that at certain penetrations the coefficient of external friction passes through a minimum. Using the notion of an extremum of a function, we shall obtain the approach corresponding to the minimum value of the coefficient of friction:

$$\frac{h}{r} = \frac{6\tau_0(1-\mu^2)(\nu+1)}{E\alpha_f} \quad (2.14)$$

The contour pressure that causes such an approach will be [37]

$$p_c = \frac{0.2\nu(\nu-1)k_1}{\Delta^\nu} \left[\frac{6\tau_0(\nu+1)(1-\mu^2)^{\frac{2\nu-1}{2\nu+1}}}{\alpha_f E^{\frac{2\nu-1}{2\nu+1}}} \right]^{\frac{2\nu+1}{2}} \quad (2.15)$$

For the most typical values of surface roughness

$$p_c = \frac{2.2 \times 10^2}{\Delta^2} \left[\frac{\tau_0(1-\mu^2)^{3/5}}{\alpha_f E^{3/5}} \right]^{5/2} \quad (2.16)$$

Analysis of formulas (2.15) and (2.16) shows that a minimum coefficient of external friction with elastic deformations in the contact areas is only feasible for materials having a low modulus of elasticity. With metals, the mechanical component of the coefficient of friction can generally be neglected. Therefore, with increasing magnitude of the penetration and, consequently, of the contour pressure, the coefficient of external static friction for metallic sliding pairs decreases in elastic contact.

The relationship between $\frac{p_c(1-\mu^2)}{E}$, corresponding to minimum values of the coefficient of external static friction, and $\frac{\tau_0(1-\mu^2)}{E}$ for various α_f and $\frac{R_{\max}}{rb^{1/\nu}}$ is represented graphically in Fig. 2.5a. The smoother the surface, the higher the magnitude of the contour pres-

sure resulting in minimum values of the coefficient of friction. An increase in the elastic modulus or hysteresis loss factor leads to a reduction of p_c corresponding to f_{\min} . The increased elastic modulus, however, commonly has the effect of decreasing the hysteresis loss factor. As a result, the relation of p_c to the modulus of elasticity proves to be more complex than that given by formula (2.16).

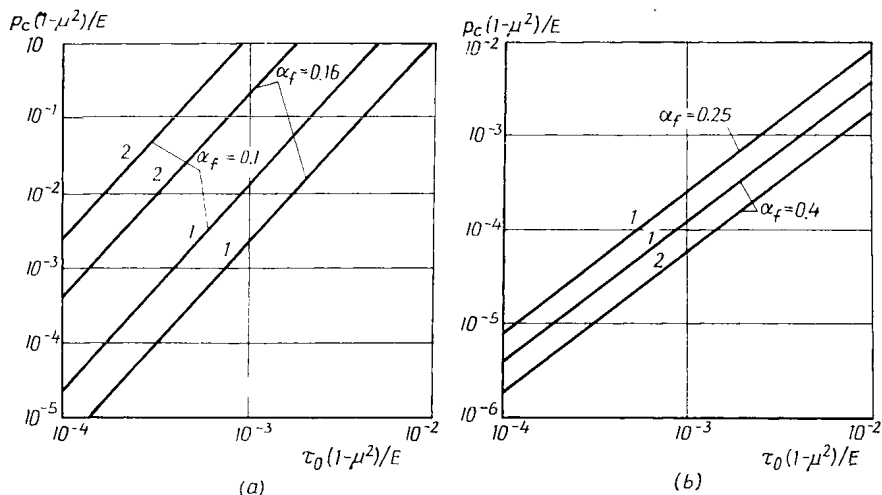


Fig. 2.5. Relationship between values of $\frac{p_c(1-\mu^2)}{E}$, corresponding to f_{\min} , and $\frac{\tau_0(1-\mu^2)}{E}$

1— $\Delta = 0.15$; 2— $\Delta = 0.07$; (a) sparse contact; (b) dense contact

The minimum coefficient of external friction is

$$f_{\min} = \frac{1.5\tau_0^{1/2}\alpha_f^{1/2}(1-\mu^2)^{1/2}}{E^{1/2}} + \beta \quad (2.17)$$

Thus, sparse elastic contact renders the minimum coefficient of external friction independent of the magnitude of the applied normal load; the coefficient is determined by the operating conditions of the sliding pair (τ_0 and β) and the mechanical properties of the material of the less rigid component in this pair.

The variation of the minimum coefficient of friction with $\frac{\tau_0(1-\mu^2)}{E}$ at different values of the effective hysteresis loss factor is shown graphically in Fig. 2.6. The frictional constant β has a marked effect on the value of the minimum coefficient of external friction. The given formulas hold true for the coefficient of external static friction and also for the coefficient of sliding friction under conditions where the sliding speed has little effect on the parameters entering into the formulas.

Dense elastic contact occurs at contour pressures higher than those found from formula (2.10), that is, when the number of contacting asperities is equal to the number of asperities in the contour area. Under the sparse-contact conditions, a closer approach causes the contact area to grow, mainly owing to an increase in the total

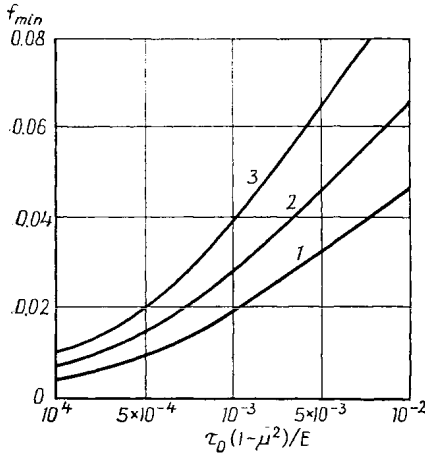


Fig. 2.6. Variation of f_{\min} with $\frac{\tau_0}{E}$
 $1-\alpha_f = 0.1$; $2-\alpha_f = 0.2$; $3-\alpha_f = 0.4$

number of contact spots, resulting from the asperities progressively coming into contact [48], and partly owing to the enlarging of separate contact spots; in contrast, under dense contact conditions the contact area increases owing to the growth in the size of separate contact spots only.

The coefficient of external static friction

$$f = \frac{2.4\tau_0(1-\mu^2)v^{1/2}}{E[v\varepsilon - (v-1)\varepsilon_d]^{1/2}} \times \left(\frac{r}{R_{\max}}\right)^{1/2} + \beta + \frac{0.2\alpha_f}{v^{1/2}} \left(\frac{R_{\max}}{r}\right)^{1/2} [v\varepsilon - (v-1)\varepsilon_d]^{1/2} \quad (2.18)$$

where ε_d = approach effective at the moment all the asperities have come into contact.

The value of ε_d as dependent on the parameters of the bearing-area curve is found [48] by the formula

$$\varepsilon_d = \frac{1}{\frac{1}{(bv)^{v-1}}} \quad (2.19)$$

In the dense contact area the value of the coefficient of friction will be a minimum with

$$\frac{h_m}{r} = \frac{1.2\tau_0(1-\mu^2)}{\alpha_f E} \quad (2.20)$$

where h_m = mean proximity, defined as

$$h_m = \frac{R_{\max}}{v} [v\varepsilon - (v-1)\varepsilon_d] \quad (2.21)$$

The contour pressure corresponding to the minimum coefficient of static friction in the area of elastic dense contact will be

$$p_c = \frac{0.25r}{v^{3/2}R_{\max}} \left(\frac{1-\mu^2}{E}\right)^{1/2} \left(\frac{\tau_0}{\alpha_f}\right)^{3/2} \quad (2.22)$$

For the most typical classes of surface roughness, that is, with $v = 2$ and $b = 2$,

$$p_c = 0.09 \frac{r}{R_{\max}} \left(\frac{1-\mu^2}{E}\right)^{1/2} \left(\frac{\tau_0}{\alpha_f}\right)^{3/2} \quad (2.23)$$

Formulas (2.15) and (2.23) lead to the conclusion that during sparse contact as compared with dense contact the contour pressures corresponding to the minimum value of the coefficient of static friction are more strongly dependent on the surface roughness, operating conditions and mechanical properties of the softer material in the sliding pair. The relationship between the contour pressure, corresponding to the minimum coefficient of friction, and $\frac{\tau_0(1-\mu^2)}{E}$ at various values of α in sparse contact is graphically shown in Fig. 2.5b.

In the dense elastic contact area, the minimum coefficient of static friction will be

$$f_{\min} = \frac{1.5\tau_0^{1/2}\alpha_f^{1/2}(1-\mu^2)^{1/2}}{E^{1/2}} + \beta \quad (2.24)$$

Thus, the minimum values of the coefficient of external static friction [see formulas (2.17) and (2.24)] coincide at identical values of τ_0 , α_f , μ and E in the areas of sparse and dense contact.

Plastic contact takes place when the average normal stresses in the areas of contact between surface asperities reach the values of Brinell hardness for the material being deformed. This condition will hold at penetrations

$$\frac{h}{r} = 5.4(1-\mu^2)^2 \left(\frac{HB}{E}\right)^2 \quad (2.25)$$

Using formula (2.25), we shall obtain the magnitude of the contour pressure that causes plastic contact:

$$p_c \geq \frac{5.4^v}{2\Delta^v} \frac{HB^{2v+1}(1-\mu^2)^{2v}}{E^{2v}} \quad (2.26)$$

For the surface finishes extensively used in engineering

$$p_c \geq 14.5 \frac{1}{\Delta^2} \frac{HB^5(1-\mu^2)^4}{E^4} \quad (2.27)$$

The relation between $\frac{p_c}{HB}$ and Δ at various $\frac{HB(1-\mu^2)}{E}$ ratios is represented in Fig. 2.7. It is apparent that plastic contact occurs at relatively low contour pressures for surfaces finished coarser than the 8th class of surface roughness. With better finishes, the contour pressure giving rise to plastic deformations in the contact area grows significantly, reaching large magnitudes for the 10th and higher classes of surface roughness.

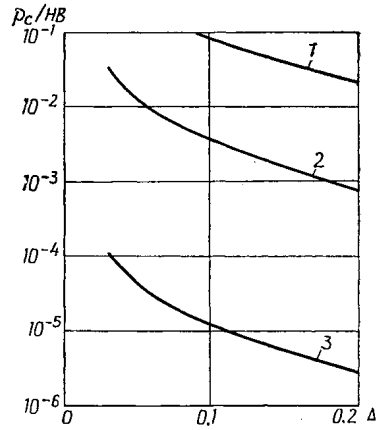


Fig. 2.7. Relationship between p_c and Δ

1 — $\frac{HB}{E} = 0.1$; $\mu = 0.5$; 2 — $\frac{HB}{E} = 0.05$, $\mu = 0.5$; 3 — $\frac{HB}{E} = 0.01$, $\mu = 0.3$

Because of their differing heights, some of the asperities, having penetrated deeper than according to formula (2.27), deform the material of the mating part plastically; the irregularities that penetrate to a smaller depth than that given by formula (2.9) deform the material elastically, and the irregularities whose penetration varies within the range given by

$$2.4(1-\mu^2)^2 \left(\frac{HB}{E} \right)^2 \leq \frac{h}{r} \leq 5.4(1-\mu^2)^2 \left(\frac{HB}{E} \right)^2 \quad (2.28)$$

deform the material elastically-plastically. Thus, no ideal plastic contact of rough solid bodies can take place. Calculations show, however, that with contacting surfaces of a lower than the 9th class of surface roughness, which deform each other plastically over a part of the contact area, the irregularities deforming the material elastically-plastically contribute to the interaction of solids insignificantly as compared with the irregularities that deform the material plastically. Analysis indicates [see formulas (2.10) and (2.11)] that surfaces finished to the 10th class of roughness normally work within the range of elastic and elastic-plastic deformations in the contact area. Therefore, to a first approximation, it can be concluded that once the magnitudes of the contour pressures determined by formulas (2.26) and (2.27) are reached, an ideally plastic contact takes place. The contact at plastic deformations can be either sparse or dense.

Sparse plastic contact occurs at contour pressures that satisfy the following condition [47]

$$\frac{14.5}{\Delta^2} \left[\frac{HB(1-\mu^2)}{E} \right]^4 \leq \frac{p_c}{HB} \leq \frac{0.5}{(\nu B^{1/\nu})^{\frac{\nu}{\nu-1}}} \quad (2.29)$$

or, for the most common surface finishes

$$\frac{14.5}{\Delta^2} \left[\frac{HB(1-\mu^2)}{E} \right]^4 \leq \frac{p_c}{HB} \leq 0.062$$

During sparse plastic contact, the force of external static friction is equal in magnitude to the resistance that results from the ploughing of the surface of the softer component in the sliding pair by the penetrating asperities and also to the resistance caused by molecular interactions in the real contact areas [36].

The coefficient of external static friction at plastic deformations in the contact areas is

$$f = \frac{\tau_0}{HB} + \beta + 0.55\nu(\nu-1) k_1 \left(\frac{h}{r} \right)^{1/2} \quad (2.30)$$

For the surface finishes used in engineering most extensively

$$f = \frac{\tau_0}{HB} + \beta + 0.44 \left(\frac{h}{r} \right)^{1/2} \quad (2.31)$$

Thus, with plastic deformations in the contact areas the molecular component of the coefficient of external friction is independent of the approach between the mating surfaces of solid bodies. The mecha-

nical component of the coefficient of friction grows with the approach. Therefore, the total coefficient of external static friction increases with the penetration in the contact areas during plastic deformation.

As the approach varies over a wide range, the coefficient of friction passes through a minimum. With materials deformable only elastically, this minimum depends on the ratio of the molecular component to the mechanical component. With materials deformable both elastically and plastically, the minimum coefficient of friction results from the transition of elastic deformations in the contact areas to plastic-elastic and purely plastic deformations. For such materials the mechanical component of the coefficient of friction is small during elastic deformations in the contact areas, while the molecular component, as it follows from the formula, decreases with greater penetrations. This component remains invariable during plastic deformations, whereas the mechanical component grows larger. Thus, in the portions of the contact area where elastic-plastic deformations take place, that is, in the penetration areas determined by formula (2.28), the coefficient of friction passes through a minimum and then grows with further penetration over the areas of plastic deformations. The exact value of the penetration at which the coefficient of friction is at its minimum cannot possibly be found, because the interaction of solids in the course of plastic deformation within the contact area is not yet clearly understood. To a first approximation, this penetration may be considered to be the arithmetic mean of the penetrations corresponding to the transition from elastic deformations to elastic-plastic deformations and from the latter to plastic deformations, that is, the minimum coefficient of friction for plastically deformable materials occurs at penetrations

$$\frac{h}{r} = 3.9 (1 - \mu^2)^2 \left(\frac{HB}{E} \right)^2 \quad (2.32)$$

For the most frequently used engineering surface-roughness classes the contour pressures causing such penetrations will be

$$\frac{p_c}{HB} = 7.5 \frac{1}{\Delta^2} \left[\frac{(1 - \mu^2) HB}{E} \right]^4 \quad (2.33)$$

Figure 2.8 presents a graph showing variation in the $\frac{p_c}{HB}$ ratio with Δ at various values of $\frac{HB}{E} (1 - \mu^2)$ for a plastically deformable material of the softer component in a sliding pair at the minimum coefficient of friction.

The minimum value of the coefficient of friction under these conditions will be

$$f_{\min} = \frac{\tau_0}{HB} + \beta + 0.9 (1 - \mu^2)^2 \left(\frac{HB'}{E} \right)^2 \quad (2.34)$$

From formula (2.34) it follows that with materials for the softer member of the sliding pair that have a high modulus of elasticity, for example, with metals having $\frac{HB}{E} \approx 0.01$, the mechanical component in the minimum coefficient of friction can usually be ignored as compared with the molecular component. Thus, the minimum coefficient of friction at the penetrations determined by equation (2.32) is equal, under these conditions, to the molecular component of the coefficient of external friction.

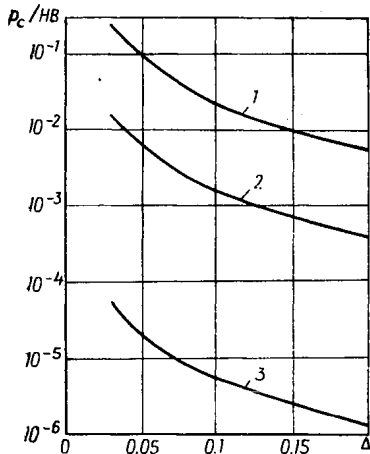


Fig. 2.8. $\frac{P_c}{HB}$, corresponding to minimum coefficient of friction for materials with high elastic modulus, as a function of Δ
 1— $\frac{HB}{E} = 0.1$, $\mu = 0.5$; 2— $\frac{HB}{E} = 0.05$, $\mu = 0.5$; 3— $\frac{HB}{E} = 0.01$, $\mu = 0.3$

of the coefficient of friction [46] is given by

$$\frac{P_c}{HB} = \left[\frac{f_{mi}}{0.55\nu(\nu-1)k_1} \right]^{2\nu} \frac{1}{\Delta^\nu} \quad (2.36)$$

For the most common engineering surface finishes

$$\frac{P_c}{HB} = \frac{2.8 \times 10^{-3} f_{mi}}{\Delta^2} \quad (2.37)$$

Formula (2.37) shows that the contour pressure conforming to the condition $f_{mi} = f_{mc}$ greatly depends on the surface roughness; namely, it grows with decreasing roughness.

Plastic dense contact takes place at contour pressures exceeding the values obtained by formula (2.29). At the area of plastic dense contact the coefficient of external static friction is given by

$$f = \frac{\tau_0}{HB} + \beta + \frac{0.54}{\sqrt{1/2}} \left(\frac{h}{r} \right)^{1/2} \left[\nu - (\nu-1) \frac{h_d}{h} \right]^{1/2} \quad (2.38)$$

In some engineering applications of tribological joints, it is essential to know the penetrations and the corresponding contour pressures at which the molecular component of the coefficient of external friction is equal to the mechanical component. This condition holds, as follows from formula (2.31), at the penetrations

$$\frac{h}{r} = 0.23 f_{mi} \quad (2.35)$$

Thus, even with the maximum possible value of the molecular component of the friction coefficient at plastic contact, $f_{mi} = 0.2$, it will be equal to the mechanical component at $\frac{h}{r} \approx 0.046$, that is, at relatively small penetrations.

The contour pressure at equal molecular and mechanical components

where h_d = approach corresponding to the transition from sparse contact to dense contact.

Plastic dense contact can occur in heavily loaded movable joints, in interference-fit joints, in packings, and the like.

2.3. FACTORS AFFECTING THE COEFFICIENT OF EXTERNAL STATIC FRICTION

The coefficient of external static friction is a complex function of the operating conditions of the sliding pair; it depends specifically on the presence or absence of a boundary-lubrication film, the magnitude of the contour pressure, the mechanical properties of the materials used, and the roughness of the mating surfaces. The contour pressure arising between rubbing bodies to a great extent depends on the design of the joint. Therefore, this design also affects the coefficient of external static friction.

2.3.1. Contour Pressure

The contour pressure in a tribological joint greatly depends on the normal load applied to the joint. Some authors [4, 50, 64, 69] indicated a decrease, while others [3, 6, 34, 51], an increase in f with increased normal load. Several investigators [16, 26, 33, 35, 54] showed that with variation of normal load over a wide range, the transition of the coefficient of friction through a minimum takes place. The last phenomenon is a general rule, and the first two are particular cases.

Depending on the design of a joint, identical normal loads can result in differing contour pressures; for this reason, analysis of the variation in the coefficient of external static friction with the normal load is advisable to carry out by using the contour pressure, which is the ratio of the normal load to the contour area of contact, rather than the normal load itself.

According to the molecular-mechanical theory of friction the variation of the coefficient of external static friction with contour pressure is determined by the type of deformation at the real contact spots.

Elastic contact. Substituting into formula (2.12) the value of the approach, we obtain the relationship between the coefficient of external static friction and the contour pressure in elastic sparse contact:

$$f = \frac{2.4\tau_0}{\frac{1}{p_c^{2v+1}}} \left[\frac{1-\mu^2}{v(v-1)k_1 5^{1/2v} E} \right]^{\frac{2v}{2v+1}} \frac{1}{\Delta^{\frac{v}{2v+1}}} + \beta$$

$$+ \frac{0.4\alpha_f}{v^2-1} \left[\frac{5p_c(1-\mu^2)}{(k_1 v)^{2v+2}(v-1)E} \right]^{\frac{1}{2v+1}} \Delta^{\frac{v}{2v+1}} \quad (2.39)$$

For the most typical surface finishes

$$f = \frac{2.1\tau_0}{p_c^{0.2}} \left(\frac{1-\mu^2}{E} \right)^{0.8} \frac{1}{\Delta^{0.4}} + \beta + 0.24\alpha_f p_c^{0.2} \left(\frac{1-\mu^2}{E} \right)^{0.2} \Delta^{0.4} \quad (2.40)$$

If the contour pressure rises during elastic contact, the molecular component of the coefficient of friction decreases and the mechanical component increases; as a result, the variation of the total coefficient of friction will in this case depend on the mutual proportion of these components.

The minimum takes place at the contour pressures determined by formula (2.15). The variation of the coefficient of friction with contour pressure at $\beta = 0.05$, $\Delta = 0.5$, $\nu = 2$, $b = 2$ and $\frac{\tau_0 (1-\mu^2)}{E} = 10^{-3}$ is shown in Fig. 2.9a. From Figure 2.9a and formulas (2.39)

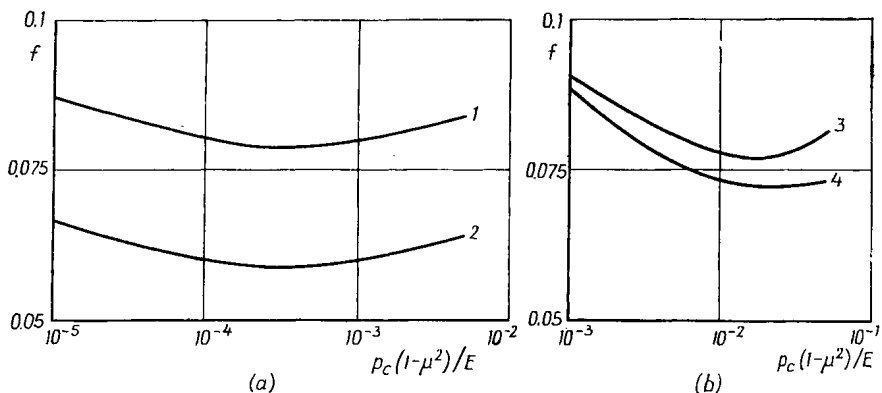


Fig. 2.9. Relationship between f and p_c for elastic dense contact (a) and sparse contact (b)

1— $\alpha_f = 0.4$; 2— $\alpha_f = 0.25$; 3— $\beta = 0.05$; 4— $\beta = 0.03$

and (2.40) it follows that the minimum coefficient of friction is possible only when the values of τ_0 and β are small, and the values of α_f of the Δ complex (see Fig. 2.5) are sufficiently large, that is, when the values of the molecular and the mechanical component are close to each other. This condition is normally satisfied with adequate boundary lubrication, when the softer component of the sliding pair exhibits a low elastic modulus (for instance, when it is made of rubber or plastic), whereas the harder component has a sufficiently rough surface. If the material of the softer rubbing member has a high elastic modulus, then within the range of contour pressures lower than those determined by formula (2.33) the coefficient of friction will decrease. As the contour pressures rise in excess of these magnitudes, an increase in the coefficient of friction can be expected during elastic-plastic and plastic contacts. With increasing contact pressure, the minimum of the coefficient of friction shifts towards the origin of coordinates. In the sparse-contact region, however, no

marked variation in the coefficient of friction with the contour pressure takes place.

During elastic dense contact the coefficient of external static friction, as follows from formula (2.18), varies with the contour pressure according to the following relationship [47]:

$$f = \frac{1.4\tau_0(1-\mu^2)^{2/3}}{E^{2/3}p_c^{1/3}} \left(\frac{r}{R_{\max}} \right)^{1/3} + \beta + \frac{0.35\alpha_f p_c^{1/3}(1-\mu^2)^{1/3}}{E^{1/3}} \left(\frac{R_{\max}}{r} \right)^{1/3} \quad (2.41)$$

The coefficient of friction as a function of the ratio of the contour pressure to the elastic modulus is represented graphically in Fig. 2.9b. Calculations are made for $\beta = 0.05$, $\beta = 0.03$, $\alpha_f = 0.4$, $\Delta = 0.05$ and $\frac{\tau_0(1-\mu^2)}{E} = 10^{-3}$. During dense elastic contact, the coefficient of external static friction changes with the contour pressure more intensively than during sparse elastic contact (Fig. 2.9). In the general case, the coefficient of external friction during dense elastic contact passes through a minimum as the pressure increases.

The contour pressure corresponding to the minimum coefficient of friction is found by formula (2.22). The minimum value of the coefficient of friction during elastic dense contact is only characteristic of materials having a low elastic modulus. For materials of a high elastic modulus (metals) the state of density during elastic deformations is not reachable.

Plastic contact. Sparse plastic contact occurs at contour pressures determined by formula (2.29). The molecular component of the coefficient of friction in the plastic contact conditions does not depend on the contour pressure. The mechanical component, as follows from formula (2.30), rises with increasing contour pressure. The total coefficient of friction varies with the contour pressure in the following way:

$$f = \frac{\tau_n}{HB} + 0.55\nu(\nu-1)k_1\Delta^{1/2} \left(\frac{2p_c}{HB} \right)^{1/2\nu} \quad (2.42)$$

or, for the most typical engineering surface finishes

$$f = \frac{\tau_n}{HB} + 0.44\Delta^{1/2} \left(\frac{2p_c}{HB} \right)^{1/4} \quad (2.43)$$

During plastic sparse contact, the coefficient of friction rises but little with the contour pressure. A graph showing the relationships between the coefficient of friction and the contour pressure is given in Fig. 2.10a. It is apparent from formula (2.43) that for surfaces with smaller roughness values, the coefficient of friction in identical conditions varies with the contour pressure less intensively. As a rule, ν is inversely related to the surface roughness; hence, the coefficient of friction varies still less intensively with the contour pressure.

Dense plastic contact takes place at pressures

$$\frac{p_c}{HB} \geq \frac{0.5}{(vb^{1/v})^{\frac{v}{v-1}}} \quad (2.44)$$

As with the sparse contact, the variation of the coefficient of external friction is due to that of the mechanical component. The following relationship between the coefficient of friction and the contour pressure can be derived from formula (2.38):

$$f = \frac{\tau_n}{HB} + 0.76 \left(\frac{R_{\max}}{r} \right)^{1/2} \left(\frac{p_c}{HB} \right)^{1/2} \quad (2.45)$$

Comparison between expressions (2.43) and (2.45) shows that the coefficient of friction is more responsive to variations of the contour

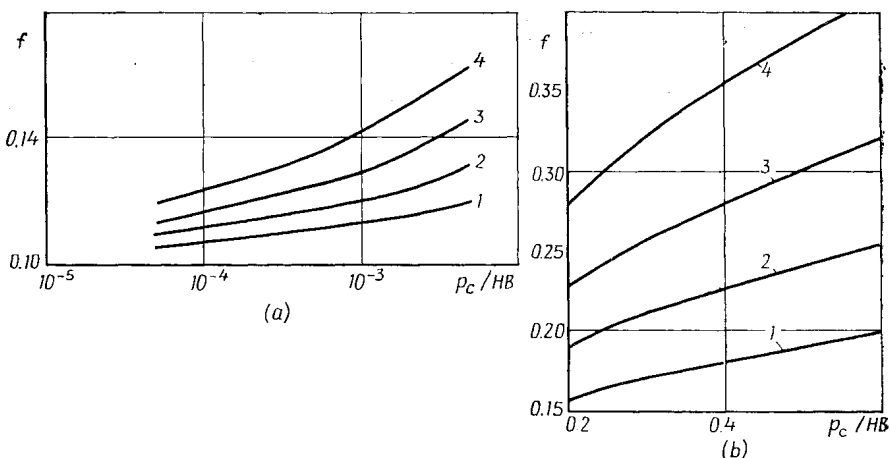


Fig. 2.10. Relationship between f and p_c during plastic sparse contact (a) and dense contact (b) at $f_{m1} = 0.1$

1— $\Delta = 0.02$; 2— $\Delta = 0.05$; 3— $\Delta = 0.1$; 4— $\Delta = 0.2$

pressure during plastic dense contact than during sparse contact. The coefficient of friction as a function of the contour pressure is graphically shown in Fig. 2.10b. As was indicated before, during elastic contact of rubbing members, in which the softer member has a low elastic modulus, the coefficient of friction generally passes through a minimum with an increase in the contour pressure. A similar relationship holds for the softer rubbing member made from a metal. In these conditions, the coefficient of friction decreases owing to a decrease in its molecular component during elastic contact and increases owing to the mechanical component during plastic contact. Hence, during the external friction of solids, the general law governing the variation of the coefficient of friction is that the latter passes through a minimum with an increase in the contour pressure. The conditions in which the coefficient of external friction rises or

decreases are determined as dependent on the parameters of operation for a sliding pair (see above).

Thus, the contradictions among various authors in interpreting the relationship between the coefficient of friction and the normal load are resolved by the molecular-mechanical theory of external friction on the basis of the interaction of solids during deformations of various types in the real contact areas.

2.3.2. Surface Roughness

Dissimilar hardness of solids in contact gives rise to penetration of the harder asperities into the surface of the softer body. The deformation of the harder body is substantially smaller than that of the softer body and can be neglected. The surface roughness of the harder body should, therefore, be taken into account when the effect of roughness on the interaction of solids is considered [18].

Distinction is made between the original roughness and the developed, or steady-state roughness [15, 17, 22]. By the original roughness is meant the surface roughness of a solid, obtained by machining. The steady-state roughness develops on the surfaces of the contacting parts as they slide against each other; it depends on the joint's operating conditions. Setting aside the consideration of the mechanism of formation of the steady-state roughness, let us consider the basic relationships between the coefficient of external static friction and surface topography.

It should be emphasized that the effect of distribution of the material across the surface layer of solids on the coefficient of external friction is of a very complex nature. The material distribution through the surface layer is estimated by the distribution of irregularities with height (the bearing-area curve parameters b and v) and by the absolute dimensions of the irregularities (parameters R_{\max} , r , R_z , and others). A rigorous theoretical relationship between the parameters of the bearing-area curve and the parameters R_{\max} and r is not yet obtained. Because they vary insignificantly for a sufficiently wide range of surface finishes, the parameters b and v can be assumed to be invariable in assessing the variation of the coefficient of friction with surface roughness.

It has been proposed recently [17] to assess the surface roughness by a complex parameter Δ , which is thought to characterize surface topography more adequately (see Ch. 1).

The variation of the coefficient of friction with surface topography is greatly influenced by the character of deformation in the real contact areas. Let us consider in more detail the relation between the coefficient of friction and surface roughness for the elastic and plastic types of contact.

Elastic contact. During elastic sparse contact the coefficient of friction is calculated by formula (2.39) or, approximately, by for-

mula (2.40). Formula (2.39) may be written in the following form:

$$f = \frac{A'}{\Delta^{\frac{v}{2v+1}}} + \beta + B' \Delta^{\frac{v}{2v+1}} \quad (2.46)$$

It is apparent from formula (2.46) that with the increasing complex parameter the molecular component decreases, and the mechanical component grows. Therefore, an increase in the complex parameter can cause the coefficient of friction, depending on the ratio of the components, to increase, or to diminish, or else, in the general case,

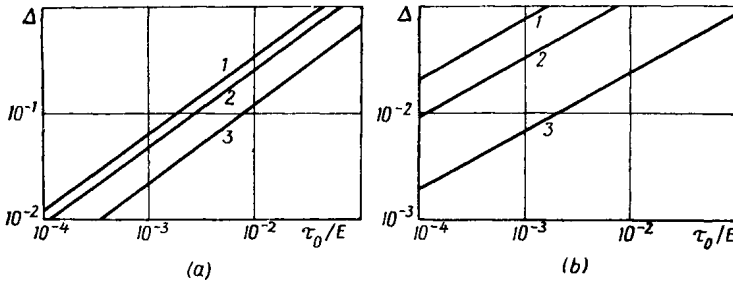


Fig. 2.11. Variation of Δ with $\frac{\tau_0}{E}$ during dense contact (a) and sparse contact (b)

$$1 - \frac{\tau_0}{p_c} = 0.1; 2 - \frac{\tau_0}{p_c} = 0.05; 3 - \frac{\tau_0}{p_c} = 0.01$$

to pass through a minimum. Calculations show that the value of the complex parameter corresponding to the minimum of the coefficient of friction is given by

$$\Delta = \frac{15\tau_0^{5/4} (1-\mu^2)^{3/4}}{p_c^{1/2} E^{3/4} \alpha_f^{5/4}} \quad (2.47)$$

The surface roughness corresponding to the minimum coefficient of friction is referred to as the optimum one.

The value of the complex parameter that corresponds to the minimum coefficient of friction is substantially affected by the characteristics determining the operation of a tribological joint (p_c , τ_0) and the mechanical properties of the softer rubbing member (α_f , E , and μ). The variation of the complex parameter, causing the minimum coefficient of friction, with the ratio $\frac{\tau_0 (1-\mu^2)}{E}$ at different p_c is shown in Fig. 2.11.

Substituting the value of the complex parameter into formula (2.39), we obtain the minimum coefficient of friction under invariable operating conditions of the joint and effective for the optimum surface roughness of the harder rubbing component

$$f = 1.5 \left[\frac{\tau_0 \alpha_f (1-\mu^2)}{E} \right]^{1/2} + \beta \quad (2.48)$$

It should be noted that the derived expressions are valid at lower contour pressures than those determined by formula (2.22).

This minimum value of the coefficient of external friction coincides with f_{\min} determined by the load. Hence, f_{\min} for a given tribological joint is independent of both the load and surface roughness and is determined by the materials of the rubbing members and the sliding conditions. During elastic dense contact the coefficient

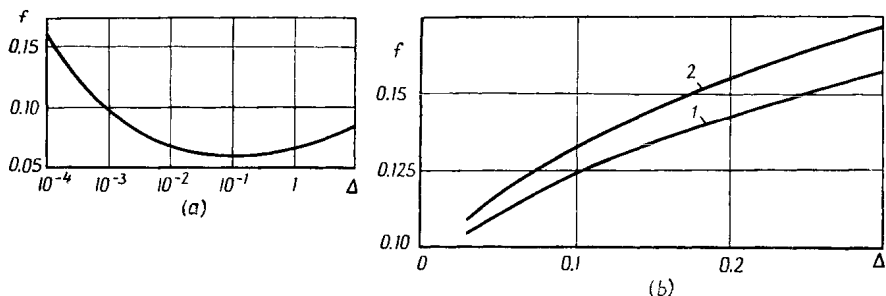


Fig. 2.12. Variation of coefficient of friction with surface roughness during sparse elastic contact (a) and plastic contact (b)

1— $\frac{p_c}{E} = 10^{-3}$; 2— $\frac{p_c}{HB} = 10^{-2}$

of friction depends, as follows from formula (2.48), on the ratio $\frac{R_{\max}}{R}$, the molecular component decreasing and the mechanical component increasing with the ratio. As in the case of sparse contact, such relationships are caused by an increase in the depth of the deformed surface layer at an invariable contour pressure. The parameter Δ , found similarly to that for sparse contact, is given by

$$\Delta = \frac{5.7\tau_0^{3/2}(1-\mu^2)^{1/2}}{E^{1/2}p_c\alpha_f^{3/2}} \quad (2.49)$$

Figure 2.11b presents the variation of Δ , corresponding to the minimum coefficient of friction, with $\frac{\tau_0}{E}$. Calculations are carried out for $\mu = 0.5$, $\alpha_f = 0.4$, $b = 2$, and $\nu = 2$. The coefficient of friction effective at the optimum roughness during dense elastic contact coincides with the minimum coefficient determined as a function of the contour pressure and the depth of penetration. The variation of the coefficient of friction with surface roughness is shown in Fig. 2.12a. Calculations are made by formula (2.40) for $\frac{\tau_0}{E} = 5 \times 10^{-4}$; $\frac{p_c}{E} = 10^{-3}$; $\alpha_f = 0.25$, $\mu = 0.5$, and $\beta = 0.05$.

It should be kept in mind that formulas (2.48) and (2.49) hold true when the softer rubbing component has a low elastic modulus. If this component is made of a high-modulus material, then the

coefficient of friction will decrease with roughness. For surfaces finished to a very small roughness ($R_z < 0.2 \mu\text{m}$), however, the coefficient of friction can rise because the area of the interaction of solids due to molecular interactions will substantially exceed the real contact area.

Plastic sparse contact. During plastic deformations in the real contact areas, the molecular component of the coefficient of external friction does not depend on surface topography. The mechanical component, as follows from formula (2.42), grows with the complex parameter Δ . Thus, during plastic sparse contact the coefficient of friction rises with surface roughness. The relationship between the coefficient of friction and Δ at various p_c is illustrated in Fig. 2.12*b*. Calculations are performed by formula (2.43) at $f_{ml} = 0.08$. Within the range of contour pressures near those determined by formula (2.33) for materials of high elastic modulus, the coefficient of friction is capable of passing through a minimum if the complex parameter varies considerably. This minimum is caused by the transition from elastic to elastic-plastic and purely plastic deformations with increasing roughness. The stated relationships are derived without regard to the effect of roughness on the frictional constants τ_0 and β of the surface and are, therefore, approximate. However, they explain satisfactorily the results of many experiments [17, 18, 53]. Consequently, they may be used for the calculation of the coefficient of friction as a function of surface roughness with a sufficient accuracy.

2.3.3. Mechanical Properties of Contacting Materials

The surface layers of the softer member in a rubbing pair are more deformable than those on the harder member; for this reason, the softer number is expected to determine the coefficient of external friction. This dependence is very complex: the mechanical properties of the softer member can be altered through either replacement or special treatment (strengthening, hardening, or the like) of its material, which obviously will affect the frictional parameters τ_0 and β . The relationships between these parameters and the mechanical properties of different materials are yet unclear. In some cases, however (for instance in boundary-lubricated conditions), the variation of the mechanical properties of the softer rubbing member does not affect markedly these parameters, and they may be considered constants. For this reason, the relationships between the coefficient of friction and the mechanical properties of the softer rubbing component in a sliding pair will be given for the elastic and plastic contact conditions at invariable frictional parameters (τ_0 and β), contour pressures, and surface roughness.

Elastic sparse contact. The characteristic by which comparison is made is the elastic modulus. The molecular component of the

coefficient of friction for the most typical surface finishes

$$f_{ml} = \frac{2.1\tau_0}{p_c^{0.2}\Delta^{0.4}} \left(\frac{1-\mu^2}{E} \right)^{0.8} + \beta \quad (2.50)$$

decreases with an increase in the elastic modulus. The rate of change for f_{ml} depends on the value of the frictional parameter β . If β is small compared with the first term of formula (2.50), then the molecular component will vary inversely with $E^{0.8}$.

If

$$\beta \gg \frac{2.1\tau_0}{p_c^{0.2}\Delta^{0.4}} \left(\frac{1-\mu^2}{E} \right)^{0.8} \quad (2.51)$$

then the molecular component of the coefficient of friction practically does not vary with E . The decrease in the molecular component with higher values of E is due to a growth in the normal stresses at the contact spot, which results from the diminishing of the real area of contact. The reduction in this area with higher elastic moduli leads to a decrease in penetration and, consequently, a decrease in the mechanical component of the coefficient of friction (the coefficient of frictional hysteresis losses remaining invariable):

$$f_{mc} = 0.24\alpha_f p_c^{0.2} \left(\frac{1-\mu^2}{E} \right)^{0.2} \frac{1}{\Delta^{0.4}} \quad (2.52)$$

With increasing values of elastic modulus the coefficient of hysteresis losses usually diminishes. For this reason the mechanical component of the coefficient of friction will be very sensitive to the variation of the elastic modulus of the softer rubbing member. Thus, with an increase in the elastic modulus of the softer rubbing member, the coefficient of external friction decreases at the expense of both molecular and mechanical components. This reduction in f as a function of the elastic modulus was obtained experimentally [47, 49].

Elastic dense contact. A similar relationship is derived for the dense contact conditions [see formula (2.41)]. The function $f = \psi(E)$ for the sparse and dense contact conditions at various β is graphically represented in Fig. 2.13. Calculations were made for invariable $\frac{\tau_0}{E_0} = 2 \times 10^{-2}$, $\frac{p_c}{E_0} = 0.02$, $\Delta = 0.12$, $\mu = 0.5$ and $\alpha_f = 0.3$. The ratios E/E_0 , where E_0 is a reference elastic modulus, are plotted on the abscissa.

Plastic sparse contact. The characteristic by which comparison is made is the Brinell hardness number. The molecular component of the coefficient of friction

$$f_{ml} = \frac{\tau_0}{HB} + \beta \quad (2.53)$$

varies inversely with the material hardness. The decrease is marked if the frictional parameter β is smaller than the first term of formula (2.53). When $\beta \gg \frac{\tau_0}{HB}$, the molecular component practically does not vary with hardness.

The mechanical component decreases with growing hardness, because the depth of penetration of the asperities diminishes. Thus, the total value of the coefficient of external friction is inversely related to the hardness of the softer rubbing member during plastic

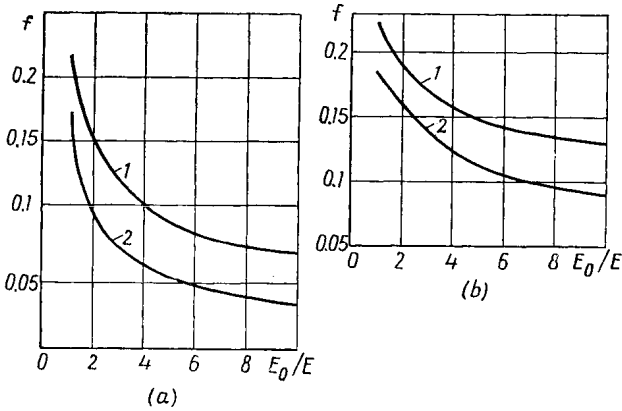


Fig. 2.13. Relationship between coefficient of friction and elastic modulus for sparse contact (a) and dense contact (b)
1— $\beta = 0.05$; 2— $\beta = 0.01$

sparse contact. The function $f = \psi(HB)$ is shown graphically in Fig. 2.14. Plotted along the abscissa is the ratio $\frac{HB_0}{HB}$, where HB_0

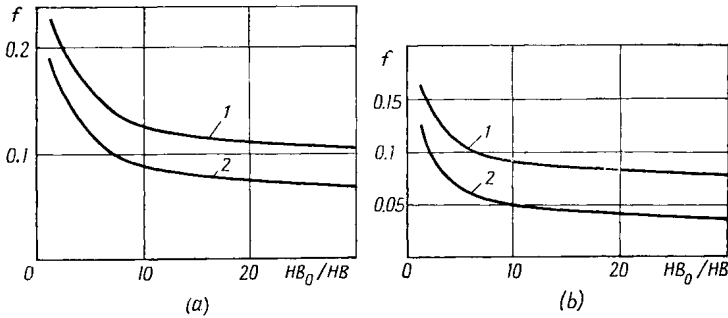


Fig. 2.14. Coefficient of external static friction vs hardness for sparse contact (a) and dense contact (b)
1— $\beta = 0.05$; 2— $\beta = 0.01$

is a suitable reference hardness number. Calculations were carried out with $\frac{\tau_0}{HB_0} = 0.1$, $p_c = 0.02HB_0$, and $\Delta = 0.1$. The higher the value of β , the less perceptibly the coefficient of external friction varies with hardness.

Plastic dense contact. In these contact conditions the coefficient of external friction varies with the material hardness in a similar way [see formula (2.45)].

The given relationships, though approximate, fit the results of experiments satisfactorily [7, 39, 46, 65].

2.3.4. Temperature of Solids in Contact

Let us consider the variation of the coefficient of external static friction with the temperature of rubbing bodies during plastic contact.

The rise of temperature brings about changes in both the molecular and the mechanical component of the coefficient of friction [38]. The character of variation of the molecular component is determined by the variation of the specific force of resistance to sliding (that is, tangential stress τ_n at the rubbing members' interface) and by the variation of the average normal stress at the contact. Using the concept of a third body, it can be stated that the tangential stress at the interface, caused by the viscosity of the third body, diminishes with rising temperature:

$$\tau_n = \tau_{n0} e^{-\gamma \Delta \vartheta} \quad (2.54)$$

where γ = temperature coefficient, τ_{n0} = value of τ_n at a certain constant reference temperature, and $\Delta \vartheta$ = variation of temperature.

During plastic contact, the average normal stress is equal to the Brinell hardness number which, depending on the temperature change, varies as follows [56, 57]:

$$HB = HB_0 e^{-\alpha \Delta \vartheta} \quad (2.55)$$

where HB_0 = hardness at a reference temperature, and α = temperature coefficient.

The values of α and γ are found experimentally by methods similar to those described below.

The molecular component of the coefficient of external static friction varies with the joint's operating temperature in accordance with the following relationship:

$$f_{ml} = \frac{\tau_{n0}}{HB_0} e^{(\alpha - \gamma) \Delta \vartheta} = f_{ml_0} e^{(\alpha - \gamma) \Delta \vartheta} \quad (2.56)$$

where f_{ml_0} = molecular component at a reference temperature.

Depending on the temperature variation, the molecular component can diminish, grow, or remain invariable.

According to the data by N. I. Amosov, under normal service conditions in air, external friction in closed tribological joints (the coefficient of mutual overlap is equal to unity) takes place at temperatures of $-150^\circ\text{C} \leq \vartheta \leq (0.1 \text{ to } 0.3) \vartheta_f$ where ϑ_f = fusion temperature. For joints with the coefficient of overlap much less than unity, external friction takes place in the temperature range of

$-40^{\circ}\text{C} < \vartheta < (0.2 \text{ to } 0.3) \vartheta_f$. At temperatures $\vartheta = (0.2 \text{ to } 0.3) \vartheta_f$, external friction ceases because an intense seizure of the rubbing bodies in the contact regions occurs.

Analysis shows that the influence of the variation in surface topography with increasing temperature on the mechanical component of the coefficient of friction can be neglected. In that case the changing temperature will affect the mechanical component through variation of the material hardness. Reduction in hardness with increasing temperature causes a greater penetration of asperities and thus, a rise in the mechanical component:

$$f_{mc} = f_{mc_0} e^{\frac{\alpha \Delta \vartheta}{2\nu}} \quad (2.57)$$

The total value of the coefficient of external static friction, as dependent on the operating temperature, will be

$$f = f_{ml_0} e^{\delta \Delta t} + f_{mc_0} e^{\frac{\alpha \Delta \vartheta}{2\nu}} \quad (2.58)$$

Hence, as a rule, the molecular component of the coefficient of external static friction decreases, and the mechanical component grows with the rising operating temperature. In general, the function $f = \psi(\theta)$ passes through a minimum during the variation of the joint's operating temperature within the range corresponding to the region of external friction.

2.4. METHODS FOR DETERMINING QUANTITIES REQUIRED FOR CALCULATION OF THE COEFFICIENT OF EXTERNAL STATIC FRICTION

The mechanical component of the coefficient of friction can be calculated accurately enough from the mechanical characteristics of the softer member in the sliding pair, the surface geometry of the harder member, and the magnitude of the contour pressure in the joint. The methods for calculating the molecular component from the characteristics of rubbing solids are not yet developed; for this reason, the component is determined experimentally.

A method for determining the molecular component of the coefficient of external friction and the frictional parameters α and β . The molecular component of the coefficient of external friction is generally given by

$$f_{ml} = \frac{\tau_n}{p_r} \quad (2.59)$$

or

$$f_{ml} = \frac{\tau_0}{p_r} + \beta \quad (2.60)$$

The molecular component for plastic contact ($p_r = HB$) should be determined experimentally. During elastic contact, the value of p_r is variable. The frictional parameters τ_0 and β , which are independent of the normal contact stress, can therefore be used for the calculation of the molecular component. Knowing the values of τ_0 and β , the calculation is made by the following formulas: for dense contact

$$f_{ml} = \frac{2.1\tau_0}{p_c^{0.2}} \left(\frac{1-\mu^2}{E} \right)^{0.8} \frac{1}{\Delta^{0.4}} + \beta \quad (2.61)$$

and for sparse contact

$$f_{ml} = \frac{1.4\tau_0(1-\mu^2)^{2/3}}{E^{2/3} p_c^{1/3}} \left(\frac{r}{R_{\max}} \right)^{1/3} + \beta \quad (2.62)$$

In determining the molecular component the following requirements have to be met: (1) the laboratory experimental conditions should be as close as possible to the actual operating conditions at the contact of the rubbing components; and (2) the average normal contact stresses with the laboratory model and with the real product should be equal, because the molecular component depends on the normal stress.

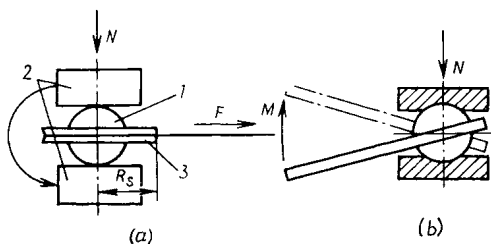


Fig. 2.15. Determining f_{ml} by means of a spherical indenter (a) and a cylindrical indenter (b)

The most extensive application has found the method described in [41]. The method satisfies the above requirements; it consists essentially in that the resistance to relative sliding, caused by the deformation of the surface layers (that is, the mechanical component of the frictional force), is eliminated or reduced to a negligible amount; f_{ml} is then found from the obtained magnitude of the molecular component of the frictional force. The method is implemented by squeezing an indenter I of a true spherical shape (Fig. 2.15a) between two flat and parallel blocks 2, rotating the indenter about its symmetry axis, and measuring the frictional force needed for the rotation. It is convenient to fix the indenter in a setting 3. The flat blocks are chosen in accordance with the requirements placed on specimens for the Brinell hardness tests, depending on the materials to be investigated and the diameter of the indenter. The indenters are either made specially for the test or selected, where possible, from ball bearings. The working surface of the blocks is processed according to the Brinell hardness of the material. If the hardness $HB < 35$, the blocks can be filed before the test with a fine-cut file. The surface of the blocks with $HB > 35$ needs to be polished.

The spherical indenter made of a harder material must have a surface finished to a high class of surface roughness (the 12th or 13th). The force of resistance to rotation is then practically equal (within 0.5 percent) to the molecular component of the frictional force. The load applied must be such as to ensure impression diameters of $0.064 \leq d/D \leq 0.6$. Taking into account that within this range of the impression diameters the average contact stress is invariable and equal to the Brinell hardness, and also that

$$N = 2\pi R_{sp} h HB \quad (2.63)$$

the loads necessary for the tests in the plastic contact conditions will vary over the range

$$0.126 \times 10^{-3} R_{sp}^2 HB \leq N \leq 1.26 R_{sp}^2 HB \quad (2.64)$$

where R_{sp} = radius of the spherical indenter.

The tangential stress caused by the measured force required to rotate the indenter about its symmetry axis normal to the working surfaces of the flat blocks is given by

$$\tau_n = \frac{3FR_s}{4\pi r_{im}^3} \quad (2.65)$$

and the molecular component of the coefficient of friction [see formula (2.59)] is given by

$$f_{ml} = \frac{3FR_s}{4Nr_{im}} \quad (2.65a)$$

where R_s = radius of the setting, and r_{im} = radius of impression.

The impression diameter can be measured with the aid of a magnifying glass suited to similar measurements in the Brinell hardness test, or with the aid of Model MIP-12 comparators or microscopes.

The values of the molecular component of the coefficient of friction for various materials in contact with a spherical indenter made of Grade IX-15 steel are given in Table 2.2.

In some cases f_{ml} can be found approximately by using a cylindrical indenter instead of a spherical one (Fig. 2.15b). The applied normal load must be taken so as to ensure the average contact pressures equal to HB . The tangential stress at the interface between a flat specimen and a cylinder, and also the molecular component of the coefficient of friction are calculated by the formulas

$$\tau_n = \frac{F_0 R_0}{2NR_{cl}} HB, \quad f_{ml} = \frac{F_0 R_0}{2NR_{cl}}$$

The drawback to this method is a lower accuracy due to likely misalignment between the specimens and the cylinder.

The frictional parameters τ_0 and β can be suitably found in rubbing test materials applied to different backings [46]. By determining the value of τ_n in one and the same sliding pair for at least two different magnitudes of the average normal stress and plotting a graph $\tau_n = \psi(p_r)$ as shown in Fig. 2.16 we find the values of τ_0 and β .

Table 2.2

Value of the molecular component of the coefficient of friction and frictional parameters τ_0 and β (after K. S. Lyapin)

Material	HB , kgf/mm ²	f_{ml}	τ_0 , kgf/mm ²	β
<i>Metals</i>				
Lead	3.3	0.140	0.274	0.057
	2.8	0.155	—	—
Silver	55	0.096	0.77	0.081
Aluminium	23	0.124	—	—
Copper	28.5	0.139	1.68	0.080
	40.0	0.125	1.8	
	52.0	0.115	1.82	
	85.0	0.100	1.70	
Nickel	70.0	0.123	0.49	0.116
	105.0	0.130	1.47	
	180.0	0.095	3.78	
Armco iron	70.0	0.139	—	—
	130.0	0.097	—	—
	65.0	0.160	—	—
Vanadium	110.0	0.103	—	—
Tantalum	78.0	0.115	2.42	0.084
Molybdenum	110.0	0.105	1.87	0.088
	186.0	0.095	2.79	0.080
	140.0	0.128	—	—
Tungsten	285.0	0.082	—	—
Niobium	32.0	0.142	0.896	0.114
Rhenium	105.0	0.095	—	—
Chromium	200.0	0.095	—	—
	100.0	0.135	1.50	0.120
Cadmium	23.0	0.096	0.943	0.055
Zinc	33.0	0.088	—	—
Magnesium	44.0	0.082	—	—
Titanium	128.0	0.100	2.82	0.078
Zirconium	190.0	0.085	—	—
	74.0	0.121		
Cobalt	130.0	0.092	—	—
	83.5	0.082	—	—

Table 2.2 (cont.)

Material	HB, kgf/mm ²	f_{ml}	τ_0 , kgf/mm ²	β
Antimony	27.0	0.127	0.73	0.100
Bismuth	7.70	0.175	0.454	0.116
Tin	4.40	0.170	0.449	0.068
Indium	0.80 0.60	0.200 0.260	0.107 —	0.066 —

Plastics (after K. S. Lyapin, V. S. Paramonov, and A. I. Smol'yakov)

Fluoroplastic	3.10	0.028	0.341	0.017
Polyethylene Grade ПЭВД	2.0 2.6	0.080 0.090	0.044 0.130	0.058 0.040
Polyethylene Grade ПЭНД	3.8	0.080	0.114	0.050
Polypropylene	3.70	0.380	0.011	0.035
Polycaprolactam	7.5	0.088	—	—
Light-coloured viniplast	12.0	0.091	0.372	0.06
Caprolon	13.0	0.065	0.195	0.05
Commercial capron	7.0	0.063	0.161	0.04
Polyamide Grade 68П	16.0	0.085	—	—
Plexiglass	16.0	0.220	—	—
Phenylon	31.0	0.065	—	—
Densified wood (unimpregnated)	—	—	0.050	0.061
Wood impregnated with industrial oil Grade 45	—	—	0.100	0.080
Wood impregnated with engine oil	—	—	0.025	0.076
Wood impregnated with fluoroplastic Grade Ф-4	—	—	0.70	0.074
Wood impregnated with ceresine	—	—	0.07	0.038
Wood impregnated with ceresine and stearic acid	—	—	0.135	0.028
Rubber	—	—	0.250	0.010
Hide:				
raw	—	—	$0.22 \cdot 10^{-4}$	0.016
dehaired	—	—	$0.20 \cdot 10^{-4}$	0.014
tanned	—	—	$1.7 \cdot 10^{-4}$	0.080

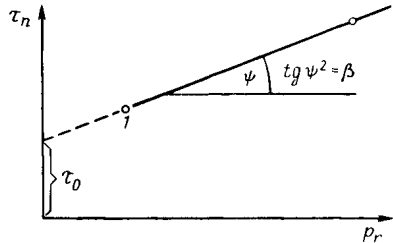
Bearing alloys

БН	25	0.102	—	—
Б83	24	0.150	—	—
ACC-6-5	—	—	1.0	0.065
A-20	—	—	1.6	0.050
Beryllium bronze	150	0.095	—	—

Table 2.2 (cont.)

Material	HB , kgf/mm ²	f_{ml}	τ_0 , kgf/mm ²	β
<i>Synthetic diamonds on various steels</i> (after A. I. Ershov)				
30XГCA	340	0.125	20.06	0.066
45	270	0.119	20.39	0.044
08X18H9T	159	0.15	3.18	0.130
40X	341	0.109	18.41	0.055
45	324	0.112	12.96	0.072

When the interchangeable-backing method is used for determining τ_n at different values of p_r on one material, a film of the material to be tested is applied to backings of various hardness. For convenient measurement the hardness of the backings should be higher than, or equal to, the hardness of the material. One value of τ_n can be found as is described above, by using plain flat specimens made from the material to be tested. To determine the second value of τ_n , it is essential to use composite specimens, that is, the film of the test material on a backing. The load is taken so as to ensure plastic deformation in the contact area. The film thickness should not exceed 10 μm in order to prevent the magnitude of the average contact stress from being appreciably affected by the test material's mechanical properties.

Fig. 2.16. τ_n and β as dependent on p_r

The values of τ_0 and β can be estimated roughly in the following way. First τ_n and p_r (from the formula $p_r = \frac{N}{\pi r^2_{im}}$) are determined during plastic contact; the normal load is then slightly relieved (by 15 to 20 percent), and these parameters are determined once more. From the found values of τ_n and p_r , the frictional constants τ_0 and β are obtained by plotting the graph $\tau_n = \psi(p_r)$. Because the values of p_r found as described are approximate, the parameters τ_0 and β will be derived from the graph $\tau_n = \psi(p_r)$ with some error. They may, however, be used for calculating the coefficient of friction to a first approximation.

In some cases, the above method for finding τ_0 and β is difficult to carry out. Then use can be made of rubbing pairs comprising a spherical (cylindrical) indenter and a plane, or two cylinders with crossed axes. From experiments with these models at two different loads in the elastic contact conditions, the molecular component of

the coefficient of friction is obtained and then from the following two equations

$$f_{ml_1} = \frac{\tau_0}{p_{r_1}} + \beta, \quad f_{ml_2} = \frac{\tau_0}{p_{r_2}} + \beta \quad (2.66)$$

the parameters τ_0 and β are determined. Where practicable, the molecular component is found for actual tribological joints, and τ_0 and β are calculated with the use of equation (2.66) and the Hertz contact pressure formula, or, for rough surfaces, the Demkin formulas (see Ch. 1).

The normal load that ensures elastic contact for a spherical indenter rubbing against a plane, with due regard for equation (2.8) and the Hertz relationship

$$h = 0.83 \sqrt[3]{\frac{N^2 (1-\mu^2)^2}{R_{sp} E^2}} \quad (2.67)$$

will be

$$N = 5R^2HB \left[\frac{HB(1-\mu^2)}{E} \right]^2 \quad (2.68)$$

For materials with a high elastic modulus at lighter loads on the spherical indenter than those found from formula (2.68), the mechanical component of the coefficient of friction may be neglected. From equations (2.66) it follows that with $f_{ml_1} > f_{ml_2}$

$$\tau_0 = \frac{2.6 (f_{ml_1} - f_{ml_2}) E^{2/3}}{(1-\mu^2)^{2/3} R_{sp}^{2/3}} \left(\frac{N_1^{1/3} N_2^{1/3}}{N_2^{1/3} - N_1^{1/3}} \right) \quad (2.69)$$

$$\beta = f_{ml_1} - \frac{6.6 (f_{ml_1} - f_{ml_2}) N_2^{1/3}}{N_2^{1/3} - N_1^{1/3}} \quad (2.70)$$

In equations (2.69) and (2.70) the subscripts 1 and 2 stand for the parameter values obtained from the first and the second experiment. The values of τ_0 and β determined by different methods under different working conditions are listed in Table 2.2.

Experimental techniques for determining surface topography parameters. Knowledge of the bearing-area curve parameters b and v is essential for calculating the coefficient of external friction, contour pressures, relationships between load and approach of the surfaces in contact, contact areas, and other contact characteristics. A method for determining these parameters from surface profile graphs is developed (see Ch. 1). This method, however, is time-consuming; moreover, the found values of b and v can be used for analysis of the frictional interaction of solids to a certain approximation only, because the parameters are found by the length of surface-irregularity sections, whereas contact occurs on the flanks of the irregularities.

The parameters b and v can be obtained experimentally [42], using the relation of approach between solids to the normal load

applied during plastic sparse contact:

$$h = R_{\max} \left(\frac{p_c}{bHB} \right)^{1/\nu} \quad (2.71)$$

If the values of h_1 and h_2 are found experimentally at two respective contour pressures p_{c_1} and p_{c_2} corresponding to plastic sparse contact [see formula (2.29)], then

$$\nu = \frac{\lg p_{c_2} - \lg p_{c_1}}{\lg h_2 - \lg h_1} \quad (2.72)$$

$$b = \frac{p_{c_i}}{HB} \left(\frac{R_{\max}}{h_i} \right)^\nu \quad (2.73)$$

To obtain the value of b , knowledge of R_{\max} is necessary. The value of R_{\max} can readily be found from a profile graph or chosen from Tables 1.6 and 1.7 with reference to the appropriate method of surface finishing. Besides, R_{\max} and consequently, b can be determined experimentally.

Experimental finding of b entails determining many other characteristics of surface topography. Analysis will show that practically all the formulas concerning the interaction of solids contain the complex parameter Δ . If the values of the coefficient of external static friction f_1 and f_2 are obtained experimentally at certain magnitudes p_{c_1} and p_{c_2} of the contour pressure during plastic sparse contact [see formula (2.29)], then, using equation (2.42), the complex parameter Δ can be expressed as

$$\Delta = \frac{(f_1 - f_2)^2 HB^{1/\nu}}{[0.55\nu(\nu - 1)k_1]^2 (p_{c_1}^{1/2\nu} - p_{c_2}^{1/2\nu})^2} \quad (2.74)$$

Substituting into this formula the values of ν , found by formula (2.72), and k_1 , found from the graph in Fig. 2.2, we calculate the parameter Δ .

With the known value of Δ , we can determine the effective curvature radius of asperities, using equation (2.71):

$$r = \frac{h_i}{i\Delta} \left(\frac{HB}{p_{c_i}} \right)^{1/\nu} \quad (2.75)$$

where h_i and p_{c_i} = values of approach and contour pressure taken from experiments for finding ν .

This method of determining the asperity curvature radius is substantially simpler and more accurate than that using profile traces [11, 22].

The value of r being known, the maximum height of surface irregularities, R_{\max} , can be found experimentally. To this end, the coefficients of friction f_3 and f_4 must be determined at certain contour pressures $p'_{c_1} > p'_{c_2}$ during plastic dense contact, that is, within the range of contour pressures higher than those determined by relationship (2.44). By applying the formula for calculating the coef-

ficient of external static friction we shall obtain

$$R_{\max} = \frac{1.7RHB(f_3 - f_4)^2}{(p'_{c_1}/2 - p'_{c_2}/2)^2} \quad (2.76)$$

Substituting the derived value into formula (2.73), we shall find the parameter b of the bearing-area curve.

Let us summarize the sequence of the experiments for determining the characteristics of surface topography. First the approach between the mating surfaces of solids is determined at two loads that correspond to contour pressures p_{c_1} and p_{c_2} causing plastic sparse contact. On applying the second load, the test specimens are set in sliding motion against each other, and the coefficient of sliding friction conforming to the contour pressures p_{c_2} and p'_{c_2} is found. The load is then increased so as to bring about the dense contact conditions, and the coefficient of friction is determined at two different pressures p'_{c_1} and p'_{c_2} . By the data obtained from five successive experiments, with the use of formulas (2.72) through (2.76), all the necessary characteristics of surface roughness are determined.

The values of the bearing-area curve parameters found from the known value of R_{\max} with the aid of formulas (2.72) and (2.73) coincide satisfactorily with the values calculated from surface profile graphs [42]. Methods for determining the contour pressure are dealt with in Ch. 1.

2.5. METHOD FOR CALCULATION OF THE COEFFICIENT OF FRICTION

The mechanical component of the coefficient of external friction can be calculated for the actual operating conditions of a sliding pair. The molecular component is calculated from the values of frictional parameters τ_0 and β obtained experimentally. Before calculating the coefficient of friction, one must have a clear notion of what type of deformation occurs in the contact areas and what type of contact (dense or sparse) takes place at a given contour pressure. Here two kinds of problems are encountered, to which we shall conventionally refer as direct and inverse. The direct problem calls for determining the coefficient of external friction by the given values of contour pressure, by the mechanical properties of the rubbing parts and by the molecular component of the coefficient of friction or the frictional parameters τ_0 and β . Alternatively, the inverse problem proceeds from the specified coefficient of friction and aims at the choice of operating conditions (that is, materials for the rubbing members and the type of lubricant, which are selected by the molecular component determined from the frictional parameters τ_0 and β); choice is also made of the surface roughness and the con-

tour pressures that ensure the given coefficient of friction for the selected materials.

The necessary calculations are advisable to make in the following sequence.

Direct problem. (1) Choose the mechanical properties of the rubbing members from the appropriate reference sources or find them experimentally.

(2) Determine the surface-roughness parameters, using Table 1.5 (for rough estimates) or the methods disclosed above.

(3) Find the values of τ_n and f_{ml} , using Table 2.2 or methods for their determining from the parameters τ_0 and β .

(4) Determine the contour pressure from the Hertz formulas, depending on the design of the joint (see Ch. 1).

(5) Using formulas (2.9) and (2.27) determine what type of deformation will take place in the contact areas.

(6) By formula (2.4) find out whether the external friction conditions will occur at the joint.

(7) With formulas (2.11) and (2.29) determine whether the contact is dense or sparse.

(8) Using the appropriate formula, calculate the coefficient of friction.

Inverse problem. (1) Select approximately from Table 2.2 the molecular component of the coefficient of friction and the materials that will suit the joint's operating conditions.

(2) Proceeding from the joint's design characteristics and the selected materials, determine the contour pressure by the Hertz relationships.

(3) Using formulas (2.9) and (2.27), roughly determine the type of deformation in the contact areas.

(4) Using formulas (2.11) and (2.29), determine whether the contact is dense or sparse.

(5) Depending on the obtained results, vary the parameters of surface roughness and the contour pressures so as not to exceed the limits of the established type of contact interaction, and make sure that the required value of the coefficient of friction is reached.

(6) Refine the value of the contour pressure on the basis of the derived data.

(7) By the obtained values of the complex parameter, choose the type of machining that ensures the required surface-roughness class.

Figures 2.17 through 2.21 give nomographs for each type of contact, which are designed to determine approximately the coefficient of friction.

The nomograph designed to determine the molecular component for elastic sparse contact by the known values of $\frac{\tau_0}{E} = 0.1$ at $\nu = 2$ and $b = 2$ is given in Fig. 2.17. By the specified values of $\frac{P_c}{E}$, the value of $f_{ml} - \beta$ is arrived at for a definite surface roughness in

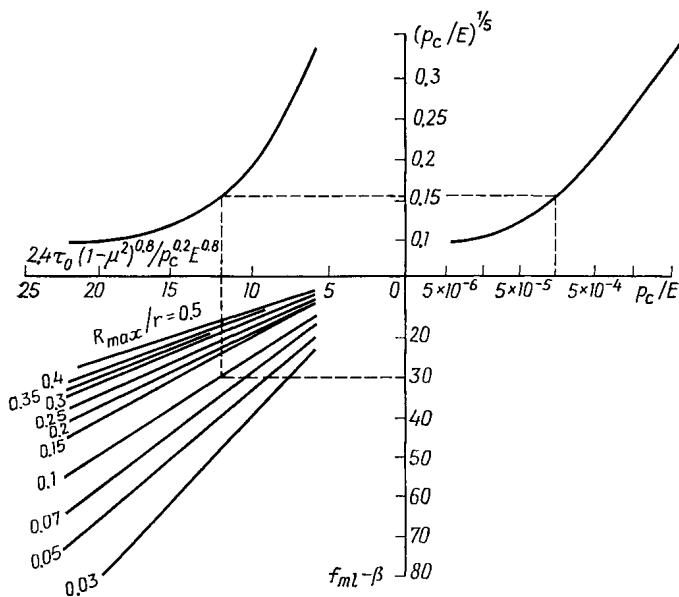


Fig. 2.17. Nomograph for determining the molecular component of the coefficient of friction

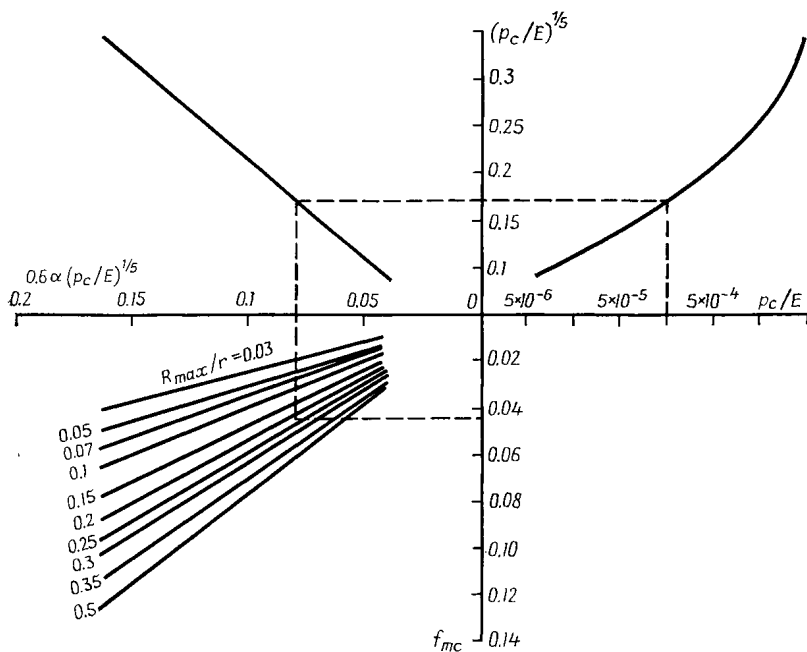


Fig. 2.18. Nomograph for determining the mechanical component of the coefficient of friction

the sequence indicated by the dash lines. The molecular component of the coefficient of friction is then found by the known value of β .

A nomograph for calculating the mechanical component of the coefficient of external friction is represented in Fig. 2.18. Here, the

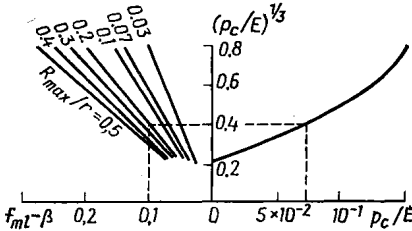


Fig. 2.19. Nomograph for determining the molecular component of the coefficient of friction during dense contact

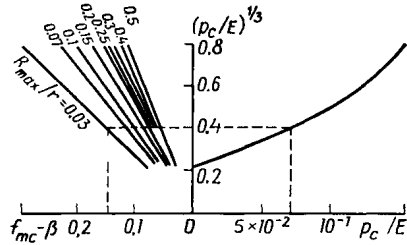


Fig. 2.20. Nomograph for determining the mechanical component of the coefficient of friction during dense contact

sequence indicated by the dash lines is followed for determining a conventional mechanical component at $\nu = 2$, $b = 2$, and $\alpha_f = 1$; multiplying this component by the hysteresis loss factor, we have f_{mc} for the material used.

Nomographs used to find the values of the molecular and mechanical components for elastic dense contact are given in Figs. 2.19 and 2.20. The sequence in which the necessary values are found is shown by the dash lines.

Figure 2.21 represents a nomograph for finding the mechanical component f_{mc} of the coefficient of friction by a given value of $\frac{p_c}{HB}$ at $\nu = 2$, $b = 2$. The sequence of operations is indicated by the dash lines. The total coefficient of friction is found by adding together the mechanical component and the molecular component, the latter being determined experimentally with due regard for the operating conditions of the given joint.

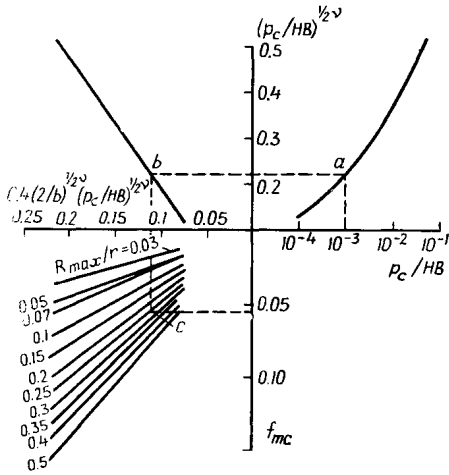


Fig. 2.21. Nomograph for determining the mechanical component of the coefficient of friction at $\nu = 2$ and $b = 2$

Example 1. Calculate the coefficient of external static friction on machine-tool guideways at a nominal pressure $p = 4 \text{ kgf/cm}^2$. The calculation is carried out according to the sequence indicated on page 89. The guideway is made from a structural steel hardened to $HB \ 250$ and machined by surface grinding

to the 9th class of surface roughness. The part movable along the guideway is made from a fluoroplastic with the following mechanical properties: $E = 10^4$ kgf/cm², $\alpha = 0.15$, $HB = 3.1$ and $\mu = 0.5$.

The surface roughness parameters must be specified for the guideway, because steel is much harder than fluoroplastic.

From Tables 1.6 and 1.7 we find $\Delta = 2.6 \times 10^{-3}$, $\nu = 1.6$, $b = 2.3$, and $\frac{R_{\max}}{r} = 0.004$. In accordance with the operating conditions (rubbing in air) we choose the frictional constants from Table 2.2. If the tabulated data do not fit the operating conditions, the frictional constants must be determined by the methods described on pages 80-87. The sliding parts have the contact area which is affected by surface waviness. With regard to waviness

$$p_c = kE^{0.8} \left(\frac{H_b}{R_b} \right)^{0.4} p_a^{0.2}$$

Assuming that the surface waveform is spherical with $k = 0.5$ and choosing $\frac{H_b}{R_b} = 10^{-5}$ for surface grinding, we shall have

$$p_c = 0.5 (10^4)^{0.8} (10^{-5})^{0.4} 4^{0.2} \approx 10.4 \text{ kgf/cm}^2$$

Using formula (2.9), let us find the type of deformation in the contact area:

$$\begin{aligned} \frac{p_c}{HB} &= \frac{2.4^{\frac{2\nu+1}{2}}}{5} \nu(\nu-1) k_1 \left[\frac{HB(1-\mu^2)}{E} \right]^{2\nu} \left(\frac{1}{\Delta} \right)^\nu \\ &= \frac{2.4^{2.1} \times 1.6 \times 0.6 \times 0.85}{5} [2.4 \times 10^{-2}]^{3.2} \left(\frac{10^3}{2.6} \right)^{1.6} = 9 \times 10^{-2} \end{aligned}$$

Hence, the contour pressure that corresponds to transition from elastic to elastic-plastic deformations, that is $p_c = 28$ kgf/cm², will exceed p_c effective at the joint. In the contact region, therefore, elastic deformations will take place. The extent of density of the contact is determined by formula (2.10):

$$\begin{aligned} p_c &= \frac{8 \times 10^{-2}}{(b^{1/\nu} \nu)^{\frac{2\nu+1}{2(\nu-1)}}} \Delta^{1/2} \frac{E}{1-\mu^2} = \frac{8 \times 10^{-2}}{(2.3^{0.6} \times 1.6)^{3.5}} \\ &\quad \times (2.6 \times 10^{-3})^{1/2} \frac{10^4}{0.75} \approx 2 \text{ kgf/cm}^2 \end{aligned}$$

The joint will work at the elastic dense contact; hence the coefficient of friction will be

$$\begin{aligned} f &= \frac{1.4\tau_0(1-\mu^2)^{2/3}}{E^{2/3} p_c^{1/3}} \left(\frac{r}{R_{\max}} \right)^{1/3} + \beta \\ &+ \frac{0.35\alpha_f p_c^{1/3} (1-\mu^2)^{1/3}}{E^{1/3}} \frac{R_{\max}^{1/3}}{r^{1/3}} = \frac{1.4 \times 0.032 \times 0.75^{0.67}}{10^{8/3} \times 10.4^{1/3}} \\ &+ 0.02 + \frac{0.35 \times 2.5 \times 0.15 \times 10.4^{1/3} \times 0.75^{1/3}}{10^{4/3}} \approx 0.044 \end{aligned}$$

Example 2. The tribological joint is a plain bearing. The shaft is made from steel Grade 45 hardened to HRC 52 and ground to the 9th class of surface roughness. The bearing liner is made from bronze Grade БрОЦС 6-6-3 with elastic modulus $E = 9 \times 10^3$ kgf/mm² and a hardness of HB 70 and reamed to the 9th class of surface roughness.

The roughness parameters must be found for the steel shaft, for it is the shaft that is the harder rubbing component. From Table 1.6 we choose $b = 0.6$, $\nu = 2$, $\Delta = 9.6 \times 10^{-2}$, $R_{\max} = 2.4$ μ m, and $r = 10$ μ m.

The bearing works with boundary oil lubrication at a speed that causes no heating. In agreement with the operating conditions, we find from Table 2.2 the molecular component of the coefficient of friction $f_{ml} = 0.06$ and $\tau_n = 4.2 \text{ kgf/mm}^2$.

According to M. N. Dobychin, the maximum stress in the bearing depends on a number of factors determining the bearing's operation.

For the materials chosen

$$n = 0.16\mu_l + 0.554 = 0.16 \times 0.3 + 0.554 \approx 0.6$$

$$c_0 = \frac{4}{\pi} \left[(1 - 0.09) + 0.91 \frac{9 \times 10^3}{2.4 \times 10^4} \right] = 1.65$$

$$\alpha' = \frac{100 \times 0.91}{0.05 \times 9 \times 10^3} = \frac{20 \times 10}{10^3} = 0.2$$

$$\begin{aligned} \varphi_0 &= 0.32 \left(\frac{1.65 + 0.12}{0.12} \right)^{0.6} \left(\frac{0.2}{1.2} \right)^{0.6} \\ &= 0.32 \times 14.7^{0.6} \times 0.17^{0.6} = 0.32 \times 5.1 \times 0.35 = 0.57 \end{aligned}$$

$$\sigma_{\max} = \sigma_{av} \left(\frac{1}{0.57} + 0.35 \right) = 2.1 \sigma_{av}$$

The average contact stress σ_{av} for the shaft diameter specified at 80 mm will be 1.25 kgf/mm^2 . Hence, $\sigma_{\max} = 2.6 \text{ kgf/mm}^2$.

The type of deformation in the contact area will be determined from formula (2.26):

$$\begin{aligned} \frac{p_c}{HB} &= \frac{0.5 \times 5.4^v}{\Delta^v} \left[\frac{HB(1 - \mu^2)}{E} \right]^{2v} = \frac{0.5 \times 5.4^2}{10^{-2}} \left(\frac{70 \times 0.91}{9 \times 10^3} \right)^4 \\ &= 5 \times 29 \times 10^{-11} \times 2.4 \times 10^3 \approx 3.5 \times 10^{-6} \end{aligned}$$

that is, $p_c = 2.5 \times 10^{-4} HB \text{ kgf/mm}^2$.

The contour pressure in the joint exceeds the value of p_c corresponding to transition from elastic-plastic to plastic deformation. Hence, the contact between the rubbing components will be plastic.

Using formula (2.4), we ascertain whether external friction conditions take place with the given values of f_{ml} , given material and surface topography of the shaft:

$$\frac{p_c}{HB} = \frac{0.125}{\Delta^2} \left(1 - \frac{6\tau_n}{HB} \right)^2 = 0.125 \times 100 \times 0.64^2 \approx 5.1$$

that is, $p_c \approx 36 \text{ kgf/mm}^2$.

As the found value of p_c exceeds that specified for the joint, the latter will work with external friction. The density of the contact is found by formula (2.29):

$$\frac{p_c}{HB} = \frac{0.5}{\left(b \frac{1}{v} v \right)^{\frac{v}{v-1}}} = \frac{0.5}{(0.6^{1/2} 2)} = 0.21$$

The contour pressure at the joint is lower than p_c obtained by calculation; therefore the contact will be plastic and sparse.

The coefficient of external friction

$$\begin{aligned} f &= f_{ml} + 0.44 \Delta^{1/2} \left(\frac{p_c}{HB} \right)^{1/4} = 0.06 + 0.44 (9.6 \times 10^{-2})^{1/2} \left(\frac{2.6}{70} \right)^{1/4} \\ &= 0.06 + 0.44 \times 0.31 \times 0.44 = 0.06 + 0.06 = 0.12 \end{aligned}$$

Example 3. The tribological joint is a disc friction clutch. The nominal pressure $p_a = 4 \text{ kgf/cm}^2$. The flywheel and the pressure plate are made from cast iron Grade C4 15-32. The bearing-area curve parameters are $b = v = 2$; $\Delta = 5.3 \times 10^{-2}$ (see Table 1.5). The hardness of the flywheel and the pressure plate is $HB \ 250$. The plate linings are made from a composite material with $HB \ 10$, and an elastic modulus of 370 kgf/mm^2 . The clutch works at $\theta = 60^\circ\text{C}$. For these conditions the molecular component of the coefficient of friction, found from Table 2.2, will be $f_{m1} = 0.15$.

Because of the low stiffness of friction linings, the nominal pressure may be assumed to be equal to the contour pressure. According to formula (2.26), the contour pressure causing plastic contact will be

$$\frac{p_c}{HB} = \frac{0.5 \times 5.4^2}{(5.3 \times 10^{-2})^2} \left[\frac{10 \times 0.75}{370} \right]^4 = 0.5 \times 10^4 \times 1.2 \times 10^{-8} = 0.6 \times 10^{-4},$$

that is, $p_c = 6 \times 10^{-3} \text{ kgf/mm}^2$.

Thus, the contour pressure obtained is lower than that effective in the friction clutch. Hence, plastic deformations occur in the real area of contact. The contour pressure corresponding to the condition in which external friction in the clutch is upset is

$$\frac{p_c}{HB} = \frac{0.125}{\Delta^2} \left(1 - \frac{6\tau_n}{HB} \right)^2 = \frac{0.125 \times 0.01 \times 10^4}{(5.3 \times 10^{-2})^2} = \frac{1.25 \times 10^{-3} \times 10^4}{28} \approx 0.45,$$

that is, $p_c \approx 4.5 \text{ kgf/mm}^2$.

The obtained value is larger than the contour pressure in the clutch; therefore, the external friction condition will be satisfied.

Dense contact in the clutch is feasible at contour pressures

$$p_c \approx 0.25HB = 2.5 \text{ kgf/mm}^2$$

Thus, plastic sparse contact takes place in the friction clutch under the given conditions. The coefficient of external friction will be

$$f = 0.15 + 0.44 (5.3 \times 10^{-2})^{1/2} \left(\frac{0.04}{10} \right)^{1/4} = 0.15 + 0.44 \times 0.23 \times 0.25 = 0.18$$

2.6. PRELIMINARY DISPLACEMENT

External static friction occurs in the preliminary displacement area. Preliminary displacement is a phenomenon of small relative displacement of the rubbing solids up to the moment when transition from rest to sliding friction starts [8, 68].

Distinction is made between the preliminary displacement a_τ^b caused by the bulk deformation of the rubbing members and the contact preliminary displacement a_τ^c . The contact preliminary displacement is caused by the change in the stress condition over the contact area of solids at the moment the displacement begins [25] and depends on the type of deformation in the contact area. Thus, the total preliminary displacement will be

$$a_\tau = a_\tau^b + a_\tau^c \quad (2.77)$$

The preliminary displacement due to bulk deformation of solids under the action of force required to bring about relative sliding is a variable quantity dependent on the point where it is detected. Its magnitude is calculated by the formula

$$a_\tau^b = \frac{\tau}{G_1} h_1 + \frac{\tau}{G_2} h_2 \quad (2.78)$$

where h_1 and h_2 = respective distances from the section at which the rubbing solids are fixed to the section where a_t^b is measured (Fig. 2.22), and G_1 and G_2 = elastic moduli in shear for the first and the second bodies, and τ = bulk shearing stresses.

The contact preliminary displacement during elastic deformation is caused by increased slipping in the contact region when a force is applied in the direction of sliding. Let us assume that the contacting bodies are plates of a certain thickness. During elastic contact, a compressive force normal to the contact interface gives rise to two areas. One area having a radius exceeding ρ' is characterized by sliding upon application of load; in the second area, whose radius is smaller than ρ' , sliding does not occur. According to [10]

$$\rho' = r \left(1 - \frac{T_i}{fN_i} \right) \quad (2.79)$$

where T_i = tangential pulling force.

With increasing T , the sliding area also increases, and with $T_i = fN_i$, the value of ρ' will be equal to zero, that is, sliding will occur over the whole contact area. In the process, the asperity is displaced tangentially by

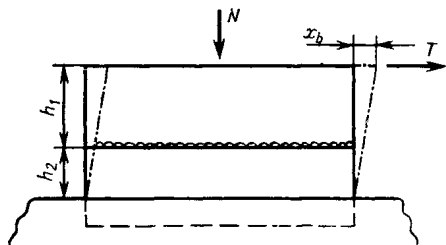


Fig. 2.22. Diagram of preliminary displacement

$$a_\tau^c = \frac{(2-\mu)(1+\mu)f_i h}{1-\mu^2} \quad (2.80)$$

The preliminary displacement of the contacting surfaces will be equal to a_τ^c at the highest asperity. Hence, in this case, the contact preliminary displacement will depend on the amount of approach and the coefficient of friction at the highest asperity, which makes its finding difficult. It can be assumed, however, to a good approximation that $f_{i, \max} = f$, which is the average coefficient of friction.

During plastic contact, the stress condition in the contact area will change, because the material will be ploughed by the asperities at the moment of displacement. If the normal load acts only, an asperity will deform the material as is shown in Fig. 2.23a. Here, the contact area will be

$$\Delta A_{r, st} = 2\pi r h_{i, st} \quad (2.81)$$

In sliding the ploughing causes the asperity to bear against the deformed material only with its frontal portion in the direction of motion. The area of contact of the asperity with the material deformed is

$$\Delta A_{r, st} = \pi r h_{i, kin} \quad (2.82)$$

Therefore, with the identical amounts of approach, which can correspond to different loads, the real area of contact in sliding will be half of that at rest. Taking into account equation (2.81), the real area of contact for a rough surface sliding over a smooth one will be

$$A_{r, st} = \frac{1}{2} A_c b e_{kin}^y \quad (2.83)$$

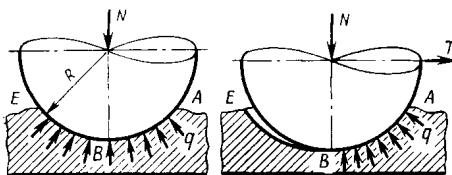
The relationship between the amounts of approach at rest and in sliding will depend on that between the respective areas of real contact. For plastic deformations in the contact areas

$$A_r = \frac{N}{p_r} \quad (2.84)$$

Therefore, the relationship between the real areas of contact at rest and in sliding will depend on the forces acting upon the rubbing bodies and on the relationships between the stresses effective in these conditions. Appropriate calculations [40] and experiments [28] show that for different materials and interaction times where rheological effects can be neglected

$$p_{r, st} = p_{r, kin} = p_r \quad (2.85)$$

Considering the fact that the sliding components are acted upon by the sum of the normal force and the tangential force causing the sliding motion, we shall have



$$A_{r, kin} = A_{r, st} \sqrt{1 + f^2} \quad (2.86)$$

Fig. 2.23. Contact of asperity at rest and during displacement

Thus, a sharp reduction of the contact area during displacement results in a closer approach of the contacting

members. This is caused by the redistribution of the contact areas due to ploughing at the initial period of sliding motion. At the rear asperity (relative to the direction of sliding) the contact area diminishes from $\frac{A_{ri, st}}{2}$ to zero, while at the frontal asperity, it increases from $A_{ri, st}$ to $A_{ri, kin}$. From formula (2.86), the following relationships between the magnitudes of approach at rest and in sliding can be derived: for a single indenter

$$h_{kin} = 2h_{st} \sqrt{1 + f^2} \quad (2.87)$$

for the contact of a rough and a smooth surface

$$h_{kin} = h_{st} (2 \sqrt{1 + f^2})^{1/\nu} \quad (2.88)$$

$$h_{kin} = h_{st} (2 \sqrt{1+f^2})^{\frac{1}{v_1+v_s}} \quad (2.89)$$

plane, corresponding to the redistribution of the real area of contact, will be the contact preliminary displacement.

$$a_{\tau}^c = \int_{h_{st}}^{h_{kin}} \sqrt{\frac{r}{2}} z^{-\frac{1}{2}} dz \quad (2.90)$$
$$a_{\tau}^c = \sqrt{2rh_{st}} [(2\sqrt{1+f^2})^m - 1] \quad (2.91)$$

where m = coefficient depending on the type of the sliding pair. For the pair consisting of a spherical indenter and a flat surface, $m = \frac{1}{2}$, for the contact of a rough surface with a smooth surface $m = \frac{1}{2\nu}$, and for two rough contacting surfaces $m = \frac{1}{2(\nu_1 + \nu_2)}$.

7-01025

indenter, $0.2r_{st}$ for the contact of a rough surface with a smooth surface, and $0.1r_{st}$ for the contact of two rough surfaces. According to [67], the average static diameter of the contact spot varies from 2 to 17 μm . Hence, the magnitude of the contact preliminary displacement is usually extremely small.

Elastic sparse contact. The contact preliminary displacement, as dependent on load [9], is

$$a_{\tau}^c = \frac{(2-\mu)(1+\mu)f_i r}{(1-\mu^2)^{0.6}} \left[\frac{5p_c}{Ev(\nu-1)k_1} \right]^{\frac{2}{2\nu+1}} \Delta^{\frac{2\nu}{2\nu+1}} \quad (2.92)$$

For the most typical surface finishes, that is with $\nu = 2$,

$$a_{\tau}^c = \frac{2.1(2-\mu)(1+\mu)f_i r}{(1-\mu^2)^{0.6}} \left(\frac{p_c}{E} \right)^{0.4} \Delta^{0.8} \quad (2.93)$$

Substituting into formula (2.91) the values of the contour pressure corresponding to the transition from elastic deformation to elastic-plastic deformations we obtain [see formula (2.9)]

$$a_{\tau, \max}^c = \frac{2.4(2-\mu)(1+\mu)rf_i}{\frac{(2\nu-1)^2}{(1-\mu^2)^{\frac{2\nu}{2\nu+1}}} \frac{\nu(2\nu-1)}{\Delta^{\frac{2\nu}{2\nu+1}}}} \left(\frac{HB}{E} \right)^{2\nu} \quad (2.94)$$

For the most typical surface finishes of metals having $\mu = 0.3$ and $\frac{HB}{E} = 0.01$, $a_{\tau, \max}^c$ is equal to $6.4 \times 10^{-8} f_i \frac{r}{\Delta^{1.2}}$.

For a single indenter, the contact preliminary displacement will be

$$a_{\tau}^c = \frac{8(2-\mu)(1+\mu)fN^{2/3}}{E^{2/3}r^{1/3}(1-\mu^2)^{1/3}} \quad (2.95)$$

Plastic sparse contact. From formulas (2.33) and (2.90), the contact preliminary displacement will be

$$a_{\tau}^c = \left(\frac{p_c}{HB} \right)^{1/2\nu} [(2\sqrt{1+f^2})^{1/2\nu} - 1] 1.41r\Delta^{1/2} \quad (2.96)$$

For plastic dense contact

$$a_{\tau}^c = \sqrt{2rR_{\max}} \left(\frac{p_c}{HB} \right)^{1/2} [(2\sqrt{1+f^2})^{1/2} - 1] \quad (2.97)$$

For a single indenter

$$a_{\tau}^c = \left(\frac{N}{\pi HB} \right)^{1/2} [(2\sqrt{1+f^2})^{1/2} - 1] \quad (2.98)$$

It should be noted that experimental data on the preliminary displacement obtained by different investigators vary considerably [1, 33, 35, 58]. These variations can be explained by the fact that the preliminary displacement consists of two components — the bulk and the contact preliminary displacement. The bulk preliminary displacement is determined by the design of both the joint and the test equipment. For this reason, the coincidence of the results

obtained on different installations and sliding pairs is impossible. The research on the contact preliminary displacement according to [46, 61] has shown a satisfactory coincidence of the experimental results with the calculated data.

REFERENCES

1. Авдеев Д. Т. Исследование предварительного смещения прессованных соединений.— «Изв. высш. учеб. заведений. Машиностроение», 1962, № 4, с. 15.
2. Айнбиндер С. Б., Логинова А. Я., Тюнина Э. Я. Трение полимерных материалов.— «Механика полимеров», 1972, № 5, с. 809—815.
3. Алисин В. В., Михин Н. М. Исследование зависимости коэффициента трения покоя от нагрузки.— «Изв. высш. учеб. заведений. Машиностроение», 1974, № 2, с. 65—69.
4. Альшиц И. Я., Бартенев Г. М. Влияние различных факторов на антифрикционные свойства полимеров.— «Вестник машиностроения», 1975, № 9, с. 39—42.
5. Билик Ш. М., Черкасская П. М. Тонкослойные антифрикционные покрытия.— В кн.: Обработка пластмасс в машиностроении. М., «Наука», 1968, с. 64.
6. Буше Н. А. К вопросу о процессах, происходящих на поверхностях трения металлических материалов.— В кн.: О природе трения твердых тел. Минск, «Наука и техника», 1968, с. 75—77.
7. Венцель С. В., Нестеренко В. А. Антифрикционные свойства некоторых приборных масел.— «Проблемы трения и изнашивания», 1974, № 5, с. 125—131.
8. Верховский А. В. Явление предварительного смещения при трогании несмазанных поверхностей с места.— «Журнал прикладной физики», 1926, т. 3, с. 311—314.
9. Влияние надмолекулярной структуры полиарилата и наполненных систем на его основе на фрикционные свойства.— «Проблемы трения и изнашивания», 1974, № 6, с. 163—167. Авт.: В. В. Коршак, В. А. Белый, И. А. Грибова и др.
10. Демкин Н. Б., Крагельский И. В. Предварительное смещение при упругом контакте твердых тел.— «ДАН СССР», 1969, т. 186, № 4, с. 812—814.
11. Демкин Н. Б. Контактное шероховатых поверхностей. М., «Наука», 1970, с. 223.
12. Дерягин Б. В. Что такое трение? М., Изд-во АН СССР, 1959, с. 243.
13. Добычин М. Н., Литвинов В. Н., Михин Н. М. Несущая способность микроконтактов при высокой плотности пятен касания.— В кн.: Жесткость машиностроительных конструкций. Брянск, 1976, № 6, с. 66—70.
14. Елин Л. В. Взаимное внедрение поверхностных слоев металлов как одна из причин изнашивания при несовершенной смазке.— В кн.: Трение и износ в машинах. Т. 13. М., Изд-во АН СССР, 1959, с. 48—58.
15. Зюльков М. И., Михин Н. М., Добычин Н. М. О механизме приработки трущихся поверхностей при исходном пластическом контакте. Труды Уральской юбилейной научной сессии. Курган, 1967, с. 221—222.
16. Каверзин С. В. Влияние температуры на начальную силу трения пары уплотнение — цилиндр. Труды фак-та Красноярского политехн. ин-та. Красноярск, 1968, с. 109—114.
17. Комбалов В. С. Влияние шероховатости твердых тел на трение и износ. М., «Наука», 1974.
18. Крагельский И. В. О трении несмазанных поверхностей.— В кн.: Трение и износ в машинах, М., Изд-во АН СССР, 1939, с. 543.
19. Крагельский И. В., Алисин В. В. Расчетный метод оценки трения и износа — эффективный путь повышения надежности и долговечности машин. М., «Знание», 1976, с. 55.

20. Крагельский И. В. Внешнее трение — друг и враг техники.— В кн.: Наука и человечество. М., «Наука», 1966, с. 355—358.
21. Крагельский И. В., Виноградова И. Э. Коэффициенты трения. М., Машгиз, 1962.
22. Крагельский И. В. Трение и износ. М., Машгиз, 1968.
23. Крагельский И. В., Михин Н. М. Об оценке фрикционных свойств материалов трущихся пар.— «Заводская лаборатория», 1968, т. 34, № 8, с. 1007—1009.
24. Крагельский И. В., Ланков А. А. О применимости формул Герца для расчета контурных площадей.— В кн.: О природе трения твердых тел. Минск, «Наука и техника», 1971, с. 307—314.
25. Крагельский И. В., Михин Н. М. О природе контактного предварительного смещения твердых тел.— «ДАН СССР», 1963, т. 153, № 1, с. 78—81.
26. Крагельский И. В. Влияние нагрузки на изменение шероховатости контактирующих поверхностей.— В кн.: Трение и износ в машинах. Т. 5. Изд-во АН СССР, 1950, с. 103—108.
27. Крагельский И. В. Молекулярно-механическая теория трения.— В кн.: Трение и износ в машинах. Изд-во АН СССР, 1949, с. 178.
28. Крагельский И. В., Михин Н. М., Ляпин К. С. Влияние нормального давления на тангенциальную прочность адгезионной связи.— «ДАН СССР», 1973, т. 209, № 4, с. 834—837.
29. Курицына А. Д. Методы исследования антифрикционных пластмасс.— В кн.: Исследования по триботехнике. М., НИИМаш, 1975, с. 49—70.
30. Куртель Р. Т. Деформация поверхностных слоев при трении.— В кн.: О природе трения твердых тел. Минск, «Наука и техника», 1971, с. 8—18.
31. Левин Б. М. Контактный метод измерения геометрии поверхностей. М., Машгиз, 1950.
32. Левина З. М., Решетов Д. Н. Контактная жесткость машин. М., Машиностроение, 1971.
33. Максак В. И. Предварительное смещение и жесткость металлического контакта. М., «Наука», 1975.
34. Митрофанов Б. П. Природа упругого предварительного смещения.— В кн.: Теория трения и износа. М., «Наука», 1965, с. 8—11.
35. Митрофанов Б. П. Соотношение между сближением и максимальным предварительным смещением для упругого дискретного контакта.— В кн.: О природе трения твердых тел. Минск, «Наука и техника», 1971, с. 322—324.
36. Михин Н. М. Трение в условиях пластического контакта. М., «Наука», 1968.
37. Михин Н. М. О зависимости коэффициента трения от нагрузки при упругом контакте.— В кн.: Контактное взаимодействие твердых тел. М., «Наука», 1971, с. 141—145.
38. Михин Н. М. О зависимости коэффициента трения от температуры.— «Изв. высш. уч. заведений. Физика», № 11, 1971, с. 146—147.
39. Михин Н. М., Ляпин К. С. Зависимость коэффициента трения от твердости и ее экспериментальная проверка.— «Изв. высш. уч. заведений. Физика», 1970, № 3, с. 50—56.
40. Михин Н. М. О расчете усилий, действующих на сферический индентор при движении по пластическому полупространству.— В кн.: Трение твердых тел. М., «Наука», 1964, с. 52—61.
41. Михин Н. М., Добычин М. Н., Ляпин К. С. Новый метод определения тангенциальной прочности адгезионного шва. Авторское свидетельство № 244686, 1969.— «Бюллетень по изобретениям», № 18, 1969.
42. Михин Н. М., Алисин В. В. Метод определения показателей кривой опорной поверхности по зависимости сближения от нагрузки при пластическом контакте.— «Изв. высш. уч. заведений. Машиностроение», 1972, № 8, с. 15-19.
43. Михин Н. М., Смольяков А. И. Исследование молекулярной составляющей коэффициента трения прессованной древесины.— «Изв. высш. уч. заведений. Лесной журнал», 1975, № 6, с. 76—80.
44. Михин Н. М., Парамонов В. С. Экспериментальные исследования

зависимости коэффициентов трения кожевенного полуфабриката от нагрузки. М., Реф. инф. «Машиностроение для легкой промышленности», 1973, № 5, с. 9—13.

45. Михин Н. М. О расчете коэффициента трения при упругом контакте. — «ФХММ», 1968, № 2, с. 204—208.

46. Михин Н. М. Внешнее трение твердых тел. М., «Наука», 1977, с. 221.

47. Михин Н. М., Комбалов В. С. Зависимость коэффициента трения от нагрузки при упругом контакте в зоне насыщения контакта. — В кн.: Контактное взаимодействие твердых тел и расчет трения и износа. М., «Наука», 1971, с. 146—153.

48. Михин Н. М., Крагельский И. В. Изменение площади фактического касания твердых тел при значительном сближении. — «ДАН СССР», 1967, т. 176, № 6, с. 1285—1287.

49. Непомнящий Е. Ф., Луарсабишвили Д. Г. Фрикционные свойства магнитных лент для вычислительной техники. — В кн.: Вопросы трения и проблемы смазки. М., «Наука», 1968, с. 131—139.

50. Павлов В. Г., Дроздов Ю. Н. Повышение долговечности узлов сухого трения. — «Вестник машиностроения», 1975, № 11, с. 34—37.

51. Рамишвили Г. Я. Сила трения как функция сближения твердых тел. — В кн.: Теория трения и износа. М., «Наука», 1965, с. 35—39.

52. Рыжов Э. В. Контактная жесткость деталей машин. М., «Машиностроение», 1966, с. 195.

53. Семенов А. П., Поздняков В. В. Методика исследования трения и адгезионного взаимодействия тугоплавких материалов при температурах до 2000°C. — В кн.: Теория трения и износа. М., «Наука», 1965, с. 332—336.

54. Трофимович А. Н., Приходько О. Г., Фомичев И. А. Сравнительные испытания термического полиамида и некоторых подшипниковых материалов. — «Проблемы трения и изнашивания», 1972, № 2, с. 132—134.

55. Френкель Я. И. Электрическая теория материи. 1924, с. 2.

56. Шишочкин В. П. О твердости металлов и их сплавов при различных температурах. — «Журнал прикладной химии», 1972, т. 2, № 6, с. 21—24.

57. Шишочкин В. П., Агеева В. А. Твердость легкоплавких металлических сплавов при различных температурах. — «Цветные металлы», 1932, № 2, с. 7—10.

58. Щедров В. С. Предварительное смещение на упруго-вязком контакте. — В кн.: Трение и износ в машинах. М., Изд-во АН СССР, 1950, с. 94—102.

59. Bowden F. P., Childs T. H. C. Friction and deformation of metals at extremely low temperatures. *Nature*, 1968, v. 219, n. 5161, p. 1333-1336.

60. Bowden F. P., Tabor D. The friction and lubrication of solids. Part II, Oxford, 1964.

61. Courtney-Pratt J. S., Eisner E. The effect of tangential force on the contact of metallic bodies. *Proc. Roy. Soc., Ser A*, v. 238, 1956, p. 529.

62. Greenwood J. A., Minschell H., Tabor D. Hysteresis losses in rubber in sliding and rolling friction. *Proc. Roy. Soc., Ser A*, 1961, v. 259, p. 480-485.

63. Holm R., Holm E., Shobert K. J. *Journ. Appl. Phys.* 1949, v. 20, p. 319.

64. Laird S., Towle K. Shear strength and friction measurement on polyethylene under high pressure. *Journ. Appl. Phys.* 1973, v. 44, n. 4.

65. Moore A. J., Tegurt W. Relation between friction and hardness. *Proc. Roy. Soc. Ser. A*, v. 212, 1952, p. 440.

66. Mordike B. L. The frictional properties of carbides and borides at high temperatures. *Wear*, 1960, v. 3, No. 5, p. 374.

67. Rabinowitz E. Investigation of size effect in sliding by means of statical techniques, *Conf. on lubr. and wear*, Lond. 1957.

68. Rankin J. S. The range of friction. *Phil. Mag.* 1926, v. 2, p. 806.

69. Whitehead J. R. Surface deformation and friction of metals at light loads. *Proc. Roy. Soc. Ser. A*, 1950, v. 201, p. 109.

CALCULATION OF WEAR RATE

3.1. GENERAL CHARACTERISTICS
OF WEAR OF MATERIALS

Wear of materials is a process of surface destruction in rubbing solids, which results in reduced dimensions of parts in a direction perpendicular to the rubbing surface. The rate of wear in sliding pairs depends on the properties of the parts' materials, the treatment of the rubbing surfaces and their quality, and also on their running conditions, that is load, temperature, lubrication, and so on.

Diverse changes occurring in the contact layer give rise to various types of wear. A specific type of wear cannot be defined by a single term; it should rather be described by several characteristics. The mechanism of surface destruction is varied.

Depending on the character of the interface medium, distinction is made between dry wear, boundary-lubrication wear, and abrasive wear. Depending on the deformation of the surface layer, wear during elastic contact, wear during plastic contact, and wear during micro-cutting are differentiated.

Thus, three characteristics should be used for the description of a specific type of wear, for example, fatigue wear at boundary friction during elastic contact.

Three phases of the wear process take place under constant rubbing conditions: the running-in period, the period of steady-state wear, and the period of severe wear.

The *running-in process* consists in that the asperities on rubbing surfaces change their shape and the material becomes work-hardened; as a result of these two processes, the conditions bringing about elastic contact set in. Ensuring elastic contact at rubbing surfaces is essential because it provides for minimum wear and a stable magnitude of frictional force.

Running-in is characterized, as a rule, by more intensive wear of rubbing surfaces and by higher heat generation, which are accompanied by changes both in surface geometry and in the physical and mechanical properties of the materials surface layers.

In the process of running-in, the asperities that are least able "to survive" under given operating conditions are destroyed intensively and new asperities differing from the original ones in shape and dimensions are formed. It is found experimentally that after running-in in various conditions for diverse sliding pairs, a stable surface roughness proper to given rubbing conditions develops, which is duplicated, rather than changed further on, during the rubbing process. The original surface roughness has no bearing on the stable roughness (Fig. 3.1).

The roughness parameters for some run-in machine parts are given in Table 1.8. The bearing-area curve parameters can be assumed to a first approximation to be $v = 2$, $b = 2$. The molecular-mechanical theory of friction has revealed a close relation between the parameters characterizing frictional interaction and the surface-geometry parameters. The stable surface roughness of a solid depends on the strength of bonds due to contact molecular interactions, elastic properties of the material, and specific normal load, and can be found by calculation from these variables (see Ch. 2). The possibility of predicting the value of stable surface roughness at the design stage enables one to specify such surface treatment methods and roughness classes as will ensure a shorter running-in period and a minimum wear of the joint in the process. Running-in is followed by the period of steady-state wear, over which the wear rate of the joint in the given rubbing conditions is at a minimum. Various investigations [4, 9, 16, 17, 18, 21] have shown that the wear particles break away as a result of numerous load cycles on a single frictional bond.

The main difficulty in understanding the nature of wear of materials is due to the fact that the sub-surface layers of rubbing parts, apart from being subject to mutual mechanical interaction, are greatly influenced by the ambience [19]. In fact, the physico-mechanical properties of the sub-surface layers differ from those of the bulk of the material. Consideration of the effect that physical, chemical, and mechanical factors have on the wear destruction of the surface layer of solids gives grounds for regarding wear as a cumula-

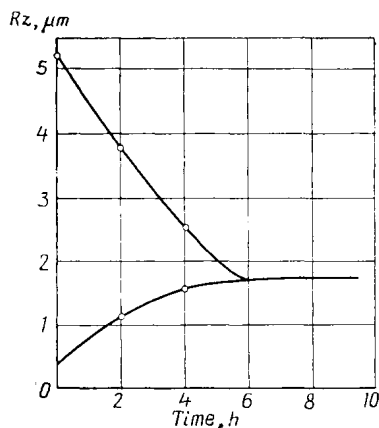


Fig. 3.1. Variation of surface geometry during running-in process for specimens from steel Grade 45 and bronze Grade ОЦС 5-5-5 with dissimilar initial roughness values in boundary friction conditions ($p_a = 30 \text{ kgf/cm}^2$, $v = 5 \text{ m/s}$)

tive process in which the effects of individual factors combine during repeated loading of the frictional bonds to result in the separation of a wear particle.

This type of wear occurs in tribological joints under various conditions; exposed to it are also joints sealed against abrasive particles and kept from severe corrosion or seizure. In general, only the cumulative mechanism of destruction can provide satisfactory explanation of wear of the harder material, caused by the softer material in a sliding pair; for instance, rubber or plastic packing wears away a steel surface, diamond cutting tool becomes worn in machining soft alloys, and so on. The formation of surface cavities during rolling friction, referred to as contact fatigue, or pitting, is a variety of cumulative wear.

3.2. PHYSICAL MODEL OF WEAR

The amount of labour consumed in repairing machine parts is substantially greater (5 times or more) than in its manufacture, because the repair process is, as a rule, poorly mechanized. Hence the requirement for increasing wear resistance of machine parts. The calculation of the wear rate, particularly at the design stage, plays an important role in predicting the wear life of parts [12].

Initially, design relationships [13] only took into consideration the effect produced by hardness and load on a material's wear resistance. Experiments show, however, that wear is affected to no lesser extent by the elastic properties of the material, the part's running conditions (load, speed, temperature), external conditions (lubrication, environment), and the joint's design features.

The sliding of an asperity against the mating body gives rise to a frontal wave of the deformed material which is subjected to a compressive stress. Behind the asperity the material is strained because of the frictional force. Thus, every portion of the material being deformed is subjected to the opposite-sign deformations. The numerous repeated deformations lead to physical and chemical changes in the surface layer and, consequently, to the breaking-away of wear particles.

Experiments with a spherical indenter sliding under load along a circular path have shown that the material of the test specimen is destroyed not immediately, but after several passes of the indenter (that is, after several interaction cycles). As the wear particles are removed and the indenter gets deeper into the material, again there is no appreciable changes on the rubbing surface during several cycles (Fig. 3.2).

The effective contact stress σ_{eff} at which the separation of wear particles occurs is proportional to the specific friction force τ :

$$\sigma_{eff} = k\tau = kf_{ml} p_r \quad (3.1)$$

where k = factor characterizing the contact stress condition; the factor depends on the nature of the material, and for brittle materials $k = 5$, whereas for highly elastic materials $k = 3$.

Wear is usually characterized by the linear wear rate:

$$I = \frac{V_{\Sigma}}{A_a L} = \frac{U}{L} \quad (3.2)$$

where L = sliding distance, and V_E = volume of worn material at the sliding distance L .

Bearing in mind that only the real area of contact takes part in the friction process, let us introduce the concept of specific wear by analogy with expression (3.2):

$$i_h = \frac{V_d}{A_r d} \quad (3.3)$$

where d = mean diameter of the contact spot and V_d = volume of the material worn off the area A_r in sliding over the distance d as a result of a single interaction between surface irregularities.

Dividing expression (3.2) by expression (3.3) and making the necessary transformations, we shall obtain

$$I = i_h \frac{A_r}{A_a} = i_h \frac{p_a}{p_r} \quad (3.4)$$

The thickness of the worn layer corresponding to a single interaction between the irregularities is

$$V_d = \frac{U_v}{n} \quad (3.5)$$

where n = number of cycles of interaction resulting in the separation of the material volume U_v .

Let us consider the contact of an absolutely rigid solid having a rough surface with a smooth, elastically-deformed part subjected to wear. The rough surface is modelled with a set of hemispherical segments of an identical radius, which are so arranged with height that the distributions of material in the surface layers of the model and the real surface are described by identical bearing-area curves. The mutual influence of the asperities is ignored because in most real joints the density of contact is very low and can be approximately estimated by the ratio of the nominal pressure to the hardness of the softer member of the sliding pair.

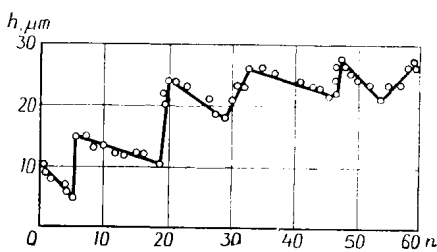


Fig. 3.2. Penetration of an indenter, as dependent on the number of loading cycles

To a first approximation, let us assume that only the volume of the penetrated asperities takes part in the deformation of the mating component (Fig. 3.3):

$$U_v = \int_0^h A_r dh = A_c R_{\max} \int_0^{\varepsilon} b \varepsilon^{\nu} d\varepsilon = \frac{A_r h}{\nu+1} \quad (3.6)$$

Substituting formula (3.6) into (3.3) and taking into account (3.5), we shall have

$$i_h = \frac{h}{(\nu+1) \frac{dn}{dh}} \quad (3.7)$$

With the irregularities being modelled by means of hemispherical segments, it can be demonstrated geometrically that for a single

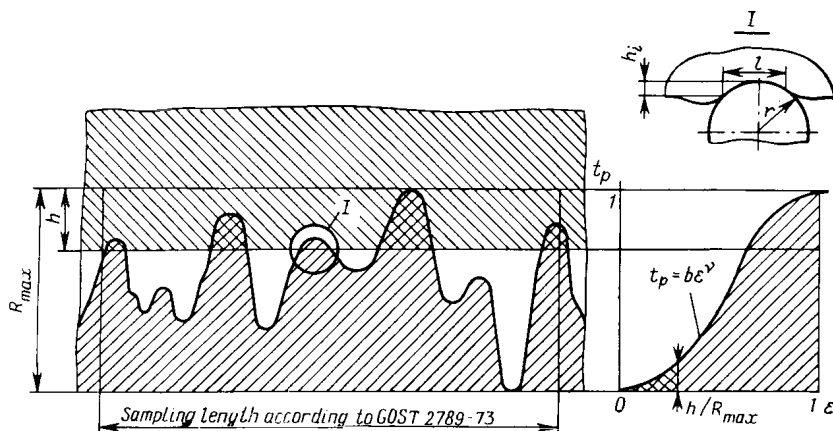


Fig. 3.3. Contact of a rigid rough solid with the flat surface of the material being deformed

irregularity

$$d \approx \sqrt{2rh}$$

Then

$$\frac{h}{d} \approx 0.7 \sqrt{\frac{h}{r}}$$

For a multiple contact, we have the following main equation for calculating the wear rate:

$$I = K_1 \alpha \sqrt{\frac{h}{r}} \frac{p_a}{p_r} \frac{1}{n} \quad (3.8)$$

where K_1 = factor determined by the geometric shape and height of individual asperities on the surfaces of solids (commonly, $K_1 \approx 0.2$) and $\alpha = \frac{A_r}{A_a}$ = coefficient of mutual overlap.

The rate of wear, I , can vary from 10^{-3} to 10^{-12} (Table 3.1).

Table 3.1

Typical values of dimensionless rate of wear I for different machine components

Wearing component	I	Note
Cylinder liners: in Model ЯМЗ-236 engine	1.8×10^{-12} 2.5×10^{-12}	Piston rings: tin-plated chromium-plated
Piston rings: tin-plated, in Model ЯМЗ-236 engine chromium-plated, in Model ЯМЗ-236 engine in Model Д-48Т engine	2.5×10^{-11} 2.5×10^{-12} 4×10^{-11}	Cast-iron cylinder liners
Automobile engine crankshafts: rod journals main journals	4×10^{-11} - 5×10^{-12} 1.6×10^{-11} - 1.8×10^{-12}	Steel on bearing metal
Stub axle spindle in steering axle of Model ЗИЛ-130 truck	1.8×10^{-9} 1.6×10^{-9}	Lubricant Grade 1-13 Metalplating lubricant
Components of Model Э-302, Э-505, Э-651, and other excavators: slewing plate swivel splined shaft gears of reversing mechanism: cylindrical bevel chain-drive sprocket in reversing mechanism claws in clutch of reversing mechanism bucket teeth	8.6×10^{-11} 5.3×10^{-10} 1.5×10^{-11} 6.3×10^{-12} 7.3×10^{-12} 6.3×10^{-10} 10^{-4} - 10^{-3}	Materials of mating components: Steel Grade 50Г—steel Grade ИХ15 Steel Grade 40Х—steel Grade 35ГЛ Steel Grade 40Х—steel Grade 45 Steel Grade 40—steel Grade 40Х Steel Grade 45—steel Grade 45 Same Same
Machine-tool guideways Shaper ram	2×10^{-9} - 4×10^{-10} 2×10^{-11}	Cast iron on cast iron Same
Cutting tools: from cemented-carbide Grade Т15К6 in air: without cutting fluid	$(1.5 \text{ to } 6) \times 10^{-8}$	Material machined: Steel Grade 40Х, $v = 150$ -230 m/min

Table 3.1 (cont.)

Wearing component	<i>I</i>	Note
T5K10 tools in air: flank wear	1.1×10^{-8}	Steel Grade 40X, $v = 180$ m/min
face wear	2.2×10^{-8}	—
The same in 5×10^{-6} Hg vacuum: flank wear	5.8×10^{-8}	—
face wear	4.1×10^{-8}	—
Tools from steel Grade P9K5 in air: flank wear	5.5×10^{-7}	Steel Grade XH35BT10, $v = 4$ m/min
face wear	6×10^{-7}	—
The same in 5×10^{-6} mm Hg vacuum: flank wear	8.5×10^{-7}	—
face wear	1.1×10^{-6}	—
Limit gauges: from cemented carbide from alloy Grade HM-332 and steel Grade Y10A	10^{-10} $(1.3 \text{ to } 2.9) \times 10^{-9}$	— —
Friction components in brakes disk-type drum-type shoe-type	8×10^{-7} - 4×10^{-10} $(2 \text{ to } 8) \times 10^{-7}$ 2×6^{-6} - 10^{-7}	— — —
Sliding bearings for boring bits	10^{-5} - 10^{-7}	—
Couplings, clutches, and limited-motion bearings subject to vibration	8×10^{-6} - 10^{-8}	Wear is caused by fretting-corrosion
Rotor blades in soil mixers: for sand for loam	$(2.1 \text{ to } 3.4) \times 10^{-8}$ $(4 \text{ to } 10) \times 10^{-8}$	— —
Tyre tread	2×10^{-8} - 10^{-9}	On asphalt covering
Rubber seals (unlubricated)	5×10^{-7} - 5×10^{-8}	On steel
Rolling elements in bearings operating in aqueous environment	$(0.7 \text{ to } 2) \times 10^{-10}$ $(1.3 \text{ to } 4.3) \times 10^{-9}$	$\sigma_{\max} < 200$ kgf/mm ² $\sigma_{\max} > 200$ kgf/mm ²

Table 3.1 (cont.)

Wearing component	<i>I</i>	Note
Bronze bushes in dampers	2×10^{-11}	—
Hinged jorns in aircraft undercarriage:		
grease Grade ЦИАТИМ-201 + Pb	1.3×10^{-10}	Steel Grade 30ХГСА
grease Grade ЦИАТИМ-201	5.2×10^{-10}	Bronze Grade БрАЖМц
Bearing bushes from self-lubricating materials:		
АМАН-4	1×10^{-9}	
П68ДМ-1.5	2×10^{-9}	
sprelaflon (made in GDR)	6×10^{-9}	
Polymer coating Grade ФБФ-74Д on steel at 400-800 kgf/cm ²	2×10^{-8} - 3×10^{-7}	

On the basis of experience [12], the following classes of wear resistance may be recommended:

Class	0	I	II	III	IV	V	VI	VII	VIII	IX
$\lg I_{\min}$	-13	-12	-11	-10	-9	-8	-7	-6	-5	-4
$\lg I_{\text{зам}}$	-12	-11	-10	-9	-8	-7	-6	-5	-4	-3

The established wear resistance classes are characterized by the main types of contact frictional interactions adopted in the mechanics of solids:

Classes I-V — elastic deformations;

Classes VI-VII — elastic-plastic deformations;

Classes VIII-IX — microcutting.

The rate of wear depends on the type of contact interaction between the mating bodies. For this reason, the elastic contact interactions must be ensured in every case. Such interactions mostly come about all by themselves, as a result of the running-in of the mating surfaces, which leads to changes in the shape and height of the contacting irregularities.

Let us consider the significance of each of the factors entering into formula (3.8). The first factor expresses the relative depth of penetration of surface irregularities; this depth determines the type of contact. For elastic contact it must be smaller than 10^{-2} and 10^{-4} with ferrous and non-ferrous alloys, respectively. It should be noted that with $\frac{h}{r} > 0.5$ external friction is impossible. The second factor determines the ratio of the real area of contact to the apparent

area. Because of surface roughness and waviness, this ratio is always smaller than unity. It ranges from 10^{-4} to 10^{-2} for metals and from 10^{-2} to 10^{-1} for elastomers (polymers, rubber). The third factor characterizes the resistance of the material to rupture with repeated frictional interactions (fatigue resistance). This factor depends on the material properties, the magnitude of stress effective at the contact, the character of the mechanical and chemical processes occurring in the contact area, and the presence of lubrication or gaseous ambience. Varying over a wide range (from 10^{-2} to 10^{-10}), this factor has a prevalent effect on the wear rate.

Let us calculate the dimensionless factors entering into formula (3.8) for the case of interaction between an absolutely rigid, rough (but not wavy) surface and an elastically-deformed body subject to wear. The rough surface is characterized by the surface-geometry complex parameter Δ and the bearing-area curve parameters b and v . From the known equation for the bearing-area curve (see Ch. 2), we obtain

$$\sqrt{\frac{h}{r}} = \left(\frac{2p_c}{p_r} \right)^{\frac{1}{2v}} \Delta^{\frac{1}{2}}$$

The second dimensionless factor $\left(\frac{p_a}{p_r} \right)$ can be calculated by using formula (3.11), where $p_a = p_c$.

Consider the last factor $\frac{1}{n}$ in formula (3.8). It is known that the number of cycles n causing a material's rupture decreases with increasing magnitude of stress. This relationship is referred to as the Veler fatigue curve. The fatigue curve is described analytically with empirical exponent-type formulas:

for elastic contact

$$n = \left(\frac{\sigma_0}{\sigma_{eff}} \right)^{t_f} \quad (3.9)$$

where σ_{eff} and σ_0 = effective and ultimate tensile stresses at a single elongation cycle and t_f = parameter of the frictional fatigue curve. It should be noted that during contact between rough surfaces, a single frictional bond is subject to random variations of the effective stress because of different asperity heights. Consideration of the statistical relationships at unstable loading of contact spots and application of the hypothesis on the linear addition of the adverse effects of fatigue allows the number of cycles up to the separation of a wear particle to be taken into account through the correction factor K_{tv} , given in the nomograph of Fig. 3.4 [12].

When calculating a material for wear resistance, the characteristics that normally are used for the estimation of the bulk strength properties of solids are not sufficient; it is necessary to know the specific characteristics of the materials for the components of the sliding pair. The exponent t_f of the fatigue curve in essence accounts

for the whole complex of physical and chemical processes that occur during sliding. It cannot yet be calculated; therefore, it is determined experimentally by the following methods.

(1) *From wear tests.*

Here, data can be used either from field wear tests or from tests on laboratory wear-testing machines, Models И-47, СМЦ2, МДП, МТП, and the like. The major drawback to this method, namely its low efficiency, is remedied by the use of multiposition wear-testing machines on which several specimens are investigated simultaneously under different loads.

(2) *From tests on equipment with localized contact, that is, on cyclo-meters [14].*

For materials that do not come into mechanical or chemical interaction with the lubricant, the ambience, or the mating component, the parameter t_f can be taken from the results of testing for the bulk fatigue life. For the most typical rubbing conditions, the values of t_f are listed in Table 3.2.

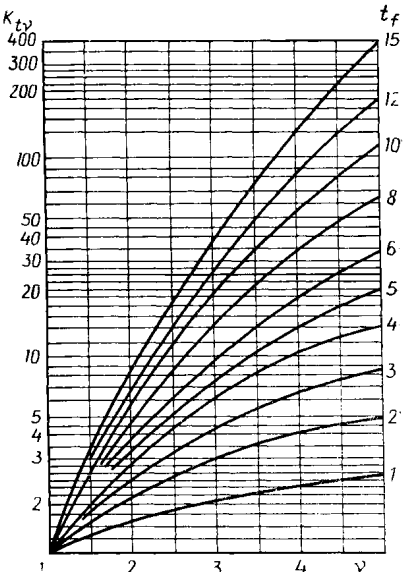


Fig. 3.4. Nomograph for determining the coefficient K_{tv}

Values of frictional fatigue parameter in sliding without lubrication on a steel specimen in air

Table 3.2

Material	σ_0 , kgf/cm ²	t_f	Material	σ_0 , kgf/cm ²	t_f
Steel Grade 45	7,000	7.9	Butadien-styrene-base rubber:		
Cast iron Grade 4HMX	6,600	4.1	for treads*	1,600	3.4
Graphite Grades:			for packings at 100°C	216	4.8
AF-1500	200	2.0	Polyformaldehyde	1,470	1.3
AO-1500	250	2.6	Polycarbonate	8,400	2.9
AMC	800	2.4	Unfilled epoxy resin	1,800	4.6
Electrographite	2,750	6.7	R82	14,200	3.1
НИГРАН	250	2.0	Fluoroplastic Grade 4	630	5.0
Rubbers with elastic moduli, E , kgf/cm ² :			Retinax Grade		
22	2,110	3.0	ФК-240	11,840	12.6
28	1,450	3.4	АФ-3АМ	27,300	2.9
32.5	8,500	3.6	Caprolon	6,300	2.6

* On concrete covering.

3.3. MAIN DESIGN RELATIONSHIPS

After transformations the main equation (3.8) for elastic contact will take the form

$$I = K_1 \alpha 2^{\frac{1}{2v}} p_a p_c^{\frac{1}{2v}} p_r^{t-1-\frac{1}{2v}} \Delta^{\frac{1}{2}} \left(\frac{k f_{ml}}{\sigma_0} \right)^{t_f} \quad (3.10)$$

The real contact pressure is calculated by the formula

$$p_r = 0.5 E^{\frac{2v}{2v+1}} \Delta^{\frac{v}{2v+1}} p_c^{\frac{1}{2v+1}} \quad (3.11)$$

The contour pressure (without regard to the effect of surface roughness on the deformation of waves [1])

$$p_c = 0.2 E^{0.8} \left(\frac{H_b}{R_b} \right)^{0.4} p_a^{0.2} \quad (3.12)$$

It is suitable to distinguish between the following varieties of contact.

(1) The contact between rough unrun surfaces which have no waviness ($p_c = p_a$). This case applies to small joints wherein the dimensions limiting the apparent contact area are commensurable with the sampling length according to GOST 2789-73; examples are watch-movement bearings, mechanical instrument components, many types of thread, pin, key and other joints. This type of contact also takes place in joints wherein one of the mating parts has a low stiffness, for instance, guide bars, single- or multi-point cutting tools, and in joints representing higher-order kinematic pairs, such as gear transmissions, cams, and wheel-and-rail pairs.

(2) The contact between rough, wavy and unrun surfaces ($p_c \neq p_a$). Examples are machine-tool guideways, disc-type brakes, and clutches.

(3) The contact between run-in surfaces. This case applies to parts of any configurations wherein an optimum roughness has developed on the rubbing surfaces, which duplicates itself as the part wears out.

Substituting the appropriate expressions for the real and contour pressures into formula (3.10), we derive formulas suitable for engineering calculations for wear resistance. For the contact of surfaces wherein $p_a = p_c$, after substituting formula (3.11) into (3.10), we shall have

$$I = K_2 \alpha K_{tv} p^{1 + \frac{t_v}{2v+1}} E^{\frac{2vt_v}{2v+1}-1} \Delta^{\frac{vt_v}{2v+1}} \left(\frac{k f_{ml}}{\sigma_0} \right)^{t_f} \quad (3.13)$$

where

$$K_2 = 0.5^{t_f-1-\frac{1}{2v}} \times 2^{\frac{1}{2v}} K_1$$

At $\nu = 2$, which conforms to a substantially normal law of height distribution of the asperities

$$I = K_2 \alpha K_{tv} p^{1 + \frac{t_f}{5}} E^{-\frac{4t_f}{5}} \Delta^{-\frac{2t_f}{5}} \left(\frac{k f_{ml}}{\sigma_0} \right)^{t_f}$$

For the elastic contact of wavy planes, with regard to (3.12), we shall obtain

$$I = K_3 \alpha K_{tv} p^{1 + \frac{t_f}{5(2\nu+1)}} E^{-\frac{2t_f(5\nu+2)}{5(2\nu+1)}} \Delta^{-\frac{\nu t_f}{2\nu+1}} \times \left(\frac{H_b}{R_b} \right)^{\frac{2t_f}{5(2\nu+1)}} \left(\frac{k f_{ml}}{\sigma_0} \right)^{t_f} \quad (3.14)$$

where $K_3 = K_2 \times 0.2^{\frac{t_f}{2\nu+1}}$ = numerical factor depending on the parameters t_f and ν (Fig. 3.5).

Ignoring insignificant departures from the proportionality between the wear rate and the nominal pressure at $\nu = 2$, we have

$$I \approx K_3 \alpha K_{tv} p E^{t_f} \times \left(\frac{H_b}{R_b} \right)^{0.1 t_f} \Delta^{0.4 t_f} \left(\frac{k f_{ml}}{\sigma_0} \right)^{t_f}$$

Let us derive an expression for the wear rate of run-in surfaces [7]. In this case, the real contact pressure will be

$$p_r \approx 0.7 \sqrt{\frac{\tau_0 E}{\alpha_h}}$$

Then the coefficient of friction without regard to the mechanical component will be

$$f \approx 1.4 \sqrt{\frac{\tau_0 \alpha_h}{E}} + \beta$$

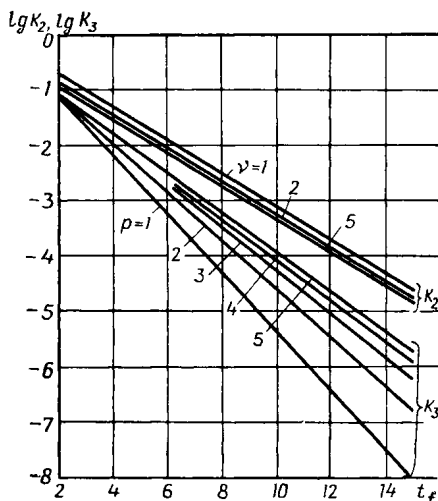


Fig. 3.5. Nomograph for determining the coefficients K_2 and K_3

Hence, the coefficient of friction for run-in surfaces does not virtually depend on the applied load and the geometry of the rubbing surfaces.

The surface roughness developed as a result of running-in [5] can be estimated by the formula

$$\Delta \approx \frac{15 \tau_0^{5/4}}{E^{3/4} p^{1/2} \alpha_h^{5/4}} \quad (3.15)$$

After substituting expression (3.15) into (3.13) we obtain

$$I = K_2 15^{\frac{2t_f}{5}} \alpha K_{tv} p E^{\frac{t_f}{2}-1} \tau_0^{1/2} \frac{1}{\alpha_h^{1/2}} \left(\frac{k f_{ml}}{\sigma_0} \right)^{t_f} \quad (3.16)$$

The derived relationships also apply to other types of sliding pairs.

Where the difference between the elastic properties of the member causing wear and the member subjected to wear is not great, it is good practice to use the effective elastic modulus

$$E_{eff} = \frac{E_1 E_2}{E_1 + E_2}$$

More accurate results will be obtained if in the above relationships the appropriate coefficients of elasticity $\Theta = \frac{1-\mu^2}{E}$ are substituted for the elastic modulus. The increase in accuracy, however, will not be significant.

The surface roughness of the component subject to wear can be allowed for by using the effective values of the roughness parameters:

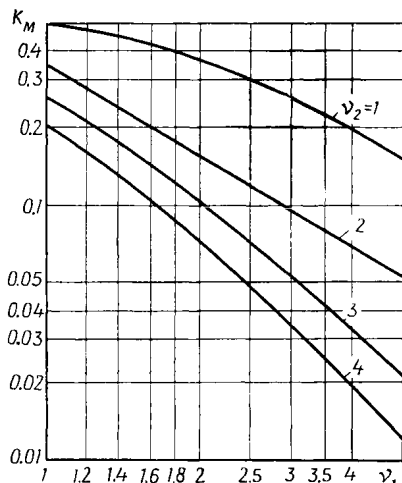


Fig. 3.6. Nomograph for determining the coefficient K_M

$$r_{1,2} = \frac{r_1 r_2}{r_1 + r_2} R_{\max_{1,2}} = R_{\max_1} + R_{\max_2}, \quad v_{1,2} = v_1 + v_2$$

$$b_{1,2} = b_1 b_2 \frac{K_M R_{\max_{1,2}}}{R_{\max_1}^{v_1} R_{\max_2}^{v_2}}$$

The coefficient K_M , as a function of v_1 and v_2 , is given in Fig. 3.6.

With $v_1 = v_2 = 2$

$$\Delta_{1,2} = \frac{1.6 (R_{\max_1} R_{\max_2})^{1/2}}{r_{1,2} (b_1 b_2)^{1/4}}$$

If the mating surfaces differ in roughness by more than two classes, the roughness of the smoother surface may be neglected.

3.4. FACTORS AFFECTING WEAR RATE

The foregoing design relationships (3.13), (3.14), and (3.16) allow the effect of the various factors on wear to be understood. For many surfaces obtained by different machining methods (see Ch. 2), as

well as for run-in surfaces, $\nu \approx 2$. The frictional fatigue parameter t_f varies within the range of $2 < t_f < 10$ for most materials. Based on the above values of ν and t_f , Table 3.3 gives the ranges of the

Table 3.3

Effect of various factors on wear*

Rubbing surface	Exponent for the quantity						
	p_a	E	Δ	$\frac{H_b}{R_b}$	f_{ml}	τ_0	α_h
Rough, nonwavy and un-run	1.4-3	0.6-7	0.8-4	—	2-10	—	—
Rough, wavy and un-run	1.08-1.4	1.9-9.6	0.8-4	0.16-0.8	2-10	—	—
Run-in	1	0-4	—	—	2-10	0.5	1-5

* For most surfaces $\nu \approx 2$, $2 < t_f < 10$.

variation of exponents (depending on ν and t_f) for the parameters that take into account various factors affecting the wear rate. Let us consider each of these factors.

Specific load (nominal pressure). For un-run surfaces, wear is a nonlinear function of the specific load, whose effect is more pronounced ($I \approx p_a^{(1.4 \text{ to } 3)}$) for surfaces with a small contact area, that is, nonwavy surfaces. Waviness substantially decreases the nonlinearity of this relationship. For run-in surfaces, the wear rate varies directly with the specific load. Thus, in the general case $I \approx p_a^{(1 \text{ to } 3)}$, which agrees with field tests [20] and with numerous laboratory tests of machine parts.

Elastic properties of the material (elastic modulus). The elastic modulus has a marked effect on the wear rate of a material, its rise leading to increase in I for materials with identical rupture strength. The exponent for the elastic modulus varies most widely and has the largest absolute value. The wider range of the variation corresponds to the contact of a nonwavy rough surface, whereas the larger absolute value of the exponent holds for a rough and wavy surface. A clear-cut relationship between the elastic modulus and the wear rate is difficult to arrive at experimentally, because the elastic modulus is also related to the materials frictional properties, particularly to the coefficient of friction, and to strength characteristics (σ_0 , t_f).

Imperfect elasticity is accounted for by the hysteresis loss factor α_h , whose knowledge is essential for predicting the wear of run-in surfaces. Some values of α_h are given in [7].

Strength characteristics of the material (σ_0 , t_f). Increase in the absolute values of these characteristics always has a benefi-

cial influence on wear life. The higher the σ_0 , the stronger the material for a single rupture; the greater the t_f , the larger the number of cycles needed to break away a wear particle.

Frictional properties of the joint (the coefficient of friction f). The wear rate depends on the coefficient of friction ($I \approx f^{t_f}$) as strongly as on the strength properties (σ_0). This relationship is not simple, because the coefficient of friction f also depends on the elastic properties of the material, surface roughness, specific load, and the parameters characterizing molecular interactions at the contact.

Roughness and waviness of surfaces. Surface geometry has a marked effect on the wear rate. Because the complex roughness parameter Δ may vary over the range of $10^{-3} < \Delta < 1$ (that is, within four orders of magnitude), and the exponent for Δ ranges from 0.8 to 4, neglect of roughness can result in an error of several orders of magnitude in the calculation of wear rate [8].

Waviness can vary the wear rate in a smaller range, because $10^{-3} > \frac{H_b}{R_b} > 10^{-6}$, whereas the value of the exponent is less than unity and can only rise fourfold, which in extreme cases gives a variation of I about two orders of magnitude. Therefore, waviness must be taken into account, even though the accuracy of determining the absolute value of the waviness parameter required for calculation is relatively low. The geometry of run-in rubbing surfaces has no effect on wear rate.

Molecular contact interaction, depending on various rubbing conditions, that is, the type of lubricant, the cleanliness of the surfaces, and the parameters and cleanliness of the gaseous environment, is accounted for by the coefficient of friction, particularly by the parameters τ_0 and β . The wear rate of friction surfaces varies with their resistance to shear. For this reason the use of lubrication extends the wear life of tribological components.

Speed and temperature factor. The effect of sliding speed on wear rate is not yet sufficiently understood. The sliding speed determines the time of existence of a single frictional bond and, consequently, the rate of the material's deformation. The toughness of the frictional bond, therefore, affects the friction and wear of materials. The intensity of heat generation and the contact temperature depend on sliding speed. The heating of surface layers in rubbing bodies causes changes in their mechanical and frictional properties, as well as in mechanical and chemical structures. For these reasons, the wear-temperature relationship should be regarded as one governed by the temperature relationships for the material's properties included in the equations for wear-rate calculations, that is, t_f , σ_0 , f and E .

The elastic modulus E varies (decreases) relatively little with increasing temperature. Depending on temperature, the coefficient of friction can diminish, rise, or remain invariable. This is explained by diverse changes in the ratio between the molecular and the me-

chanical component of the coefficient of friction. The variation of t_f with temperature is still unclear. For this reason, t_f should be determined under temperature conditions similar to those which will be effective in the actual friction joint.

Particularly worth mentioning are the critical points at the curves that represent the relationship between the wear rate and the parameters characterizing the generation of heat at the contact, namely, temperature, speed and load. When the contact temperature reaches a certain level during simultaneous action of mechanical and chemical factors, fundamental changes take place in the material, and its surface layers acquire essentially new mechanical properties [15] that are accompanied by a stepwise change of several orders of magnitude in the wear rate (Fig. 3.7). To identify such critical points, experiments on frictional heat resistance must be conducted wherein the empirical relation of the coefficient of friction and the wear rate to the temperature effective near the rubbing surface must be obtained.

The disclosed calculation applies to a stable motion in unlubricated frictional conditions and during boundary friction.

The results of calculation of the wear rate in various sliding pairs by this method show a satisfactory agreement with experimental data [11]. Random variations in the parameters entering into the equations may be considered one of the causes of scattering. The maximum possible discrepancy is of about one order of magnitude.

The proposed calculation method offers the designer the following advantages: — the life expectancy of a movable joint can be calculated; — the influence of the various process variables and physicomaterial properties of materials and lubricants on wear can be revealed; — experimental results obtained in some conditions can be corrected for other conditions.

Calculation example. Calculate the wear rate of an axial seal consisting of a flange made from steel Grade 45 and a polycarbonate packing ring. The flange frictional surface is machined by cylindrical grinding, and the roughness parameter $Ra = 0.2$. The nominal pressure is 5 kgf/cm^2 . The coefficient of friction equals 0.2. Determine the wear of the packing ring over a sliding distance of 100 km.

The physico-mechanical properties of polycarbonate under the given running conditions: $E = 12,000 \text{ kgf/cm}^2$, $\sigma_0 = 8,400 \text{ kgf/cm}^2$, and $t_f = 2.9$.

The flange surface roughness is characterized by the complex roughness parameter $\Delta = 0.01$ (see Ch. 1) and $v = 2$. Calculate I by formula (3.13), with $\alpha = 1$, $K_{tv} = 2.4$:

$$I = 0.2 \times 0.5^{1.65} \times 2^{0.25} \times 2.4 \times 12,000^{1.32} \times 0.01^{1.16} \left(\frac{3 \times 0.2}{8,400} \right)^{2.9} = 2 \times 10^{-9}$$

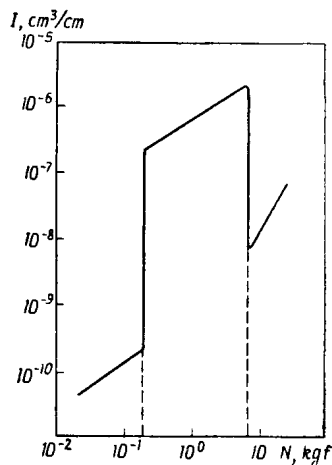


Fig. 3.7. Variation of wear rate with load for steel having 0.52% C at $v = 2.6 \text{ m/s}$ (after N. Welsh)

Then the wear of the packing ring over a sliding distance of 100 km will be

$$U = IL = 2 \times 10^{-9} \times 10^9 = 0.2 \text{ mm}$$

REFERENCES

1. Алисин В. В., Комбалов В. С. Учет волнистости поверхностей при расчете площадей касания. — «Надежность и контроль качества», 1975, № 8, с. 38—48.
2. Денисова К. Е., Гонтарь И. Н., Романов В. М. Износостойкость зубчатых колес из пластмасс. — «Вестник машиностроения», 1971, № 3, с. 48—49.
3. Дроздов Ю. Н. К расчету зубчатых передач на износ. — «Машиноведение», 1969, № 2, с. 84—88.
4. Исследование структуры фрикционных материалов. М., «Наука», 1972. Авт.: З. В. Игнатьева, И. В. Крагельский, И. М. Любарский и др.
5. Комбалов В. С. Влияние шероховатости твердых тел на трение и износ. М., «Наука», 1974.
6. Крагельский И. В. Некоторые понятия и определения, относящиеся к трению и изнашиванию. М., Институт машиноведения, 1957.
7. Крагельский И. В., Алисин В. В. Расчетный метод оценки трения и износа — эффективный путь повышения надежности и долговечности машин. М., «Знание», 1976.
8. Крагельский И. В., Комбалов В. С., Алисин В. В. Влияние размера поверхности касания на трение и износ. — В кн.: Механика и физика контактного взаимодействия. Вып. 1. Калинин, Калининский политехнический ин-т, 1975, с. 4—14.
9. Крагельский И. В., Непомнящий Е. Ф. Теория износа высокоэластичных материалов. — В кн.: Пластмассы в подшипниках скольжения (исследования и опыт применения). М., «Наука», 1965, с. 49—56.
10. Крагельский И. В., Непомнящий Е. Ф., Харач Г. М. Физико-механические свойства полимеров, обеспечивающие высокую износостойкость узлов трения. — В кн.: Обработка пластмасс в машиностроении. М., «Наука», 1968, с. 42—54.
11. Крагельский И. В., Непомнящий Е. Ф., Харач Г. М. Корреляция расчетной оценки износа поверхностей трения с экспериментом. «ДАН СССР», т. 185, № 4, 1969, с. 802—804.
12. Крагельский И. В., Харач Г. М. О расчете износа поверхностей трения. — В кн.: Расчетные методы оценки трения и износа. Брянск, Приокское книжное изд-во, Брянское отделение, 1975, с. 5—47.
13. Крагельский И. В., Щедров В. С. Развитие науки о трении. М., Изд-во АН СССР, 1956.
14. Логинов А. Р. Методы оценки характеристик фрикционной усталости материалов. — В кн.: Исследования по триботехнике. М., НИИ информации по машиностроению, 1975, с. 217—225.
15. Любарский И. М., Палатник Л. С. Металлофизика трения. М., «Металлургия», 1976.
16. Марченко Е. А., Непомнящий Е. Ф., Харач Г. М. Циклический характер накопления искажений II рода в поверхностном слое как физическое подтверждение усталостной природы износа. «ДАН СССР», 1968, т. 118, № 5, с. 1103—1104.
17. Радчик А. С., Радчик В. С. О деформации поверхностных слоев при трении скольжения. «ДАН СССР», 1958, т. 119, № 5, с. 933—935.
18. Ратнер С. Б. О роли усталостных процессов при истирании полимерных материалов. «ДАН СССР», 1963, т. 150, № 4, с. 150—154.
19. Ребиндер П. А. Физико-химическая механика — новая область науки. М., «Знание», 1958.
20. Решетов Д. Н. Детали машин. М., «Машиностроение», 1973, с. 655.
21. Rosenaw L. Fatigue wear as a rate process. Wear, vol. 6, No 5, 1963, p. 33-340.

CALCULATION OF TRIBOLOGICAL JOINTS FOR WEAR

4.1. WEAR IN TRIBOLOGICAL JOINTS

4.1.1. Basic Laws of Wear in Materials

The wear calculation of machine parts must be based on the physical laws of wear effective both for the materials used in a given joint and for given operating conditions. The first step in the calculation is establishing the limiting conditions that determine the type of wear in the joint so that unallowable types of wear (for instance, seizure) are avoided. Secondly, analytical relationships for the rate of wear in sliding pairs must be employed, the relationship used being considered as a function of random variables, since each of the parameters governing the wear rate tends to scatter.

The calculation of joints for wear is primarily intended for estimating the distribution of pressure and linear wear over the rubbing surface; it must also assess the change in the relative position of the mating parts that has resulted from their wear, and relate the wear of the materials to that of the parts, to the functional properties of machine units and to the design and dimensions of joints.

The calculation also requires knowledge of the development of wear in time. For most cases, the relationship between the time t taken by the wearing process and the amount of wear U can be assumed to be linear; then the time rate of wear

$$\gamma = \frac{U}{t} = \text{const}$$

According to the fatigue theory of different types of wear (elastic contact, plastic contact, or microcutting), the linear rate of wear is proportional to the pressure in the contact area:

$$I = k p^m$$

where $1 < m < 3$; for run-in surfaces, $m \approx 1$.

In abrasive-wear conditions, there is also a linear relationship between the linear wear rate and the pressure, expressed, according to M. M. Khrushchov, as $I = kp$, that is, the linear wear U does not depend on the speed of the relative sliding over identical rubbing path: $U = kpL$.

Dividing both parts of this equation by the time of operation of the joint, we obtain

$$\gamma = kp v \quad (4.1)$$

where k = coefficient that characterizes the wear resistance of the material and the running conditions of the joint (lubrication, protection of the rubbing surfaces against fouling, and so on).

The time wear rate (γ) and the linear wear rate (I) are related by the equation $\gamma = vI$.

These laws can be used for the wear calculation of many machine parts (slideways, plates in friction clutches, lead screws and nuts, slotted links in crank mechanisms, and the like). In the general case, the time wear rate can be expressed as a power function:

$$\gamma = kp^n v^n \quad (4.2)$$

Commonly, for abrasive wear $n = 1$.

The value of the coefficient k is affected primarily by the materials of the sliding pair, geometry of the surfaces in contact, and lubrication (see Ch. 3).

4.1.2. Wear of the Surface and Joint

The main characteristic for the assessment of *wear of a surface* is the *linear wear* (U), which is defined as the change in the part's dimension in a direction perpendicular to the rubbing surface. Generally, wear does not spread uniformly over the surface; for this reason, $U = f(x, y)$, where x and y are the coordinates of the rubbing surface.

Wear occurs during the sliding of two mating surfaces which wear away simultaneously with the result that their mutual position alters.

Wear of a joint is a characteristic of the mutual approach of the mating parts as they wear away. Wear of this type is measured by one or several geometric parameters that cause the change in the relative position of the mating parts, resulting from their wear.

Wear of joints is directly responsible for the loss of the original functional characteristics by a machine or mechanism. The design and kinematic features of a given sliding pair are of great importance, because they control the character and direction of displacement (approach) that is likely to result from wear.

Figure 4.1 shows diagrams for determining wear in typical sliding pairs. For rotational components that run in wear-resistant bearings, the direction $x-x$ of the likely mutual approach is known beforehand (Fig. 4.1a).

In this case, wear of the joint is characterized by a single parameter U_{1-2} , which is the amount of the relative approach of the worn parts 1 and 2 in the direction $x-x$.

Since the approach of the parts is possible only in the direction $x-x$, the sum of the amounts of wear of the parts, measured in the

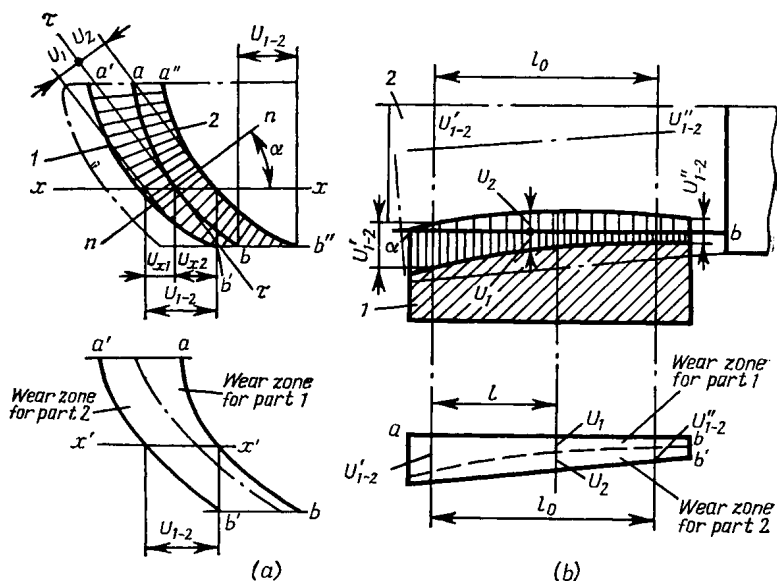


Fig. 4.1. Wear of joints and mating surfaces

(a) direction of the mutual approach of mating parts is predetermined; (b) mating parts self-align as they wear

direction of the possible approach, is bound to be constant and equal to the amount of wear of the whole joint, that is, $U_{x1} + U_{x2} = U_{1-2} = \text{const.}$

This relationship might be called the *condition of contact of bodies*, because it characterizes one important feature of the joint's wear process, namely, that the worn surfaces of the parts are in full contact, regardless of their shape. Because the contact surface $a'b'$ and $a''b''$ is common for the two parts, one can construct a region, usually referred to as the region of mutual penetration, that characterizes the volume of the worn material in each of the mating parts. The region of mutual penetration is a diagram of wear that is outlined by the curve of the original, not worn surface ab , with $a'b'$ and $a''b''$ brought into coincidence (see the lower part of Fig. 4.1a).

From the condition of contact, the following equations hold for any point of the surface:

$$U_{1-2} = \frac{U_1 + U_2}{\cos \alpha} \quad \text{or} \quad \gamma_{1-2} = \frac{\gamma_1 + \gamma_2}{\cos \alpha} \quad (4.3)$$

where U_1 and U_2 = wear of parts at a given point, measured in a normal direction $n-n$ to the rubbing surface, α = angle between the normal to the rubbing surface and the direction of possible approach, γ_{1-2} = time rate of wear in the joint, and γ_1 and γ_2 = time rates of wear of the parts at a given point.

For joints wherein the direction of mutual approach is not predetermined and the relative position of the mating parts is controlled by the character of the acting forces and the shape of the worn surface, different relationships will be valid.

A typical example of such a joint is an assembly of a shaft and a sliding bearing (Fig. 4.1b). As the parts wear away, the shaft lowers and tilts in the bearing, changing its position. A new position of the shaft, determining the wear of the joint, can be defined in two ways: either by the displacement of a point on the shaft axis and the angle of axis inclination, or by two linear parameters U'_{1-2} and U''_{1-2} .

The points on the shaft axis, at which the above values are measured, may be chosen arbitrarily.

The values of U'_{1-2} and U''_{1-2} are measured in a direction perpendicular to the original position of the axis of rotation without regard to the small inclination angle of the shaft that results from wear.

In order to find the relationship between the parameters characterizing wear of the joint (U'_{1-2} and U''_{1-2}) and wear of the mating parts (U_1 and U_2) at some point with a coordinate l , let us consider the region of mutual penetration for this case (see the lower part of Fig. 4.1b). Here

$$U_1 + U_2 = U'_{1-2} \left(1 - \frac{l}{l_0}\right) + U''_{1-2} \frac{l}{l_0} \quad (4.4)$$

where l_0 = distance between the points where the parameters U'_{1-2} and U''_{1-2} defining the wear of the joint are measured.

A more complex case of wear takes place where both parameters U'_{1-2} and U''_{1-2} are a function of the relative position of the mating parts.

4.1.3. Classification of Joints by Wear Conditions

Solving the problems associated with wear of machine components requires a clear understanding of the fact that the design of a joint has a marked effect on the distribution of wear over the rubbing surface and on the character of interaction between the worn surfaces. In many cases the influence of the design factors on the shape of a worn surface proves greater than the influence of the nature of wear in materials.

For instance, the shape of the worn surface in straight slideways depends on the acting forces, the character of relative motion, and the shape and dimensions of the slideways, rather than on the materials they are made from.

When developing a machine, the design engineer needs the wear calculation methods suitable for the various joints the machine is to incorporate, so that he is able to arrive at appropriate design decisions. A classification of typical joints by their wear conditions is given in Table 4.1. According to the nature of the likely approach of the parts, that results from wear of their surfaces all the joints are divided into two types. The type I joints have additional non-

Table 4.1

Classification of joints by wear conditions

Type	A		B		
	1st group	2nd group	3rd group	4th group	5th group
I					
II					

Note: A — invariable contact conditions; B — variable contact conditions.

wearing or little-wearing guideways that provide for the approach of the worn parts in the specified direction $x-x$ only. In the type II joints, the parts are self-aligned, and their relative position depends on the shape of the worn surface. In such joints the effect of wear on the functional properties of the sliding pair is more pronounced.

Under this classification, all joints are further divided into five groups, depending on whether the frictional and wearing conditions are identical for the points of the mating surfaces, which move along one and the same path. With the 1st-group joints, the points moving along the same path wear away identically for each of the two parts (for instance, wear in rotational surfaces loaded centrally). Related to the 2nd group are joints wherein the wearing conditions are identical for points moving along the same path for one of the mating parts only (examples are sliding bearings and block-

type brakes). Placed in the 3rd group are joints representing a lower-order kinematic pair (slideways, crank mechanisms), and in the 4th group, joints representing a higher-order kinematic pair (antifriction bearings, cam mechanisms). With the 3rd- and 4th-group joints, the wearing conditions are not identical for all points of both mating parts: therefore, nonuniform wear is very likely in such joints.

Related to the 5th group are parts in contact with a solid substance or environment, such as soil, rock, or a part being machined. Here, wear of one surface only, which is acted upon by an abrasive or some other ambience is studied; the shape of the work surface will depend on the character of interaction (the diagram of loads or velocities) with the ambience. All the joints can also be broken down into two categories: *A* — such as have constant contact conditions, and *B* — such as have variable contact conditions (see the calculation methods below).

Joints of all the types referred to above are encountered in machinery and equipment (Table 4.2).

Table 4.2

Examples illustrating the classification of joints by wear conditions

Group	Type of joint	
	I (direction x-x specified)	II (self-aligning)
1	Cone and friction clutches	Plates of friction clutches
2	Lead screw and nut	Shaft and plain bearing; shoe brakes with self-aligning shoes; circular slideways (eccentrically loaded)
3	Piston rings and cylinder liner	Straight slideways; slider and slotted link
4	Toothed gearing; cam and cam follower	Wheel and rail; rolling bearings and guideways
5	Rigidly clamped cutting tools	Ploughshares; self-aligning cutting tools

The type and group to which a joint belongs determines the method of its calculation for wear and makes it possible to relate the design of the joint to its expected wear characteristics.

4.2. WEAR CALCULATION METHODS FOR TRIBOLOGICAL JOINTS

4.2.1. The Use of the Contact Condition

The following methods of wear calculation are applicable.

(a) *By the pressure* (average or maximum) effective at the rubbing surface; the obtained values are compared with the allowable ones, taken, as a rule, from practice.

The pressure is though a major, but not the only factor that determines the rate of wear. For this reason, calculations by pressure give but rough data on the dimensions of joints; in some instances, such calculations can even lead to erroneous conclusions about the ways of improving the wear resistance of the joint to be developed.

(b) *By the amount of wear and the shape of the worn surface.*

This calculation method indicates the main routes to extending the wear life of the joint both at the design stage and in service.

When determining the shape of the worn surface, the quantities to find are the amount of wear of the rubbing surfaces at every point, the diagram of pressure p at the interface, and the variation in the parts' relative position resulting from wear, that is, wear of the joint. These calculations are based on the laws of materials' wear and take into account the configuration of the joint.

In order to make the method clear, let us consider the wear calculation of a conical joint (Fig. 4.2) for linear laws of wear [see formula (4.1)].

Let us determine the character of the diagram of pressures in this instance. The origin of coordinates is suitable to locate at the cone apex, the y axis being directed along the cone generatrix. The speed of relative sliding at a given point of the rubbing surface will be

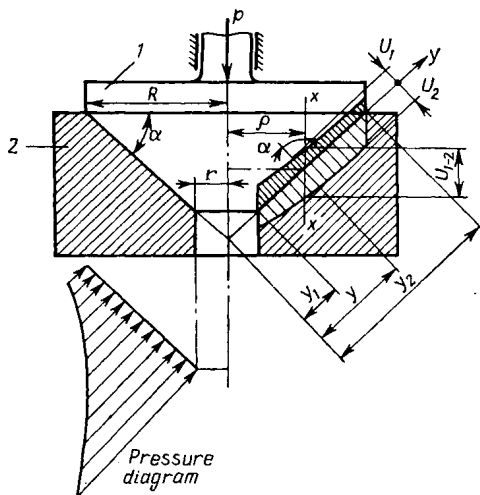


Fig. 4.2. Wear diagram for conical surfaces

$$v = 2\pi r n = 2\pi n y \cos \alpha$$

and relationships (4.1) will take the form

$$\left. \begin{aligned} \gamma_1 &= k_1 p \, 2\pi n \cos \alpha \cdot y \\ \gamma_2 &= k_2 p \, 2\pi n \cos \alpha \cdot y \end{aligned} \right\} \quad (4.5)$$

Applying formula (4.3), we shall have

$$\gamma_{1-2} = \frac{\gamma_1 + \gamma_2}{\cos \alpha} = (k_1 + k_2) \, 2\pi n p y$$

whence

$$p = \frac{\gamma_{1-2}}{2\pi n (k_1 + k_2) y} \quad (4.6)$$

From this equation it follows that the pressure diagram has a hyperbolic form since $\gamma_{1-2} = \text{const.}$

To find the values of γ_{1-2} , let us determine the relationship between the force P and the pressure p distributed over the rubbing surface:

$$P = \int_S p \cos \alpha \, dS = 2\pi \int_{y_1}^{y_2} p \cos \alpha \rho \, dy = 2\pi \cos^2 \alpha \int_{y_1}^{y_2} p y \, dy$$

where

$$y_1 = \frac{r}{\cos \alpha}, \quad y_2 = \frac{R}{\cos \alpha}, \quad \rho = y \cos \alpha$$

Substituting into this formula the values of p from formula (4.6), and integrating and solving the equation for γ_{1-2} , we shall obtain

$$\gamma_{1-2} = \frac{P n (k_1 + k_2)}{(R - r) \cos \alpha} \quad (4.7)$$

With this formula, the time rate of wear (or the amount of wear $U_{1-2} = \gamma_{1-2} t$) can be calculated for the joint, depending on its operating conditions (P and n), its dimensions and form (R , r , α), and the characteristics of wear for the materials of the mating parts (k_1 and k_2).

The pressure diagram can be calculated by the formula derived from relationships (4.6) and (4.7):

$$p = \frac{P}{2\pi (R - r) \cos \alpha} \frac{1}{y} \quad (4.8)$$

The configuration of the worn surface can be obtained from equations (4.5), substituting the value of p from equation (4.8):

$$\begin{aligned} U_1 &= \gamma_1 t = k_1 \frac{P n}{R - r} t \\ U_2 &= \gamma_2 t = k_2 \frac{P n}{R - r} t \end{aligned} \quad (4.9)$$

Similar design relationships can be arrived at for the joints of other types and for other laws of wear (see Table 4.3). The wear calculation for the 2nd-group joints is considered in [5].

Table 4.3

Type of joint	Wear law	Pressure diagram p	Shape of worn surface	Time rate of wear, γ_{1-2}
Disc-type surfaces	(1)	$\frac{P}{2\pi(R-r)} \frac{1}{\rho}$	$U_1 = k_1 \frac{Pn}{R-r} t; \quad U_2 = k_2 \frac{Pn}{R-r} t$	$\frac{(k_1 + k_2) Pn}{R-r}$
	(2) $n=1$	$\frac{m}{\sqrt{\frac{\gamma_{1-2}}{(k_1 + k_2) 2\pi n} \frac{1}{\rho}} = \frac{A}{m \sqrt{\rho}}}$ ($A = \text{const}$)	$U_1 = \gamma_{1-2} \frac{k_1}{k_1 + k_2} t$ $U_2 = \gamma_{1-2} \frac{k_2}{k_1 + k_2} t$	$(k_1 + k_2) \frac{\left(2 - \frac{1}{m}\right)^m Pmn}{\left(R - \frac{1}{m} - \frac{2}{r} - \frac{1}{m}\right)^m (2\pi)^{m-1}}$
Conical surfaces	(1)	$\frac{\gamma_{1-2}}{2\pi n(k_1 + k_2)} \frac{1}{y}$	$U_1 = k_1 \frac{Pn}{R-r} t; \quad U_2 = k_2 \frac{Pn}{R-r} t$	$\frac{P(k_1 + k_2)n}{(R-r) \cos \alpha}$
	(2) $n=1$	$\frac{m}{\sqrt{\frac{\gamma_{1-2}}{2\pi n(k_1 + k_2)} \frac{1}{y}}}$	$U_1 = \gamma_{1-2} \frac{k_1 \cos \alpha}{k_1 + k_2} t$ $U_2 = \gamma_{1-2} \frac{k_2 \cos \alpha}{k_1 + k_2} t$	$\frac{k_1 + k_2}{\cos \alpha} \left[\frac{\left(2 - \frac{1}{m}\right) P}{2\pi \left(R - \frac{1}{m} - \frac{2}{r} - \frac{1}{m}\right)} \right]^m \frac{2\pi n}{m}$
Spherical surfaces (with radius of sphere R)	(1)	$\frac{\gamma_{1-2}}{2\pi n(k_1 + k_2) R} \operatorname{ctg} \alpha$	$U_1 = \gamma_{1-2} \frac{k_1 \cos \alpha}{k_1 + k_2} t$ $U_2 = \gamma_{1-2} \frac{k_2 \cos \alpha}{k_1 + k_2} t$	$\frac{4Pn(k_1 + k_2)}{R(\sin 2\alpha_2 + 2\alpha_2 - \sin 2\alpha_1 - 2\alpha_1)}$
	(2) $n=1$	$\frac{m}{\sqrt{\frac{\gamma_{1-2} \cos \alpha}{(k_1 + k_2) 2\pi n R \sin \alpha}}}$	$U_1 = \gamma_{1-2} \frac{k_1 \cos \alpha}{k_1 + k_2} t$ $U_2 = \gamma_{1-2} \frac{k_2 \cos \alpha}{k_1 + k_2} t$	$\frac{Pm(k_1 + k_2)n}{(2\pi)^{m-1} R^{2m+2} \left[\int_{\alpha_1}^{\alpha_2} \frac{1}{1 + \frac{1}{m} d\alpha} \right]^m}$

Note: Here n = rotational frequency, rpm, and α_1 and α_2 = coordinates of contact arc for spherical surface.

The calculation shows that the parameters of a worn joint, that determine its functional properties, are not only dependent on the law of wear for a given pair of materials, but also on the design features and shape of the joint.

4.2.2. Rectilinear Guideways

Nonuniform wear is typical of rectilinear guideways (the 3rd group of joints). Contact may be effected over a part of the surface only, which makes analytical calculations difficult. It is the deviation of form due to wear, however, that upsets the proper action of many joints (for instance, machine-tool guideways).

The problem of wear calculation for guideways can be solved with an accuracy sufficient for practical purposes when based on the following assumptions:

(1) The amount of wear (U) is proportional to the sliding distance (s) and the magnitude of pressure (p):

$$U_1 = k_1 ps, \quad U_2 = k_2 ps$$

where U_1 and U_2 = respective amounts of wear for the bed slideways and the carriage (or table).

(2) The initial pressure diagram remains invariable in the process of wear, that is re-distribution of pressure due to wear is insignificant.

(3) The distribution curve $\varphi(x)$ defining the motion of a slide along the ways is known. The motion is associated, for instance, with machining different parts. The ordinates of the curve characterize the fraction of the total sliding distance that corresponds to a given position of the slide.

For instance, if identical parts are processed on the machine and the slide moves over a constant distance, then each section of the guideways is allotted an equal part of the whole sliding distance and the distribution curve will be represented by a straight line parallel to the abscissa. If the machine works different parts, the distribution curve will reflect the travel of the slide in machining these parts, and consequently, the character of loading the machine. The curve $\varphi(x)$ showing the peculiarities of operation of the given machine can be found from an analysis of the operating conditions.

For determining the shape of the worn surface of the bed ways and the slide (or a slide block), let us assume the following designations (Fig. 4.3): $U(x)$ = sought-for amount of linear wear of the bed ways (U_1) along the length (x), $[0 \leq x \leq (L + l_0)]$, $U(l)$ = sought-for amount of linear wear of the slideways (U_2) over the length l ($0 \leq l \leq l_0$), L = maximum travel of the slide, l_0 = length of the slideways, $p = f(l)$ = equation of the pressure diagram, $y = \varphi(x)$ = distribution curve for the total sliding distance (referred to the left-hand end of the slide), s = sliding distance travelled by every point of the slideways over a given length of time, k =

coefficient of wear showing the amount of linear wear in μm at a pressure of 1 kgf/cm^2 over a sliding distance of 1 kilometer for a given pair of materials in the given wearing conditions, k_1 = coefficient of wear for the bed's material, and k_2 = coefficient of wear for the slide's material.

The function $U(l)$ is determined on condition that every point of the slideways wears away throughout the whole sliding distance s and is acted upon by a constant pressure $p = f(l)$. Therefore, the wear distribution curve will be similar to the pressure diagram; it is expressed by the equation $U(l) = k_2 s f(l)$.

The main cause of the loss of machine accuracy is the shape of the worn bed ways defined by the function $U(x)$. To find this function, let us consider how a section of bed ways with an abscissa x wears out (Fig. 4.3). The motion of the slide

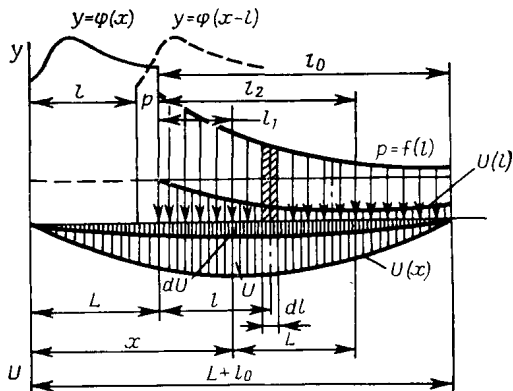


Fig. 4.3. Wear diagram for slideways

results in that the section of the bed ways wears out under the action of pressures determined by the portion of the pressure diagram $f(l)$ which passes over the section with the coordinate x as the slide moves. Each element of the pressure diagram with a coordinate l wears the bed ways by an amount proportional to $pdl = f(l) dl$. To find an elementary amount of wear, dU , caused by the action of pdl , it is necessary to determine the section of the total sliding distance that is traversed by the pressure-diagram element pdl in the process of wear of the bed-way section defined by the coordinate x . To this end, we shall make use of the distribution curve $y = \varphi(x)$. Because the equation of this curve characterises the displacement of the left-hand end of the slide ($l = 0$), the equation for a point of the slide with the coordinate l will take the form $y = \varphi(x - l)$, and the fraction of the sliding distance, that corresponds to the point defined by the coordinate x , will be equal to $s\varphi(x - l)$.

Therefore, the amount of wear at the point x due to the action of the pressure-diagram element pdl will be

$$dU = k_1 s \varphi(x - l) f(l) dl$$

To find the wear at the point x , resulting from the action of the whole pressure-diagram section from l_1 to l_2 , it is necessary to add

together the elementary sections pdl within the above limits:

$$U(x)=k_1s\int\limits_{l_1}^{l_2}\varphi(x-l)f(l)dl\tag{4.10}$$

This formula is a general one for various cases. The limits of integration are chosen depending on what section of the pressure diagram has effect on a given point of bed ways, defined by the coordinate x (Table 4.4).

Table 4.4

Limits of integration in formula (4.10)

$\frac{L}{l_0}$	Section	Limits of section	Limits of integration	
			l_1	l_2
>1	I	$0\leq x\leq l_0$	0	x
	II	$l_0\leq x\leq L$	0	l_0
	III	$L\leq x\leq l_0+L$	$x-L$	l_0
<1	I	$0\leq x\leq L$	0	x
	II	$L\leq x\leq l_0$	$x-L$	x
	III	$l\leq x\leq l_0+L$	$x-L$	l_0

The formula reveals the influence of the main factors on the shape of worn guideways, namely, k characterizes the wear resistance of materials and the wearing conditions; s , the work load of the machine in time, $p=f(l)$, the design of the slide in terms of both the disposition of forces (the form of the pressure diagram) and their magnitude, and $\varphi(x)$, the machine operating conditions, for instance, the processing operations performed on the machine.

Guideway calculation formulas for different cases are given in Table 4.5.

4.2.3. Joints with Variable Contact Conditions

Variable contact conditions are typical of joints related to higher classification groups (see Table 4.1). Here, a change in external factors (forces, speeds, contact conditions, and the like) with respect to each section of the surface has a major effect on the distribution of wear over the rubbing surface.

A typical example of such joints is a cam-follower pair with a roll- or edge-type follower. Cam mechanisms are extensively used in different types of machinery, especially in automatic machines. Nonuniform wear of the cam profile results in upsetting the kinematics of the motion and additional dynamic loading, and frequently causes the failure of the whole mechanism.

Table 4.5

Guideway calculation formulas

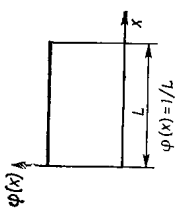
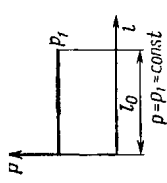
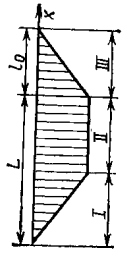
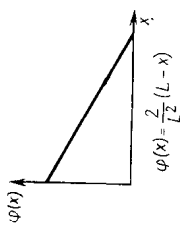
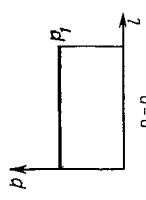
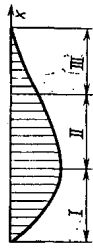
$\frac{L}{l_0}$	Distribution curve $\varphi(x)$	Specific pressure diagram $f(l)$	Shape of worn guideway	Section	Section equation $U(x) = k_s \int_{l_1}^{l_2} \varphi(x-l) f(l) dl$
> 1				I II III	$k_s p_1 \frac{x}{L}$ $k_s p_1 \frac{l_0}{L}$ $k_s p_1 \frac{1}{L} (L + l_0 - x)$
				I II III	$k_s p_1 \frac{x^2}{2Ll_0}$ $k_s p_1 \frac{l_0}{2L}$ $k_s p_1 \frac{1}{2Ll_0} [l_0^2 - (x-L)^2]$
				I II III	$k_s p_1 \frac{1}{L^2} (2Lx - x^2)$ $k_s p_1 \frac{l_0}{L^2} (2L + l_0 - 2x)$ $k_s p_1 \frac{1}{L^2} (L + l_0 - x)^2$
				I II III	

Table 4.5 (cont.)

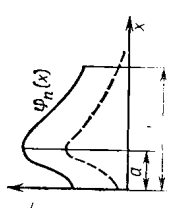
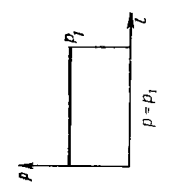
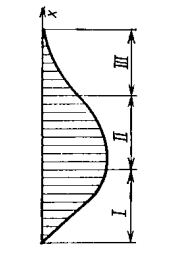
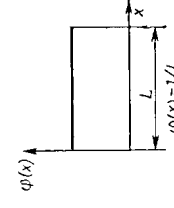
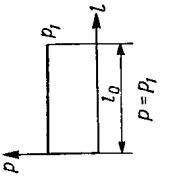
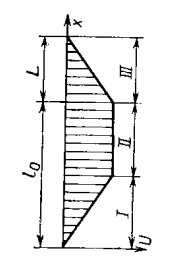
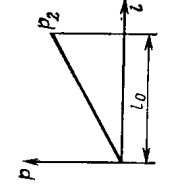
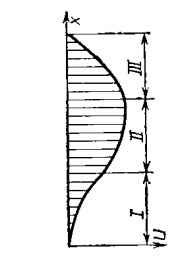
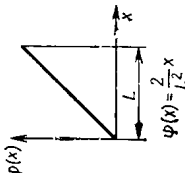
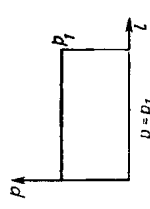
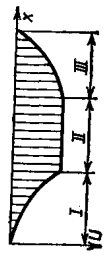
$\frac{L}{l_0}$	Distribution curve $\varphi(x)$	Specific pressure diagram $f(l)$	Shape of worn guideway	Section	Section equation $U(x) = k_s \int_{l_1}^{l_2} \varphi(x-l) f(l) dl$
> 1				I II III	$k_s p_1 M \left[\Phi \left(\frac{x-a}{\sigma} \right) + \Phi \left(\frac{a}{\sigma} \right) \right]$ $k_s p_1 M \left[\Phi \left(\frac{x+a}{\sigma} \right) + \Phi \left(\frac{a+l_0-x}{\sigma} \right) \right]$ $k_s p_1 M \left[\Phi \left(\frac{L-a}{\sigma} \right) + \Phi \left(\frac{a+l_0-x}{\sigma} \right) \right]$
< 1				I II III	$\frac{k_s p_1}{L} x$ $k_s p_1$ $\frac{k_s p_1}{L} (l_0 + L - x)$
				I II III	$\frac{k_s p_2}{2L l_0} x^2$ $\frac{k_s p_2}{2l_0} (2x - L)$ $\frac{k_s p_2}{2l_0} [l_0^2 - (x-L)^2]$

Table 4.5 (cont.)

$\frac{L}{l_0}$	Distribution curve $\varphi(x)$	Specific pressure diagram $f(t)$	Shape of worn guideway	Section	Section equation $U(x) = ks \int_{l_1}^{l_2} \varphi(x-t) f(t) dt$
< 1				I II III	$ks p_1 \frac{x^2}{l_1^2}$ $ks p_1$ $ks p_1 \frac{L^2}{l_1^2} [L^2 - (x - l_0)^2]$
				I II III	$ks p_2 \frac{x^3}{3l_0 L^2}$ $ks p_2 \left(x - \frac{2}{3}L\right)$ $ks p_2 \frac{L^2}{3l_0^2} [3(L^2 + l_0^2)x - x^3 - 2l_0^3 - 2L^3]$

Designations: $\varphi_n(x)$ = normal (Gaussian) distribution law; Φ = Laplace normalized function; $M = \frac{1}{\Phi\left(\frac{a}{\sigma}\right) - \left(\frac{L-a}{\sigma}\right)}$.

Let us consider a method of estimating the wear of a cam profile, taking, by way of example, a cam mechanism with a straight reciprocating follower with a point-shaped tip (Fig. 4.4). This pair belongs to joints of the 4th group, type II, because the follower guide-ways determine the x - x direction for the possible approach of the components as they wear, and the contact condition according to

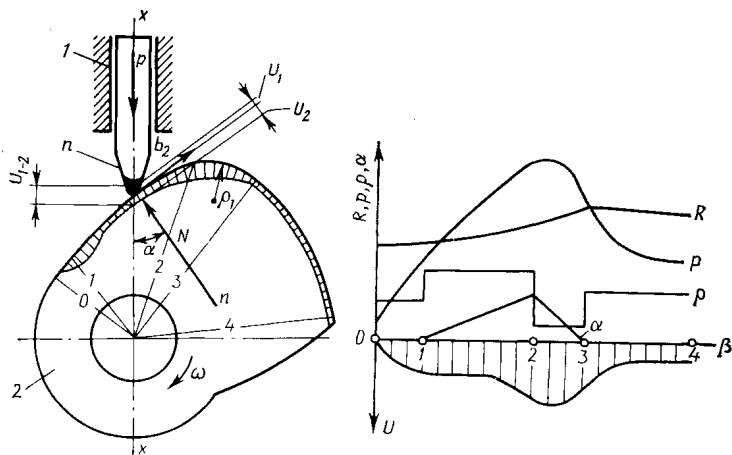


Fig. 4.4. Wear diagram for a cam mechanism

relationships (4.3) holds for this case. Wear of the follower tip has little effect on the variation of its law of motion, and the main cause of the variation will be the cam wear. The laws of wear of materials such, for instance, as expressed by the equation (4.2), also need to be used in calculating the form of the worn surface, and they must be applied to each section of the surface. Here, however, the following factors should be taken into account.

(1) The contact stress σ_c in the contact area is governed by the Hertz law.

(2) The normal load is a function of load P acting upon the follower and pressure angle α :

$$N = P \frac{\cos \varphi_2}{\cos (\alpha + \varphi_1 + \varphi_2)}$$

where φ_1 and φ_2 = respective angles of friction in the cam and follower pair and the follower guideways. The pressure angle α is different for different sections of the profile. The load P can be calculated for each point of the cam profile, for instance, as a function of either the angle of rotation β , or the length of the developed profile.

(3) The cam-profile radius of curvature, ρ_1 is different for different sections of the profile.

(4) The sliding speeds of the follower along the cam profile vary, and at a constant angular velocity of the cam, $\omega = \text{const}$, the relative tangential sliding speed v_r will be

$$v_r = \frac{\omega R}{\cos \alpha}$$

where R = cam radius ($R = \text{var}$).

It is just this speed that enters into the original wear relationship. If this relationship is expressed as a function of the sliding distance, then the latter is defined by the developed length of the cam profile.

Thus, if the basic wear relationship for the materials at a given type of friction is put down as, for instance,

$$\gamma = k\sigma_c^m v_r$$

then the form of the cam's worn surface $U = \gamma t$ is determined by directly substituting into the formula the original values of P , α , R and ρ from the above relationships, taking into account that these parameters are variable and depend on the cam's angle of rotation β . An instance of graphical representation of the original parameters of the cam and of the form of its worn surface for the operative section (characteristic profile points 2-4) is given in Fig. 4.4. Wear U_{1-2} of the joint, which is measured by a single parameter in the direction $x-x$ and determines the distortion of the law of the motion being transmitted, can be found by formula (4.3) wherein U_1 , U_2 , and angle α are functions of the cam's angle of rotation.

4.2.4. Running-in of Inaccurate or Deformed Parts

When mating parts are manufactured or assembled with low accuracy or are deformed, no full contact of their surfaces can be ensured. As a result, the parts will undergo the running-in process at the initial period of their work. Here running-in involves the enlargement of the rubbing area due to wear of the joint, rather than a change in the surface roughness. This type of running-in is referred to as *macro-running-in*.

A diagram of the macro-running-in process for a deformed disc-type part is shown in Fig. 4.5. At the initial period of contact (Fig. 4.5a), the load P can be concentrated in a limited area and cause a rather intensive wear. As the mating surfaces wear away (Fig. 4.5b, c), the contact area grows larger and the load becomes distributed all over it.

The running-in period will be longer where more wear-resistant materials are used. For this reason, beneficial properties of new materials may prove unutilized in practice; moreover, they can give rise to undesirable phenomena, unless measures to shorten the running-in period are taken. For instance, with a deformed shaft, the edge-contact pressures can be effective for a long time in a sliding

bearing made from a wear-resistant material owing to a prolonged running-in period. Here, the wear-resistant shaft needs to be made stiffer or a self-aligning bearing is required.

Let us consider a method for calculation the length of the running-in period, t_{ri} , as applied to two disc-type surfaces whose initial shapes do not coincide because of inaccurate manufacture or deformation.

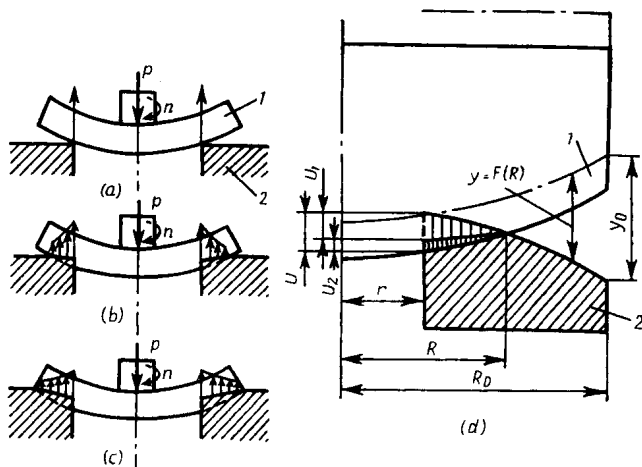


Fig. 4.5. Diagram of running-in for inaccurately machined or deformed parts

If the discs are in full contact, their wear can be determined by formula (4.9), considering the disc as a kind of a conical surface ($\alpha = 0$).

As during the running-in period the radius R continuously varies with time, the relationship should be expressed in a differential form:

$$dU = k \frac{Pn^2}{R-r} dt \quad (4.11)$$

A diagram for determining wear of the surfaces at a given instant of the running-in period is shown in Fig. 4.5d. The radius R changes with time till it reaches the maximum value $R = R_0$.

The relationship between the respective increments of radius, dR , and wear, dU , can be derived if the equation of the initial clearance between the surfaces is known. This equation can generally have the form $y = F(R)$.

If the clearance is caused by the deformation of one of the parts, the function will represent the equation of the part's elastic line.

In the course of running-in, wear grows with gradually diminishing initial clearance y ; therefore $dU = dy$, and then $dU = F'(R) dR$.

Substituting this expression into equation (4.11), we shall have

$$dt = \frac{(R-r) F'(R)}{kPn} dR$$

The length of the running-in period

$$t_{ri} = \frac{1}{kPn} \int_r^{R_0} (R-r) F'(R) dR \quad (4.12)$$

or, taking into account that the rate of wear of the joint during full contact of the discs is given by $\gamma_{1-2} = k \frac{Pn}{R_0-r}$ [see formula (4.7)], we shall have

$$t_{ri} = \frac{1}{\gamma_{1-2}(R_0-r)} \int_r^{R_0} (R-r) F'(R) dR$$

This formula illustrates the above statement, namely, that the higher the wear resistance of the materials (that is, the lower the time rate of their wear, γ_{1-2}), the longer the running-in period.

In many cases, $F(R)$ can be expressed by a power function. $F(R) = c(R-r)^m$ at $R=r$, $F(R) = 0$.

Substituting the value of the derivative $F'(R) = cm(R-r)^{m-1}$ into formula (4.12) and making the necessary transformations, we shall obtain

$$t_{ri} = \frac{cm}{(m+1)kPn} (R_0-r)^{m+1} \quad (4.13)$$

During the running-in period wear of the joint as a function of time does not obey a linear relationship

$$U = \sqrt[m+1]{c \left[\frac{(m+1)kPn}{m} \right]} t^{\frac{m}{m+1}}$$

The inaccuracy of the initial contact of the mating parts can be characterized by the maximum clearance y_0 (see Fig. 4.5d):

$$y_0 = \frac{m+1}{m} \gamma_{1-2} t_{ri} \quad (4.14)$$

This formula enables one to solve practical problems concerning the required accuracy of the initial contact of mating parts.

For example, if the form of the initial contact conforms to a parabolic equation ($m=2$), the running-in period is not to exceed $t_{ri} = 50$ h, and the time rate of wear γ_{1-2} of the joint at full contact, according to the operating conditions, is equal to 10^{-4} mm/h, then the allowable value of y_0 , computed by formula (4.14), will be

$$y_0 = \frac{3}{2} 10^{-4} \times 50 = 0.0075 \text{ mm}$$

Thus, the tolerance on the clearance proves very strict even at a high wear rate of a material.

4.2.5. Pairs with Small Relative Displacements

Small relative displacements of mating surfaces (oscillatory motion) are encountered in some mechanisms and can also be caused by vibrations. The type of wear typical of the latter case is fretting-corrosion of kinematically stationary joints.

Where the variation in the x -coordinate for the wear and pressure diagrams can be neglected, the specific feature of the calculation of

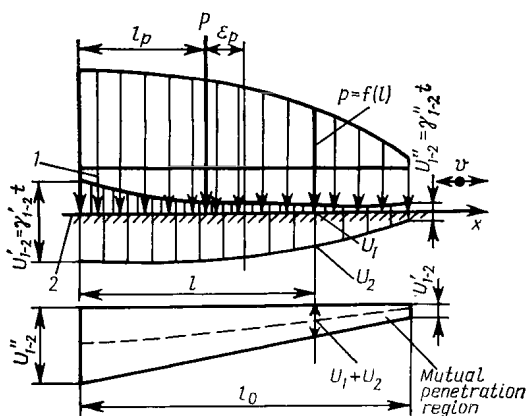


Fig. 4.6. Diagram for calculating wear of parts that execute straight oscillatory motion

such joints is that the condition of contact can be used and, as a result, the shape of the worn surface can be calculated more accurately.

A calculation diagram for this case is shown in Fig. 4.6. The contact condition based on the area of mutual penetration is expressed by formula (4.4).

Let us consider the given problem for the law of wear according to the equation (4.2) which, in regard to pressure is expressed as a power function with $n = 1$:

$$\gamma = kp^mv$$

For the sum of the time wear rates, we shall have $\gamma_1 + \gamma_2 = (k_1 + k_2)vp^m$ from the law of wear; $\gamma_1 + \gamma_2 = \gamma_{1-2}' \left(1 - \frac{l}{l_0}\right) + \gamma_{1-2}'' \frac{l}{l_0}$ from the contact condition given by formula (4.4).

By equating the right-hand sides of these equations, we shall obtain an expression for p , which, in conjunction with the static-

equilibrium equations, will give a system of equations:

$$p^m = \frac{1}{v(k_1 + k_2)} \left[\gamma'_{1-2} \left(1 - \frac{l}{l_0} \right) + \gamma''_{1-2} \frac{l}{l_0} \right] \quad (4.15)$$

$$P = a \int_0^{l_0} p \, dl \quad (4.16)$$

$$Pl_p = a \int_0^{l_0} pl \, dl \quad (4.17)$$

where a = width of the guideways, and l_p = coordinate of the point of application of the force P .

In this way a system of three equations in three unknowns (p , γ'_{1-2} , and γ''_{1-2}) is obtained; its solution will give all the necessary parameters of the worn joint.

The described method illustrates the general approach to the solution of the problem of wear in joints when statics equations are not sufficient for the assessment of the pressure diagram. The surface contact condition forms an additional equation that allows the unknown parameters to be determined.

Let us solve the problem for a linear wear law, that is, with $m = 1$.

Substituting the value of p from (4.15) into equations (4.16) and (4.17) and integrating them, we shall derive two equations from which the values of the parameters γ'_{1-2} and γ''_{1-2} of the worn joint can be obtained.

After transformation we shall have

$$\gamma_{1-2} = \frac{Pv(k_1 + k_2)}{al_0} \left(1 \pm 6 \frac{\varepsilon_p}{l_0} \right) \quad (4.18)$$

where ε_p = offset for the point of application of the force P . This formula joins two formulas in one, and with the plus sign we obtain $\gamma_{1-2} = \gamma'_{1-2}$, whereas with the minus sign, $-\gamma_{1-2} = \gamma''_{1-2}$.

Substituting these values of γ'_{1-2} and γ''_{1-2} into formula (4.15), we have an expression for the pressure diagram, which, after being transformed, will take the form

$$P = p_m \left(1 + 6 \frac{\varepsilon_p}{l_0} - 12 \frac{\varepsilon_p^2}{l_0^2} \right) \quad (4.19)$$

where $p_m = \frac{P}{al}$ = mean pressure on the rubbing surface at $\varepsilon_p = 0$ and $p = p_m = \text{const.}$

Thus, the pressure diagram has a linear character for the given wearing conditions. It is generally a trapezoid, which at $\varepsilon_p = l_0/6$ is transformed into a triangular diagram ($p_{\min} = 0$). Formula (4.19) for the pressure diagram is similar to those obtained from statics equations alone, but under the assumption that the pressure

diagram is linear. In this case, no such assumption has been made (it would mean the addition of an equation to a statically indeterminate problem), and formula (4.19) is obtained under other assumptions, namely, that wear is proportional to the pressure. With $m \neq 1$, the pressure diagram will not be linear [6].

4.3. WEAR CALCULATION WITH ALLOWANCE FOR STIFFNESS

4.3.1. Contact Problem for Wearing Joints

The above-considered methods for determining the pressure diagram effective in the contact zone and the form of the worn surface were based (for the 1st- and 2nd-group joints) on the use of the contact condition for their wear.

However, the deformation of the surface layers, which determines the character of the pressure diagram for stationary joints and for movable joints during the initial period of their operation, has not been taken into account.

At the same time, the surface contact condition, which gives an additional equation for the calculation of wear, can also be applied to the case of contact between two stationary surfaces under the assumption that the contact occurs over the whole apparent area, and the deformation of the surface irregularities in the contact area plays a predominant part. Here, in fact, a full contact of the mating parts proves to take place with any type of deformation and, consequently, conditions (4.3) and (4.4) will apply when linear wear U is substituted for linear contact deformations δ for the same points on the surface. With contact deformations and wear considered jointly, the contact conditions will be given by the following equations:

where the direction of possible approach of the mating parts is predetermined (Fig. 4.7a)

$$\Delta_{1-2} = \frac{(U_1 + U_2) + (\delta_1 + \delta_2)}{\cos \alpha}$$

where the rubbing surfaces are self-aligning (Fig. 4.7b)

$$(U_1 + U_2) + (\delta_1 + \delta_2) = \Delta_1 \left(1 - \frac{l}{l_0}\right) + \Delta_2 \frac{l}{l_0}$$

where Δ_{1-2} , Δ_1 , and Δ_2 = magnitudes of mutual approach of the parts with allowance for the deformation and wear of the surfaces.

Solving the contact problem requires knowledge of the laws of the surface-layer deformation as well as the basic laws of wear for the materials. The relationship between the contact displacement δ and the pressure p exerted on the surface is mostly expressed

by a power function:

$$\delta = \lambda p^n \quad (4.20)$$

where λ and $n = \text{constants}$ depending on the surface geometry and the properties of the materials* [3].

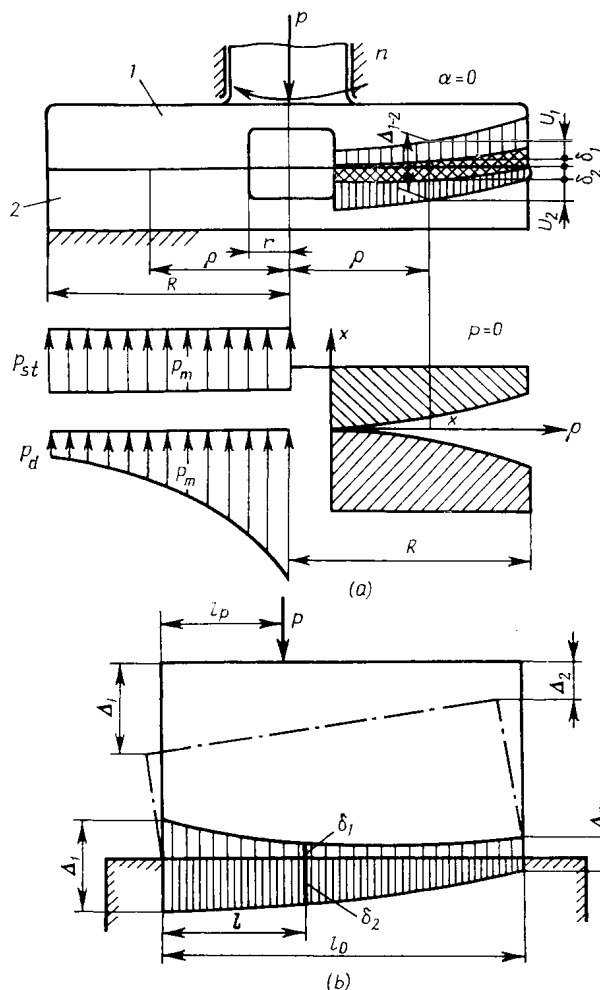


Fig. 4.7. Contact condition for surfaces with regard to contact rigidity

The pressure diagram that is determined by the conditions of contact rigidity is referred to as static, and the diagram depending on the law of wear is referred to as dynamic.

Let us consider a stationary joint shown in Fig. 4.6. All the conclusions made with respect to wear of the joint can also be applied

* Calculation of the constants λ and n by the specified values of roughness parameters and mechanical properties of materials is given in Ch. 1.

to the contact deformation. Thus, formula (4.19) for the pressure diagram will take the same form if the value of the exponent n in the law of deformation (4.20) will be equal to unity. To estimate the amount of mutual approach during contact deformation of surfaces, formula (4.18) can be used with the substitution of λ for $(k_1 + k_2) v$ and the amount of approach Δ for γ_{1-2} .

Here the static and dynamic pressure diagrams are similar in character, and no redistribution of internal forces in the contact area will occur. Such will be the case when the speed of relative sliding in various portions of the contact area is constant or differs from the average rate insignificantly and has no effect on the variation of the contact pressure diagram in the process of wear. Thus the relationships for the deformation of two surfaces and their wear at small relative displacements (see Fig. 4.6) can be used for calculation of a drum-and-brake-shoe assembly in an axial section because the peripheral speed on the frictional surface does not depend on the coordinate l ($v = 2\pi nR = \text{const}$) and has no influence on the form of the worn surface.

4.3.2. Transition of Static Pressure Diagram into Dynamic One

Taking by way of example a contact of disc-type surfaces, let us consider the case in which the pressure diagram for a stationary joint differs radically from that of a movable joint. The discs can be calculated by the formulas applicable to conical surfaces, with $\alpha = 0$ and $y = \rho$.

The pressure diagram in the course of wear is hyperbolic [see formula (4.8)], whereas for the stationary joint it will be rectangular ($p = \text{const}$, see Fig. 4.7a) owing to the character of deformation of the surface layers. The hyperbolic character of the p -diagram with the worn joint means that the surface layers in the area of larger radii ρ will be subject to a smaller deformation. For this reason, after the discs are stopped and the load is removed, the shape of the surface will be different from a plane. This shape is such that the pressure diagram obeys equation (4.8) also at a static load. Under the assumption that contact deformations obey relationship (4.20), the equation of the distorted surface in a cross section will be

$$x = \lambda \left[\frac{P}{2\pi(R-r)} \right]^n \left(\frac{1}{R^n} - \frac{1}{\rho^n} \right)$$

Equation (4.20) can be used for the assessment of the character of a dynamic pressure diagram by measuring the departure of the rubbing-surface shape from a plane upon removing the load. Such experimental investigations were conducted, for instance, by Professor G. Danov and his pupils in Bulgaria.

Thus the static pressure diagram will gradually change into the dynamic one as the surfaces wear away. Let us consider this process with disc-type surfaces for linear laws of wear ($m = n = 1$).

Let us apply the contact condition, with contact deformations and wear being effective simultaneously.

Since the worn and deformed surfaces must coincide upon being re-joined, then for any point of the rubbing surface

$$(\delta_1 + \delta_2) + (U_1 + U_2) = \Delta = \text{const}$$

With regard to the laws of deformations and wear, we shall have

$$(\lambda_1 + \lambda_2) p + (k_1 + k_2) 2\pi n \rho t p = \text{const}$$

Differentiating with respect to ρ and considering that $p = f(\rho)$, we obtain

$$(\lambda_1 + \lambda_2) \frac{dp}{d\rho} + 2\pi n t (k_1 + k_2) \left(\rho \frac{dp}{d\rho} + p \right) = 0 \quad (4.21)$$

Let us designate

$$B = \frac{\lambda_1 + \lambda_2}{2\pi n (k_1 + k_2) t}$$

Integrating equation (4.21), we shall derive the following formula for the pressure diagram:

$$p = \frac{c}{B + \rho} \quad (4.22)$$

The constant c is found from the statics equation $P = 2\pi \int_r^R p \rho d\rho$.

Substituting into this equation the value of p from formula (4.22) and integrating, we shall have

$$c = \frac{P}{2\pi \left(R - r - B \ln \frac{B+R}{B+r} \right)} \quad (4.23)$$

Finally, from formulas (4.22) and (4.23)

$$p = \frac{P}{2\pi \left(R - r - B \ln \frac{B+R}{B+r} \right)} \frac{1}{B + \rho}$$

The latter formula leads to the following conclusions.

1. With $B = 0$ ($t = \infty$), we have formula (4.8) for $\alpha = 0$ and $y = \rho$, that is the transition from a static pressure diagram to a dynamic one will last for an infinitely long period of time.

2. With $B = \infty$ ($t = 0$), the second factor turns into zero, that is, p does not depend on ρ , and a static pressure diagram (rectangular) is obtained.

The rate of the transition depends on the ratio of the discs radii (the wider the disc, the slower the transition), and on the properties

of the materials [6]. For more wear-resistant materials and for those with a low contact rigidity, the transition of the pressure diagram passes slower. In all instances, however, the initial period

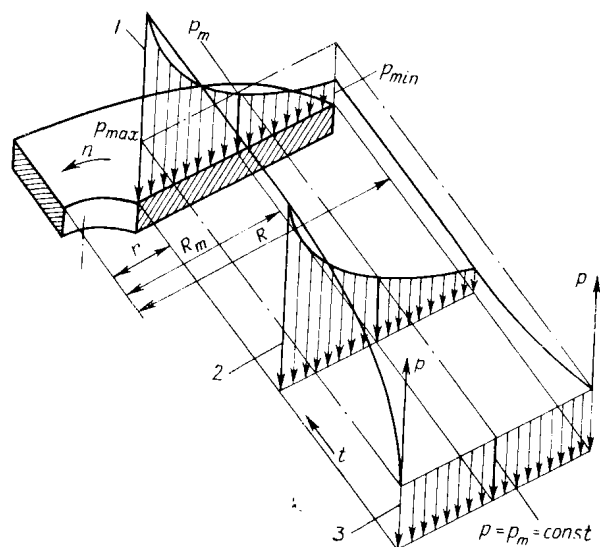


Fig. 4.8. Transition of static pressure diagram to dynamic diagram for disc-type surfaces

1—dynamic diagram; 2—intermediate diagram; 3—static diagram

of work is characterized by a more active transition of the p -diagram (Fig. 4.8).

4.3.3. Rigidly Linked Joints

Engineering mechanisms commonly have several tribological joints whose wear can progress differently. If the wear of each joint has no influence on that of the other elements, the joints can be analysed and calculated independently, and then the total effect of wear in all the joints on the functional parameters of the mechanism can be estimated. There is, however, a large number of mechanisms and assemblies wherein wear of individual surfaces is interrelated and cannot be considered separately. A typical example of such mechanisms is statically indeterminate systems with wearing supports.

With a high stiffness of links, it is the wear conditions that will play the major part, and the operation of each of the joints should be assessed with regard to their total wear. Such joints will be referred to as rigidly linked.

Let us take as an example a centrally-loaded table with two pairs of annular guideways disposed at different radii (Fig. 4.9). The

table will lower as the guideways wear. Their wear, however, cannot be considered separately on the basis of the reactive forces in the guideways, found beforehand. The interrelated wear will occur if wear of each joint in the x - x direction is identical, that is

$$U_1 = U_2$$

This condition determines the magnitude of reactive forces P_1 and P_2 in the guideways and the character of wear in the whole mechanism. It will replace an additional equation of deformations, which is used in calculating statically indeterminate systems. Thus, if linear laws of wear are followed in the considered instance, then the wear of a disc-type joint is calculated by the formula given in Table 4.3. Using relationship (4.9), we shall obtain

$$\frac{(k_1 + k_2) P_1 n}{R_1 - r_2} = \frac{(k_3 + k_4) P_2 n}{R_2 - r_1}$$

whence

$$\frac{P_1}{P_2} = \frac{k_3 + k_4}{k_1 + k_2} \cdot \frac{a_1}{a_2}$$

where a_1 and a_2 = width of the guideways; and k = coefficient of wear for the appropriate combinations of materials and wearing conditions.

If $k_1 + k_2 = k_3 + k_4$, that is, the wearing conditions and materials for each pair are identical, then the magnitudes of the reactive forces only depend on the width of the guideways and are proportional to it.

With regard to the statics equation $P = P_1 + P_2$, we shall deduce that the rate of wear in the direction x - x for a table with two annular guideways will be

$$\gamma = \frac{Pn(k_1 + k_2)}{a_1 + a_2} \quad (4.24)$$

Hence, for the given law of wear, γ depends on the width of the guideways rather than on their radii. This fact suggests that the calculation of guideways by allowable pressures, which is extensively used in practice, for instance, in designing machine tools, may lead to erroneous conclusions. According to this method, it is thought appropriate to arrange the guideways at larger radii in order to reduce the pressure through an increased area of the rubbing surface. Formula (4.24) shows, however, that the wear resistance cannot be improved in such a way because the speed of relative sliding will rise with the guideways area.

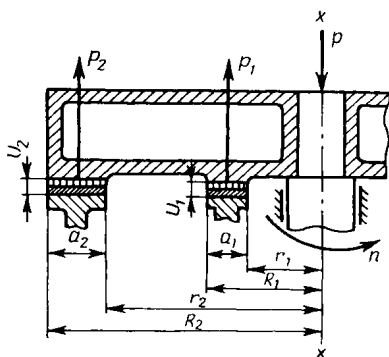


Fig. 4.9. Wear diagram for table annular guideways exemplifying rigidly linked joints

4.4. CALCULATION OF WEAR LIMITS

4.4.1. The Allowable Amounts of Wear

In order to calculate a machine's life expectancy it is essential to establish the limiting values for wear, U_{\max} , allowable in separate machine parts and joints.

Three groups of criteria for wear limits may be differentiated:

(1) as a result of wear, the machine can function no longer (a breakage, wedging, or failure in a mechanism occurs);

(2) wear brings the machine into the condition wherein it fails in a short period of time (impacts and vibrations emerge, the rubbing surfaces wear away rapidly, temperature in machine units rises);

(3) because of wear the machine's functional characteristics go beyond the specified limits (the quality of product deteriorates, productivity is lost, efficiency falls and noise increases).

The wear limits criteria are associated in some instances with the operation of a given joint or part, and in others, with the operation of several parts of a mechanism or unit.

For parts restored during periodic scheduled repairs the allowable amounts of wear, U_{al} , will be smaller than or equal to the limiting U_{\max} , as the part must not fail during the last between-repair period. If the length of the between-repair period, that is, the time between two scheduled repairs, is T_1 , then wear of a part during this time will increase by γT_1 . For this reason, the allowable amount of wear, U_{al} , which is the starting point from which the part should be recovered in periodic repairs will be

$$U_{al} = U_{\max} - \gamma T_1$$

Taking into account that $\gamma = U_{al}/T$, where T is the before-repair period of operation of the part, we shall have

$$U_{al} = U_{\max} - \frac{U_{al} T_1}{T}$$

whence

$$U_{al} = \frac{U_{\max}}{1 + \frac{T_1}{T}} = U_{\max} \frac{k}{k+1} \quad (4.25)$$

where k = a given scheduled repair since the moment of the last repair, that is, the time of the part operation $T = kT_1$.

Example 1. The part has a carburized layer 0.8 mm deep and a limiting amount of wear, U_{\max} , equal to 0.65 mm (80 per cent of the layer depth). Check whether the part must be repaired if in measurement during a third scheduled repair its wear proved to be 0.55 mm.

Find U_{al} by formula (4.25):

$$U_{al} = 0.65 \frac{3}{3+1} = 0.49 \text{ mm}$$

Hence, the repair is necessary, because, although its wear is smaller than U_{\max} , the part will not last up to the next scheduled repair.

Tribological components in modern machinery mostly belong to the 3rd group with respect to determining U_{\max} . The limiting condition often results from impaired characteristics of the machine rather than its breakages or failures. Machining accuracy, which is essential for machine tools, is an example of such characteristics.

Analytical relationships for U_{\max} can be obtained by establishing a relation between functional errors in the machine and the parameters defining the size and shape of the worn surface.

Examples of calculation for maximum allowable wear are given in [5] and [7]. The limiting condition is determined by assessing the shape of the worn surface, wear of the joint, and their influence on the joint's performance.

4.4.2. Wear Limits for Multi-Link Mechanisms

For many mechanisms consisting of a large number of kinematic pairs, the wear limiting condition is determined under the assumption that the position of the end link is within the specified tolerance band Δ . Wear of individual links determines the departure of the end link from the specified position. Depending on the design and kinematics of the mechanism, the effect of wear of a given surface on the position of the end link can be estimated by the transmission ratio i_k . Therefore, with a mechanism that has n wearing links, the following equation can be put down:

$$\sum_1^n U_k i_k = \Delta + e \quad (4.26)$$

where e = possible compensation for wear.

The wear limit U_{\max} should be established for one (the most wear-prone) part or for several parts on condition that $\Delta \leq \Delta_{al}$.

If one of the joints wears at a rate γ_x , then the relationship between its wear U_x and error Δ must be derived. To this end, we multiply both sides of equation (4.26) by $\gamma_x = U_x/T$:

$$U_x \frac{\sum_1^n U_k i_k}{T} = (\Delta + e) \frac{U_x}{T}$$

whence

$$U_x \sum_1^n \gamma_k i_k = (\Delta + e) \gamma_x$$

or

$$U_x = (\Delta + e) \frac{\gamma_x}{\sum \gamma_h i_h} = \frac{\Delta + e}{\sum_{h=1}^n \left(\frac{\gamma_h}{\gamma_x} \right) i_h} \quad (4.27)$$

By this formula the wear limit can be computed for any sliding pair, because with $\Delta = \Delta_{al}$ wear will be $U_{\max} = U_{x, \max}$.

Example 2. Consider a mechanism consisting of four links with transmission ratios $i = 1$ and an allowable positional deviation of the end link, Δ_{ql} equal to 0.3 mm. Let the ratio of the time wear rates for separate links, which is found experimentally, be $\gamma_1 : \gamma_2 : \gamma_3 : \gamma_4 = 1 : 3 : 7 : 4$. As the link 3 wears away most rapidly, calculate the limit wear $U_{3, \max}$. From formula (4.27), with $e = 0$, we shall have

$$U_{3, \max} = \frac{0.3 \times 7}{1 + 3 + 7 + 4} = 0.14 \text{ mm}$$

Note that by determining U_{\max} for one of the links, we take into account wear in all the links.

In order to increase the allowable value of U_{\max} and, consequently, the service life of the whole mechanism, let us introduce a wear compensating device, which makes up for wear by an amount $e = 3$ mm. Compute U_{\max} for this case:

$$U_{3, \max} = \frac{(0.3 + 3) \times 7}{1 + 3 + 7 + 4} = 1.55 \text{ mm}$$

It can be seen that the wear life of the mechanism has increased 11 times.

4.5. CALCULATION FOR RELIABILITY OF JOINTS

4.5.1. Reliability Parameters

With U_{\max} known, the wear life T of a tribological joint can be computed by the formula

$$T = \frac{U_{\max}}{\gamma}$$

This calculation, however, is complicated by the fact that the time wear rate γ is a random variable that can range widely.

The above-described wear relationships are essentially functions of random arguments, because the external factors (load, sliding speeds), materials properties (hardness, ultimate strength), and operating conditions are random variables. Therefore, the calculation of service life with respect to wear is a prediction determining the wear life and the respective probability of a joint's failure-free operation.

This problem is solved on the basis of the probability and product reliability theories.

Let us consider the most typical instance where a change in the parameter U of a product is caused by wear and follows a linear law

$$U = \gamma t \quad (4.28)$$

Here the rate of wear, γ , depends, as a rule, on a large number of random variables, such as load, temperature, operating conditions and the like. Therefore, it typically obeys the normal distribution law, that is,

$$f_0(\gamma) = \frac{1}{\sigma_\gamma \sqrt{2\pi}} \exp \left[-\frac{(\gamma - \gamma_m)^2}{2\sigma_\gamma^2} \right]$$

where $f_0(\gamma)$ = probability density, γ_m = mean value (mathematical expectation) of the rate of the process, and σ_γ = standard (root-mean-square) deviation.

With regard to the scatter of a product's initial parameter, for instance, the manufacturing accuracy of a rubbing-surface equation (4.28) should be expressed in the form $U = a + \gamma t$, where a is the initial parameter of the product (the rubbing surface).

Therefore, the wear life is generally a function of two independent random variables a and γ :

$$T = \frac{U_{\max} - a}{\gamma}$$

If each of the variables a and γ obeys a normal distribution law, then wear U for a given value of $t = T$ will also conform to a normal distribution with a mathematical expectation $U_m = a_0 + \gamma T$ and a standard deviation $\sigma_U = \sqrt{\sigma_a^2 + T^2 \sigma_\gamma^2}$, where a_0 is the mathematical expectation and σ_a , the standard deviation of the random variable a .

A diagram of wear process in this instance is shown in Fig. 4.10. The probability $P(T)$ of failure-free operation of a product over its service period $t = T$ is the main characteristic of reliability and depends here on the probability characteristics of the wear process. To calculate $P(T)$, let us consider the probability of determining the amount of wear in the range from 0 to U_{\max} . This probability is numerically equal to the area under the curve $f(U) = f(\gamma t)$, that lies within the limits $0 \leq U \leq U_{\max}$. Since $f(U)$ obeys a normal distribution law, this area can be computed with the aid of the normalized Laplace function Φ_0 which is tabulated [10].

Thus, the following relationship can be given [8]:

$$P(T) = 0.5 + \Phi \left(\frac{U_{\max} - a_0 - \gamma_m T}{\sqrt{\sigma_a^2 + \sigma_\gamma^2 T^2}} \right) \quad (4.29)$$

The calculation of the probability of trouble-free operation, $P(T)$, by this formula is made, as a rule, in two variants.

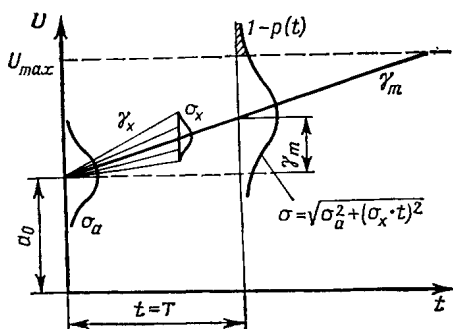


Fig. 4.10. Diagram for assessing reliability in the case of a linear wear law

(1) With the wear life $t = T_l$ being specified, calculation is made of the probability of failure-free operation, $P(t = T_l)$, which serves as a characteristic of product reliability. In this case all the parameters determining the argument in the Laplace function are known, and $P(T)$ is computed by using the tables of the function.

(2) For products that are to meet stringent reliability standards, it is customary to specify $P(T)$ and to calculate the wear life T_l satisfying the given requirement for trouble-free operation. Here the value of T , which enters into the argument of the Laplace function, is sought from formula (4.29). The argument of the Laplace function will be the quantile U_α of the normal distribution, that is, the value corresponding to the given probability $P(T)$. Quantiles of normal distribution can be found from tables [10].

For determining T , we shall derive from formula (4.29) the quadratic equation

$$U_\alpha \sqrt{\sigma_0^2 + \sigma_Y^2 T^2} = U_{\max} - a_0 - \gamma_m T \quad (4.30)$$

Thus, the order of calculation is that the value of U_α appropriate for the specified value of $P(T)$ is chosen from the tables for the quantiles of normal distribution, and then the wear life T is computed by equation (4.30).

4.5.2. Example of Calculation for Wear Life and Probability of Failure-Free Operation

Let us consider an example of use of the above formulas for calculation of product reliability parameters.

Example 3. Calculate the wear life (γ -percentage life T_γ) of a wear part for a specified probability of failure-free operation, $P(t)$, ranging from 0.9 to 0.9999.

Initial data.

1. The part's wear U obeys linear relationship (4.1).

2. Nominal (average) operating conditions: $p_m = 16$ kgf/cm² and $v_m = 2$ m/s.

From analysis of the load ranges likely to occur in service it is found that the loads obey a normal distribution law and, within the 6 σ -zone, have the following variations: $p = 16 \pm 4.5$, that is, $\sigma_p = 1.5$ kgf/cm², and $v = 2 \pm 0.6$, that is, $\sigma_v = 0.2$ kgf/cm².

3. Tests of samples in the average service conditions have shown that for 100 h of operation the average amount of wear was 2 μ m, that is, $\gamma_m = 2 \times 10^{-2}$ μ m/h.

It should be noted that these data can also be obtained by calculation, for instance, by the formulas derived by Prof. I.V. Kragelsky (see Ch. 3). Average values will be sufficient to find from the tests.

4. The average value of k is obtained on condition that $\gamma_m = k p_m v_m$; $2 \times 10^{-2} = k \times 16 \times 2$, whence $k = 6.25 \times 10^{-4}$.

5. The dimension a_0 of the part is made accurate to within ± 3 μ m, that is, $\sigma_0 = 1$ μ m.

6. From the part's operating conditions the maximum allowable wear $U_{\max} = 10$ μ m is found, for instance, by the method disclosed above. This

wear is calculated with reference to the nominal dimension a_0 ; for this reason, T_m should be determined with $a_0 = 0$.

Solution.

The average wear life of the part will be

$$T_m = \frac{U_{\max}}{\gamma_m} = \frac{10}{2 \times 10^{-2}} = 500 \text{ h}$$

For determining the variance of the wear process $D_k = \sigma_k^2$ at $k = \text{const}$, we apply the theorem on the variance of independent noncentred random variables [1]:

$$D_\gamma = D(kpv) = k^2 D(pv) = k^2 [D(p) D(v) + p_m^2 D(v) + v_m^2 D(p)]$$

or

$$\sigma_\gamma = \sqrt{D(kpv)} = k \sqrt{p^2 \sigma_v^2 + p_m^2 \sigma_v^2 + v_m^2 \sigma_p^2}$$

$$= 6.25 \times 10^{-4} \sqrt{2.25 \times 0.04 + 256 \times 0.04 + 4 \times 2.25} = 2.77 \times 10^{-3} \text{ } \mu\text{m/h}$$

Then, we substitute into formula (4.30) the values of $U_{\max} = 10 \text{ } \mu\text{m}$, $a_0 = 0$, $\gamma_m = 2 \times 10^{-2} \text{ } \mu\text{m/h}$, $\sigma_0 = 1 \text{ } \mu\text{m}$, and $\sigma_\gamma = 2.77 \times 10^{-3} \text{ } \mu\text{m/h}$ and solve the quadratic equation for T . The obtained values are listed in Table 4.6.

Table 4.6

Results of product wear life calculation

Specified value of $P(T)$	Quantile (from table in [10])	Wear life $T_l = T$, h	Specified value of $P(T)$	Quantile (from table in [10])	Wear life $T_l = T$, h
0.5	0	500	0.999	3.090	345
0.9	1.282	435	0.9999	3.719	315
0.99	2.326	385			

The above calculations lead to the following conclusions: first, the wear life must be chosen fairly accurately, for even its small variations can have a marked effect on the probability of failure-free operation; and second, there is a region of high reliability, where the probability of failure-free service is close to unity. Taking as the basis the initial data on the product, the likely service conditions, and the results of the assessment of wear rate, the described method makes it possible to calculate the product's wear life for the specified probability of failure-free operation, to indicate measures that will bring about a major improvement in reliability, and to assess the weight of each factor in quantitative terms.

4.5.3. Predicting the Wear of Joints

The above-considered wear-calculation methods enable the design engineer to estimate the likely wear process and take account of the influence of the main factors as early as at the product development stage.

Determining the wear coefficients k , which, as is well known, depend on a large number of factors, poses a particular difficulty. Finding these coefficients by the relationships derived from the study of physics of wear is most desirable (see Ch. 3).

Where the values of the wear coefficients for specific materials are unavailable, one may use the following techniques in wear calculations.

(1) Make comparative calculations to find how much the wear resistance of the given pair will be increased compared with a basic similar joint or with several design versions.

(2) Estimate the value of the coefficient k on the basis of service data for similar sliding pairs, or by predicting a likely increase in wear resistance from the use of new materials whose variations in mechanical properties and structure are known.

(3) Specify the linear or time rate of wear by establishing the necessary class of wear resistance and place the requirements before production and maintenance engineers for the use of such sliding-pair designs and operating conditions as will keep the wear rate within the prescribed limits.

(4) Test the specimens of the mating materials and use the obtained data for the calculation.

The calculation of individual joints forms a basis for predicting the performance of the whole mechanism.

4.5.4. Effect of Wear on Functional Properties of a Machine

Wear in joints and mechanisms of a machine leads to a gradual deterioration of its performance. The performance of a product is determined by its ability to carry out the specified functions, retaining the values of the parameters within the limits established by the specifications.

The machine's functional parameters are very diverse and depend on the purpose and design of the machine. For instance, in metal-cutting machine tools the functional parameters are the machining accuracy and surface finish; in engines, efficiency and power under different operating conditions; in a number of machine tools, production rates, and so on. The more complex and advanced the machine, the larger the number of parameters characterizing its performance.

As the machine wears out, its original parameters deteriorate, the rate of their change being different. In order to estimate the deterioration of performance of the machine as a whole due to wear, it is essential to establish a relationship between the wear and service life of individual units and the parameters of the machine.

Taking into account that any modern machine is subjected during its service life to repair, adjustment and other types of maintenance

by which its performance is restored, the machine's wear can be estimated from two different standpoints:

(1) By the total time (and, respectively, cost) spent on restoring the performance (the length of service life).

(2) By the probability of retaining the original parameters of the machine within the prescribed limits during the specified service period (the failure-free operation).

The first criterion may be represented by the coefficient of usage (coefficient of durability) K_d , which is found from the formula

$$K_d = \frac{T_o}{T_o + \sum \tau_{dti}} \quad (4.31)$$

where T_o = time of operation of the machine during the whole period of service, $\sum \tau_{dti}$ = total machine downtime caused by failures (repair, adjustment, and so on) during the whole period of service.

The coefficient of durability is a dimensionless quantity ($K_d \leq 1$), and the larger its value, the more durable the machine.

In order to find K_d , it is necessary to establish its relation to the service life of machine parts.

The downtime due to repair of a given part or joint will be

$$\tau_{dti} = \frac{T_o}{T_i} \tau_i$$

where T_i = service life of the i th part (joint) of the machine, τ_i = time (or labour) consumption for the repair of the i th part (joint), including dismantling, assembly, and adjustment.

The ratio T_o/T_i shows how many times during the period T_o the given part was repaired.

Substituting the value of τ_{dti} into formula (4.31), we obtain the coefficient of durability expressed through the service life and the time required for the repair of machine parts:

$$K_d = \frac{1}{1 + \sum \frac{\tau_i}{T_i}} \quad (4.32)$$

In periodic scheduled repairs, when a group of parts are repaired simultaneously, T_i is taken to mean the time up to the next repair and τ_i , the time consumed in repair.

From formula (4.32) it follows that the main method for increasing the durability of a machine is the reduction of the time spent in repair and the extension of the service life of the component parts.

In most machines and mechanisms, the service life is determined by wear of their joints.

4.5.5. Diagram for Calculation of a Machine for Reliability

The calculation for reliability and service life with respect to wear includes the following stages (Fig. 4.11).

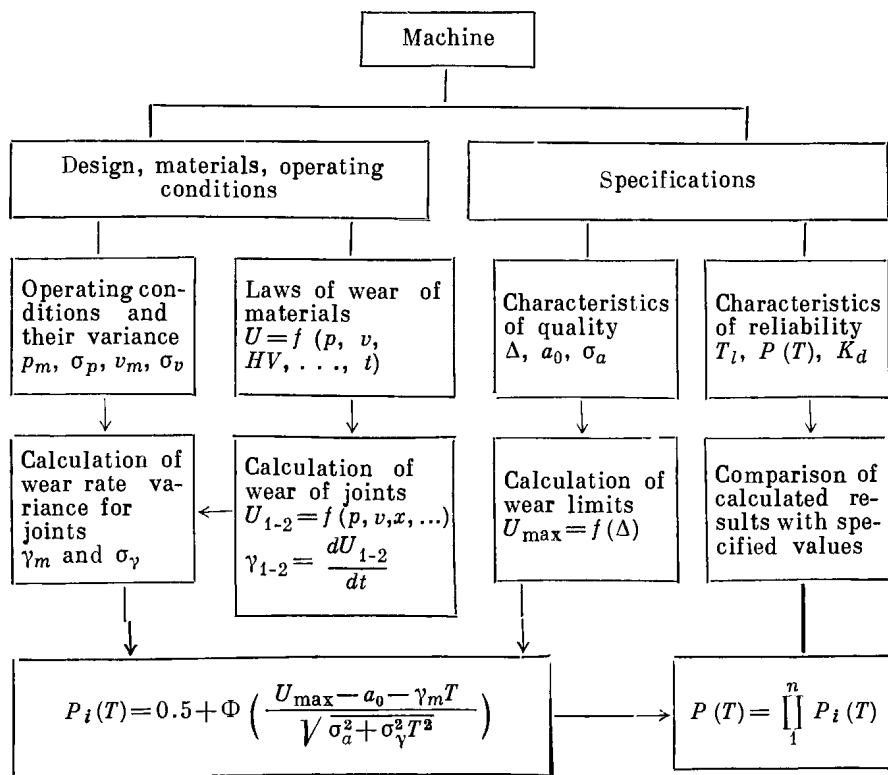


Fig. 4.11. Sequence of machine design calculation for wear life and reliability

(1) Specifications are established for the machine parameters, including:

- the characteristics of reliability and durability, that is, the service life T_l and the allowable values for the probability of trouble-free service, $P(t)$, the total machine downtime for the service period or the coefficient of durability, and also the allowable expenditures on the machine repair and maintenance;

- the characteristics of the machine quality, that is, accuracy of operation, efficiency, production rates, quality of machine manufacture (a_0 , σ_a), and the like.

(2) The basic physical laws of wear are established that characterize the machine's service conditions and can be used in calculations for wear.

(3) Wear calculation is made on the basis of the physical law of wear and the design of the joint. The end parameters of the joint are determined depending on its type. For instance, where guideways are subject to wear, the distribution of wear along the sliding surface and the respective change in the path of the slide are calculated.

(4) The wear limits are established for the component parts. This calculation is made with regard to machine specifications, primarily to the required accuracy of operation of the machine.

(5) Feasible ranges of operating conditions for the machine as a whole and for its components are estimated. Subject to determination are not only the mean values of loads, speeds, and so on, but also their variance.

(6) On the basis of the above data and wear relationships, the average rates and variance of wear for each of the joints are determined.

(7) The probability of failure-free operation is calculated for a given output parameter, for instance, by formula (4.29).

(8) In calculating the probability of failure-free operation, $P_i(t)$, for several (n) end parameters of the machine, for instance, for different characteristics of accuracy, the total probability (with the parameters being independent) is assessed as

$$P(t) = \prod_{i=1}^n P_i(t)$$

After they are calculated, the characteristics of reliability are compared with the allowable values established by the machine specifications.

If the reliability characteristics — service life and $P(t)$ — do not meet the specifications, then it is determined in which parts and by what amount the probability of trouble-free service needs to be increased during the required service life to meet the appropriate specification values.

Product designers are well familiar with such methods for increasing the service life of machinery as the use of wear-resistant materials, provision of adequate lubricating systems, protection of rubbing surfaces against fouling, compensation for wear, and application of quick-replaceable parts and units. Currently, some other directions of the development of modern machinery are becoming increasingly popular. Let us indicate the main of them.

(1) Designs are worked out in which wear affects the operation of a mechanism or machine to the least possible degree.

(2) The principle of uniform wear of surfaces, which is one of the methods for implementing the previous, more general principle, contributes in many instances to an extended service life.

(3) Invariable conditions at the rubbing surface (temperature, load, and the like) guarantee the correct function, low wear and the absence of unallowable types of wear with many critical joints. For this reason, devices that provide for such conditions are emerging.

(4) The action of external agents, primarily forces, is transferred from the critical joints to less critical ones for increasing the service life and accuracy of operation.

(5) Compensation for wear tends to be automated, which is a new line in machine development.

Wear calculation of machine joints and mechanisms is an important prerequisite for making optimum decisions at the design stage if tribological components are to ensure the required reliability of machine characteristics in the specified service conditions.

REFERENCES

1. Вентцель Е. С. Теория вероятностей. М., «Наука», 1969.
2. Крагельский И. В. Трение и износ. М., «Машиностроение», 1968.
3. Левина З. М., Решетов Д. Н. Контактная жесткость машин. М., «Машиностроение», 1971.
4. Проников А. С. Блок-схема возникновения отказа.— «Надежность и контроль качества», 1976, № 5, с. 12—17.
5. Проников А. С. Износ и долговечность станков. М., Машгиз, 1957.
6. Проников А. С. Контактная задача для сопряженных поверхностей деталей машин.— В кн.: Трение и износ в машинах. Сборник XV. М., Изд-во АН СССР, 1962, с. 375—391.
7. Проников А. С. Основы надежности и долговечности машин. М., Изд-во стандартов, 1969.
8. Проников А. С. Расчет показателей надежности при постепенных (износных) отказах.— «Надежность и контроль качества», 1973, № 2, с. 3—13.
9. Технологическая надежность станков. Под ред. Проникова А. С. М., «Машиностроение», 1971.
10. Шор Я. Б., Кузьмин Ф. И. Таблицы для анализа и контроля надежности. М., «Советское радио», 1968.

CHOICE OF MATERIALS FOR RUBBING PARTS

There are many materials suitable for tribological components. Antifriction materials, which allow the operation of movable joints with a limited lubrication or without it, are of the greatest importance. The most effective and promising among such materials are polymers, carbon-graphites, metal-ceramics and various compounds on their base.

The main requirements for antifriction materials are dictated by the necessity to ensure the following functional properties of tribological joints: maximum or specified magnitudes of strength and stiffness; maximum or specified reliability and service life; minimum mass, noise, and loss of energy; low metal content; high manufacturing processability, minimum cost; and suitable assembly and maintenance.

Tribology has amassed a wealth of experience which allows the general principle of selecting materials for rubbing components to be formulated and the selection sequence outlined (Fig. 5.1). This sequence is convenient to break down into four stages described below. Let us briefly consider the main factors relating to the problem.

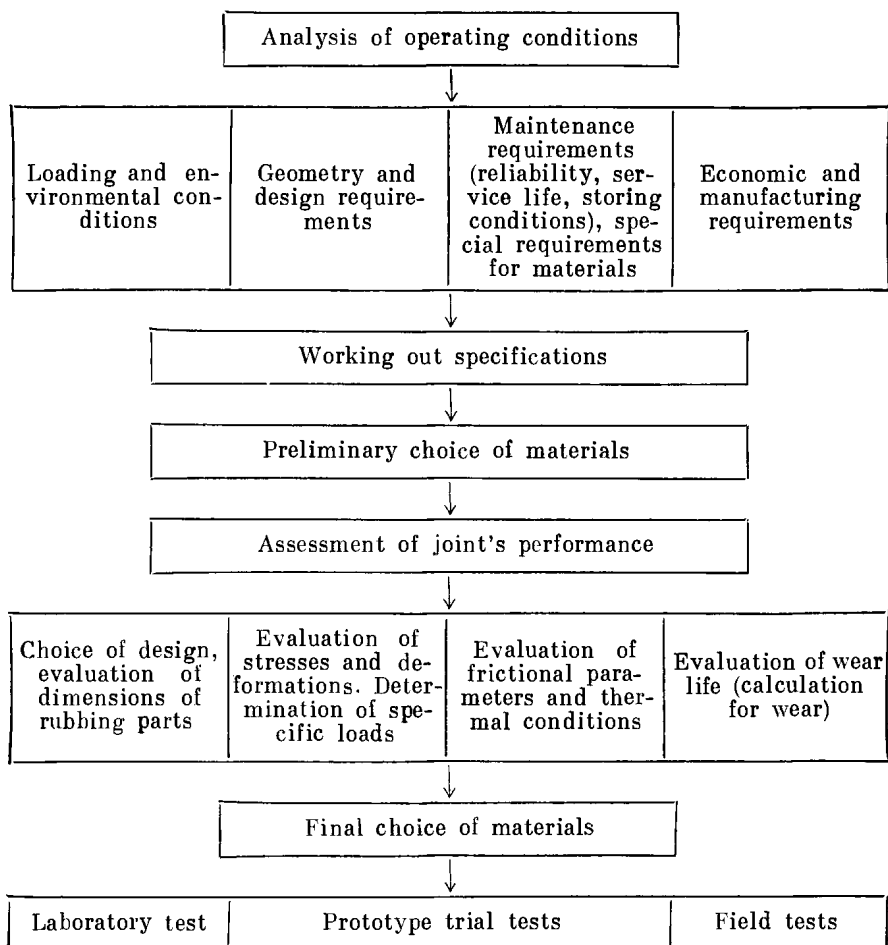


Fig. 5.1. Exemplary sequence of choice of materials for rubbing parts

5.1. ANALYSIS OF OPERATING CONDITIONS AND DRAWING UP OF SPECIFICATIONS

Developing the specifications for a tribological unit requires primarily a thorough statement and analysis of the operating conditions. The latter may include the load and speed factors, storing and environmental conditions, data on permissible accuracy limits, reliability and service-life requirements, expected consumption rates, and the like (see Table 5.1 given by way of example).

When working out the specifications, the following factors should be taken into account:

- friction is a source of energy losses, and this factor is crucial for the performance of miniature electric motors, gyroscopes,

Table 5.1

Specification sheet*Enterprise:* Electric-motor factory*Unit:* Brush and commutator assembly, drawing No. 1174A (enclosed)*Brief description of the unit:* The brush and commutator assembly is used in a d.c. fractional-horsepower motor designed for driving various automatic systems.*The task is to choose the material for the brush.* A similar brush is made from the MF-33 Grade material based on graphite, copper, tin, and lead, and impregnated with bakelite varnish.

No.	Characteristic	Existing unit (prototype)	Unit to be developed
<i>I. Loading and environmental conditions</i>			
1	Lead (kgf/cm ²) and its application	0.5, along brush axis	Up to 2
2	Rotational frequency, rpm	3,000	9,000
3	Loading conditions (duration and periodicity of loading)	Lengthy, recurrently short, reversible	Lengthy, recurrently short, reversible
4	Acceleration, g	1G	30
5	Atmospheric conditions	Normal	Humidity up to 98%
6	Temperature, °C	20-40	Up to 100
7	Work medium and its concentration	Air	Vacuum to 10 ⁻⁵ mm Hg
8	Electric action	Nominal current density not over 20 A/cm ²	Current density up to 30 A/cm ²
9	Ingress of foreign matter (abrasive, etc.)	Inadmissible	Undesirable
10	Mating component (material, hardness, surface roughness, etc.)	Copper Grade M1 GOST 859-66, HB 75, Ra 0.16-1.25 μm	
11	Overall dimensions	25 mm dia × 45 mm	
12	The required accuracy and its variation in service	Close contact of the brush to exclude sparking is essential	
13	Special requirements on the design (combining working functions, interaction with other units)	—	—
14	Other requirements	—	—

II. Service requirements

15	Reliability characteristics	Startup failures in air must be excluded	Startup failures at elevated humidity (98%) must be excluded
16	Service life, h	200	500
17	Necessity and feasibility of performance control	—	—
18	Energy efficiency (coefficient of friction)	0.20-0.25	0.18-0.20
19	Noise level	—	As low as possible

Table 5.1 (cont.)

No.	Characteristic	Existing unit (prototype)	Unit to be developed
20	Damping capacity	—	—
21	Toxicity	—	—
22	Ionizing radiation	—	—
23	Giving off gases	—	Undesirable
24	Long-term storage necessity (temperature, humidity, type of slush, wrapping)	Storage at high humidity upsets stability of contact	Stable characteristics must be secured in storage at a humidity of 98%
25	Other requirements	—	—

III. Cost and manufacturing requirements

26	Production volume	Small-batch production	Quantity production
27	Price, roubles	0.16	0.12-0.14
28	Energy consumption in manufacture	—	—
29	Production rates, pieces per hour on one machine	20	50
30	Mass, g	0.15	Up to 0.2
31	Appearance and finish	No special requirements	Smooth surface
32	Other data	—	—

tensioning devices in textile machinery, and so on; friction is also a major source of heating in rubbing surfaces and machine parts as a whole, which is important at low heat dissipation in vacuum; friction, for instance, causes electrification in polymer fibres and fabric in the process of their manufacture, and friction is a source of vibration and noise, which is a limiting factor for designing movable joints in film projectors, textile machinery, sound-recording apparatus and other acoustic devices;

— wear alters the geometry of mating parts and, consequently, adversely affects the accuracy of joints; it weakens the load-supporting sections of parts; it is also accompanied with formation of by-products that can have an adverse effect on the performance of the main units of machinery (for instance, commutator bars in electric motors may become short-circuited, a vacuum system clogged, or vibrations may arise);

— the interaction of rubbing parts may give rise to unfavourable results, for instance, seizure and fusing of surface layers or progressive pitting of mating surfaces, which leads to a catastrophic failure of the joint.

It is also essential to know where, when, and how long rubbing parts will be kept before going into service. For instance, exposure to sun rays may cause accelerated ageing in parts made of polymers;

Table 5.2

General data on physico-mechanical and frictional properties of materials for tribological components

Group of materials	Ultimate strength, kgf/cm ²		Maximum working temperature, °C	Limiting value of $p v$ criterion, kgf/cm ² × m/s	Coefficient of friction	Specific properties	Applications
	in compression	in tension					
Polymer-base materials: thermoplastics	—	700-800	100-120	0.2-1.0	0.15-0.40	High processability, chemical resistance, wear resistance	Tribological parts (bearings, gears, cams, etc.)
	800-1,000	—	250-300	2-5	0.10-0.40	Increased heat resistance, low cost	Plain bearings, rolling bearing components, structural parts, etc.
Carbon-graphite materials	200-400	140-250	300-450	2-4	0.20-0.35	High thermal and electric conductivity, heat resistance, and chemical resistance	Sealing components, bearing liners in hydraulic pump and air-driven engines, frictional components in aircraft and chemical equipment
Metal-ceramics	2,500-2,800	—	300-500	6	0.25-0.40	High thermal resistance and conductivity	Tribological components working at high temperatures
Laminated materials	—	—	300-350	18-36	0.10-0.15	High thermal conductivity and load capacity (up to 1,400 kgf/cm ²)	Plain bearings in heavily loaded tribological units

sharp changes in humidity may lead to distortion of rubbing surfaces. An incorrectly chosen environment may turn out to be aggressive with respect to the material of a rubbing part. It is also important to properly select the material of the mating counterpart and to specify optimum values of roughness for both mating surfaces. The more carefully the operating conditions are analyzed and specified, the easier the selection of the material can be.

5.2. PRELIMINARY CHOICE
OF MATERIAL

5.2.1. General Data

It is advisable to select first of all the group of materials that meet the joint's specifications most fully. Materials based on polymers, and also laminated, carbon-graphite and metal-ceramic materials find the widest application for the rubbing components of machinery, mechanisms, and instruments that are to operate without positive lubrication. Some general data on these materials are given in Table 5.2.

5.2.2. Polymer-Base Materials

Materials of this group are extensively used in tribological joints. Applications include gear wheels, cages and balls in antifriction bearings, rubbing members in sliding bearings, cams, guideways, fasteners, and other parts. The use of plain polymers for rubbing components is decreasing. Comparative data on the coefficients of friction and the wear rate for some polymer-base materials are listed in Table 5.3 and 5.4. While making use of the tables, however,

Table 5.3

Antifriction properties of some polymer materials
(polymer on metal without lubrication)

Material	Coefficient of friction		Relative wear
	static	kinetic	
Polyamides	0.20-0.25	0.25-0.30	200
Polyformaldehyde	0.15	0.20	65
Polytetrafluoroethylene	0.10	0.15	8
Polycarbonate	0.30	0.40	2,500
Polyurethane	0.30	0.40	340
Styrene acrylonitrile	0.30	0.35	3,000
Phenolic-resin-base moulding compound	0.15-0.20	0.25	30

Table 5.4

Antifriction properties of thin-layer coatings
(load 40 kgf/cm², sliding speed 1 m/s, oil lubrication)

Polymer	Coefficient of friction	Polymer	Coefficient of friction
Polyamides	0.040-0.050	Polyacrylate	0.040
Aromatic polyamide	0.030	Epoxy resin Grade 3II-5	0.032
Polycarbonate	0.032	Fluoroplastic Grade 42JI	0.032

it should be borne in mind that the antifriction properties of one and the same material can vary substantially, depending on its operating or testing conditions. The material of the mating part has a marked effect on wear of a bearing made from a polymer. For instance, if wear of a specimen made from polytetrafluoroethylene working in a pair with a carbon-steel specimen is assumed to be unity, then the relative amount of wear for the same polymer mated with cast iron, stainless steel, chromium coating, or an aluminium alloy will reach 2, 3, 20, and 50, respectively. The best properties exhibit composite materials that contain polymers as a binding substance (matrix) and various functional fillers that are intended to impart the required frictional, mechanical, and other properties to the material.

The main advantages of thermoplastic-base antifriction materials are excellent processability, low cost, and good damping properties. Rubbing components can be manufactured from thermoplastics by such highly efficient methods as die-casting, extrusion, centrifugal casting, anion polymerization of the monomer directly in the mould (for large components), and deposition of antifriction coatings from polymer melts and dispersions.

Thermosets are more temperature-resistant and strong. They are processed largely by compression and injection moulding. Powdered thermosetting compounds can be applied in the form of thin-layer coatings.

Polyamides are used for making most rubbing components. Soviet industry produces mouldable polyamides, Grades П-68 (П-610, GOST 10589-73), П-12JI (ТУ* 6-05-1309-72), П-125Б (ТУ 6-05-211-898-73), П-66 (OST** 6-06-369-74), П-АК-93/7, П-АК-80/20, and П-АК-85/15 (GOST 19459-74), capron (ТУ 6-06-309-70), and bar shaped polyamide — caprolon Grade B (MRTU*** 6-05-988-66). Polyamides can perform in the temperature range of -40 to $+80^{\circ}\text{C}$

* An acronym meaning technical specifications.

** An acronym meaning a standard adopted in a particular branch of industry.

*** An acronym meaning interbranch technical specifications.—*Editor's notes.*

for a long time, and in the range of 100 to 120° C, for a short time. They are resistant to chemical attack by mineral and organic oils, fats, hydrocarbons (kerosene, benzine, benzol), aldehydes, ketones, concentrated or weak alkalines, weak acids, and ethers, but are dissolved in concentrated acids (sulphuric, muriatic, formic, acetic), phenolics, fluorinated and chlorinated alcohols.

Polyamide components are resistant to the action of cyclic and impact loads, work well and wear out little on hardened steel. When sliding on non-ferrous metals, especially aluminium, they wear intensively. The coefficient of friction without lubrication is 0.1 to 0.2, with oil lubrication, 0.050 to 0.1, and with water lubrication, 0.08 to 0.15.

Polyamides, however, are rather hygroscopic, which has the effect of altering the dimensions of parts, and this property must be taken into account when rubbing members are to work in water or in a humid atmosphere. Upon dehydration the original dimensions are practically restored. The maximum absorption of moisture can reach 3.3 percent for П-68, 1.75 percent for П-12, 6.5-7.0 percent for caprolon Grade B, 7.2 percent for П-66, and 10 to 11 percent for capron.

To improve strength characteristics, polyamides are reinforced, and for better antifriction properties they are filled with solid lubricants.

Soviet industry produces the following grades of reinforced antifriction polyamides: П-610-BCM (ТУ П-510-68), ПHC-610-710, ПHC-610-ДМ-1.5 (ТУ 6-05-1034-74), and КГ-10 (ТУ П-455-65), АТМ-2 (ТУ 6-05-031-502-74), НГП-610, and НГП-АК-80/20 (ТУ 60-67). In these composites graphite, molybdenum disulphide, and talc are used as solid lubricants, and finely chipped glass fibre as a reinforcing filler. Data on physical and mechanical properties of polyamides are presented in Tables 5.5 through 5.7.

The linear expansion coefficient and water absorption of filled and reinforced polyamides is 50 to 67 percent, the coefficient of dry friction, 120 to 200 percent, and the rate of wear, 20 to 50 percent of those of unfilled polymers.

Polyamides can be used very efficiently as thin-layer coatings. Such coatings can be obtained from solutions, suspensions, pastes, aerosols, and by plating. Methods of producing antifriction coatings from powdered polyamides find the widest application. The best antifriction characteristics are exhibited by polycaproamid and caprolon-B coatings (Table 5.8).

These characteristics are greatly affected by the thickness of the layer (whose optimum value depends on physical and mechanical properties of the polymer and the surface roughness of the mating member), and also by the joint's design and operating conditions. A polycaproamid coating 0.3 mm thick is considered to be close to optimal (Table 5.9). With a smaller thickness, the damping capacity of the coating decreases and specific loads rise; with a thickness

Table 5.5

Physico-mechanical properties of polyamides

Characteristic	И-610	Capron	И-12И	И-12В	Caprolon Grade B	И-66	И-АК-93/7
Density, g/cm ³	1.10	1.13	1.02	1.02	1.15-1.16	1.14	1.14
Flexural stress, kgf/cm ²	800-900	900- 1,000	500-700	—	1,200- 1,500	1,000- 1,200	1,000- 1,200
Breaking stress, kgf/cm ² :							
in tension	450-600	580-650	350-400	—	800-1,000	800-900	600-700
in shear	500-580	650	400-550	450	700-900	800	600-700
in compression	550	600	—	—	—	—	550-600
Ultimate elonga- tion, %	700-900	850- 1,100	600-630	—	1,000- 1,100	—	1,000- 1,200
Elastic modulus, kgf/cm ²	100-150	80-150	70-300	250-300	10-30	20-40	80-100
Impact strength, kgf cm/cm ² :							
without not- ching	10,000- 12,000	15,000	12,000- 18,000	8,000	20,000- 30,000	—	15,000- 16,000
with notching	80-125	100-120	80-90	50-60	150-160	90-100	100-130
Hardness, kgf/cm ² , at a load of 36.5 kgf	4.5-10	5-10	5-10	50-60	4-6	4.9-8	3-5
	1,000- 1,500	1,000- 1,100	740-780	500-800	1,400- 1,500	1,100- 1,800	1,000- 1,200

exceeding the optimum value, the coefficient of friction increases, while the load-carrying capacity and wear resistance diminish due to inadequate heat removal and, hence, worse thermal conditions in the joint.

Extremely thin coatings (less than 50 μm thick) are promising; however, they are still to be studied. In contact with hard, smooth surfaces, such coatings are capable of sustaining very high specific loads.

Fluoroplastics and fluoroplastic-base composites have found numerous applications in engineering for tribological components.

Fluoroplastics exhibit exceptionally high resistance to chemical attack: they are practically unaffected by acids, oxidizers, alkalis and solvents. Fluoroplastics are only sensitive to molten alkaline metals and their complexes with ammonia, naphthalene, pyridine, and also to elementary fluorine at elevated temperatures. At temperatures over 350° C fluoroplastics react with alkaline metals and their compounds (oxides and carbonates), and with oxides of some other metals (lead, cadmium, copper).

Table 5.6

Thermo-physical properties of polyamides

Characteristic	П-160	Capron	П-66	Caprolon Grade B	П-АК-93/7	П-АК-85/15	П-12П П-129
Melting point, °C	213-220	210-218	252-265	220-226	237-243	224-230	178-180
Thermal resistance, °C:							
at a bending load, kgf/cm ² :							
18.5	45-60	45-50	55-60	60-70	50-55	45-50	42-45
4.6	161	—	—	—	—	—	135-140
according to Vicat	195-208	190-200	220	190-210	220-230	210-220	140
according to Martens	55-60	55-60	75-76	74-75	55-60	50-60	45
Heat capacity, cal/(kg °C)	0.20	0.45	—	—	0.40-0.50	—	0.38
Coefficient of thermal conductivity, kcal/(m h °C)	0.2326-0.2093	0.246	0.240	0.2675-0.3373	0.2326-0.2559	—	0.200-0.2442
Linear expansion coefficient, $\alpha \times 10^{-5}$, 1/°C	11-12	8-10	1-9.8	6.6-9.8	10-12	9-12	1.25

Table 5.7

Physico-mechanical properties of filled and reinforced polyamides

Grade	Density, ρ , g/cm ³	Bending stress, kgf/cm ² (GOST 4648-71)	Breaking stress, kgf/cm ²		$E \times 10^4$, kgf/cm ²	Impact strength without notching, kgf \times cm/cm ²
			in tension	in compression		
ПHC-610-T10	1.16	600-700	500-600	800-1000	3.2	50-80
ПHC-610-T20	1.25	600-800	500-600	800-1000	3.5-4.0	25-40
ПHC-610-T40	1.33	600-800	550-630	—	—	15-20
ПHC-610-T10	1.15	500-700	500-600	800-900	3.0	50-80
ПHC-610-DM1,5	1.12	500-700	500-600	800-1,000	3.0	50-80
КТ-10	1.14	600-700	650-800	800-1,000	—	18-50
П-610-BC	1.35	1,600-2,000	1,100-1,400	1,000-1,200	8.0	30-50
П-610-BCA	1.35	1,600-2,000	1,100-1,400	1,000-1,200	8.0	20-50
П-610-BCM	1.35	1,600-2,000	1,100-1,400	—	8.0	20-50
П-610-BCФ	1.15	1,400-1,900	900-1,000	1,100-1,200	6.0-7.0	15-25
П-6-BC	1.35	1,700-2,200	1,200-1,600	1,100-1,300	8.0-10.0	30-60
П-12-BC	—	1,200-1,400	1,000	—	5.6-6.0	25-30
АТМ-2	1.38	1,100-1,270	500-520	1,100-1,280	—	11-20

Table 5.8

Properties of polyamide coatings

Parameter	Capron	Caprolon Grade B
Breaking stress in tension, kgf/cm ²	500-600	600-650
Ultimate elongation, %	25-60	—
Microhardness, kgf/mm ²	9.5-13,0	10-13.5
Strength of adhesion to phosphatized steel surface, kgf/cm ²	400-600	350-500
Coefficient of friction on steel ($v=0.5$ m/s, $p=100$ kgf/cm ² , oil lubrication)	0.015-0.020	0.009-0.02
Wear, $\mu\text{m/km}$ ($v=0.5$ m/s, $p=55$ kgf/cm ²)	0.55-0.85	0.45-0.65

Table 5.9

Effect of layer thickness on antifriction properties of polycaproamide coating

Parameter	Coating layer thickness				
	0.2	0.3	0.4	0.5	0.6
Maximum normal pressure, kgf/cm ²	75	140	120	95	70
Coefficient of friction	0.020	0.018	0.030	0.055	0.065
Wear, $\mu\text{m/km}$	0.58	0.66	0.72	0.76	0.56

In rubbing against metals, the coefficient of friction of fluoroplastics, particularly of polytetrafluoroethylene, is very low: it does not exceed the usual friction coefficients for lubricated metal sliding pairs. Soviet industry produces a variety of fluoroplastics for rubbing components, namely, fluoroplastic-4 (polytetrafluoroethylene), GOST 10007-72; fluoroplastic-4Д, GOST 14906-69; fluoroplastic-4М, TU II-207-68; fluoroplastic-40, MRTU 6-05-817-68, TU II-272-70, TU 6-05-041-383-72 and TU II-193-68; fluoroplastic-3 and 3М, GOST 13744-76; fluoroplastic-30, TU II-236-70; and fluoroplastic-2 and 2М.

In spite of the low coefficient of friction, the application of plain fluoroplastics is limited by their low strength and unsatisfactory manufacturing properties. Various combinations of fluoroplastics with other materials have found use in engineering.

Introduction of different fillers at 15 to 30 percent by volume allows wear to be markedly reduced. The most extensively applicable

fillers are conventional and graphitized coke, man-made graphite, molybdenum disulphide, glass fibre, and metal powders.

Mechanical properties of filled fluoroplastics are given in Table 5.10.

Table 5.10

Properties of filled fluoroplastic-base materials

Parameter	Pure PTFE	Ф4С14 - 15% glass fibre	Ф4С15М5 - 15% glass fibre and 5% MoS ₂	Ф4К20 - 20% coke	Ф4К15М5 - 15% coke, MoS ₂	Ф4М15 - 15% MoS ₂
Density, g/cm ³	2.2	2.21	2.14	2.14	2.19	2.25
Breaking stress in tension, kgf/cm ²	200	140	142	130	155	135
Ultimate elongation, %	350	300	250	120	150	250
Brinell hardness, kgf/mm ²	3.8	5	6	4	6	5
Deformation under a load of 100 kgf/cm ² during 24 h at 22°C, %	6.6	3.5	3.8	2.9-3.0	3.6	4.3
Maximum value of ν , kgf cm/(cm ² s) at ν , cm/s:						
5	45	350	400	500	600	500
50	65	450	500	700	700	500
500	90	550	620	1,100	1,100	400
Allowable value of ν (wear 0.127 mm dur- ing 100 h)	100	130	150	325	500	185
Relative wear resis- tance	1	250	275	625	1,000	560

Industry manufactures a number of low-friction materials: composite Ф4К20 (ТУ 6-05-1412-71), composite Ф4Г21М7 (ТУ 02-14-6-71), composite Ф4С15 (ТУ 6-05-041-363-72), low-friction materials 7В-2А (TsMTU 01-51-69), АФГ-80ВС (TsMTU 01-45-69), АФГМ (TsMTU 01-46-69), ФН-3 (ТУ П-495-66), ФН-202 (ТУ П-644-68), АМИП-15М (ТУ П-407-65), and АМИП-30М (ТУ П-407-65).

Fluoroplastics are widely used in the form of varnishes, suspensions, and pastes for making antifriction materials.

Soviet industry produces fluoroplastic-4А suspension (МRTU 6-05-1246-69), varnish ФБФ-74 (ТУ 6-05-1617-73), paste ПФМ-75 (ТУ 6-05-041-335-71), fluoroplastic-4М suspension (ТУ 6-05-041-508-74), and fluoroplastic-4МД suspension (ТУ 6-05-041-508-74).

Fluoroplastics find extensive application as antifriction fillers in different composites based on thermoplastic and thermosetting

polymers, offering a substantial decrease in the coefficient of friction and wear of the joint.

Polyolefins are the most commonly used polymers. The main among them, polyethylene and polypropylene, combine satisfactorily a good mechanical strength, adequate chemical resistance, and low gas and moisture absorption.

Polyolefins are resistant to acids and alkalis and insoluble in organic solvents at 20°C. Strong oxidizers (for instance, nitric acid), liquid and gaseous chlorine and fluorine destroy polyolefins. At elevated temperatures they are soluble in many organic solvents, particularly in aliphatic and aromatic hydrocarbons and their halogen derivatives.

Industry produces the following grades of polyolefins: high-pressure polyethylene ПЭВД (GOST 16337-77), low-pressure polyethylene ПЭНД (GOST 16338-77), medium-pressure polyethylene ПЭСД, and polypropylene (MRTU 6-05-1105-67).

Numerous composites are obtained on the basis of polyolefins by introducing various additives and fillers. The latter are most commonly carbon black, rubber, glass, fibre, and sawdust. The resulting materials exhibit high wear resistance, and their coefficient of friction is 0.1-0.15.

The choice of a composite should be in keeping with GOST 16337-77, GOST 16338-77 and MRTU 6-05-1105-67. Physico-mechanical properties of some polyolefins are presented in Table 5.11.

Powdered polyethylene is frequently introduced into composite materials to improve their antifriction properties. A drawback to polyolefins is their low temperature resistance: the rubbing components made of them can function at temperatures not over 60°C, and, momentarily, up to 80°C.

Pentaplast is used for high-accuracy engineering components (gear wheels, cup packings, ring packings, and others).

Articles made of pentaplast can operate at temperatures up to 120-130°C for a long time, and up to 135-150°C momentarily. Pentaplast is highly resistant to chemical attack (at 20-27°C) by nitric acid (60 percent), perchlorethylene, sodium hydrate (40 percent), sulphuric acid (92 percent), phenols and dichlorophenols, hydrogen chloride, hydrosilicofluoric acid (up to 45 percent), hydrofluoric acid (up to 40 percent), fats, hydrocarbons (kerosene, diesel fuel, mineral oils), and catalysts. It cannot resist, however, strong oxidizers at boiling temperature, fuming nitric acid, oleum, chloro-sulphonic acid, and 85-98 percent sulphuric acid at 60°C with injection of chlorine. Pentaplast is soluble at temperatures over 100°C in cyclohexanone and chlorobenzene, in boiling dioxan, and in dimethylformamide at 110-120°C. Pentaplast is processed by all conventional methods on equipment used for working thermoplastics.

Industry makes pentaplast in a wide range of molecular masses according to TU 6-05-1422-71. Data on physico-mechanical properties of pentaplast are listed in Table 5.12.

Table 5.11

Physico-mechanical properties of polyolefins

Parameter	ПЭВД	ПЭНД	ПЭСД	Polypropylene
Density, g/cm ³	0.918-0.930	0.949-0.955	0.96-0.97	0.90-0.91
Breaking stress, kgf/cm ² :				
in tension	100-170	220-300	280-350	250-400
in static bending	120-170	200-350	—	—
in shear	140-170	—	—	—
Ultimate elongation, %	500-600	300-800	200-800	200-800
Elastic modulus in bending, %	1,200-2,600	6,500-7,500	8,000-10,000	6,700-11,900
Brinell hardness, kgf/mm ²	1.4-2.5	4.5-5.8	5.6-6.5	6.0-6.5
Brittle point, °C	From -80 to -120	From -100 to -150	—	From -5 to -15
Thermal resistance according to Vicat, °C	80-90	—	—	—
Notch impact strength, kgf cm/cm ²	—	2.0-12.0	—	33-80
Moisture absorption at 20°C, %	0.15 (during 1 year)	0.06 (during 2 years)	—	0.5 (during 0.5 year)

Table 5.12

Physico-mechanical properties of pentaplast

Parameter	Value	Parameter	Value
Density, g/cm ³	1.4	Impact strength, kgf cm/cm ² :	
Breaking stress, kgf/cm ² :		injection moulded specimens at a temperature, °C:	
in tension (50 mm/min) at a temperature °C:		-50	8
-50	780	0	10
0	650	20	140
20	400-550	compression moulded specimens at 20°C	20-40
100	250	Brinell hardness, kgf/mm ²	8-11
in compression	850	Moisture absorption during 30 days, %	0.01
in static bending	600-850		

For sliding pairs of pentaplast-on-pentaplast and pentaplast-on-steel Grade 5, the coefficient of friction at a temperature of 20°C and a pressure of 50 kgf/cm² is equal to 0.14 and 0.12, respectively. Physico-mechanical properties of pentaplast are improved by introducing mineral fillers. Promising as fillers are graphite, micro-powdered mica, glass fibre, and chromium oxide. Characteristics of the main properties of filled pentaplast are presented in Table 5.13.

Table 5.13

Properties of filled pentaplast

Parameter	Filler, %				
	Mica		Glass fibre 2-5 mm, 10	Chromium oxide, 15	Graphite, 15
	15	25			
Breaking stress in tension (50 mm/min), kgf/cm ²	630	615	670	560	530
Ultimate elongation, %	25	15	20	19	17
Elastic modulus in bending, kgf/cm ²	24,200	32,600	21,070	13,400	22,000
Impact strength, kgf cm/cm ²	40-50	25	30	140	40-50
Brinell hardness, kgf/mm ²	13.9	14.8	12.3	9.8	10.0

Polyformaldehyde is widely used for gear wheels, pinions, sleeves, clutches, and other engineering components.

Polyformaldehyde parts can operate at temperatures up to 120°C. The material is highly resistant to organic solvents. At temperatures below 60°C it is soluble in hexafluoroacetonehydrate, and at 100-180°C, in phenols, halogen hydrocarbons, acetic anhydride, methylene diacetate, and other compounds. It is resistant to hot water, salt solutions, sea water, alkalis, and organic acid solutions. Mineral acids cause decomposition of the polymer. Polyformaldehyde products exhibit high stiffness, dimensional stability, and high resistance to wear and ageing.

Polyformaldehyde is processed by injection moulding. Soviet industry produces polyformaldehyde (MRTU 6-05-1018-66) and copolymers based on formaldehyde — CФД — and trioxan — CTД — (TU 6-05-1543-72). Also in production are trial batches of polyformaldehyde filled with glass fibre, polytetrafluoroethylene, molybdenum disulphide, and carbon black. The coefficient of friction of unfilled polyformaldehyde on steel without lubrication is 0.3-0.35.

The main physico-mechanical properties of polyformaldehyde are given in Table 5.14. Introduction of fluoroplastic (15-20 percent) into polyformaldehyde reduces wear by a factor of 3 to 4 and the coefficient of friction by a factor of 1.5 to 2.

Table 5.14

Physico-mechanical properties of polyformaldehyde

Parameter	Value	Parameter	Value
Density, g/cm ³	1.41	Elastic modulus in tension, kgf/cm ²	(25 to 29) × 10 ⁸
Melt flow index, g/10 min	2-30	Impact strength with notching, kgf cm/cm ²	
Breaking stress, kgf/cm ² :		Brinell hardness, kgf/mm ²	5-9
in tension	650-700	Thermal resistance, °C, at a load, kgf/cm ² :	12-13
in compression	1,450	4.6	160
in static bending	1,250	18.5	115-120
Ultimate elongation, %	10-15		

Polycarbonate finds many applications in general engineering, instrument-making, radio engineering, and electrical engineering, for machine-tool, instrument, and computer components and so on. The polymer is highly resistant to exposure in atmosphere. It is suitable for use in tropical environments, and its properties remain practically unchanged upon long exposure to light, heat, or vacuum, and after sharp temperature rises.

Polycarbonate is a promising material for cryogenics applications in gaseous and liquid nitrogen, hydrogen, and helium ambiances at temperatures of down to -253°C. It has high impact strength and dimensional stability, and low creep. It is sensitive, however, to cyclic loads and has a low fatigue strength. Maximum water absorption of polycarbonate immersed in water does not exceed 0.4 percent, and when held in the atmosphere, 0.2 percent. It is resistant to water solutions of mineral acids and salts, as well as oxidizers; insoluble in aliphatic and cycloaliphatic hydrocarbons and oils, aliphatic alcohols, ethers, and carbon acids; resistant to aqueous solutions of soaps, deterines, bleaches, animal fats, and vegetable oils. Organophile bases, such as ammonium hydroxide or amines, saponify polycarbonate, and aqueous solutions of strong alkalis destroy it. Polycarbonate is soluble in 1,1,2,2-tetrachloroethane, methylenechloride, chloroform, thiophene, dioxan, and it swells in benzene, chloro-benzene, toluene, acetone, and the like.

Produced by Soviet industry are polycarbonates diflon (TU 6-05-1668-74) and diflon CTH (TU 6-05-211-937-74) containing 25 percent by mass of glass-fibre reinforcement.

Physico-mechanical properties of polycarbonates are given in Table 5.15.

Table 5.15

Physico-mechanical properties of polycarbonates

Parameter	Injection mouldable diflon	Diflon CTH-30	ДАК
Density, g/cm ³	1.2	1.40	1.2
Breaking stress, kgf/cm ² :			
in tension	600-700	900-1,100	500-550
in compression	800-900	1,200-1,400	700-800
in static bending	900-1,000	1,500-2,000	800-1,000
Ultimate elongation, %	50-100	4-5	30-50
Elastic modulus in tension, kgf/cm ²	(22 to 24) × 10 ³	(60 to 70) × 10 ³	—
Impact strength, kgf cm/cm ²	120-140	35-45	90-110
Brinell hardness, kgf/mm ²	10-11	15-16	—
Moisture absorption, %	0.4	0.2	—
Maximum operating temperature, °C	135	150	220-240*
Cold resistance, °C	-100	-100	—
Coefficient of friction on steel	0.3	—	0.15-0.2
Wear on network, mm ³ /(m cm ²)	0.13	0.01	0.0003-0.003

* Melting point.

Addition of fluoroplastic (from 15 to 20 percent) to polycarbonate reduces its coefficient of friction by a factor of 2 to 3 and wear by a factor of 10 to 30.

A new low-friction material ДАК, which is diflon modified by fluoroplastic-4, is developed at the Research Institute of Polymer Materials (NIIPM).

The material retains the physico-chemical, physico-mechanical and dielectric properties of polycarbonate, whereas its antifriction characteristics are improved 1.5 to 2.0 times. It is processed by injection moulding, extrusion, and other methods.

The ДАК is produced in the form of solid, nontransparent granules from white to light-brown in colour. Products made from this material lend themselves to machining.

The antifriction polycarbonate ДАК is recommended for structural components operating in tribological joints without lubrication, namely, sleeves, gears, valve components, and others.

Polyarylates are essentially thermoplastic polymers suitable for making rubbing parts by casting and injection moulding. Most proper for the purpose are Soviet-produced polyarylates Д-3, Д-4, and Д-39 (ТУ 6-05-211-72); their physico-mechanical properties are presented in Table 5.16.

Polyarylates exhibit relatively high temperature resistance; rubbing components made of them can operate for a long time at 160 to 180°C and momentarily at 230°C. They also have good resistance to ionizing radiations, and good dielectric properties; they

Table 5.16

Physico-mechanical properties injection mouldable polyarylates

Parameter	Д-3	Д-4	Д-4С
Density, g/cm ³	1.197	1.197	1.217
Breaking stress, kgf/cm ² :			
in tension	850-900	450-500	500-600
in compression	900-1,200	800-1,000	900-1,100
in static bending	1,000-1,200	500-600	800-1,000
Ultimate elongation, %	10-20	10-15	12-15
Elastic modulus in tension, kgf/cm ²	(6 to 7) × × 10 ³	(8 to 10) × × 10 ³	(10 to 12) × × 10 ³
Impact strength, kgf cm/cm ²	50-80	30-50	80-100
Brinell hardness, kgf/mm ²	20-25	19-20	25-30
Moisture absorption in 24 h, %	0.02	0.02	0.15
Coefficient of friction	—	0.4	—

melt at 255 to 285°C, begin oxidizing at 250 to 270°C, and decompose at 450°C. Cold resistance is -100°C. the coefficient of thermal conductivity, about 0.2 kcal/(m h). Shrinkage of polyarylate products is from 0.6 to 1.0 percent. Grades Д-3 and Д-4 polyarylates are capable of long-term resistance to mineral and organic acids (except for H₂SO₄), alcohols, aliphatic hydrocarbons, oils, and fuels. They are soluble in tetrachlorethane and its mixture with phenol, and are decomposed by concentrated alkali solutions. For improved wear resistance and lower coefficient of friction polyarylates are filled with solid lubricants.

Polyimides are heat resistant thermosetting polymers, used as binders for producing low-friction composites (see Table 5.17).

On the basis of polyimides ПИМ-67 (ТУ П-622-69) and ПИМ-69 (ТУ П-279-70), Soviet industry makes filled composites ПИМ-67-ДМ-3 and ПИМ-69-ДМ-3 containing 3 percent molybdenum disulphide, and ПИМ-67-Г-10 and ПИМ-69-Г-5 loaded with graphite. These materials feature high resistance to radiation, do not oxidize at temperatures up to 275°C, properly resist organic and neutral oils, but decompose in concentrated acids and alkalis and during prolonged boiling in water. Rubbing parts made of polyimide composites are capable of functioning at 220 to 260°C for a long time. Polyimide articles are shaped mainly by compression moulding; thanks to low shrinkage (0.7 to 1.0 percent), this method ensures high accuracy of product. The composites are also readily machined.

NIIPM has developed a new low-friction, self-lubricating material, grade ПАМ-15. This filled polyimide can be used for structural antifriction components, such as pinions in speed reducers, which withstand up to 20-fold vibration overloads during operation in air, in CO₂ or in a 10⁻⁶-mm Hg vacuum; other applications of this material include plain and antifriction bearings for work within

Table 5.17

Physico-mechanical properties of polyimide-base moulding compounds

Parameter	IIM-67	IIM-69	IIM-67-ДМ-3	IIM-67-Г-10	IIM-69-ДМ-3	IIM-69-Г-5
Density, g/cm ³	1.39-1.44	1.38-1.44	1.43-1.45	1.44-1.46	1.43-1.45	1.44-1.47
Breaking stress, kgf/cm ² :						
in tension	1,100-1,300	950-1,250	900-1,300	700-980	850-1,200	700-900
in compression	2,000-2,300	2,100-2,400	2,100-2,300	1,500-1,900	2,300-2,500	1,800-2,300
in bending at a temperature, °C:						
20	1,800-2,300	1,800-2,300	1,600-2,200	1,200-1,800	1,600-2,000	1,300-1,700
250	500-900	600-1,000	440-870	430-750	600-800	500-600
Ultimate elongation, %	9-20	4-7	6.5-15	5-8	—	—
Elastic modulus in bending, kgf/cm ²	(29.70 to 36) × 10 ³	—	—	—	—	—
Impact strength, kgf cm/cm ²	60-120	60-100	20-80	8-30	30-50	20-40
Brinell hardness, kgf/mm ²	18-28	20-27	21-31	23-33	21-28	22-30
Upper range of operating temperatures, °C	220-250	235-265	220-250	250	220-250	220-250
Thermal resistance according to Vicat, °C	280	280	280	280	280	280
Coefficient of friction	0.33-0.35	0.35-0.40	—	—	—	—
Moisture absorption in 24 h, %	0.18-0.29	0.2-0.3	—	—	—	—

the temperature range from -196°C to $+250^{\circ}\text{C}$. The material is a composite including polyimide resins ПМ-67 or ПМ-69 and a solid lubricant (Table 5.18). Pinions and bearing bushes are machined from compression moulded blanks.

Table 5.18

Physico-mechanical properties of self-lubricating polyimides

Parameter	ПМ-15-69 at temperature, $^{\circ}\text{C}$			ПМ-15-67 at temperature, $^{\circ}\text{C}$		
	-196	+20	+110	-196	+20	+110
Breaking stress in tension, kgf/cm^2 , not lower than	1,020	644	550	1,100	800	600
Elastic modulus in compression $E \times 10^{-4}$, kgf/cm^2	9.07	6.23	2.85	—	—	—
Brinell hardness, kgf/mm^2	40	33	20	—	30	19
Specific impact strength, kgf cm/cm^2	8.8	7.8	7.8	—	16	—
Coefficient of friction on Model МН-1М testing machine ($p = 50 \text{ kgf/cm}^2$, $v = 0.5 \text{ m/s}$)	—	0.18	—	—	0.18	2
Coefficient of friction on Model УТН-1М testing machine ($p = 22 \text{ kgf/cm}^2$, $v = 0.5 \text{ m/s}$) in air, 5 mm Hg	—	—	—	—	0.292	—

Aromatic polyamides are used for rubbing components in unfilled or filled (by fluoroplastic, graphite, molybdenum disulphide, and other solid lubricants) form. They are characterized by high strength and heat resistance. Soviet industry makes aromatic polyamides under a trade name of "Phenylon", grades П, C1 (ТУ 6-05-221-101-74) and C2 (ТУ 6-05-221-226-72) in the form of fine powders from which products are compression and injection moulded (C1 and C2). The linear expansion coefficient within the range from -70 to $+300^{\circ}\text{C}$ varies from 18×10^{-6} to $40 \times 10^{-6} 1/^{\circ}\text{C}$, and the coefficient of thermal conductivity, from 0.16 to 0.23 $\text{kcal/(m h }^{\circ}\text{C)}$. Phenylon is resistant to many organic liquids, oil, benzine, weak acid and alkali solutions. The moisture absorption of Phenylon is similar to that of polyamides; a Phenylon part can absorb up to 10 percent

water and its dimensions can increase by two percent. The coefficient of friction of unfilled Phenylons is about 0.4. Filling with fluoro-plastic or graphite allows the coefficient of friction to be reduced to 0.15-0.20, and wear resistance, increased by almost one order of magnitude. Oil lubrication can lower the coefficient of friction down to 0.015. Phenylon joints are capable of proper functioning within the temperature range from -50 to $+200^{\circ}\text{C}$. Successful applications of phenylon include plain bearings, sealings, thrust bearings ball-bearing cages, cams, fine-module gears, valve components, and other products. The main physico-mechanical properties of Phenylon are presented in Table 5.19.

Table 5.19

Physico-mechanical properties of compression-moulded phenylon specimens

Parameter	Phenylon II	Phenylon C1	Phenylon C2
Density, g/cm^3	1.33	1.33	1.33
Breaking stress, kgf/cm^2 :			
in tension	1,000-1,200	1,100-1,200	1,200-1,400
in bending	1,300-1,500	1,500-1,700	2,200-2,400
in shear	800	910	1,200
Ultimate elongation, %	4	5	6.6
Elastic modulus, kgf/cm^2	$(30 \text{ to } 33) \times 10^3$	$(32 \text{ to } 33) \times 10^3$	$(30 \text{ to } 32) \times 10^3$
Yield point in compression, kgf/cm^2	2,100-2,300	2,200-2,300	2,100-2,300
Impact strength, kgf cm/cm^2	20-30	30-40	40-50
Hardness, kgf/cm^2	31-33	26-30	28-29
Thermal resistance according to Vicat, $^{\circ}\text{C}$	270	275	290
Cold resistance, $^{\circ}\text{C}$	-70	—	—

Plain epoxy and furan polymers are not applicable for rubbing components. They acquire antifriction properties when filled, mostly with graphite and molybdenum disulphide. Industry produces a low-friction moulding compound II-1-9 (TU MBO 023146) which is shaped into products by injection and compression moulding methods.

High filler content moulding materials ЭНГ-30 and ЭНГ-25 (filled with graphite) and ЭНМ-25 (filled with molybdenum disulphide) are developed for work in aggressive environments (Table 5.20). These materials are processed by casting at atmospheric pressure and by compression moulding. The operating temperature range for rubbing components made from epoxy resins is from -100 to $+150^{\circ}\text{C}$.

Materials based on furan polymers have higher resistance to temperature and chemical attack as compared with epoxy polymers (Table 5.21). Compression-moulding compounds ФАФФ-31ГЭ, ДФГ-

Table 5.20

Properties of epoxy moulding compounds

Parameter	II-1-9	ЭНМ-25	ЭНГ-25	ЭНГ-30
Breaking stress, kgf/cm ² :				
in tension	—	400-500	500-600	400-500
in compression	1,700-2,000	1,700-1,800	1,600-1,650	1,200-1,400
in static bending	1,000-1,300	1,000-1,200	1,200-1,400	800-1,000
Impact strength, kgf cm/cm ²	9-12	14-16	15-16	12-14
Brinell hardness, kgf/cm ²	30	—	—	—
Thermal resistance (Vicat), °C	—	125-135	120-130	125-135

Table 5.21

Physico-mechanical properties of materials based on furan polymers

Parameters	ФАФФ-31FЭ	ДФГ-1	ДФ-1	ДФ-2
Density, g/cm ³	1.6-1.65	1.70-1.75	1.75-1.82	1.6-1.9
Moisture and volatiles content, %	1.0-1.5	1.0-1.5	0.4-0.5	0.25-0.5
Particle size distribution (%) in passing through sieve with mesh size, mm:				
2.0	100	100	100	100
0.5	70	70	70	Not specified
Breaking stress, kgf/cm ² :				
in compression	1,000-1,400	1,000-1,410	1,000-1,400	1,000-1,400
in static bending	—	—	—	290
Minimum impact strength, kgf cm/cm ²	—	—	—	2.5
Brinell hardness, kgf/mm ²	—	—	—	20
Thermal resistance (Martens), °C	230-280	230-300	250-300	230
Flowability (Raschig), mm	—	—	—	60-110
Wear resistance, mm ³ /(m·cm ²)	8.1-8.3	8.0-8.3	7.5-7.8	7.4-7.6
Shrinkage, %	0.4-0.5	0.4-0.5	0.2-0.4	0.2-0.5

1, ДГ-1 (ТУ II-741-71) and ДГ-2 (ТУ 6-05-211-812-74) find applications as plain bearings, groove gaskets, piston rings, and other components designed for use in chemically aggressive (acid and alkali) environments and in air at temperature from -100 to $+200^{\circ}\text{C}$.

The compound is available in the form of a black powder; the surface of the mouldings is smooth, without swellings and cracks, and variation in hues is allowable.

The coefficient of friction of epoxy- and furan-polymer-base compounds without lubrication is 0.15 to 0.25 and with lubrication presented by production environments may become as low as 0.05. On the basis of polyvinyl furfural, a Soviet-formulated polymer, the IMMS of the Byelorussian Academy of Sciences has developed a family of ПБФК-type self-lubricating compounds. These are mouldable powders shaped into products by compression moulding. The optimum processing conditions are: the moulding temperature $180 \pm 10^\circ\text{C}$, and the moulding pressure, 1,200 to 1,400 kgf/cm². Physico-mechanical properties of the ПБФК-9 compound (ТУ 88 БССР-05-74) are listed in Table 5.22. The material can work

Table 5.22

Physico-mechanical properties of ПБФК compound

Parameter	Value	Parameter	Value
Density, g/cm ³	3.0	Linear expansion coefficient (within the range from 20 to 200°C), 1/°C	$(1.84 \pm 0.4) \times 10^{-5}$
Ultimate strength in compression, kgf/cm ²	1.100 ± 100	Coefficient of thermal conductivity, W/m °C	
Brinell hardness, kgf/mm ²	21 ± 1	Maximum coefficient of friction	
Impact strength, kgf cm/cm ²	2.5 ± 0.5		

for a long period at 180 to 200°C, and for a short time at up to 250°C. Its performance in vacuum is good, and in water, poor.

Antifriction plastics type AMAH are developed in the Research Institute of Element-Organic Compounds and in the Research Institute of Mechanical Engineering of the USSR Academy of Sciences. The compounds are produced under trade names of AMAH, ЭСТЕРАН, ТЕКАН, and БИЛАН. These are multi-component materials that make use of binders in the form of polymers specially formulated for the purpose, or chosen from the known types having high thermal, radiation, and chemical resistance along with good processing characteristics. The main properties of these materials are given in Table 5.23.

The materials are processed by compression and injection moulding at a pressure ranging from 400 to 1,000 kgf/cm² and a temperature varying from 230 to 500°C, depending on the binder used. The best anti-friction properties show up in contact with hard steel components (30 to 40 HRC) of a high surface roughness class.

Table 5.23

Physico-mechanical properties of type AMAH plastics

Parameter	ЭТЕПАВ-1	ТЕСАВ-6	ЭТЕПАВ-21	ВИЛАН-20
Density, g/cm ³	3.6	3.5	3.1	3.0
Impact strength, kg cm/cm ²	1.5	2.5	3.0	3.0
Brinell hardness, kgf/mm ²	25	28-30	22-25	25
Coefficient of friction	0.05	0.06	0.08	0.1
Ultimate strength in compression, kgf/cm ²	800	1,000	800	1,000
Linear wear rate*	—	0.7×10^{-9}	0.5×10^{-9}	—
Maximum operating temperature, °C	220	300	200	300

* The dimensionless ratio of the height of the worn-off layer to the friction distance during end-to-end sliding; the test conditions are: $v = 2$ m/s, $p = 2$ kgf/cm².

The type AMAH compounds are benzine- and oil-resistant, vibration-resistant, not sensitive to moisture and can be stored for a long time. They are only sensitive to attack by strong acid- or alkali-type oxidizers.

The most preferable applications encompass dry-friction units working in a vacuum within the temperature range from -200 to $+300^{\circ}\text{C}$. The performance of the materials in self-lubricating antifriction-bearing cages is studied best. The compounds are also used for plain bearings designed to run at high rotational speeds (up to 16,000 rpm) but light loads, or, alternatively, at low speeds and heavy loads (up to 200 kgf/cm²). Known applications also include light-loaded gears and feeding elements for transfer lubrication systems in heavily loaded metal gear transmissions.

Wood-base materials are finding ever increasing application for tribological components, primarily for bearings, slideways and like parts. Wood is a natural polymer material having a particular formation wherein highly stout cellulose fibres are bound by lignin into a stiff and strong capillary and porous structure. Such a structure presents wide possibilities of improving the properties of wood by its purposeful filling and rational combining with other materials. Among new lines of research in this direction is combination of densifying and impregnating with various active substances, such as metal compounds, polymers, and others.

Impregnation with polymers offers dimensional stability, reduced moisture absorption, and higher strength. Metal fillers markedly improve thermal conductivity, whereas oils and surface-active

substances sharply decrease the coefficient of friction and the rate of wear. Properties of such wood-base materials are given in Table 5.24. Type АПД materials developed in IMMS according to TU-88-

Table 5.24

Physico-mechanical properties of wood-base materials

Parameter	Wood impregnated with polyethylene dissolved in oil Grade MC-20 АПД-1	Wood impregnated with synthetic binder	Wood impregnated with stearate (Grade II) in engine oil	Wood impregnated with stearate (Grade II) in organo-silicon compound	Wood impregnated with copper salts and their oxides and glycerine АПД-2
Density, g/cm ³	1.15-1.25	1.4-1.45	1.3-1.4	1.3-1.4	1.1-1.15
Ultimate strength in compression with grain, kgf/cm ²	11-12	13-15	14-16	12-15	10-11
End-face Brinell hardness, kgf/mm ²	10-11	24-25	16-18	16-18	10-11
Thermal resistance (Vicat), °C	180	200	180	220	180
Volume pressing-off when held in water during 30 days at T = 20°C, %	60-75	1.5-2	16-20	10-15	100
Moisture absorption during 30 days in wet conditions (W = 95%)	10-12	1.5-2	4-8	3-6	25-30
Coefficient of friction in self-lubrication	0.08-0.12	0.08-0.14	0.06-0.12	0.09-0.12	0.03-0.04
Linear wear rate	0.7×10^{-9}	1.53×10^{-9}	0.32×10^{-9}	0.84×10^{-9}	0.55×10^{-11}
Maximum allowable friction temperature, °C	90-100	150-160	130-140	200-210	80-90

BSSR-11-76 are used for flange-type wood-plastic plain bearings, which showed good performance in supporting rollers on belt conveyors operating in dusty environments at foundries, building sites, and in agricultural production.

The potential of polymers for use as tribological components is far from being limited by the above-described polymer materials.

Some promising lines in research and development of new anti-friction materials are currently directed toward formulating composites based on new heat-resistant, highly strong polymer binders; compounding materials loaded with active fillers able to control friction directly in the course of rubbing interaction; and devising methods of local filling in order to obtain products with the required bulk and surface properties.

5.2.3. Laminated Materials

These are complex-structure materials consisting of a hard backing, an intermediate layer, and an antifriction surface layer. Metal-fluoroplastic laminates and bearing components made from them find the most extensive application. Developed and produced in the USSR is a laminate with a structural steel substrate (TU 27-01-01-71). The backing made from steel Grade 08кп or 10кп (GOST 1050-74) is coated on both sides with a layer of copper Grade M1 (GOST 859-66) or brass Grade Л90 (GOST 15527-70). A porous layer of spheroidal bronze powder (9 to 11 percent Sn) with particles 0.063 to 0.16 mm in diameter is sintered onto the steel backing. The bronze layer is then impregnated with a compound containing 75 percent fluoroplastic Grade 4-ДБ (ТУ П-40-59) and 25 percent molybdenum disulphide (MTU 06-1-68). The compound is also used to form the operative surface layer. Table 5.25 gives the main

Table 5.25

Dimensions of metal-fluoroplastic band, mm

Total thickness	Thickness			Width	Length
	steel backing	layer I	fluoroplastic layer		
1.10 1.60 2.60	0.75 1.30 2.30	0.35	0.06	75-100	500-2,000

dimensions of Soviet-made metal-fluoroplastic laminated strip.

The major advantages offered by metal-fluoroplastic laminates are: the capability of working without lubrication at temperatures from -200 to $+280^{\circ}\text{C}$, low coefficient of friction (0.02 to 0.25), even at the starting moments, high strength and thermal conductivity, low material content, resistance to many industrial liquids, gases, solvents, and oils. The laminate adequately operates in vacuum and in inert gases.

Metal-fluoroplastic band is used for fine stamping of such components as unsplit plain-bearing bushes, rolled-up sleeves, ball-joint components and spherical pads, bearings, and components for separable pin joints.

Proper judgement must be used when specifying clearances in metal-fluoroplastic bearings, because, apart from thermal expansion, there is a hazard of extrusion of the fluoroplastic out of the porous substrate and into the clearance. A number of recommended clearances for metal-fluoroplastic bearings are listed in Table 5.26.

A study of service life of 30-mm diameter bearings has shown that the wear limit is reached at $pv = 4$ (kgf/cm) (m/s) in 100 to

Table 5.26

Recommended clearances for metal-fluoroplastic bearings

Inner diameter, mm	Design diametral clearance, μm	Specified clearance, μm		
		min	max	average
10-18	30	30	100	65
18-30	35	35	125	80
30-40	40	40	140	90
40-50	45	45	145	95

800 h, $pv = 3$ (kgf/cm) (m/s) in 200 to 2,000 h, and $pv = 2$ (kgf/cm) (m/s) in 400 to 4,000 h. Minimum wear is achieved when the bearing is mated with a metal shaft finished to a surface roughness of 0.6 to 1.5 μm .

Field experience shows that metal-fluoroplastic bearings are most efficient to apply without lubrication at high specific loads and low sliding speeds; in mechanisms with hydrodynamic or gas lubrication under severe starting conditions; in cases where self-oscillations may arise; and in some other cases. Metal-fluoroplastic bearings serve many engineering applications. In aircraft, for instance, they are used in rotary joints of control systems and in hinged-bolt assemblies; in textile machinery, in place of lubricated needle roller bearings; in automobiles, as swivel axles in the ГАЗ-53 Model trucks, and as sleeves in brakes and friction clutches in the ЗИЛ-130 Model trucks; such bearings are also applicable in looms and sewing machines, in high-load electric motors, as gas bearings in various instruments, and in other equipment.

Close in characteristics to the above-described Soviet-made material are some metal-polymer laminates developed in other countries.

Laminated band materials produced by Glacier in the United Kingdom are extensively used in various countries. The widest acceptance has gained the DU-type laminate, which is a bimetallic band having a steel base coated with a tin bronze layer whose pores are filled with fluoroplastic containing 20 percent lead. The material sustains static pressures up to 3,200 kgf/cm². The coefficient of friction varies within 0.05 to 0.1 at low speeds, and reaches 0.2 at high speeds. The recommended values of pv for bearings made from the DU laminate are given in Table 5.27.

A metal-fluoroplastic laminate named Sprelaflon is developed and put into production in the GDR. The material is a steel band with a pressed-on antifriction layer containing fluoroplastic-4 (37 percent), metallic lead (50 percent) and phenol-formaldehyde resin binder (13 percent). At a specific load of 20 to 65 kgf/cm² and a rotational speed up to 1,000 rpm, the coefficient of dry fric-

Table 5.27

Permissible values of pv (kgf/cm²) (m/s) for bearings made from Grade DU material

Typical applications	Shaft from soft steel		Shaft from hardened steel (<i>HB</i> 540)	
	Service life, h			
	1,000	10,000	1,000	10,000
Thrust bearings	8.8	4.25	10.6	5.3
Guideways	4.25	2.1	4.6	2.5
Plain bearings:				
at a constant load whose point of application is fixed relative to the bearing bush	5.65	4.25	8.8	6.7
at a load turning relative to the bearing bush	8.8	6.7	10.6	8.5
at a fixed load and oscillating shaft	10.6	8.15	11.7	8.5

tion is from 0.1 (low speeds) to 0.24 (high speeds); the wear resistance of the laminate is tens of times that of an integral specimen of the same composition.

Laminates with cloth, film, felt, gauze, and other backings, which are used as semi-finished products for making integral bearings and packings, for lining working surfaces in metal casings, and on slideways, are finding ever increasing application.

Materials of this group include: bronze-wire gauge impregnated with fluoroplastic carrying various filler reinforcements; fluoroplastic fabric wherein the side opposite to the rubbing surface is provided with interwoven cotton threads that allow the plastic to be bound to its backing with phenol-formaldehyde resin; fluoroplastic film which is coated with half-vulcanized rubber, whereafter they can be adhesive bonded together by pressing and heating; and felt which is coated with a 0.7-mm thick fluoroplastic layer.

5.2.4. Carbon-Graphite Materials

Carbon-base antifriction materials are available in the following main types: roasted and graphitized carbon (metal impregnated or not), graphite-plastics, and graphite-fluoroplastics. High thermal resistance and specific heat, good antifriction properties, and proper machinability make for successful application of this family of structural materials in tribological joints.

Carbon-base and graphite-fluoroplastic materials. Roasted carbon-base low-friction materials have a higher hardness and strength

but lower thermal conductivity than graphitized materials (see Ch. 12); their linear expansion coefficient is lower than that of metals, and the coefficient of friction is 0.05 to 0.10.

The tensile strength of graphitized antifriction materials markedly rises with increasing temperature (at 2,500°C it is about twice that at 20°C), whereas the coefficient of friction drops by a factor of three.

Carbon-base antifriction materials are resistant to chemical attack by almost all acids (up to their boiling temperature), salt solutions, and all organic solvents; their resistance to concentrated solvents of caustic alkalis is limited.

The amount of wear over 100 h of operation at maximum allowable specific pressures and speeds in dry rubbing conditions in air at room temperature is as follows (μm):

Carbon-base materials (roasted and graphitized)	50
The same materials impregnated with metals	30
Graphite-fluoroplastic materials	30

The performance of carbon-base antifriction materials substantially depends on the composition and moisture content of the gaseous ambience. With the presence of films or droplets of condensed moisture on the rubbing surface, wear and coefficient of friction of carbon-base antifriction materials rise about 10 times, and with metal-impregnated materials, twofold.

Upon impregnation with a metal, carbon-base materials become stronger, impenetrable to liquids and gases at high pressures, and, in some cases, give better performance in rubbing conditions.

Graphite-fluoroplastic antifriction materials have elastic-plastic deforming characteristics. They are less strong but more dense and impenetrable to liquids and gases than carbon materials.

Data on the permissible values of specific pressures and speeds for various grades of antifriction materials during rubbing in air at room temperature are given in Table 5.28.

Grade AΦΓM material is developed specifically for work in dried gases.

In liquid environments use is only made of impenetrable materials, such as carbon-base metal-impregnated ones, and graphite-fluoroplastic material Grade 7B-2A.

Antifriction graphite-plastic self-lubricating materials are heavily filled composites based on powdered carbon solid-lubricant fillers bound with resins of increased thermal resistance. These materials are used for tribological components operating in dry-friction conditions, as well as in water, kerosene, lubricating oils, and liquid oxygen.

Physico-mechanical properties of materials Grades AMC-1, AMC-3 and AMC-5 are listed in Table 5.29. These materials have high mechanical strength typical of epoxy resins, high temperature

Table 5.28

Maximum permissible loads and velocities for antifriction materials

Material	Recommended material of mating part	p , kgf/cm ²	v , m/s
AO-1500 AO-600	Pearlitic cast iron, chromium plated	15-20 10-15	10 10
АГ-1500 АГ-600	Steels of all grades and hardness, chromium plated	10-15 10-12	30 20
AO-1500-CO5 AO-1500-B83	Cast iron, steel, chromium plated	25-35 35-40	15 10
АГ-1500-CO5 АГ-1500-B83 АГ-1500-БрС30 7B-2A	Steel, chromium plated	20-25 15-20 15-20 10-15	25 20 20 5
АФГМ АФГ-80BC	Cast iron, steel Cast iron, steel, chromium plated	15-20 10-15	5 5

resistance inherent in silicon resins, low coefficient of friction, and high wear resistance.

With the specific load varying from 10 to 50 kgf/cm² at a sliding speed of 0.5 m/s, the coefficient of friction of materials Grades AMC-1 and AMC-2 decreases from 0.2-0.3 to 0.05-0.1.

The long-term temperature resistance of materials Grades AMC-1 and AMC-3 is 180 to 200°C.

The material Grade AMC-3 is to be preferred for operation in water, kerosene, and other media. The AMC-1 is designed for dry-friction applications at normal humidity, and the AMC-5 is advisable for service at high specific loads in various liquid media.

These materials find application in axial seals, piston rings, sealing glands of oxygen pumps, air-distributor rings of cigarette production machines, and other components.

5.2.5. Metal-Ceramic Materials

Metal-ceramic products are used for plain bearings, linings, and other tribological parts that require high wear resistance and low coefficient of friction. Wide application of metal-ceramics is accounted for, first, by their adequate gas and liquid permeability, which makes them self-lubricant materials suitable for operation in environments fouled by solid matter and, second, by good processability and sufficient accuracy of products.

Table 5.29

Physico-mechanical properties of graphite-plastics

Parameter	AMC-1	AMC-3	AMC-5
Density, g/cm ³	1.74-1.8	1.78-1.8	1.3-1.45
Ultimate strength in compression, kgf/cm ² at a temperature, °C:			
20	1,800-2,100	80-1,100	1,400-1,500
200	300-400	260-320	400-500
Ultimate strength in bending, kgf/cm ²	500-700	250-350	1,800-2,000
Brinell hardness, kgf/mm ²	40	35	35
Water absorption, % by mass	0.1-0.2	0.01	0.1
Specific impact strength, kgf cm/cm ²	3-7	3-5	30-40
Coefficient of thermal conductivity, kcal/m h °C	3-5	10-15	0.4-0.8
Linear expansion coefficient $\alpha \times 10^5$ 1/°C	3-5	3-5	3-5
Allowable operating temperature, °C, during service life, h:			
> 1,000	180-200	180-200	180-200
< 100	270-350	270-350	270-350
Kerosene permeability, cm ³ cm/(cm ² atm s)	10 ⁻⁶	10 ⁻⁶	—
Wear rate at a specific pressure up to 5 kgf/cm ² and a sliding speed up to 2 m/s, m/m	—	10 ⁻¹¹	10 ⁻¹⁰

Current metal-ceramics can be broken down conventionally into two groups:

1. Porous alloys based on iron and graphite (iron-graphite), bronze and graphite (bronze-graphite), aluminium and graphite (aluminium-graphite). Some of these composites also incorporate other solid lubricants (boron nitride, tungsten carbide) or sulphurous metals WS₂, MoS₂, Cu₂S, FeS, CoS, TiS₂, and SnS. The chemical content of these alloys is: 88 to 99 percent base metal, 0.3 to 4 percent graphite, and 1.5 to 10 percent additives.

2. Alloys based on iron, copper and other metals impregnated with various polymers, usually with teflon or polytetrafluoroethylene. The content of polymers is from 1.5 to 10 percent.

Produced in this country is iron-graphite of the following grades: ЖГр-0.3; ЖГр-1; ЖГр-3; ЖГр-7; ЖГр-2Д2.5; ЖГр-1.5Д5; ЖГр-2Д10. Ferrum sulphide (10 to 15 percent) is introduced into the last three grades for improving antifriction properties. There are other two grades, ЖГр-1Дс-3 and ЖГр-3ЦС-4, which use as additives 3 percent Cu₂S and 4 percent ZnS, respectively.

Iron-graphites are applicable at working pressures not exceeding 100 to 150 kgf/cm² and temperatures up to 150°C. The linear expansion coefficient is (9 to 11) $\times 10^{-6}$ 1/°C. The coefficient of friction against

steel with and without lubrication is 0.07 to 0.09. Iron-graphite differs from other antifriction metal-ceramics in that its structure is sensitive to variations in graphite content and to processing conditions. Iron-graphite with a ferrite structure has a lower wear resistance. A pearlitic structure containing about 1 percent combined carbon and 1.5 percent graphite exhibits the highest hardness and strength among the iron-graphites.

Bronze-graphite is characterized by the lowest allowable working pressure among metal-ceramic antifriction composites (60 to 80 kgf/cm²), a minimum temperature range (60 to 80°C), and a minimum coefficient of friction of 0.04 to 0.07 (without lubrication) and 0.05 to 0.07 (with lubrication). The linear expansion coefficient is (12 to 17) 10⁻⁶ 1/°C. Lead bronze allows a buildup of pressure up to 260 kgf/cm² and works at temperatures up to 80°C. The coefficient of friction with lubrication is 0.05.

Polymer impregnated materials, such as БРО10ФГ and БРО46ФГ (containing respectively from 5 to 10 and from 0 to 1.5 percent fluoroplastic) make it possible to increase the maximum working temperature up to 150°C, retaining the allowable working pressure proper to the chosen type of metal-ceramic composite.

Table 5.30

Physico-mechanical properties of some antifriction metal-ceramic materials

Grade	Density, g/cm ³	Porosity, %	Ultimate strength, kgf/mm ²		HB
			in compression	in tension	
ЖГр-1-20	6.0-6.3	17-23	14-18	40-45	60-100
ЖГр-2-20	5.8-6.2	17-23	14-16	38-42	50-80
ЖГр-3-20	5.5-6.2	17-23	12-14	30-35	50-80
ЖГр-3-Д	5.7-6.2	22-27	25-35	120-130	70-100
ЖГр-Дс-3	6.2-6.3	18-22	—	90-120	90-120
БрОГ10-2	6.0-6.8	20-25	—	50-60	18-20
АЖГр-6-3	2.6-2.8	5-10	—	14-15	20-24

Grade	Impact strength, kgf m/cm ²	Coefficient of friction with lubrication	Permissible load, kgf/cm ² , at $v = 1-3$ m/s	Maximum temperature, °C
ЖГр-1-20	0.3-0.6	0.06-0.09	34-38	100-120
ЖГр-2-20	0.25-0.35	0.06-0.09	34-38	100-120
ЖГр-3-20	0.18-0.22	0.04-0.06	40-45	100-140
ЖГр-3-Д	0.4-0.8	0.04-0.07	50-70	120-150
ЖГр-Дс-3	0.4-0.5	—	80-100	Up to 150
БрОГ10-2	—	0.004-0.008	25-30	80-90
АЖГр-6-3	0.4-0.5	0.005-0.008	40-60	100-120

Carbon-metal materials Grades AO and AI are advisable to use in dry-rubbing against cast-iron and chromium-plated surface in gaseous and water-vapour environments, the AI Grade being applicable also in a pair with any steels. The coefficient of friction for these materials is 0.1 to 0.2, and wear is proportional to the coefficient of friction. Ultimate compressive strength for these materials is from 800 to 1,100 kgf/cm², whereas for iron-graphite it is from 6,000 to 8,000 kgf/cm².

Aluminium-graphites contain copper or iron additives. Aluminium-graphite Grade AIГp-6-3, for instance, incorporates 6 percent, and the AIГ-10-3 incorporates 10 percent copper. These materials are noted for a comparatively low coefficient of friction (0.005 to 0.008), the smallest density among metal-ceramics (2.6 to 2.9 g/cm³) and low permissible specific loads (40 to 60 kgf/cm²).

The main physico-mechanical properties of available metal-ceramic composites are given in Table 5.30.

5.3. ASSESSMENT OF PERFORMANCE OF TRIBOLOGICAL JOINTS AT DESIGN STAGE

After the materials tentatively estimated as meeting the specifications are chosen, design calculation and assessment of performance of the joint should be made. Primarily, the optimum dimensions and design of the joint must be determined. Depending on the type of rubbing part (a gear wheel, a bearing, a seal, a contact brush, or a guideway) and its main specifications established by the assignment, the part is commonly calculated for strength and deformation and checked for friction (thermal conditions) and wear; alternatively, calculation for frictional parameters and checking for strength and deformational properties may be made. Design calculation methods for specific components are given in the relevant chapters of this handbook.

An important part of dimensional calculation is the determination of clearances in joints. Here, it should be noted that more stringent accuracy requirements, on the one hand, involve the hazard of jamming as the joint heats and becomes deformed and, on the other hand, incur sharp increases in production costs.

When estimating the load capacity of the joint in order to find an optimum variant, one should keep in mind that the joint's performance can be sufficiently improved by the correct design and manufacture of the rubbing parts. The part under development should have an appropriate surface roughness; it should be provided with reinforcement at weaker, failure-prone portions, with special design features for lubrication and disposal of wear particles, with additional heat-removal elements (if needed), and so on.

Let us illustrate the above considerations with examples of combined polymer and metal-polymer components.

High processability of plastics extends the possibility of making multi-purpose parts combining, for instance, the functions of a gear wheel and a fan (Fig. 5.2*a, b*), the latter being used for cooling the adjacent bearing units. An integral cast gear wheel can be provided with a claw clutch for transmitting torque (Fig. 5.2*c*). A plastic component in the form of a toothed rim combined with a sliding bearing (Fig. 5.2*g*) gives improved performance. Metal frame elements interposed between the rim and the bearing portion ensure

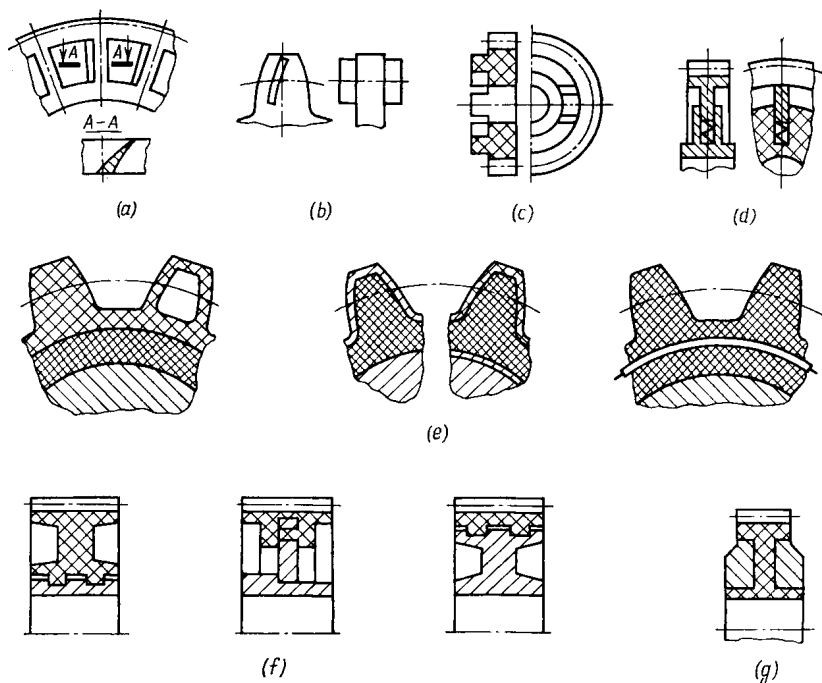


Fig. 5.2. Combined polymer and metal-polymer gear designs

(a) and (b) with spoke- and face-type fan blades, respectively; (c) gear and claw-clutch combination; (d) gear with an elastic toothed rim placed on floating spokes; (e) design versions of a gear with radially compliant elastomer pads; (f) plastics gears with metal hubs; (g) plastics gears with a sliding bearing

high stability in the dimensions of the thin-walled bearing sleeve and adequate removal of heat from the rubbing area.

Also of interest is a gear design wherein an elastic toothed rim is capable of considerable radial displacements in the meshing area (Fig. 5.2*d*). The same effect is achieved in a gear wheel with a plastics toothed rim connected with the hub through an elastic pad from rubber or some other elastomer (Fig. 5.2*e*). Gears with an elastic toothed rim are suitable for engagement with several mating gears simultaneously and have improved load-carrying capacity.

One promising way to increase the load capacity of polymer gears and improve their functional characteristics is the use of metal

reinforcing elements taking the bulk of the load in operation. Such gear designs make it possible to combine the strength and stiffness of a metal frame with the high antifriction properties and damping capacity of plastics.

Reinforced metal-polymer gears feature improved flexural strength of teeth and better heat-removal properties, which makes them suitable for applications in vital, heavily loaded machine units.

Plastics gears with metal hubs in the form of sleeves and discs (see Fig. 5.2*f*) have found the most extensive use.

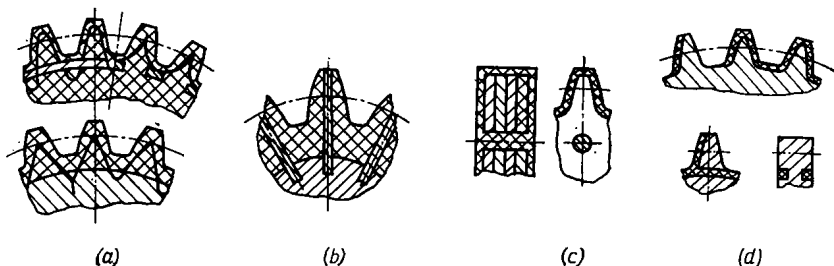


Fig. 5.3. Metal-polymer gears

(a) with crimped metal band and wire reinforcement; (b) with radially disposed reinforcing strips; (c) with a set of toothed metal discs; (d) with a gear-shaped metal frame

In order to increase the flexural strength of teeth, reinforcing elements are introduced into every tooth. The teeth are reinforced by a crimped metal band strengthened with metal rings (Fig. 5.3*a*) or secured to a stamped shouldered flat disc. The crimped band may be fixed to tooth-like projections on the metal disc; these projections may be stamped out directly on the cylindrical hub.

The use of reinforcing elements made as stamped strips radially disposed along the whole length of teeth (Fig. 5.3*b*) offers a substantially higher flexural strength and the capability for work in heavily loaded transmissions.

A high strength is provided by a frame in the form of a set of toothed discs held together by means of rivets, welding, or a polymer material let into suitable holes in the discs (Fig. 5.3*c*).

Among current designs of metal-polymer gear wheels, is one wherein teeth are faced with a polymer applied to the metal frame by die casting (Fig. 5.3*d*). The frame is a gear wheel with teeth whose thickness is diminished over the entire depth of tooth by an amount equal to the thickness of the polymer layer. A combined adhesive and mechanical fixing of the facing on the frame is most effective as it offers a 1.5 times higher load-carrying capacity per unit tooth width than with the facing fixed only mechanically.

The efficient methods of adhesive bonding of the facing are based on the use of intermediate adhesive layers (sublayers), which are phosphate films, hard facings obtained from powdered polymers, and the like.

The best results are given by sublayers deposited from polymer solutions. This method offers metal-polymer bonds whose strength equals the cohesion strength of the material being applied. Moreover, the metal-polymer structure proves to be more resistant to liquid media and atmospheric ambience and has an improved fatigue resistance.

A significantly lower level of noise and vibration is achieved by the use of composite gears having elastic vibration-damping elements placed between the hub and the toothed rim. These elements are commonly made from plastics or rubber.

The rim can be elastically connected with the hub through steel leaf-type or cylindrical elements in combination with a shock-ab-

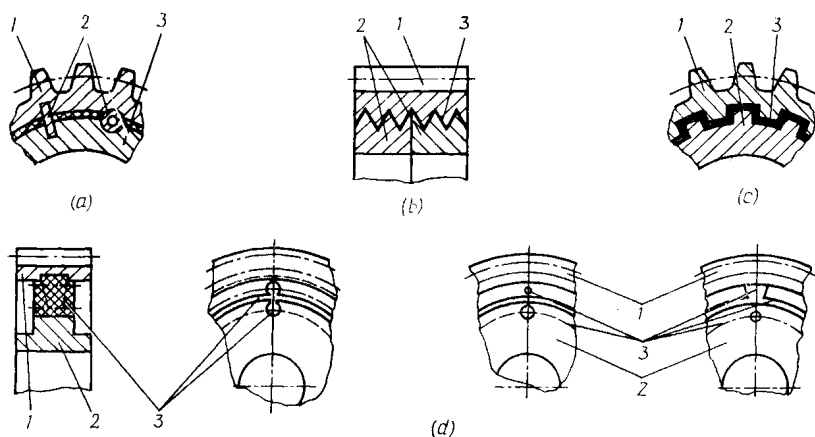


Fig. 5.4. Composite gears

(a) with a damping elastomer layer; (b) with a vibration-damping thermoplastic structural layer; (c) toothed rim spline-joined with the hub through a vibration-damping structural rubber pad; (d) toothed rim joined to the hub by means of slots or recesses; 1—rim; 2—hub; 3—elastic element

sorbing layer of elastomer (Fig. 5.4a), which here takes no part in transmitting torsional moment. Alternatively, connection between the rim and the hub can be effected directly through a load-carrying vibration-damping layer located in a suitable space provided between the components. This space, into which polymer is poured, is made in the form of grooves, slots or recesses of suitable dimensions and shape (Fig. 5.4d), threaded or splined mating profiles (Fig. 5.4b and c, respectively), or the like. A composite-gear transmission is less sensitive to manufacturing and assembly errors and to misalignment of the gears in operation; it provides for a more uniform distribution of load along the gear tooth width as compared with integral steel gears.

The load-carrying capacity of sliding bearings significantly depends on their design and the relations between the dimensions of

the main components determining the distribution of load over the contact area, on heat-removal conditions, damping capacity, and the like. A bearing wherein the antifriction lining is applied to the stationary rubbing component has a higher load capacity and lower frictional losses than that in which the movable rubbing component, for instance, the shaft, carries the antifriction lining. The latter type of sliding pair is preferable to use in precision ma-

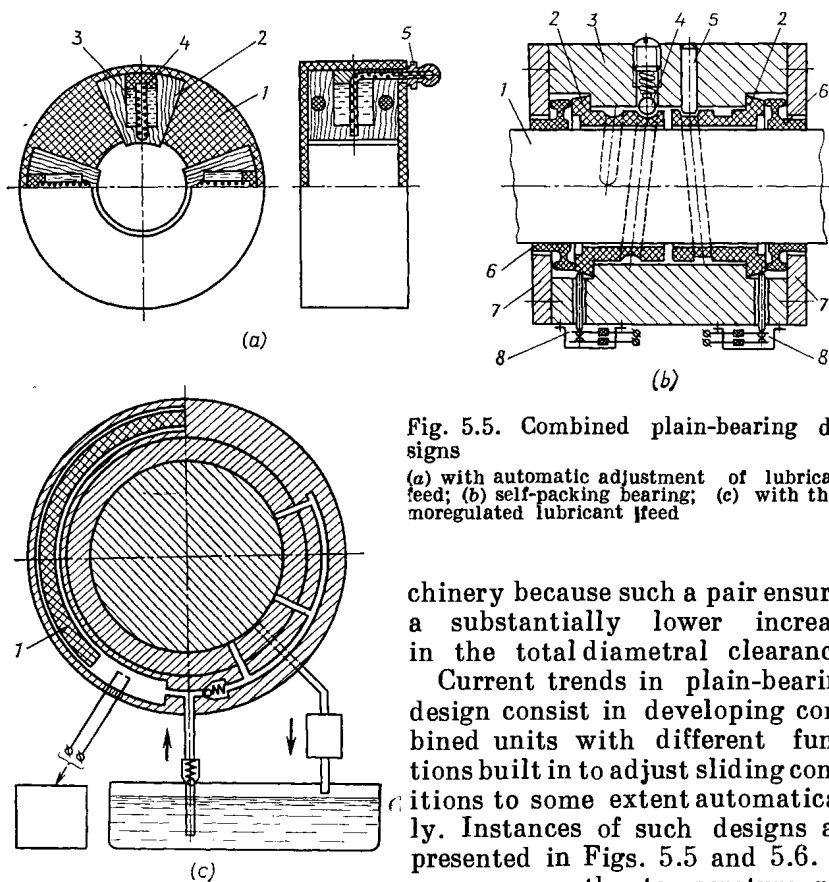


Fig. 5.5. Combined plain-bearing designs

(a) with automatic adjustment of lubricant feed; (b) self-packing bearing; (c) with thermoregulated lubricant feed

chinery because such a pair ensures a substantially lower increase in the total diametral clearance.

Current trends in plain-bearing design consist in developing combined units with different functions built in to adjust sliding conditions to some extent automatically. Instances of such designs are presented in Figs. 5.5 and 5.6. In some cases, the temperature rise

in the contact area can be used to advantage for self-regulation of oil feed to the rubbing surfaces (Fig. 5.5a). The sliding bearing consists of a housing 1 made from a thermoplastic (polypropylene or the like) and antifriction inserts 2 made from filled densified wood. Perforated tubular elements 4, filled with a heat-decomposing gas-forming substance, for instance, $\text{Ca}(\text{HCO}_3)_2$, are built into oil-containing cavities 3 made in the inserts. The thermoconductive elements are provided with nipples 5 for supplying the gas-forming substance and oil.

The use of gas-forming compounds decomposed by heat makes it possible to produce an inert atmosphere together with a sealing pressure in the joint.

Figure 5.5*b* shows a self-packing plain bearing that makes use of the selective transfer effect. Self-packing is achieved by using frictional forces (moments) that inevitably arise between the shaft journal and the bearing bushes and cause axial displacements of the bushes, required for closing axial seals and actuating signal contacts. During rotation of the shaft journal 1, the bearing bushes 2 tend to turn relative to the housing 3. When turning, the bushes slide with their helical grooves relative to a spring-loaded ball 4 or a pin 5 and thus shift axially, pressing packings 6 against covers 7 to seal the bearing on its end faces. The axial displacement of the bushes constantly makes up for wear in the seals and, eventually, causes contacts 8 to close, thus giving warning of wear of the seals or faulty operating conditions in the bearing.

An ingenious design solution to the problem of thermoregulation and compensation for lubricant losses is illustrated in Fig. 5.5*c*. Here, heat generated by friction is transformed through the expansion of a thermoelement 1 into mechanical energy used for the delivery of lubricant. The advantage of this design is a leakproof and self-contained lubricating system.

Research has shown that the use of thin polymer films instead of solid polymer bearings provides for better removal of heat from the friction area, higher load-carrying capacity, and reduced friction losses. The application of polymer-coated bearings enables one to specify smaller diametral clearances, higher loads and speeds, and to solve some other design problems.

Plain bearings with a thin polymer lining are intended for lightly loaded movable joints operating without additional lubrication, where a good damping capacity is required, for instance, in motion-picture cameras, centrifuges, and other equipment. Such a bearing (Fig. 5.6*a*) comprises a pedestal body 1, a bearing cap 2, and a crimped floating liner 4, coated with a thin plastics layer 5 and put over a shaft journal 2. Holes 6 are provided on the working surfaces and the sides of the liner for better circulation of lubricating medium. As running conditions and load vary during operation, the liner slides on either its outside or inside surfaces. The notable feature of this design is a bellows-shaped liner with creased flanks. Under dynamic loads the liner changes its shape, thus damping vibrations and ensuring optimum operating conditions.

One variety of this type of sliding bearing features a liner pressed around the shaft journal and has tubes inserted axially at an angle to the shaft axis. The tubes extend beyond the liner end faces and carry at one of their ends blades forming an impeller for setting up a flow of a coolant medium. In this way, better heat removal and an extended service life of the bearing are achieved. The bearing unit (Fig. 5.6*b*) incorporates a pedestal body 1, a bearing cap 2,

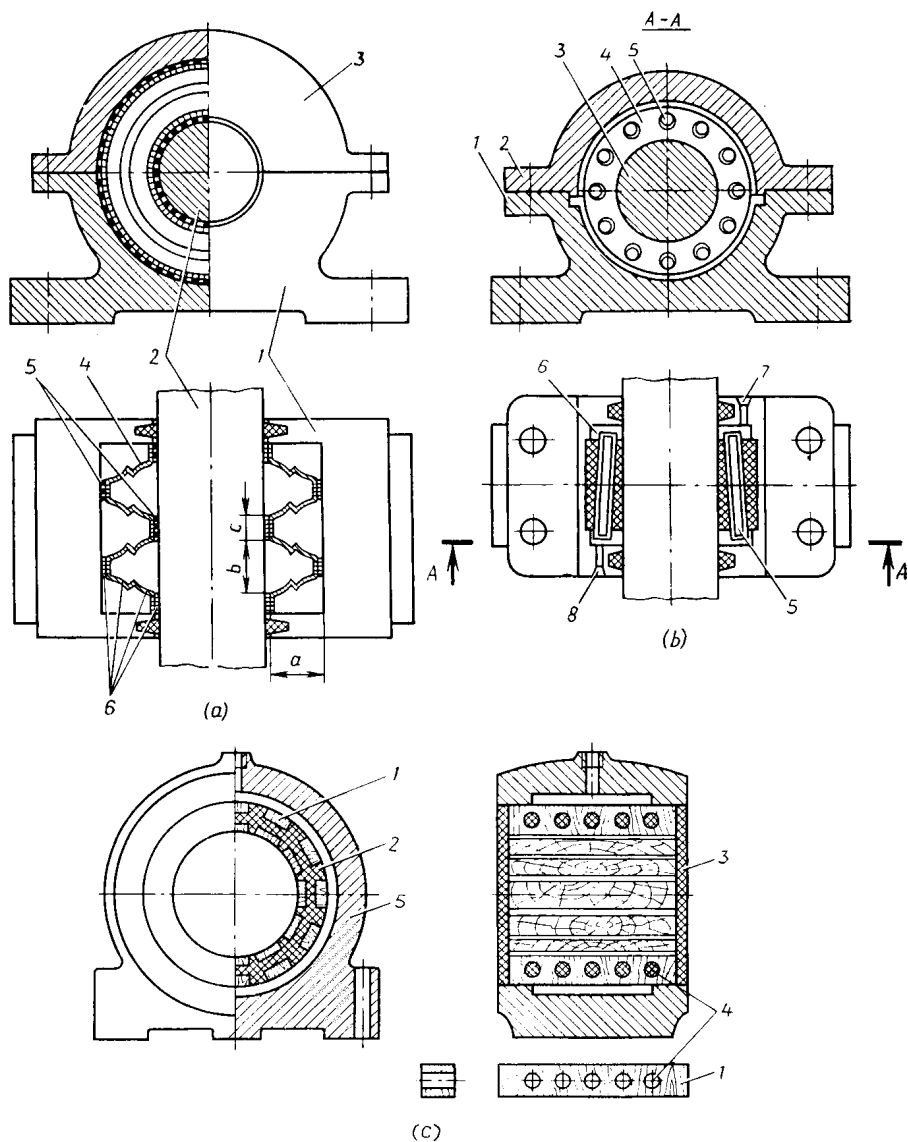


Fig. 5.6. Combined plain bearings

(a) with a thin damping lining on the operating surface; (b) with improved heat removal; (c) with densified-wood liner inserts

a plastics liner 4, an oil reservoir 6 and air valves 7. The liner 4 secured on a shaft 3 contains tubes 5 with blades. Depending on the properties of the liner and bearing-housing materials, the bearing unit can work with or without lubrication. In order to intensify the removal of heat through the tubes 5, the ends of the tubes ex-

tending from the liner end faces are twisted to form blades with such a shape and angle of inclination that air or lubricant are sucked into the tubes on one side and a vacuum making for intensified heat exchange is produced on the opposite side. In this way, with increasing rotational frequency and higher heat generation, the removal of heat is intensified automatically; when the bearing runs dry, cooled air is sucked in and exhausted into the ambience through the valves 8. The diameter of the tubes is selected depending on the liner wall thickness and the unit's operating conditions.

Densified and impregnated wood, which at present finds an ever increasing use, contributes to the development of the most advanced designs of bearings and processes for their manufacture both in automated mass production and in repair jobs.

The use of sliding bearings from densified wood in the form of solid bushes, particularly large ones, entails a low utilization of the high-quality material, high costs of machining, and the need for expensive fixtures. An original bearing unit design that meets specific operating conditions of densified-wood bearings is shown in Fig. 5.6c. The unit consists of a housing 5, a set of rectangular liner inserts 7 from a self-lubricating densified wood, a shell 2 from a thermoplastic material, polymer connecting elements 4, and thermoplastic end-face covers 3.

Elastic axial and radial fixing of the liner inserts reduces stresses in the unit due to dynamic and temperature factors. The shape of the bearing's outside surface may vary in accordance with the conditions of use; it is determined by the shape of the mould. To manufacture such bearings, inserts of densified wood, made to fairly wide dimensional tolerances, are placed in appropriate slots of the mould so as to be supported at their end faces, and a thermoplastic polymer is injected into the mould, suitable grooves being formed between the inserts on the inner surface of the bearing for collecting lubricant and particles of the worn material and abrasives.

Experience has shown that insert-type densified-wood bearings function satisfactorily in abrasive and chemically-aggressive environments at speeds ranging from 0.25 to 1.0 m/s and loads up to 40 kgf/cm².

5.4. THE FINAL CHOICE OF MATERIAL

The results of field tests give the main criterion for the final selection of the material for a rubbing part. However, before the field tests, the materials that have been previously chosen on the basis of a tentative estimation should be bench-tested in standard conditions, and also in conditions simulating the operating ones to the maximum possible extent. Such tests will allow the range of ma-

materials feasible for use in the specified conditions to be reduced significantly.

Standard methods enable one to make a comparative assessment of the available materials with minimum time and money expenditure; the results of this assessment, however, are not sufficient to decide whether a given material is suited to an actual tribological component. It should be taken into account that, depending on the chosen test techniques, different results may be obtained on identical specimens. For this reason, in laboratory research on the frictional properties of materials, the character of specimens' interaction, their speed and loading conditions should be similar to the operating ones.

The next stage in selecting materials for rubbing components is the testing of prototype parts under conditions simulating the operating ones as close as possible. The results are to show the feasibility of making a batch of prototype components for field tests which will give the final answer — of what material and design a given rubbing part should be for adequate performance in newly developed or modernized equipment.

REFERENCES

1. Ахматов А. С. Молекулярная физика граничного трения^{*} М., Физматгиз, 1963.
2. Белый В. А., Довгяло В. А., Юркевич О. Р. Полимерные покрытия. Минск, «Наука и техника», 1976.
3. Вайнштейн В. Э., Трояновская Г. И. Сухие смазки и самосмазывающиеся материалы. М., «Машиностроение», 1968.
4. Виноградов Г. В. Антифрикционные полимерные материалы. — В кн.: Энциклопедия полимеров, т. 1. М., «Советская энциклопедия», 1972.
5. Гриб В. В., Кутейникова З. А., Симонов Г. А. Твердые смазки и самосмазывающиеся материалы для узлов трения приборов времени. «Обзорная информация», вып. 2. М., 1972.
6. Коршак В. В. Термостойкие полимеры. М., «Наука», 1969.
7. Крагельский И. В. Трение и износ. М., «Машиностроение», 1968.
8. Курицына А. Д., Истомина И. П. Композиционные материалы и покрытия на базе фторопласта-4 для сухого трения в подшипниках скольжения. С-IX «Новые материалы в машиностроении». М., 1971.
9. Материалы в машиностроении. Справочник под общей ред. И. В. Кудрявцева, т. 5, под ред. В. А. Попова, С. И. Сильвестровича и И. Ю. Шейдемана. М., «Машиностроение», 1969.
10. Мошков А. Д. Пористые антифрикционные материалы. М., «Машиностроение», 1968.
11. Техничко-экономическая эффективность и опыт использования пластмассовых деталей механического привода. Минск, БелНИИНТИ, Госплан СССР, 1976. Авт.: Коновалов Э. Я., Лапицкий И. М., Старжинский В. Е., Щербakov С. В.
12. Трение и износ материалов на основе полимеров. Минск, «Наука и техника», 1976. Авт.: Белый В. А., Свириденко А. И., Петроковец М. И., Савкин В. Г.
13. Семенов А. П., Савинский Ю. Э. Металло-фторопластовые подшипники. М., «Машиностроение», 1976.

14. Справочник по пластическим массам. Под ред. В. М. Катаева, В. А. Попова, Б. И. Сажина. М., «Химия», 1975, т. I, II.
15. Энциклопедия неорганических материалов. Киев, «Наукова думка», 1977, т. 1, 2.
16. Ясь Д. С., Подмоков В. Б., Диденко Н. С. Испытания на трение и износ. Киев, «Техника», 1971.
17. Tribology. Handbook. Ed. by M. J. Neale. Butterworths, London, 1973, p. 557.

METALS FOR RUBBING COMPONENTS

6.1. STRUCTURAL CHANGES OF METALS IN FRICTION

6.1.1. General

In modern engineering, most rubbing components are made of metals. Further advance in technology may bring about new processing methods and nonmetal materials, but in the foreseeable future metals will remain predominant materials for rubbing components. The reason for it is that metals, as a rule, meet the various operating requirements for rubbing surfaces to a greater extent than other materials. The advantages of metals are their relatively favourable combination of strength and plasticity, the ability to form various compounds with one or several elements, etc. Depending on the chemical nature of the elements and conditions the composite system exists in, metals can form solid solution, eutectic mixtures, and chemical compounds with other metals or nonmetals. Each of these combinations exhibits different properties, specifically, different frictional characteristics.

6.1.2. Structure and Properties

The properties of metals are determined by their atomic arrangement and structure. In modern physical metallurgy the term structure is very broad: it encompasses the phase composition, the type and character of crystal lattice, the number of defects and character of their distribution within the crystal lattice (substructure).

The wear resistance of metals also largely depends on their structure and properties of individual microvolumes characterized by different structural constituents. The prevalent type of these constituents, their amount, morphology, and positional relationships have a great effect on wear resistance.

Characteristics of the main structural constituents of steel and cast iron are given in Table 6.1.

More often than not, the hardness and wear resistance of alloys grow higher with increasing carbon content.

As seen from Table 6.1, each of the structural constituents has a distinct set of properties which must be taken into account when considering the methods of processing a given metal for various frictional conditions of its operation.

An important wear-resistance characteristic of metals is the type of crystal lattice and the orientation of the direction of sliding in friction relative to the different crystallographic axes. In general, the structural constituents, the anisotropy of crystals, the impurities and defects — all this in combination with external conditions determines the physical, mechanical and processing properties of metals and alloys.

6.1.3. Metal Strengthening

Metals, as delivered from metallurgical plants, usually lack the properties needed to resist wear.

In modern engineering, rubbing metal parts undergo strengthening treatment by various methods. Such methods are heat treatment, thermochemical treatment, surface strengthening by plastic deformation, etc.

Given below are the main types of heat treatment of metals used for rubbing components [2, 10, 24, 25].

Annealing is an operation in which equilibrium (stable) structures in steel are obtained by cooling from a temperature above the A_{c3} point or from that within the transformation region, prolonged holding at these temperatures, and slow cooling at a specified rate. Annealing changes the degree of dispersion of the phases and considerably increases the structural stability of the ferrite-cementite mixture, reduces its hardness, and improves its plasticity and toughness. Annealing is used to prepare the structure of steel for subsequent heat treatment operations (hardening), to remove internal stresses and to improve machinability. Diffusion annealing levels out the chemical nonuniformity of steel.

Normalizing is a process of heating steel to from 30 to 50°C above the A_{c3} point, holding at this temperature and subsequently cooling in the air. Normalizing results in the finer structures and improved mechanical properties of low- and medium-carbon steels. It is often used to prepare the structure for subsequent hardening and sometimes (for parts with small cross-sectional areas) to substitute for the first hardening operation after carburizing.

Hardening is an operation in which nonequilibrium structures are obtained in steel through the transformation of austenite on its sharp

Table 6.1

Characteristics of metal (steel and cast iron) structural constituents and their effect on performance of tribological components [3.16]

Structural constituent	Characteristic	Hardness		Effect of structural constituent on wear resistance
		additional subdivisions of constituents	HV	
Ferrite	Solid solution of carbon in α -iron	1. Pure iron and ferrite in carbon steel	50-135	Ferrite-base steel and cast iron have low hardness and wear resistance
		2. Alloyed ferrite	100-270	
Austenite	Solid solution of carbon in γ -iron	In alloy steel	150-220	Tends to strengthen under cold plastic deformation. Hence, despite their low hardness, austenite-base alloys have good wear resistance under impact, severe crushing, and plastic deformation conditions
Carbides	Chemical compound of iron and carbon—cementite (6.67% C); in alloys, chemical compound of iron, carbon and alloying elements	1. Cementite 2. Complex carbides in alloy steels	1,000-1,150 1,100-1,300	Depending on forming conditions, carbides have different morphology and dispersity. As components of ferrite-carbide mixture (pearlite), carbides are essential to wear resistance of steel and cast iron
Pearlite	Mixture of ferrite and cementite	Pearlite: granular lamellar sorbite sorbite troostite	160-190 190-230 230-260 250-300 300-400	Hardness and wear resistance of alloys rise with the amount of carbides in the structure. Structures with lamellar pearlite are more wear-resistant than those with carbides in granular form
Martensite	Supersaturated solid solution of carbon in α -iron, formed in non-diffusing transformation	In carbon and alloy steels	800-900	Martensite provides high hardness and strength, and serves as a base of numerous wear-resistant iron-carbon alloys

Table 6.1 (cont.)

Structural constituent	Characteristic	Hardness		Effect of structural constituent on wear resistance
		additional subdivisions of constituents	HV	
Graphite	Crystal modification of carbon	Found in cast iron in three varieties: lamellar floccular spheroidal	Low	Graphite inclusions serve as lubricant reducing friction
Eutectic in cast iron	Mechanical mixture	1. Graphite-base (ferrite+graphite)	130	—
		2. Phosphide-base [pearlite+phosphide (Fe_3P)+cementite]	775	—
		3. Carbide-base (cementite+pearlite)	900-1,000	—

Note. The hardness values in this table are approximate and relative. The hardness of structural constituents depends on the content of carbon and alloying elements.

supercooling at a rate higher than critical. Hardening is effected by heating the metal to a temperature within the critical temperature range or above the critical point Ac_3 , holding at this temperature and quickly cooling. The treatment results in the formation of the nonequilibrium structures of martensite and troostite and of a number of intermediate structures. Their formation depends on the chemical composition of a given grade of steel, the cooling rate, and the temperature at which the steel ends its martensitic transformation (point M_h). Hardening is used to obtain high hardness and other necessary mechanical and physical properties. Most hardened parts undergo subsequent tempering. Hardening is widely used for parts subject to friction and wear.

Tempering is heating and holding hardened parts below the critical point Ac_1 (below the transformation region), and subsequent cooling. As a result, the nonequilibrium hardening structures change over to more stable structures, whereby the required mechanical properties are obtained or internal stresses are removed.

Artificial ageing is the heating and prolonged holding of parts at low temperatures (mainly from 150 to 180°C). The properties of steel and alloys are changed through internal processes without significant changes in the microstructure. The process is used for components and tools to improve strength and provide for the stability of shape.

Subzero treatment is a deep cooling of hardened parts. Here, the retained austenite changes into martensite to a fuller extent. The operation is used to increase the hardness, fatigue strength, wear resistance and the stability of shape of some hardened steels.

In addition to heat treatment, use is made of thermomechanical treatment. This is effected either at elevated or at low temperatures. In the first process, the treated metal becomes stronger and more wear-resistant than in conventional heat treatment. The second process involves deformation of supercooled austenite within its high-stability region and subsequent hardening. This type of treatment provides for greater hardness, contact fatigue strength, and maintained properties at temperatures of up to 500°C. The process is used for high-alloy bearing steels.

The strengthening of metals and alloys is the result of the strengthening of either all or the weakest atomic bonds that determine the strength of crystalline solids. The changes in the energy, length and character of the chemical bond, that take place during metal strengthening, are accompanied with slight changes in the atomic radii, interplanar distances and crystal lattice spacings. These quantities vary with temperature and pressure, which causes a very effective change of strength and other physical properties. This is especially the case with multicomponent, heterogeneous alloys where connection between similar or dissimilar crystal lattices emerges in various forms. In such cases the physical properties of alloys are other than weighted means of the specific properties of the individual alloy components or structural constituents; they are determined by complex laws of interaction resulting in energy changes.

In practice, depending on frictional conditions and the required properties of the parts to be treated, heat treatment may include several of the above operations performed in sequence.

For instance, use may be made of (1) annealing, hardening, and tempering; or (2) two-stage hardening with tempering after each stage; or (3) carburising with subsequent hardening, etc.; or (4) special combinations of mechanical and thermal treatment. These processing techniques make it possible to obtain the optimum structure and properties of metals and so provide the necessary strength and wear resistance of the product.

6.1.4. Secondary Processes in Friction

In friction, the structure of the metal in the active layer and hence, its properties undergo changes. These changes are due to the nature of external friction itself, which involves plastic deformation, the transformation of mechanical energy into thermal energy, etc. As a result, the metal on the rubbing surface may get instantly heat-

ed and then cooled as it comes out of the point of contact. According to B. D. Grozin, a metal layer 100 μm thick is heated by friction at a rate of 4×10^5 to 10^4 $^{\circ}\text{C/s}$ and then cooled at a rate of 10^3 to 10^4 $^{\circ}\text{C/s}$.

Depending on the combination of mechanical and thermal actions and their intensity, a whole range of $\alpha \rightleftharpoons \gamma \rightleftharpoons K$ transformations may take place in the structure. Specifically, these are the precipitation or dissolution of the excess phase; quick-running diffusion processes, which cause a local change in the chemical composition and consequently, a secondary hardening or tempering; the processes of carbide recrystallization, coagulation, and coalescence; etc. Some of these processes, such as recrystallization and coagulation, result in lower wear resistance of the metal. Due to the very short time of heating and cooling of the metal during friction, there may form intermediate unstable structures ("white layer", etc.) characteristic of a highly stressed state. Not only does the change of the metal structure and properties in individual microvolumes take place, but also, as a consequence, the change of the friction process itself.

Thus, the wear resistance of a metal is determined not only by its structure in the initial state (that is, before friction), but also by the

Table 6.2

Secondary structures in the active layer

Structure	Brief characteristic
Secondary austenite	Forms in the process of friction mainly from the initial martensitic structure and often in the presence of retained austenite. Its crystal lattice has a greater parameter than that of the initial (before friction) austenite (3,601 to 3,610 \AA for steel Grade Y10, according to B. D. Grozin), and it has a higher microhardness
Secondary martensite	This is the product of decomposition of secondary austenite. It is more readily etched than the initial martensite; its microhardness is from 850 to 925 kgf/mm^2 and higher
"White layer"	The development of this structure is due to local impulse load and thermal effects. It cannot be etched by common chemicals and possesses a high microhardness—of the order of 900-1,300 kgf/mm^2 and higher

Note. The hardness of secondary structures depends on the type and dispersity of the initial structure (before friction), on the conditions and intensity of friction, on the chemical composition of steel (the content of carbon and alloying elements).

structure that is formed under the combined action of the individual processes induced by friction [15].

The main secondary structures formed in friction are given in Table 6.2.

Of great importance is the process of formation, destruction and reproduction of oxide films on the rubbing surface.

The interaction between the active, plastically deformed surface layers of the metal and the oxygen contained in the ambient air or the lubricant adsorbed on the rubbing surface results in chemically adsorbed films, solid-solution films, or metal oxides. Their removal from the rubbing surface is a steady process wherein a dynamic balance between the destruction and reproduction of oxide films takes place [11]. During this process, wear debris (metal particles) break loose from the rubbing surface as a result of the repeated loading of individual frictional bonds. The chemical composition of the oxides which form in friction is given in Table 6.3.

Table 6.3

Oxides formed in friction [15]

Oxide composition	Formation temperature, °C	Micro-hardness, kgf/mm ²	Oxide composition	Formation temperature, °C	Micro-hardness, kgf/mm ²
α -Fe ₂ O ₃	200	—	α -Fe ₂ O ₃ +Fe ₃ O ₄	400-570	500
γ -Fe ₂ O ₃	200	1,000	Fe ₃ O ₄ +FeO	570	300

Depending on the joint construction, some quantity of wear debris can be retained on the rubbing interface. These particles on the one hand are subject to deformation and on the other, have some effect upon the process.

This effect may sometimes prove significant. Table 6.4 presents the approximate composition of wear debris [23].

Table 6.4

Phases found (+) in wear debris in friction of steel Grade 45

Test conditions	α -Fe	α -Fe ₂ O ₃	γ -Fe ₂ O ₃	Fe ₃ O ₄	γ -Fe ₂ O ₃ ·H ₂ O	Fe ₃ C
Friction in air, T=293 K	+	+	+	—	+	—
Friction in vacuum: T=293 K	+	+	—	+	—	+
T=77 K	+	+	—	—	—	+

Note. α -iron is found by an X-ray diffraction analysis; the other phases are found by an electron diffraction examination.

Table 6.5

Modern physical methods of metal structure studies [14, 22]

Method	Brief description
Optical metallography	Examination in the bright and the dark field for qualitative analysis of alloy phase composition; quantitative analysis of phase composition, size, shape, and distribution (magnification range $100\times$ to $2000\times$)
Microhardness	Complementary to optical metallography, serves to identify different alloy phases and to determine the degree of strengthening of each phase in the structure under test
X-ray diffraction analysis	A direct method of alloy phase composition analysis (mainly by photography); study of fine metal structure (using a diffractometer), i. e., analysis of the degree of soundness and the dominant orientation of crystallites, detailed study of structural changes in alloys caused by heat treatment and machining
Electron diffraction examination	Similar in purpose to X-ray diffraction analysis but provides information about the thinner metal layers (for layers under $1,000\text{ \AA}$ in thickness). Thin metal films and foils are observed by transillumination, which is more accurate than by reflection, but the latter allows massive specimens to be observed without preparation
Electron microscopy	Provides high resolution which makes it possible, with appropriate specimen preparation, to observe structural changes on a near-atomic level. Allows magnifications of up to $100,000\times$ and over. Investigation using replicas gives detailed information on metal microstructure that cannot be revealed by optical microscopy, on disperse structures, specifically, hardened-metal structures, and on their distribution, which makes it possible to establish qualitative and quantitative relations between the structure of metals and their properties or their behaviour in service. Electron fractography can provide information about fatigue fracture and even its progression. Scanning electron microscopy allows direct observation of specimens (without the use of replicas), and, with a special attachment, the distribution of chemical elements on the specimen surface.

6.1.5. Main Methods of Metal Structure Analysis

At present, the metal on a rubbing surface is studied by the physical methods presented in Table 6.5.

Table 6.5 (cont.)

Method	Brief description
X-ray spectrum analysis	<p>Diffraction electron microscopy provides a direct method of phase-composition analysis for thin metal films and foils. As a method complementary to the electron diffraction examination, it allows identification of each alloy phase and gives information about the fine structure of the specimen, i. e., makes it possible to study the grain boundary structure, dislocation reactions, and interaction of dislocations with different phases of the alloy</p> <p>Allows research into distribution of different chemical elements in a specimen, providing a resolution of the order of a few micrometers.</p> <p>The method is important for solving many problems in physical metallurgy, such as the study of micro-segregation and identification of inclusions in industrial alloys</p>
Continuous radiography method	<p>A variety of the X-ray diffraction analysis, adapted to investigation of rubbing surfaces. The equipment can be brought close to the sliding interface to fix the metal condition at the moment following disengagement of a given surface point from the counterface. The method allows fixation (by photography or with the use of ionization counters) of the material structure under conditions almost resembling those of friction and just before intensive cooling upon coming out of the contact zone.</p>
Mass-spectrometry	<p>Uses the release of gases as an indicator of processes running in the friction contact zone</p>

6.1.6. Recommendations

Mechanical properties and examples of use of metal structural materials are described in [46, 48].

Measures to increase wear resistance should be aimed at reducing the molecular and mechanical components of the friction force. To achieve this, the following guidelines are used in practice.

(1) When developing new materials, it is expedient to provide a structure where hard particles are dispersed in a relatively soft matrix (the Sharpy-type structure), which helps to localize seizure.

(2) For parts with a hardness of over 50 HRC, tempered martensite is the optimal structure. Below that hardness, better wear resist-

ance is exhibited by a steel having the structure of hardened troostite (preferably, acicular troostite).

(3) In heavy-duty components subjected to case hardening with a low-temperature tempering, the presence of a dense carbide network at the grain boundaries is impermissible. Here, an additional heat-treating operation, normalizing, is recommended between carburizing and hardening.

(4) A heat-treatment process and the steel structure and substructure should be developed so as to provide, in addition to strength, sufficient plasticity for increased resistance to plastic deformation and local destruction. With this in view, it is necessary to consider the permissible amount of retained austenite in the structure.

For a number of cases a combination of the "unhardened" γ -phase with the "strain-hardened" α -phase is optimal.

6.2. THERMO-CHEMICAL TREATMENT AS A MEANS FOR INCREASING THE WEAR RESISTANCE OF METALS

6.2.1. Process Features

Improved antifriction properties and wear resistance of metals are achieved by thermo-chemical treatment (TCT) through diffusive saturation or modification of metal surfaces with chemically active compositions, using chemical reactions.

TCT can be effected in solid, liquid, or gaseous media. The process duration depends on the chemical composition of the medium used and temperature. With respect to process features and results, TCT of metals falls into two principal groups.

(1) TCT used for increasing wear resistance through greater surface hardness of rubbing parts. This type of treatment includes the widely used processes of carburizing, nitriding, cyaniding, borating, etc.

These are employed primarily for improving resistance to abrasive wear.

(2) TCT intended mainly for improving antiscuff properties by forming thin surface layers enriched with chemically active substances; these layers prevent seizure and scoring in friction. This type of TCT is exemplified by sulphidizing, sulphocyaniding, impregnating the surface with selenium, tellurium, treatment in a cadmium-iodide bath. These processes do not increase surface hardness, or increase it but slightly; their effect is in reduced coefficient of friction and localized scoring. The processes are used for rubbing components which are to operate under conditions where scoring is possible and where lubrication is limited or impracticable to use [5, 13].

Table 6.6

Carburization of low-carbon and alloy steels

Type	Medium	Temperature, °C	Duration, hrs	Depth of layer, mm
Gas carburizing	Mixture of endogas with city gas: 16-20% CO, 12-16% CH ₄ + C ₂ H ₆ , 30-40% H ₂ , 20-30% N	950	6-12	0.6-1.4
	Natural gas, liquefied mixtures of propane and butane	910 930	2-3.5 8-9	0.8-1.15 1.0-1.2
Pack carburizing	70-76% charcoal, 20-25% barium carbonate, 3.5% calcium carbonate (GOST 2407-73)	920-930	5.5-16.0	0.6-1.8
	Carburizer: 10-15% BaCO ₃ , 3.5% CaCO ₃ (GOST 5535-76). Grain size 3.5-10 mm. Moisture content ≤ 5-6%			
Liquid carburizing	Salt bath: 78-85% Na ₂ CO ₃ (or K ₂ CO ₃), 10-15% NaCl and 6-8% SiC (carborundum)	880-900	0.5	0.15-0.20

6.2.2. TCT Processes and Their Application

Carburizing is used for low-carbon plain and alloy steels with 0.08 to 0.30 percent carbon. In the carburized layer, the carbon content usually ranges from 0.8 to 1 percent, depending on steel grade.

Carburizing with subsequent tempering at 170 to 200°C provides a surface hardness of 60-64 *HRC* for carbon steels, and 58-61 *HRC* for alloy steels (Table, 6.6).

Carburized and hardened parts made of alloy steels are well to subject to work hardening in order to cause the transformation of retained austenite into martensite. After heat treatment, the carburized layer should have the structure of acicular martensite with fine carbide grains and a small amount of retained austenite. Such a structure is favourable to an increase in wear resistance [16].

Low-carbon carburized steels are used for light-duty applications, such as piston pins, connecting-rod forks, camshafts, worms, gears with a maximum cross-section of up to 25 mm. Alloy steels are used for similar components with a cross section of up to 35 mm in medium-load applications. Medium-strength alloy steels are used for

Table 6.7

Nitriding of typical machine components made of various steels

Steel grade	Nitriding conditions		Nitriding results		Typical components	
	Temperature, °C	Process duration, hrs	Minimal surface hardness, HV	Depth of layer, mm		
38XM10A	510 510 540 540	35 55 35 42	950	0.30-0.35 0.50-0.55 0.45-0.50 0.50-0.70	Turbine, engine, and instrument components: steam-turbine valve stems, internal combustion engine liners; bushings, pins, shafts, gears, spindles, etc.	
38XM	480	25		600		0.25-0.35 0.25-0.35
35XM	520	10				
34M1A						
40X	500	48	450	0.45-0.50	Shafts, gears, etc.	
20X13	530-580 550	20 55	800 —	0.25-0.27	Parts subjected to impact loads (valves, etc.)	
08X18H10T	600 560 600-650	75 50 5	700 — —	0.20-0.40 0.15 0.10	Fasteners and other parts working at elevated temperatures	
34XH1M	510 530	25 10	600	0.45-0.50	Parts of large cross-section for high loads	
34XH3M	500	50		0.50-0.60		
38XH3MΦA	445 495	50-65 70				
35XH1M2Φ	505	20	480	0.50-0.60	Crankshafts, valves, connecting rods, bolts, gears, etc.	
36XH1MΦ	560	30				
40XHMA	500	50	550	0.45-0.50		
45XHMΦ	500	50				
38XH3BA	500	50				
18X2H4BA	500	55	650	0.45-0.50	Critical components of high strength and toughness, subjected to variable cyclic loads: crankshafts, gears, connecting rods, pins, etc.	
30X2H2BΦA	500	35		0.25-0.30		

Table 6.7 (cont.)

Steel grade	Nitriding conditions		Nitriding results		Typical components
	Temperature, °C	Process duration, has	Minimal surface hardness, HV	Depth of layer, mm	
30XBA 25X5MA	500	55	650	0.5-0.55	Plungers and bushings
	530	36	800	0.35-0.45	
	550	12	800		
15X11MΦ	530	10		0.35-0.45	Vaness, rods, bushings working at up to 560°C
15X12BMΦ (9H802)	580	18	HRA 82.5	0.30-0.35	
4X14H14B2M (9H69)	570-630	25-35	750	0.10-0.20	Fittings, engine valves, fasteners working at up to 600°C

gears up to 75 mm in cross-section operating with impacts, and high-strength alloy steels are used for heavy-duty gears up to 120 mm in cross-section.

Nitriding serves to saturate the surface layer with nitrides to a depth of 0.25 to 0.7 mm and so to increase its hardness to 500-900 HV. This improves resistance to wear, corrosion, and cavitation. On the other hand, the nitrided layer features increased brittleness. It is also structurally unstable when exposed to 400-500°C for a long time. Nitriding leads to some dimensional changes in treated parts, which can be compensated for by stock allowances.

Nitriding conditions, depending on grades of steel and on their application, are given in Table 6.7.

Carbonitriding and cyaniding. These processes have an advantage of higher saturation speed over gas carburizing. The surface layer becomes more wear-resistant owing to the presence of nitrogen and finer grains. Cyaniding in salt baths is advantageous as to processing speed, but it has a substantial drawback: the toxic salts require precautions on the part of personnel.

Carbonitriding and cyaniding conditions and their effects on various steels are given in Tables 6.8 and 6.9, respectively.

The surface-layer structure obtained by high-temperature cyaniding features a carbonitrided zone or carbonitride inclusions. Low-temperature cyaniding mainly provides saturation with nitrogen, the layer of carbonitrides being insignificant.

Borating. In this process, a surface hardness of HV 1,400-1,500 and microhardness of HV 2000 are achieved for steel, resulting in high wear resistance.

Borating is used mainly for plain medium-carbon steels and also for alloy steel Grades 30XTC, 40XC, and 50T.

Table 6.8

Carbonitriding of structural steels

Gas medium	Steel grade	Temperature, °C	Process duration, hrs	Depth of layer, mm	Heat treatment and hardness
Endogas 80-90%, natural gas 5-8%, ammonia 2.5-5%	25XFT	850	5.25	0.5-0.7	Cooling in furnace to 825°C, quenching in oil at 180°C, tempering at 170°C, $HRC \geq 60$
	25XFM	850	9.00	0.8-1.0	
Mixture of kerosene and ammonia vapours	20X 18FT 18X2H4BA	850	3-4	0.6-1.0	Quenching directly from furnace, HRC 52-62
Decomposition products of triethanolamine	Steel Grades 10 and 20	840	3	0.35	$HRC \geq 60$
Pyrolysis products of triethanolamine	Medium-carbon steels	600	6-10	0.15-0.40	Surface microhardness: $H290$ for steel Grade 45, $H560$ for steel Grade 30X2HBΦA

The high wear resistance is retained in heating up to 900°C; in addition, corrosion resistance of carbon high-chromium and austenitic steel is improved.

Borating conditions and effects are given in Table 6.10 [16].

Sulphidizing and sulphocyaniding. Sulphidizing in salt baths has found the greatest use owing to simple equipment and a relatively rapid process.

Among the various mix formulations for sulphidizing baths developed in different countries, the most efficient are the sulphidizing baths used in this country, which contain no toxic reagents.

Sulphidizing produces a considerable antiscuff effect, allowing greater seizure loads, and reduces the coefficient of friction. Wear resistance is increased from 2 to 5 times.

The most common method for assessing the quality of sulphidizing is testing on a four-roll friction testing machine, where measurements are taken of the seizure load, the coefficient of friction, and the wear rate [5].

The most widely used mix formulations for sulphidizing and sulphocyaniding baths and the effects are presented in Table 6.11.

Table 6.9

Cyaniding structural steels

Bath content	Process temperature, °C	Process duration, hrs	Depth of layer, mm
<i>High-temperature cyaniding</i>			
For small-depth cyaniding:		0.50	0.10-0.15
(a) in melting: 50% NaCN, 50% NaCl, in processing:	840	1.00	0.15-0.25
20-25% NaCN, 20-25% NaCl, 20-50% Na ₂ CO ₃	870	0.50 1.00	0.20-0.25 0.25-0.30
(b) in melting: 9% CN-melt Grade ГИПХ, 36% NaCl, 55% CaCl ₂ ; in processing: 0.4-1% CN	840	0.50 1.00	0.15-0.20 0.20-0.30
	870	0.50 1.00 2.00	0.20-0.30 0.30-0.40 0.45-0.55
For variable-depth cyaniding:			
in melting: 10% NaCN, 24% NaCl, 50% BaCl ₂ ; in processing:	840	1.30 1.00	0.25-0.30 0.50-0.60
8-12% NaCN, 10% Na ₂ CO ₃ , 15% BaCl ₂ , 30-50% Ba ₂ CO ₃ , 30-50% NaCl	900	2.00 4.00	0.70-0.80 1.00-1.20
For deep cyaniding:			
in melting: 8% NaCN, 10% NaCl; 82% BaCl ₂ ; in processing:	900	0.40 0.75 1.00	0.20-0.75 0.30-0.50 0.50-0.60
38% NaCN, 22% NaCl; 40% BaCO ₃	950	1.50 2.00 3.00 4.00 5.00-6.00	0.50-0.80 0.80-1.00 1.00-1.10 1.20-1.30 1.40-1.60
<i>Low-temperature cyaniding</i>			
For small-depth cyaniding:			
in melting: Durferrit NS and Durterrit NS ₂ salts; in processing: 50% KCN, 42-48% KCNO, 1% Na ₂ CN ₂ , K ₂ CO ₃ —balance (Tennifer process)	570	1.00-3.00	0.15

Table 6.10

Borating of steels

Medium		Process conditions		Results	
state	composition	tempera- ture, °C	process dura- tion, hrs	surface hardness	depth of layer, mm
Solid	80% boron carbide, 0.5-1% ammonium chloride, quartz sand—balance	950	6	—	0.12-0.14
	50% boron carbide, 50% cryolite as bin- der	1,200	2-3*	H1000	0.12
Liquid	Electrolysis bath, 100% borax	930-950	2-6	HV 1400-1,550	0.15-0.35
	60-70% borax, 30-40% boron carbide	900-1,100	5-20	—	0.15-0.85
Gaseous	Diboron 1 and hydro- gen 1: (25 to 75)	800-850 900-1,100	4 2-6	> H1800	0.20 0.07-0.16
	Boron trichloride and hydrogen 1:20	850	3-6		0.11-0.20

* Duration, min.

The best results are obtained in treating carbon and low-alloy steels and irons, a lower effect is produced by sulphidizing chromium and stainless steels and titanium alloys, although substantial improvements are evident even here.

Sulphocyaniding is a process wherein the surface layer is saturated both with nitrides and sulphides. The process results in improved antiscuff properties (although somewhat less effective than those obtained in sulphidizing), and increased wear resistance (for some metals higher than in sulphidizing).

TCT methods for titanium alloys. Of all metals used in mechanical engineering, titanium alloys exhibit the poorest antifriction properties and the highest tendency to scuffing. TCT methods used for steel prove ineffective for titanium alloys; however, without special TCT techniques or lubricants with special additives, the application of titanium alloys in movable joints, is, as a rule, impermissible.

Table 6.11

Sulphidizing and sulphocyaniding

Process	Bath formulation	Process temperature, °C	Seizure load for steel Grade 45, kgf
Sulphidizing in NIIKHIMMASH 2/6 No. 1 bath	1.8% NaCNS (KCNS), 5.5% Na ₂ S ₂ O ₃ , 41.7% KCl, 51.0% Na ₂ SO ₄	560	> 500
Low-temperature sulphidizing	69% KCNS, 22% Na ₂ S ₂ O ₃ , 9% NH ₄ CNS	200	100-140
Sulphocyaniding in ENIMS bath	73% K ₄ Fe (CN) ₆ , 10% Na ₂ S ₂ O ₃ , 17% NaOH	560	100-120
Sulphocyaniding in NIITAvtoprom bath	44% K ₂ CO ₃ , 54% CO (NH ₂) ₂ , 2% Na ₂ S	580	400-500
Sulphocyaniding in SATS baths: No. 1	34% NaCN, 7% Na ₂ S ₂ O ₃ , 16% Na ₂ CO ₃ , 16% K ₂ CO ₃ , 27% NaCl + KCl	560	250-300
No. 2	25% NaCN, 1.2% NaCNO, 2% NaCNS, 2.2% Na ₂ S, 34.8% Na ₂ CO ₃ , 34.8% NaCl + KCl	560	250-300
No. 3	95% NaCN, 5% Na ₂ S ₂ O ₃	560	150-200
No. 4	4% NaCN, 5% NaCNO, 2% NaCNS, 47% Na ₂ CO ₃ , 40% NaCl + KCl	560	150-200
"Durferrit Sofumi": No. 1	30% NaCN, 7% NaCNO, 60% NaOH, 3% S	560	180-200
No. 2	30% NaCN, 16% NaCNO, 4% Na ₂ S, 25% Na ₂ CO ₃ , 25% NaCl + KCl	560	200-250
No. 3	35% NaCN, 11% NaCNO, 10% CaS, 15% NaCl + KCl, 15% BaCl ₂ , 25% CaCl ₂	560	200-250
No. 4	30% NaCN, 7% NaCNO, 60% NaOH, 3% S	560	150-200

Table 6.11 (cont.)

Process	Bath formulation	Process temperature, °C	Seizure load for steel Grade 45, kgf
"Atelier Partiot": No. 1	4% NaCN, 15.5% NaCNO, 35% Na ₂ CO ₃ , 45% NaCl + KCl, 0.5 S	560	150-200
No. 2	16% NaCN, 21% NaCNO, 40% Na ₂ CO ₃ , 22.7% NaCl + KCl, 0.3% S	560	180-200

Notes. 1. Seizure load for untreated steel Grade 45 is 15 to 20 kgf.

2. Process duration 1 h for the NIIKHIMMASH 2/6 No. 1, and 3 hours for all the other baths.

Thermochemical treatment methods for titanium alloys and the antiscuff properties obtained are given in Table 6.12.

The maximum effect is obtained by treatment in the NIIKHIMMASH cadmium-iodide bath, which makes it possible to use titanium alloys in sliding couples with and without lubrication [5].

6.2.3. Assessing the Effectiveness of TCT

The effect produced by thermochemical treatment of metals for sliding components is expressed in terms of reduced coefficient of friction, increased seizure load and improved wear resistance. The absolute numerical values of these parameters for different TCT methods are inevitably relative in character. The effectiveness of TCT for the same materials varies depending on the movable joint design and operating conditions, such as sliding speed, pressure, temperature. For this reason, the most acceptable approach is to compare the above-mentioned parameters determined for treated metals with those for untreated ones. For instance, the effectiveness of TCT can be expressed as the ratio of the coefficient of friction f , seizure load P , and wear resistance k of treated metals to the same quantities f_0 , P_0 and k_0 obtained for untreated metals. These quantities can be measured on conventional friction testing machines. For instance, the coefficient of friction and wear resistance can be determined on the Amsler wear machines, Model MN, and the seizure load, on four-ball or four-roller type machines.

Data on comparative effectiveness of the various TCT methods are given in Table 6.13.

Thermo-chemical treatment of titanium alloys

Table 6.12

Process	Distinguishing features	Treatment resultt		Operating conditions		
		depth of layer (thickness of coating), μm	microhardness, kgf/mm^2	lubrication requirements	pressure kgf/cm^2	sliding speed, m/s
Sulphidizing in NIUKHIMMASH 2/6 No. 1 bath	Chemical interaction between titanium and molten salts, formation of titanium sulphides and oxides	10-20	—	Operation without lubricants permitted	100-150	10
Treatment in NIUKHIMMASH cadmium-iodide bath	Chemical interaction between titanium and molten salts	20-30	—		400-500	10
Thermal oxidizing	Chemical interaction between titanium or its alloys and oxygen at 700 to 800°C	30-60	700-800	Lubrication or anti-friction varnish coating required	75-100	1
Nitriding	Chemical interaction between titanium or its alloys and nitrogen at 850 to 950°C	150-250	600-1,200	Operation with or without lubricants possible	100	10
Chromium plating	Deposition of chromium on titanium alloys by electroplating	50-150	900-1,400		100	2
Chemical nickel coating	Deposition of nickel on titanium alloys in special alkaline or acidic solutions	15-30	700-800	Lubrication with mineral oils required	75	2
Molybdenum or tungsten coating	Thermal dissociation of vapours of molybdenum or tungsten carbonyl in vacuum on surface heated to over 200°C	20-200	Soft coatings—200-400, hard coatings—1,500-3,000	Lubrication with mineral oils or greases required	50	0.5
Double-layer coating with molybdenum disulphide or tungsten disulphide	Thermodiffusion coating with molybdenum or tungsten and subsequent sulphidizing to form molybdenum disulphide or tungsten disulphide	—	—	Operation without lubricants permitted	300	2

Table 6.13

Effectiveness and application of thermochemical treatment (TCT)

TCT process	Materials	Tribological components	Effect of TCT		
			f/f_0	p/p_0	h/h_0
Carburizing	Carbon and alloy steels	Gears, sprockets, cams, worms, piston rings	0.8-1.0	1.0-1.5	2-3
Nitriding	Alloy steels	Turbine components, plungers, crankshafts, connecting rods, bolts	0.8-1.0	1.0-1.5	2-4
Carbonitriding and cyaniding	Carbon tempered steels and alloy steels	Threaded parts, bushings, connecting rods, cutting tools	0.7-0.8	1.5-2.0	2-5
Borating	Medium carbon and alloy steels	Bushings, pump components, chain links, nozzles for fluids			2-5
Sulphocyaniding	Carbon alloy steels and stainless steels	Piston rings, liners, bushings, gears and worm wheels, pump components, threaded parts, joint pins	0.5-0.6	4-5	2-5
Sulphidizing	Carbon steels and cast irons		0.4-0.5	5-10	1.5-3.0
Treatment in cadmium-iodide bath	Titanium alloys	Threaded parts, bushings	0.5-0.6	5-10	—

6.3. FRICTION AND WEAR OF METALS AT HIGH SLIDING SPEEDS

Problems involving friction and wear of materials at sliding speeds in excess of 50 m/s arise in aircraft and missile engineering, turbines, instrument making, transport, and metal cutting. According to data available from the USA, friction at high speeds is mostly characterized by an extremely short-term contact interaction of rubbing surfaces. For example, the acceleration of a projectile in the bore of a light-gas gun takes from 10^{-5} to 10^{-4} s, the movement of a bullet in a rifle bore lasts from 10^{-3} to 10^{-2} s, the acceleration and

friction braking of launching trolleys in a rocket track takes from 1 to 10 s; the effective braking of aircraft and railway trains lasts from 20 to 40 s.

Research into friction and wear of solids rubbing at high sliding speeds shows that there takes place an intensive heat generation which can be as high as 130 MW/m^2 at $v = 500 \text{ m/s}$. The heat generation intensity per unit time per unit apparent contact area is expressed as $q = f p_a v$.

The materials of rubbing components cannot warm up throughout during the short-term processes of high-speed friction, and the heat is absorbed by thin surface layers only.

The thickness of the surface layer absorbing the heat is found from the formula [8]

$$\delta = 1.94 \sqrt{at}$$

where a = thermal diffusivity.

The great intensity of heat flow, and the small thickness of the heat-absorbing layer result in a heat shock with a high temperature gradient at the contact.

The temperature at the sliding interface can reach the melting point of one of the rubbing materials, which begins to melt on the surface. The presence of this effect has been reported in [1, 4, 6, 21].

The time necessary for melting to begin is found from the expression [1]

$$t_m = \frac{\pi}{4} \frac{\lambda^2 (\vartheta_m - \vartheta_0)^2}{aq_1}$$

where t_m = time it takes the material to begin melting under the action of a constant heat flux q_1 normal to the sliding surface; and λ = thermal conductivity of the material.

Table 6.14 gives values of t_m for different metals under the action of the heat flux $q_1 = 12 \text{ MW/m}^2$ [1].

It follows from the data of Table 6.14 that antifriction materials for high-speed friction should have fusible components, while friction materials, refractory components.

A model of the melting of a slider under the action of a given heat flux q_1 in high-speed friction is shown in Fig. 6.1. It is assumed that the melt is at once transferred onto the counterface and the melting boundary moves into the slider at a rate S .

In a certain time t^* from the beginning of melting, the region with a thickness $z_1^* = S(t^*)$ has melted. The melting rate S is a variable, and so is the thickness of the melted layer, n . The average

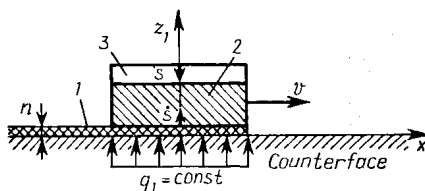


Fig. 6.1. Physical model of the melting of a solid on its rubbing surface in high-speed sliding

1—molten layer; 2—heating region $\vartheta(z_1, t)$; 3—region with initial temperature ϑ_0

Table 6.14

Metal melting caused by heat flux ($v_0 = 0^\circ\text{C}$)

Material	$\lambda, \frac{\text{W}}{\text{m}^\circ\text{C}}$	$\alpha \times 10^6, \frac{\text{m}^2}{\text{s}}$	$\vartheta_m, ^\circ\text{C}$	$\frac{\lambda^2 \vartheta (t_m - \vartheta_0)^2}{a}$ (MW/m ²) ² s	t_m, s
Bismuth	7.7	6.4	271	0.72	0.004
Lead	30.2	20.4	327	4.77	0.026
Tin	58	31	232	5.85	0.032
Zinc	95	30	420	52	0.28
Cast iron	29	6.9	1,200	175	0.95
Aluminium	235	82	660	294	1.6
Steel Grade Y10	37	7.5	1,460	390	2.1
Steel Grade 45	38	7.5	1,480	422	2.3
Steel Grade 10	42.8	8.1	1,500	510	2.8
Armko iron	43.6	8.5	1,530	525	2.9
Copper	365	100	1,083	1,560	8.5
Tantalum	64	22	2,990	1,660	9.1
Molybdenum	129	46	2,625	2,500	13.6
Tungsten	128	47	3,380	3,980	21.7

thickness of this layer is

$$n_{av} = \frac{z_1^* l}{L^*}$$

where l = slider dimension in the direction of sliding; and L^* = sliding distance from the beginning of melting.

The presence of the molten layer in the contact zone signifies that friction at high sliding speeds is hydrodynamic by nature.

Theoretical analysis of the melting problem (Stefan's problem) involves the determination of the melting rate \dot{S} , which has an effect on the molten layer thickness and, hence, on the force of viscous friction and on the wear rate. It follows then that small values of the friction coefficient at high sliding speeds can be attributed to a low shear resistance of the rubbing surfaces highly heated in the contact zone and to the melting there.

Given below are values of the coefficient of friction depending on sliding speeds in the bore of a rifle, f_r [26], and an artillery gun, f_g [27]:

$v, \text{ m/s}$	0	85	340	720	930
f_r	0.3	0.07	0.054	0.051	—
f_g	0.27	0.052	0.031	0.022	0.021

The relationships between the coefficient of friction and the sliding speed obtained in the testing of magnetic rail brakes [20], on a Beams high-speed centrifuge [4], and on a long slideway are given in Table 6.15.

The diagram of the coefficient of friction versus sliding speed at different pressures for specimens of Grade 10 steel moving on a long slideway made of steel Grade 65 is shown in Fig. 6.2.

Table 6.15

Coefficient of friction depending on sliding speed

Test conditions	Material	f at v , m/s					
		50	100	200	300	400	500
Magnetic rail brake [20] Beams' ultra- centrifuge [4]	Steel	0.04	—	—	—	—	—
	Bismuth*	0.12	0.07	0.04	—	—	—
	Antimony*	0.25	0.18	0.14	0.1	0.07	—
	Steel**	0.12	0.10	0.08	0.06	0.05	0.04
	Copper**	0.23	0.17	0.12	0.09	0.08	0.07
	Titanium carbi- de**	0.22	0.16	0.11	0.08	0.06	0.05
Long slide- way	Aluminium oxi- de**	0.17	0.15	0.13	0.12	0.11	0.10
	Steel Grade 10 ($p_a = 150$ kgf/cm ²)	0.05	0.035	0.03	0.025	0.022	0.02

* Low loads (0.2 kgf).

** High loads (up to 8 kgf).

Studies of wear at high sliding speeds [1, 7] have shown that the wear rate grows with sliding speed and pressure, lying within the range of $I = 10^{-7}$ to 10^{-5} . The wear rate, as dependent on sliding

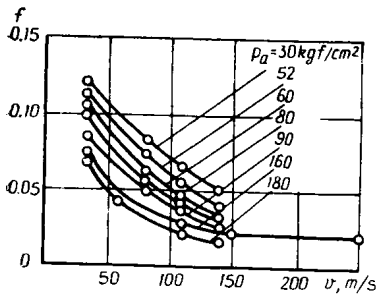


Fig. 6.2. Effect of sliding speed and pressure on the coefficient of friction for steel Grade 10

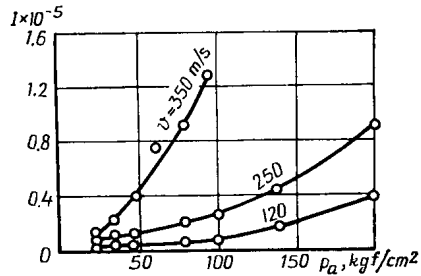


Fig. 6.3. Effect of sliding speed and pressure on the wear rate of copper rubbing against steel

speed and contact pressure p_a for copper specimens is shown in Fig. 6.3. The tests involved the sliding of the specimens at a constant speed during $t = 1$ s [1].

Depending on wear resistance at high sliding speeds, metals can be arranged in the following series [4]: tungsten, tungsten-molybdenum alloys, molybdenum, tantalum, armko iron, steel, cast iron, copper, aluminium, zinc, bismuth, tin, lead.

REFERENCES

1. Балакин В. А., Балакина Н. А. Оплавление твердого тела при высокоскоростном трении. — В кн.: Среда и трение в механизмах, вып. II. Таганрог, радиотехн. ин-т, 1976, с. 16—26.
2. Бернштейн М. Л. Термомеханическая обработка металлов и сплавов. М., «Металлургия», 1968, т. 1 и 2.
3. Блантер М. Е. Металловедение и термическая обработка. М., Машгиз, 1963.
4. Боуден Ф. П., Тейбор Д. Трение и смазка твердых тел. М., «Машиностроение», 1968.
5. Виноградов Ю. М. Трение и износ модифицированных металлов. М., «Наука», 1972.
6. Горюнов В. М. Исследования трения при нестационарном высокоскоростном режиме. — В кн.: Новое в теории трения. М., «Наука», 1966, с. 91—97.
7. Горюнов В. М., Чичинадзе А. В. Износ металлических материалов при высокоскоростном нестационарном трении. — В кн.: Расчет и испытание фрикционных пар. М., «Машиностроение», 1974, с. 98—102.
8. Дроздов Ю. Н. Тепловой аспект проблемы задира катящихся со скольжением тел. М., «Машиностроение», № 2, 1972, с. 71—79.
9. Журавлев В. Н., Николаева О. И. Машиностроительные стали. Справочник. М., «Машиностроение», 1968.
10. Контер Л. Я., Артамонова В. В., Штейн А. С. Влияние НТМО на теплоустойчивость и контактную выносливость высоколегированных подшипниковых сталей. МИТОМ, 1976, № 3, с. 59—61.
11. Костецкий Б. И. Трение, смазка и износ в машинах. Киев, «Техніка», 1970.
12. Крагельский И. В., Виноградова И. Э. Коэффициенты трения. М., Машгиз, 1955.
13. Крагельский И. В. Трение и износ. М., «Машиностроение», 1968.
14. Любарский И. М., Воскобойников Д. Б., Голдштейн Л. Я. — В кн.: Износ и трение металлов и пластмасс. М., «Наука», 1964, с. 79—86.
15. Любарский И. М., Палатник Л. С. Металлофизика трения. М., «Металлургия», 1976.
16. Материалы в машиностроении. Справочник, т. 2, М., «Машиностроение», 1967, с. 96—137.
17. Металловедение и термическая обработка. Справочник. М., «Металлургиздат», 1961, т. 1 и 2.
18. Мягков В. Д. Краткий справочник конструктора. Л., «Машиностроение», 1975.
19. Надежность и долговечность машин. Киев, «Техніка», 1975. Авт.: Костецкий Б. И., Носовский И. Г., Бершадский Л. И., Караулов А. К.
20. Натурные испытания фрикционного материала для магнитореельсового тормоза. Труды МИИТ. Вып. 315, 1968, с. 135—143. Авт.: Б. К. Быков, Э. Д. Браун, О. В. Бесценная, М. Д. Фокин.
21. Полосаткин Г. Д., Грибанов С. А. Измерение температуры на поверхности резца при скоростях до 800 м/с. — «Известия вузов. Физика», 1965, № 3, с. 173—174.
22. Приборы и методы физического металловедения. Пер с англ. под ред. Ф. Вейнберга. М., «Мир», вып. 1, 1973, вып. 2, 1974.
23. Проблемы трения и изнашивания. Киев, «Техніка», 1973 МВ и ССО УССР, сб. № 3, с. 44—48. Авт.: Островская Е. Л., Любарский И. М., Удовенко В. Ф. и др.
24. Филинов С. А., Фиргер И. В. Справочник термиста. М.-Л., «Машиностроение», 1964.
25. Шмыков А. А. Справочник термиста. М., Машгиз, 1961.
26. Groch G., Plake E. Zeitschrift für das gesamte Schiess und Sprengstoffwesen, 1940, S. 31-33.
27. Boundary Lubrication. An Appraisal of World Literature. Compiled and Edited by F. F. Ling, E. E. Klaus, R. S. Fein. New York, 1969, p. 10-14.

METALLIC ANTIFRICTION MATERIALS

7.1. BRIEF CHARACTERISTICS OF BEARING ALLOYS

The most common antifriction materials used for bearings are tin, lead, copper, aluminium and zinc alloys. Steels and cast irons are used for the purpose less frequently.

7.1.1. Babbitt Metals

The oldest bearing materials are soft alloys based on tin and lead. The first bearing alloy was developed by I. Babbitt, an American inventor, in 1839. It contained 82 to 84 percent Sn, 5 to 6 percent Cu, and 11 to 12 percent Sb. As this alloy had been the first in the use of soft, white antifriction alloys in engineering, all subsequent alloys based on tin and lead were named babbitt metals. These alloys, also referred to as white metals, have low hardness (*HB* 13-32), low melting point (240 to 320°C) and increased softening at elevated temperatures (*HB* 9-24 at 100°C); they readily run in and exhibit high antifriction properties. At the same time they have low fatigue strength, which affects bearing life.

Two groups of alloys are standardized in the USSR (see Table 7.1). The babbitt metals that found the most extensive use abroad (in the USA) are given in Table 7.2.

The physical, mechanical, and antifriction properties of babbitt metals are treated in detail in [27], and are not described here. The choice of a bearing alloy should be made with regard to the thickness of the bearing lining. A heterogeneous microstructure of the B83 type alloys having big, hard, cubic crystals of SnSb (β -phase) fails to provide adequate resistance to fatigue damage in thin bearing linings (under 1 mm in thickness) under the action of cyclic

Table 7.1

Composition (%) of babbitt metals used in the USSR**A. Babbitts according to GOST 1320-74**

Grade	Sn	Sb	Cu	Cd	Ni	As	Pb
B88	Balance	7.3-7.8	2.5-3.5	0.8-1.2	0.15-0.25	—	—
B83		10.0-12.0	5.5-6.5	—	—	—	—
B83C		9.0-11.0	5.0-6.0	—	—	—	1.0-1.5
B16	15.0-17.0	15.0-17.0	1.5-2.0	—	—	—	Balance
BH	9.0-11.0	13.0-15.0	1.5-2.0	0.1-0.7	0.1-0.5	0.5-0.9	
BC6	5.5-6.5	5.5-6.5	0.1-0.3	—	—	—	

B. Babbitts according to GOST 1209-73 (lead—balance)

Grade	Sn	Ca	Na	Mg	Al
BKA	—	0.95-1.15	0.7-0.9	—	0.05-0.20
BK2	1.5-2.1	0.30-0.55	0.2-0.4	0.06-0.11	—
BK2III	1.5-2.1	0.65-0.90	0.7-0.9	0.11-0.16	—

Table 7.2

Composition (%) of babbitt metals used in the USA

Grade	Sn	Sb	Pb	As
SAE11	86.0 (min)	6.0-7.5	0.5	0.1
SAE12, ASTM2	88.25 (min)	7.0-8.0		—
SAE13	5.0-7.0	9.0-11.0	Balance	0.25
SAE14, ASTM7	9.25-10.75	14.0-16.0		0.6
SAE15, ASTM15	0.9-1.25	14.0-15.5		0.8-1.2

Note. Impurities 0.2%.

loads [3]. The plastic deformation builds up in individual local volumes of the β -phase crystals, this leading to residual strain in the babbitt layer. It is difficult for the crystals of the hard component that takes up the load to penetrate into the plastic matrix in the thin alloy layer. The size of such crystals is often commensurable with the layer thickness, reaching several tenths of a millimeter. The

layer of the soft, plastic matrix under the crystals develops a greater ability to withstand plastic deformation with the aid of its backing (the bearing housing). In individual areas where brittle crystals of the β -phase accumulate, a probability arises that pressure from the journal to the bearing housing may be imparted directly through these crystals. Then the β -phase proves to be a weak spot, with cracks developing in the SnSb crystals. These microdefects form pockets of stress concentration which give rise to further fatigue cracking in continued cyclic loading.

Babbitts for thin-walled bearing linings should comply with the following requirements:

(1) they should have no sharply inhomogeneous structure. Single-phase alloys with adequate resistance to crushing can be used for the purpose;

(2) since thin-walled precision linings should operate mainly in fluid-friction conditions, the antifriction properties become less significant than resistance to fatigue failure, which must be adequately high;

(3) for better running-in, preference should be given to a babbitt layer of reduced hardness (*HB* 15-20), bearing in mind that resistance to crushing in a thin layer increases owing to the influence of its backing;

(4) the required bearing life depends considerably upon the strength of adhesion of the babbitt lining to the backing. This strength is determined by the ability of the tinning to stand fatigue failure.

Some alloys developed and used in the USSR for thin-walled bearing linings are presented in Table 7.3.

Table 7.3

Composition (% , lead — balance) of babbitts used for thin bearing linings

Grade	Sn	Sb	As	Cu
COC6-6	5.5-6.5	5.5-6.5	—	—
BC2	1.5-2.5	9.0-10.0	0.5-0.8	—
БК2 with the addition of remelt	1.5-2.1	0.15-0.3 Na	0.04-0.09 Mg	0.08-0.30

Bearings with babbitt linings over 3 mm thick are used for relatively light operating conditions. The babbitt layer of such bearings (alloy Grades Б83, Б16, БН, БКА) can easily run-in and provides compensation for inaccuracies arising in the manufacture, assembly, and service. Examples are sliding bearings in railway vehicles, in powerful low-speed marine engines, in compressors, etc.

7.1.2. Copper-Base Alloys

This relatively large group of alloys used as antifriction materials is represented by bronzes (with and without tin) and brasses. Bronze bearings come in monometallic and bimetallic varieties. Monometallic bearings (linings, bushings, etc.) are made of bronzes with adequate strength and hardness. Bronze alloys used for the purpose are divided into those with a high (up to 10 percent) and a low (up to 3 percent) tin content. The alloy components include Zn, Pb, Ni, P and some others. In the USSR, the pertinent State Standard (GOST 613-65) specifies the composition of low-tin bronze grades. The grades with a high tin content are produced to special specifications. The compositions of the most commonly used grades of bronze are given in Table 7.4.

Table 7.4

Composition (% , copper — balance) of the most common cast tin bronzes

Grade	Sn	Zn	Pb	Application
Standard bronzes				
БрОЦНЗ-7-5-1*	2.5-4.0	6.0-9.5	3.0-6.0	In tribological joints at loads up to 25 kgf/cm ²
БрОЦНЗ-12-5	2.0-3.5	8.0-15.0	3.0-6.0	
БрОЦС5-5-5	4.0-6.0	4.0-6.0	4.0-6.0	Antifriction components
БрОЦС4-4-17	3.5-5.0	2.0-6.0	14.0-20.0	
БрОЦС3.5-7-5	3.0-4.5	6.0-9.5	3.0-6.0	
Special bronzes				
БрОЦ10-2	9.0-11.0	1.0-3.0	—	Critical antifriction components
БрОЦ10-1**	9.0-11.0	—	—	
БрОЦН40-2-3***	9.0-11.0	—	2.0-3.25	
БрОЦ10-10	8.0-10.0	6.0-11.0	—	
БрОЦ16-5	15.0-17.0	4.0-6.0	—	
БрОЦ18-12	7.0-9.0	—	11.0-13.0	

* Contains 0.5-2.0% Ni.

** Contains 0.4-1.0% P.

*** Contains 3.0-4.0% Ni.

Assembled bushings, face bearing discs, and other antifriction components are made of wrought tin alloys; these are itemized in Table 7.5.

In bimetallic bearings the antifriction layer is made of bronzes with an increased lead content and without tin or with a small amount of tin. The first type is exemplified by a widely used bronze Grade БрС30 which contains 30 percent Pb; the second type contains 22 percent Pb and 1 percent Sn. For monometallic bearings use is sometimes made of lead bronze Grade БрОС5-25 (5 percent Sn and 25 percent Pb).

Table 7.5

Composition (% , copper — balance) of wrought bronzes

Grade	Main components, %			GOST or Specifications (TU)
	Sn	P	Ni	
БрОФ6.5-0.15	6.0-7.0	0.1-0.25	—	GOST 5017-74
БрОФ6.5-0.4	6.0-7.0	0.3-0.4	—	
БрОФ7.0-0.2	7.0-8.0	0.1-0.25	—	GOST 5017-74
БрОФ8.0-0.3	7.5-8.5	0.25-0.35	0.1-0.2	TU 48-21-214-72
БрОФ6.5-0.4	6.0-7.0	0.3-0.4	0.1-0.2	GOST 5017-74
БрОЦСЧ-4-2.5*	3.0-5.0	—	—	

* Contains 3.0-5.0% Zn and 1.5-3.5% Pb.

Alloys containing no tin have also found relatively wide use. Some of them are not only as good as those with tin, but also have better properties. The chemical composition and application of such alloys are presented in Table 7.6.

Table 7.6

Composition (%) of tinless bronzes

Grade	Cu	Sb	Pb	P	Alloys replaced	Application
БрCyФ6-12-0.3	81.7	6.0	12.0	0.3	БрОС8-12 БрОС10-10	Bushings, valve spools, sliders and other components operating at high sliding speeds
БрCyHЦСФ-3-3-20-0.2	69.3	3.5	20	0.2	БрОС10-10 БрОС8-12	Bearings exposed to sea and fresh water and aggressive liquids
БрCyH6-2 БрCyФ6-1	91.3 93.0	6.0 6.0	— —	— 1.0	БрОФ10-1	Antifriction components
БрКМц3-1	96.0	—	—	—	БрОЦ10-2 БрОЦ4-3 БрОЦ8-4 БрОЦС6-6-3 БрОЦС5-5-5	Springs, bushings, and form castings

Note. Bronze БрCyH6-2 also contains 2.0% Ni and 0.7% Zn; bronze БрКМц3-1 contains 3.0% Si and 1.0% Mn, and bronze БрCyHЦСФ-3-3-3-20-0.2 contains 3.5% Zn and 3.5 Ni.

For heavy-duty rubbing components (in road construction machines, heavy machine tools, movable joints of thermal engineering equipment, etc.) use is made of high-strength aluminium bronzes [14]. The composition and mechanical properties of some aluminium bronze grades used in the Soviet engineering industries are given in Table 7.7.

Table 7.7

Composition (%) and properties of aluminium bronzes

Grade	Al	Ni	Mn	Fe	σ_t , kgf/mm ²	δ , %	Casting method
БрАМц9-2Л	8-10	—	1.5-2.5	—	40	20	K
БрАМц10-2	9-11	—	1.5-2.5	—	50	12	S, K
БрАЖ9-4Л	9-10	—	—	2-4	40	10	S
БрАЖМц10-3-1.5	9-11	—	1.0-2.0	2-4	50	12	K
БрАЖН10-4-4Л	9.5-11.0	3.5-5.5	—	3.5-5.5	60	5	K
БрАЖН11-6-6	10.5-11.5	5.0-6.5	—	5.0-6.5	60	2	K

Designations. K—permanent mould casting; S—sand casting.

Brasses (alloys of copper with zinc and some other metals) are used as antifriction materials to a lesser degree than bronzes. The alloys known as silicon brasses, manganese brasses [24, 27], and aluminium ferrous brasses (GOST 17711-72) have found application as antifriction materials. Their chemical composition, properties, and applications are given in Table 7.8.

Table 7.8

Composition (% , zinc — balance) and properties of antifriction brasses

Grade	Cu	Mn	Pb	σ_t , kgf/mm ²	δ , %	Application
ЛАЖ60-1-1Л*	58-61	0.1-0.6	—	40	20	Fittings, bushings, bearings
ЛКС80-3-3**	77-81	—	2.0-4.0	30-40	15-25	Bearings, bushings
ЛМцС58-2-2	57-60	1.5-2.5	1.5-2.5	30-42	20	Bearings, bushings and other components, including backings for railway vehicle bearings

* Contains 0.8-1.5% Al; 0.8-1.5% Fe.

** Contains 2.5-4.5% Si.

Copper-base alloys are very common materials all over the world. They differ very little in chemical composition. To illustrate that, Table 7.9 presents standard bronze grades employed in the FRG [32] and in the USA [33].

Table 7.9

Composition (%) of bronzes used in FRG and USA

Grade	Standard	Cu	Pb	Sn	Zn	Other elements
<i>Bronzes used in FRG</i>						
GCuPb22Sn	DIN4716	84	22	1	—	—
GCuPb10Sn	DIN4716	80	10	10	—	—
GCuSn7ZnPb	DIN4705	83	6	7	4	—
GCuSn10	DIN4705	90	—	10	—	—
GCuSn8	DIN47662	92	—	8	—	—
CuZn31Si	DIN47660	68	—	—	31	1AS
CuAl19Mn	DIN47665	88	—	—	—	3Mn
<i>Bronzes used in USA</i>						
Leaded copper	SAE480	65	35	—	—	—
Leaded copper	SAE48	70	30	—	—	—
Lead-tin bronze	AMS4840	70	25	5	—	—
Semi-plastic bronze	SAE67	78	16	6	—	—
Red brass castings	SAE40	85	5	5	5	—
Bronze bearing castings	SAE660	83	7	7	3	—
Phosphor bronze	SAE64	80	10	10	—	1.0P
Hard bronze	SAE62	88	2	—	2	—
Hard bronze	SAE620	88	4	—	4	—
Leaded gun metal	SAE65	88	2	10	—	—
Aluminium bronze	ASTMB148-52-9C	85	—	—	—	4Fe, 11Al

7.1.3. Aluminium-Base Alloys

The use of aluminium-base bearing alloys in the USSR and other countries has markedly increased over the past decade. These alloys have a fairly adequate fatigue strength, good resistance to corrosion in the presence of lubricants, relatively high resistance to scoring, and good antifriction properties. Such qualities can account for the trend towards the substitution of these alloys for lead- and tin-base antifriction alloys and lead bronzes.

Aluminium alloys are used for monometallic parts (bushings, bearings, pin joints, etc.) and for bimetallic bearings. The latter are stamped from a bimetallic (laminated) strip or band with an aluminium lining bonded to the steel backing during their plastic deformation in rolling. Monometallic bearings are made of relatively strong and hard alloys, whereas plastic alloys of lower hardness are used for bimetallic-bearing linings.

Aluminium alloys are mainly classified by microstructure [3]. Such a classification is more indicative of the alloys' antifriction properties, since the role of soft structural components in reducing wear and improving the antiscoring properties of rubbing components is universally acknowledged. The group I contains alloys having inclu-

sions of hard structural components (FeAl_3 , Al_3Ni , CuAl_2 , Mg_2Si , AlSb , silicon, etc.) in the alloy's plastic matrix. The alloys of the group II have soft inclusions in addition to hard ones.

In the USSR, aluminium-base alloys are standardized by GOST 14113-69 (Table 7.10).

Table 7.10

Composition (% , aluminium — balance) of aluminium antifriction alloys

Group	Grade	Ni	Mg	Sb	Cu	Si	Sn	Ti
I	AH-2.5	2.7-3.3	—	—	—	—	—	—
	ACM	—	0.3-0.7	3.5-6.5	—	—	—	—
II	AO9-1	—	—	—	1.0	—	9.0	—
	AO3-1	0.4	—	—	1.0	1.85	3.0	—
	AO9-2	1.0	—	—	2.25	0.5	9.0	—
	AO9-2B	—	—	—	1.75	—	9.0	0.02-0.10
	AO20-1	—	—	—	1.0	—	20.0	0.02-0.10

In other countries, the group II alloys have been used wider, but the group I alloys have also found relatively extensive use over the past few years. Detailed data on the chemical composition of the alloys are given in [19]; those on the most common alloys are presented in Table 7.11.

Table 7.11

Composition (% , aluminium—balance) of aluminium-base alloys used in various countries

Grade	Sn	Ni	Cu	Si	Cd	Pb	Mg
SAE770 (USA)	6.5	1.0	1.0	—	—	—	—
SAE780 (USA)	6.5	0.5	1.0	1.5	—	—	—
SAE781 (USA)	—	—	—	4.0	1.0	—	—
AS-15 (UK), SAE783 (USA)	20.0	—	1.0	≤ 0.15	—	—	—
Al-Pb alloy	—	—	≤ 1.0	—	—	≤ 8.0	—
KS1275 (FRG)	—	1.0	≤ 1.0	13.0	—	—	1.0
AS-78 (UK)	—	—	1.0	11.0	—	—	—

With the emergence in recent years of high-power engines in the automotive, tractor, and transport engineering industries, urgent need has arisen for bearing materials with improved resistance to scoring. To solve the problem, special alloys of aluminium with tin are being developed in the USSR, Japan, Great Britain, and the USA. Such alloys contain up to 30 and even 40 percent Sn. Methods of ob-

taining alloys which contain Pb are also at the development stage. According to Pratt [30], alloys of this type exhibit good resistance to scoring in the presence of ultra-thin layers of lubricant, but this property is the most fully realized with a Pb content of 14 percent and over. A method for obtaining bearing materials from alloys of aluminium with lead (up to 30 percent Pb) in granular form [19] has been developed in the USSR. The grains are formed in a barrel with round holes, which rotates at 1,500 rpm. A stream of liquid alloy breaks into drops which get through the holes into water and solidify at a rate of 10^2 to 10^4 °C/s.

The subsequent processing of the grains is done by various methods. Extrusion in worm-type extruders has proved effective. The blanks obtained lend themselves to forming by pressure; they are rolled together with steel strips for subsequent manufacture of bimetallic bearings.

7.1.4. Zinc-Base Alloys

Although they have been known as antifriction materials since long ago, zinc-base alloys have found limited use. However, these alloys have some valuable features, which often make it possible to utilize them instead of bronzes and babbitts.

Zinc-base alloys having a low melting point (about 400°C) soften on heating to a greater extent than bronze and aluminium alloys, and so run in easier. For this reason, zinc-alloy bearings cause less wear to the mating journals in the presence of abrasive particles. The latter penetrate into the rubbing surface of the bearing, this resulting in reduced damage to the journal from microcutting.

Zinc alloys are readily processed for both monometallic and bimetallic products. A zinc alloy can be bonded to a steel backing by casting [20] or by rolling [3]. The bonding of the molten alloy to the steel backing is effected by a layer of liquid zinc applied by the hot zinc-plating method.

Bearings and other components made of zinc alloys are obtained by casting and forming (rolling, pressing) methods. The chemical composition of standard alloys (GOST 21437-75) and their properties in cast or wrought states are presented in Table 7.12.

As distinct from bronze and aluminium alloys, zinc alloys have increased strength and plasticity after hot rolling at 250 to 300°C, their fatigue strength being also improved. For instance, the IIAM9-1.5 Grade cast alloy in the form of round specimens subjected to rotation and alternating bending showed a fatigue strength of 5.0 kgf/mm², whereas in similar conditions the fatigue strength of the rolled alloy increased to 10-11 kgf/mm² [3].

Zinc-base alloys as antifriction materials have found wide-spread use in the USSR, particularly in railway vehicles [3, 20]. In

other countries zinc alloys are utilized for this purpose on a relatively small scale. The chemical composition of some common zinc alloys used in these countries is given in Table 7.13.

Table 7.12

Composition (% , zinc — balance) of standard zinc alloys used in the USSR

Grade	Main components			Properties					
	Al	Cu	Mg	cast alloys			wrought alloys		
				σ_t , kgf/mm ²	δ , %	HB	σ_t , kgf/mm ²	δ , %	HB
				not less than					
ЦАМ9-1.5	9.0-11.0	1.0-2.0	0.03-0.06	25	1.0	95	30	10.0	85
ЦАМ10-5	9.0-12.0	4.0-5.5	0.03-0.06	25	0.4	100	35	4.0	90

Table 7.13

Composition (% , zinc — balance) of zinc alloys used in various countries

Grade	Chemical composition, %			
	Al	Cu	Mg	Mn
1010 (FRG)	9-11	0.6-1.0	0.02-0.05	—
410 (FRG)	3.7-4.3	0.6-1.0	0.02-0.05	—
Japan	10	2	—	0.2
Alzen 305 (Austria)	30	5	—	—

7.1.5. Ferrous Alloys

Steels as antifriction materials are employed relatively rarely and only for very light operating conditions at low specific pressures and sliding speeds. Being hard and having a high melting point, steel poorly runs in and tends to seize with the mating journal and develop scoring. The usual grades are the so-called copper steels with a low carbon content, or graphitized steels having inclusions of free graphite. The chemical composition of some steel grades recommended as substitutes for bronze in light operating conditions [15] is given in Table 7.14.

Cast iron is used for bearings and other rubbing parts in greater quantities and varieties than steel. The antifriction properties of cast iron are largely determined by the structure of the graphite constituent. Iron with graphite in a globular or thick-plates form is more wear-resistant than that with thin graphite plates. The structure of an antifriction cast iron should have the minimal amount of

Table 7.14

Composition (% , iron — balance) of antifriction steels

Grade	Cu	Al	C	Si	Mn	S	P
Copper steel	32	2.5	0.1	—	—	—	—
Graphitized steel	—	—	1.6	1.0	0.3	≤ 0.03	≤ 0.03

free ferrite (under 15 percent) and no free cementite [18]. The chemical composition of the most commonly used cast iron grades is given in Table 7.15.

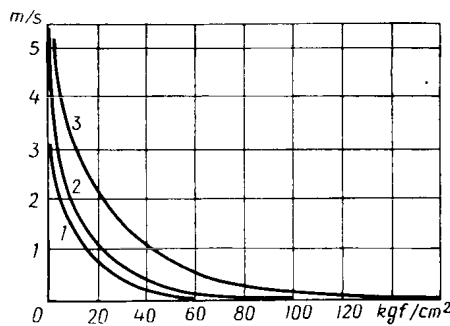


Fig. 7.1. Graphs of sliding speed vs permissible specific load for antifriction cast irons

1—Grade И5; 2—Grades ЧЧ1 and ЧЧ2; 3—Grade Б

Table 7.15

Composition (% , iron — balance) and hardness of the most common antifriction cast irons (GOST 1585-70)

Grade	C	Si	Mn	Ni	Cr
AЧC-1	3.2-3.6	1.3-2.0	0.6-1.2	0.3-0.4	0.2-0.4
AЧC-2	3.2-3.8	1.4-2.2	0.4-0.7	0.2-0.4	0.2-0.4
AЧC-3	3.2-3.8	1.7-2.6	0.4-0.7	≤ 0.3	≤ 0.30
Malleable AЧK-1	2.3-3.0	0.5-1.0	0.6-1.2	—	—
High-test cast iron AЧБ-1*	2.8-3.5	1.8-2.7	0.5-1.2	—	—

Grade	Cu	P	S	HB
AЧC-1	1.5-2.0	0.15-0.30	≤ 0.12	180-262
AЧC-2	—	0.15-0.4	≤ 0.12	180-229
AЧC-3	—	0.15-0.4	≤ 0.12	160-190
Malleable AЧK-1	1.0-1.5	0.2	≤ 0.08	187-262
High-test cast iron AЧБ-1 *	≤ 0.7	0.2	≤ 0.03	—

* Contains ≥ 0.03% Mg.

Composition and main specifications of metal-ceramic bearings

Grade	Composition, %	Density, g/cm ³	Porosity, %	σ_t , kgf/mm ²	σ_c , kgf/mm ²	HB	Impact strength, kgf/cm ² (specimens without notches)	Coefficient of friction with lubrication	Permissible load, kgf/cm ² (at $v = 2-3$ m/s)	Maximum permissible working temperature, °C
Porous iron	100 Fe	6.0-6.5	18-22	12-14	30-40	40-55	1.6-2.0	0.019-0.023	40-45	100-120
ЖГр-1-20пф	99.0 Fe + 1.0 graphite	6.0-6.3	17-23	14-18	40-45	60-100	0.3-0.6	0.06-0.09	34-38	100-120
ЖГр-2-20пф	98.0 Fe + 2.0 graphite	5.8-6.2	17-23	14-16	38-42	50-80	0.25-0.35	0.06-0.09	34-38	100-120
ЖГр-3-20пф	97.0 Fe + 3.0 graphite	5.5-6.0	17-23	12-14	30-35	50-80	0.18-0.22	0.04-0.06	40-45	100-140
ЖГр-3-Д-3	94.0 Fe + 3.0 graphite + 3.0 copper	5.7-6.2	22-27	25-35	120-130	70-100	0.4-0.8	0.04-0.07	50-70	120-150
ЖГр-3-Ц-4	93.0 Fe + 3.0 graphite + 4.0 ZnS	5.4-5.8	17-23	12-14	75-80	60-100	0.15-0.25	0.001-0.0075	80-100	up to 150
ЖГр-4-Д-3	96.0 Fe + 1.0 graphite + 3.0 Cu ₂ S	6.2-6.3	18-22	—	90-120	90-120	0.4-0.5	—	80-100	up to 150
АЖГр-6-3	90 Al + 6 Fe + 4 graphite	2.6-2.8	5-10	—	14-15	20-24	0.4-0.5	0.005-0.008	40-60	100-120
АМГ-10-3	87.0 Al + 10.0 Cu + 3.0 graphite	2.8-2.9	5-10	—	23-24	30-35	—	—	35-50	100-120
БрОГ10-2	88 Cu + 10.0 Sn + 2 graphite	6.0-6.8	20-25	—	50-60	18-20	—	0.004-0.008	25-30	80-90

Note. Пф ~ perlitic-ferritic structure.

Antifriction cast iron is limited in application to light operating conditions. The recommended ranges of specific pressures and sliding speeds are shown in Fig. 7.1 (the grades cited are specified by GOST 1585-70).

7.1.6. Sintered Alloys

Diverse porous antifriction components are produced by pressing or rolling with subsequent sintering of ferrous or copper-base powders. Prior to mounting, such components are saturated with oil. As a rule, components of this type are used for operation with a scanty lubricant supply, although they provide stable performance with copious quantities of lubricant (fluid friction) as well [17].

Self-lubricating powders of graphite, molybdenum disulphide, boron nitride, and some others are indispensable additives to the ferrous and copper-based components. A ferrous composition usually contains graphite which, depending on its grade, has a significant effect on the mechanical and antifriction properties. Table 7.16 presents the properties and chemical composition of the most common porous alloys based on iron, aluminium and copper.

7.2. COMPARATIVE EVALUATION OF BEARING MATERIALS PROPERTIES

7.2.1. Fatigue Strength

Engine bearings, various bushings, pin joints, and other components break down owing to the formation and development of fatigue cracks. The effect manifests itself as through cracks in monometallic bearing (Fig. 7.2a) and as pitting of the antifriction layer in bi-metallic bearings (Fig. 7.2b). Another effect, as distinct from this macrocracking, is the breaking of individual asperities, which is classified as fatigue wear [13] due to repeated excessive deformation.

The breakdown of bearings due to the pitting of the antifriction layer has especially often been observed in recent years with the development of heavy-duty engines for automobiles, tractors, ships, diesel locomotives and so on. Increased loads and high rotational speeds have placed new, higher demands on bearing performance.

Fatigue failure of bearings occurs mainly under the action of pulsating compressive stresses. Despite distinctions in the properties of various bearing alloys, the character of fatigue defects is basically the same. In all cases surface destruction emerges at the spots with maximum contact stresses, surface defects, or microstructure deficiencies. A crack grows into the lining depth, extends down to the backing and then expands throughout the interface layer, which

as a rule is weaker than the main lining metal. Cracking in antifriction layers develops slower than in structural parts, so bearings have a comparatively longer life.

The process of fatigue cracking in bearings runs under specific conditions. The sliding surface of the antifriction layer is subject to

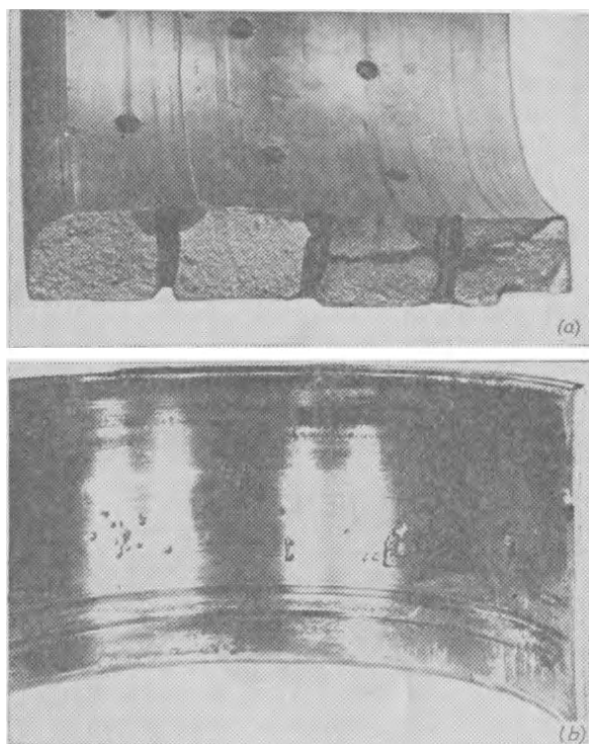


Fig. 7.2. Fatigue failures
(a) of a monometallic bushing from zinc alloy Grade IIAM9-1.5; (b) of a leaded bronze bearing lining of the Model M756 diesel engine

variable loads transmitted through a lubricant film having a definite surface activity. The frictional conditions vary from fluid to boundary and even dry friction. Substantial variations are also observed in the temperature of the rubbing surfaces. Therefore fatigue processes in bearing materials are determined not only by cracking due to variable loading, but also by heat-, corrosion- and friction-induced stresses. Considered below are the factors influencing the process of fatigue.

The character and magnitude of load. In an actual bearing carrying an unstable load, the acting forces vary depending on the angle of journal rotation; in addition, long-term maximum loads due to gas pressure and inertial forces also have substantial variations. Si-

multaneously, the bearing is subjected to the action of static compressive stresses due to its pretightening, and to heating stresses which are particularly tangible when the linear expansion coefficients of the bearing and of the housing are substantially different. The failure of bearings, as mainly dependent on the action of inertial forces, is reported in [7, 8]. This can account for fewer bearing break-

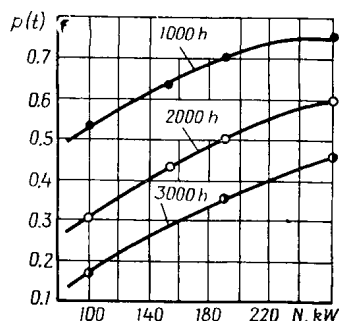


Fig. 7.3. Relationship between reliability function $P(t)$ and load with various running times for Model ЧН25/34 diesel-engine bearings

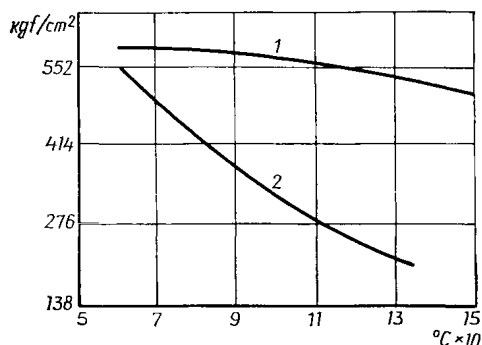


Fig. 7.4. Fatigue strength as a function of test temperature (determined on the Sapphire Model testing machine)
1—for aluminium tin alloy; 2—for tin-base white metal

downs with increased operating loads of the Model ЧН25/34 mode-rate-speed marine diesel engine [7], as illustrated in Fig. 7.3.

The emergence and development of cracks is considerably influenced by tensile stresses. The latter often result from bearing design features, operating conditions, etc.

Depending on the material, bearings respond differently to heating. With soft babbitt-metal bearings, the fatigue strength sharply drops with increased temperature, which is shown on the diagram in Fig. 7.4. The same level of heating only slightly reduces the fatigue strength of aluminium and copper alloys.

With bimetallic bearings, temperature variations lead to a change in the magnitude and direction of residual stresses in the antifric-tion layer [28]. The temperatures of bimetallic strips, at which residual stresses change direction (change-over from tensile to compressive stresses upon heating) are given in Table 7.17.

As operating temperatures usually exceed $60^{\circ}C$, residual compressive stresses are bound to occur in bearings of aluminium and zinc alloys.

Temperature variations within the range causing the change of stress direction may promote the formation of fatigue cracks. A discrete character of friction leads to local overheating areas where maximum contact stresses arise from the action of external forces. In

Table 7.17

Heating temperatures at which residual stresses change direction

Grade	Plate thickness, mm	Ratio between thicknesses of alloy layer and Armko iron layer	Number of specimens	Average temperature, θ , °C, of the beginning of plastic deformation on heating, and respective specimen deflection, Δh , mm				Average temperature at which residual stresses change from tensile to compressive, °C	
				initial test		subsequent tests		initial test	subsequent tests
				t	Δh	t	Δh		
AO9-1	4.6	1 : 2.0	6	85.6	0.476	115.7	0.786	32.8	47.8
	6.2	1 : 2.8	3	90.0	0.257	105.6	0.360	35.0	42.8
	8.0	1 : 3.4	4	92.0	0.300	130.0	0.556	36.0	55.0
	10.0	1 : 4	4	75.7	0.170	143.5	0.440	27.9	61.8
ЦАМ9-1.5	4.6	1 : 2	3	74.0	0.53	97.1	0.823	37.0	38.5
	6.2	1 : 2.8	3	93.3	0.26	128.3	0.462	46.6	54.2

this case, combined stresses may exceed the permissible level. Consequently, fatigue cracking may develop after a short period of service.

Physical properties of alloys. In addition to the difference in linear expansion coefficients, which determines the level of residual stresses in bimetallic bearings, the value of the elasticity modulus is sometimes taken into account when evaluating fatigue strength. For some groups of alloys a change in the chemical composition leads to a change in the modulus of elasticity. Such, for instance, are lead-base alloys containing antimony. Using this distinctive feature, a criterion of fatigue strength was suggested [21] for lead-base alloys:

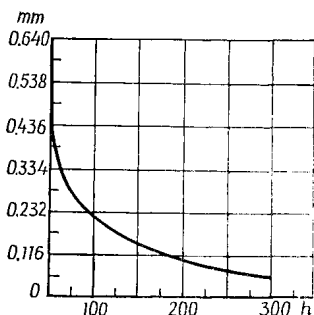


Fig. 7.5. Relationship between babbitt-layer thickness and bearing life (mean load 93 kgf/cm²)

$$\varepsilon_{-1} = \sigma_{-1}/E$$

where σ_{-1} = fatigue limit.

In agreement with this criterion, alloys with a smaller modulus of elasticity will have a greater fatigue strength at equal deformations.

Bearing design features. The thickness of an antifriction lining is significant for its fatigue strength. The greatest fatigue strength is found in linings several hundredths of a millimeter thick (Fig. 7.5). Such layers of soft metal are regarded as surface coatings. Being deposited on a strong backing, they facilitate running-in and often wear out sooner than develop fatigue failures. In such situations, the

strength of babbitt metal is commensurable with that of lead bronze or aluminium alloys. The bearing design features (width-to-diameter ratio, configuration of sliding surfaces, oil grooves, coolers, diametrical clearances in different sections, etc.) are selected with a view to improving the hydrodynamic characteristics, and hence, the fatigue strength. The aim is to arrive at a design which excludes boundary friction, providing reduced maximum pressures in the lubricant film. An instance of such a design is bearings without any grooving in the Model Д100 diesel locomotive engine. The oil film thickness was increased three times, resulting in a sharply increased life of the bearings, which have the БК2 Grade babbitt linings.

The formation and spreading of fatigue cracks is also caused by burrs, nicks, dents, scratches and other surface defects, which are sources of stress concentration. The stresses are especially tangible in bearings where the antifriction lining is mechanically attached to the housing. Thus, for instance, blisters in the babbitt lining of railway carriage bearings cause cracking already after two months of running [3].

Lubrication. In the process of friction, the lubricant acts upon the bearing and journal materials and affects the service properties of the bearing. For instance, oils containing organic acid solutions cause selective corrosion of the lead constituent in lead bronze bearings [9] and so reduce the fatigue strength. The corrosion intensifies with rising temperature and with water getting into the oil. The grade of oil has a significant effect on lead corrosion. For example, tests of lead bronze on the Model ДК2 ХАММ testing installation [3] showed that its corrosion in oil Grades М12 and М12Б was considerably stronger than in other oils (Fig. 7.6).

For some bearing materials the aggressive action of a lubricant with antisludge additives capable of removing oxide films from the antifriction alloy also reduces the fatigue strength. An example is a shorter useful life of Grade БК2 lead-babbitt bearings in diesel locomotive engines with the use of oils containing Grades ВНИИ ПИ-366 and ЦИАТИМ-339 additives.

Fatigue strength data. A great body of information has been collected on the fatigue strength of bearing materials. Resistance to cracking for various bearing materials was determined by testing specimens in testing machines, laboratory installations, and other devices simulating the operation of bearings.

Table 7.18 presents data on the fatigue strength of various bearings reported by Glacier Metal Co.

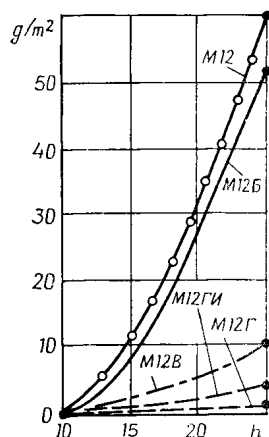


Fig. 7.6. Corrosive effect of oil as a function of its oxidation

Table 7.18

Fatigue strength of bearing alloys

Test equipment	Antifriction material	Fatigue strength, kgf/mm ²	Fatigue strength relative to that of babbitt
Laboratory installation (test for 10 ⁷ cycles)	Tin babbitt	1.40	1.00
	Cu-35% Pb	2.66	1.90
	Al-6.5% Sn-1% Ni-1% Cu, cast	4.23	3.05
Underwood testing machine	Tin babbitt	0.56-1.05	1.00
	Cu-35% Pb	1.05-1.75	1.73
	Tin babbitt, 0.1 mm thick	1.40-2.80	2.60
	Cu-Pb with Sn or Ag	2.10-2.80	3.02
	Aluminium alloys	2.80-3.50	3.92
Viking testing machine	Tin babbitt (7% Sb, 8% Cu)	1.33	1.00
	Lead babbitt (1% Sn, 15% Sb, 1% As)	1.30	0.97
	Cu-Pb lined with alloy Pb+10% Sn, 0.04 mm thick	2.87	2.16
	Cu-Pb lined with alloy Pb-5% In, 0.04 mm thick	2.87	2.16
	Cu-30% Pb, sintered	2.38	1.79
	Al-20% Sn-1% Cu, bimetal lining on steel backing	3.22	2.42
	Cu-22% Pb-4% Sn, sintered	3.85	2.90

Of interest are also data from the same company on maximum pressures that can be taken up by bearings without pitting

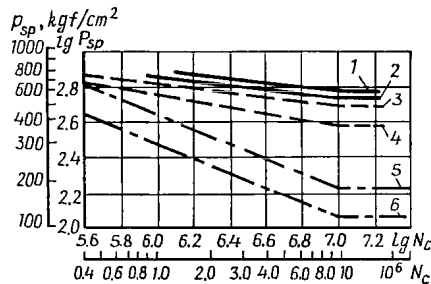


Fig. 7.7. Fatigue curves for bearings of various materials (journal made of steel Grade 45, induction hardened to *HRC* 56-58, lubrication with oil Grade ДП114)

1, 3, 5—for alloy Grades AO20-1, BpC30 and B83, respectively, tested at a speed of 7 m/s;
2, 4, 6—for the same alloys tested at a speed of 9 m/s

(Table 7.19) and relative fatigue characteristics for various bearing alloys (Table 7.20).

Extensive research has recently been conducted [10] into the fatigue strength of bearing linings (Table 7.21). The data can be used

with a fair degree of confidence for the selection of bearing alloys.

Table 7.22 also presents test data on the fatigue strength of various bearings.

In testing bearings at the ЦНИИИ research institute, fatigue strength diagrams were constructed for two journal rotational speeds. The tests were carried out on a modified Sapphire testing machine which makes it possible to change load and rotational speed within a wide range. The results are shown in Fig. 7.7.

Table 7.19

Permissible specific pressures on bearings made of various materials

Antifriction material	Specific pressure causing pitting, kgf/cm ²	Ratio between maximum specific pressure for given material and that for tin babbitt
<i>Underwood testing machine</i>		
Tin babbitt	70	1.00
Cadmium alloys	75	1.07
Lead bronze	120	1.70
Thin babbitt layer (0.07 mm thick)	180	2.60
Lead bronze with addition of silver or tin	210	3.00
Aluminium alloys	270	3.90
Silver	300	4.35
Bronze	600	8.70
<i>Glacier testing machine</i>		
Tin babbitt (7% Sb, 3% Cu)	140	1.00
Lead babbitt (15% Sb, 1% Sn, 1% Cu)	140	1.00
Lead bronze with soft lining	300	2.10
Alloy 70% Cu, 30% Pb, metal ceramic	250	1.80
Alloy 60% Cu, 40% Pb, metal ceramic	220	1.55
Alloy 74% Cu, 22% Pb, 4% Sn, metal ceramic	400	2.90
Alloy 20% Sn, 1% Cu, aluminium—balance	340	2.40

Table 7.20

Relative wear life of various alloys

Antifriction material	Relative wear life	Recommended minimum hardness of journals, HB
Tin babbitt	1.0	160
Lead babbitt	1.0	160
Lead bronze (sintered, with electrodeposited lead-tin alloy)	1.8	230
Lead bronze (sintered) without lining	1.9-2.1	280
Lead bronze (sintered) with fused lead-tin alloy lining	1.9-2.1	280
Aluminium-tin alloy (20% Sn, 1% Cu)	2.5	200

Table 7.21

Fatigue limits of antifriction linings

Antifriction alloy	HB	Fatigue limit, kgf/mm ² , for bearing	
		52.7 mm in diameter, 29.5 mm in length	54.0 mm in diameter, 20.5 mm in length
Tin babbitt (SAE12) 0.25 mm thick	28-33	3.5	—
Lead babbitt (SAE15) 0.25 mm thick	17-22	3.5	—
Aluminium alloy:			
20% Sn, 1% Cu	38-43	9.1-10.5	10.5
10% Pb, 4% Si	—	9.1-10.5	—
6% Sn, 1% Cu, 1% Ni	42-47	9.8-10.5	—
6% Sn, 1% Cu, 1% Ni, lined with alloy Pb+10% Sn, 0.025 mm thick	—	10.85	—
Sintered lead bronze (30% Pb), lined with alloy Pb+10% Sn 0.025 mm thick	40-50	11.2-12.6	11.9
Cast lead bronze (24% Pb, 1% Sn), lined with alloy Pb+10% Sn+2% Cu 0.025 mm thick	50-60	—	11.9
Aluminium alloy (11% Si, 1% Cu, 1% Mg, 1% Ni), lined with alloy Pb+10% Sn 0.025 mm thick	55-65	> 12.6	—

7.2.2. Running-in

Rubbing surfaces run in through plastic deformation and wear. Plastic deformation develops mainly in bearings with a soft anti-friction layer and relatively loose fitting. With greater hardness of a bearing alloy at working temperature and higher resistance to local plastic deformations, it takes longer for the bearing to run in, all other things being equal. The properties of bearing alloys at working and room temperatures are given in Table 7.23.

The run-in process can be expressed by the wear rate or operating temperature as a function of running time (Fig. 7.8).

In the presence of abrasive particles, the run-in process accelerates as the path of the particles moving between the journal and the lining grows in length. The latter depends on the sliding speed and on the penetration of the particles into the antifriction layer. The penetration is determined by the lining hardness and the relation between the rate of work-hardening of the material and that of its loosening under the action of the heat generated as the particles are pressed into the lining surface. The latter effect largely depends on the temperature of recrystallization, whose values for a number of alloys are given in Table 7.23.

Table 7.22

Fatigue strength of bearing alloys (data by the Zavolzhsk Motor Works)

Chemical composition of bearing lining material	Thickness of active layer, mm	Fatigue strength, kgf/cm ²	Relative fatigue strength
Alloy COC 6-6 (6% Sb, 6% Sn, Pb—balance)	0.37	135	1.0
	0.16	150	1.1
	0.10	164	1.22
	0.07	187	1.38
	0.04	220	1.63
Durex-100 type bearings (40% Ni and 60% Cu sintered and lined with alloy COC6-6)	0.08-0.12	170	1.26
Alloy AO20-1 (1% Cu, 20% Sn, Al—balance)	0.3-0.4	470	3.5
	0.63	430	3.18
	0.13	540	4.0
Alloy AMO-1-6 (1% Cu, 6% Sn, 0.5% Ni, Al—balance)	0.3-0.4	555	4.11
The same lined with alloy 90%Pb+10% Sn 0.01-0.02 mm thick	0.3-0.4	555	4.11
Glacier bearings (30% Pb, 70% Cu, sintered and lined with alloy 90% Pb+10% Sn 0.01-0.2 mm thick)	0.35	430	3.18
Vanderwell bearings (23% Pb, 1.5% Sn, 0.5% Fe, Cu—balance), lined with alloy 90% Pb+10% Sn 0.033 mm thick	—	430	3.18
The same, with lining 0.019 mm thick Glucobearings (21.5% Pb, 1.5% Sn, 0.3% Fe, Cu—balance), lined with alloy 8.5% Sn + 2% Cu + Pb 0.026 mm thick	—	510	3.78
	—	550	4.07

Table 7.23

Properties of bearing alloys at elevated temperatures

Grade	Mechanical properties						Recrystallization temperature, °C
	at +20°C			at +100°C			
	σ_c , kgf/mm ²	δ , %	HB	σ_c , kgf/mm ²	δ , %	HB	
Б83	9.1	6.0	29.0	6.1	15.2	14.5	80
Б16	8.6	0.2	27.4	5.6	0.4	17.5	100
БКА	11.8	2.5	20.0	7.8	10.0	16.0	120
ЦАМ9-1.5	32.2	4.0	98	20.0	7.4	50.0	180
АО20-1	5.0	12.8	36	4.0	15.0	30.0	200
БрС30	8.4	5.0	28.0	7.4	6.0	26.0	300

The run-in process will also accelerate if wear is accompanied by the transfer of metal and the formation of protective metal films, which can be observed in alloys having a soft structural constituent (BpC30, AO20-1, AO9-1, and some others). When seizure is accompanied by tearing in depth, and build-up of the material occurs, the run-in process is impeded. This effect does not take place if the rule of a positive gradient of mechanical properties, formulated by I. V. Kragelsky [13], is obeyed. The running-in is more effective when the interaction between sliding surfaces involves the loosening of the antifriction alloy at the contact areas, which takes place in frictional conditions bordering on seizure [11]. The running-in process is also facilitated in selective transfer conditions [5], when interaction with the lubricant at the sliding interface leads to a selective corrosion of the alloy's chemically more active constituents. In copper alloys such constituents are zinc, tin, etc.

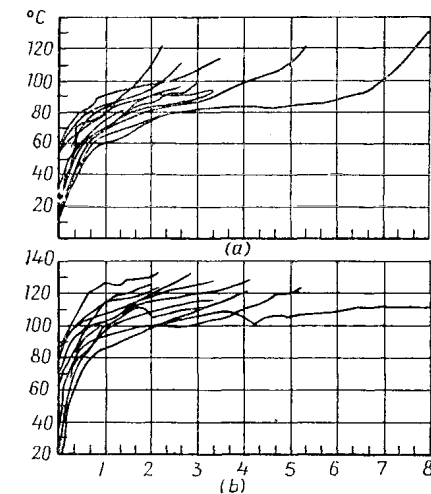


Fig. 7.8. Variation of temperature with time during tests of babbitts in railway vehicle sliding bearings (a) alloy Grade BKA; (b) alloy Grade BC1

the alloy's chemically more active constituents. In copper alloys such constituents are zinc, tin, etc.

7.2.3. Wear Resistance

Most data on the wear resistance of bearing alloys pertain to a steady-state operation of the rubbing parts.

Information on wear is given as comparative data obtained in testing various tribological joints under laboratory and actual service conditions. Some data on comparative wear resistance of various antifriction alloys are given below.

Table 7.24

Relative wear of shaft journals

Bearing alloy	Relative wear of journal	Bearing alloy	Relative wear of journal
Babbitt Grade E83	1.0	Aluminium alloy Grade AO9-2 with lining (10% Sn, 90% Pb)	1.95
Leaded bronze Grade BpC30	4.0	Alloy Grade AO9-2 with lining containing molybdenum disulphide	1.45
Aluminium alloy Grade AO9-2	3.5		

Table 7.24 presents relative values of wear for steel shaft journals run in various bearings, as obtained in testing on the Underwood test rig; the test pressure was 50 kgf/cm², journal hardness HB 160-170, and lubrication with oil Grade ДП-11 [4].

The properties of lead bronze and aluminium-tin alloys have been evaluated, as applicable to automobile engines. According to the data reported in [29], automobile engine bearings made of alloy Grade AO20-1 after 10⁶ km of run were found to have smaller clearance changes (Table 7.25).

Table 7.25

Wear of automobile engine bearings

Antifriction material	Clearance increase, mm	
	maximum	average
Binary lead bronze with soft-metal linings	0.014	0.013
Aluminium-tin alloy (20% Sn, 1% Cu)	0.010	0.009

Comparison data obtained in the USSR on the linear wear of automobile engine bearings for two bearing materials (babbitt metals, Grades COC6-6 and AO20-1) are given in Table 7.26.

Table 7.26

Wear of engine bearings in the USSR-made automobiles

Characteristics	Wear rate $I \times 10^4$, $\mu\text{m}/\text{km}$	
	in Gorky city	in Moscow
Average wear of:		
crankshaft journals in steel-aluminium bearings	4.03	2.10
upper steel-aluminium bearings	0.78	0.80
lower steel-aluminium bearings	0.37	0.30
Overall increase of diametrical clearance in steel-aluminium bearings	5.18	3.20
Average wear of:		
crankshaft journals in bearings with standard COC 6-6		
Grade alloy linings	3.24	1.50
upper standard bearings	2.34	2.20
lower standard bearings	1.34	2.00
Overall increase of diametral clearance in bearings with standard linings	6.92	5.70
Ratio between diametral clearance increase values for steel-aluminium bearings and standard bearings	0.75	0.56

Table 7.27

Wear of bearings in engines made by the Chelyabinsk Motor Works

Alloy	Running time, h	Average wear or bearing linings	Average wear of journals	Average journal ovality	Increase of average oil clearance
		mm			
AO9-1	2509	0.025	0.012	0.002	0.034
	3242	0.045	0.010	—	0.045
	2323	0.014	0.018	0.006	0.030
	2365	0.018	0.015	0.006	0.060
ACM	3774	0.082	0.081	—	0.080
	2599	0.052	0.029	0.007	0.073
	2500	0.014	0.027	0.007	0.025
	2500	0.087	0.009	—	—

Of interest are data on wear of the bearings of Models Д108 and Д130 tractor engines, obtained by specialists of the Chelyabinsk tractor factory (Table 7.27).

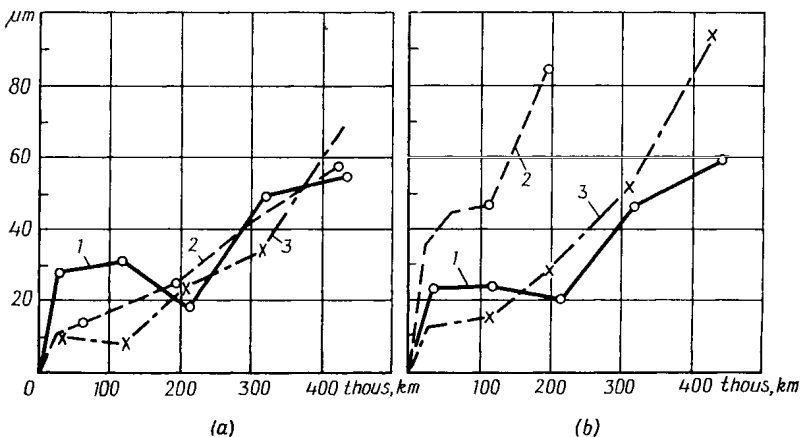


Fig. 7.9. Wear of various antifriction alloys in diesel locomotive engine bearings (a) in crankpin bearings; (b) in main journal bearings; 1—alloy Grade AO9-2; 2—alloy Grade AO3-1; 3—alloy Grade BK2 on a bronze backing

The wear resistance of some antifriction alloys used for heavy-duty locomotive diesel engines is shown in the graphs of Fig. 7.9.

7.2.4. Compatibility of Sliding-Pair Elements

In operation involving boundary or dry friction, resistance to wear and scoring is largely determined by the materials of the bearing and the journal, and by the type of lubricant. The sliding-pair

materials are selected with regard to their compatibility. This is the property of the materials in a given pair, with a given lubricant or without lubrication, to adapt themselves to one another in the process of relative motion so that the required useful life is achieved and any damage to the rubbing surfaces, causing breakdown, is excluded. The compatibility of rubbing materials has been studied by several authors [3, 12, 16, 25].

A prolonged stable operation of rubbing components without any substantial damage is observed in the fluid friction conditions, although corrosion and cavitation of the rubbing surfaces can sometimes be found. Actually, bearings often work in the semi-fluid friction conditions, where both the bulk and the surface properties of oils are effective at the same time. The relative share of boundary and fluid friction in this regime depends on operating conditions (speed, load, oil temperature) which are defined by a dimensionless parameter $\frac{\eta n}{p}$, surface roughness parameters, and, to some extent, the grade of oil. The influence of the bearing and journal materials mainly consists in the ability to form, in the boundary friction conditions, more or less stable boundary films that can increase or reduce friction.

Bowden [2] has found that in boundary friction a chemical interaction of metals with fatty acids contained in oils takes place in addition to a physical adsorption of polar oil molecules. By the ability to react with oil, metals are divided into active (Sn, Cu, Zn, Pb, Al, etc.) and inactive (Ag, Au, Pt, etc.). The first form with fatty acids chemical compositions like metallic soaps, which are good lubricants. Such soaps, produced by chemical reaction with oils, are capable of retaining boundary films up to much higher temperatures. Unlike the boundary films formed by physical adsorption, the soap-base films restore themselves in the process of their disintegration or wear.

The strength of an oil film and the ability to protect the rubbing surfaces from seizure depend on the temperature in the contact zone. The response of the tribological joint to an increase in temperature varies with the oil grade, viscosity, and purity, and it is determined by the materials of the bearing and the journal, and by their surface roughness.

For aluminium and copper alloys, the critical temperature at which desorption of the boundary layer takes place increases with the addition of alloying elements [16]. The friction characteristics (f , M_f) substantially vary with oil temperature. Special tests [19] made it possible to assess the effect of a number of factors, including the materials of rubbing parts, on the emergence of a regime which involves disruption of the oil film. The results of the tests are given below. Figure 7.10 depicts relationships between the friction characteristics and temperature for three types of alloys differing in hardness. The highest temperatures at which boundary friction sets

in have been observed with babbitt metal Grade BK2, the lowest temperature, with the hard zinc alloy, the ACM Grade alloy taking an intermediate position. Lead bronzes have been found to differ sharply from aluminium-tin alloys and aluminium-lead alloys. It

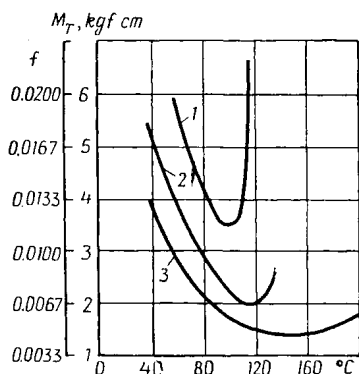


Fig. 7.10. Variation of the friction moment and friction coefficient with the temperature of the diesel engine oil Grade II11 in friction on soft steel (*HB* 150) 1—for alloy Grade IIAM9-1.5; 2—for alloy Grade ACM; 3—for babbitt Grade BK2

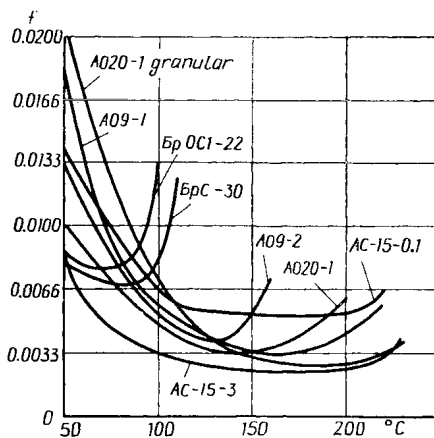


Fig. 7.11. Variation of the coefficient of friction with oil temperature for various alloys

can be easily seen on the graph in Fig. 7.11. Lead bronzes induce the transitional regime at lower oil temperatures. The chemical composition of the tested alloys is given in Table 7.28.

Table 7.28

Composition (% , aluminium — balance) of alloys tested for oil film breaking conditions

Alloy	Sn	Cu	Ni	Si	Pb	HB
AC15-0.5	0.5	—	—	—	15	35
AC15-3	3	—	—	—	15	42.1
AO20-1rp	17-23	0.7-1.2	—	—	—	40.6
AO20-1	17-23	0.7-1.2	—	—	—	20.1
AO9-1	8-10	0.8-1.2	—	—	—	31.6
AO9-2	8-10	2-2.5	0.8-1.2	0.3-0.7	—	54.0
БрО30 *	—	70	—	—	30	34
БрОС1-22 *	1	77	—	—	22	48

* No aluminium.

All other things being equal, the same bearing alloy behaves differently depending on the journal material and the type of lubricant. The introduction of surface active fatty acids into an oil leads to a markedly increased transitional temperature. This influence is well noticeable in Fig. 7.12. The degree of this influence differs depending on the type of alloy. The soft lead babbitt Grade BK2, is more responsive to it.

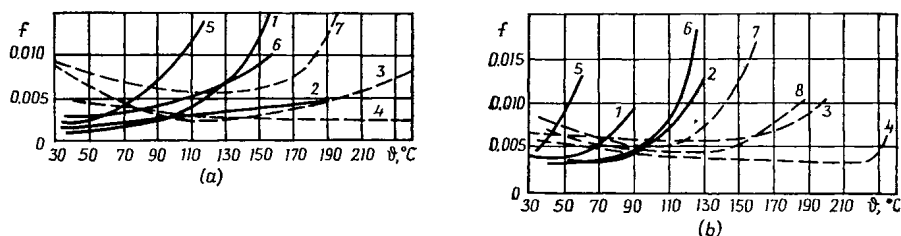


Fig. 7.12. Effect of oil temperature on the coefficient of friction on steel (a) babbitt Grade BK2; (b) alloy Grade A9-2; 1, 2, 3, 4—friction of unhardened steel journal lubricated, respectively, by vaseline oil, vaseline oil with stearic acid (1%), diesel oil, diesel oil with stearic acid; 5, 6, 7, 8—friction of hardened steel journal lubricated likewise

7.2.5. Resistance to Scoring

The type of bearing material has an effect on scoring and the extent of damage it causes to the rubbing surfaces.

A necessary condition for the development of scoring is the disruption (desorption) of the boundary oil film when, according to [4], contact stresses τ approach the limiting values. The occurrence of boundary friction and the strength of the boundary film are largely determined by the bearing and journal materials. In this respect the best materials are soft babbitt metals, and then, alloys having soft structural components (Grades AO20-1, AO9-1, BpC30, etc.). Hard antifricition alloys without soft metal inclusions, as a rule, show poorer behaviour. For this reason, bearings made of such materials are provided with thin soft-metal linings (0.01 to 0.03 mm thick). The chemical composition of the most common linings used in England is given in Table 7.29.

After desorption of the oriented layers of the surface-active agents' molecules, areas are formed on the rubbing surfaces where friction runs without lubrication. At this stage, the behaviour of the materials depends on the resistance to seizure.

Because the seizure of two surfaces in friction is accompanied with an intensive heat generation, the surface layers get heated rather rapidly up to the melting of the metal or of its fusible structural constituent.

Antifricition alloys can be arbitrarily split into three groups, each having its peculiar seizure and antiscoring behavior. These groups are described in Table 7.30.

Table 7.29

Composition of bearing soft coatings

Coating	Chemical composition, %			
	Pb	Sn	Cu	In
Tin	—	100	—	—
Lead-tin	90 89 87*	10 10 10*	— 1 3*	— — —
Lead-indium	95	—	—	5

* One of the longest-wear-life coatings.

Table 7.30

Seizure and damage in bearings of different materials

Group of materials	Melting point, °C	Character of seizure	Character of bearing surface damage	Character of journal surface damage
Tin- and lead-base alloys	≤ 350	In thin surface layer	Light score marks and pits	Transfer of friction material, no pits and score marks
Zinc-base alloys. Aluminium-base alloys with soft structural constituents (tin, lead, cadmium)	≤ 650	In thin surface layer and tearing in depth	Small and deep score marks and pits	Score marks and sometimes pits
Aluminium-base alloys without soft structural constituents, and copper-base alloys*	≤ 1,000	Accompanied by tearing in depth	Score marks and pits	Score marks and sometimes pits

* With copper melting, journal embrittlement failure due to adsorption-reduced strength is sometimes observed.

Iron-base alloys (steels and cast irons) on seizure develop significant defects on rubbing surfaces, such as cold welding of individual spots and severe tearing in depth of the material.

The process of the seizure of mating surfaces is accompanied by intensive plastic deformations. Depending on operational condi-

tions, the antifriction alloy may either be strengthened, which is determined primarily by its increased hardness, or its hot deformation above the recrystallization point may occur if heat generation is adequate. In this case no strengthening is observed. The extent of strengthening due to plastic deformation for the most part determines the extent of damage caused by seizure.

Special experiments carried out on the VMC Model testing device to evaluate resistance to seizure in friction made it possible to assess the ability of some antifriction alloys to be strengthened [19].

The resistance to seizure in friction was characterized by the value of the load applied to move two plates (one of steel and the other of the alloy under test), at which the formation of welded junctions [19] was fixed. The results made it possible to arrange various antifriction alloys in the order of the rising seizure load as follows: BK2, B83 AO20-1, AO9-1, ИАМ10-5, ИАМ9-1.5, AO9-2, and AC15-0.5.

7.3. SELECTION OF BEARING ALLOYS

Bearing alloys are selected depending on service conditions and other parameters. Recommendations for use of various alloys are treated in monographs [3, 6, 18, etc]. The most detailed recommendations are given for the application of babbits. A. K. Zaitsev has determined the permissible static load on babbit bearings, equal to half the value of the limit of proportionality in compression, found at working temperature (75°C); he also suggested a universal criterion for selecting a bearing material, that is, the product $p v$ (pressure by speed)*. This criterion has been used up to now, and, depending on its values, operating conditions for bearings have been classified as light, moderate, normal, heavy and extra-heavy. Heavy conditions are defined by $p v = 300$ (kgf/cm²) (m/s). Other sources allow for much heavier permissible loads and higher permissible speeds [18].

The range of application of various bearing alloys in the fluid friction conditions is determined by their fatigue strength. For soft babbit metals, the materials with the best antifriction properties, the fatigue strength is increased by reducing the thickness of the lining, by lowering the oil temperature, by using a bronze or brass backing which provides a smaller difference in the linear expansion coefficients, by machining to a higher degree of accuracy and better surface finish, and by some other measures.

Depending on these factors, the same material can operate under different working conditions. Thus, for instance, the babbits can stand pressures [31] given in Table 7.31.

* Although the $p v$ criterion has found extensive practical use, it is nevertheless very approximate and not always confirmed by experimental data. A more general characteristic is $p^n v^m$ (see Ch. 4).

Table 7.31

Permissible pressures on bearings, depending on babbitt layer thickness

Babbitt layer thickness, mm	Pressure, kgf/cm ²		
	normal working conditions	heavy working conditions	maximum permissible pressure
0.4	105	70	140
0.05-0.12	140	105	245

Different permissible pressures on bearings are also specified for harder alloys [31] in accordance with operating conditions and lining arrangements (Table 7.32).

Table 7.32

Permissible pressure on bearings, depending on bearing material and working conditions

Material	Pressure, kgf/cm ²		
	normal conditions	heavy conditions	maximum permissible pressure
Leaded bronze	210	140	280
Cast aluminium alloy	245	175	385
Aluminium alloy on steel backing, with a lining of soft metals	280	175	490

In the general case, the manufacturing methods and construction of bearings should be taken into account, as well as the operating conditions (p and T , °C). These factors have been used in [3] for a schematic classification of alloy application conditions (Table 7.33).

REFERENCES

1. Алексеев Н. М., Крагельский И. В. Задача о движении штампа по пластическому полупространству с учетом упрочнения в связи с вопросами заедания пар трения.— В сб.: Исследования по триботехнике. М., 1975, с. 5—11.
2. Боуден Ф. П., Тейбор Д. Трение и смазка. М., Машгиз, 1963. Пер. с англ.
3. Буше Н. А. Подшипниковые сплавы для подвижного состава. М., «Транспорт», 1967.
4. Галашев Н. Н. Исследование алюминиевых сплавов для подшипников судовых дизелей.— «Труды Ливта» Сборник статей молодых научных работников. Л., 1968, с. 18—22.
5. Гаркунов Д. Н., Крагельский И. В., Поляков А. А. Избирательный перенос в узлах трения. М., «Транспорт», 1969.
6. Зайцев А. К. Типовые баббиты, стандартные и новые. М., Цветметиздат, 1932.

Table 7.33

Recommendations for use of bearing alloys

Material	Operating conditions			Recommended manufacturing and design requirements			Operating conditions classified in points
	pressure, kgf/cm ²	rotational speed, m/s	oil temperature, °C	alloy layer thickness, mm	fitting accuracy	journal hardness HB	
Tin- and lead-base alloys							
All grades of babbitt metals	10-50	2-5	≤ 50	Tenths of a mm	—		Mechanical (in slots)
	10-50	5-10	≤ 60				
Babbitts, Grades	50-100	5-10	≤ 75	Hundredths of a mm		—	Tinning
	50-120 80-150	≤ 10 ≤ 15	≤ 80 ≤ 100	Thousandths of a mm			
Copper-, aluminium-, and zinc-base alloys							
Zinc-base alloys on steel backing							
Aluminium-base alloys on steel backing	150-250	≤ 15	≤ 100	$\begin{matrix} < 1 \\ < 0.5 \end{matrix}$	Thousandths of a mm	≥ 300	Rolling or casting
Cast aluminium bearings (II-group alloys)		≤ 15	≤ 100	—		≥ 200	—
Lead bronze on steel backing	150-250	≤ 20	120	< 0.5		≥ 400	Metallurgical
Aluminium-base alloys of the III group on steel backing	200-300	≤ 20	120			≥ 400	Rolling or casting

7. Захаров Р. С., Яцковский Е. Н. Определение надежности подшипников коленчатого вала судовых ДВС.— «Труды Николаевского кораблестроительного института», 1970, вып. 34, с. 102—107.
8. Захаров С. М. Гидродинамические режимы смазки подшипников дизеля 2Д100.— «Вестник ЦНИИ МПС», 1965, № 2, с. 25—29.
9. Зуидема Г. Г. Эксплуатационные свойства смазочных масел. Пер. с англ. М., Гостехиздат, 1957.
10. Изготовление и испытание подшипников с антифрикционным слоем из высокопрочных алюминиевых сплавов.— «Труды НАМИ», вып. 82, 1966, с. 50—70. Авт.: Н. М. Рудницкий, Ю. А. Рассадин, А. Д. Курицына и др.
11. Карасик И. И., Силин Л. В. Оценка прирабатываемости материалов по предельным режимам нагружения. М., «Экспресс-стандарт», 1973, № 20, с. 10—12.
12. Костецкий Б. И. Трение, смазка и износ в машинах. Киев, «Техніка», 1970.
13. Крагельский И. В. Трение и износ. М., «Машиностроение», 1968.
14. Литейные бронзы. Л., «Машиностроение», 1973. Авт.: К. П. Лебедев, Л. С. Райнес, Г. Ф. Шеметев, А. Д. Горячев.
15. Лунев А. А. Литейные медистые антифрикционные стали.— «Литейное производство», 1955, № 5, с. 15—18.
16. Матвеевский Р. М. Температурная стойкость граничных смазочных слоев и твердых смазочных покрытий при трении металлов и сплавов. М., «Наука», 1971.
17. Мошков А. Д. Пористые антифрикционные материалы. М., «Машиностроение», 1968.
18. Петриченко В. К. Антифрикционные материалы и подшипники скольжения. М., Mashgiz, 1954.
19. Подшипники из алюминиевых сплавов. М., «Транспорт», 1974. Авт.: Н. А. Буше, А. С. Гуляев, В. А. Двоскина, К. М. Раков.
20. Применение цинкового сплава взамен бронз и баббитов. М., Трансжелдориздат, 1961. Авт.: П. Г. Абрамов, Н. А. Буше, В. А. Двоскина, М. С. Кручинин.
21. Рудницкий Н. М. Выносливость материалов для подшипников скольжения автомобильных двигателей. М., Mashgiz, 1955.
22. Семенов А. П., Савицкий Ю. Э. Металлофторопластовые подшипники. М., «Машиностроение», 1976.
23. Семенов А. П. Схватывание металлов. М., Mashgiz, 1958.
24. Смирягин А. П., Смирягина Н. А., Белова А. В. Промышленные цветные металлы и сплавы. Справочник. М., «Металлургия», 1974.
25. Хрущов М. М., Бабищев М. А. Исследование изнашивания металлов. М., Изд-во АН СССР, 1960.
26. Хрущов М. М. Усталость баббитов. М., Изд-во АН СССР, 1943.
27. Шпагин А. И. Антифрикционные сплавы. М., Metallurgizdat, 1956.
28. A. Buske. Aluminium Lager in Motorenbau.— «Motortechnische Zeitschrift», 1954, Jahrgang, 15, s. 337.
29. Campbell Y. The development and testing of engine bearings.— «IAAE Journal», 1964, vol. 24, No. 11-12, p. 182—193.
30. Pratt G. G. New developments in bearing materials.— «SAE Preprints», Internat. Autom. Eng. Congress, Jan. 13-17, 1969, No. 690112.
31. I. B. Mohler. Al on steel bearings Diesel. Power 31, No. 9, 1953.
32. E. Roemer. Werkstoffe und Schichtaufbau bei Gleitlagern.— «Zeitschrift für Werkstofftechnik», 1973, Bd. 4, No. 8, s. 434-442.
33. Sliding-Bearing Materials.— «Machine Design», 1974, vol. 46, No. 15, p. 37-44.

MANUFACTURING METHODS FOR IMPROVING THE WEAR RESISTANCE OF MATERIALS AND TRIBOLOGICAL JOINTS

8.1. GENERAL

Contact interaction between rubbing parts is influenced by geometrical and physico-mechanical characteristics of their mating surfaces. The first include surface roughness (microirregularities), waviness, errors of form (macroirregularities), the direction of asperities, and dimensional accuracy; the second include microhardness, the extent and depth of work hardening, etc.

The effect of surface roughness on wear is mainly observed during the running-in of mating parts, when the size, shape, and direction of asperities undergo changes. Hence, it is wise for the product designer to specify the machining method that can provide, at the manufacturing stage, the optimum surface roughness which is usually found after running-in. The results will be shorter running-in time and longer wear life of the joint.

The required bearing surface area of a part cannot be ensured by specifying the surface roughness alone; the processing method that makes it possible to obtain the surface with the necessary parameters should also be specified.

Considering that surface roughness in a longitudinal direction mostly differs from that in a transverse direction, the surface quality should be assessed with regard to the direction of the asperities left by machining. The effect of this direction on wear life is variable for different friction conditions and roughness values. In fluid friction and with a small height of surface irregularities their direction does not matter, but with greater roughness the direction of irregularities parallel to the direction of relative motion becomes more beneficial.

In boundary friction of surfaces with a small height of irregularities arranged parallel to the direction of relative motion, seizure of the

surfaces occurs, and wear proves to be greater than it is for surfaces with mutually perpendicular directions of irregularities. However, for rubbing surfaces of greater roughness, when no seizure takes place, parallel directions of surface irregularities give minimal wear.

The value of the friction coefficient is also influenced by the height and direction of surface irregularities. It reaches its maximum when both rubbing surfaces have irregularities directed perpendicular to the direction of motion. When the surface irregularities are different in direction, intersecting at right or other angles, the coefficient of friction is minimal.

The wear life of mating surfaces depends considerably on their waviness, whereas the surface pattern formed by scraping, vibration roller treatment or other processing methods provides for lubricant retention.

The errors of form (macroirregularities), dimensional errors, and errors of position of a given surface are determined by machining accuracy.

The accuracy of machining depends on various factors inherent in the machining process (elastic and thermal deformations of the structural loop comprising the machine, the fixture, the cutting tool, and the part being machined; gradual wear of the cutting tool; etc.).

Machining errors are determined either approximately, by using reference data on the accuracy of machining of various surfaces, or analytically, by calculation based on the analysis of elementary machining error components.

Errors of form and position are controlled by the limits specified by GOST 10356-63. It must be taken into account, however, that form errors equal in magnitude but different in geometrical character (convex, concave, deviations in one or two planes, the character of clearance changes in fitting parts having a specific positional relationship and form deviations, etc.) may affect the wear life of a given joint differently.

For this reason, surface macrogeometry should be assessed not only by the maximum deviations from the true geometrical form, but also by the actual form of the surface over its nominal area; in assemblies allowance must be made for the relative position taken by the macroirregularities of the mating surfaces.

The accuracy of a tribological joint, specified by the engineering drawing and determined by the amount of clearance between the mating parts, largely depends on the relationship between the height of surface irregularities and the machining tolerance on each part. It must be taken into account that during running-in the height of surface irregularities may decrease (when greater than the optimal value) by 65 to 75 percent, so that the mating parts' dimensions exceed the tolerance limits, and an additional amount of clearance results in a completely changed character of fit, i.e., in a loss of accuracy (the

joint comes out with a fit of, for instance, the 3rd tolerance grade instead of the specified 2nd tolerance grade, with a running fit instead of a close sliding fit, etc.). Therefore, in all critical assemblies where the specified fit must be maintained over a long period of service, the components should be machined for a definite optimum roughness of the rubbing surfaces.

Wear resistance also depends on the microhardness of the surface layer. The preliminary strengthening (strain hardening) of the surface layer metal reduces its deformation and wear due to friction and the diffusion of surface layers due to mechanical and molecular interactions. It also inhibits the mutual plastic deformation of the surface layers on the mating parts that gives rise to their cold welding, or seizure, which is the most intensive type of wear. Preliminary surface strengthening improves wear resistance not only in friction with lubrication, but also in dry friction, increasing wear life 1.5 to 2 times and more. It is especially so with the more plastic and relatively soft steels, in which even a slight increase in microhardness due to surface strengthening markedly reduces wear.

The real contact area changes until the bearing capacity reaches a certain value which depends on the relationship between this area, the yield point (σ_y) for the softer material, and the external force that creates pressure on the sliding interface. The value of σ_y for a given metal closely relates to its microhardness. During the running-in period, rubbing surfaces develop the optimum microhardness of the surface layers and also obtain the optimum roughness. The favourable effect of surface strengthening on wear resistance has its limit. Excessive microhardness as a result of overstrengthening brings about increased wear due to metal flaking. Hence, surface strengthening in the course of machining or special treatment (burnishing with rollers or balls, shot peening, etc.) should be closely controlled to exclude overstrengthening.

Each method for processing machine parts has definite surface strengthening capabilities (Table 8.1).

8.2. MACHINING METHODS

For each machining method, a better surface finish leads to increased real contact areas. The height of surface irregularities in a longitudinal direction, R_l , is often commensurable with that in a transverse direction, R_{tr} . In some cases R_l can not only be equal to R_{tr} but also exceed it. This is observed in machining with a cutting tool with a built-up edge. Vibration also affects R_l to a greater degree than R_{tr} ; its variation changes R_l by 250 to 700 percent and R_{tr} by 50 to 100 percent.

Values of surface roughness and waviness parameters for various machining methods are given in Ch. 6. The effect of machining me-

Classification and capabilities of surface strengthening methods

Strengthening principle	Strengthening method	workpiece material	dimensional accuracy	Capabilities					thickness of hardened or deposited layer, mm	
				surface roughness class according to GOST 2789-73	hardness of surface obtained	magnitude and sense of residual stresses in surface layer, kgf/cm ²				
							min	max		
Strengthening by plastic deformation of surface layer (work hardening), improving its physico-mechanical properties, changing the magnitude and sense of residual stresses in surface layer, improving surface microgeometry by cold working	Shot peening	Cast iron, steel, nonferrous and titanium alloys	Retained from preceding operation	2-7	Increased by 20-40%	Compressive stresses 40-80		0.4	1.0	
	Shot-and-abrasive blasting			5-8				0.2	0.6	
	Centrifugal working			Improved by one-two classes	Increased by 15-60%			0.3	0.7	
	Roller burnishing			7-11	Compressive stresses 60-80		1.0	20.0		
	Vibratory burnishing						Increased by 20-50%	1.0	35.0	
	Ball burnishing		1-3				0.3	5.0		
	Broach burnishing			9-11				0.3	5.0	
	Peening						0.5	35.0		
	Hardening by cutting		7-9	2-4			Increased by 20-30%	0.05	0.5	
	Vibro-impact working		4-5	3-5	Compressive stresses 30-70		0.1	0.7		
	Hydraulic vibro-impact working		Retained from preceding operation	4-7					Increased by 20-40%	
				5-8					Increased by 20-40%	

Table 8.1 (continued)

Strengthening principle	Strengthening method	Capabilities						
		workpiece material	dimensional accuracy	surface roughness class according to GOST 2789-73	hardness of surface obtained	magnitude and sense of residual stresses in surface layer, kgf/cm ²	thickness of hardened or deposited layer, mm	
							min	max
	Tumbling			8-10	Increased by 10-15%	Compressive stresses 10-20	0.05	0.1
	Hydrotumbling			8-10	Increased by 20-40%	Compressive stresses 20-40	0.1	0.3
	Vibro-tumbling			10-12	Increased by 10-15%	Compressive stresses 10-15	0.05	0.2
	Ultrasonic strengthening			Improved by two-four classes	Increased by 50-90%	Compressive stresses 80-100	0.1	0.9
	Hydropolishing			8-11	Increased by 20-30%	Compressive stresses 30-70	0.01	0.20
	Diamond bur-nishing				Increased by 30-60%		0.01	

Table 8.1 (continued)

Strengthening principle	Strengthening method	Capabilities						
		workpiece material	dimensional accuracy	surface roughness class according to GOST 2789-73	hardness of surface obtained	magnitude and sense of residual stresses in surface layer, kgf/cm ²	thickness of hardened or deposited layer, mm	
							min	max
Strengthening by thermochemical treatment, changing physico-chemical properties and structure of surface layer, changing the magnitude and sense of residual stresses in surface layer	Carburizing	Low-carbon steel	Warpage 0.05-0.15 mm	Downgraded by one-two classes	HRC 60-70	Compressive stresses 40-100	0.5	2.0
	Nitriding	Steel, cast iron	Warpage 0.05-0.10 mm		HV 650-1200		0.05	0.60
	Cyaniding	Steel			HRC 60-75		0.01	2.5
	Aluminizing		Warpage 0.05-0.15 mm		—	—	0.05	0.5
	Chromizing			Microhardness 1,600-2,000	—	0.02	0.30	
	Siliconizing	Steel, cast iron		—	—	0.02	0.03	
	Sulphidizing		Warpage 0.05-0.10 mm	No change		0.05	1.00	

Table 8.1 (continued)

Capabilities							
Strengthening principle	Strengthening method	workpiece material	dimensional accuracy	surface roughness class according to GOST 2789-73	hardness of surface obtained	magnitude and sense of residual stresses in surface layer, kgf/cm ²	thickness of hardened or deposited layer, mm min max
Strengthening by heat treatment of surface layer, improving its physical co-mechanical properties and structure, the changing the magnitude and sense of residual stresses	Flame hardening	Steel	Warpage 0.03-0.4 mm	Downgraded by one class	HRC 40-70	Compressive stresses 30-80	0.5 10.0
	Induction hardening		Warpage 0.03-0.07 mm	No change	HRC 40-70		0.2 10.0
Strengthening by hard-facing with wear-resistant materials	Manual oxy-acetylene deposition	Steel, cast iron, nonferrous alloys	Significant deformation	Rough surface	HB ≥ 200 to 400	Tensile stresses 10-50	0.5
	Manual arc-welding deposition	Steel, cast iron, nonferrous alloys					2.0
	Arc-welding bimetalization	Steel, nonferrous alloys	7-9		HB 250-450		1.0 3-5

Table 8.1 (continued)

Capabilities						
Strengthening principle	Strengthening method	workpiece material	dimensional accuracy	surface roughness class according to GOST 2789-73	hardness of surface obtained	magnitude and sense of residual stresses in surface layer, kgf/cm^2
						thickness of hardened or deposited layer, mm min max
Strengthening by hard-facing with wear-resistant materials	Hidden-arc welding deposition	Steel, cast iron, nonferrous alloys	Significant deformation			1.5 40.0
	Electroslag welding deposition				HB 500-650	2.0 40.0
	Vibratory arc-welding deposition		Insignificant deformation		HB 500-650	0.3 3.0
Strengthening by spraying surfaces with wear-resistant materials	Gas metal spraying	Metals and nonmetals	No deformation		$HB \geq 120-420$	0.3 15.0
	Electrical metal spraying					1.3 15.0
	Plasma metal spraying	Steel, cast iron, nonferrous alloys	Insignificant deformation		$HB \geq 500-2,000$	0.3 20-30

Table 8.1 (continued)

Strengthening principle	Strengthening method	workpiece material	dimensional accuracy	Capabilities				
				surface roughness class according to GOST 2789-73	hardness of surface obtained	magnitude and sense of residual stresses in surface layer, kgf/cm ²	thickness of hardened or deposited layer, mm	
							min	max
Strengthening by electroplating surfaces with wear-resistant materials	Chromium plating	Steel, cast iron, nonferrous alloys	No deformation, accuracy retained from preceding operation	6-8	HB 500-1,200	Tensile stress 20-60	0.01	1.0
	Hard nickel plating				HB 550-650	—	0.05	2.0
	Acierage				HB 120-600 HV 2,200	—	0.2 0.1	5.0 0.3
	Borating	Steel		4-7	HB 40-120	—	0.05	2.0
	Deposition of thin alloy layers	Steel, cast iron, nonferrous alloys						
	Enamelling	Steel, cast iron, nonferrous alloys, aluminium and its alloys		—	Microhardness 600-700	—	0.001	0.012
	Deep oxidation	Aluminium and its alloys		—	Microhardness 400-450	—	0.01	0.2-0.3

Table 8.1 (continued)

Capabilities								
Strengthening principle	Strengthening method	workpiece material	dimensional accuracy	surface roughness class according to GOST 2789-73	hardness of surface obtained	magnitude and sense of residual stresses in surface layer, kgf/cm ²	thickness of hardened or deposited layer, mm	
							min	max
Strengthening by chemical deposition of wear-resistant materials	Coating with nickel, chromium, cobalt- and cobalt-nickel	Cast iron, steel, nonferrous metals	No deformation	6-10	Microhardness 800-950	—	0.01	0.3
	Enamelling	Steel, cast iron	Insignificant deformation	3-5	—	—	0.05	0.3
Strengthening by deposition of nonmetallic coatings	Paint and varnish coating	Metals and nonmetals	No deformation				0.15	0.3
	Coating with plastics and special materials							

ods on surface roughness and strengthening is characterized in Tables 8.2. and 8.3.

Table 8.2

Effect of machining methods on properties of surface layers

Machining method	Degree of strain hardening*, %	Depth of strain hardening, μm
Turning (normal and high-speed)	120-150	30-50
Fine turning	140-180	20-60
Milling with face cutters	140-160	40-100
Milling with plain cylindrical cutters	120-140	40-80
Drilling and counterboring	160-170	180-200
Reaming	—	150-200
Broaching	150-200	20-75
Gear hobbing and shaping	160-200	120-150
Gear shaving	—	≤ 100
Circular grinding:		
unhardened carbon steel	140-160	30-60
low-carbon steel	160-200	30-60
hardened steel	125-130	20-40
Surface grinding	150	16-35

*Surface microhardness in percent of core microhardness.

Table 8.3

Effect of cutting conditions on surface quality and service properties of machine parts

Cutting conditions	Effect on geometric characteristics of workpiece surface	Effect on physico-mechanical properties of workpiece surface layer	Effect on service properties of parts
Cutting speed	Roughness of machined surface is increased within one-two classes when machining is done at cutting speeds conducive to formation of built-up edge	As cutting speed grows (up to certain limits), the depth of strain-hardened layer increases. At high speeds (from 200 to 600 m/min) the reverse process occurs and the depth of strain hardening decreases. In machining alloy steels and low-ductility steels, residual compressive stresses set in at cutting speeds of 400 to 600 m/min. With steel Grades 20 and 45 compressive stresses occur at 500 to 800 m/min and negative rakes	With increase of cutting speeds and reduction of surface roughness to optimum values, wear and corrosion resistance improve. Fatigue strength is increased with higher degree and depth of strain hardening and with greater residual stresses

Table 8.3 (continued)

Cutting conditions	Effect on geometric characteristics of workpiece surface	Effect on physico-mechanical properties of workpiece surface layer	Effect on service properties of parts
Cutting feed	Surface roughness in increased with feed rate within one-two classes	Residual stresses and the depth of strain hardening grow with feed rate	Higher feed rates reduce wear resistance as surface roughness increases to its optimal values. Fatigue strength is improved
Depth of cut	Machining of ductile metal with small depths of cut (0.1 to 0.2 mm) on surface layers work-hardened in previous operations reduces surface roughness within one-two classes (in finish machining)	No significant effect on the depth of strain hardening	No tangible effect
Coolant	Heat removal, decrease of cutting temperature, and adsorbed lubricating film reduce wear and adhesion, which lowers surface roughness within one-two classes	—	—
Tool rake angle	Increased deformation of surface layer due to unfavourable rake results in increase of surface roughness within one class	Tools with negative rake angles of 15 to 45° induce residual compressive stresses in surface layers	Machining with tools having negative rake angles from 15 to 45° leads to increased fatigue strength
Relief angle	Increased area of contact between tool and workpiece leads to greater friction and increased surface roughness (within one class)	With relief angle increased from 3 to 15° the depth of strain hardening decreases	Relief angles from 3 to 15° have no considerable influence on wear resistance. Fatigue strength may somewhat decrease

Table 8.3 (continued)

Cutting conditions	Effect on geometric characteristics of workpiece surface	Effect on physico-mechanical properties of workpiece surface layer	Effect on service properties of parts
Entering angle	With entering angle increased from 30 to 60°, surface roughness grows significantly in roughing, and within one-two classes in finishing	Decrease of entering angle from 90 to 45° results in reduced depth of strain hardening	Smaller depth of strain hardening and greater surface roughness reduce fatigue strength
End cutting edge angle	With increase in end cutting edge angle, surface roughness grows significantly in face milling (within one class in roughing and within one-two classes in finishing)	—	Smaller depth of strain hardening and greater surface roughness reduce fatigue strength
Side cutting edge slope angle	Unfavourable side cutting edge slope angle may result in scratching of machined surface by chips (surface roughness increased within one-two classes in roughing and within one-two classes in finishing)	—	—
Nose tip radius	With radius of tool nose rounding increased from 0.5 to 4 mm, surface roughness is reduced (within one class in roughing and within one-two classes in finishing)	—	Wear resistance improves as surface roughness reaches optimum values; fatigue strength increases
Change in cutting edge finish due to wear	As tool wears, surface roughness grows within one class	Tools with carefully lapped cutting edges make for reduced depth of strain hardening	Wear resistance and fatigue strength change until surface roughness and strain hardening reach optimum values
Cutting edge radius due to wear	As cutting edge radius grows due to wear, surface roughness increases within one class	Growing wear of cutting edge results in greater depth of strain hardening and residual stresses	Greater depth of strain hardening and higher residual stresses improve fatigue strength
Cutter runout	Deep furrows are formed on machined surface (waviness)	—	Service properties may be downgraded

Table 8.3 (continued)

Cutting conditions	Effect on geometric characteristics of workpiece surface	Effect on physico-mechanical properties of workpiece surface layer	Effect on service properties of parts
Tool material	Adhesion of workpiece metal to tool face, caused by physical affinity of metals, results in increased surface roughness. With carbide- and ceramic-bit tools surface roughness is reduced	—	—
Mechanical properties of workpiece material	Increased workpiece hardness reduces surface roughness (within one-two classes in roughing and finishing). This effect is more pronounced in low-speed operations (broaching) than in such operations as turning and milling	With harder workpiece material its volume subject to plastic deformation decreases. In softer steels plastic deformation extends deeper, residual stresses grow	Increased hardness and strength of material, higher residual stresses in surface layer and reduced surface roughness make for greater fatigue strength
Structure of workpiece material	For fine-grained low-carbon steels, low cutting speeds are conducive to reduced surface roughness. At high speeds, surface roughness decreases in change-over from coarse-grained structure to fine-grained one. For medium-carbon steels, thin lamellar pearlitic structure results in reduced surface roughness. For high-carbon steels, except for steel Grade IX-15, nodular and thin lamellar pearlitic structures are optimal	—	Reduced grain size improves service properties
Vibration of MFTW (machine-fixtured-tool-workpiece structural loop)	Vibrations of the structural loop as a whole and of its components result in surface roughness increased within one class in roughing and one-two classes in finishing	—	Vibration of MFTW structural loop may result in markedly impaired service properties

8.3. SURFACE TREATMENT BY PLASTIC DEFORMATION

The accuracy and surface quality obtained by various cold working methods are given in Tables 8.4 to 8.6. Depending on the type of tool, surface quality can be varied within a fairly wide range.

Table 8.4

Finishing of external cylindrical surfaces by cold working

Working method	Treated work within size ranges, mm	Capabilities				
		accuracy (tolerance grade)	surface roughness class	degree of work hardening, %	maximum depth of work hardening, μm	
Burnishing by cemented carbide plates	Axles, rigid plain and stepped shafts $d > 20$, l unlimited	Not for working to size	8-9	50-60	600	
Burnishing by diamond tools	Axles, shafts $5 < d < 50$, l unlimited	2-1	11-12	20-25	1,000	
Burnishing by spring-action single-roller tools	Axles, rigid plain and steeped shafts			20-40		
Burnishing by spring-action single-ball tools ($d_{ball}=10$ mm)	Axles, plain shafts of low stiffness					
Burnishing by spring-action multi-ball tools	Axles, plain shafts $d > 8$, l unlimited		Not for working to size	8-11		5,000
Burnishing by spring-action three-roller tools	Axles, plain and stepped shafts of low stiffness $d > 20$, l unlimited				20-50	
Burnishing by rigid multi-roller tools	Axles, radially-balanced plain and stepped shafts $d > 20$, l unlimited	3-2	8-12		15,000	
Impact burnishing by inertial-action ball heads	Axles, shafts $d > 10$, l unlimited	Not for working to size	8-10	15-30	500	
Vibratory burnishing by spring-action single-ball tools	Axles, shafts of low stiffness $d > 10$, $l < 50$		3-12	20-50	5,000	

Note. The processes are used for finishing and surface strengthening. Burnishing by rigid multi-roller tools is also used for sizing.

In general, all methods of surface cold working improve the wear life of the treated parts. The reason is an increased surface hardness combined with a special pattern left on the surface.

Table 8.5

Finishing of cylindrical holes by cold working

Working method	Purpose	Treated work within size ranges, mm	Capabilities			
			accuracy (tolerance grade)	surface roughness class	degree of work hardening, %	maximum depth of work hardening, μm
Broach burnishing Burnishing: by spring-action single-ball tools by spring-action multi-ball tools by rigid adjustable ball-type tools by spring-action roller-type tools by rigid non-adjustable tools with cylindrical rollers by rigid adjustable tools with cylindrical and tapered rollers by rigid impact-action non-adjustable roller tools by vibrating spring-action tools Impact burnishing by inertial-action ball heads	S, F	Through holes $d < 100$, $l < 50$ Bushing-type parts with through holes $d < 100$, l unlimited	2-4	8-9 9-10	40-50 20-40	5,000
	F, St	Through holes $d > 20$, $l < 100$	Not for working to size	9-11	20-50	2,000
	S, F	Through holes $d > 40$, l unlimited			20-40	
	F, St	Through holes $d > 20$, l unlimited			20-50	
	S, F	Medium-stiffness parts with through holes $d > 60$, l unlimited	3-2	10-11	20-40	5,000
		Through and blind holes $d > 6$ to 8, $l < 30$	Not for working to size 2-4 and better			
		Rigid, parts with blind holes $d > 20$, l unlimited				15,000
	F, St	Through holes $d > 20$, l unlimited	3-2	9-11	20-50	5,000
		Low-stiffness parts with through holes $d > 70$, l unlimited	Not for working to size	8-10	20-40	2,000
		Holes $d > 70$, l unlimited			15-30	500

Designations. S — sizing; St — strengthening; F — finishing.

Table 8.6

Cold working of flat surfaces

Working method	Purpose	Treated parts within size range, mm	Capabilities		
			surface roughness class	degree of work hardening, %	maximum depth of work hardening, μm
Burnishing: by spring-action ball and roller type tools by multi-ball tools rigid spring-action by multi-roller tools at high pressure by ball on shaping machine by roller on planing machine Simultaneous face milling and burnishing by ball Vibratory burnishing of end faces	F, St	End faces of rotational parts; d unlimited	9-12		5,000
	S, F, St F, St	Plate-type parts; overall dimensions unlimited			
	S, F, St	Annular end faces of rotational parts; $d < 300$	10-12	20-40	8,000
	F, St	Long flat surfaces; overall dimensions unlimited	9-11		5,000
	S, F, St	Long flat surfaces; overall dimensions unlimited	7-9		1,000
	F, St	Discs and thrust bearings; d and l unlimited	8-10	20-50	2,000

Note. For designations refer to Table 8.5.

Diamond burnishing is used for steel, nonferrous metals and alloys. As diamond is brittle, the treatment should not be employed for interrupted surfaces. This process is not used for parts with considerable form deviations in a transverse direction and parts with variations in surface hardness (in excess of *HRC* 4-5), because a consistent surface quality is difficult to obtain.

The form of the treated part in a longitudinal direction and that in a transverse direction change but slightly.

Ball and roller burnishing is used for working cylindrical surfaces, grooves, fillets, flat and form surfaces. Dimensional changes due to the treatment and its accuracy depend on the workpiece configuration, the burnishing tool, and the process conditions, and also on the accuracy of form, dimensions, and surface finish obtained in the preceding operation. In burnishing stiff workpieces, the amount of dimensional changes depends on the initial condition of the surface. The effect of burnishing conditions on the surface quality is disclosed in Table 8.7.



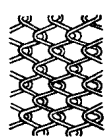
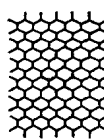
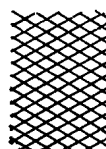


Table 8.7

Effect of burnishing conditions on surface quality

Working conditions	Roughness of treated surface	Degree of work hardening (rise in hardness)	Depth of work hardening
Increase of workpiece rotational speed from 10 to 60 m/min	No effect	Slightly rises	Slightly increases
Increase of burnisher longitudinal feed from 0.3 to 1.00 mm	Slightly grows	No effect	Slightly decreases
Increase of burnisher pressure from 20 to 5,000 kgf	At first decreases (within one class) and then remains unchanged	Considerably rises	Considerably increases
Increase in the number of working passes	At first without change (for two-three passes) and then may grow	At first (up to three passes) rises, and then falls (overworking)	At first slightly increases and then remains unchanged
Increase in diameter of burnisher roller	Decreases	Decreases	Decreases

Table 8.8

Surface patterns obtained by vibratory burnishing

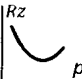
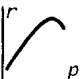
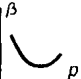
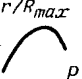
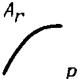
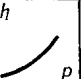
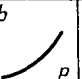

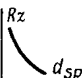
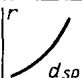
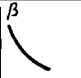
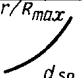
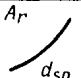
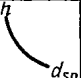


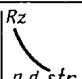
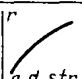
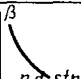
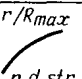
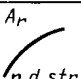
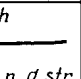
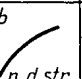
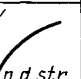
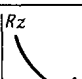
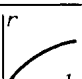
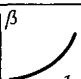
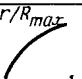
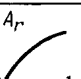
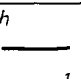
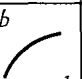
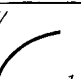
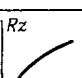
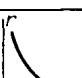
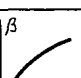
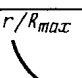
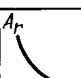
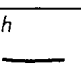
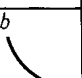
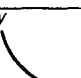
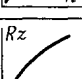
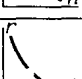
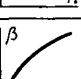
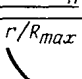
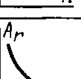
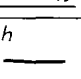
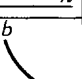
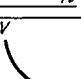
With groove geometry retained			With groove geometry renewed	
grooves do not touch	grooves touch	grooves intersect	hexagonal	tetragonal
Schematic view				
				
Profile chart				
				

Broach burnishing is done with small or large amount of interference. In the first case the extent of plastic deformation does not affect the whole thickness of the part. Such a treatment improves the surface finish and reduces the form errors and dimensional variations of holes by 30 to 35 percent in a batch of parts. Plain, thin-walled cylindrical sleeves and bushings are worked with large amount of interference. The plastic deformation acts on the whole part.

Vibratory burnishing allows five different surface patterns to be obtained, as shown in Table 8.8. In addition, their combinations are possible (one of the first three with one of the last two). The treatment produces a new microrelief on the surface and a system of grooves which retain lubricant and reduce the area of contact for operation without lubricant.

By changing the processing conditions it is possible to obtain practically any regular surface pattern (Table 8.9). The surfaces treated

Qualitative influence of vibratory burnishing conditions on surface geometric parameters Table 8

Working conditions	Surface roughness parameters					Groove parameters		
	R_z	r	β	r/R_{max}	A_r	h	b	V
Burnisher pressure, p								
Radius of burnisher sphere, $d_{sp}/2$								
Number of oscillations per unit time, n (double strokes)								
Oscillation amplitude, l								
Workpiece rotational speed, n								
Feed, s								

Note. h , b , and V =depth, width, and volume of grooves, respectively.

by vibro-burnishing feature asperities outlined by large radii and having almost equal height in longitudinal and transverse directions. The contact area with equal heights of surface irregularities is larger than that of machined or conventionally burnished surfaces. Consequently, the smoothing out of the vibro-burnished surfaces in the course of running-in proceeds with their minimal approach.

Electromechanical strengthening is used for steel and cast iron parts.

The treatment is more efficient for steels with a high carbon content. With some steel grades the surface hardness rises 4.5 times over the initial value, the hardened layer being 0.2 to 0.3 mm deep.

The best levelling-out of asperities is achieved at a roller speed of 10 to 15 m/min, a roller pressure of 20 to 75 kgf and with three working passes. The surface finish is improved by two to three classes, and no changes in the form of the part are observed. The wear resistance of normalized steels after the electromechanical strengthening treatment is 4 to 10 times that of such steels after polishing or grinding. For hardened steel Grade IX15 wear resistance can be increased 2 times.

Electromechanical strengthening is an effective surface treatment method for cast iron parts. It provides the 8th or 9th surface roughness class (an improvement by three to four classes on the roughness left after machining). Surface finish becomes better with the working pressure increased from 10 to 60 kgf/cm², the working speed increased to 120 m/min, and with three working passes.

The strengthened layer is 0.8 mm deep, with its microhardness raised 1.5-2 times.

After running-in, the surfaces treated by the electromechanical strengthening method exhibit improved wear resistance.

8.4. HEAT TREATMENT (SURFACE HARDENING)

This type of treatment is normally used to form a hard wear-resistant surface layer in specific regions on parts made of medium- and high-carbon and pearlitic steels, malleable, gray and high-test cast iron containing not less than 0.6 percent carbon. The depth of hardening is prescribed to be not less than 1.5 to 2 mm.

Flame hardening is applicable to both cylindrical and flat parts. It is commonly used to surface harden large steel parts, such as cast gears, worms, rolls, crankshaft journals. The advantages of the method are simple equipment and ease of processing, minimal distortion and the absence of oxidation after hardening, and the possibility of obtaining a uniform layer with hardness gradually changing through the depth.

Induction hardening. The passage of electric current without contact with the part being treated allows a clean surface to be obtained. A thin oxide film does not downgrade the surface quality. Such a treatment is effected by two methods. The first method involves the heating of the whole area to be hardened. This is used for disc-shaped parts or for local hardening (plain shafts, crankshafts, camshafts, splined shafts, gears, control levers, etc.). The method is very efficient.

The second method consists in that one portion of the surface is heated and cooled after another rather than the whole surface at once.

This method is used for hardening rolls for cold rolling, straightening rolls, large shaft journals, axles, engine cylinder liners, large piston rings, machine tool frames. The method allows both external and internal surfaces to be treated.

The advantages are that it is possible to obtain a hardened layer of from hundredths of a millimeter to 10 mm and over with a fine-grained structure without overheating; the greatest production rates are ensured as against other hardening methods; the process lends itself to automation and can be incorporated into a production line or an automatic transfer line.

8.5. SURFACE COATING

Electroplating is widely used for increasing wear resistance (chromium plating, acierage, nickel plating, etc.).

Chromium plating is one of the most commonly used methods for increasing the wear resistance of steel parts. The deposit has low coefficient of friction and high hardness (*HB* 1,000-1,100). Chromium plating reduces friction and, consequently, heat generation in sliding pairs. The wear life of chrome-plated parts is prolonged 5 to 15 times. The deposit has a poor wettability with oil. The retention of oil is improved by developing pores, channels, or indentations on the plated surface.

The shear strength of adhesion of chromium to steel, cast iron, nickel and brass for carefully prepared surfaces can reach 30 kgf/mm². However, steels with a high tungsten and cobalt content, and also high-carbon steels and high-silicon iron are not plated with chromium.

Wear-resistant chromium plates come in the following varieties: poreless, poreless over a knurled surface, porous, spot-type, and screen porous. A chromium plate can be made porous by etching. All types of bright chromium plates can be etched; the plate to be etched must be not less than 0.06 mm thick, otherwise etching down to the base metal is possible.

In the absence of sharp corners, a chromium plate of less than 0.05 mm thick gives an exact reproduction of the surface relief, including surface roughness. The surfaces to be plated are prepared by any of the following methods: fine grinding, honing, lapping, or polishing. Where the plate is to be thick in excess of 0.05 mm, fine grinding suffices.

According to treatment conditions, the plate may come out with point-type and channel-type pores, the cross-section of the channels being 0.05 by 0.05 mm. The point-type pores provide for better

oil retention, and therefore such plates are used for heavy-duty applications, e.g., upper compression piston rings in engines. Plates with the point-type porosity rapidly run in, but their wear resistance is somewhat lower than that of platings with the channel-type porosity. The latter plates are often used for cylinder liners. Wear of porous chromium-plated liners and piston rings is lower than that of unplated ones by a factor of 4 to 7, and for chromium-plated steel parts, wear decreases by a factor of 3 to 5. In addition to porous chromium plates, poreless plates deposited on knurled surfaces are used. Their wear life is 1.5 to 2 times that of porous plates, whereas the chromium consumption is lower, coming to 30-50 percent of chromium required for channel-type porous plates.

Chrome-plated parts are often ground and lapped. Where a considerable layer of chromium should be removed, to retain porosity grinding is done in two stages: preliminary grinding after chromium deposition and finish grinding after etching.

The chromium plating process and equipment are determined by the size, shape, and permissible wear of the parts to be plated, as well as by the required quality of the plate itself. Machine-tool components manufactured to the 2nd tolerance grade in most cases are permitted to wear by 0.1 mm on diameter, and parts of the 3rd tolerance grade, by 0.2 mm. Therefore, the diametral thickness of the plate should be somewhat greater than 0.1 mm in the first case and 0.2 mm in the second. Parts of the 3rd tolerance grade should be plated true to size, whereas parts of the 2nd tolerance grade, with a grinding allowance (about 0.08 mm on the diameter).

Chromium plating is widely used in the manufacture and repair of vehicle components. The permissible wear of such components ranges from 0.1 to 0.2 mm. The nominal dimensions are well to restore by chromium plating just within these limits.

Chromium plating is not advisable to use for parts operating in combination with babbitts, fine-grained cast irons, and soft or medium-hard steels at moderate pressures and with lubrication. The same also applies to parts working in combination with titanium. In some cases chromium is 4 to 5 times as wear-resistant as nitrided steel and 10 to 15 times as structural steel. Chromium plating, however, cannot replace full hardening and case hardening. Carburized and hardened steels are chrome-plated because of greater wear and corrosion resistance of chromium.

Each type of chromium plate should be used in the most advantageous conditions. For instance, poreless plates are advisable for parts operating with adequate lubrication at moderate sliding speeds. In other conditions a smooth chromium surface is inoperable, as it develops scores and scratches.

The wear resistance of chrome-plated parts does not improve if the working temperature changes the hardness of chromium. For this reason, forging dies, for instance, are chrome-plated where the working temperature does not exceed 500°C.

Acierage. Plates of this type can be very hard (HV 600-650), approaching the hardness of steel, which is why this process is sometimes called steeling.

The process has found the most extensive use for depositing metal on outworn surfaces of steel and cast iron parts to restore the initial dimensions. The electrolyte components are readily available, the process speed is high, and the deposit thickness can reach 8 mm. Where greater hardness is required, as, for instance, in restoring carburized parts, the deposit itself is either carburised or chrome-plated.

To obtain wear-resistant iron deposits with improved mechanical properties and structure directly from baths, use is made of electrolytes that contain manganese and nickel.

Hard nickel plating. This is used to increase the wear resistance of rubbing components and restore their dimensions. Nickel plates are less hard than chromium ones and relatively easy to run in; they have a greater toughness and may be up to 2 mm thick. The linear expansion coefficient of nickel is close to that of steel, whereas with chromium it is several times as great. The process requires a less powerful (by a factor of 3 to 4) d.c. source, and its power consumption is lower by a factor of 20 than that required by chromium plating.

The electrodeposition of a hard, wear-resistant alloy of nickel and phosphorus has also found application. The plate has a 30-percent lower coefficient of friction in sliding on cast iron than the chromium plate has on steel. In dry friction, the plate exhibits a wear resistance which is 3 times that of hardened steel Grade 45 and by 10 to 20 percent lower than that of chromium.

Parts of various metals, when rubbing against phosphorus-nickel plates, wear less by a factor of 4 to 5 than when rubbing against steel and less by 20 to 40 per cent than when rubbing against chromium. Hard nickel plating is used for strengthening and restoring crankshafts, machine tool spindles, piston pins, cylinder liners, etc.

Oxidation (deep) is a process of obtaining oxide films of over 60 μm in depth that have high microhardness (400 to 500) and wear resistance. The process is used for increasing the wear life of gears, motor components in textile machinery and other machine parts made of aluminium and its alloys with not more than 4.5 percent Cu and 7 percent Si. Oxidation of such parts and their use with lubricants increase the wear life from 5 to 10 times.

8.6. HARD-FACING

The method is used to strengthen newly manufactured parts as well as to restore worn machine parts and prolong their life. Hard-facing makes it possible to replace high-alloy steel by low-alloy and plain carbon steels, and, in the case of non-ferrous metals, to reduce their consumption and simplify construction.

Hard facing with tubular electrodes

Electrode		Average composition of deposits, %	Physical properties	Application
Grade	Filler			
ЭТН-1	Blast-furnace ferromanganese	2.0-2.5 C; 20-26 Mn	Hard and tough deposit. Microhardness of main material (without work hardening) is 500 to 700 kgf/mm ² , that of carbides, 1,200 to 1,400 kgf/mm ² ; Microhardness of work-hardened material is 700 to 900 kgf/mm ² . The thickness of facing layer deposited in one pass is up to 6 mm	Steel (carbon content under 0.35%) and cast iron parts: stonebreaker jaws, rims, hammers, excavator bucket teeth, caterpillar bogie wheels in excavators and tractors
ЭТН-2	Stalinite	2.4-2.5 C; 5-6 Mn; 5-6 Cr	Hard deposit. Mean microhardness is 800 to 900 kgf/mm ² . Facing layer deposited in one pass can be up to 6 mm thick. Blades are hard-faced with layers of not more than 4.5 mm thick	Steel and cast iron parts: blades in bulldozers, scrapers, and graders; rolls, snails, and wheels in dredgers; blades in mortar mixers, disintegrators, and asphalt mixing plants; ripper teeth
ЭТН-3	Blast-furnace ferromanganese with 6-7% nickel added	2.0-2.5 C; 20-26 Mn; 1.5-3 Ni	Hard deposit of high toughness. Microhardness of main material is 500 to 700 kgf/mm ² , that of carbides, 1,200 to 1,400 kgf/mm ²	Steel and cast iron parts, particularly those subject to sharp and heavy impact loads
ЭТН-4	Tungsten carbide (as second layer, the first layer is deposited with electrodes ЭТН-2)	—	Thickness of each layer of 1.5 to 2.0 mm. Mean microhardness of outward layer is 1,400-1,600 kgf/mm ²	Blades and cutters of high-speed earthmoving equipment used for frozen grounds; stonebreaker jaws for basalt and other hard rocks; blades of toothless dippers
ЭТН-5	Mixture Grade KBX-10	—	Hard deposit with wear resistance greater than that of ЭТН-4. Mean microhardness is 1,500 to 1,700 kgf/mm ²	The same as of the ЭТН-4 Grade electrodes

The method involves the fusion of a hard metal with the base metal, which provides for good adhesion of the two. The minimum thickness of the hard layer can be about 0.25 mm, but the maximum thickness is practically unlimited. The process provides for high production rates. Hard-facing materials are wire of high-carbon, alloy and high-alloy steels (GOST 10543-75) and metal electrodes (GOST 10051-75). The application of tubular electrodes is described in Table 8.10, and data on their wear resistance are given in Tables 8.11 and 8.12.

Table 8.11

Wear resistance of some materials and hard-facing deposits

Material	Microhardness	HRC	k_1	k_2
Steel Grade 65Г:				
unhardened	260-285	—	1.15	1.0
hardened	285-400	—	1.70	1.0
Chilled cast iron	470	—	2.8	1.15
Hard facing with electrodes Grade ЭТН-1:				
without work hardening	750	30-40	4.8	1.9
main material work-hardened to 50%	900	30-40	5.8	2.2
Hard facing with electrodes Grade Т-620	880-1,030	49-56	—	2.1
Tungsten carbide Grade BK6	2,200-2,400	76-78	—	5.5-6
Hard facing with electrodes Grade ХАДН	980-1,150	55-58	—	2.2
Chromium plating*	1,200	—	7	3.0-3.3
Hard facing with tubular electrodes:				
Grade ЭТН-3	800-950	30-40	—	2.2
Grade ЭТН-2	800-950	40-55	—	2.2
Grade ЭТН-4	400-1,600	62-64	—	2.6
Grade ЭТН-5	500-1,700	60-66	—	2.8

Designations. Wear resistance coefficients: k_1 with reference to steel Grade Cr3; k_2 with reference to steel Grade 65Г.

* Rubbing without impacts.

The oxy-acetylene process is used for strengthening parts made of steel Grades 35, 40 and 45. The process is also recommended for low and medium-alloy steel Grades 20X, 20X3, 18XFT, 30X, 35X, 40X (chromium steels), 20XH, 40XH, 12XHA3 (chromium-nickel steels), and 15X (chromium-vanadium steels). The process is most widely used for hard-facing with a hard metal of the Sormite* type and

* Sormite is the trade name of a family of hard iron-base alloys developed in the USSR.— *Translator.*

Table 8.12

Wear resistance of various materials and hard-facing deposits

Material of hard-facing deposit and its conditions	Substrate material	Composition of deposit, %	Thickness of electrode casing, mm	Microhardness, kgf/mm ²			HRC	k ₁	k ₂	k ₃
				H ₀	H _c	H _m				
Steel Grade Cr6 hardened and tempered	—	0.38-0.50 C	—	—	—	480-500	—	3.85	1.0	0.16
Tungsten carbide Grade BK6	—	94 WC-6 Co	—	—	2,800	—	—	23.8	6.2	1.0
Chilled cast iron, outer layer	—	3.0-3.5 C	—	250	800	470	—	3.3	0.85	0.17
Hadfield steel before work hardening	—	1.0-1.4 C; 10-14 Mn	—	—	—	500	—	4.0	1.0	0.17
Hadfield steel work-hardened to 50%	—	10-14 Mn	—	—	—	750	—	1.6	1.6	0.26
Hard-facing with carbonic tubular electrodes										
80% iron chips 20% ferrochromium	Cr3	1.33 C	—	—	—	—	52	—	—	—
		4.3 Cr	0.8	—	—	1,070	55	9.1	2.4	0.38
Hard-facing with manganese tubular electrodes										
100% blast-furnace ferromanganese	Cr3	2.64 C; 26 Mn; 0.93 Si	0.65	625	1,530	908	42-46	6.7	1.8	0.2
93% blast-furnace ferromanganese and 7% nickel		2.4 C; 19.1 Mn; 1.87 Ni	0.65	678	1,600	797	27-30	6.1	1.6	0.26
100% blast-furnace ferromanganese		2.1 C; 21 Mn	0.8	625	1,355	775	40-41	6.1	1.6	0.26
93% blast-furnace ferromanganese and 7% nickel		2.57 C; 26 Mn; 2.68 Ni	0.8	813	1,510	910	22	6.8	1.8	0.28

Table 8.12 (cont.)

Material of hard-facing deposit and its condition	Substrate material	Composition of deposit, %	Thickness of electrode casing, mm	Microhardness, kgf/mm ²			HRC	k ₁	k ₂	k ₃
				H ₀	H _c	H _m				
Hard-facing with tubular electrodes filled with Stalinite										
100% Stalinite (hand deposition)	Cr3	2.9 C; 5.5 Mn 6.5 Cr; 2.45 C;	0.8	625	977	790	50	6.7	1.8	0.28
		5.9 Mn; 5.2 Cr	0.8	—	—	898	54	7.6	2.0	0.32
100% Stalinite (machine deposition)	Cast iron Cr3	3.1 C; 5.0 Mn; 5.2 Cr	0.8	—	—	826	55	7.0	1.8	0.29
		2.47 C; 6.4 Mn; 5.4 Cr	0.8	—	—	940	40	7.7	2.0	0.32
Hard-facing with tungstic tubular electrodes										
100% tungsten carbide (hand deposition)	Cr3	—	0.8	1,400	2,300	1,550	62-64	13.1	3.4	0.55
Hard-facing with chromous tubular electrodes										
55% ferrochromium, 40% iron chips, 5% refined graphite	Cr3	2.3 C; 10.8 Cr	0.75	—	—	808	48	6.8	1.8	0.28
55% ferrochromium, 40% iron chips, 5% refined graphite	—	2.17 C; 8.0 Cr	0.65	678	1,206	884	52	7.5	2.0	0.31
Hard-facing with solid electrodes and chromium plating										
Electrodes Grade MBTV, 5 mm dia, thinly coated	—	1.7 C; 23-25 Mn	—	640	1,470	—	—	—	—	—
Electrodes Grade T-620	Cr3	3 C; 18.0 Cr	—	813	1,190	—	49-56	6.8	1.8	0.29
Electrodes Grade T-620		3.1 C; 18.0 Cr	—	736	1,355	—	51-56	6.7	1.8	0.29
Chromium plating	—	—	—	—	—	1,200	—	10.2	2.5	0.43

Designations. k₁, k₂, and k₃ = wear resistance coefficients with reference to steel Grade 20, steel Grade Cr6, and cemented carbide Grade BK6, respectively; H₀, H_c, and H_m = microhardness of main material and carbides, and mean microhardness, respectively.

Designations. k₁, k₂, and k₃ = wear resistance coefficients with reference to steel Grade 20, steel Grade Cr6, and cemented carbide Grade BK6, respectively; H₀, H_c, and H_m = microhardness of main material and carbides, and mean microhardness, respectively.

with various high-temperature materials of tools and machine parts whose working surfaces must have high hardness and wear resistance. Hard-facing with Sormite is advisable for carbon steels, especially for steel Grade Y8A. Alloy tool steel Grades 5XHM, 3XBA, 4XBC etc., can also be processed, although low-alloy structural steels, such as Grades 40XH, 40X, etc., lend themselves to the process easier.

Hard-facing with Sormite is also used for road and construction machine parts which require high wear resistance.

The hard layer thickness is specified in accordance with operating conditions and permissible wear of the surface: for parts subject to abrasive wear it should not exceed 2.5 to 4 mm, for cutting tool edges, 1.5 to 3 mm, and for tools subject to small impact loads, 2 mm. Hand processing capability is from 0.25 to 0.5 mm.

Sormite No. 1 is normally used for layers 0.5 to 5 mm thick, and Sormite No. 2, for those 1.5 to 3.5 mm thick. A facing thick in excess of 1.5 mm is usually formed in several layers, because a single layer placed at once tends to mix with the base metal. Where the permissible wear of a part is greater than the maximum possible thickness of the Sormite layer, the surface is first faced with a filler metal with properties similar to those of the base metal, and only then with Sormite.

The arc-welding process is used both in manufacture and in repair practice. The types and grades of electrodes for processing machine parts of steels and alloys are specified by GOST 10051-75. The properties guaranteed by the electrodes are valid for the second or third layer. Mechanized processing is effected with consumable electrodes.

Workpieces that undergo mechanized processing normally require no special surface preparation.

The electroslog process. A high-alloy hard layer is obtained mainly by using filler materials (wire of solid cross-section, castings, sintered and electrode wire). For high-alloy steels, the most suitable flux is AH-22, for carbon and alloy steels, AH-8 GOST 9087-69 and crushed fluorite.

The process is usually combined with positive forming of the metal-bath surface by an iron mould, pad, or slider.

The electroslog process offers advantages over arc welding; the amount of the base metal in the hard layer is reduced (from 30-40 percent to 10-15 percent), the flux requirements are lower, the power losses are reduced; the process provides for higher efficiency; the slag skin requires no removal since the process is run in a single pass.

The process is expedient where considerable amounts of facing metal must be deposited on parts coming in large lots. The most commonly processed parts are those with flat, conical, and cylindrical surfaces.

The vibratory arc-welding process makes it possible to form hard layers 0.3 to 3 mm thick without overheating the parts being treated. The hard metal is transferred from a vibrating electrode in

small portions as a result of frequent arc discharges produced on breaking the circuit.

The material is wire 1.5 to 2.5 mm in diameter of carbon, low- and medium-alloy steels, and also some high-alloy steels. The process is applied in the manufacture and dimensional restoration of machine parts made of carbon and alloy steels. The service properties of the hard layer can be improved by finish machining (grinding and electromechanical burnishing or polishing, etc.).

8.7. METAL SPRAYING

According to the heat source used to melt the metal, metal spraying is classified into gas, electrical and plasma types.

Plasma spraying has greater manufacturing capabilities than the other methods. Coating materials are aluminium oxides, tungsten, molybdenum, niobium, intermetalloid compounds, silicides, various carbides, borides, etc. Materials which are coated include metals, ceramics, plastics, glass, wood, etc. A flow of plasma-forming gas containing no oxygen allows the metallization of materials without their decomposition and prevents the oxidation of the material being coated. The plasma flow makes it possible to obtain alloys of different materials, including refractory ones, and to apply multi-layer coatings. The surface being coated heats to no more than 200°C, which excludes workpiece warpage. The energy characteristics of the plasma flow are easily adjustable in accordance with processing requirements, which is impracticable with gas spraying.

The most common use of plasma spraying is in deposition refractory compositions.

The process is capable of providing coatings 0.02 mm in thickness and more (up to 15 mm and even thicker).

A part is prepared for metallization by cleaning and roughing the surface to be coated. The most commonly used methods are sand blasting and cutting a thread with rough surface.

The coating is applied by special spray guns. Depending on application, use is made of the following wire grades:

Restoration of worn rubbing surfaces
working in contact with antifriction
alloys in the presence of lubrication

Steel Grades V12, V10,
V8 (at high pressures);
steel Grades 60, 50 (at
low and medium pressures)

Restoration of worn joint faces . .

Steel Grades 40, 30 10

Protection from water and atmospheric corrosion

Zinc, cadmium

Protection from corrosion in aggressive media	Lead (in sulphuric acid) Aluminium (in nitric acid)
Deposition of sprayed antifriction linings	Bimetallic wire: lead-aluminium, lead-copper, copper-steel; zinc
Filling of cracks in iron, steel, and non-ferrous alloy castings	Zinc, low-carbon steel (in non-aggressive media)

The necessary dimensional accuracy and surface finish of machine parts with a sprayed metal layer can be achieved by machining on metal-cutting machine tools.

Machining allowances and the minimum thickness of the coating layer left after machining are given in Table 8.13. The strength of

Table 8.13

Machining allowances and minimal thickness of coating (on radius, mm) after machining

Workpiece diameter, mm	Turning to size	Turning and subsequent grinding		Grinding without preliminary turning	Minimum thickness of coating
		turning allowance	grinding allowance		
Up to 25	0.50	0.50	0.15	0.35-0.40	0.60
26-50	0.60	0.60	0.15	0.40-0.45	0.60-0.65
51-75	0.65	0.65	0.15	0.45-0.50	0.65-0.70
76-100	0.75	0.75	0.20	0.50-0.57	0.75-0.80
101-125	0.80	0.80	0.20	0.57-0.65	0.80-0.85
126-150	0.90	0.90	0.20	0.65-0.72	0.85-0.90
151 and more	1.00	1.00	0.20	0.80-0.85	0.95-1.00

adhesion between the deposit and the base metal mainly depends on the quality and method of surface preparation for spraying (Table 8.14), and on the materials of the coating and the base. Sprayed metal layers exhibit greater wear resistance than the initial metals. This can be attributed to increased hardness (Table 8.15) and to channels and pores in the layer, which facilitate lubrication.

The spraying of self-fluxing carbides, especially that involving plasma spraying with subsequent melting of the deposit, is finding ever increasing use.

The chemical composition of self-fluxing powders for spraying is specified by GOST 21448-75.

The surface being coated should have a definite roughness that provides for the maximum strength of adhesion of the coating to the base. Three main methods are recommended for surface preparation: turning (for solids of revolution), blasting with steel particles, and blasting with iron shots (both used for any open surface).

Table 8.14

Strength of adhesion (kgf/cm²) of coating to substrate, depending on preparation method (workpiece—steel shaft)

Method of surface preparation	Direction	
	tangential	axial
Sand blasting	620	345
Hatching with chisel with subsequent sand blasting	739	820
Blasting with steel chips	840	—
Shot blasting	710	1,040
For threaded features, cutting threads with rough surfaces	965	1,800
The same for rounded thread, with flattening the crests	2,120	1,440
Winding wire and subsequently sand blasting	1,930	—
Spark erosion treatment	—	915-1,100
Electric arc treatment	—	250

Table 8.15

Some physico-mechanical properties of substrate and sprayed coating materials

Material	σ_t , kgf/mm ²	δ , %	σ_c , kgf/mm ²	HB
Zinc	11.27 (3.24)	65 (1.3)	(13.00)	25 (32)
Aluminium	9.16 (3.45)	45 (1.1)	(20.40)	20 (44)
Copper	22.55 (3.10)	58 (0.0)	—	50 (97)
Brass	31.68 (2.64)	60 (0.0)	(52.50)	59 (103)
Lead	1.41 (1.37)	64 (1.5)	—	—
Steel Grade 40	(10.00-18.00)	—	(105.00-153.00)	158 (230)

Note. Figures in parentheses pertain to sprayed metal.

The maximum strength-of-adhesion values before and after deposit melting for various surface preparation methods with the same surface roughness parameters ($R_a = 20-35 \mu\text{m}$; $R_p = 40-80 \mu\text{m}$; $R_{\text{max}} = 100-170 \mu\text{m}$; $S_m = 400-450 \mu\text{m}$) are given in Table 8.16.

The cutting conditions and tool geometry providing for the maximum strength of bonding are presented in Table 8.17 (the base materials are steel Grades Cr3 and 45, the adhesion strength before melting is 3.5 kgf/mm², after melting 18 to 21 kgf/mm²).

Melting is done to turn the sprayed layer into a solid condition and to create its metallic bond with the base material. The melting process is normally effected in two stages: the preliminary heating

Table 8.16

Strength of adhesion to substrate

Surface roughness parameter $S_m, \mu m$	Shear strength of adhesion (kgf/mm ²) of unfused and fused (figures in parentheses) coatings to surfaces prepared by			
	turning	blasting		
		with shots	with steel chips	with quartz sand
340	2.0 (11.7)	2.0 (11.4)	1.9 (11.2)	0.9 (4.9)
390	2.3 (13.1)	2.5 (13.5)	2.3 (13.0)	6.9 (5.2)
430	2.4 (14.0)	2.6 (16.1)	2.5 (14.6)	1.2 (6.8)
470	2.5 (14.5)	2.5 (14.1)	2.7 (15.0)	1.3 (7.2)
520	2.6 (14.5)	2.4 (13.7)	2.4 (14.0)	1.0 (7.1)
570	2.3 (13.0)	2.2 (13.0)	2.4 (12.1)	0.8 (6.0)
610	2.1 (12.2)	2.0 (11.8)	2.1 (12.0)	0.7 (5.4)
640	1.8 (11.4)	1.9 (11.0)	1.7 (11.5)	0.6 (5.0)

Table 8.17

Surface preparation for metal spraying

Turning (tool bit-cemented carbide T15K6)								Blasting with steel chips				Blasting with cast-iron shots		
$v, m/min$	$s, mm/rev$	t, mm	φ°	φ_1°	R, mm	γ°	ρ, mm	l, mm	b, mm	$p, kgf/cm^2$	T, min	D, mm	$p, kgf/cm^2$	T, min
65-75	0.4-0.55	0.4-0.7	45	45	0.3-0.8	0+4°	0.05-0.1	1.5-3.0	0.5-1.5	4-5	5-8	0.8-1.2	4-5	5-8

Designations. v = cutting speed, s = feed, t = depth of cut; φ = side cutting edge angle, φ_1 = end cutting angle, R = tool nose radius, γ = rake angle, ρ = cutting edge rounding radius, l = size of steel chip lengthwise, b = size of steel chip crosswise, p = compressed-air pressure, D = iron shot diameter.

of the coated part to 800-900°C, and the final heating of the sprayed layer to 1030-1080°C when the liquid phase (eutectic) begins to appear.

The machining of the *CHFH* and *BCHFH* type coats having a bulk hardness of *HRC* 58-68 and a microhardness of individual boride, carboboride, and carbide inclusions of up to 4,000 kgf/mm² should be performed exclusively by diamond grinding wheels. Grinding by abrasive wheels is not practical because of low productivity (slow feeds and speeds and frequent wheel dressing required) and inadequate surface quality.

These alloys should be preliminarily ground by diamond wheels with metal bonds, (Types MO16, MO13, and MB1), using diamonds (Grades ACKM, ACK, and ACB) having grain sizes 200/160 and

250/200. The wheels ensure a stable surface finish of $(0.16 \text{ to } 0.3) = \mu\text{m } Ra$ and minimal diamond requirements as compared with organic-bonded diamond wheels.

The recommended grinding conditions are: $v_{wheel} = 35\text{--}50 \text{ m/s}$, $v_{work} = 25\text{--}35 \text{ m/min}$, $s_{long} = 1 \text{ m/min}$, $s_{cross} = (0.08 \text{ to } 1.5) \text{ mm/double stroke}$ [(0.01 to 0.03) mm/double stroke in final passes], and copious coolant (5 percent emulsol in water). Finish grinding should be done by the face of the cup-type grinding wheels, elastic grinding sticks, and endless abrasive bands, with a 20-percent aqueous solution of emulsol.

For instance, a shaft 1,500 mm in diameter is ground by a 150 mm dia wheel. The wheels to be used are with the ACO, ACP, and ACM Grade diamonds, the B1 and BP Grades organic bonds, and grain sizes 28/20 to 125/100. The minimal surface roughness [(0.04 to 0.02) $= \mu\text{m } Ra$] is achieved at a longitudinal feed of $s_{long} < 0.27 \text{ mm/rev}$, a grinding pressure of 3 to 6 kgf, and wheel grain sizes $K = 28/20\text{--}63/50$.

Polishing is done with diamond bands [elastic sticks having a steel base, a rubber underlayer, and an elastic diamond band (ACO) with rubber bonds Grades P9 and P4, or endless diamond bands]. Cloth-base diamond bands are impractical to use for grinding the hard coatings because of high diamond consumption (one band is spent on machining two or three workpieces 80 dia \times 40 mm). For grinding with elastic sticks use is made of the CФГ-100 Type superfinishing head mounted on an engine lathe. The sticks oscillate with an amplitude of 3 mm, and 1,400 double strokes/min, with a large volume of coolant being applied (a mixture of 79% Kerosene, 20% spindle oil, and 1% oleic acid).

The best surface finish [(0.03 to 0.015) $= \mu\text{m } Ra$] is achieved at $v_{work} = (25 \text{ to } 30) \text{ m/min}$, $T = 25\text{--}35 \text{ s}$, $p = 3 \text{ to } 4 \text{ kgf/cm}^2$, and $K = 28/20\text{--}63/50$. Similar machining conditions should be used when grinding with endless rubber-bonded diamond lands (bond Grades P9 and P4).

Diamond grinding is equally effective for all self-fluxing Ni-Cr-B-Si carbides. The ПГ-XH80CP2 and ПГ-XH80CP3 Grade alloys can also be machined with silicone-carbide grinding wheels. Rough grinding is carried out with the K325-40 CM1K-CM2K Type wheels and finish grinding, with the K310-16 CM1-CM2 Type wheels.

Self-fluxing coatings are highly wear resistant. For instance, coating-to-steel friction pairs (in boundary friction conditions) provide a 4- to 9-times increase in wear life at specific loads of 15 to 100 kgf/cm² and sliding speeds of 8 to 54 m/min as compared with steel-to-steel and steel-to-cast iron pairs; wear of steels rubbing against the coatings decreases by a factor of 1.5 to 2.5.

Data on wear of self-fluxing coatings are given in Tables 8.18 and 8.19.

The coefficient of friction in coating-to-steel pairs is reduced by a factor of 1.8 to 2.2 with the initial surface roughness of (0.16 to

Table 8.18

Wear resistance of self-fluxing coatings (lubrication with grease Grade BHHH HII-410)

Sliding distance, km	Wear (μm) for sliding couples			
	steel Grade XBF-steel Grade XBF	steel Grade XBF-coating Grade CHFH	steel Grade 45-coating Grade CHFH	steel Grade 40X-coating Grade CHFH
$p = 15 \text{ kgf/cm}^2, v = 54 \text{ m/min}$				
1.68	1.0-1.0	0.5-0.4	0.5-0.3	0.6-0.4
3.37	1.5-1.5	1.0-0.6	0.6-0.4	0.8-0.5
5.05	2.0-2.0	1.5-0.7	1.0-0.5	1.0-0.6
10.1	2.5-2.5	2.0-0.8	1.5-0.6	1.4-0.6
20.2	3.0-3.0	2.5-0.8	2.0-0.7	1.9-0.7
25.3	3.2-3.2	2.7-0.9	2.1-0.7	2.1-0.7
$p = 50 \text{ kgf/cm}^2, v = 54 \text{ m/min}$				
1.68	3.0-3.0	1.2-0.5	0.8-0.3	0.8-0.3
3.37	4.0-4.0	2.0-0.8	1.3-0.5	1.2-0.4
5.05	5.0-5.0	2.5-1.0	1.5-0.5	1.6-0.5
10.1	6.0-6.0	3.0-1.1	2.0-0.7	2.1-0.7
20.2	7.0-7.0	3.3-1.2	2.3-0.8	2.3-0.7
25.3	7.5-7.5	3.4-1.3	2.5-0.8	2.5-0.8

Table 8.19

Wear resistance of self-fluxing coatings (lubrication with oil Grade II-12A)

Sliding distance, km	Wear (μm) for sliding couples			
	steel Grade 48A-steel Grade 45	steel Grade 48A-coating Grade CHFH	steel Grade 45-coating Grade CHFH	steel Grade 40X-coating Grade CHFH
$p = 15 \text{ kgf/cm}^2, v = 54 \text{ m/min}$				
1.68	2.0-2.5	1.5-0.3	0.5-0.3	0.4-0.3
3.37	2.4-3.0	2.5-0.4	0.8-0.4	0.7-0.4
5.05	3.5-3.8	3.5-0.5	1.0-0.5	1.0-0.5
10.1	4.0-4.3	3.9-0.5	1.5-0.6	1.4-0.6
20.2	4.4-4.0	4.0-0.6	2.0-0.7	1.9-0.7
25.3	4.6-5.3	4.2-0.7	2.1-0.7	2.0-0.7
$p = 50 \text{ kgf/cm}^2, v = 54 \text{ m/min}$				
1.68	2.0-2.5	2.0-0.3	0.8-0.3	0.8-0.3
3.37	3.0-3.5	3.0-0.5	1.3-0.5	1.3-0.4
5.05	4.0-4.5	3.5-0.6	1.5-0.5	1.4-0.5
10.1	4.5-5.0	4.0-0.6	2.0-0.7	2.0-0.6
20.2	5.0-5.5	4.5-0.6	2.3-0.8	2.3-0.7
25.3	5.2-5.8	4.7-0.8	2.5-0.8	2.5-0.8

0.3) $\mu\text{m } Ra$, and by a factor of 2 to 10 with the surface roughness obtained after running in.

The Ni-Cr-B-Si self-fluxing coatings are most effective where a part must be protected simultaneously against wear, an aggressive medium, and a high temperature (up to 800°C). The coatings are widely used to prolong the wear life of various machine components: pumps, fan blades, casting-machine plungers, valves in hydraulic systems, cams, dies, screws for abrasives conveyors, etc.

Coatings of the BСНГН Grade alloy filled with tungsten carbide providing very high hardness are effective to apply for protecting parts subject to a combined abrasive, erosive, and mechanical action.

The use of self-fluxing hard materials in tribological joints prolongs their life from 5 to 30 times.

REFERENCES

1. Аскинази Б. М. Упрочнение и восстановление деталей электромеханической обработкой. Л., «Машиностроение», 1977.
2. Елизаветин М. А., Сатель Э. А. Технологические способы повышения долговечности машин. М., «Машиностроение», 1969.
3. Елизаветин М. А. Повышение надежности машин. М., «Машиностроение», 1973.
4. Маталин А. А. Технологические методы повышения долговечности деталей машин. Киев, «Техніка», 1971.
5. Рыжов Э. В. Технологическое управление геометрическими параметрами контактирующих поверхностей.— В кн.: Расчетные методы оценки трения и износа. Брянск. Приокское книжное изд-во, Брянское отделение, 1975.
6. Сагарда А. А., Чеповецкий И. Х., Мишнаевский Л. Л., Алмазно-абразивная обработка деталей машин. Киев, «Техніка», 1974.
7. Справочник металлста. Т. 2. М., «Машиностроение», 1977.
8. Справочник технолога-машиностроителя. Т. 1. М., «Машиностроение», 1972.
9. Старосельский А. А., Гаркунов Д. Н. Долговечность трущихся деталей машин. М., «Машиностроение», 1967.
10. Шнейдер Ю. Г. Образование регулярных микрорельефов на деталях и их эксплуатационные свойства. Л., «Машиностроение», 1972.
11. Ящерицын П. И., Рыжов Э. В., Аверченков В. И. Технологическая наследственность в машиностроении. Минск, «Наука и техника», 1977.

LUBRICANTS AND ADDITIVES

9.1. ENGINE OILS

Oils used to lubricate piston-type internal combustion engines are called engine oils. These are lubricants containing a base oil and synthetic additives which improve the properties of the base oil or impart to it the required new properties. The composition and viscosity of the base oil and also the types and concentrations of the additives generally determine the service properties of engine oils. The basic components of engine oils have a viscosity of 3.5 to 22 cSt at 100°C. The concentration of engine-oil additives is varied within a wide range (from several percent in light-duty oils to 25-30 percent in oils for marine diesel engines operating on heavy, high-sulphur fuels).

The general characteristic necessary to select an engine oil in accordance with its operating conditions are contained in the standard grade designations of engine oils established by GOST 17479-72.

The standard grade designations comprise the following symbols. The initial letter M stands for engine oil. The figure next to it indicates the nominal oil viscosity in centistokes at 100°C. For all-weather oils, this figure is the denominator of a fraction whose numerator indicates the viscosity limits in centistokes at -18°C. After the figure or the fraction comes one of the first six letters of the Russian alphabet; in addition, the letters Б, В and Г may be provided with subscripts 1 and 2. The letters indicate the field of application of the oil, i.e., its group in accordance with operating conditions. Altogether, GOST 17479-72 specifies 11 classes of engine oils by viscosity and 12 groups by operating conditions.

Let us give some examples of decoding engine oil designations. Oil Grade M-12Г₁ is an engine oil having a viscosity of 12 cSt at

100°C, group Γ_1 ; oil Grade M-6₃/10B is a high-viscosity all-weather oil with a viscosity of 10 cSt at 100°C and from 2,600 to 10,400 cSt at -18°C, group B.

9.1.1. Classification by Viscosity and the Main Principles of Oil Selection

According to viscosity, engine oils are divided into seven seasonal classes and four all-weather classes. Viscosity values for each class are given in Table 9.1.

Table 9.1

Viscosity classes of engine oils

Viscosity class	Viscosity, cSt, at temperature °C		Viscosity index
	100	-18	
6 8 10 12 14 16 20	6±0.5 8±0.5 10±1.0 12±0.5 14±1.0 16±1.0 20±2.0	Unspecified	≥ 90
4 ₃ /6 4 ₃ /8 4 ₃ /10 6 ₃ /10	6±0.5 8±0.5 10±0.5 10±0.5	2,600 > v ≥ 1,300 10,400 > v ≥ 2,600	≥ 125

The classification also specifies values of the viscosity index, a conventional quantity that characterizes the relationship between oil viscosity and temperature. The greater the viscosity index, the smaller is the change of viscosity with temperature. In addition, the viscosity index of seasonal oils defines the degree of purity of the base oils used to produce them. The high viscosity index of all-weather oils is achieved with the aid of special additives that increase viscosity at high rather than low temperatures. Engine oils that can be used for automobile and tractor engines in winter as well as in summer, and also special oils for use in engines operating at very low subzero temperatures are obtained by adding high-molecular polymers and copolymers into a thin mineral oil.

The choice of an engine oil by viscosity is made considering two typical regimes of engine operation in which the oil viscosity is at

its maximum and minimum, namely, the start-up of the engine cooled to ambient temperature, and long-term operation at peak power output.

It has been found experimentally that the maximum viscosity of an engine oil that makes it possible to start up an engine equals 2,500 to 5,000 cP. The minimum oil viscosity on the surfaces of the hottest rubbing components which ensures proper lubrication is 2 to 4 cP.

Table 9.2 compiled on the basis of the data given in [54], presents

Table 9.2

Equivalent-viscosity temperatures for different engine oils

Viscosity class SAE J300	SAE 10W	SAE 20W	SAE 30	SAE 40	SAE 50
Viscosity class GOST 17479-72	6*	6-8	10-12	14-16	20
Minimum temperature of cold start, °C	-23	-18	-10	0	+5
Maximum temperature of oil in crankcase, °C	90	110	135	150	160

* Lower limit.

approximate temperature values at which engine oils of different viscosity classes have equivalent viscosities.

The average values of the maximum temperatures of engine parts and oil in the crankcase [57] are given in Table 9.3.

Table 9.3

**Maximum temperatures of rubbing parts and oil
in engine crankcase, °C**

Test point	Carbu- rettor engines	Diesel engines	Test point	Carbu- rettor engines	Diesel engines
Piston groove for upper compression ring	180-300	250-290	Cylinder wall	—	200-230
Camshaft cam	120-195	180-220	Crankshaft main bearing	140-170	115-170
			Oil in crankcase	130-160*	100-150

* Oil cooler allows the temperature of oil to be reduced by 23°C on the average.

Engines used at ambient temperatures above 0°C or in the engine rooms of vessels, power plants, etc., should be lubricated with class 10 to 20 engine oils. Preference should always be given to an oil with the minimum necessary viscosity. The use of an oil with excessive viscosity results in increased fuel consumption due to friction losses and intensive wear during engine starts if the engine is started up infrequently and the oil is not pumped through the engine prior to its starting.

Where the use of an engine involves frequent starts after relatively short downtime intervals (under two hours), it is well to select an oil whose viscosity is one class higher than the required minimum value (2 to 4 cP). For an oil of greater viscosity it takes longer to run off the rubbing surfaces, which ensures a reduction in start-up wear. With prolonged downtime periods, the positive effect of greater oil viscosity becomes insignificant.

Oils of the 10th and 12th classes are expedient to use in high-speed vehicle engines; those of the 14th to 16th classes, in medium-speed diesel and marine engines; and class 20 oils, for lubrication of cylinders in marine crosshead engines.

One particular reason for the use of oils of higher viscosity in engines with large-diameter cylinders is that such oils provide for better sealing of the clearances between the piston rings and grooves and so prevent the leakage of gases from the combustion chamber.

For engines run at subzero temperatures, use is made of winter oils of classes 6 and 8 or of all-weather oils of classes 4₃/10 and 6₃/10. The latter oils and also class 8 oils are used in summer as well.

Automotive engines of the carburettor type should be lubricated with class 4₃/6 oils in winter at low subzero temperatures, with class 8 or 6₃/10 in winter and summer in moderate-climate regions, and with class 12 oils in summer in hot-climate regions. Automotive and tractor engines of the diesel type should be lubricated with class 6 oils in winter at low subzero temperatures, and with class 8 and classes 10 to 12 oils in moderate-climate regions in winter and summer, respectively.

The latest development outside this country is wide-range all-weather oils (SAE 10W/50 and SAE 20W/50), which are equivalent in viscosity to oils 4₃/20 and 6₃/20 according to the classification of GOST 17479-72. Such oils can be used in Western Europe's climate all the year round for lubricating modern and prospective automobile engines, specifically for prolonged highway riding at maximum speeds [54]. For prospective models the maximum temperature of oil in the crankcase is predicted at 160°C. However, it should be reduced by all means to the following values to maintain the required periods between oil changes: 130 to 135°C for oils of the 10th through 20th classes; 115°C for class 8 oils, and 100°C for denser oils. Temperatures in excess of these limits sharply increase the rate of oil oxidation.

9.1.2. Classification by Service Properties and the Main Principles of Selection

The principal properties of engine oils which determine their fitness for engines of different types and different degrees of boosting used in various operating conditions include:

- antisludge properties, i.e., the ability to prevent the formation of sludge on hot surfaces and the coking of piston rings;
- wear-resistant properties;
- dispersion properties, i.e. the ability to prevent the formation of low-temperature sediment in the crank-case, oil piping, oil filter and other areas during low-load operation of the engine;

$P_{eff}, \text{kgf/cm}^2$

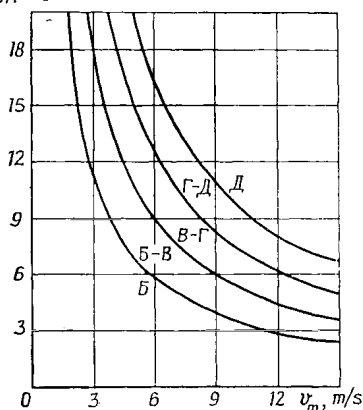


Fig. 9.1. Selection of oil group depending on engine boosting level

ing on the field of application, is established by GOST 17479-72. Oils of groups B_1 and B_2 , B_1 and B_2 , Γ_1 and Γ_2 are used, respectively, for engines of the carburettor type and diesel type with low, medium, and high degree of boosting. Oils of groups B , B and Γ are universal and can be used both for carburettor and diesel engines.

The correspondence of an oil to a given group is established by a number of standard tests carried out on special installations or test engines. The testing procedures for each group are listed in GOST 17479-72, and described in [33].

The recommended fields of application for the various groups are given in GOST 17479-72 descriptively, without any quantitative definition of engines with low, medium, and high degree of boosting. For more accurate selection of an oil according to the degree of engine boosting, use may be made of the graph in Fig. 9.1, which has been constructed on the basis of the data given in [61]. For this purpose, the designations of the groups of service properties according to the

- anticorrosion properties, i.e., the ability to prevent corrosion of the crankshaft bearing linings;

- antioxidation properties, i.e., resistance to oxidation at high temperatures;

- neutralizing properties, i.e., the ability to neutralize acids forming in the process of oil oxidation and condensed from the end products of fuel combustion.

Commercial grades of engine oils with the required properties are obtained by varying the chemical composition of the oils and the amount of additives in them.

The classification of oils into groups by service properties, depend-

US and UK military specifications were replaced by the standard group designations according to GOST 17479-72, using the interchangeability diagram [33].

The engine boosting criterion, which is the product of the piston mean velocity, v_m and the mean effective pressure, p_{eff} , has been taken as an attribute indicative of the severity of operating conditions for oil in an engine. Four similar boosting-criterion curves have been constructed and five regions obtained on the p_{eff} versus v_m graph. Each curve represents the boosting criterion of the engine installation used to test oils of a given group for classification. Each region indicates the oil groups whose boosting criterion falls into this region. It should be noted that oils of the lowest group are applicable in combination with a fuel containing up to 0.4 percent sulphur, whereas oils of the higher groups are operable with a fuel having up to 1 percent sulphur. For two-stroke engines the values of the boosting criterion should be doubled.

The assortment of USSR-made engine oils, their main characteristics and applications are given in [45].

The classifications and interchangeability of engine oils made in the USSR and other countries are considered in [33].

9.2. TRANSMISSION OILS FOR AUTOMOTIVE APPLICATIONS

Oils of this type are used for lubricating the mechanical and hydromechanical transmissions of land vehicles.

Typical forms of damage of transmission gears and bearings are pitting of the working surfaces and, at high contact temperatures, scuffing.

An effective measure against scuffing is extreme-pressure additives in oils; as for fatigue life of teeth surfaces, it may be prolonged by increasing the oil viscosity.

When selecting an oil by viscosity, it must be taken into consideration that the viscosity and the behaviour of the oil at low temperatures determine the possibility of starting the vehicle at a low temperature without warming up the transmission; they also determine the consumption of fuel and the ease of draining the oil.

9.2.1. Viscosity and Its Dependence on Temperature

The required viscosity and low-temperature properties of the oil to be used are determined by the temperature conditions of the service and storage of the vehicle, the transmission design features and the specific engine power (per unit vehicle mass).

The classification of USSR-made automotive transmission oils by viscosity and service conditions, adopted by the CMEA countries (PC-3999-73), is given in Table 9.4. together with the respective oil grades.

Table 9.4

USSR-made transmission oils, as grouped by viscosity and service conditions according to the PC-3999-73 classification adopted by CMEA countries

Viscosity classes		TM-1	TM-2	TM-3	TM-4	TM-5
SAE	USSR					
75W	6	—	—	—	—	—
80W	9	—	ТС ₃ -9-ДФ-11	ТСЗП-8, ТС-10-ОТП	ТС ₃ -9ГИП	—
85W	12	—	—	—	—	TM5-12 TM5-12PR
90	18	Nigrol 3	ТЭ-15-ЭФО ТС 14.5-ДФ-11	ТСП-14 ТАП-15В, ТСП-15К	ТС-14.5- chloref-40 ТАД-17, ТСЗП-16А	ТАД-17И
140	34	Nigrol Л		Oil for gear- boxes and steering gear cases GOST 4002-53	Oil for hy- poid gears GOST 4003-53	

Note. Oil Grades TM-1 without additives; oil Grades TM-2 with antiwear additives; oil TM-3 with extreme-pressure additives; oil Grades TM-4 and TM-5 for hypoid gears; Grades TM-4 with chlorine-containing additives and free sulphur, Grades TM-5 with multicomponent chlorine-phosphorous additives.

It is important that for transmission oils used within a wide temperature range the viscosity-temperature curve should be gradual. For the range of temperatures where oils obey the Newton law

$$\tau = \eta \frac{dv}{dh}$$

(where h = thickness of the oil film, cm; η = dynamic viscosity and v = velocity, cm/s) the relationship between the kinematic viscosity and the temperature of oil is determined by the Walter law [18, 36]

$$\lg \lg (v + 0.8) = A - B \lg T$$

where ν = kinematic viscosity, cSt, and A and B = constants depending on the hydrocarbon content of oils.

The relationship between kinematic viscosity and temperature, according to the Walter law, for several grades of transmission oils is shown in Fig. 9.2. Given the value of viscosity at two different temperatures, the nomograph can be used to find the viscosity at

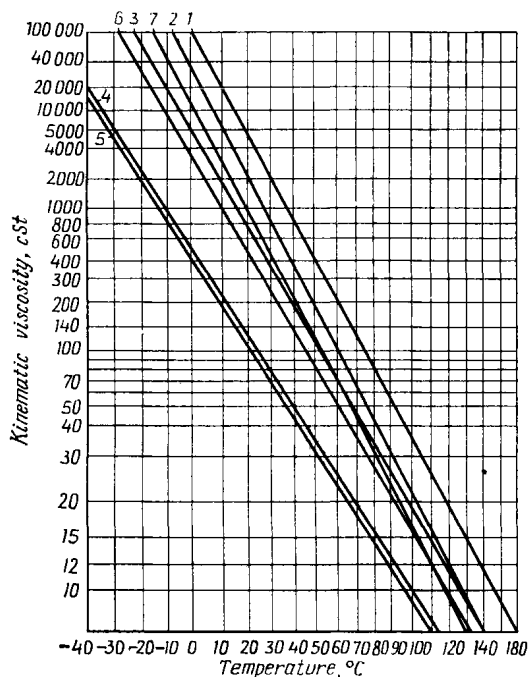


Fig. 9.2. Kinematic viscosity of transmission oils as a function of temperature (Walter's law)

1—industrial oil (Nigrol II); 2—sulphurized oil for hypoid gears; 3—oil Grade ТАД-17М; 4—oil Grade ТСз-9-ГНП; 5—oil Grade ТСП-8; 6—oil Grade ТСП-14; 7—oil Grade ТАП-15В

any temperature within the range defined by the Newton law. The gradient of the curves, i.e., the factor B in the Walter equation, depends on the hydrocarbon content of the oils and the degree of their freedom from resinous compounds and heavy aromatic hydrocarbons.

Untreated residual oils, e.g., industrial oil and sulphurized oil for hypoid gears feature high gradients of the viscosity temperature curves, i.e., sharp changes of viscosity with temperature. The TAP-15B Grade oil is similar to these oils in viscosity-temperature characteristics. Transmission oils produced from the Baku crudes have a higher gradient of the viscosity-temperature characteristic than the oils of selective refining (Grades ТАД-17М and ТСП-14) produced from the crudes of the Ural-Volga and Western-Siberia oil fields.

The ТС₃-9ГП and ТС3П-8 Grade oils have an extremely low-gradient characteristic and are intended for cold-weather use.

The viscosity index (VI) defines the viscosity-temperature properties of oils for the temperature range above the freezing point:

$$VI = \frac{(L - v_{50}) 100}{L - H} + P$$

where v_{50} = kinematic viscosity of oil at 50°C, P = correction, which has a marked effect on VI only when its values are negative,

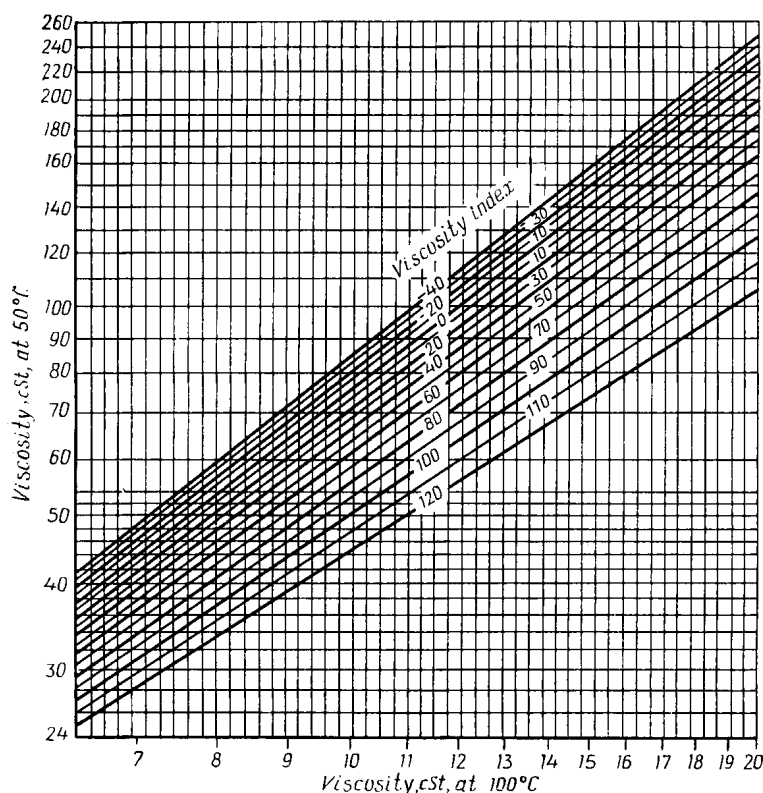


Fig. 9.3. Nomograph for determining the viscosity index of oils with viscosities of up to 20 cSt at 100°C

L = viscosity in centistokes at 50°C of an oil which has $VI = 0$, and H = viscosity in centistokes at 50°C of an oil which has $VI = 100$. L and H are found from tables [36, 43] using the viscosity value at 100°C for a given oil. Approximate values of VI are given in the nomographs of Figs. 9.3 and 9.4 [30, 36].

Unrefined oils have a low and even negative VI , which signifies that their viscosity changes sharply with temperature.

A high viscosity index (above 80) is typical of highly refined oils.

Except for low-temperature oils with polymer additives, which, irrespective of the hydrocarbon content, always have a high viscosity index, the VI for low-viscosity oils is indicative of the hydrocarbon

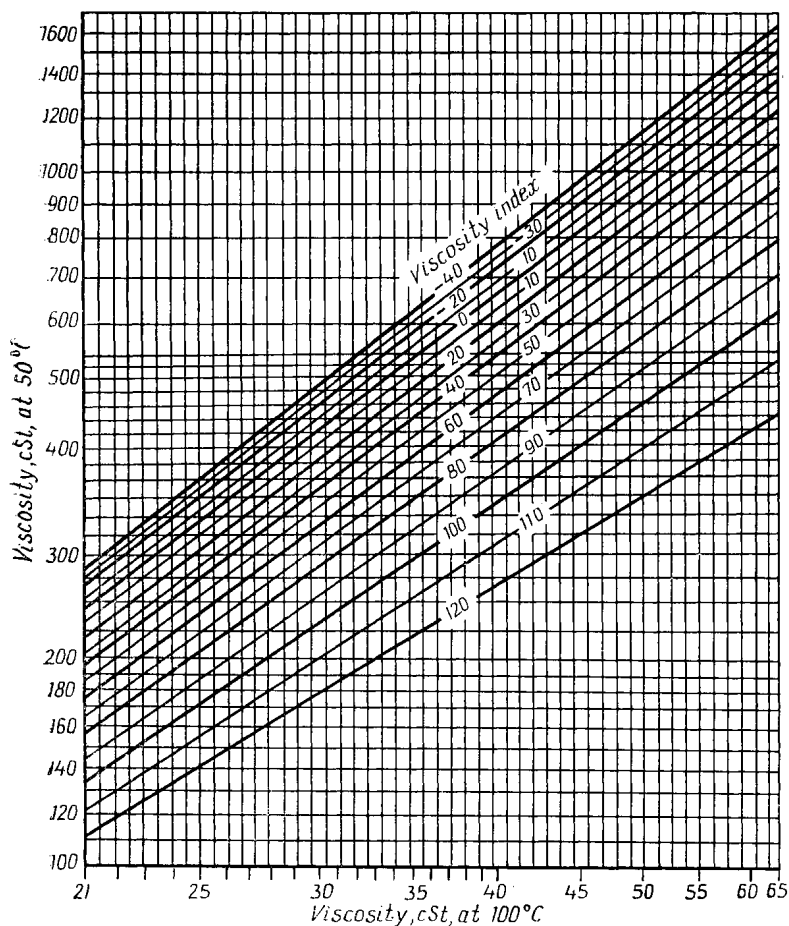


Fig. 9.4. Nomograph for determining the viscosity index of oils with viscosities of over 20 cSt at 100°C

concentration and the level of refining, which determines the thermo-oxidation stability of the oil.

At low temperatures approaching the oil congealing point, viscosity depends on shear velocity gradient.

Table 9.5 and Fig. 9.5 give data on the losses of energy in overcoming internal friction in an oil film. These losses grow with decreasing temperature, i.e., with increasing structural viscosity,

Table 9.5

Energy losses in GAZ-51 Model truck gearbox in first gear [16]
[summer transmission oil (TU 38101 529-75),
input shaft speed 1 rpm]

Cause of energy losses	% of overall torque at temperatures, °C	
	0	-15
External friction	17.8	6.7
Internal friction in oil flow	82.2	93.3
Friction in bearings and seals	20.5	14.4
Friction in gear mesh	61.7	78.9

while the external friction in useful work (e.g., in moving the vehicle) remains constant (Fig. 9.5) [16].

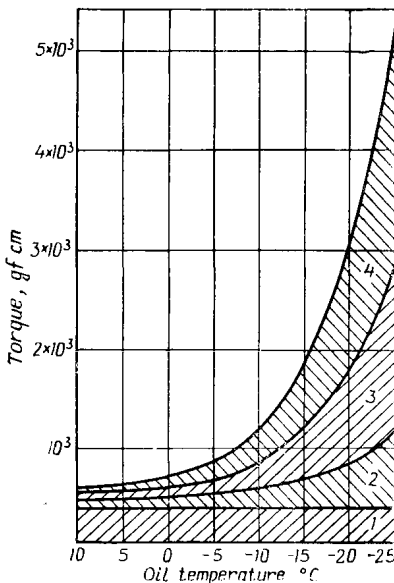


Fig. 9.5. Distribution of energy losses in an automobile transmission lubricated with transmission oil Grade II in operation at low ambient temperatures

1—in external friction; 2—in internal oil friction in sliding contact; 3—in friction in oil flow formed by gears rotation; 4—in friction in oil flow formed as oil is forced out of gear mesh

With a dynamic viscosity in excess of 4,000 to 5,000 P, starting a vehicle without warming up the transmission presents great difficulties [16].

According to K. S. Ramaya, the dynamic viscosity of mineral and vegetable oils has the following relationship with the absolute temperature:

$$\eta = \exp \left(A + \frac{B}{T} \right)^2 \text{ or } \sqrt{\lg \eta} = \left(A + \frac{B}{T} \right)$$

Figure 9.6 illustrates relations between dynamic viscosity and temperature for several oil grades: oil Grade TC3П-8 provides the starting of land vehicles at temperatures of up to -55°C , Grades TCII-14 and ТАД-17И, up to -30° , Grade ТАII-15В, up to -22°C , and a hypoid transmission oil, up to -18°C without warming up the transmission. Normally, the dynamic viscosity of transmission oils made in the USSR is rated at 5°C above their congealing point.

With increasing pressure the viscosity of oil grows exponentially:

$$\eta = \eta_0 e^{\alpha p}$$

where η = dynamic (or absolute) viscosity at pressure p , η_0 = dynamic viscosity at atmospheric pressure, and α = pres-

sure coefficient of viscosity, equal to $\frac{1}{\eta} \frac{d\eta}{dp}$ (cm s²/gf), which for mineral oils can be from 0.0015 to 0.004 [48]. Roughly, a growth in pressure of 3,500 kgf/cm² produces a two-fold increase in viscosity.

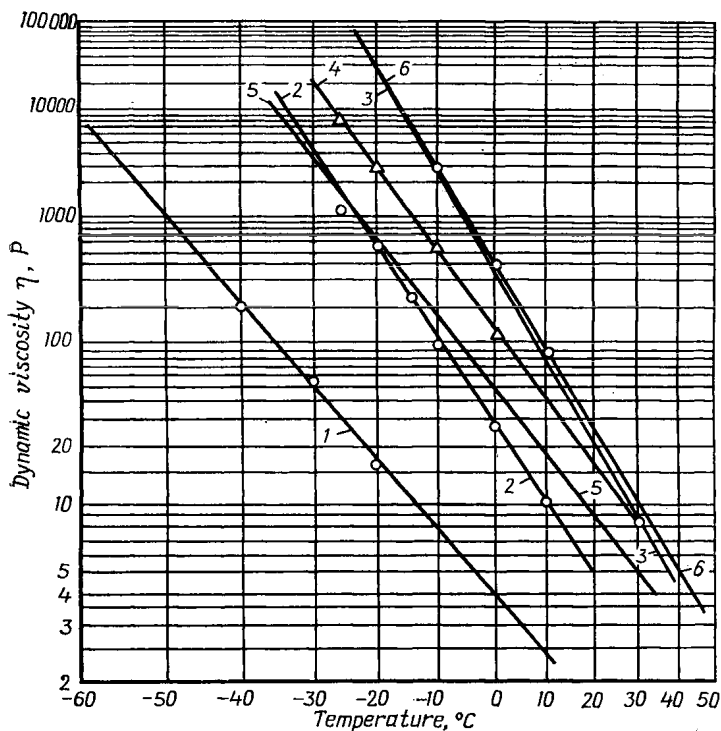


Fig. 9.6. Relation between dynamic viscosity and temperature for transmission oils

1—Grade TC3II-8; 2—Grade TCH14; 3—industrial oil (Nigrol 3); 4—Grade TAPI-15B; 5—Grade TAD-17H; 6—sulphurized oil for hypoid gears

At high contact pressures on transmission gear teeth two effects take place that increase the hydrodynamic load capacity: the increase in viscosity with pressure and elastic deformation of the teeth contact surfaces.

9.2.2. Basics of Oil and Additive Selection

Transport vehicle transmissions, especially those in automobiles, feature high specific pressures (up to 30,000 kgf/cm²) on gear teeth and variable operational conditions. Specifically, frequent changes in automobile speed are unfavourable to the hydrodynamic lubrication conditions in the meshing teeth of the transmission. Wear, and

sometimes scuffing, of the teeth in the gear transmissions of transport vehicles using plain oils prove that hydrodynamic and contact-hydrodynamic lubrication are not typical of them. A substantially increased wear life of transmission gears can be achieved through the introduction of antiwear and extreme-pressure additives into transmission oils.

The temperature at which chemically active antiwear additives begin reacting with metal is critical for their proper choice. The additives should react with the metal surface at the contact temperature and not at the bulk temperature of the oil. Therefore, the choice of additives and doped oils must be made with due regard for temperatures at the sliding interface.

For the cases being discussed, the contact temperature can be approximately calculated by the Blok formula [11, 18, 50]. The method and an example of calculation of the contact temperature of the first-gear teeth in a heavy truck are given in Table 9.6.

The temperature value calculated by the formula of Table 9.6 is a temperature rise due to the heat generated in friction. The actual tooth surface temperature results from the initial gear temperature and the calculated contact temperature. Table 9.7 gives calculated values of the contact temperature for the transmission gears of automobiles and tractors. These values indicate that contact stresses at the pitch point are not the only factor to be reckoned with in selecting oil additives. Other important factors are the relative speed of sliding of the teeth flanks in contact and the contact pressures at the spots of maximum heat generation. Depending on the gears rotational frequency, accuracy and finish, the coefficient of friction may range from 0.03 to 0.1.

According to experimental data, the temperature of the bearings of the automotive final-drive hypoid gears can be about 200°C, while the oil bulk temperature is about 150°C. The teeth contact temperature is likely to reach the maximum of the calculated values given in Table 9.7.

In tractors, gear-teeth contact temperatures are the lowest, and the oil bulk temperature does not exceed 100°C. Hence, the scuffing of gears in tractor transmissions is found infrequently, and the main kind of teeth surface damage is fatigue pitting and wear. For this reason, oils with extreme-pressure additives are inexpedient to use for tractor transmissions; here effective are additives that reduce wear in moderate friction conditions.

Table 9.8 presents seizure load values and temperatures of the oil running from the tooth contact zone, as obtained in testing USSR-made transmission oils in the IAE-3^{1"}/₄ Model gear testing machine.

For modern oils with additives containing sulphur and phosphorus (two right-hand columns in Table 9.8), gear teeth scuffing occurs at greater loads, but pitting of teeth develops before seizure. The high

Table 9.6

Calculation of contact temperatures in gear mesh for
first gear of heavy truck

Parameter	Designation	Unit	Formula	Actual value
Number of teeth:				
pinion	z_p	—	—	12
gear	z_g	—	—	51
Normal module	m_n	cm	—	0.5
Gear ratio	i	—	$\frac{z_g}{z_p}$	4.25
Active tooth face width	b	cm	—	3.8
Reference circle diameter:				
pinion	d_{rp}	cm	$z_p m$	6
gear	d_{rg}	cm	$z_g m$	25.5
Pressure angle	α_s	—	—	22°20'
Base circle diameter:				
pinion	d_{bp}	cm	$d_{rp} \cos \alpha_s$	5.55
gear	d_{bg}	cm	$d_{rg} \cos \alpha_s$	23.58
Pinion pitch circle diameter	d_p	cm	$\frac{2A}{i+1}$	5.54
Centre distance	A	cm	$\frac{d_{bg} + d_{bp}}{2}$	5.54
Torque on pinion shaft	M_p	kgf/cm	—	11.960
Rotational speed:				
pinion	n_p	rpm	—	924
gear	n_g	rpm	—	217
Tooth linear load	q	kgf/cm	—	1,226
Addendum circle:				
pinion	D_{ep}	cm	—	7.47
gear	D_{eg}	cm	—	26.3
Tooth pressure angle at contact point:				
pinion	$\cos \alpha_{ep}$	—	$\frac{d_{bp}}{D_{bp}}$	0.73
	$\operatorname{tg} \alpha_{ep}$	—	—	0.932
gear	$\cos \alpha_{eg}$	—	$\frac{d_{bg}}{D_{bg}}$	0.90
	$\operatorname{tg} \alpha_{eg}$	—	—	0.484
Distance along path of contact:				
from gear to pinion-tooth addendum	e_p		$\frac{d_{bp}}{2} (\operatorname{tg} \alpha_{ep} - \operatorname{tg} \alpha_s)$	1.43
from pinion to gear-tooth addendum	e_g		$\frac{d_{bg}}{2} (\operatorname{tg} \alpha_{eg} - \operatorname{tg} \alpha_s)$	0.86

Table 9.6 (cont.)

Parameter	Designation	Unit	Formula	Actual value
Position of contact point on contact path:				
pinion	e'_p	cm	$e_p - 0.3 m_n$	1.28
gear	e'_g		$e_g - 0.3 m_n$	0.71
Curvature radius at contact point:				
on pinion-tooth addendum	ρ'_p		$\frac{d_{bp}}{2} \sin \alpha_s + e'_p$	2.33
on gear-tooth dedendum	ρ''_g		$\frac{d_{bg}}{2} \sin \alpha_s - e'_p$	3.70
on gear-tooth addendum	ρ'_g		$\frac{d_{bg}}{2} \sin \alpha_s + e'_g$	5.69
on pinion-tooth dedendum	ρ''_p		$\frac{d_{bp}}{2} \sin \alpha_s - e'_g$	0.34
Speeds of motion of tooth profile at contact point:				
pinion-tooth addendum	v'_p	cm/s	$\frac{\pi n_p}{30} \rho'_p$	216
pinion-tooth dedendum	v''_p		$\frac{\pi n_p}{30} \rho''_p$	31.4
gear-tooth dedendum	v''_g		$\frac{\pi n_g}{30} \rho_g$	80
gear-tooth addendum	v'_g		$\frac{\pi n_g}{30} \rho'_g$	124
Sliding speeds of tooth profiles at contact points:				
on pinion-tooth addendum	—		$v'_p - v''_g$	136
on gear-tooth addendum	—		$v''_p - v'_g$	93.6
Half-length of contact line:				
on pinion-tooth addendum	b_{1ap}	cm	$1.52 \sqrt{\frac{q}{E} B^*}$	0.045
on gear-tooth addendum	b_{1ag}		$1.52 \sqrt{\frac{q}{E} C^{**}}$	0.021
Coefficient of friction	f	—		0.1
Thermal conductivity for steel	λ	kgf cm/(cm s °C)	—	4.2
Density of steel	γ	kgf/cm ³	—	0.0078
Specific heat for steel	c	kgf cm/(kg °C)	—	7,000

Table 9.6 (cont.)

Parameter	Designation	Unit	Formula	Actual value
Temperature at contact point on pinion-tooth addendum (gear-tooth dedendum)	Θ_{ap}	°C	$0.83 \frac{fqG^{***}}{\sqrt{\lambda\gamma cb_{1ap}}}$	275
Temperature at contact point on gear-tooth addendum (pinion-tooth dedendum)	Θ_{ag}	°C	$0.83 \frac{fqH^{****}}{\sqrt{\lambda\gamma cb_{1ap}}}$	281
Contact load:				
on pinion-tooth addendum	P_{ap}		$\frac{q}{2b_{1ap}}$	12,600
on gear-tooth addendum	P_{ag}	kgf/cm ³	$\frac{q}{2b_{1ap}}$	28,000
Pinion and gear hardened and ground, HRC	—	—	—	58-65

$$*B = \frac{\rho'_p \rho''_g}{\rho'_p + \rho''_g}; \quad **C = \frac{\rho'_g \rho''_p}{\rho'_g + \rho''_p}; \quad ***G = \frac{v'_p - v''_g}{\sqrt{v'_p} + \sqrt{v''_g}}; \quad ****H = \frac{v'_g - v''_p}{\sqrt{v'_g} + \sqrt{v''_p}}$$

Table 9.7

Contact temperatures in automotive gears

Application	Gear	Contact load, kgf/cm ²	Relative sliding speed of tooth profiles at contact point, cm/s	Contact temperature, °C
Five-ton truck	First	16,100	25.4	110
Heavy truck	First	12,600	136	275
Planetary gear of hydro-mechanical transmission	Heaviest-loaded pair	14,900	136	115
	Transfer box	21,300	583	330
Wheel tractor	Final drive	8,700	42.5	130
	Seventh gear	6,300	256	68
Tracked tractor	Final drive	7,000	50.2	60

Table 9.8

Seizure load and the temperature of oil leaving the contact zone of gear mesh. Test on Model IAE-3 $\frac{1}{4}$ " gear-testing machine (after Yu. A. Rosenberg)

Parameter	ТЭ-15-3ΦО ТУ 38 101-521-75	Sulphurized oil for hypoid gears, ГОСТ 4003-53	ТСП-14, ТУ 38 101-488-74	ТАП-15В ТУ 38 101-176-74	ТСП-8 ТУ 38 101-313-72	ТАП-17и, ТУ 38 101-306-72	Oil for hypoid gears with additive CΦA (pilot grade)
Seizure load, kgf/mm ²	190	280	225* 251**	210* 220**	251	314	320
Temperature of oil, °C	100	173	161* 171**	158* 173**	155	> 200	> 200

* With additive ОТП.

** With additive ЛБ-23к.

temperature of the oil emerging from the contact zone (over 200°C) indicates that additives of this type are capable of reaction and efficient at high contact temperatures, which is why scuffing develops progressively at the final stages of loading rather than immediately.

9.2.3. Types and Properties of Additives

There are three types of oil additives which improve friction conditions: antifriction additives, which reduce friction and increase the efficiency of transmissions and also friction additives which provide the specified coefficient of friction, antiwear additives which reduce wear of rubbing surfaces at moderate temperatures or loads, and extreme-pressure additives, which prevent or reduce the effect of scuffing of rubbing surfaces at high contact loads and temperatures.

(1) *Antifriction additives* are essentially surface-active agents which are adsorbed on the metal surface and retained there by weak van-der-Waals forces. Hence, the adsorbed films can hold on rubbing surfaces at temperatures of under 140°C [12].

The additives, which include fatty acids, their ethers and salts, and natural or synthetic fats, are expedient to use for worm gearings where the maximum efficiency and the specified thermal capacity must be ensured.

Friction additives, which provide $f_{stat} < f_{kin}$ and so exclude stick-slip in friction, contain sperm oil (a scarcity), aluminium stearate, nitroderivatives of phosphoric, thiophosphoric, and dithiophosphoric acids, and amine salts of dialkyl dithiophosphoric acids (Grade

Table 9.9

Extreme-pressure and antiwear additives for transmission oils

No.	Grade	Chemical description	Weight concentration in oil, %	Standard (Specifications)	Application
1	ОТН	Sulphurized tetramers of propylene	5-6	OST 38-01-8-71	Automotive transmission oils
2	КННХ-2	Sulphurized polyolefines	3-4.5	—	
3	ЛЗ-23к	Ethylene-bis-isopropylxanthogenate	5	GOST 11883-77	
4	ЛЗ-ТИБ/6	5-neopentyl-4-tertiary butyl-1,2-4 dithio-cyclopentene-4-thion-3		TU 38 20-70	Cutting fluids, automotive transmission oils
5	АБЭС	Bis-(alkylbenzylthio)-ethane	3.5-3.8	TU 38 101327-72	Oils for gear transmissions in ground vehicles and industrial equipment
6	Chlorparaffin	Chlorinated paraffin wax	5-10	TU 6-01120-67	Oils for industrial gear reducers
7	Sovol	Pentachlorodiphenyl	5-10	MRTU 6-01-333-69	Transmission oils for various machines
8	Sulphol	Bis-(trichloroamyl)-sulphide	4-5	TU 6-03113-64	Oil for running-in gears and worm gearings
9	ЛЗ-28	Trichloramylbutyl xanthogenate	6	TU 38-30131-71	Transmission oils for ground vehicles
10	ЛЗ-309/2	Trichloramyl diisopropyl dithiophosphate	9-10	TU 38-30169-73	Automotive transmission oils for low temperatures
11	ВИР-1	Multi-component additive	6.5	—	Oils for hypoid gears in passenger cars
12	Chloref-40	Dibutyl ether of trichlormethyl phosphonic acid	2	—	Oils for hypoid gears in trucks
13	ДФ-11	Zinc isobutylisooctyl dithiophosphate	0.8-3	OST 38-129-73	Oils for automotive gearboxes, fluids for hydromechanical transmissions, engine oils, components for multi-purpose additives

Table 9.9 (cont.)

No.	Grade	Chemical description	Weight concentration in oil, %	Standard (Specifications)	Application
14	ВНИИ НП-354	Zinc dioctylphenyl dithiophosphate	5	TU 38-1-1181-68	Engine oils. Oils for gear transmissions
15	ДФ-1	Barium dialkyl dithiophosphate	3-3.5	GOST 10644-63	Engine oils. Fluids for hydrodynamic transmissions
16	МНИ-ИП-22К	Calcium dialkylphenyl dithiophosphate	4.5	GOST 9832-77	Oils for engines and transmissions
17	АДТФ	Amine salt of dialkyl dithiophosphoric acid	0.25-0.35	—	Oils for hydro-mechanical transmissions in vehicles, oils for machine tool guideways
18	ЭФО	Zinc and barium salts of aryl dithiophosphonic acid	5	GOST 14625-69	Tractor transmission oil

АДТФ, No. 17 in Table 9.9). These agents are effective in small concentrations and also provide antiwear functions.

(2) *Antiwear additives* are derivatives of phosphorous, phosphonic, and, especially, phosphoric acids [8], specifically the ethers of phosphoric, thiophosphoric, and dithiophosphoric acids, their amides, amine or metallic (especially zinc) salts.

Two types of zinc salts of dithiophosphoric acids are available: zinc dialkyl dithiophosphate (Grade ДФ-11, No. 13 in Table 9.9) and zinc dialkyl phenyl dithiophosphate (ВНИИ НП-354, No. 14 in Table 9.9). Barium dithiophosphate (Grade ДФ-1, No. 15 in Table 9.9) serves as an antisludge and antioxidant additive to a greater extent than an antiwear one. The ЭФО Grade additive (No. 18 in Table 9.9), which is a mixture of zinc and barium salts of dithiophosphonic acid with aromatic radicals, is widely used in tractor transmission oils. The additive is very cheap.

Unlike barium and zinc dithiophosphate additives—Grades ДФ-1, ДФ-11, and ВНИИ НП-354—the МНИ ИП-22к Grade additive, which is calcium dialkylphenyl dithiophosphate (No. 16 in Table 9.9), may cause corrosion of copper at elevated temperatures (130 to 150°C).

Table 9.10

Temperature of additives decomposition and reaction with metals, antiscuff and antiwear properties of additives in oil Grade TC-14.5, as found by testing on a four-ball test machine

Additive	Temperature, °C			Concentration in oil, % by weight	Antiscuff properties found by tests			Wear of balls mm, under load of 20 kgf for 4 h
	decomposition	reaction with iron	reaction with copper		ОПШ	P _c , kgf	P _c , kgf	
<i>Sulphur-containing additives</i>								
Bis-(dialkylbenzyl-disulphides (e.g., ABC-2)	205-236*	175-226*	164-182*	3	63.8	79	355	0.6-0.8*
ОТП АБЭС	182 227	178 202	135 194	5 3.5-3.8	66.8 56.3	68 69	398 355	0.6 0.7
ЛЗ-23К	198	195 239 245	188	5	69.1	112	398	0.97
Bis-(isopropyl-xanthogenate)	147 167 —	118 191 259	110 145 191	3	72.7	89	447	1.1
БТК	259 275	234 248	134	5	68.4	100 112	355	0.83
ЛЗ-ТИБ	259	248	132	3-4	70.9	100	398	0.8
<i>Chlorine-containing additives</i>								
Chlorinated paraffin wax	200	135	130	8 (from 5 to 10)	60.4	100	355	1.0
Sulphol	291	156	183	4	75	112	447	1.0
ЛЗ-28	235	150	160	6	79.4	112	562	0.83
ЛЗ-309/2	185	158	163	8	74.2	100	447	0.45
Sovol	—	—	—	5	41	89	224	0.8
<i>Phosphorus-containing additives</i>								
Chloref-40 ₁	225	135	—	2	86	141	631	0.45
ДФ-11	197 232	197 234	—	3	48.8	100	282	0.33
ВНИИ НП-354	—	—	—	4	38.3	79	224	0.35
ЭФО	—	—	—	4	40.8	89	224	0.3

* Depending on the length of alkyl radicals.

The ethers and salts of phosphoric, thiophosphoric, and dithiophosphoric acids are operable at up to 200°C; above this limit they are subject to thermal decomposition (Table 9.10 and Fig. 9.7).

Surface-active agents derived from hydrocarbons can also reduce wear but at lower temperatures. The greater thermal stability of phosphoric-acid derivatives is due to their chemical adsorption on

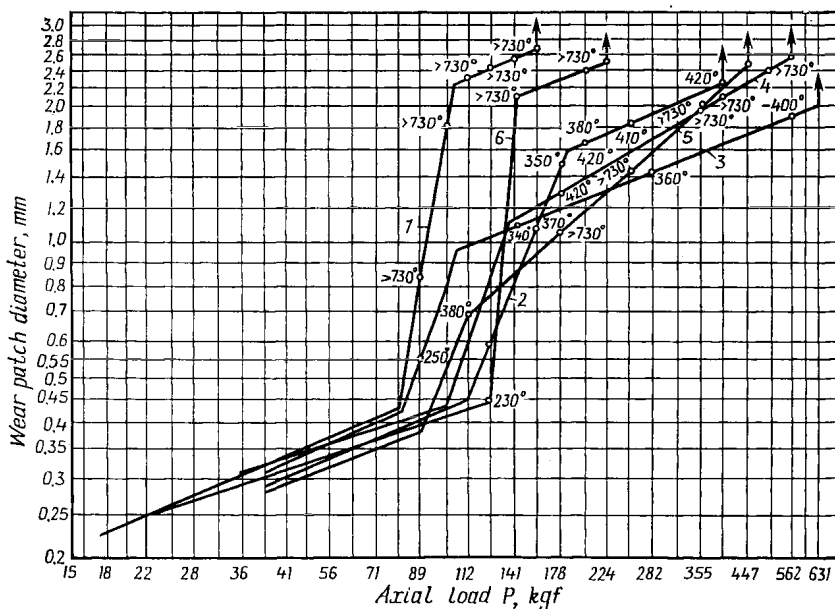


Fig. 9.7. Wear as a function of load in testing oils with sulphur-containing additives on a four-ball testing machine (the temperatures shown are measured at the wear spot centre)

1—plain oil Grade TC-14.5; 2—oil Grade TC-14.5 with 5% of additive Grade ИБ-6/9; 3—oil Grade TC-14.5 with 5% dibenzyl disulphide; 4—sulphurized oil for hypoid gears; 5—oil Grade TC-14.5 with 5% of additive Grade ДФ-11

rubbing surfaces, whereas hydrocarbon derivatives are adsorbed physically.

If follows from the data of Table 9.7 that phosphoric-acid derivatives can be fairly effective additives to oils for spur and helical-gears in most of automotive transmissions.

However, these additives, except for the derivatives of trichloromethyl phosphoric acids (see No. 12 in Table 9.9), are ineffective as extreme-pressure agents because they do not weaken the scuffing of rubbing surfaces, although they increase the seizure load (Fig. 9.7, curves 5 and 1).

(3) *Extreme-pressure additives* prevent the scuffing of rubbing surfaces at high contact temperatures and loads.

Plastic deformations in friction give rise to the formation of juvenile surfaces, and vacancies in the metal crystalline lattice lead to the seizure and scuffing of the surfaces. Chemically active extreme-pressure additives react with the juvenile surfaces, they fill the crystalline lattice vacancies and thereby prevent seizure, localizing the process in microvolumes.

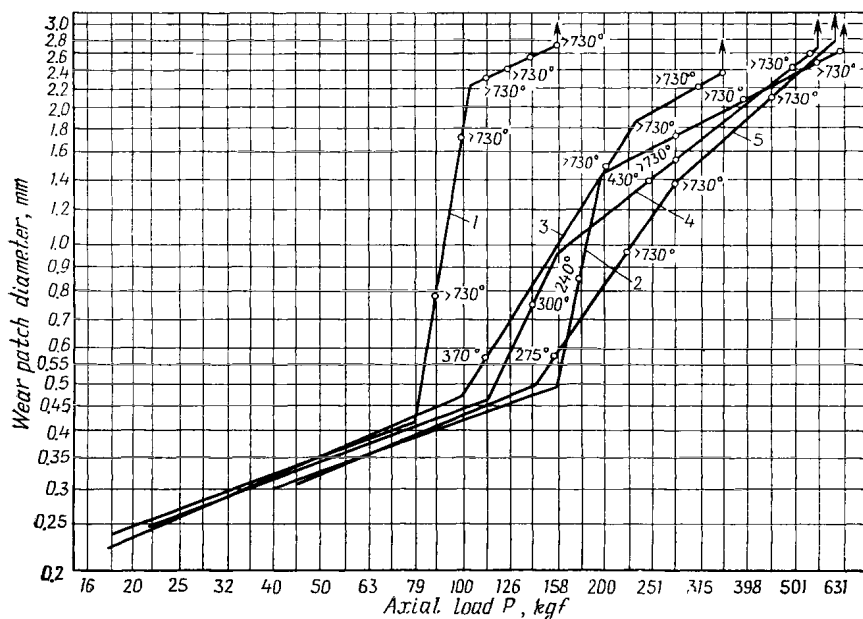


Fig. 9.8. Wear as a function of load in testing oils with chlorine-containing additives on a four-ball testing machine (the temperatures shown are measured at the wear spot centre)

1—plain oil Grade TC-14.5; 2—oil Grade TC-14.5 with 1% of the Chloref-40 additive; 3—oil Grade TC-14.5 with 10% chlorinated paraffin; 4—oil Grade TC-14.5 with 4% Sulfol; 5—oil Grade TC-14.5 with 4% Sulfol and 3% ДФ-11

A good antiscuffing effect is provided by organic derivatives of sulphur and chlorine, and also by compositions containing both these elements.

The oil bulk temperature normally does not exceed 150°C, and therefore, compositions used as extreme-pressure additives must be capable of reaction with metal at temperatures above 150°C. In sliding friction at the beginning of scuffing the temperature at a point contact may reach 200°C and more, depending on the presence and character of additives in the oil (Figs. 9.7 and 9.8).

As can be seen from Table 9.10, chlorine-containing additives begin reacting with iron at 130 to 180°C; consequently, most additives of this type are fit for use at oil bulk temperatures up to 130°C and moderate contact temperatures (Fig. 9.8).

Additives containing sulphur, as a rule, react with iron at about 200°C and more (Table 9.10). An exception are some highly aggressive organic derivatives of sulphur, which, because of their aggressiveness, are not used as extreme-pressure additives. Sulphur-containing additives are effective in the most severe operating conditions, i.e., at 200°C and more (see Fig. 9.7). Moreover, they exhibit the greatest ability to reduce surface failure and temperature under scuffing conditions.

When selecting additives, the aim is to obtain a doped oil offering a set of optimal properties rather than the maximum effect in a single area. Modern oils should perform a number of functions, so they should contain multi-component additives. Such an optimum combination is obtained by introducing phosphorous-containing components which improve antiwear properties of the oil under moderate friction conditions and increase the magnitude of seizure loads, as well as sulphur-containing components which mitigate the process of scuffing and reduce its scale and the contact temperature. Modern oils should also contain inhibitors to prevent the oxidation and corrosion of copper and steel in the presence of moisture, and also foam suppressors and, in some cases, special friction and antisludge components (e.g., oils for hydromechanical transmissions).

9.2.4. Requirements for Transmission Oils

Base oils and additives should be selected according to the operating temperatures, ambient temperatures, and design features of transmissions (Tables 9.4, 9.9, 9.10 and 9.11).

Low-temperature oils with a viscosity of 5.5 to 12 cSt at 100°C and with good viscosity-temperature characteristics are obtained by thickening base oils with polymeric additives (polymethacrylates, polyisobutylenes, normal polybutenes, etc.).

Especially stringent requirements as to viscosity-temperature characteristics and low-temperature properties are placed on oils for hydrodynamic and hydromechanical transmissions, because these oils serve as working fluids in automotive hydraulic torque converters and hydraulic control systems. The oils must provide low resistance to shaking and allow easy pumping through small-diameter conduits. In hydromechanical transmissions, oil serves to lubricate planetary gears and friction-clutch discs. Hence, the oil should have special frictional properties, which are provided by introducing additives that ensure $f_{st}/f_{hin} < 1.0$ and smooth engagement of the clutch (Table 9.11). The oil must also contain antisludge agents for keeping the discs clean and free of skidding.

The available grades of transmission oils and their applications are given in Tables 9.12 through 9.16.

Table 9.11

Selection of oil depending on operating conditions

Viscosity, cst, at 100°C	Application	Viscosity- tempera- ture char- acteris- tics	Low-temperature properties	Antiscuff properties	Anti- wear prop- erties	Fric- tion prop- erties	Oxida- tion stabi- lity	Additives
6.5-7.5	Hydromechanical transmission	Excel- lent $VI \geq 140$	Excellent for summer and all-weather use in temperate climate, $\eta_{-40} \leq 500$ P for cold climate $\eta_{-50} \leq 400$ P	Good in lubri- cation systems when the oils are also used for main-drive gears where $\theta_c \geq 350^\circ\text{C}$ Poor for low- load planetary gears where $\theta_c < 200^\circ\text{C}$	Excel- lent	$f_{st}/f_{kin} < 1.0$	Excel- lent	For highly load- ed gears at $\theta_c \geq 200^\circ\text{C}$, ex- treme-pressure, antiwear, fric- tion, antioxi- dant, defoam- ing, and anti- sludge All but exte- reme-pressure
6.5-7.5	Hydrodynamic trans- missions	Good, $VI \geq 90$	—	Not required	Good	Not re- quired	Excel- lent	Antiwear, anti- oxidant, anti- sludge and de- foaming
14-18 22-34	Automotive transmis- sions working at temperatures and loads that require no additives in oil	$VI \geq 80$	$\theta_s^* \leq -25^\circ\text{C}$	—	—	—	—	—

Table 9.11 (continued)

Viscosity, cSt, at 100°C	Application	Viscosity- tempera- ture cha- racteris- tics	Low-temperature properties	Antiscuff properties	Anti- wear proper- ties	Fric- tion proper- ties	Oxida- tion stabi- lity	Additives
	Tractor transmission components operating at $\theta_c \leq 150^\circ\text{C}$, whose typical surface failu- res are wear and fa- tigue pitting:							
9-11 14-20	for cold climate for temperate climate	$VI \geq 100$ VI_{-40-95} for trucks, $\eta_{1-20} \leq 2,000$ P for cars	$\theta_s \leq -40^\circ\text{C};$ $\eta_{-35} \leq 2,000$ P $\theta_s = -15$ to -20°C $\eta_{-15} \leq 2,000$ P	—	Good	—	—	Antiwear and, for low-tempe- rature oils, thickeners
9-11	Truck transmissions operating at $\theta_c \geq$ $150^\circ\text{C};$ — for cold climate	$VI \geq 100$	Excellent $\theta_s = -40^\circ\text{C};$ $\eta_{-40} \leq 2,000$ P $\theta_s \leq -25^\circ\text{C};$ $\eta_{-20} \leq 1,000$ P	—	—	—	—	Extreme-pres- sure
14-15	— for temperate cli- mate	$VI \geq 80$		Good	—	—	—	

Table 9.11 (continued)

Viscosity, cSt, at 100°C	Application	Viscosity- tempera- ture cha- racteris- tics	Low-temperature properties	Antiscuff properties	Anti- wear proper- ties	Friction proper- ties	Oxida- tion stabi- lity	Additives
14-16 12-14	Transmissions of heavy trucks and tra- cked vehicles opera- ting at $\theta_c \geq 200^\circ\text{C}$: — for temperate climate — for cold climate	$VI \geq 90$ $VI \geq 100$	$\theta_s \leq -25^\circ\text{C}$ $\eta_{-20} \leq 800 \text{ P}$ $\theta_s \leq -40^\circ\text{C}$ $\eta_{-40} \leq 1000 \text{ P}$	Good	Good	—	Good	Extreme-pres- sure, antiwear, and, for low- temperature oils, thickeners
9-11	Hypoid gears in trucks for cold climate	$VI \geq 120$	$\theta_s = -50^\circ\text{C}$; $\eta_{-45} \leq 2,000 \text{ P}$	Excellent	Good	—	—	Extreme-pres- sure, thickener, and multi-pur- pose additives
17-19 12-14	Hypoid gears in pas- senger cars: — for temperate climate — for cold climate	$VI \geq 90$ $VI \geq 120$	$\theta_s = -55^\circ\text{C}$; $\eta_{-20} \leq 1,000 \text{ P}$ $\theta_s \leq -40^\circ\text{C}$; $\eta_{-35} \leq 800 \text{ P}$	Good	Good	—	Good	Extreme-pres- sure, antiwear, antioxidant, corrosion inhi- bitor, and, for low-tempera- ture oils, thickeners

Designations. θ_c = contact temperature; θ_s = setting temperature.

Table 9.12

Oils without additives

Main parameters	Grade TC-14.5, TU 38 101110-71	Industrial oil (Nigrol JI and 3) TU 38 101529-75	Testing methods
Kinematic viscosity, cSt, at 100°C	≥ 14.5	18-32	GOST 33-66
Setting point, °C	-25	3 = -20	GOST 20287-74
Dynamic viscosity, P, not more than	650 (at -20°C)	JI = -5	GOST 1929-51

Table 9.13

Oils for hydromechanical transmissions

Main parameters	Grade A, TU 38 101179-71	Grade IT-50, TU 38 101487-74	Testing methods
Kinematic viscosity, cSt, at: 100°C	Not specified (5-8.2)	Not specified (5-6.5)	GOST 33-66
50°C	23-30	11-14	
-20°C, not more than	2,100	—	Reference table for viscosity index values (Standardgiz, 1960) GOST 20287-74
Viscosity index, not less than	—	80	
Setting point, °C	-40	-28	

Table 9.14

Oils with antiwear additives for automobile gearboxes and tractor transmissions

Main parameters	Grade TC ₈ -9-IT-11, TU 38 101159-71	Grade TC-14.5- IT-11, TU 38 101294-72	Grade T3-15-300, TU 38 101521-75	Testing methods
Kinematic viscosity at 100°C, cSt	9.0	14.5-15.5	15±1	GOST 33-66
Viscosity index, not less than	120	80		[43]
Setting point, °C, not higher than	-50	-25	-18	GOST 20287-74

Table 9.14 (continued)

Main parameters	Grade TC ₈ -9-ДФ-11, ТУ 38 101159-71	Grade TC-14.5- ДФ-11, ТУ 38 101294-72	Grade TC-1-ЭФФ, ТУ 38 101521-75	Testing methods
Dynamic viscosity, P, not more than	2,000 (at -45°C)	800 (at -20°C)	2,000 (at -15°C)	GOST 1929-51
Antiscuff properties:				
ОПИ*	40	42	—	GOST 9490-75
И ₃	34	37	—	—
P _c , kgf	200	200	—	—
Diameter of wear spot on spheres, mm for 4 hours of test at P=20 kgf	—	0.45 (at 130°C)	—	Method ВНИИ НП

* Test data.

Table 9.15

Oils with extreme-pressure additives for trucks and heavy tracked vehicles

Main parameters	Grade TC-10-ОТН ТУ 38 101148-72	Grade ТАИ-15В, ТУ 38 101176-74	Grade ТЦИ-14, ТУ 38 101488-74	Gearbox oil, GOST 4002-53
Kinematic viscosity, cSt, at temperature, °C:				
100	≥ 10	15±1	14-15	20.5-32.4
50	—	—	—	—
-45	—	—	—	—
Viscosity index	—	—	—	—
Setting point, °C	-40	-20	-25	-20
Dynamic viscosity, P, not more than	3,000 (at -15°C)	3,000 (at -20°C)	1,000 (at -20°C)	—
Antiscuff properties:				
ОПИ*, not less than	60	60	60	—
И ₃	~53	~52	53-62	—
P _c kgf, not less than	398	355	398	—

Table 9.15 (continued)

Main parameters	Grade TC3H-8, TU 38 101386-72	Grade TC3H-9 TU 38 101386-73	Grade TCH-15K, draft TU	Testing methods
Kinematic viscosity, cSt, at temperature, °C:				
100	7.5-8.5	≥ 9	≥ 15	GOST 33-66
50	—	≥ 36	—	—
-45	$\leq 25,000$	—	—	—
Viscosity index	—	120	90	[43]
Setting point, °C	-50	-50	-25	GOST 20287-74
Dynamic viscosity, P, not more than	—	2,500 (at -40°C)	800 (at -20°C)	GOST 1929-51
Antiscuff properties:				
ОПН*, not less than	50	60	60	
M_3	45-48	52-54	55-62	GOST 9490-75
P_c kgf, not less than	282	316	355	

* Experimental data.

Table 9.16

Oils for hypoid gears

Main parameters	Grade TC ₃ -9, TU 38 101386-72 (for trucks)	Sulphurized oil for hypoid gears in pas- senger cars	Grade TCH-14c, TU 38 101270-72 (for trucks)	TC3H-16A, TU 38 401101-75	Grade TAJI-17H TU 39 101306-72 (for passenger cars)	Testing methods
Kinematic visco- sity, cSt, at tem- perature, °C						
100	≥ 9	20.5- 32.4	≥ 14.0	≥ 15.0	≥ 17.5	GOST 33-66
50	≤ 36	—	—	—	100-120	
Viscosity index, not less than	120	—	—	120	95	[43]
Setting point, °C, not more than	-50	-20	-25	-38	-25	GOST 20287-74
Dynamic visco- sity, P, not more than	2,500 (at	—	800 (at -20°C)	1,500 (at	—	GOST 1929-51

Table 9.16 (continued)

Main parameters	Grade TC ₉ -9, ТУ 38 101386-72 (for trucks)	Sulphurized oil for hypoid gears in pas- senger cars	Grade TCI ₁₁ -14c, ТУ 38 101270-72 (for trucks)	TC3II-16A, ТУ 38 401101-75	Grade TAI ₁₁ -17II ТУ 39101306-72 (for passenger cars)	Testing methods
Antiscuff proper- ties:	-45°C)			-35°C)		
ОПН*, not less than	80	—	80	70	70	GOST 9490-75
И ₃	63-70	—	65-72	62-65	62-68	GOST 9490-75
P _c , kgf, not less than	398	—	447	398	398	—
Wear of spheres, mm, for 4 h at temperature, °C:						
not more than 130°	—	—	—	—	0.4	
not more than 150°	—	—	—	0.5	—	Method ВНИИ НП

* Experimental data.

9.3. INDUSTRIAL OILS

The purpose of industrial oils is to reduce the coefficient of friction in the rubbing components of machine tools, presses, steel-mill roll stands, and other industrial equipment. In addition, industrial oils must remove heat from rubbing parts, protect them against corrosion, clean them, and serve as a sealing medium, while developing no foam in contact with air, etc.

Oils used for critical applications can be regarded as a kind of structural material whose properties have a bearing on the performance of rubbing parts often in the same degree as those of the materials of these parts.

Industrial oils are conventionally classified by viscosity into the following three groups [4, 41]:

—low-viscosity oils, with a viscosity of from 6 cSt at 20°C to 10 cSt at 50°C;

—medium-viscosity oils, with a viscosity of from 10 to 58 cSt at 50°C;

—high-viscosity oils, with a viscosity of from 58 cSt at 50°C to 96 cSt at 100°C.

For the past ten years the trend has been towards the viscosity index increased from 85 to 95-105 and even to 120-140. This is due to the fact that base oils with a high viscosity index exhibit improv-

Grade	Chemical description	Concentration in oil, % by weight	GOST or TU	Purpose
<i>Antioxidants</i>				
ЛАНИ-317	Zinc dialkyl dithiophosphate based on isopropyl alcohol and alcohols obtained by direct oxidation of synthin with 12-16 carbon atoms	0.7-3.5	VTU TH3 139-64	Antioxidant, antiwear, anticorrosive
Ionol	4-methyl-2,4-ditertiary butylphenol	0.2-0.7	GOST 10894-76	Antioxidant
<i>Antirust additives</i>				
AKOR-1	Based on oils AC-9.5, DC-8, and DC-11, with addition of 1-10% stearine during alkalization (GOST 6484-64)*	5-20	GOST 15171-70	Anticorrosive, improving slushing properties
B 15/41	Acid ester of alkenyl succinic acid and ethylene glycol	0.1-0.3	TU 6-148666-72	Antirust in high humidity
<i>Bodying agents</i>				
ПИБ	Product of low-temperature polymerization of isobutylene	By selection*	TU MXII 1764-54	Thickening and increasing viscosity index
КП-5	Concentrate ПИБ in oil:		TU 38 101209-72	
КП-40	КП-5 av. mol. wt. 4,000-6,000			
П-20	КП-40 av. mol. wt. 9,000-15,000		TU 604270-68	
ПМАД	П-20 av. mol. wt. 15,000-25,000			
	28-35% polymethacrylate concentrate in oil Grade И-20А	0.1-0.3		Depressor, thickening and increasing viscosity index
<i>Foam inhibitors</i>				
ПМС-200А	Methyl silicone liquid	0.002-0.007	TU 602718-72	
<i>Friction ("anti-stick-slip") additives</i>				
Aluminium stearate	Aluminium salt of stearic acid	0.7-2.2	TU 38 101322-72	
<i>Antifriction additive</i>				
МВЧ-4	Molybdenum disulphide	0.5-3.0	ТУ ИМТ 06-1-68 GOST 8225-73	
КП; ГС-4	Colloidal graphite compound with dispersed-phase graphite Grade ГС-4	1.0-2.0		

* Concentration is determined depending on base-oil viscosity, mechanical destruction, etc.

Table 9.18

Service properties of industrial oils [34]

Properties	Agent	Application
Antiscuff	Extreme-pressure additives	Mechanisms working at high temperatures and loads
The same for impact loads	Extreme-pressure additives or high-viscosity oils	Mechanisms subjected to impact loads
Antiwear	Antiwear additives	Mechanisms whose wear life is determined by wear or rubbing surfaces
Running-in	Additives facilitating running-in	Running-in of newly assembled mechanisms
Antifriction	Special additives or synthetic oils	Low-efficiency mechanisms, worm gearings, leadscrew-nut transmissions
Protection against relaxation oscillations in friction	Special additives increasing the friction coefficient with rising speed of sliding	Guideways of machine tools and other machines with low-speed motions; mechanisms with friction clutches
Viscosity: high viscosity index	Highly refined oils with high viscosity index obtained from special crude oils and thickeners for thin base oils	Mechanisms working within wide temperature ranges where oil viscosity must be as stable as possible
Compressibility: reduced	Oils of appropriate fractional composition and hydrocarbon content	Hydraulic drives
increased		Mechanisms subjected to impact loads
Low setting point	Thin oils, oils made from special crudes, paraffin-free oils and depressants	Outdoor applications in regions with low subzero temperatures, with centralized lubrication systems having long oil conduits
Stability against ageing:		
at normal temperatures	Highly refined oils and antioxidants	Heavy complex machinery with large-capacity oiling system (rolling mills, etc.)
at high temperatures	Synthetic oils with antioxidants	Mechanisms working at ambient temperatures of 120-150°C
Foaming (low)	Defoaming agents	General-purpose
Demulsification (low)	Demulsification inhibitors	Equipment where water can get into oil (steel mills, etc.)
Anticorrosive	Corrosion inhibitors	Mechanisms working in humid atmosphere and with water in oil; also in presence of environmental aggressive media
Protective	Antirust additives	
No reaction with non-metals	Oils with minimum amount of aromatic hydrocarbons	Mechanisms with seals and other parts made of rubbers having low stability to oil

Table 9.18 (continued)

Properties	Agent	Application
Tackiness	Special and polymeric additives	Textile and food processing equipment. Open mechanisms. Watches and instruments oiled for life
Ease of removal	Surface-active additives	Textile machinery
Nonflammability	Nonflammable oil emulsions or synthetic oils	Equipment working under fire-hazardous conditions (hydraulic systems, high-temperature enclosures, coal mines, etc.)
Nontoxicity	Nontoxic and nonodorous additives	Every application
Stability to aeration	Special additives	Hydraulic systems, machines and mechanism where this property is required

ed response to additives of various chemical compositions which upgrades their quality and makes for reduced additives consumption in the production of additive-blended oils.

The principal advantages of base oils of high viscosity index are as follows [17]:

- highly reliable performance of machine parts provided within a wide range of working temperatures;
- oils can be used over a long period without change, which reduces their consumption;
- multi-purpose use of oils is possible;
- good response to additives, etc.

Additive-type industrial oils are made up of mineral base oils and additives of various compositions.

The properties of the main USSR-made additives for industrial oils are given in Table 9.17. Extreme-pressure and antiwear additives are characterized in Table 9.9.

The use of industrial oils with extreme-pressure and antiwear additives provides for reduced metal consumption, prolonged running between repairs, increased efficiency and productivity, longer service life and reliability of equipment.

Wear and scuffing may arise in semi-fluid, semi-dry, and boundary friction. These types of surface damage are typical of heavy-duty gear transmissions, sliding bearings starved of lubrication or made of materials with poor antifriction properties, and also antifriction bearings run under unfavourable conditions, particularly with pre-loading. Frictional conditions are the dominant factor for the selection of oils by service properties. The main service properties of industrial oils are given in Table 9.18; their brief characteristics and service significance are given in handbooks [22, 23, 41], and quality specifications, in [5, 24, 49].

9.3.1. Main Properties

Viscosity. Industrial oils are selected mainly by viscosity.

For conversion of different viscosity units, calculation of viscosity change with temperature or determination of viscosity index, use should be made of the pertinent formulas, nomographs, tables, and diagrams given in Appendix 1 of handbook [41, pp 895-905].

When selecting an oil, account must be taken of three critical viscosity values: the optimal value at a normal working temperature, the minimum value at the highest working temperature, and the maximum value at the lowest working temperature at which a cold start must be ensured.

Variation in oil viscosity in excess of a definite range adversely affects the performance of machines.

For instance, oils used in the hydraulic systems of NC machine tools must be changed when the viscosity deviates from its specified value by ± 10 percent. In ordinary hydraulic systems an increase in oil viscosity of up to 25 to 30 percent is permissible [6, 22, 49].

In hydrodynamic design of tribological joints and selection of oils for them, use is usually made of kinematic viscosity, which is an indispensable attribute in specifications for all mineral oils.

Values of the kinematic and the dynamic viscosity of some mineral oils are given in Table 9.19.

Table 9.19

Kinematic and dynamic viscosities of industrial oils

Oil grade	Viscosity at 50°C		Oil grade	Viscosity at 50°C	
	kinematic, cSt	dynamic, $\frac{\text{H} \times 10^3}{\text{s/m}^2 (\text{Pa s})}$		kinematic, cSt	dynamic, $\frac{\text{H} \times 10^3}{\text{s/m}^2 (\text{Pa s})}$
И-5А	4-5	3.4-4.3	ИГП-91	88.0-94.0	77.5-82.8
И-8А	6-8	5.2-6.9	ИГП-114	110.0-118.0	96.9-104.0
И-12А	10-14	8.6-12.0	ИГП-152	147.0-158.0	130.2-140.0
И-20А	17-23	14.6-19.8	ИГП-182	175.0-190.0	156.0-169.4
И-25А	24-27	20.9-23.5	ИНСп-20	18.0-25.0	15.8-21.9
И-30А	28-33	24.5-28.9	ИНСп-40	35.0-45.0	30.8-39.7
И-40А	35-45	30.7-39.4	ИНСп-65	60.0-70.0	53.2-62.0
И-50А	47-55	41.2-48.2	ИНСп-110	100.0-120.0	88.6-106.3
И-70А	65-75	57.3-66.1	ИСПи-25	23.7-27.0	20.6-23.5
И-100А	90-118	79.3-104.0	ИСПи-40	34.2-40.5	30.1-35.6
ИГП-4	3.4-4.4	2.8-3.7	ИСПи-65	60.8-68.1	53.5-60.0
ИГП-6	5.5-7.5	3.9-6.3	ИСПи-110	109.5-118.5	97.6-105.6
ИГП-8	7.0-9.0	6.0-7.7	ИРп-40	35-40	30.8-35.2
ИГП-18	16.5-20.5	14.2-17.6	ИРп-75	72-80	64.2-71.3
ИГП-30	28.0-31.0	24.2-26.8	ИРп-150	140-160	124.7-142.5
ИГП-38	35.0-40.0	30.5-34.8	ИТП-200	216-240	198.0-224.4
ИГП-49	47.0-51.0	41.2-44.7	ИТП-300	304-357	258.1-340.9
ИГП-72	70.0-75.0	61.7-66.1			

Pressure has a substantial effect on oil viscosity (Fig. 9.9). Here, viscosity was measured using quartz resonators [12]. The viscosity of the tested oils at all temperatures grows with pressure differently; it is greater with the increase in pressure and decrease in temperature.

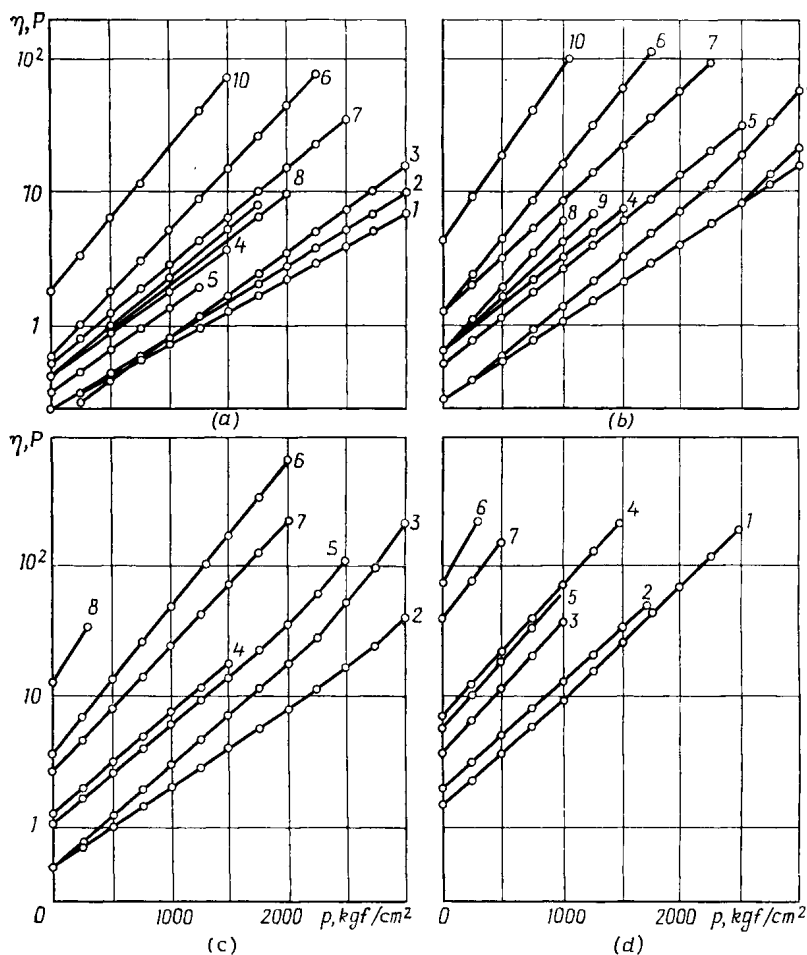


Fig. 9.9. Effect of pressure on viscosity of oils
(a) 0°C ; (b) -10°C ; (c) -20°C ; (d) -40°C ; 1—oil Grade AMF-10; 2—oil Grade MFE-10-A; 3—oil Grade PM; 4—oil Grade PML; 5—oil Grade BMT3; 6—oil Grade MBII; 7—transformer oil; 8—oil Grade ВИ-6; 9—oil Grade ИГП-6; 10—oil Grade АУП

This quality is essential for lubrication of mechanisms operating at high specific loads and high pressures in movable joints; it must be taken into account in design, since it has a favourable effect on the lubricating properties of oils, providing a strong lubricant film between rubbing surfaces.

Resistance to oxidation. In service, the physical and chemical properties of oils must not change significantly. One of the most typical changes is oil oxidation. The result is the increased corrosive action and greater viscosity of oil, or the formation of insoluble residues therein.

The process of oil oxidation is accelerated under the effect of high temperatures or catalysts, i.e., metals and metal salts of organic acids, formed in the interaction of oxidation products with the metal. The organic acids formed in oxidation may have a favourable effect on oil. Subsequently, however, a monomolecular layer of metallic soaps emerges on the metal surfaces. In addition, asphaltenes and other polymeric compounds are formed by the oxidation process. These changes are accompanied with an increase in the viscosity of the oil, its darkening, and sedimentation. However, the process of oxidation can be retarded by introducing various antioxidants in the oil.

The action of oxidation inhibitors consists in the disruption of the chain as the additive reacts with the oil molecule being oxidized; as a result, the additive itself becomes oxidized. In this process, the additive molecule decomposes, the energy of the oxidized oil molecule dissipates, and the chain reaction comes to an end.

The rate of oil oxidation (as well as that of the chemical reaction) practically doubles as the temperature rises by 10°C. The higher the temperature of the oil and the longer it remains in a mechanism, the higher is the rate of oxidation and the greater is the amount of oxidation products accumulated in the oil. All this may affect the normal operation of the mechanism (by causing contamination, corrosion, blocked oil circulation in the system, etc.).

The stability of an oil against oxidation depends on the method of its production and on the chemical composition; it is achieved by the selection of the basic material, the degree of refining (Fig. 9.10) and sometimes by introducing special antioxidation additives (see Table 9.17, and also the ДФ-1 and ДФ-11 Grade additives in Table 9.9).

As shown in Fig. 9.10, the oxidation stability of highly refined oils is several times greater than that of lightly refined oils. The former also exhibit a better response to antioxidants.

The main criterion used for the evaluation of oil stability is the acid number, which for most plain industrial oils must not exceed 0.05 to 0.5 mg KOH/g. Additive oils can have a relatively high acid number, and for such oils, e.g., the ИГП Grade, the stability is evaluated by an increase of 0.5 mg KOH/g in the acid number against its initial value. The rate of change of the acid number is much more significant than its absolute value at any time during the oil service life. As an example, for some plain mineral oils, the rate of increase in the acid number is specified at up to 2 mg KOH/g in 600 hours and over.

The results of oxidation tests of the ИГП Grade additive industrial oils by the ASTM D-943 method are shown in Fig. 9.11. The

tests were run for 1,000 hours at 95°C in a flow of oxygen and in the presence of copper, iron, and water. The oils under test had the same level of viscosity (20 cSt at 50°C) but different mineral bases

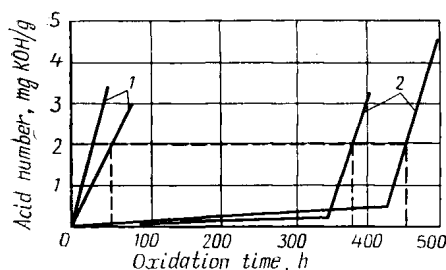


Fig. 9.10. Oxidation stability of additive oils, depending on the level of refining the base oil

1—light refining; 2—high refining

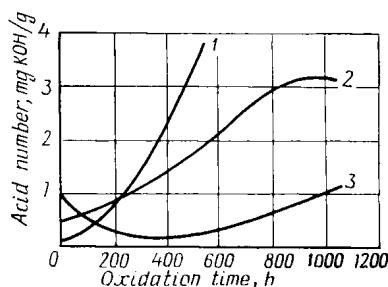


Fig. 9.11. Testing of oils by the ASTM D-943 method

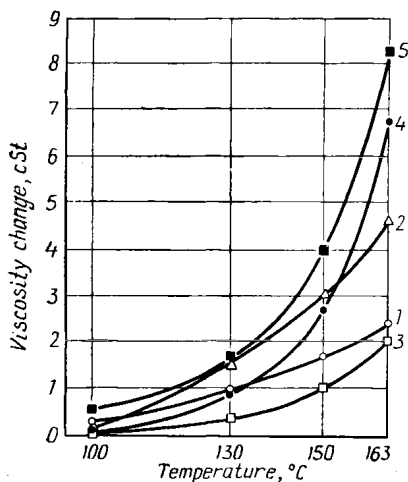
1—plain oil Grade IB-85; 2—oil Grade ИПН based on the IB-85 Grade oil; 3—oil based on the IB-95 Grade oil

refined to a variable degree. Characteristically, the acid number of the oils on a highly refined base (Grade IB-95) changed gradually, whereas that of the oils on a lightly refined base (Grade IB-85) sharply rose from the beginning of the test and in 1,000 hours reached 3 mg against 1 mg KOH/g for the IB-95 Grade base oil. In the plain IB-85 Grade oil the acid number reached 2 mg KOH/g already in 390 hours.

The oxidation stability of industrial oils is essential where these are used for a long time without change in closed-circuit lubrication systems. Data on the oxidation stability of various oils of this type make it possible properly to select an oil and to determine the possibility of its replacement with another oil. Figure 9.12 shows the results of comparison tests of some oils with a viscosity of 28 cSt at 100°C, the oils having similar in physico-chemical properties but differing in processing and hydrocarbon content.

Fig. 9.12. Change of oil viscosity with temperature

1—oil Grade И-28 from the Baku crudes; 2—oil Grade И-28 ФНПЗ; 3—oil Grade И-28; 4—oil Grade ВИ-250; 5—oil Grade ИС-28 from sulphurous crudes



The different character of the change of viscosity with temperature as the oils were oxidized in the ДК-2 Model oxidation tester

revealed low-gradient viscosity-temperature curves for the oils (Grades К-28, П-28, П-28ФНПЗ) produced from crudes with a low sulphur content, and steeper curves for the oils (Grades ВМ-250, ПС-28) produced from crudes with a high sulphur content. At 100°C, however, the viscosity of the oils after oxidation changes but slightly, not in excess of 0.5 cSt. In closed-circuit lubrication systems the temperature of oils similar to the П-28 Grade normally does not exceed 100°C, so that only a slight change in the acid number and viscosity of the tested oils can be expected.

Anticorrosive properties. Organic acids contained in mineral oils and also those formed as a result of oxidation during service in quantities that exceed the permissible limits may cause corrosion. Nonferrous metals and alloys used for bearing liners are particularly sensitive to the corrosive attack of such acids. In some cases corrosion can be caused by active sulphurous compounds (e.g., in additive-blended oils) and by mineral acids and alkalis left over after oil processing. Oils are evaluated for anticorrosive qualities by the permissible values established for the acid number, the content of water-soluble acids and alkalis, the extent of corrosion of copper and steel test plates, the ability to resist moisture, the hydrolytic stability, corrosion in the presence of water, etc.

The acid number signifies the presence of organic acids in an oil, whereas water-soluble acids and alkalis detected by the reaction of an aqueous extract from the oil indicate the presence of mineral acids and alkalis. The extent of corrosion of copper and steel plates is determined by the condition of the surfaces after prolonged holding (from 3 to 72 hours) in the oil at elevated temperatures. The surface condition is directly indicative of the corrosive activity of the oil, especially if it contains chemically active sulphurous compounds. Moisture resistance characterizes the ability of an oil to protect rubbing surfaces against moisture which in the presence of oxygen may give rise to metal corrosion.

Antiscuff and antiwear properties. The effect of oils on wear of materials in laboratory conditions is determined by the testing on friction machines of simple-shape specimens—spheres, cylinders, rolls, and flat sliders.

In the Soviet engineering practice use is made of the ЧИИМ Model four-ball friction machines, where an overall wear index is determined, characterizing the rate of wear under loads within the range from P_h (the load at which scoring marks initially appear) to P_c (the load at which scoring develops into surface failure). The antiscuff properties of oils are determined on such machines by the procedure established by GOST 9490-75.

The antiwear properties of oils are also determined on the ЧИИМ Model machines; the procedure involves the measurement of the wear spot diameter (in mm) on the bottom balls.

The antiscuff and antiwear properties of some current grades of additive-type industrial oils are described in Table 9.20.

Table 9.20

Antiwear and antiscuff properties of modern additive oils

Oil		Application	Additive	Antiscuff properties according to GOST 9490-75		Antiwear properties: wear spot diameter, mm
Grade	TU			P_c	ОПН	
ИГП-18 ИГП-38 ИГП-72 ИГП-91 ИГП-114 ИГП-182	38 101413-73	Hydraulic systems of metal-cutting and metal-forming machine tools, lubrication of light-duty gear transmissions and other units where oil should have high oxidation stability	Antioxidant, antiwear, antirust and defoaming agents	29 29 30 31 31 31	21 23 25 27 29 29	0.45 0.48 0.42 0.45 0.39 0.42
ИГСп-18 ИГСп-38	38 101238-72	The same as for the ИГП Grade oils, and also in hydraulic systems which require oils with high antiscuff properties	The same as in the ИГП Grade oils plus extreme-pressure additive	30 31	31 32	0.45 0.45
ИНСп-20 ИНСп-40 ИНСп-65 ИНСп-110	38 101-76	Lubrication of machine-tool slideways at low-rate feeds (1-200 mm/min) and various industrial applications	"Anti-stick-slip", antifric-tion, extreme-pressure, and adhesion agents	30 31 32 34	31 32 35 42	1.04 0.94 0.88 1.04
ИРп-40 ИРп-75 ИРп-150	38 101286-72 38 101451-74	Lubrication of gear transmissions and industrial mechanisms working at medium loads	Antioxidant, extreme-pressure, anticorrosion, defoaming, and antiwear agents	35 36 37	46 60 67	0.42 0.51 0.86
ИТП-200 ИТП-300	38 101292-72	Lubrication of gear transmissions and heavy-duty worm gearings	Antioxidant, extreme-pressure, and antifric-tion agents	37 37	60 64	0.54 0.52

Defoaming properties. These define the ability of oils to release air and other gases without foam formation. The latter shortens the service life of oils since it intensifies their oxidation. The cooling ability of oil is reduced and its leakage through seals is increased. The defoaming properties of oils are determined by the ASTM D-892 procedure as the tendency to foaming and the stability of the foam (cm^3).

9.3.2. Modern Oil Assortment

General-purpose industrial oils standardized by GOST 20799-75 are the distillate and residual mineral oils (or their mixtures) of light refining without additives. They are used as lubricants for diverse industrial equipment where there is no need for special additive oils. They are also used as base oils in the production of additive oils.

Table 9.21 presents the main physico-chemical properties of the general-purpose industrial oils according to GOST 20799-75, and Table 9.22, the corresponding oil grades according to formerly existing standards and specifications.

The **ИГП Grade oils** (see Tables 9.19 and 9.20) comprise highly refined additive oils with a wide viscosity range. These oils offer improved viscosity-temperature properties (viscosity index over 90), thermooxidation stability, slower ageing when heated, reduced tendency to foaming, moisture stability, etc.

The **ИГЦп Grade oils** (see Table 9.20) differ from the ИГП Grade oils by the presence of an extreme-pressure additive. The specifications for the ИГЦп Grade oils include working load rates and maximum oil-film disruption pressures.

The **ИHCп Grade oils** (see Tables 9.19 and 9.20) are regularly refined additive oils. They are highly efficient in eliminating stick-slip and therefore are intended for lubricating slideways where low-speed motions (1 to 200 mm/min) are involved.

The **ИСПп Grade oils**, TU 38 101293-72 (see Table 9.19) are obtained from lightly refined oils by introducing additives which improve antiscuff, antiwear and antifricition properties. These oils are used for lubricating gear transmissions and slideways functioning at relatively high speeds (over 200 mm/min).

The **ИПп Grade oils** (see Tables 9.19 and 9.20) are intended for gear transmissions and mechanisms in industrial equipment operating at medium loads. Antiscuff and antiwear characteristics for these oils are specified.

The **ИТП Grade oils** (see Tables 9.19 and 9.20). Not more than 1 percent sulphur due to the additives is permitted in the oils.

The **ИЦп Grade oils** are used to lubricate the chains of overhead and floor conveyors which periodically pass through drying chambers with a temperature of 180 to 200°C. These are high-viscosity residual oils with a viscosity of 20 to 40 cSt at 100°C. The ИЦп-20

Table 9.21

**Main physico-chemical properties of general-purpose industrial oils
(GOST 20799-75)**

Parameter	Oil grades									
	И-5А	И-8А	И-12А	И-20А*	И-25А	И-30А	И-40А**	И-50А	И-70А	И-100А
Kinematic viscosity at 50°C, cSt	4-5	6-8	10-14	17-23	24-27	28-33	35-45	47-55	65-75	90-118
Viscosity index, not less than	—	—	—	85	85	85	85	85	85	85
Setting point, °C, not more than	-25	-20	-30	-15	-15	-15	-15	-25	-10	-10
Flash point, as determined in closed crucible, °C, not less than	120	130	165	180	180	190	200	200	200	210
Coking capacity, %, not more than	—	—	—	—	0.15	0.15	0.15	0.20	0.40	0.45
Ash content %, not more than	0.005	0.005	0.005	0.005	0.005	0.005	0.005	0.005	0.005	0.005
Acid number, mg KOH per gram of oil, not more than	0.05	0.05	0.05	0.05	0.05	0.05	0.05	0.05	0.05	0.05
Sulphur content of oils made from sulphurous crudes, %, not more than	0.1	0.1	0.1	1.0	1.0	1.0	1.1	1.1	1.2	1.2

* For oil of this grade made to State Quality Mark specifications, viscosity index ≥ 100 and flash point $\geq 190^\circ\text{C}$.

** For oil of this grade made to State Quality Mark specifications, viscosity index ≥ 97 and flash point $\geq 210^\circ\text{C}$.

Notes. 1. No water, mechanical impurities, water-soluble acids, alkalis, and solvents are permitted in all the grades.

2. For data accumulation purposes, provision has been made for determining oil colour in calorimeter Model ИИТ, oxidation stability according to GOST 18136-72, and density according to GOST 3900-47.

3. With users consent, some oil grades made from Baku and Kazakhstan crudes may have deviations from GOST 20799-75 in viscosity index.

Grade oil (15 to 20 cSt at 100°C) is a highly refined mineral oil made from sulphurous crudes and containing an antifriction additive. The ИИИ-40 Grade oil (40 to 45 cSt at 100°C) is a mineral oil made from sulphurous crudes and having a number of additives, one of these being a sulphur-containing extreme-pressure agent.

The ВИИИ ИИ-801 Grade oil (TU 38 116-66) is used to run-in gear transmissions and worm gear sets [8]. The oil is based on the И-40А Grade oil and contains not less than 5 percent Sulphol as an extreme-pressure additive and 0.5 to 1 percent Akor-1 as an anticorrosive additive. Sulphol has the ability to increase wear of rubbing

Table 9.22

Grades of general-purpose industrial oils without additives (GOST 20799-75) and respective oil grades according to formerly used standards

Grades according to GOST 20799-75									
И-5А	И-8А	И-12А	И-20А	И-25А	И-30А	И-40А	И-50А	И-70А	И-100А
Grades according to former standards									
Velosit, GOST 1840-51	Vaseline oil, GOST 1840-51	И-12, GOST 1707-51	И-20, GOST 1707-51	И-25, ТУ 38 1272-69	И-30, GOST 1707-51	И-45, GOST 1707-51	И-50 (СУ) GOST 1707-51	И-65, ТУ 38 1272-69	ИСТ-14, GOST 8675-62
	Sewing-machine oil, GOST 973-50	И-12, GOST 8675-62	И-20, GOST 8675-62	—	И-30, GOST 8675-62	И-45, GOST 8675-62	И-50, GOST 8675-62	—	И-110, ТУ 38 1272-69
—	—	И-12, ТУ 38 1272-69	—	—	—	И-40, ТУ 38 1272-69	И-45, ТУ 38 1272-69	—	—
—	—	—	—	—	—	—	И-50 (СУ) МРТУ 38 1233-66	—	—

Table 9.23

Interchangeability of USSR-made industrial additive oils with those produced by major companies in other countries

USSR	Foreign maker			
	Oliofiat	Shell	Mobil	Esso
ИГП-2		Spindel oil 33	Velocite 3	
ИГП-4	RAX-11	Tellus 11	Velocite 4	Spinesso 32
ИГП-6	RAX-15	Tellus 13	Velocite 6	Spinesso 34
ИГП-8	RAX-15	Tellus 15	Velocite 6	Spinesso 36
ИГП-14		Tellus 23	Velocite 10	
ИГП-18	RZA-27	Tellus 27	DTE Light	Teresso 43
ИГП-30	RZA-40	Tellus 29	DTE Medium	Teresso 47
ИГП-38	RZA-50	Tellus 33	DTE Heavy Medium	Teresso 52
ИГП-49	RZA-65	Tellus 41	DTE Heavy	Teresso 56
ИГП-60	RZA-65	Tellus 41	DTE 103	Teresso 65
ИГП-72	RZA-95	Tellus 69	DTE Extra Heavy	Teresso 65
ИГП-91	PZA-120	Tellus 72	DTE 88	Teresso 85
ИГП-114	RZA-150	Tellus 72	DTE 105	Teresso 100
ИГП-152	RZA-200	Tellus 75	EI 61L	Teresso 120
ИГП-182	RZA-240	Tellus 75	DTE AA	Teresso 140
ИГСп-18	RCS-27	Tonna 27		Febis K43
ИГСп-38	RCS-50	Tonna 33		Febis K48
ИНСп-20		Tonna 27	Vactra 1	
ИНСп-40		Tonna 33	Vactra 2	
ИНСп-65		Tonna 41	Vactra 3	
ИНСп-110		Tonna 72	Vactra 4	
ИСПи-25	EP 35/S	Tonna 27		Febis K48
ИСПи-40	EP 50/S	Tonna 33		Febis K53
ИСПи-65	EP 85/S	Tonna R41		—
ИСПи-110	EP 150/S	Tonna 72		Febis K73
ИРп-40	EP 50/P	Macoma 33	Compound AA	Pen-O-Led EP1
ИРп-75	EP 100/P	Macoma 68	Compound BB	Pen-O-Led EP2
ИРп-150	EP 150/P	Macoma 72, 73	Compound DD	Pen-O-Led EP3
ИТП-200	EP 300/P	Macoma 75, 76	Compound EE, PP	Pen-O-Led EP5
ИТП-300	EP 400/P	Macoma 82	Compound GG	Pen-O-Led EP6
ИЦп-20	XTO Me-	—	—	—
ИЦп-40	diu Rothen 2000p			

surfaces at the initial stage of running, which accelerates the running-in of the surfaces and provides for their polishing and reduced temperature in the transmission.

The use of the БНМН ПП-801 Grade oil for running in globoidal reducing gears instead of the commonly used cylinder oil Grade 52 makes it possible to cut the running-in time by a factor of 4, to improve considerably the quality of the rubbing surfaces, to increase the teeth contact pattern area by 10 to 30 percent, and to reduce the oil temperature during the running-in period.

The П-8П Grade oil based on mineral oils with the addition of 3 to 5 percent Sovol is intended for heavy-duty toothed gearings in rolling-mill stands. As distinct from normally used high-viscosity oils, this oil has a lower-gradient viscosity-temperature characteristic, particularly within the range from $+20^{\circ}\text{C}$ to -30°C , which is essential for normal functioning of the closed-circuit lubrication systems of mill stands with long oil conduits (90 to 100 m and more). The П-8П Grade oil was found to influence the rate of wear of gear teeth in the same degree as the ПС-28 Grade oil and cylinder oils. With equal loading and comparable teeth hardness values, the specific wear of the teeth of roll-stand gears and reducing gears lubricated with the ПС-28 Grade is 35 to 50 percent of that observed in operation with high-viscosity lubricants. The oil provides for better heat removal and reduced pressure in the system (by 0.4 to 0.6 kgf/cm² as compared with high-viscosity oils).

All additive oils are free from water, mechanical impurities and water-soluble acids and alkalis.

As the current trend is towards increased production and consumption of additive oils for lubricating industrial equipment, their assortment will be diversified and undergo unification. At the same time, their growing ability to perform in different applications will promote the universal use of the oils and make it possible to reduce their variety within a factory.

The export and import of industrial equipment have necessitated a comparison of USSR-made additive oils with those made by the leading manufacturers in other countries. Table 9.23 presents data on the interchangeability of such oils. The results of tests of some imported oils are given in Table 9.24.

9.4. GREASES

9.4.1. Properties

By their properties greases hold an intermediate position between solid lubricants and oils. Greases generally include two components: a fluid base (mineral, vegetable, synthetic, and other oils) and a thickener (solid hydrocarbons, various salts of high-molecular fatty acids, i.e., soaps, dispersed-phase silica gels and bentonites, and

Results of testing imported oils

Table 9.24

Oil grade	Kinematic viscosity, cSt, at temperature, °C		Viscosity index	Flash point (open crucible), °C	Coking capacity, % by mass	Acid number, KOH per gram of oil	Ash content, % by mass	Sulphur content, %	Colour in NPA marks	Set-ting point, °C	Antiscuff properties		Wear spot diameter, mm
	50	100									ОП	P _c	
Velocite 4	4.20	1.70	69	140	0.004	0.07	None	0.364	1.0	-10	13.3	27	4.40
Velocite 6	7.36	2.63	102	158	0.034	0.10	0.023	0.270	1.0	-22	14.5	27	0.98
Vacuoline 1405	20.13	5.24	108	206	0.022	0.15	None	0.463	2.5	-14	17.8	27	0.95
Vacuoline 1409	37.86	8.20	108	228	0.052	0.06	0.004	0.640	2.5	-14	17.1	26	0.95
Vactra No. 2	40.10	8.80	113	230	0.176	1.54	0.045	0.045	> 8.0	-26	26.3	33	0.69
Mobilgear 630	105.49	46.16	94	232	—	0.99	0.092	0.864	6.0	—	51.7	34	0.91
Mobilgear 636	296.96	32.79	85	280	—	0.505	0.146	2.31	> 8.0	-7	59.2	36	0.37
Mobil DTE 24	20.55	5.19	100	208	—	1.13	0.21	0.924	1.0	-24	20.5	29	0.39
Mobil DTE Heavy													
Medium	36.04	7.80	104	230	0.06	0.20	0.022	0.990	1.5	-12	22.1	28	0.45
Tellus 33	39.71	8.16	97	230	0.134	0.84	0.104	1.05	2.5	—	—	—	—
Macoma 37	50.0	8.60	63	181	4.4	6.35	3.54	1.464	> 8.0	-26	38.95	33	0.94
Macoma R 68	75.85	11.92	75	191	2.8	5.31	1.62	1.79	> 8.0	-24	67.6	42	1.32
Tegula 72	114.30	16.76	87	226	—	2.70	5.58	0.62	1.5	-16	—	—	—
Valvata J-81	305.70	35.62	97	306	1.1	0.10	None	0.35	> 8.0	-4	28	23	—
Energol HP-20	35.05	7.40	95	220	0.226	0.58	0.097	1.65	3.5	-16	30	20	0.38
Energol HP-40	63.20	10.90	85	234	0.300	0.52	0.10	1.82	4.5	-24	33	31	0.40
Energol HLP 40	8.40	2.80	83	164	0.028	0.20	None	0.68	4.5	-28	20.6	29	0.43
Energol HLP 65	20.60	5.40	114	212	0.034	0.21	0.01	0.52	1.0	-28	22.7	29	0.37
Energol HLP 80	27.20	6.50	111	220	0.138	0.24	0.02	0.50	1.5	-30	26	30	0.37
Energol HP 20C	39.35	8.10	97	224	0.134	0.65	0.05	2.14	—	-28	34	21	0.64
Energol RD 150	57.19	10.46	93	220	0.260	0.36	None	1.60	5.0	-30	42.7	32	1.07
Energol GR 700 EP	300.90	28.20	57	280	1.696	0.22	0.035	2.17	> 8.0	-8	49.4	35	0.45

other organic and inorganic substances). Greases also contain additives which improve their service qualities. Various fillers (graphite, molybdenum disulphide, powdered metals and their oxides, mica, etc.) are often introduced into greases.

In the process of grease production, the thickeners, specifically soaps, form a three-dimensional structure whose cells hold the oil. Owing to this structure, greases under moderate loads behave as solids (they do not flow under gravity, and stay in place on inclined and even vertical surfaces); under loads which overcome the structural strength, greases flow like oils. However, when the load is removed, the grease stops flowing and again acquires the properties of a solid. This is a very important feature which gives greases advantages over oils.

The main advantages are the ability to remain in unsealed tribological joints and to operate within wider temperature and speed ranges, higher lubricity, better anticorrosion properties, the ability to function in contact with water and aggressive media, and higher cost-effectiveness.

The drawbacks to greases are poor cooling effect, greater tendency to oxidation, and more complicated delivery to a joint to be greased.

A knowledge of grease properties and special features, with due consideration for operating conditions and movable joint construction, makes possible the proper selection of a grease for a given application.

The main characteristics of greases which are most commonly specified in the USSR and other countries are given below.

Shear strength (τ , gf/cm²) is the minimum force that must be applied to deform the structure of grease and to initiate its flow. The specified values are established by GOST 7143-73. The magnitude of the shear strength and the temperature characteristic of a grease determine its ability to hold in a joint and to move into the friction zone. To some extent this value has an effect on the starting torque in bearings. **Consistency** (η , P) characterizes the flow of a grease after the bonds in its structure have been upset as a result of the critical force application. Consistency values are determined by GOST 7163-63. The consistency of greases depends not only on temperature, but also on flow conditions, i.e., the rate of deformation. Rising temperatures and increased deformation rates reduce the consistency of greases. Consistency is especially sensitive to changes in the rate of deformation. At a constant temperature, a 10- to 100-fold increase in the deformation rate produces a drop in consistency by a factor of from several hundred to several thousand.

Since the consistency of greases depends on their deformation, the concept of effective consistency is used. This is the viscosity of a Newtonian liquid (oil) whose resistance to a shear stress equals that of a given grease at the same temperature.

The consistency of greases is important when they are to be placed into tribological joints at low temperatures; it affects the magnitude

of starting and running torques in bearings, has an effect on the capability of the greases of being pumped through lubricant conduits, etc.

Mechanical stability. The change of the bulk mechanical properties of greases, such as shear strength, under a mechanical action and after subsequent relaxation is called the mechanical stability of greases.

This is an important performance characteristic of greases, particularly of those used in universal joints, flat guide ways, sliding bearings, etc., because the whole amount of grease in the joint is in action. A mechanically unstable grease, i.e., one that is highly susceptible to deformation and does not recover its initial properties after the load has been removed, is likely to flow out of the joint and cause its premature damage. The mechanical stability of greases is specified by GOST 19295-73.

Colloidal stability. This is the ability of a grease to retain oil in its structure under the action of external forces. Colloidal stability is specified by GOST 7142-74 as the amount (in percent) of the released (pressed-out) oil.

Greases with a high colloidal stability can release no oil during prolonged storage and service. A small amount of the released oil is always favourable to rubbing parts, as it improves their lubrication. However, when oil is released from a grease considerably, i.e., when the grease has a low colloidal stability, it flows out of the joint and leaves over the thickener, which solidifies and thus impairs lubrication.

Vaporability is determined by GOST 9566-74 as the amount of oil (in percent) evaporated from a grease in a strictly specified time. The loss of oil due to evaporation results in an increased relative content of the thickener in the grease and hence, in its higher shear strength and consistency, and it also brings about changes in other service properties of the grease.

Water resistance. This is the ability of greases to resist dissolution in water, to absorb no water from the environment, to resist washing-off by water, and to retain their properties in contact with water. A standard method for determining water resistance has yet to be agreed upon. Wherever necessary, a special procedure is resorted to in each specific case (boiling the grease in water, washing it off a revolving bearing or a plate with a controlled water jet, etc.).

Load capacity of the lubricant film is closely interrelated with friction and wear phenomena and therefore with the laws they obey. This is a very important attribute of a lubricant, which embraces a complex of properties that are found in boundary layers of the lubricant at the interface with metal, i.e., in boundary friction conditions. The complex includes the critical temperature of disruption of the lubricant film, the critical pressure it can withstand, its plastifying action and adhesive forces, antifricition, antiwear, and antiscuff properties, etc.

Because greases always contain surface-active agents, to say nothing of special additives, their lubricating efficiency is much higher than that of the oils that are used as the base.

The load capacity of the lubricant film in a boundary layer for various greases is determined by testing for friction and wear, which also includes evaluating the antiwear and anticuff properties on the ЧИИМ-3 Model friction machine according to GOST 9490-75.

Anticorrosion properties are characterized by the corrosive action of greases on metals. According to GOST 5757-67, these properties are evaluated by immersing metal plates in a grease, holding them there at a specified temperature, and then inspecting visually for corrosive effects. The emergence of corrosion spots and points, a considerable darkening of the plates, and also a change of the colour and appearance of the grease at the interface with the metal indicate that the grease has inadequate anticorrosion properties.

Dropping point. The minimum temperature at which a drop of a grease heated under specified conditions falls out of the Ubbelohde thermometer is called dropping point. It shows only an indirect relation to the grease melting point and for this reason has no physical meaning. The method for its determining is established by GOST 6793-74.

Greases with a dropping point of up to 100°C have been found to have their maximum usable temperature lying 15 to 20°C below the dropping point. But with the advent of greases whose dropping point is much higher than 100°C, e.g., lithium greases (170 to 200°C), mixed barium-calcium greases (230 to 260°C), bentonite and silica-gel greases (no dropping point), this characteristic has become of no practical importance. Thus, for instance, the maximum usable temperature for lithium greases comes to 110-130°C, and for mixed calcium greases, to 150-160°C.

The dropping point is sometimes indicative of the type of thickener used in a grease, and hence, may indirectly point to its possible field of application.

Penetration. The penetration number is the depth to which a cone of standard dimensions and mass (150 g) sinks under gravity into a grease in five seconds at 25°C. The procedure is established by GOST 5346-50, the unit of measurement is one tenth of a millimetre.

This characteristic is mostly used in foreign practice, and sometimes in the USSR. Penetration is an arbitrary empirical parameter having no physical meaning and showing no relation to service properties of a grease. It often happens that greases markedly different in chemical composition and properties have equal or close penetration numbers. The latter can be used for evaluating the uniformity of various batches of the same grease.

Water content. For most greases the presence of water in them is impermissible. However, some greases (hydrated calcium, calcium-sodium) contain water as an indispensable component. Greases with hydroscopic thickeners, e.g., sodium soaps, may also contain

water in small quantities (up to 0.5 percent), which do not affect their properties.

The qualitative water content in greases is determined by GOST 1548-42, and the quantitative content, by GOST 2477-65.

Mechanical inclusions. There is no consensus about what can be regarded as mechanical inclusions. However, all foreign inclusions, such as abrasives, which add to the wear of rubbing surfaces, saw dust or cloth fibres, which clog grease conduits or grease guns and so hinder the access of grease to its destinations, are impermissible. The amount of mechanical inclusions in greases is determined by several procedures prescribed by GOST 1036-75, which involve dissolving a grease in hydrocarbon solvents with subsequent weighing the sediments left on a filter. The permissible amount of the sediment for various greases should not exceed 0.1 to 0.5 percent. Mechanical inclusions that cannot be dissolved in hydrochloric acid are checked for in accordance with GOST 6479-73. Normally, the presence of such inclusions in greases is not permitted. According to GOST 9270-59, optical microscopy of a thin film of grease spread over an object glass plate is employed to determine the amount and size of foreign inclusions. The first two methods are used for general-purpose greases, and the third, for greases applied in precision tribological units, instrument bearings, etc.

The amount of free acids and alkalis. In the production of greases where soaps are used as thickeners, chemically neutral greases are difficult to obtain. A surplus of free acid or alkali is always present therein. A considerable amount of one or the other not only adversely affects the rheological properties of greases but also causes corrosion of the rubbing parts. Two standard methods are used to determine the amount of free acids or alkalis in greases: one for water-soluble ones (GOST 6307-75) and the other for organic (GOST 6707-76). A small amount of free organic acids and alkalis is permitted, whereas water-soluble ones are not permitted at all.

For some greases the specifications contain some other quality characteristics. These, however, are not general and do not reflect in full the service properties of the greases.

Data on greases are treated in greater detail in [38, 40, 41].

The thickener accounts for from 8 to 25 percent of the grease mass only. However its type and properties are crucial to the service properties of greases and so determine their field of application. For this reason, the greases given in Table 9.25 are grouped by the type of thickener.

Having realized the vital effect of the thickener on grease properties, a due attention should be paid to oils which go for greases. Low-temperature greases are produced from low-viscosity mineral and synthetic oils. For greases used at temperatures over 200°C, use is made of polysiloxanes, etc. General-purpose greases contain mainly industrial oils, residual oils, and their mixtures.

Table 9.25

Properties of greases

Trade name of grease	Standard	Viscosity, P, at 10 s ⁻¹ and temperature, °C		Shear strength, gf/cm ² , at temperatures, °C		Colloidal stability, %	Range of working temperatures, °C	
		subzero	0	20	80		from (-)	to (+)
Hydrated calcium (Ca-) greases								
Press-Solidol C Solidol C	GOST 4366-76	—	500-1,000	1.2-2.5	0	2-10	40	50
	GOST 4366-76	—	1,000-2,000	2-5	0	1-5	30	60
Press-Solidol YC-1 Solidol YC-1 Graphite grease YCca Contact grease	GOST 1033-73	—	600-1,000	1.2-2.5	0	7-15	40	50
	GOST 1033-73	—	1,500-2,000	3-6	0	5-13	30	70
	GOST 3333-55	—	2,000-4,000	4-7	0	—	—	70
	TU 38 USSR 2-001979-72	—	—	(240)	—	1-3	—	65
ИП-1Л (summer) ИП-1З (winter) ЦИАТИМ-208	GOST 3257-74	—	1,000-2,000	2-5	0	5-15	40	70
	GOST 3257-74	—	500-1,000	1.3-3.0	0	10-18	15	65
	GOST 16422-70*	15,000-18,000 at -30	—	—	—	—	40	100
Complex calcium (kCa-) greases								
Uniol-1	TU 38 USSR 2-01-150-73	—	1,000-2,000	3-6	1.5-5.0	1.5-3	30	150
	TU 38 USSR 2-01-219-75	—	800-1,500	2-4	0.8-2.5	2-4	30	130

Table 9.25 (continued)

Trade name of grease	Standard	Viscosity, P , at 10 s ⁻¹ and temperature, °C		Shear strength, gf/cm ² , at temperatures, °C		Colloidal stability, %	Range of working temperatures, °C	
		subzero	0	20	80		from (-)	to (+)
Uniol-3M	TU 38 101605-75	5,000-8,000 at -30; ≤2,000 at -50	500-800	4-6	1.5-4.0	5-10	60	150
Dispersol-1	TU 38 USSR 2-01-144-72	—	—	(200-310)	—	7-15	40	100
ЦИАТИМ-221	GOST 9433-60*	≤8,000 at -50	—	—	1.0-1.5	—	60	150
ВНИИ НП-207	GOST 19774-74*	≤14,000 at -30	—	—	0.7-1.5	—	60	160
Sodium (Na-) greases								
Fatty Konstalin УТ-1	GOST 1957-73	5,000-7,000 at -15	1,500-3,000	—	1.0-2.5	—	20	110
Fatty Konstalin УТ-1	GOST 1957-73	8,000-12,000 at -15	2,500-5,000	—	1.5-3.5	—	20	110
ЯНЗ-2	GOST 9432-60	5,000-7,000 at -15	1,200-2,000	2.5-5.0	1.8-3.0	—	30	100
1-13	GOST 1631-61	6,000-10,000 at -15	2,000-5,000	4-8	1.5-2.5	—	20	110
1-ЛЗ	GOST 12811-67*	6,000-10,000 at -15	≤5,000	4-8	1.5-2.5	—	20	110
ЛЗ-ЦНИИ	GOST 19791-74	12,000-16,000 at -30	—	4-6	—	—	40	110
ДТ-1	TU 38 USSR 2-01116-76	—	—	(315-345)	—	—	30	110
КСВ	TU 38 USSR 2-01115-76	11,000-15,000 at -15	7,000-8,000	4-6	0.5-1.5	4-8	30	110
Aircraft engine grease НК-50 (СТ)	GOST 5573-67*	25,000-30,000 at -15	—	—	1.8-2.5	—	15	150
Textile machinery grease ИТ	OST 38.1.38-74	4,000-6,000 at -30	—	1.3-1.6**	—	—	30	80

Table 9.25 (continued)

Trade name of grease	Standard	Viscosity, P , at 10 s ⁻¹ and temperature, °C		Shear strength, gf/cm ² , at temperatures, °C		Colloidal stability, %	Range of working temperatures, °C	
		subzero	0	20	80		from (-)	to (+)
Liner grease ВЛ	GOST 5078-49*	—	1,100-1,300 (at 20)	1.5-2.5**	—	—	15	120
ВНИИ НП-228	GOST 12330-66	5,000-8,000 at -40	—	0.5-1.5	0.5-1.0	—	45	150
ВНИИ НП-257	GOST 16105-70*	2,000-2,500 at -50	—	0.8-1.0	≥ 0.8**	—	60	150
Lithium (Li-) greases								
ЦИАТИМ-201	GOST 6267-74	2,000-3,000	800-1,500	3-5	1.0-2.5	20-30	60	90
ЦИАТИМ-203	GOST 8773-73	3,000-8,000	1,000-2,000	3.5-7.0	1.5-3.0	6-12	50	100
ЦИАТИМ-202	GOST 11110-75	10,000-15,000 at -30	—	2-3	1.2-1.5**	—	40	110
ВНИИ НП-242	TU 38 1-01-359-73	4,000-10,000 at -15	3,000-5,000	4.5-6.5**	1.0-1.5	—	30	100
Litol-24	GOST 21150-75	10,000-15,000 at -30	2,000-2,800	6-8	2.0-4.5	8-12	40	120
Litol-459/5	TU 38 101-207-75	—	5,000-7,000	—	12-16	1-4	40	130
Fiol-1	TU 38 101-247-76	2,300-5,500 at -20	800-1,500	2-3	1.0-1.5	15-20	40	120
Fiol-2	TU 38USSR 2-01-188-74	4,000-8,000 at -20	1,000-2,200	3-5	1.5-2.5	10-15	40	120
Fiol-2M	TU 38 101233-75	4,000-8,000 at -20	1,000-2,200	3-5	1.5-2.5	10-15	40	120
Fiol-3	TU 38 USSR 2-01-189-74	8,000-15,000 at -20	2,000-3,000	6-8	2-4	8-12	40	120
ЛЦП-15	TU 38 USSR 2-01-224-75	7,500-15,000 at -20	1,500-3,000	5-7	2-4	10-15	40	130
ЛЦ-31	GOST 5.575-70	3,500-5,000 at -15	2,500-3,000	4-7	2-3	—	40	120

Table 9.25 (continued)

Trade name of grease	Standard	Viscosity, P, at 10 s ⁻¹ and temperature, °C		Shear strength, gf/cm ² , at temperatures, °C		Colloidal stability, %	Range of working temperatures, °C	
		subzero	0	20	80		from (-)	to (+)
No. 158	TU 38 101320-77	1,000-15,000 at -15	3,000-5,000	2-5	0.3-0.8	8-10	30	100
БНЗ-3	GOST 5.1343-72	—	3,500-5,000	—	2.5-3.0**	—	30	100
ЛПС-П	TU 38 USSR 2-01-145-75	—	800-1,500	1.5-3.0	0.8-1.2	15-20	30	120
Severol	TU 38 4.018-74	5,000-7,000 at -30; ≤20,000 at -50	1,000-1,600	7-9	3-6	15-20	60	120
ОКБ-422-7	GOST 18179-72*	≤10,000 at -10	—	10-15	≥1.5**	—	30	120
ВНИИ НП-274	GOST 19337-73	≤2,900 at -50	—	2.0-3.5	≥1.0**	—	30	110
ЖРО	TU 32 ИТ-520-73	8,000-15,000 at -50	—	—	1.5-2.5	—	40	120
ЛДС-1	TU 38 4.01-29-75	6,000-9,000 at -40	1,000-1,600	—	1-3	10-15	40	120
Aluminium (Al-) greases								
Rotary-press grease (ИР)	OST 38 1.37-74	30,000-35,000 at -30	—	—	1-2**	—	25	65
AMC-1	GOST 2742-75	—	7,000-10,000	(300-350)	—	—	—	65
AMC-3	GOST 2742-75	—	15,000-30,000	(200-250)	—	—	—	65
ЗЗС	TU 38 101474-74	—	15,000-20,000	(270-335)	—	—	—	70
Threaded-assembly grease P-2	TU 38 101332-73	—	—	—	1-2**	—	30	50
Barium (Ba-) greases								
ШРБ-4	TU 38 USSR 2-01-143-72	8,000-10,000 at -20	800-1,200	2-4	0.8-1.2	6-10	40	150

Table 9.25 (continued)

Trade name of grease	Standard	Viscosity, P, at 10 s ⁻¹ and temperature, °C		Shear strength, gf/cm ² , at temperatures, °C	Colloidal stability, %	Range of working temperatures, °C		
		subzero	0			20	80	from (-)
Mixed-soaps greases								
ЭП-176	TU 38 10196-76	12,000-17,000 at -15	5,000-8,000	—	1.5-3.5	—	25	100
MC-70	GOST 9762-76	25,000-50,000 at -50	2,000-2,300	—	0.0-0.5	—	50	65
ЛЗ-162	TU 38 101315-72	—	—	—	≥ 2.6**	3-6	25	130
P-402	TU 38 101330-73	—	—	—	≤ 90**	—	50	200
P-416	TU 38 101385-73	—	—	—	—	5-10	40	100
P-413	TU 38 101330-73	—	—	—	≤ 90**	—	30	200
Non-soap greases								
ВНИИ НП-231	TU 38 101173-71	4,500-5,500 at -40	—	2.5-4.0**	≥ 1.0	—	60	250
ВНИИ НП-246	GOST 18852-73	4,000-5,000 at -40	—	2.5-5.0**	0.7-0.25	—	80	200
Graphitol Aerol	TU 38 2-01-172-74 TU 38 USSR 2-01-171-74	—	5,000-8,000 3,000-7,000	3.5-6.0 3-7	2-4 2.5-5.0	2-4 1.5-3.0	20 20	160 160
Siol	TU 38 101-52-74	1,500-2,000 at -20	—	—	1.4-1.8**	—	30	130
ВНИИ НП-279	GOST 14296-69*	10,000-30,000 at -30	—	—	0.5-0.8	—	45	50
Silicol	TU 38 USSR 2-01-149-73	—	3,000-5,500	≥ 5	3-5	1.5-3.0	45	160
Limol Paste (grease)	TU 38 USSR 2-01-146-75	—	—	(310-340)	—	2-6	—	250
ВНИИ НП-232	GOST 14068-68	—	—	—	—	2-4	—	250

Table 9.25 (continued)

Trade name of grease	Standard	Viscosity, P, at 10 s ⁻¹ and temperature, °C		Shear strength, gf/cm ² , at temperatures, °C		Colloidal stability, %	Range of working temperatures, °C	
		subzero	0	20	80		from (-)	to (+)
Hydrocarbon greases								
ГОИ-54п	GOST 3276-74	15,000-25,000 at -50	700-1,400	0.8-2.5**	0	—	50	50
	GOST 8551-74	36,000-50,000 at -15	250-300**	4-8**	0	—	20	60
ЦИАТИМ-205	GOST 19537-74	—	15,000-40,000	—	—	—	—	45
	TU 38 101480-76	—	—	—	—	—	—	45
	GOST 5656-60	—	30-50	—	—	—	—	—
	GOST 5570-69	—	20,000-25,000	—	—	—	25	50
	GOST 20458-75	—	—	—	—	—	60	50

* Greases Torsiol-35 and Torsiol-35Э usable up to -35°C are also available (TU 38 USSR 2-01-214-75).
 ** At 50°C .

Notes. 1. Permissible storage time in years for greases kept in maker's containers is 0.5 for Dispersol-1, Silicol, Torsiol-35Э; 1 for КСБ, P-2, Torsiol-35, Aerol 39C; 1.5 for 1-13; 2 for contact grease, Uniol-1, Uniol-2, ЛЗ-162, ЛЗ-ПНН, P-416, ВНИИ НП-207, ЯНЗ-2, P-113, P-402, ДТ-1, No. 39y; 2.5 for НК-50; 3 for ИП-1Л, ИП-13, ИТ, Uniol-3М, ШРЕ-4; 5 for all the others.
 2. The greases do not dissolve in water when boiled for 1 h, except for water-soluble sodium greases; grease ДТ-1 absorbs water and emulsifies, grease ЦИАТИМ-203 does not dissolve in water but tends to emulsify; greases Uniol-1, Uniol-2, Uniol-3М, ЦИАТИМ-221, and ВНИИ НП-207 do not dissolve in water but tend to absorb it slightly; grease ЛЗ-31 is insoluble but its synthetic ether is subject to decomposition.
 3. Figures in parentheses in column "Shear strength" give penetration values at 25°C .

9.4.2. Assortment and Application of Greases

A great variety of greases are used for movable joints in industrial equipment, agricultural machinery, vehicles, etc.

The properties of various greases are given in Table 9.25, and their composition and field of application are given below.

Hydrated calcium-base (Ca-) greases are the most common type of grease. They are used in industrial equipment, hoisting machines, vehicles, etc.

Press-Solidol Grades C and YC-1 are mixtures of industrial oils (Grades 20, 30 and 40) or oil distillates, thickened with Ca-soaps of synthetic fatty acids. They are used in automobile chassis and steering linkage, and in other mechanisms, with delivery through grease guns. Fatty Solidols perform better than synthetic ones.

Solidol Grades C and YC-2 are the same in composition; they are universally used for mechanisms and machines working under normal conditions.

Graphite grease Grade YCca consists of cylinder oil thickened with Ca-soaps of synthetic fatty acids, and 10 percent of Grade II graphite. It is used for low-speed heavy-duty mechanisms, leaf springs, automotive suspensions, open gears, bore-bit bearings, etc.

The grease is not fit for precision applications (antifriction bearings, etc.).

Contact grease is a mixture of industrial oils (Grades 12 and 20) thickened with Ca-soaps of synthetic fatty soaps and 30 percent of Grade II graphite. It is used for lubrication of fish plates at rail joints for consistent electric conductivity.

The III-1I (summer) and III-13 (winter) Grade greases are composed of light cylinder oils thickened with Ca-soaps of cottonseed oil and hydrogenated fat with small additions of Na-soaps of the same fats and a soap of sulphurized cottonseed oil. The greases are used for bearings of rolling-mill stands fitted with centralized lubrication systems; they can be used in place of fatty and synthetic Solidols.

The ЦИАТИМ-208 Grade grease comprises Nigrol-type oils thickened with Ca-soaps, oxidized petrolatum, and acidol.

Complex calcium (kCa-) greases. *Uniol-1 grease* consists of residual oils of the MC-20 Grade thickened with kCa-soaps of heat treated synthetic fatty acids and acetic acid, and also antioxidants and some other additives. This is a multi-purpose grease for high-temperature heavy-duty applications; it is used in industrial equipment, tunnel furnaces, hot conveyors, etc. Also used as a multi-purpose lubricant for automobiles and tractors. The grease has high antiscuff properties.

Uniol-2 grease has the same composition. It is used in the centralized lubrication systems of mining and metallurgical equipment; has high antiscuff properties.

Uniol-3M grease is a mixture of a mineral oil and polysiloxane liquids, thickened with kCa-soaps of heat treated synthetic fatty and acetic acids. It also contains antioxidants and MoS_2 . As distinct from Uniol-1, this grease is used as an all-weather lubricant for basically the same mechanisms when these are operated at low temperatures, e.g., in the Arctic regions.

Dispersol-1 grease consists of a mineral oil thickened with kCa-soaps of stearic and acetic acids, and ceresine. The grease is used for lubricating the window raisers in the BA3 Model cars. When thinned out with white spirit, the grease is used for dip lubrication of automobile door locks and other components during assembly.

The ЦИАТИМ-221 Grade grease is a polyethylsiloxane liquid thickened with kCa-soaps of stearic and acetic acids. It is used for light-duty antifriction bearings working at elevated temperatures. The grease does not affect rubber.

The ВНИИ НП-207 Grade grease is a mixture of a polyethylsiloxane liquid and a synthetic hydrocarbon oil thickened with kCa-soaps of synthetic fatty acids and acetic acid. It contains an antioxidant. Its application is the same as that of the ЦИАТИМ-221 Grade grease, but it provides for better performance at high temperatures.

Sodium-base (Na-) greases. *Fatty Konstalin Grades YT-1 and YT-2* consists of light cylinder oils thickened with Na-soaps of castor oil. These are used for antifriction bearings and other applications where the working temperatures exclude the use of Solidols.

The ЯНЗ-2 Grade grease consists of industrial oil Grade 12 thickened with Na-soaps of synthetic fatty acids, a small quantity of Ca-soaps of these acids and also sodium sulphonate. The grease is used for automobile wheel bearings, electric motor bearings, etc.

The 1-13 Grade grease is a mixture of industrial oils having a solidification point of under 38°C thickened with Na-soaps of castor oil. It also contains a small amount of Ca-soaps of castor oil. The field of application is the same as that of the ЯНЗ-2 Grade grease.

The 1-ПЗ Grade grease is basically the same as the 1-13 Grade, but with an antioxidant. It is used for the axle roller bearings of railway vehicles.

The ПЗ-ЦНИИ Grade grease consists of spindle oil Grade AY and industrial oil Grade 50, thickened with Na-soaps of castor oil. It also contains some addition of Ca-soaps of castor oil, an antioxidant and a multi-purpose additive. The grease has improved running-in and antiscuff qualities, and it is used in the same applications as the 1-ПЗ Grade.

The ДТ-1 Grade grease consists of castor oil thickened with Na-soaps of natural fats, an antioxidant, MoS_2 , and colloidal graphite. It is used for lubricating components of automobile hydraulic drives (hydraulic clutch cylinder, brake pressure regulator, hydraulic

brake master cylinder, etc.) during assembly. The grease has improved antiscuff and antiwear qualities.

The KCB Grade grease consists of industrial oil Grade 50 thickened with Na-soaps of natural fatty acids. It contains copper flakes and additives that neutralize the copper as a catalyst of grease oxidation. The grease is used to lubricate electric switches, e.g., turn indicator switches in the BA3 Model cars.

The HK-50 Grade aircraft engine grease (CT) contains residual oil Grade MK-22 thickened with Na-soaps of inedible fat and hydrogenated fat, and also colloidal graphite. It is used as a summer lubricant for aircraft landing gear bearings.

The IT Grade grease is a textile machinery grease which is a perfume oil thickened with Na-soaps of hydrogenated fat. It is used for the ring bearings of ring spinning frames.

Liner grease Grade BII consists of industrial oil Grade 20 thickened with Na-soaps of hydrogenated fat and Grade II graphite. The grease is used for lubrication of liners mounted into gun bores and of muzzle brake threads.

The BHHI HP-228 Grade grease is a mixture of dioctyl sebacate and oil Grade MC-14 thickened with Na-soap of stearic acid. It contains anticorrosive, extreme-pressure and antioxidant additives. The grease is used for high-precision applications, e.g., gyroscope rotor bearings, it is operable at rotational speeds of up to 60,000 rpm and a vacuum of up to 0.1 mm Hg. The grease has a long service life.

The BHHI HP-257 Grade grease is a mixture of a polysiloxane liquid and an ester thickened with Na-soaps of stearic acid. It contains sodium nitrite, antioxidants, and MoS_2 . The grease is used for miniature bearings and low-output reducing gears of electromechanical instruments; it is fit for operation in a vacuum of up to 10^{-9} mm Hg at subzero temperatures.

Lithium base (Li-) greases. *The ЦИАТИМ-201 Grade grease* contains instrument oil Grade MBII thickened with lithium stearate, and an antioxidant. The grease is used for low-powered mechanisms operating at low temperatures. This is the main lubricant employed for aircraft instruments.

The ЦИАТИМ-203 Grade grease is a mixture of transformer oil with vinypol, thickened with a Li-soap of stearic acid and sulphurized sperm oil. It contains extreme-pressure additives. The grease is used similarly to the ЦИАТИМ-201 Grade, but can stand higher loads.

The ЦИАТИМ-202 Grade grease is a mixture of transformer oil and oil Grade MC-14, thickened with Li-soaps of stearic acid and castor oil. The grease is used for antifriction bearings working at rotational speeds of up to 30,000 rpm.

The BHHI HP-242 Grade grease consists of industrial oil Grade И-50A thickened with lithium stearate, an antioxidant, and MoS_2 . The grease is used for electric motor bearings. It has improved antiwear properties.

Litol-24 is a mixture of spindle oil Grade AY and industrial oil Grade 50 or a mixture of distilled and residual oils of West Siberia crudes, thickened with lithium oxystearate. It contains antioxidants and gelling agents. The grease is used for the principal tribological joints in vehicles, industrial equipment, electrical machinery, etc. Generally, it requires no change since its life is as long as that of the mechanism it lubricates.

Litol-459/5 consists of a residual oil similar to the MC-20 Grade thickened with lithium oxystearate. It contains an antioxidant and features high mechanical stability. The grease is used for lubricating ignition distributors.

Fiol-1, *Fiol-2*, and *Fiol-3* are mixtures of spindle oil Grade AY and industrial oil Grade 50 thickened with lithium oxystearate. The greases contain an antioxidant and a gelling agent. *Fiol-1* is used for forced lubrication by a grease gun or through a centralized system, and also for lubricating flexible cables in automobiles, e.g., for carburettor and ventilation control cables. *Fiol-2* is used for various movable joints (antifriction and sliding bearings, gear transmissions, etc.) of industrial equipment.

Fiol-2M is basically the same in composition as *Fiol-2*, but contains MoS_2 and has improved antiscuff properties. The grease is used in some automotive and machinery applications.

The JCU-15 Grade grease is a mixture of oil Grade AY (or industrial oil Grade 12) with industrial oil Grade 50 thickened with Li-soaps of a hydrated castor oil. It contains an antioxidant, a gelling agent, and also powdered zinc oxide. The grease has improved antiscuff properties. It is used for accelerator drive pin and universal joints, clutch control levers, the spline fittings of the input shaft of automobile speed gear boxes, propeller shafts, window raisers. The grease can substitute for *Litol-24*; in most cases it requires no change or replenishment.

The JI3-31 Grade grease is a mixture of a synthetic ethereous oil and Sovol thickened with lithium stearate. It contains antioxidants. The grease is used for various applications involving antifriction bearings. In sealed bearings it is utilized for the whole bearing life. No contact with water is permitted.

No. 158 grease consists of residual oil Grade MC-20 thickened with a Li-soap of stearic acid and castor oil and also with copper phthalocyanine. It also contains calcium stearate and rosin. The grease is used for electrical equipment bearings, automobile needle bearings, etc.

The BH3-3 Grade grease consists of industrial oil Grade 50 thickened with Li-soaps of stearic acid and castor oil. It also contains an antioxidant and sulphurized castor oil. The grease offers improved antiscuff properties; it is used for lubricating roller bearings in mining equipment.

The JC-1II Grade grease is a mixture of industrial oil Grade 12 and 50 thickened with lithium oxystearate. The grease contains a

combination of additives which improve its antiwear and antioxidant properties. The grease also has high antiscuff properties. It is corrosion-active in the presence of water. The grease is used for heavily loaded mechanisms in foundry and metal-forming equipment and the like, fitted with centralized lubrication systems.

Severol is a mixture of an industrial oil and a polysiloxane liquid, thickened with lithium stearate. Contains an antioxidant and an extreme-pressure additive. It is a general-purpose grease for diverse low-temperature applications.

The OKB-122-7 Grade grease consists of a mixture of mineral oil Grade MC-14 and a polysiloxane liquid, thickened with lithium stearate and ceresine. The grease is used as a lubricant in various instrument applications.

The ВННН НП-274 Grade grease consists of liquid chlorosiloxane thickened with lithium stearate and oxystearate. The grease is stable at extremely low subzero temperatures; it features a low vapour pressure. The grease is used for miniature bearings and low-power reducing gears; it is fit for operation in a vacuum of up to 10^{-9} mm Hg.

The ЖПО Grade grease comprises spindle oil Grade AY thickened with Li-soaps of stearic, oxystearic and oleic acids and sulphurized castor oil. It has an antioxidant. The grease exhibits improved antiwear properties; it is used for railway vehicle bearings.

The ЛДС-1 Grade grease is a mixture of mineral oil Grade ACB-5 and synthetic ether, thickened with lithium oxystearate. It contains a gelling agent and an antioxidant. The grease is used for sealed antifriction bearings in electric motors designed for long-term operation (up to 20 thousand hours) under medium and light loads.

Aluminium-base (Al-) greases. *Rotary-press grease (ИР)* contains a residual oil similar to the MC-20 Grade, thickened with Al-soaps of stearic acid. The grease is used for lubricating printing press bearings.

The AMC-1 and AMC-3 Grade greases consist of cylinder vapour oil Grade 52 thickened with Al-soaps of stearic and oleic acids. The grease is used for marine applications and for slushing mechanisms exposed to sea water.

The 39C Grade grease consists of cylinder vapour oil Grade 52 thickened with Al-soaps of heat-treated synthetic fatty acids and with petrolatum. The grease is used for corrosion protection of power-line lightning conductors, high-voltage line fittings, etc.

The P-2 Grade grease for threaded assemblies is a mixture of industrial oil Grade 50 and instrument oil Grade MBA, thickened with an Al-soap of stearic acid. It contains graphite, and powdered lead, zinc, and copper as fillers. The grease is used for sealing screw joints of casing pipes and the pump-and-compressor piping of wells. It is toxic.

Barium-base (Ba-) greases. *The ИРБ-4 Grade grease* consists of industrial oil Grade 20 thickened with a complex Ba-soap of acetic

acid and acids derived from cotton oil. The grease contains antioxidants and has high antiscuff properties. It is used for lubricating front suspension ball joints, steering rod ends in the BA3 Model cars, etc.

Complex-soap base greases. *The ЭМ-176 Grade grease* is a mixture of oil Grade AY and residual oil Grade MC-20, thickened with lithium, zinc, lead and aluminium soaps of synthetic fatty acids and castor oil. It contains graphite and pentaerythritol. The grease has high antiscuff properties, it is used for lubricating bearings in vertical and horizontal type electrical machines.

The MC-70 Grade grease consists of instrument oil Grade MBA thickened with barium and aluminium soaps of stearic acid and ceresine. The grease is used for mechanisms exposed to sea water.

The ЛЗ-162 Grade grease consists of spindle oil Grade AY thickened with lithium, zinc, and aluminium soaps of heat-treated synthetic fatty acids. It contains mica and rosin. The grease is used for fittings of flowing oil and gas wells.

The P-402 Grade grease is a mixture of industrial oil Grade 50 and a polysiloxane liquid, thickened with lithium and aluminium soaps of stearic acid. It is filled with graphite Grade II and powdered lead, zinc, and copper. The grease is used for sealing threaded fittings of casing pipes and those of pump-and-compressor piping in bore wells at temperatures lower than -30°C and, for deep wells, over 100°C . The grease is toxic.

The P-416 Grade grease consists of a spindle oil thickened with zinc and lithium soaps of stearic acid. The grease is filled with powdered zinc or its compounds. It is used to prevent scoring and facilitate assembly and disassembly of oil-rig components with coarse threads. The grease is toxic.

The P-113 Grade grease is similar in composition to the P-402 Grade. It is filled with powdered lead and its compounds. The field of application is the same as that of the P-416 Grade; used for deep wells where the temperature is over 100°C . The grease is toxic.

Non-soap greases. *The БННН НН-231 Grade grease* is a polysiloxane liquid thickened with carbon black. The grease is used for low-speed sliding and antifriction bearings, worm gearings and screw drives.

The БННН НН-246 Grade grease consists of polysiloxane liquid thickened with a pigment. The grease is used for high-speed light-duty rolling bearings and low-power gear transmissions. It is fit for operation in vacuum.

Grafitol consists of residual oil Grade MC-20 thickened with a dispersed-phase modified silica gel. It contains colloidal graphite as a filler. The grease is used for hinges of drying-chamber doors, for exhaust fans, and some other industrial applications. It has good antiscuff properties.

Aerol consists of residual oil Grade MC-20 thickened with a dispersed-phase modified silica gel. It contains molybdenum disulphide

and anticorrosive additives. The grease is used for chain conveyors in drying chambers and for other industrial applications. It has good antiscuff properties.

Siol is a mixture of industrial oil Grades 12 and 50 thickened with butoxyl. It contains MoS_2 and antioxidants. The grease is used for high-speed bearings in textile machinery.

The *ВННН НН-279 Grade grease* consists of a synthetic hydrocarbon oil thickened with silica gel. The grease is used as a lubricant for rolling bearings, sliding bearings and other tribological units where increased resistance to oxidation is required.

Silicol consists of a polysiloxane liquid thickened with a dispersed-phase modified silica gel, and sulphurized castor oil.

The grease is used for fans of carburizing furnaces and for other industrial applications.

Limol is a mixture of residual oil Grade MC-20 and cable oil Grade C-220 containing a large quantity of molybdenum disulphide and stabilized with a modified dispersed-phase silica gel. The grease is used to facilitate assembly and disassembly of screw joints and to run in rubbing parts. The applications include sliding bearings, universal joints gear and screw drives.

The *ВННН НН-232 Grade grease* (paste) comprises industrial oil Grade 20, a large quantity of MoS_2 , and lithium stearate as a stabilizer. The field of application is similar to that of *Limol*.

Hydrocarbon greases. The *ГОИ-54н Grade grease* consists of instrument oil Grade MBII thickened with ceresine. It contains an antirust additive. It is used in ordnance applications and for slushing precision mechanisms.

The *ЦНАТМ-205 Grade grease* is a mixture of medicinal vaseline oil and perfume oil, thickened with highly refined ceresine. The grease is used for seal packings, threaded assemblies and other applications exposed to aggressive media. Its guaranteed life is 10 years.

The *ИБК Grade grease* is a mixture of cylinder oil, petrolatum, and ceresine, containing an antirust additive. The grease is used for slushing metal articles and outside surfaces of machinery in transportation and long-term storage.

The *БТБ-1 Grade grease* is a mixture of spindle oil, paraffine, and ceresine, containing antirust, gelling, and adhesive agents. The fields of application are basically the same as those of the *ИБК Grade*, including, in addition, the protection of vehicle accumulator battery terminals, e.g., in the BA3 Model cars. The grease is superior to the *ИБК Grade* in stability at subzero temperatures.

The *ЕВН-1 Grade grease* is a mixture of spindle oil Grade AY and grease Grade ГОИ-54н, containing colloidal graphite. It is used similarly to liner grease Grade BJL.

No. 39y is a mixture (melt) of transmission oil, petroleum ceresine and condensation products of triethanolamine with stillage residues Grade ЧЖК. The grease is employed for lubrication of steel cables

during their manufacture and use. It is not fit for cables of hoisting equipment with movable pulleys.

Torsiol-55 is a mixture of a polysiloxane liquid, residual oil extracts, and petroleum ceresines, containing antirust additives. The application is the same as that of No. 39y, but it is used for equipment working at low temperatures, e.g., in the Arctic regions.

9.5. SOLID LUBRICANTS AND COATINGS FOR OPERATION IN VACUUM

9.5.1. Solid Lubricants

These are materials that ensure lubrication between two surfaces rubbing with dry or boundary friction under extreme conditions. Solid lubricants may belong to neither of the rubbing parts (e.g., solid lubricants in powdered form), or they may fill the composite material or coating of one or both rubbing parts. High heat resistance, good adhesion to metals, and low rate of evaporation in vacuum qualify solid lubricants for efficient use in vacuum, optical, and electronic systems. These lubricants are gaining recognition in general engineering, instrument making, and vacuum metallurgy.

Lamellar solid lubricants pertain to anisotropic compounds in which the strength of interatomic bonds is substantially different in different directions. The theoretical principles of solid lubricants are treated in numerous works [27, 9, 7, 56, 58].

Molybdenum disulphide (α — MoS_2) is crystallized in a hexagonal system. The molybdenum atoms are situated between two layers of the sulphur atoms. The distance between the nearest molybdenum and sulphur atoms is 2.41 Å, and the shortest distance between the sulphur atoms in parallel layers is 3 Å.

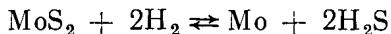
Main properties

Density, g/cm ³	4.8
Mohs hardness	1.0 to 1.5
Sublimation point, °C	450
Melting point, °C	1,185
Linear expansion coefficient within 50-700°C, 1/°C	7×10^{-6}
Thermal conductivity, kcal/(cm s °C)	4.9×10^{-3}
Magnetic properties	diamagnetic
Chemical stability	dissolvable in aqua regia, oxidizes in concentrated H_2SO_4 and HNO_3

In air, MoS_2 oxidizes to MoO_3 and S or SO_2 . Such oxide films begin forming at 350°C, and rapid oxidation of MoS_2 takes place at temperatures of over 480°C. In vacuum, MoS_2 remains stable up to 1,100°C.

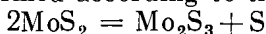
Fluorine reacts vigorously with MoS_2 , chlorine turns MoS_2 into MoCl_2 on heating, whereas bromine practically does not react with MoS_2 .

Hydrogen reduces solid MoS_2 directly to metal, without intermediate transformations:



Molybdenum disulphide is highly stable against radiation: when exposed to a dose of 5×10^9 rad, it shows no signs of damage.

A moderate heating of MoS_2 in an electric furnace in the absence of air results in Mo_2S_3 formed according to the reaction



Friction in air at surface temperatures above 400°C leads to a partial oxidation of MoS_2 to MoO_3 .

Values of specific characteristics τ_0 and β for sintered bronze specimens coated with MoS_2 films of different thickness in rubbing against steel Grade IX15 are given in Table 9.26.

Table 9.26

Adhesion of MoS_2 coatings, depending on their thickness

Sample No.	Coating thickness, μm	Mean contact stress, kgf/mm^2	τ_n , kgf/mm^2	f_{adh}	τ_0 , kgf/mm^2	β
1	Uncoated bronze	65	4.65	0.078	0.03	0.049
2	2-16	60	3.30	0.055		
3	14-18	56	3.06	0.054		
4	60-64	35	1.69	0.051		
5	74-85	29	1.51	0.052		
6	MoS_2 in bulk	3.8	0.19	0.050		

Tungsten disulphide is crystallized in a hexagonal system. The crystal lattice of WS_2 is similar to that of MoS_2 where the molybdenum atoms are replaced by the tungsten atoms. Tungsten disulphide has a greater thermal stability (up to 510°C in air) and resistance to oxidation than molybdenum disulphide (Table 9.27). Its load-carrying capacity is 3 times that of MoS_2 .

Tungsten disulphide is chemically neutral, it is insoluble in almost all media, including water, oils, alkalis and nearly all acids. The few chemicals it is sensitive to are free gaseous fluorine and hot sulphuric and hydrofluoric acids. WS_2 is a non-toxic material and it does not cause corrosion to metals.

The limitation to the use of WS_2 is its cost, which, according to some British sources, is three times the cost of MoS_2 .

The use of tungsten disulphide as an additive to oils for producing colloidal suspensions is somewhat difficult because of its high density ($\rho = 7.4 \text{ g/cm}^3$), which is 8 times that of mineral oils. For instance, in an oil-base suspension containing 50 percent (by mass) of graphite,

Table 9.27

Characteristics of solid lamellar lubricants

Solid lubricant	d, Å	c, Å	$\frac{c}{d}$	Density, g/cm ³	Compressibility modulus, kgf/cm ² *	Temperature, °C			Electrical conductivity	Friction coefficient***
						oxidation in air	decomposition in vacuum	melting		
Graphite	2.46	6.75	2.74	1.4-1.7	50,500	455	—	3,652**	High	0.04
BN	2.52	6.69	2.66	2.25	22,800	800-900	—	3,000**	Low	0.67
MoS ₂	3.16	12.32	3.90	4.8	85,000	400	1,100	1,185	Semi-conductor	0.03
MoSe ₂	3.288	12.90	3.92	6.9	—	400	—	1,200		0.02
WSe ₂	3.290	12.97	3.94	9.22	—	350	—	1,200		0.02
WS ₂	3.187	12.525	3.9	7.4	—	510	1,400	—		—
NbSe ₂	3.439	25.188	7.32	6.25	—	350	—	800	High	0.06
CdJ ₂	4.26	6.86	1.61	5.7	—	—	—	388	—	—
PbJ ₂	4.55	6.89	1.51	6.16	—	—	—	412	—	—
BiJ ₃	7.50	20.65	2.75	5.7	—	—	—	408, 439	—	—
Sb ₂ S ₂	4.589	7.5	1.2	5.67	—	—	—	552	—	0.17
AgJ	3.838	11.223	2.92	4.64	—	—	—	550	—	0.14

* Found in pressed specimens.

** Material begins subliming.

*** Tests were conducted in nitrogen at 71°C, sliding speed 1.1 m/s, pressure 10.5 kgf/cm²; boron nitride was tested at 538°C.

MoS₂ or WS₂, the volume of these components will be 36, 15.5, and 11 percent, respectively.

At atmospheric pressure and temperatures of over 400°C use is recommended of WS₂, whereas at lower temperatures MoS₂ is to be preferred as a cheaper material. In vacuum, WS₂ and MoS₂ exhibit practically the same properties, and possess lubricating ability at up to 1,320°C.

In a vacuum of 10⁻¹⁰ mm Hg, molybdenum disulphide is stable at up to 1,100°C; its decomposition takes place at temperatures above 1,400°C.

9.5.2. Self-Lubricating Materials

In accordance with the molecular-mechanical theory of friction, low friction and wear are ensured if the rule of the positive gradient of mechanical strength is observed, that is, the strength of the emerging molecular bonds must be lower than that of the underlayers: $\text{grad } \sigma_x > 0$ [46, 7, 25].

This rule is always realized when oils or greases are introduced between rubbing surfaces, because the shear strength of the lubricant is much lower than that of the metal it covers. In a pair of rubbing surfaces a positive gradient can be achieved by coating with a film (metallic or nonmetallic) and by using a self-lubricating monolithic material which in the process of friction also ensures a positive gradient of mechanical strength, owing to its active filler or to squeezing out a lubricant (Maslyanit) [13]. Still another method is the use of a resin with a solid lubricant (Grade АФ-3ам). All these phenomena are intensified with rising friction temperature which, in turn, produces structural changes in the surface layers, selective diffusion, evaporation and, hence, a change in the coefficient of friction and wear.

Analysis of the data of Table 9.26 indicates that the adhesion component of the friction coefficient remains practically unchanged (variation within 10 percent) with a change in film thickness δ of from 2 to 85 μm , whereas the tangential strength of the adhesion bond changes sharply from 3.3 kgf/mm² (with $\delta = 2$ to 6 μm) to 1.51 kgf/mm² (with $\delta = 74$ to 85 μm), that is, more than by a factor of two. The reason for this decrease is a change in the normal contact stresses.

From the production standpoint, the advantages of self-lubricating polymer materials over metals are unlimited sources of basic materials, reduced (by a factor of 2 to 5) capital investments, reduced (by a factor of 5 to 10) labour consumption in making parts without chip removal on a batch or mass production basis, and reduced (by a factor of up to 5) losses of material.

As compared with liquid lubricants, self-lubricating materials are capable of operating over a wider range of temperatures and ensure permanent lubrication during storage.

The drawbacks to self-lubricating polymer materials are the poor transfer of heat generated in friction for lack of liquid-lubricant circulation, and a friction coefficient exceeding that in hydrodynamic friction.

The main trend in developing self-lubricating polymers is towards multicomponent materials [7, 25, 13].

The content of the components in these materials is determined by the service properties, working temperatures, friction conditions, service life, load capacity, working medium, manufacturing feasibility, and cost effectiveness of a given material.

Self-lubricating polymers feature a higher rate of evaporation in vacuum than metal-ceramics and materials with a solid-lubricant surface layer.

The evaporation of material must be taken into account when selecting self-lubricating materials for operation in a high vacuum. In some cases self-lubricating polymers having a high rate of evaporation are not fit for vacuum applications.

Metal-ceramic compositions with solid-lubricant components or

Table 9.28

Properties of self-lubricating materials

Properties	Unit of measurement	AΦ-3aM	AMAH-2	AMAH-4	Esteran-33
Rate of linear wear in steady sliding (mean value)	—	4×10^{-9}	7×10^{-9}	1×10^{-9}	2×10^{-8}
Counterface material	—	Steel Grade 20X13	Steel Grade 20X13	Steel Grade 20X13	Steel Grade 20X13
Counterface roughness	—	$Ra \leq \leq 0.32 \mu\text{m}$	$Ra \leq \leq 0.32 \mu\text{m}$	—	—
Friction coefficient in steady sliding	—	0.12	≤ 0.12	≤ 0.1	0.08
Pressure	kgf/cm ²	2	2	2	2
Sliding speed	m/s	2	2	2	2
Hardness of self-lubricating material, <i>HB</i>	kgf/mm ²	28-30	—	27-29	22
Hardness of counterface, <i>HRC</i>	kgf/mm ²	32-35	32-35	32-35	32-35
Compressive strength	kgf/cm ²	—	1,500	900	1,000
Impact strength	kgf cm/cm ²	—	1.5	27-29	3
Linear expansion coefficient	$\alpha \times 10^{-5} \text{ } 1/^{\circ}\text{C}$	—	1.2	2.0	—
Density	g/cm ³	2.1	3.7	3.2	3.2
Thermal conductivity	kcal/m h $^{\circ}\text{C}$	0.25	—	0.516	—
Maximum permissible working temperature	$^{\circ}\text{C}$	350	300	300	120

coatings deposited onto the rubbing surface by various methods are more suitable for operation in vacuum.

There is a special group of heat-resistant materials in which a solid-lubrication surface layer is formed, e.g., by thermochemical

treatment [26, 14]. High thermal stresses in tribological joints operating in vacuum impose limitation on wear, loads and clearances.

Metal-ceramic materials and materials with a solid-lubricant layer are preferable for high-vacuum applications.

Data on self-lubricating polymer materials for rubbing components are given in Table 9.28. The range of commercially available materials is much wider.

9.5.3. Frictional Characteristics of Solid Lubricants and Self-Lubricating Materials

When rubbing on a hard surface in air, graphite ensures good lubrication, but it is inefficient in vacuum, as shown in Table 9.29 [58]. The coefficient of friction for both natural and pyrolytic graphite is 2 times higher in vacuum than in air. The reason is the adhesion of graphite layers to each other.

As seen from Table 9.29, boron nitride, which is also lamellar in

Table 9.29

Data on friction of graphite and boron nitride [58]

Solid lubricants	Friction coefficient		Vacuum, mm Hg
	in air	in vacuum	
Natural graphite	0.19	0.44	6×10^{-9}
Pyrolytic graphite	0.18	0.50	2×10^{-9}
Hot-pressed boron nitride	0.25	0.70	2×10^{-9}

structure, in vacuum has a coefficient of friction of up to 0.70. The lamellar structure as such is not enough to explain the difference in the lubricating efficiency of solid lubricants in air and in vacuum. One of the reasons is the presence of adsorbents coming to the sliding interface from the ambient air, and the lack of these in vacuum renders graphite and boron nitride inoperable.

The distance between the atoms in parallel layers of graphite (3.44 \AA) is greater than this distance in the boron nitride lattice. For this reason, the interlayer bonds in graphite are weaker than in boron nitride. An indirect proof of this is the coefficient of friction for graphite being lower than that for boron nitride as observed under identical test conditions. The effect of adsorbed surface films on the lubricating efficiency of lamellar structures has been extensively studied [9, 55, 58].

The relation between the coefficient of friction and temperature for tungsten molybdenum, niobium, and tantalum selenides in air at different values of the relative humidity and in vacuum is shown in Fig. 9.13 [14]. The tests were run in air and in vacuum at two

specific loads, 0.6 and 2 kgf/cm², at a sliding speed of 1.5 m/s. Friction was effected between the external cylindrical surface of a steel

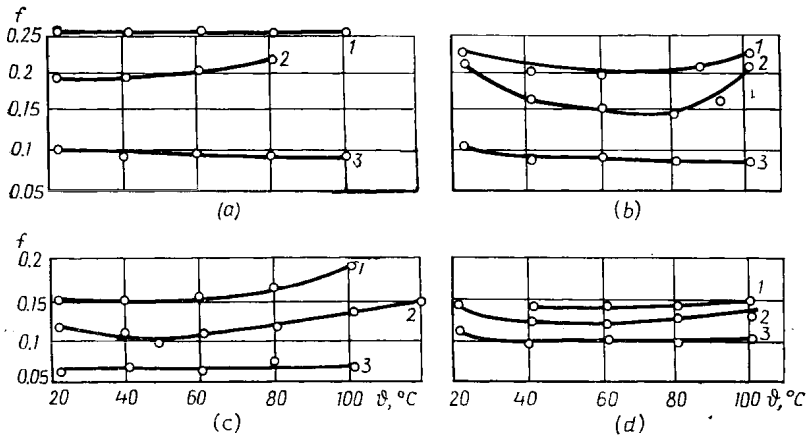


Fig. 9.13. Effect of temperature on friction coefficient for (a) tantalum diselenide; (b) molybdenum diselenide; (c) niobium diselenide and (d) tungsten diselenide

1—relative humidity 100%; 2—relative humidity 50%; 3—vacuum 10^{-7} mm Hg

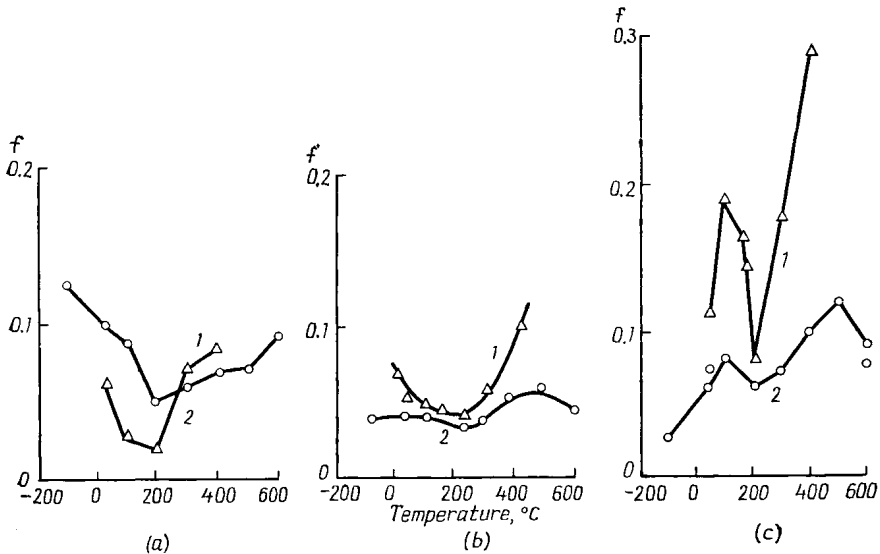


Fig. 9.14. Coefficient of friction of thin molybdenum disulphide film on (a) molybdenum, (b) tungsten, and (c) copper

Δ —in air; \circ —in vacuum

specimen (10 mm in diameter and 10 mm in length) and the end face of a cylindrical solid-lubrication insert (8 mm in diameter). The steel specimens were made of steel Grade 15X18H12C4TЮ with a surface finish of from 0.63 to 0.32 μ m Ra .

As seen from Fig. 9.13, the frictional behaviour of the tungsten, molybdenum, niobium, and tantalum diselenides within the specified region of loads (0.2 to 12 kgf/cm²) and temperatures depends on adsorbed surface films. Fig. 9.14 shows the effect of temperature on the coefficient of friction for a thin molybdenum-disulphide film on molybdenum, tungsten, and copper substrates [60]. These data

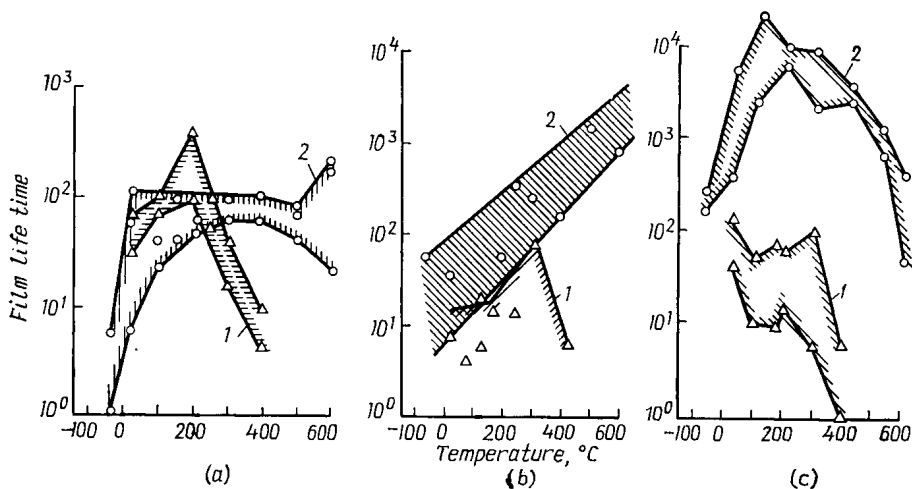


Fig. 9.15. Life time of thin molybdenum disulphide film on (a) molybdenum, (b) tungsten, and (c) copper at different temperatures
1—in air; 2—in vacuum

demonstrate the influence of the substrate and, therefore, the influence of interaction between a solid lubricant and a metal. The service life of a thin molybdenum-disulphide film on molybdenum, tungsten, and copper substrates, depending on temperature in air and in vacuum, is shown (in semi-logarithmical coordinates) in Fig. 9.15. The substrate hardness also has an effect on the coefficient of friction, so that with greater hardness of the substrate the coefficient decreases. The distinguishing features of MoS₂ are its strong adhesion to the substrate and its exceptionally high compressive strength. The layer of MoS₂ withstands dynamic pressures of up to 10⁴ kgf/cm² and static pressures of up to 3×10^4 kgf/cm², which allows it to be used up to the yield point of many metals. A new class of solid lubricants with still further improved stability in vacuum and reduced rate of evaporation has more and more often been reported upon in the literature. The solid lubricants WSe₂ and MoS₂ exhibit high thermal stability in air and in vacuum and high resistance to corrosion. Relationships between the friction coefficient and temperature for MoS₂, MoSe₂ and MoTe₂ are shown in Fig. 9.16 [58]. With molybdenum disulphide, the coefficient of friction remains low up to 550°C, and beyond this point it begins

rising sharply. At 730° in vacuum, molybdenum disulphide begins dissociating into molybdenum and sulphur. The rise of the friction coefficient at 550°C points to the effect of additional heating due to friction, which is typical of the testing procedure. Molybdenum diselenide is more stable against heating than molybdenum disulphide.

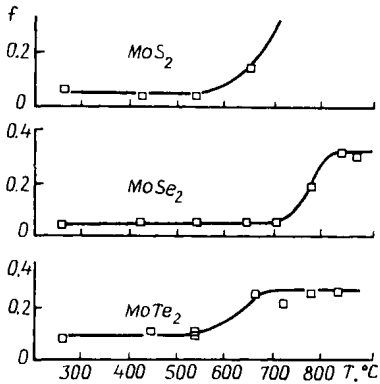


Fig. 9.16. Coefficient of friction as a function of temperature for thin films of MoS_2 , MoSe_2 , and MoTe_2 in a vacuum of 10^{-8} to 10^{-6} mm Hg at a sliding speed of 2.0 cm/s and a load of 100 gf

With self-lubricating materials in vacuum applications, the moment of friction in the movable joints rises after their prolonged stand-still. Hence, the design of low-power vacuum mechanisms involves the selection of materials with a minimum increase in the starting friction coefficient.

The AMAH-2 Grade material [7] has a stable and low coefficient of friction in vacuum, but its starting friction coefficient can be as high as 0.44. For sliding bearings, the AMAH-2 Grade material is used in combination with steel Grade 20X13 hardened to HRC 35 and finished to not worse than $0.32 \mu\text{m Ra}$. The bearing bush is finished to 1.25 to $2.5 \mu\text{m Ra}$.

The M-801 Grade material is a solid-lubricant diffusion coating of MoS_2 35 to 40 μm thick on a molybdenum substrate, obtained by thermochemical treatment [26].

The high thermal stability in vacuum and nearly equal thermal expansion coefficients of the materials of rubbing parts and the coating (e.g., the Mo-MoS₂-Mo system) present interesting possibilities for many vacuum applications. In addition to these advantages, the Mo-MoSe₂-Me (or Mo-MoSe₂-Mo) system have a low rate of evaporation in vacuum and a small difference between the starting and sliding friction coefficients (see Table 9.30).

Table 9.30

Frictional characteristic of materials with solid lubricant films

Material	Friction conditions	760 mm Hg, 20°C		(2 to 3) × 10 ⁶ mm Hg		Source (Reference No.)
		f_{st}	f_{kin}	f_{st}	f_{kin}	
AMAH-2	$p = 2 \text{ kgf/cm}^2$ $v = 4 \text{ m/s}$	0.44	0.18	0.1	0.1	[7]
M-801 (Mo-MoS ₂ -Mo)	$p = 7.8 \text{ kgf/cm}^2$ $v = 0.265 \text{ m/s}$	0.4-0.5	0.1	0.15	0.05	[26]
Mo-MoSe ₂ -Me	$p = 0.3-3 \text{ kgf/cm}^2$ $v = 0.02 \text{ m/s}$	0.13	0.12	0.1	0.1	[14]

Figure 9.17 illustrates the change of friction coefficients with temperature for sulphides and selenides, as these were heated up to 600°C. Powders of these lubricants were rubbed onto the surface of a specimen obtained from a powdered iron, Grade ПЖМ1, by pres-

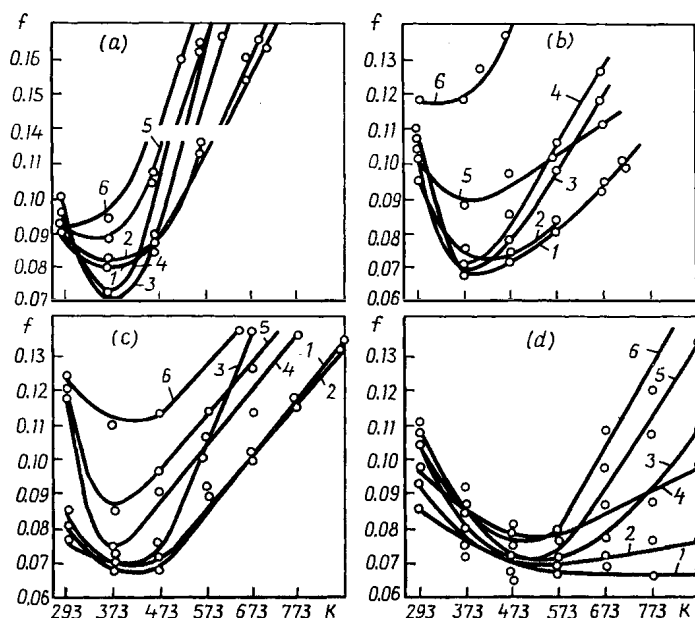


Fig. 9.17. Coefficient of friction as a function of temperature in friction of sulphides and selenides of high-temperature metals in (a) air, (b) nitrogen, (c) argon, and (d) vacuum

1—native MoS_2 ; 2— MoS_2 ; 3— WS_2 ; 4— MoSe_2 ; 5— WSe_2 ; 6— NbSe_2

sing and sintering in a hydrogen medium. The layer of the lubricants was 80 to 100 μm thick, the counterface was copper Grade M1, the pressure, 10 kgf/cm^2 , sliding speed, 0.004 m/s, and vacuum, 10^{-5} mm Hg.

The lubricating action is interpreted with respect to the atomic structure of the tested substances [28].

9.5.4. Solid-Lubricant Coatings with Polymer Binders

Solid-lubricant coatings commercially produced for use in air and in vacuum are given in Table 9.31.

The physico-mechanical properties of solid-lubricant films are largely determined by their structure which can be modified for best results by various methods, namely, by changing the binder, by introducing fillers, by heat treatment, by changing the orientation, etc. In all the materials of Table 9.31 the filler is molybdenum

Solid lubricant coatings with polymer binders (after L.N. Sentyurichina)

Coating	Standard	Binder material	In atmospheric conditions				In high vacuum				
			life, min	mean deviation, %	<i>f</i>	sliding distance, km	life, min	mean deviation, %	vacuum, mm Hg	<i>f</i>	sliding distance, km
ВНИИ НП-209	TU 38 10186-75	Organosilicon resin <i>k</i> = 1	110	±9	0.04-0.09	5.8	15	±6	5×10^{-9} - 10^{-7}	0.05-0.08	0.78
ВНИИ НП-213	TU 38 10187-75	Organosilicon resin <i>k</i> = 0.5	290	±7	0.05-0.09	15.2	50	±10	2×10^{-8} - 10^{-7}	0.04-0.08	2.6
ВНИИ НП-212	TU 38 101594-75	Urea-formaldehyde resin <i>k</i> = 0.5	380	±10	0.06-0.12	20	400	±9	10^{-8} - 5×10^{-8}	0.02-0.06	21
ВНИИ НП-229	OST 38 128-73	Sodium silicate <i>k</i> = 0.5	230	±15	0.05-0.12	12	350	±12	10^{-8} - 8×10^{-8}	0.02-0.05	18.5
ВНИИ НП-230	TU 38 101558-75	Epoxy resin <i>k</i> = 0.5	300	±12	0.05-0.12	15.7	270	±15	2×10^{-8} - 8×10^{-8}	0.02-0.06	14

Note. k = ratio between the amounts of MoS_2 and binder.

disulphide Grade MBЧ (TsMTU 06-1-68) with a grain size of 1 to 7 μm . The optimal ratio between the binder and the filler varies with different materials. The substrate material is steel (Grades 20X13, 45), cast iron (Grade БПЧ), etc. The optimal underlayer finish is 1.6 to 3.2 μm R_z , with the film thickness being 20 to 30 μm . The properties of a number of solid-lubricant coatings are described in [37]. The kind of binder has a significant bearing on the thermal stability of solid-lubricant films.

The lubricity of MoS_2 -base films at high temperatures depends, among other things, on the extent of their oxidation. The following binders are generally used: inorganic (sodium silicate, ceramics, compounds of aluminium, lead, etc.), organic (based on epoxy, phenolformaldehyde, butyral, polyurethane and other resins), and organosilicon. The maximum thermal stability (up to 800°C) is provided by inorganic binders; organosilicon binders are stable against heat in air (up to 300°C), but their stability in vacuum is limited to 150°C. Organic binders operate within the temperature range from -100 to +400°C; within this large class a binder with the required thermal properties can always be selected. The most favourable operating conditions for organic binders are those under which the binder undergoes transition into a highly elastic state.

Antifriction fillers can be represented by materials containing oxygen, chlorine, sulphates, phosphates, fluorine, sulphur, selenium, etc. The most efficient fillers are disulphides, diselenides, and chlorides, which provide high wear resistance, low friction coefficients, and stability in air and in vacuum. The wear life of solid-lubricant coatings is influenced by the nature of the binder and its resistance to tribocracking in vacuum, and by the presence of moisture in the material [46].

9.5.5. Soft Metal Coatings

These are used for lubricating purposes in precision tribological joints of optico-mechanical instruments and in sliding electric contacts operating in vacuum. A low evaporation rate and the possibility of providing high-accuracy fits allow these coatings to be employed in high vacuum within a wide range of working temperatures. Coatings of this type, functioning as solid lubricants, have also found application in movable joints operating within a wide temperature range at high specific loads.

Such coatings are disadvantageous in that they cannot regenerate as they wear unless special measures are taken, have high coefficients of friction, and are less efficient in the transfer of heat from the sliding interface than fluid lubricants. The frictional characteristics of rubbing surfaces with thin metal coatings are rather difficult to evaluate, because they depend substantially on the type of deformation in the contact [1, 62].

In friction of soft metal coatings in vacuum the following phenomena can be found on the specimens: plastic flow and tearing in depth. The first is characterized by stable friction (the coefficient

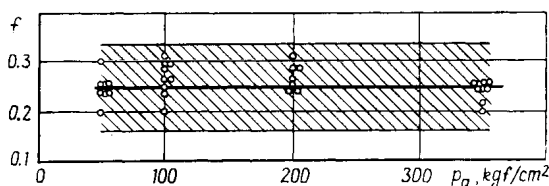


Fig. 9.18. Effect of pressure on the friction coefficient of gold-plated B-95 alloys specimens

of friction during testing did not vary in excess of 5 to 10 percent about its mean value) and by small surface roughness. For instance, the rubbing surfaces of tin and lead films on an underlayer of steel

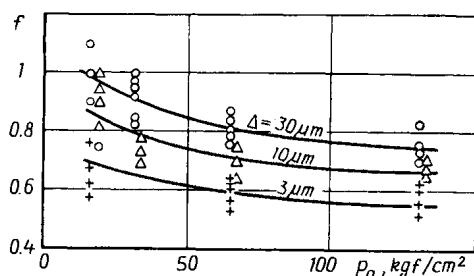


Fig. 9.19. Effect of pressure on the friction coefficient for a specimen of steel Grade 20X13 with a gold coating 3, 10 and 30 μm thick rubbing against a counterface of steel Grade 20X13 in vacuum

Grade 20X13 were found to have a surface roughness of 0.32 to 0.63 $\mu\text{m Ra}$, and that of silver film, 0.08 to 0.16 $\mu\text{m Ra}$. No transfer of film particles onto the counterface was observed by visual inspection.

Phenomena of the second type are accompanied with a significant variation in the coefficient of friction; the rubbing surface of the film becomes rough, with traces of pulls of film particles from it and smears

on the counterface. Here, the surface roughness substantially depends on both the load and the film thickness.

Shown in Fig. 9.18 is the coefficient of friction as a function of the load on a specimen of steel Grade 20X13 with a gold coating 1 to 10 μm thick which rubbed against an anodized counterface made of alloy Grade B95 in the plastic compression regime. The microhardness of the gold plating was 80 kgf/mm^2 . Within the range of pressures from 3 to 350 kgf/cm^2 , the coefficient of friction was found to depend neither on the coat thickness, which varied from 3 to 30 μm , nor on the load. The relationship obtained is typical of all the observed cases of friction in the plastic-flow conditions (with the coat thickness being $\geq 1 \mu\text{m}$), and it is characterized by the lack of any marked dependence of the friction coefficient on the coat thickness and load.

When tearing in depth takes place, the coefficient of friction substantially depends on the coat thickness and load. As the first is reduced and the second increased, the coefficient of friction decreases. Figure 9.19 shows how the friction coefficient depends on the specific load in friction of a specimen of steel Grade 20X13 with a gold coating 3, 10 and 30 μm thick against a counterface of the same steel. When the thickness of the coat is lowered under the point of transition from tearing in depth to plastic flow, the coefficient of friction levels off and no longer depends on the coat thickness and load.

REFERENCES

1. Алексеев Н. М. Металлические покрытия опор скольжения. М., «Наука», 1973.
2. Башта Т. М. Машиностроительная гидравлика. М., «Машиностроение», 1974.
3. Башта Т. М. Объемные насосы и гидравлические двигатели гидросистем. М., «Машиностроение», 1974.
4. Бадыштова К. М., Чесноков А. А., Иванкина Э. Б. Современные индустриальные масла для промышленного оборудования. М., ЦНИИТЭНефтехим, 1974, с. 4.
5. Бонер Ч. Дж. Редукторные и трансмиссионные масла. М., «Химия», 1967.
6. Брон Л. С., Тартановский Ж. Э. Гидравлический привод агрегатных станков и автоматических линий. М., «Машиностроение», 1967.
7. Вайнштейн В. Э., Трояновская Г. И. Сухие смазки и самосмазывающиеся материалы. М., «Машиностроение», 1968.
8. Виноградова И. Э. Противоизносные присадки к маслам. М., «Химия», 1972.
9. Влияние температуры на характеристики трения некоторых сульфидов, селенидов и теллуридов тугоплавких металлов.— В сб.: Трение и изнашивание при высоких температурах. М., «Наука», 1973, с. 133—138. Авт.: Ковальченко М. С., Сычев В. В., Ткаченко Ю. Г. и др.
10. Детали и механизмы металлорежущих станков. Под ред. Д. Н. Решетова. М., «Машиностроение», 1972.
11. Детали машин. Справочник. Под ред. Н. С. Ачеркана. М., Машгиз, 1953, кн. 1, с. 654.
12. Дьяченко Б. П. Измерение вязкости жидкости кварцевыми резонаторами.— «Измерительная техника», 1970, № 8, с. 20.
13. Износостойкость высоконаполненных реактопластов в условиях сухого трения.— В сб.: Тезисы докладов Всесоюзной научной конференции. Ч. II. Ташкент, Ташк. политехн. ин-тут, 1975. Авт.: Кутьков А. А., Гойтемиров Р. У. и др.
14. Исследования фрикционных свойств диселенидов вольфрама, ниобия и тантала на воздухе и в высоком вакууме.— В сб.: Тезисы докладов конференции «Повышение износостойкости и срока службы машин». Киев, 1970, с. 154, 155. Авт.: Трояновская Г. И., Лобова Т. А., Сергеева Л. М.
15. Кичкин Г. И., Виленкин А. В. Масла для гидромеханических коробок передач. М., «Химия», 1969.
16. Климов К. И., Кичкин Г. И. Трансмиссионные масла. М., «Химия», 1970.
17. Кореляков Л. В., Школьников В. М. Современные высокоиндексные масла из нефтяного сырья. М., ЦНИИТЭНефтехим, 1972, с. 5—15.
18. Коулман В. Расчет конических и гиповидных зубчатых колес на заедание. Экспресс-информация, сер. Детали машин, 1966, № 37.
19. Крагельский И. В. Трение и износ. М., «Машиностроение», 1968.

20. Крагельский И. В., Швецова Е. М. Влияние скорости скольжения на изнашивание металлов. В кн.: Трение и износ в машинах. Вып. X. М., Изд-во АН СССР, 1955, с. 5—34.
21. Кудрявцев В. Н. Зубчатые передачи. М.—Л., Машгиз, 1957.
22. Лосиков Б. В. Нефтепродукты. Свойства, качество, применение. Справочник. М., «Химия», 1966, с. 480—501.
23. Лосиков Б. В., Пучков Н. Г., Энглин Б. А. Основы применения нефтепродуктов. М., Гостоптехиздат, 1959, с. 438—450.
24. Мэнли Л. В., Коппенхофер Р. М. Изменяющиеся требования к индустриальным маслам и смазкам. Обзорный доклад на VIII Мировом нефтяном конгрессе. М., ВНИИ ОЭНГ, 1971.
25. Научные принципы создания антифрикционных самосмазывающихся пластмасс.— В сб.: Тезисы докладов Всесоюзной научной конференции, ч. II. Ташкент, Ташк. политехн. ин-тут, 1975. Авт.: Коршак В. В., Грибова И. А. и др.
26. Некоторые результаты испытания покрытий и композиций материалов на основе дисульфида молибдена в вакууме при высокой температуре.— В кн.: Трение и изнашивание при высоких температурах. М., «Наука», 1973, с. 138—142. Авт.: Дрожжина М. П., Духовской Е. А., Ермаков А. Т. и др.
27. Оболенчик В. А. Селениды. М., «Металлургия», 1972.
28. О механизме смазочного действия сульфидов и селенидов тугоплавких металлов.— «Физико-химического механика материалов», 1973, № I, с. 58—61. Авт.: Самсонов Г. Ц., Берсегян Ш. Е., Ткаченко Ю. Г. и др.
29. Опоры осей и валов машин и приборов. Под ред. Н. А. Спицина и М. М. Машкова. М., «Машиностроение», 1970.
30. Папок К. К., Рогозин Н. А. Словарь по топливам, маслам, смазкам, присадкам и специальным жидкостям. М., «Химия», 1975.
31. Петрусевиц А. И. Зубчатые передачи. Червячные и винтовые передачи.— В сб.: Детали машин. Под ред. Н. С. Ачеркана. Изд. 2-е. Кн. 1. М., Машгиз, 1953, с. 199—433.
32. Петрусевиц А. И. Роль гидродинамической масляной пленки в стойкости и долговечности поверхностей деталей машин.— «Вестник машиностроения», 1963, № 1, с. 20—26.
33. Резников В. Д., Григорьев А. И. Классификации и взаимозаменяемость отечественных и зарубежных моторных масел. Тематический обзор. Сер. «Переработка нефти». М., ЦНИИТЭНефтехим, 1976.
34. Розенберг Ю. А. Влияние смазочных масел на надежность и долговечность машин. М., «Машиностроение», 1970, с. 9—11.
35. Розенберг Ю. А., Виноградова И. Э. Смазка механизмов машин. М., Гостоптехиздат, 1960.
36. Рыбак Б. М. Анализ нефтей и нефтепродуктов. М., Гостоптехиздат, 1962.
37. Сентюрихина Л. Н., Опарина Е. М. Твердые дисульфид-молибденовые смазки. М., «Химия», 1966.
38. Синицын В. В. Подбор и применение пластичных смазок. М., «Химия», 1974.
39. Синтез и некоторые свойства халькогенидов вольфрама и тантала.— В сб.: Халькогениды, вып. 2. Киев, «Наукова думка», с. 61—76. Авт.: Зеликман А. Н., Крейн О. Е., Лобова Т. А.
40. Состав и свойства пластичных смазок. М., ЦНИИТЭНефтехим, 1970. Авт.: Вайншток В. В., Фукс И. Г., Шехтер Ю. Н., Ищук Ю. Л.
41. Справочник по применению и нормам расхода смазочных материалов. Под ред. Е. А. Эминова. Кн. 1 и 2. М., «Химия», 1969, с. 11—59 и 895—950.
42. Старосельский А. А., Гаркунов Д. Н. Долговечность трущихся деталей машин. М., «Машиностроение», 1967.
43. Таблица значений индекса вязкости. Стандартгиз, 1960.
44. Температурная стойкость новых твердых смазочных покрытий при трении в вакууме.— В сб.: Трение и изнашивание при высоких температурах. М., «Наука», 1973, с. 129—132. Авт.: Матвеевский Р. М., Сентюрихина Л. Н., Попов С. А. и др.

45. Товарные нефтепродукты, их свойства и применение. Справочник. Под ред. Пучкова Г. Н. М., «Химия», 1971 с. 72—106.
46. Трение и износ в вакууме. М., «Машиностроение», 1973. Авт.: Крагельский И. В., Любарский И. М. и др.
47. Трение и износ материалов на основе полимеров. Минск, «Наука и техника», 1976. Авт.: Белый В. А., Свириденко А. И., Петроковец М. И. и др.
48. Фукс Г. И. Вязкость и пластичность нефтепродуктов. М., Гостоптехиздат, 1951.
49. Хаттон Р. Е. Жидкости для гидравлических систем. М., «Химия», 1965, с. 16—18.
50. Часовников Л. Д. Передачи зацеплением. М., «Машиностроение», 1969.
51. Черножуков Н. И., Крейн С. Э., Лосиков Б. В. Химия минеральных масел. М., Гостоптехиздат, 1959.
52. Эрнст В. Гидропривод и его промышленное применение. М., Машгиз, 1963.
53. Bartel A. Inzureichende Schmierung als haufige Ursache fur Maschinen-ausfalle. Metall, 1971, Bd. 25, N. 8, S. 935—938.
54. Bartz W. J. "VDI-Zeitschrift", 1974, N 2, S. 127-134.
55. Brayant P. J., Gutshall P. Z., Taybor L. H., A study of mechanisms of graphite friction and Wear — "Wear", 1964, No. I, vol. 7, p. 118-128.
56. Braithwaite E. R. Solid Lubricants and Surfaces, Pergamon Press, 1964.
57. Debuan F. "Mineraloeltechnik", 1973, N. II.
58. Donald H. Buckley "Friction, Wear and Lubrication in Vacuum", Washington, NASA Lewis Research Center, 1971.
59. Horst Mauser. Mit weniger Schmierstoffen besser schmieren Ingenieur digest, Neft, 3, Mars, 1974, 13, Gahrgang, S. 39-44.
60. Yuko Tsuya. Microstructure of Wear, Friction and Solid Lubrication, Technical Report of Mechanical Eng. Laboratory Jgusa Sufinami-ku. Tokyl, Japan, 1975, No. 3. 107.
61. Peter A., Henshaw B. W. "Ind. Lubric. and Tribol." 1973, 25, No. 6, p. 230-235.
62. Rabinowicz. Variation of Friction and Wear of Solid Lubrication Films with Thickness. ASLE Transactions, vol. 10, No. 1, January 1967, p. 1-9.

THERMAL STABILITY OF BOUNDARY LUBRICATION FILMS AND SOLID LUBRICANT FILMS

As defined by GOST 18283-72, boundary lubrication is a mode of lubrication in which friction between two surfaces moving relative to each other is determined by the properties of the lubricant that differ from the bulk properties and depend upon interaction between the materials of the rubbing surfaces, the lubricant, and the environment.

Boundary lubrication films can be formed on rubbing surfaces as a result of physical adsorption, chemisorption and chemical reactions. For instance, organic substances having a molecular chain structure, whether fluid or plastic, at the same temperature in the boundary condition on the metal surface acquire elasticity, passing into another state of aggregation, either quasi-solid or quasi-crystalline [1]. The best protection of rubbing surfaces is ensured by a solid boundary layer [2, 9, 10].

One of the most important factors that affect the frictional properties of rubbing materials is the temperature produced by their friction. This temperature heats the rubbing surfaces and the boundary lubrication film. In some cases, rubbing parts may have a high bulk temperature due to specific operating conditions typical of a given application.

For this reason, data on the temperature ranges of boundary-lubrication films are essential in both the selection of a lubricant for particular uses and the development of new lubricants. GOST 17604-72 specifies a method of determining the thermal stability of lubricants in friction. The method involves testing a lubricant in a point contact of hardened steel specimens at a constant

contact load of 200 kgf/mm² and at a constant and very slow sliding speed of about 0.2 mm/s in order to avoid frictional heat generation. The bulk heating of the rubbing parts and the lubricant is effected from an external source.

In these conditions, the bulk temperature of the specimens practically equals the temperature at the contact. The temperature is stepped up by increments of 10-20°C. The test at each step is run for 1 min. The coefficient of friction and the temperature are measured during each test, and the stationary specimens are measured for wear after the test has been completed. The thermal stability of lubricants is evaluated by two parameters established for the purpose. The first is the critical temperature ϑ_{cr} at which a sharp increase in the friction coefficient is observed. The result is a stick-slip motion and intensive wear of the specimens. The critical temperature signifies that the lubricant film is broken and the metal surfaces are in direct contact (see Figure 10.1, curve 1). The second parameter is the temperature ϑ_{ch} of a chemical modification of the rubbing surfaces, at which layers having a low shear strength and serving as a lubricant emerge on the surfaces upon decomposition of a chemically active oil additive and chemical reaction between the decomposition products and the metal. This temperature is indicative of the drop in the coefficient of friction and of the end of its sharp changes (Fig. 10.1, curve 2). The dot-dash line sections on the curves define the temperature regions where stick-slip motion takes place. Both transition temperatures have a physical explanation. At the critical temperature, the oil molecules in the boundary layer become disoriented and desorbed and so lose the ability to separate the rubbing surfaces. This process is governed by the laws of reversible thermodynamic processes and is related to the heat of adsorption. At the chemical modification temperature, a solid-lubricant type film forms on the rubbing surfaces. This film reduces the coefficient of friction and stabilizes it at high temperatures. The formation of such a film is connected with irreversible chemical reactions and the properties of the metals and the active oil additives.

The above-mentioned characteristics determined by the standard procedure can be used as the basic data in comparative performance tests for selecting an optimum type of lubricant within specified temperature limits.

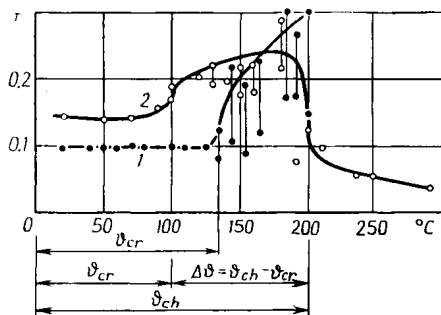


Fig. 10.1. Variation of the coefficient of friction with temperature in testing vaseline oil blended with 0.1% stearic acid (1) and with 1.5% chlorinated paraffin (2)

These lubricant characteristics are determined on the MACT-1 Model testing machine now commercially available for industrial use. Several methods (Fig. 10.2) can be employed, which provide for testing specimens of various materials (steels, alloys, and plastics).

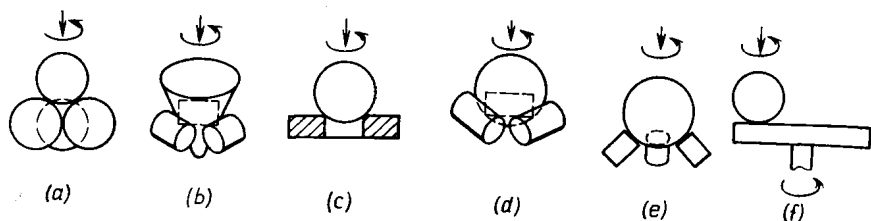


Fig. 10.2. Friction methods used in testing lubricants for temperature stability (a) four balls; (b) four rollers (one tapered and three cylindrical); (c) sphere and annular disc; (d) sphere and three rollers; (e) sphere and three flat surfaces; (f) sphere and revolving disc

With point contact methods, specific loads can range from 80 to 200 kgf/mm² (methods *a* through *d* in Fig. 10.2), and with a sphere rubbing on an annular specimen, from 0.4 to 5 kgf/mm². Low sliding speeds and bulk heating allow the temperature near the contact zone to be measured accurately with a thermocouple and to be assumed to be equal to the contact temperature without any tangible error. Testing in air is conducted within the temperature range from 20 to 350°C.

10.1. INFLUENCE OF THE NATURE OF OIL, ADDITIVE AND GREASE

Critical temperatures for mineral and synthetic oils, additives, and also for some normal alcohols and fatty acids are given in Table 10.1 [9]. Analysis of the data of Table 10.1 reveals no functional relation between the critical temperature and the physico-chemical properties of mineral and synthetic oils.

Assuming a linear dependence of the critical temperature on the viscosity of mineral oils, it is possible, using the method of the least squares, to obtain a regression line corresponding to the formula $\vartheta_{cr} = 0.335 \nu_{50} + 113.6$ (here, ν_{50} is oil viscosity at 50°C). The correlation coefficient of 0.335 is indicative of a loose relationship between the critical temperature and the viscosity of the oils. A similar calculation of the relationship between ϑ_{cr} and the molecular mass shows the lack of connection between them (the correlation coefficient being 0.145 with the regression formula $\vartheta_{cr} = 0.118 M_m + 91.5$ for the six oils with the given values of molecular mass M_m).

Table 10.1

Critical temperatures and physico-chemical properties of synthetic and mineral oils, alcohols, and fatty acids tested in friction of balls made of hardened steel Grade IIIX15

Oil	Molecular mass M_m	Flash point, °C	Acid number, mg KOH per gram	Viscosity, cSt, at temperature, °C			Critical temperature, °C
				20	50	100	
Mineral oils							
Vaseline instrument oil Grade MBII, GOST 1805-76	—	120	0.14	—	7.7	—	100
Transformer oil, GOST 982-68*	—	145	0.07	30	9.8	2.6	180
Spindle oil Grade AY, GOST 1642-75	310	165	0.07	49	13	4.0	165
Compressor oil Grade XΦ-12, GOST 5546-66*	—	160	0.03	—	18	—	160
Turbine oil Grade II, GOST 32-74	—	180	0.02	99	22.4	5.11	120
Vaseline medicinal oil GOST 3164-52*	430	185	—	140	27.8	6.2	20
Turbine oil Grade 30YT, GOST 32-74	—	180	0.02	—	30	—	140
Industrial oil Grade 50A, GOST 20799-75	450	200	0.02	—	54	—	140
Oil Grade ДС11 (0.14% S), GOST 8581-63*	—	200	0.02	—	—	11.0	145
Automotive oil Grade AK-10, GOST 21757-76	425	200	0.28	—	70	9.6	150
Automotive oil Grade AK-15, GOST 21757-76	—	215	0.42	—	123	15	140
Nafta-paraffin fraction of oil Grade MC-20 (НПФ MC-20)	—	—	—	—	92	14	155
Aircraft oil, GOST 21743-76	—	200	0.25	792	111.5	16.7	140
Aircraft oil from Grozny crudes, GOST 21743-76	487	250	0.05	1.135	156	19.93	165
Aircraft oil from Emba crudes, GOST 21743-76	560	255	0.1	1.389	158	20.7	210
Cylinder oil (bright stock), TU MHII 233-47	—	275	—	—	—	30	140
Synthetic oils							
Polyether oil Grade 36/1 TU 38 101295-75	—	195	0.5	3,000 at -40°C	—	3.0	160
Ethyl polysiloxane liquid No. 5	—	300	none	—	260	—	20

Table 10.1 (continued)

Oil	Molecular mass M_m	Flash point, °C	Acid number, mg KOH per gram	Viscosity, cSt, at temperature, °C			Critical temperature, °C
				20	50	100	
Methyl phenylsiloxane liquid	—	300	none	—	310	—	20
Ethylene glycol	—	170*	—	—	—	—	125
<i>Alcohols and acids</i>							
Nonanol ($C_9H_{19}OH$)	144	213*	—	—	—	—	60
Mixture of alcohols, from octanol to arachic alcohol, C=8 to 20	130-298	194-250	—	—	—	—	92
Mixture of alcohols, from arachic alcohol to high-molecular alcohols, C > 20	298	210-250	—	—	—	—	115
Valerianic acid $CH_3(CH_2)_3COOH$ (C-5)	102	186	549	—	—	—	100
Caprylic acid $CH_3(CH_2)_6COOH$ (C-8)	144	237	389	—	—	—	120
Caprynic acid $CH_3(CH_2)_8COOH$ (C-10)	772	268	326	—	—	—	130
Palmitic acid $CH_3(CH_2)_{14}COOH$ (C-16)	256	—	219	—	—	—	160
Mixture of acids, from stearic to pentacosanoic acid (C=18 to 25)	284-382	—	147-197	—	—	—	200

* Boiling point.

For normal alcohols and saturated fatty acids, the critical temperature grows with the number of carbon atoms in the molecular chain and the molecular mass of a compound, and for fatty acids, it also grows with decreasing acidity.

Given in Table 10.2 are test data on chemically active additives dissolved in an inactive medicinal vaseline oil (6 mmol of an additive in 100 g of the oil). The additives were tested in friction between steel Grade IIIX15 spheres. The table presents some physico-chemical properties of the additives and the content of chemically active agents therein. The introduction of the additives produces a positive effect, i.e., a higher critical temperature due to their chemisorption and reduced coefficient of friction after the lubricant film has been broken and the chemically modified film formed at a definite tempe-

Table 10.2

Results of testing chemically active additives (friction of balls made of steel Grade MX15) [3, 6, 9]

Additive	Density d_4^{20}	Content, %			Thermographical analysis		Friction test		Additive content in vaseline oil, %
		P	Cl	S	decomposition temperature, °C	temperature range of first- order exo- thermic reac- tion with powdered iron, °C	critical tempera- ture, °C	chemical-mo- dification temperature of rubbing surfaces, °C	
Tributyl phosphite (C_4H_9O) ₃ P	0.949	12.46	—	—	78	110-170	100	155	1.5
Tributyl phosphate (C_4H_9O) ₃ P=O	0.976	9.95	—	—	236	290*	100	None	1.6
Dibutyl ether of methylphosphi- nic acid $CH_3P(OC_4H_9)_2$	0.978	10.4	—	—	125	125-190	70	120	1.25
Dibutyl ether of trichloromethyl- phosphinic acid $CCl_3P(OC_4H_9)_2$ (Chloref-40)	1.218	9.7	30.8	—	207, 225 [3]	133-170	—	150	1.36
Di(trichloromethylsulphide) $CCl_3(CH_2)_4S(CH_2)_4CCl_3$ (syolphol)	S**	—	55.3	8.1	200, 291 [3]	136-160	75	170	2.3
Trichloropentyl-diisoamyl dithio- phosphate $CCl_3(CH_2)_4S-$ $-P(OC_5H_{11}-i)_2$ \parallel S	1.174	6.8	24.3	14.5	208	140-170	90	180	2.66
JT3-6/9 ($C_4H_9OCSCH_2$) ₂ \parallel S	—	—	—	40	230 [3]	201-226	110	None	1.5
Chlorinated paraffin	—	—	38	—	200 [3]	135	120	200	1.5
Diphenyl disulphide $(CH_2)_3CS-SC-(CH_2)_5$	S**	—	—	28	—	—	100	150	3.0
Dichlorodiphenyl disulphide $CCl(CH_2)_4CS-SC(CH_2)_4CCl$	—	—	24	21.6	222	—	60	170	3.0
Dibromodiphenyl disulphide $(CBrCH_2)_4CS-SC(CH_2)_4CBr$	—	—	42	16.6	—	—	60	190	3.0

* End of reaction.

** Solid.

perature (all except for tributylphosphate and additive Grade ЛЗ-6/9). The optimum result was obtained with the Chloref-40 additive. Here the temperature of chemical modification of specimen surfaces proved lower than that of desorption of the chemisorbed molecules, and the additive active elements interacted with the steel surfaces be-

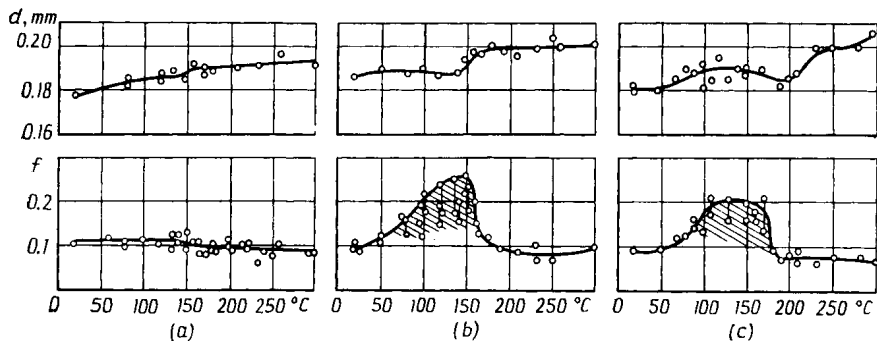


Fig. 10.3. Effect of temperature on friction coefficient f and wear patch diameter d for vaseline oil blended with additives
(a) 1.86 % Chloref-40; (b) 2.3 % Sulfol; (c) 2.66 % trichloropentyl diisooamyl dithiophosphate
friction of hardened steel balls)

fore the beginning of the desorption process. As a result, a low coefficient of friction was obtained at all test temperatures, and only at temperatures above 150°C (the chemical modification temperature) a slight increase of wear was observed. Figure 10.3 shows relationships between the friction coefficient and the wear patch diameter for a base oil with three different additives.

Comparison of the critical temperatures for oils with additives similar in chemical composition shows that ϑ_{cr} and ϑ_{ch} do not depend on the percentage of active agents in the additives. For some additives, ϑ_{ch} is in good agreement with the temperature ranges

Table 10.3

Critical temperatures of greases (maximum test temperature 300°C)

Grease	ϑ_{cr}	Grease	ϑ_{cr}
1-13, GOST 1631-61	30	ВНИИ НП-248, TU 40120-71	20
НК-50, GOST 5573-67*	43	ВНИИ НП-271, TU 38-1-299-69	150
ГОИ-54, GOST 3276-74	105	ВНИИ НП-228, GOST 12330-66	270
ЦИАТИМ-201, GOST 6267-74	90	ВНИИ НП-286, TU 38 101181-71	280
ЦИАТИМ-221, GOST 8773-73	190	ВНИИ НП-263, GOST 19832-74	300
ЦИАТИМ-231, GOST 9433-60	280	ВНИИ НП-274, GOST 19337-73	300
Litol 24, TU 38 101207-75	160	ВНИИ НП-293, TU 38-1-301-69	300

of the first exothermic reaction of the additives with iron, which were obtained through thermographical analysis (see Table 10.2).

Data on the thermal stability of a number of greases (with friction of hardened spheres made of steel Grade IIIX15) are given in Table 10.3.

10.2. INFLUENCE OF THE RUBBING SURFACE MATERIAL

The effect of the chemical composition of steels on the thermal stability characteristics of lubricants can be seen from the data on friction tests by the four-roller method, that are given in Table 10.4. The specimens made of steels containing about one percent C and alloyed with Cr, Ni, and W up to 10 atomic percent were, ex-

Table 10.4

Thermal behaviour of oils, depending of chemical composition of lubricated steels (testing at $p=150 \text{ kgf/mm}^2$, $v=0.035 \text{ cm/s}$)

Steel grade	Alloying elements content, at. %	HV	Critical temperature, °C					Temperature of chemical modification, °C		
			Spindle oil Grade AY	Vaseline oil with additives				Vaseline oil with additives		
				0.1% stearic acid	1.5% tributyl phosphate	1.5% chloro-paraffin	1% J13-23K (GOST 11883-77) and 4.3% S	1.5% tributyl phosphate	1.5% chloro-paraffin	1% J13-23K (GOST 11883-77) and 4.3% S
Y10	—	890	20	100	20	20	20	180	200	105
III X15	1.66	705	140	132	100		90		200	240
10X4.5	4.54	623	120	165	205		175	300	230	
10X5.6	5.80	566	130	150	240	120	230		235	300
10X9.5	9.70	583	130	130	180		190		260	
10H1	0.92	777	50	100						230
10H2	1.84	712	20	80		50		200	220	220
10H3.5	3.29	738	20	80	20		20	280	230	200
10H9	8.48	480	20	50		20		300	240	220
10B1	0.352	830	60	100	80	45	20	260	210	220
10B3.5	1.075	916	100	110	120	105	80	250	220	240
10B7.5	2.22	825	130	120	250	110	160	250	220	270
10B10	3.21	807	140	160	300	135	155	300	205	300

cept for two standard ones, specially cast and forged. Then the specimens, both the rollers and the cone, were ground and lapped to a surface finish of the 12th-13th class [6].

The presence of Cr and W in carbon steel increases the critical temperature of the boundary layers of mineral oils and additive oils. Specifically, an increase in the content of W leads to increased ϑ_{cr} ; as for Cr, the maximum critical temperatures for mineral oil and for oils with fatty-acid additives are achieved with a definite optimum content of Cr. Additions of Ni to steel either have no effect on ϑ_{cr} , or lower it.

The alloying of steels with Cr or W markedly increases the temperature of chemical modification of the rubbing surfaces by phosphoric and sulphuric additives. The introduction of Ni only slightly increases ϑ_{ch} for chloric and sulphuric additives, and for a phosphoric additive ϑ_{ch} sharply rises only with a Ni content of over 2 atomic percent.

Then it appears a good practice to add to steels the carbide-forming elements (i.e., Cr and W) in order to ensure a high critical temperature of lubricant layers. These elements increase the structure heterogeneity of the steels, which reduces their tendency towards

Table 10.5

Copper-base alloys ($p = 175 \text{ kgf/cm}^2$)

Main constituent and alloying elements	Alloying elements content, at. %	Annealing temperature, °C	Microhardness after machining, kgf/mm ²	ϑ_{cr} , °C	Main constituent and alloying elements	Alloying elements content, at. %	Annealing temperature, °C	Microhardness after machining, kgf/mm ²	ϑ_{cr} , °C
Copper	—	650	44	200	Sb	0.25 0.42 1.32	450	64.2 68.5 70.8	190 205
Al	1.05 5.76 10.42 16.25	650	44 58 68 79	165 120 240 250	Sn	0.118 0.30 0.58 1.16 2.77	650	46 48 57 56 68	205 240 300
Si	1.34 4.52 10.53	650	48 50 110	150 300	Zn	1.46 4.78 9.95 19.2 39.6	450	53.9 62.4 67.7 75.7 82.6	200 115 20
P	0.308 0.82 1.82	450	64.2 68.5 70.8	175 195 190					

seizure, promotes structural imperfections and microdistortions of the crystalline lattices, and so gives rise to adsorption centres on the rubbing surfaces. Nickel alloys readily react with additives containing P, Cl, and S, and can be used for heavy-duty applications. For chromium and tungsten alloys used under similar conditions it is advisable to employ oils with chloric additives.

Tables 10.5 and 10.6 present the critical temperatures of lubricant boundary layers in friction of hardened steel Grade IX9, with H_{100} of 1,000 kgf/mm², on copper and aluminium alloys (solid solutions). A sphere 12.7 mm in diameter made of this steel was run on an alloy ring at a speed of $v = 0.04$ cm/s; the lubricant was oil Grade Д1 blended with 0.1 percent of stearic acid.

Table 10.6

Aluminium-base alloys, $p = 40$ kgf/cm²

Main constituent and alloying elements	Alloying elements content, at. %	Annealing temperature, °C	Hardness, HV	Critical temperature		Main constituent and alloying elements	Alloying elements content, at. %	Annealing temperature, °C	Hardness, HV	Critical temperature	
				without removal of oxide film	oxide film removed before tests					without removal of oxide film	oxide film removed before tests
Aluminium Grade AB000	—	550	14.0	20	240	Sn	0.16	200	35.3	20	200
							0.24		35.6		
							0.49		33.3		
							1.26		35.0		
							2.31		33.6		
Si	0.028 0.106 0.714	550	14.2 16.4 24.6	110 140 230	265		5.14		33.6		
Cu	0.089 0.226 0.423	550	16.3 19.8 25.1	180 180 185	170 185 220	Sb	0.011	600	13.9	80	250
							0.037		15.2	140	
							0.095		15.6	230	260
Zn	0.207 0.353 2.430 4.530	550	14.5 14.2 17.7 36.4	40 110 185 180	250 230 — 210		0.183 0.455		15.6 19.3	—	230

For copper alloys (Table 10.5) the introduction of Sn in any of the concentrations leads to increased ϑ_{cr} , and that of P and Sb in general produces little effect. No direct correlation is observed between ϑ_{cr} and alloy hardness. A possible explanation of the effect of the alloying elements on the thermal stability of lubricant layers is different properties of oxide films formed on the rubbing surfaces,

their structure, density, plasticity, and their disintegration due to plastic deformations. Other important factors are the ability to form boundary layers with strong adsorption bonds or provide for interaction between the lubricant and the alloy surface through the oxide film.

The influence of natural oxide films is particularly strong for aluminium-base alloys (Table 10.6). With plain aluminium Grade AB000 having natural oxide films on the rubbing surface, the disintegration of the lubricant layer was observed at room temperature; when oxide films were removed beforehand by friction in oil against a loaded steel ball having a deliberately rough surface, the disintegration of the lubricant boundary layer was found to occur at 240°C. With aluminium alloys having oxide films, the introduction of Cu, Zn, Sb, and Sn in the alloys (over 2 percent) produces a sharp increase of ϑ_{cr} which, as a rule, is directly proportional to the content of the alloying element. With the oxide film removed, only Si and Sb provide a critical temperature that is higher than in the case of the plain aluminium; the content of these elements in the alloys has no significant effect. The alloys containing Sn were tested only at temperatures below 200°C because of their relatively low melting point (228.3°C). The higher the content of an alloying element in an aluminium alloy, the closer is ϑ_{cr} in the presence of the oxide film to ϑ_{cr} with the oxide film removed.

10.3. INFLUENCE OF GAS MEDIUM

The ambient gas medium has a substantial effect on the formation and strength of boundary lubricant layers in friction of steel surfaces [4, 9].

Figures 10.4 and 10.5 illustrate the results of tests by the four-sphere method on the RT-4 Model testing machine ($v = 0.03$ mm/s, $p = 200$ kgf/mm²) [9]. The specimens and the boundary layer of a mineral or synthetic oil with or without additives were bulk heated in air and in helium (~ 0.0004 percent oxygen). The antiscuff and tribochemical properties of the lubricants are markedly improved in friction in the inert gas medium. An increase in the thermal stability of the oils in helium can be attributed to the effect of the optimum oxidation conditions, because in air the excess of oxygen gives rise to thermooxidation processes which alter the chemical composition of the oils and, hence, their properties. The shortage of oxygen showed no influence on the efficiency of chemical interaction between phosphoric and chlorine-phosphoric oil additives and the steel surfaces.

The combined action of the base oil, the additives that modify the rubbing surfaces, and the ambient gas medium is essential for increasing the thermal stability of the boundary lubricant layers.

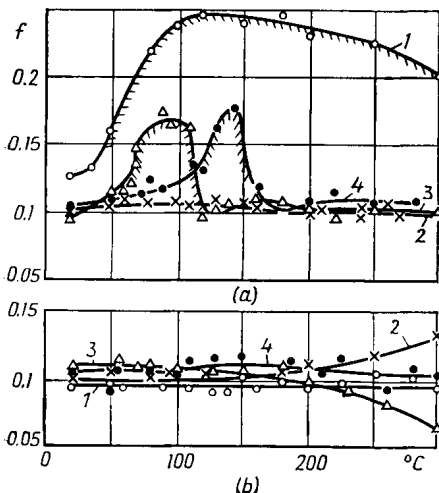


Fig. 10.4. Effect of temperature on the coefficient of friction in testing plain and additive-blended vaseline oils in (a) air and (b) helium
1—no additive; 2—Chloref-40; 3—dibutyl ether of methyl-phosphinic acid; 4—tributylphosphate

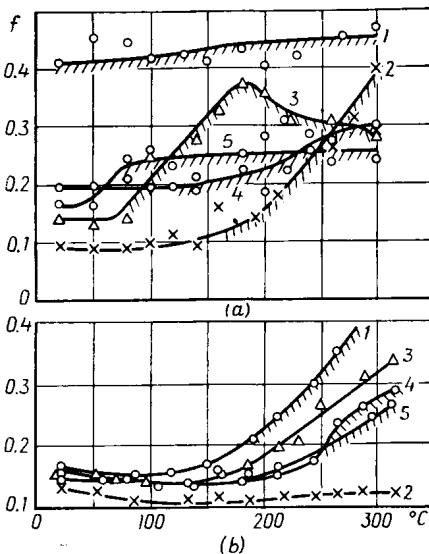


Fig. 10.5. Effect of temperature on the coefficient of friction in testing polymethylsiloxane liquid Grade IIMC-300 ($v_{50} = 171.5$ cSt), plain and with additives, in (a) air and (b) helium

1—no additive; 2—Chloref-40; 3—dibutyl ether of methyl-phosphinic acid; 4—tetra-chloropentane; 5—tributylphosphate

10.4. THERMAL STABILITY OF SOLID LUBRICANT COATINGS

The current assortment of oils and greases provides for the operation of tribological joints up to 250-300°C. However, even at such temperatures prolonged use of hydrocarbon, organosilicon, and also chloro- and fluorocarbon compounds can result in their oxidation and thermal decomposition and, hence, in the loss of lubricating efficiency.

The lubrication of rubbing components operating at higher bulk temperatures is ensured by solid lubricant coatings which have now found industrial application. These are graphite-base films for use in air, and molybdenum-disulphide base films for use in vacuum and inert gases. The working temperature ranges of solid lubricant films deposited by different methods are given in Table 10.7 (friction of a steel slider 8 mm in diameter on a revolving disc with a solid lubricant film) [9].

Generalized relationships between the friction coefficients and temperature for the data of Table 10.7 on molybdenum-disulphide

Table 10.7

Temperatures of destruction of solid lubricant coatings in friction against hardened steel Grade 9X18M ($H_{100}=800$, $P=0.54$ kgf, $v=0.1$ m/s)

Coating	Binder of method of deposition	Thickness, μm	Substrate material	Stable for 3×10^5 test cycles at temperature, $^{\circ}\text{C}$	Temperature, $^{\circ}\text{C}$, and number of cycles, n , resulting in destruction
<i>Vacuum 10^{-5} to 10^{-6} mm Hg. Lubricant—MoS_2</i>					
ВНИИ НП-229, OST 381. 28-73	Sodium silicate	20	Steel Grade 12X18H9T	500	600, $n=15,000$
ВНИИ НП-213, TU 38 10187-75	Organosilicon resin			500	600, $n=16,000$
ВНИИ НП-250, TU 38 101470-74				600	700, $n=1,000$
Molybdenum disulphide coating [7]	Polyimide resin			500	700, $n=100$
Molybdenum disulphide coating [5]	No binder; deposition by detonation method	30-50		500	600, $n=100$
M801 [12]	No binder; thermochemical deposition	30	Molybdenum	700	—
<i>Air. Lubricant—graphite</i>					
ВНИИ НП-251, TU 38 40135-75	Polyimide resin	20	Steel Grade 12X18H9T	350	400, $n=16,000$

coatings tested in vacuum are shown in Fig. 10.6. Each point of the curves corresponds to the coefficient of friction as found after 30,000 revolutions of the disc. Where the film failed earlier than that, the figure at the failure point indicates the corresponding number of revolutions. The dashed line running parallel to the axis of abscissas at the level of a friction coefficient of 0.2 defines the temperature region for each film where this is fully operable. The lower coefficients of friction at all test temperatures are provided by the molybdenum disulphide coating (Grade M801) applied to a molybdenum substrate by a thermochemical method.

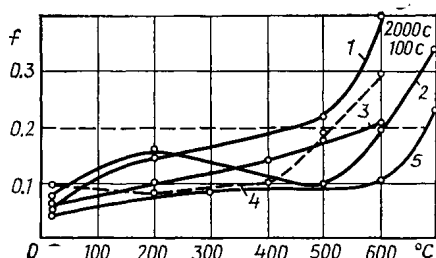


Fig. 10.6. Effect of temperature on the coefficient of friction for solid-lubricant coatings

1—ВНИИ НП-229; 2—ВНИИ НП-250; 3—molybdenum disulphide with polyimide resin; 4—molybdenum disulphide without binder; 5—M801

REFERENCES

1. Ахматов А. С. Молекулярная физика граничного трения. М., Физматгиз, 1963.
2. Боуден Ф. П., Тейбор Д. Трение и смазка твердых тел. М., «Машиностроение», 1968.
3. Виноградова И. Э. Противозносные присадки к маслам. М., «Химия», 1972.
4. Виноградов Г. В. Опыт исследования противозадирных свойств углеводородных смазочных сред. — В кн.: Методы оценки противозадирных и противозносных свойств смазочных материалов. М., «Наука», 1969, с. 3—41.
5. Матвеевский Р. М., Астахов Е. А., Краснов А. Н. Нанесение антифрикционного покрытия из дисульфида молибдена детонационным способом. — В сб.: Защитные покрытия на металлах. Вып. 6. Киев, «Наукова думка», 1972, с. 144—148.
6. Матвеевский Р. М., Буяновский И. А., Лазовская О. В. Исследование температурных пределов защитных свойств смазочных материалов при трении. — В кн.: Износостойкость. М., «Наука», 1975, с. 51—75.
7. Матвеевский Р. М., Лазовская О. В., Попов С. А. Антифрикционные свойства и долговечность твердых смазочных покрытий при трении в условиях повышенных температур. — В сб.: Повышение износостойкости деталей машин. Хабаровск, 1972, с. 20—28.
8. Матвеевский Р. М., Лазовская О. В. Температурная стойкость смазочных слоев при трении легированного алюминия по стали. — «Машиноведение», 1968, № 6, с. 78—85.
9. Матвеевский Р. М. Температурная стойкость граничных смазочных слоев и твердых смазочных покрытий при трении металлов и сплавов. М., «Наука», 1971.
10. Ребиндер П. А. О значении граничных условий в физико-химической механике процессов обработки пластических материалов. — В сб.: Обработка пластмасс в машиностроении, М., «Наука», с. 7.
11. Сентюрихина Л. Н., Опарина Е. М. Твердые дисульфидмолибденовые смазки. М., «Химия», 1966.
12. Смазочные свойства покрытия дисульфида молибдена диффузионного типа. — «Вестник машиностроения», 1974, № 12, с. 35—36. Авт.: Ермаков А. Т., Лобанов Б. П., Макаров Ю. В., Матвеевский Р. М.

